1-1-2018

Titanocene(III) Complexes: Promising Reagents for the Design of Sustainable Catalytic Processes

Godfred Kwesi Delali Fianu
Lehigh University, gfianu2002@yahoo.co.uk

Titanocene(III) Complexes: Promising Reagents for the Design of Sustainable Catalytic Processes

by

Godfred Delali Kwesi Fianu

A Dissertation

Presented to the Graduate and Research Committee

of Lehigh University

in Candidacy for the Degree of

Doctor of Philosophy

in

Department of Chemistry

Lehigh University

September 3, 2017

Approved and recommended for acceptance as a dissertation in partial fulfillment of the requirements for the degree of Doctor of Philosophy

Godfred Delali Kwesi Fianu

Titanocene(III) Complexes: Promising Reagents for the Design of Sustainable Catalytic Processes

August 16, 2017

Defense Date

Dr. Robert A. Flowers, II
Dissertation Director

Approved Date

Committee Members:

Dr. David A. Vicic

Dr. Marcos Pires

Dr. Patrick C. Wernett

ACKNOWLEDGMENTS

My sincerest gratitude goes to my advisor, mentor, and boss Dr. Robert A. Flowers II. Thank you for putting up with me all these years. Your patience, grace, support, and timely interventions, have helped shaped me into who I am as a research scientist and a thinker. As you say, “I am a distinguished professor”, but I say, you are a distinguished human being and you inspire me just by observing how you live your life, as a family man and as a boss. You have always treated me with respect and I am sincerely grateful for your constant encouragement, optimism, genuine passion, and desire to see me succeed, even when projects did not seem to work. I am truly blessed and greatly honored to have you in my life as an advisor and a lifelong mentor. Again, thank you and God will continually bless you and your family to prosper in all you do.

I also want to thank our collaborator Dr. Andreas Gansäuer and his group especially Sven, Ruben, and Dina for all the wonderful research we did together. Your contribution to these projects are immense and have expanded our understanding of titanocene(III) chemistry. I cannot thank you enough. I also thank my committee members Dr. David Vicic, Dr. Marcos Pires and Dr. Patrick Wernett for all their support.

I want to thank the past members of my group; Dr. Sadasivam Dhandapani, Dr. Kimberly Choquette, Dr. Niki Patel, Dr. Gabrielle Haddad-Weiser, and Dr. Tesia Chciuk for all their support and friendship. Sada, I am truly grateful for you taking the time to teach me most of the techniques I use today as a research scientist. It was a pleasure and an honor working with you and learning from you. Niki a.k.a. Niki Flash, Gabby a.k.a.

Empress, and Tesia a.k.a. Tesh Money, thank you so much for all the fun times and being great colleagues and friends. I am honored to call you my friends and may God bless you in all you do.

I also want to thank the current members of my group; Dr. Sandeepan Maity, Dr. Lawrence Courtney, Caroline Bartulovich, and Darian Waugh. Sandee, Darian, and Caroline, you guys make coming to lab a great experience and I am honored to call you my friends and colleagues. I also want to thank all the undergrads; Hollie Garber, Daniel Enny, Kyle Schipper, and Mari Flanigan for all their hard work. I hope I was a good mentor to all of you and may you find success in your future endeavors.

I will also like to acknowledge Lehigh Chemistry Department for all their support. I sincerely want to thank Dr. Rebecca Miller. You were the very first person I met when I came to Lehigh and you made me feel at home. Thank you for showing me kindness and a genuine interest in my progress as a graduate student. I also want to thank Marge, Jane, JoAnn, Jennifer, and Sharon for all their hard work and for making sure the department run smoothly as a well-oiled machine.

I am immensely grateful to my family, church members, and friends for all their support and prayers. To my parents, I want to say thank you for raising and instilling in me discipline, hard work, and respect for all. We did not have much growing up but you taught us that if we worked hard, we will succeed in life. I cannot thank you enough for all your prayers and encouragement. I hope to continually make you proud. To my sisters, Cynthia and Antoinette, words cannot express my gratitude for all your support and guidance. Having you around is a blessing and a privilege. You guys keep me

grounded and I am forever indebted to you both. We are forever untied by blood and may we continue in love for one another.

Finally, thanks be to God, my Creator and Father in Heaven, His son and my savior Jesus the Christ, and the comforter, Holy Spirit. All I am, and all I can ever be, comes from, and is, in Him.

TABLE OF CONTENTS

LIST OF FIGURES

LIST OF TABLES

LIST OF SCHEMES

LIST OF ABBREVIATIONS

Tetrahydrofuran	THF
Acetonitrile	MeCN
Dimethoxyethane	DME
Hexanes	Hex
Ethyl acetate	EtOAc
Dimethylformamide	DMF
Cyclic Voltammetry	CV

ABSTRACT

Titanocene(III) complexes are important single-electron reductants that have been used extensively for a variety of stoichiometric as well as catalytic reactions. Owing to their intrinsic ability to alternate between the +3 and +4 oxidation states, titanocene(III) complexes are attractive reagents for designing efficient atom-economical processes.

In this dissertation, a detailed mechanistic study of an atom-economical radical arylation of amino-epoxides, catalyzed by titanocene(III) chloride, to form indoline derivatives is presented. Information gleaned from our mechanistic studies, which include the role of salt additives and the turnover-limiting step, was used to further fine-tune and enhance this radical arylation process to incorporate a wider range of amino-epoxides including electron deficient epoxides, which were recalcitrant to the arylation process.

Also, an in-depth understanding of the impact of solvent and of ligands attached to titanocene(III) obtained from our mechanistic studies has led to the discovery of cationic titanocene(III) complexes as viable, stable catalysts, for performing the radical arylation of amino-epoxides to form indoline products. Finally, the development and mechanistic study of a procedurally straightforward, inexpensive, and mild approach for the reduction of aldehydes, ketones, and esters to their respective alcohols via a titanocene(III) borohydride-PMHS system is presented.

Chapter 1. Introduction

1.1 Titanium

Titanium is the ninth most abundant element in the earth's crust and was first discovered in 1791 by William Gregor and later named in 1795 by Martin Heinrich Klaproth.[1,2] This dark gray lustrous metal is mostly found in igneous rocks and in minerals such as rutile (TiO_2), ilmenite ($FeTiO_3$), perovskite, anatase, brookite, benitoite ($BaTiSi_3O_9$), and sphene or titanite ($CaTiSiO_5$).[1,2] It is commercially extracted *via* the Kroll process, which is a method whereby titanium tetrachloride is reduced with magnesium.[1] Titanium metal is ductile and is generally alloyed with other metals to make strong and lightweight materials for many applications including parts of aircrafts and missiles.[1,2] Titanium is also inert and resistant to corrosion. As a result, it is used for propeller shafts, rigging, and other parts of ships exposed to salt water.[1] Complexes developed with titanium are generally inexpensive, non-toxic, environmentally friendly, and have numerous applications in industry.[3] In addition to the inexhaustible applications of titanium metal in industry, inorganic and organic titanium compounds have been used extensively by researchers to carry out interesting transformations to form compounds of biological and synthetic relevance.[4]

1.2 Application of titanium complexes in organic synthesis

1.2.1 Inorganic titanium complexes

Titanium oxides and titanium halides are classic examples of inorganic titanium complexes. Titanium dioxide is found in gemstones such as rutile, brookite, and anatase. Titanium dioxide is used in paints, in inks, and in plastics. It is also used as a ceramic colorant, as a source of titanium metal, and for welding-rod coatings.[2] Titanium

tetrachloride is the most commonly used titanium halide salt. It is a colorless liquid with a penetrating acid odor and reacts with air and moisture to produce dense white fumes. Due to this phenomenon, it is used to produce smoke screens and is also used to iridize glass.[1] Titanium tetrachloride is a Lewis acid and has been used to facilitate asymmetric carbonyl reductions with concomitant C-C bond forming reactions, and cyclization processes as shown in scheme 1.1.[3,5–7] It has also been used as a precursor in the synthesis of organometallic compounds such as titanocene complexes (Scheme 1.2).[8]

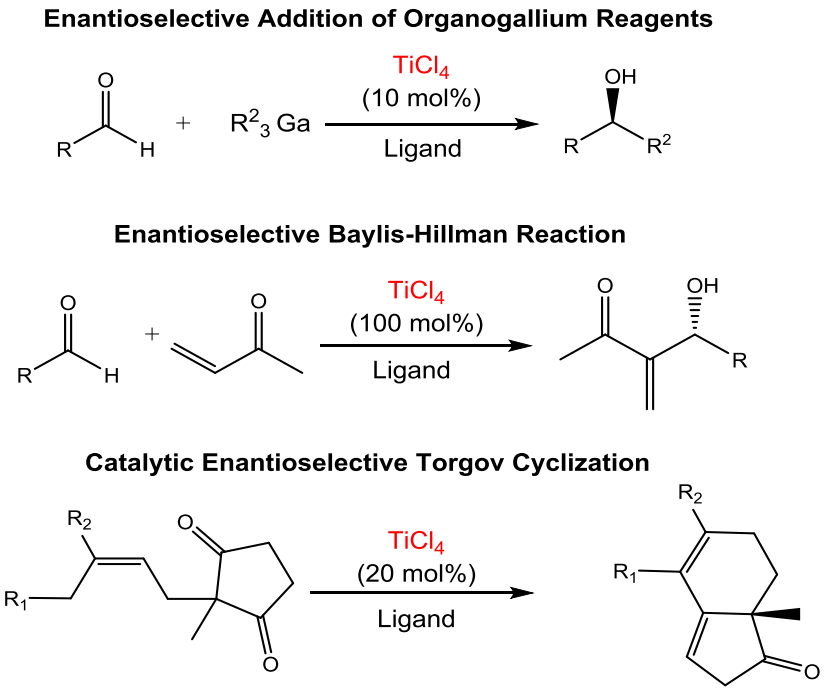

Scheme 1.1. Titanium tetrachloride as a Lewis acid[3]

Titanium trichloride, a single electron reductant, is another example of an inorganic titanium halide, which has been employed for multiple reductions,[9] including the reduction of carbonyls to their respective alcohols (Scheme 1.3).[10] Fürstner and coworkers have reported the formation of indoles *via* carbonyl couplings catalyzed by

$TiCl_3$ (Scheme 1.3).[11–13] Like $TiCl_4$, titanocene trichloride has also been used as a precursor in the synthesis of titanocene complexes (Scheme 1.3).[8]

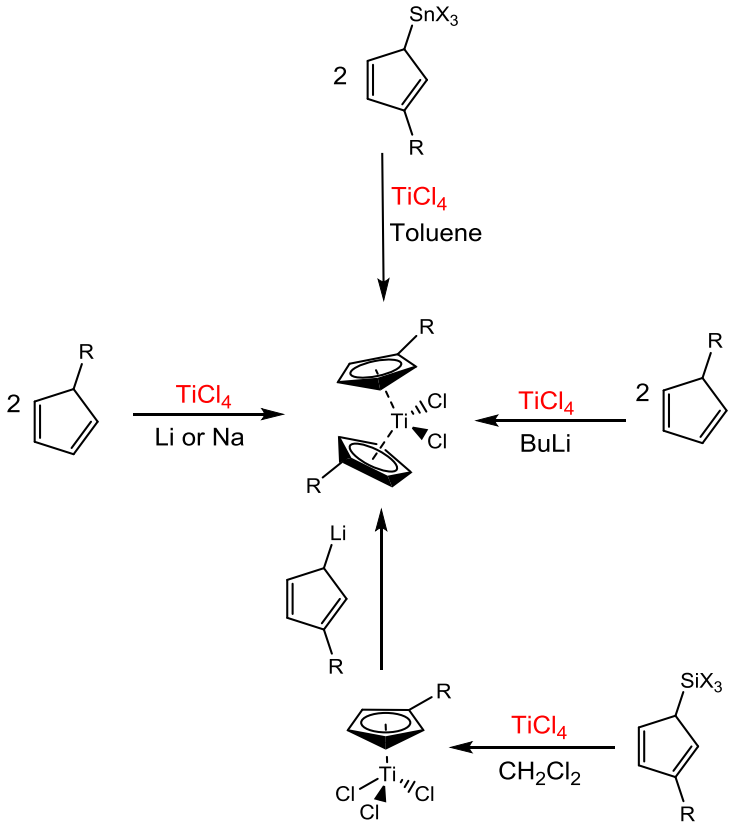

Scheme 1.2. $TiCl_4$ as precursor in the synthesis of titanocene complexes[8]

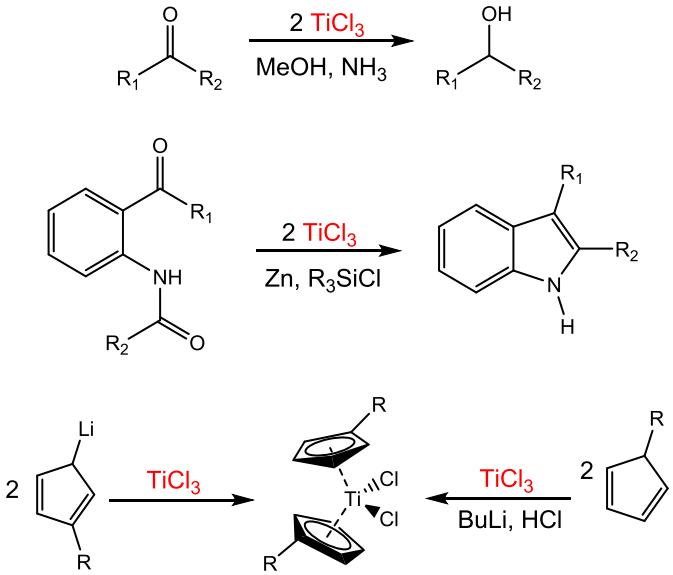

Scheme 1.3. Applications of $TiCl_3$

1.2.2 Organic titanium complexes

Titanium alkoxides are the most ubiquitous organotitanium compounds used by chemists to facilitate multiple transformations.[3] A popular chemical reaction that employs a titanium alkoxide is the Sharpless epoxidation, which is an enantioselective epoxidation of allylic alcohols with an alkyl hydroperoxide catalyzed by a titanium(IV) alkoxide in concert with a chiral tartrate ester (Scheme 1.4).[3,14,15] Titanium(IV) isopropoxide has also been used with a hydride source to reduce carbonyls to their respective alcohols[3,16] and to carry out enantioselective additions to carbonyls (Scheme 1.5).[3] Titanocene(III) chloride is another example of an organic titanium complex that has been employed by organic chemists and will be discussed in the next section.

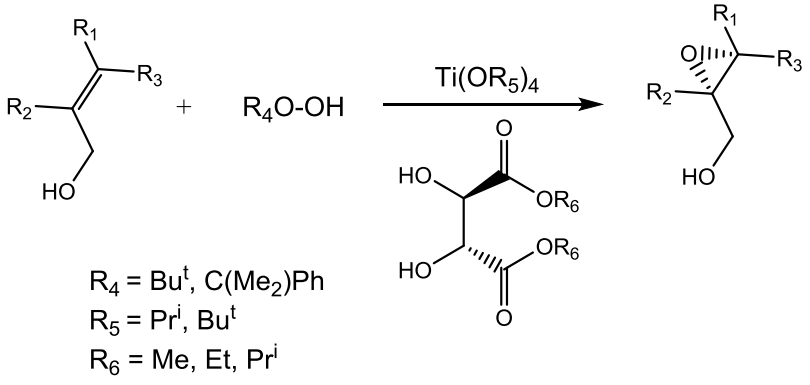

Scheme 1.4. Sharpless Epoxidation[3]

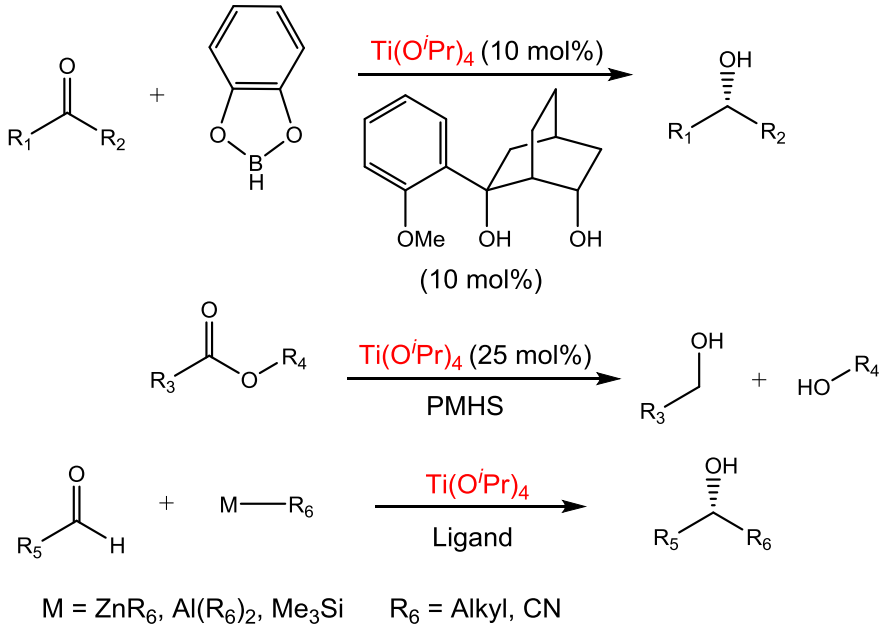

Scheme 1.5. Application of $Ti(O^iPr)_4$

1.3 Introduction to titanocene(III) chloride (Cp_2TiCl)

Cp_2TiCl is prepared either by a reaction between $TiCl_3$ and thallium cyclopentadienide[17] or by stirring commercially available titanocene dichloride (Cp_2TiCl_2) with Mn or Zn dust in tetrahydrofuran (THF). The latter is normally considered as the convenient method.[18] Cp_2TiCl is sensitive to air and moisture and as a result, reactions are performed under inert atmosphere. In the late 1980's and early 1990's, Rajanbabu and Nugent reported a series of works that highlighted the potential of titanocene(III) chloride, also known as Bis(cyclopentadienyl)titanium(III) chloride (Cp_2TiCl), in organic syntheses.[17,19] Since then, researchers have considered the application of Cp_2TiCl, which has been dubbed the Nugent reagent, with great interest.[18,20–22] Titanocene(III) chloride (Cp_2TiCl) has been shown to innately undergo reversible single electron transfer reactions between the Ti(III)/Ti(IV) redox couple,[23]

which makes it an attractive reagent for single-electron transfer (SET) processes, some of which are discussed in the next section.

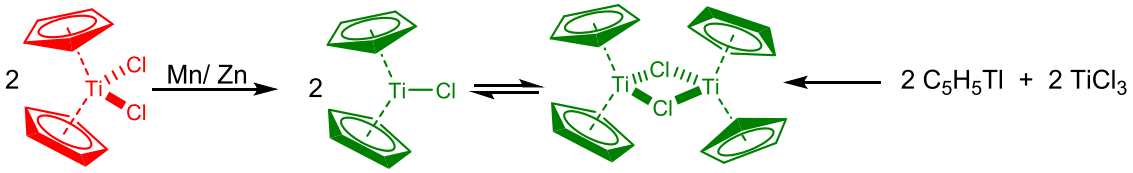

Scheme 1.6. General methods for making Cp_2TiCl

1.3.1 Application of titanocene(III) chloride in organic synthesis

1.3.1.1 Radical epoxide openings

Nugent and Rajanbabu, in their seminal work, showed that Cp_2TiCl readily opens epoxides to form β-titanoxy radicals that partake in multiple single electron transformations such as the reduction of epoxides to form alcohols and *5-exo* cyclizations with concomitant alcohol formation (Scheme 1.7).[17,19,24] Gansäuer and coworkers further developed protocols whereby catalytic amounts of Cp_2TiCl were used to carry out the same transformations in the presence of a suitable radical trap and hydrochloride salt (Scheme 1.8).[25–29] Gansäuer and coworkers have also reported *3-exo* and *4-exo* cyclizations catalyzed by Cp_2TiCl (Scheme 1.9).[30,31] Furthermore, Cuerva and coworkers showed that Cp_2TiCl also facilitates *6-endo* and *7-endo* cyclizations *via* epoxide openings to form β-titanoxy radical intermediates (Scheme 1.9).[32–37] These processes serve as key intermediates in the total syntheses of many biological compounds[22] such as antitumoral alkaloids,[38] lignans,[39] terpenes,[40] and antibiotics.[41]

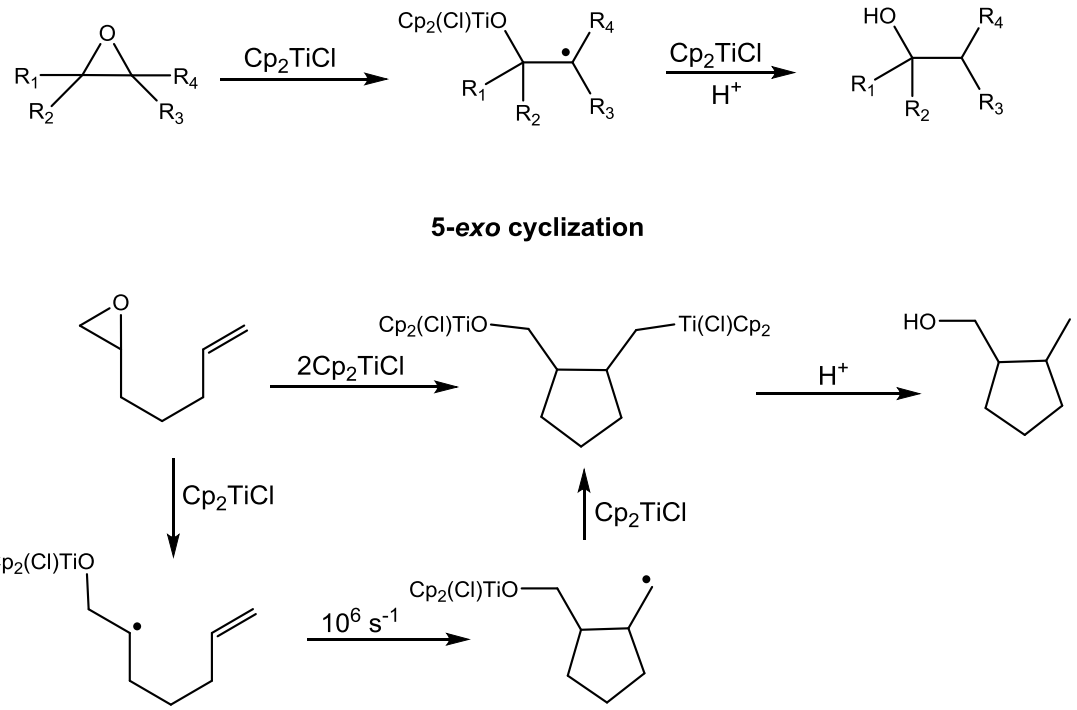

Scheme 1.7. Radical epoxide ring opening with Cp_2TiCl

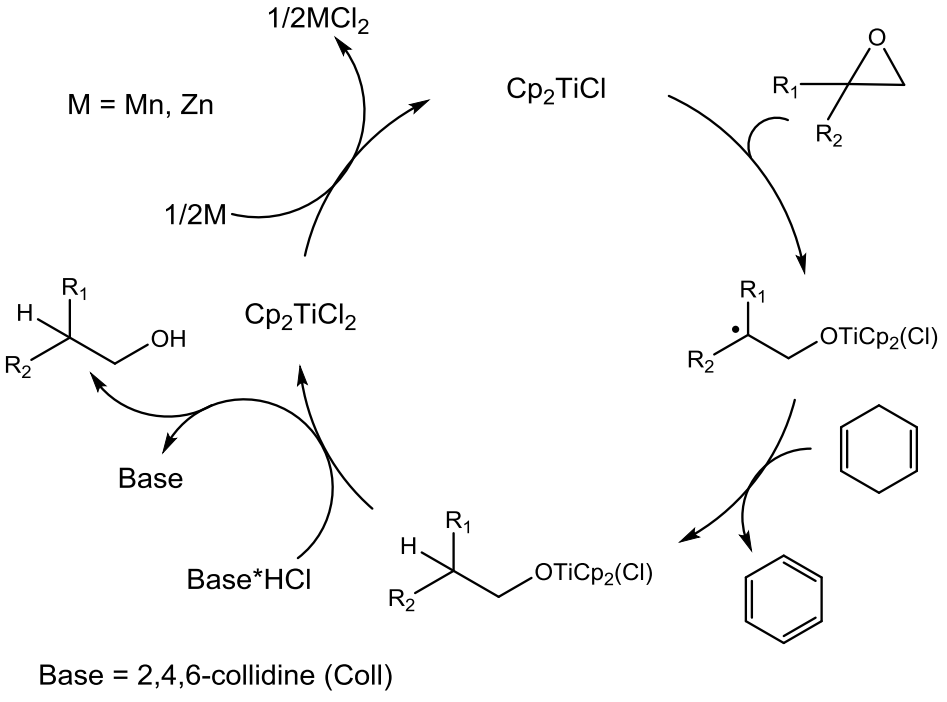

Scheme 1.8. Epoxide opening with catalytic Cp_2TiCl[20]

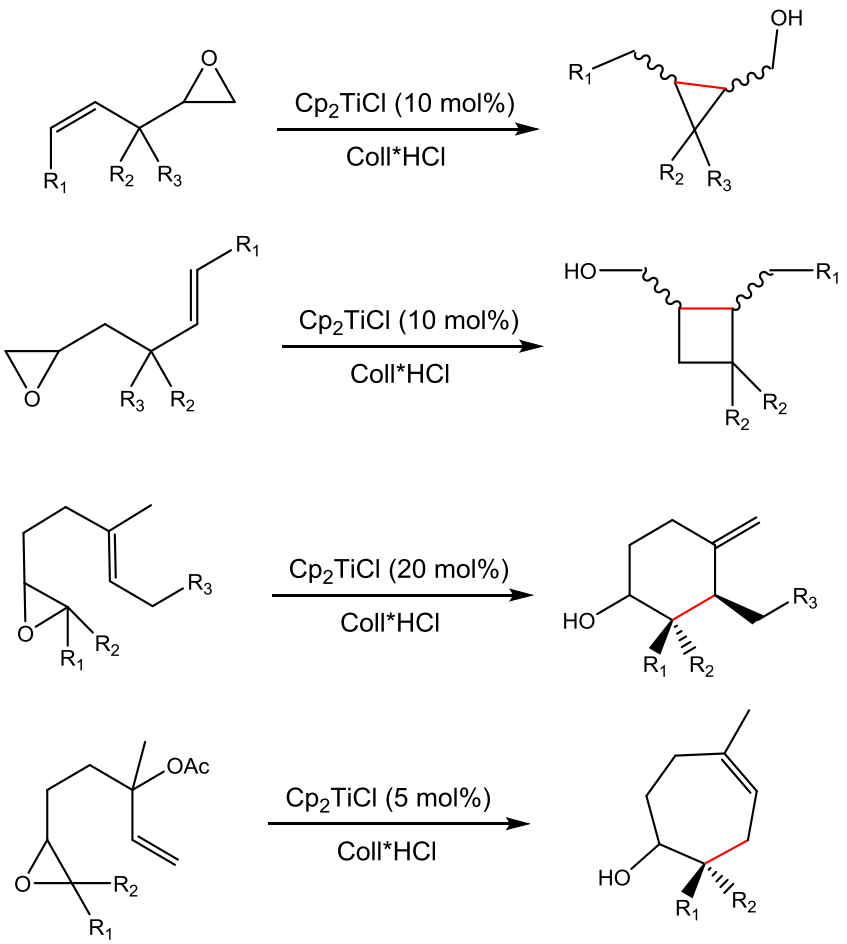

Scheme 1.9. *3-exo, 4-exo, 6-endo,* and *7-endo* cyclizations catalyzed by Cp_2TiCl

1.3.1.2 Oxetane reductions

Gansäuer and coworkers performed computational and synthetic experiments to investigate oxetane ring openings catalyzed by Cp_2TiCl. They discovered that the activation energies for opening oxetane were higher than that for opening epoxides (17 to 19 $kcalmol^{-1}$ for oxetanes and 9 $kcalmol^{-1}$ for epoxides).[42] Thus, making the reduction of oxetanes much slower than epoxides. Also, the resulting γ-titanoxy radical from opening oxetanes was found to act more as a free radical because it was less sterically hindered than the β-titanoxy radical formed from the reduction of epoxides.

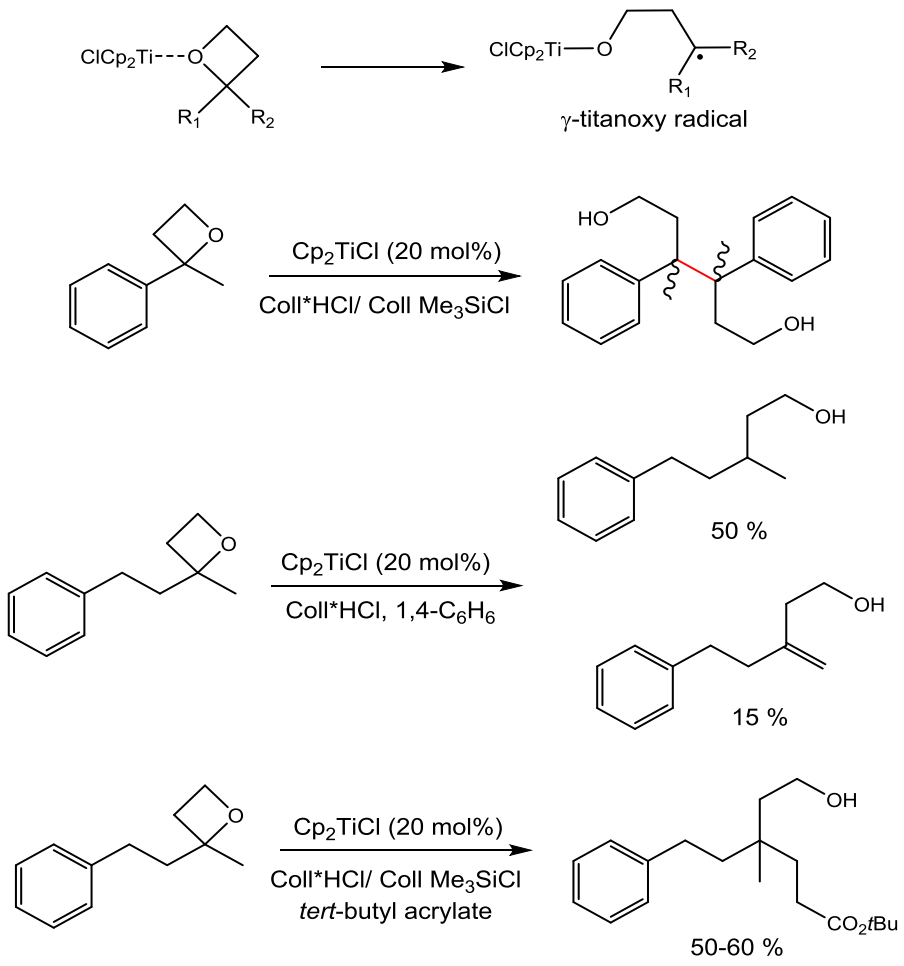

Scheme 1.10. Cp_2TiCl mediated oxetane ring opening

In a series of experiments performed under different conditions as shown in scheme 1.10, the titanocene(III) chloride catalyzed reduction of oxetanes resulted in dimerization reactions, simple reductions, and additions to acrylates. It is important to note that the titanocene catalyzed reduction of oxetanes to facilitate C-C bonds is not efficient. Nevertheless, Cp_2TiCl has been demonstrated to open oxetanes.[42]

1.3.1.3 Reductive coupling of allylic halides

Barrero and coworkers reported a Wurtz-type homocoupling of terpenic allylic halides catalyzed by Cp_2TiCl. Interestingly, they found that direct dimerization *via* the

coupling of two allyl radical species, formed by Cp_2TiCl initially abstracting a halide, was not a mechanistic pathway toward product formation. Instead, the dimerized product was facilitated *via* an allyl titanium intermediate, which is formed when the allyl radical species is abstracted by another Cp_2TiCl (Scheme 1.11).[43] The process was employed in the asymmetric synthesis of β-Onocerin, which is a natural product extracted from leguminous plants (Scheme 1.12).[43]

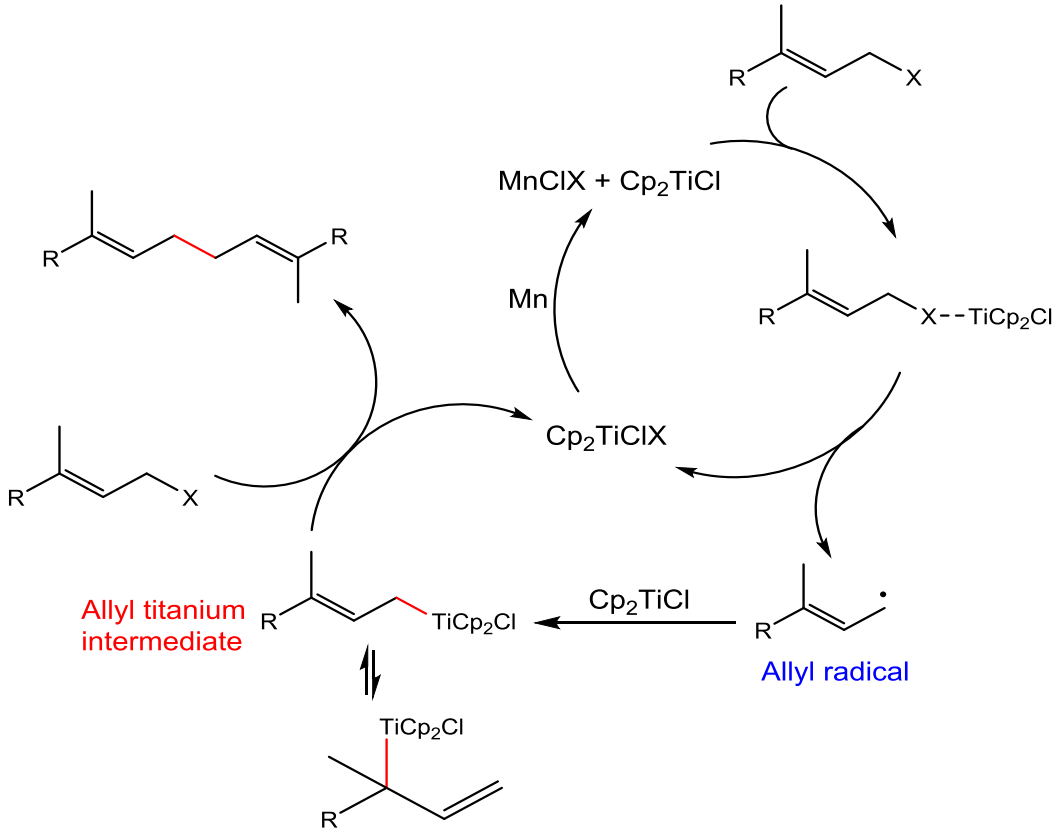

Scheme 1.11. Proposed catalytic cycle for homocoupling of allylic halides by Cp_2TiCl

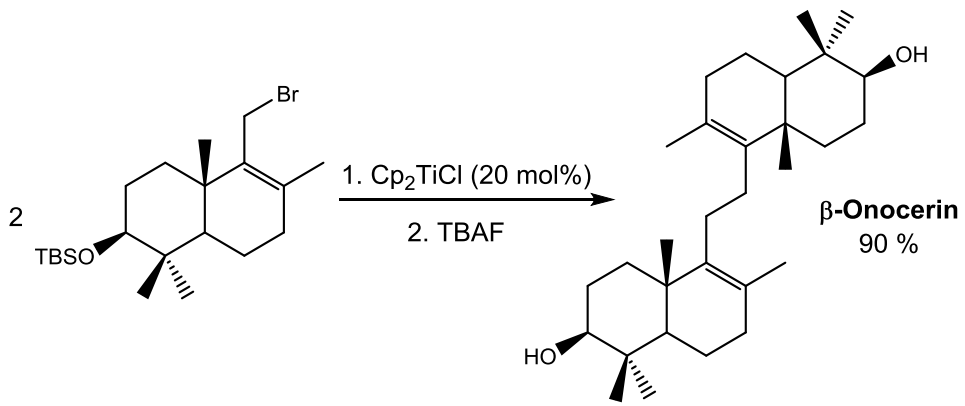

Scheme 1.12. Asymmetric synthesis of β-Onocerin

1.3.1.4 Reformatsky additions

Reformatsky additions are well established in literature as a method to synthesize β-hydroxy esters *via* a zinc catalyzed reaction of aldehydes or ketones with α-halo esters.[44] Little and coworkers reported a novel method for performing Reformatsky reactions under mild and environmentally friendly conditions with inexpensive Cp_2TiCl (Scheme 1.13).[45] In their proposed reaction mechanism, the halide on the α-halo ester is abstracted by Cp_2TiCl resulting in the formation of a radical intermediate, which reacts with another Cp_2TiCl to form the enolate. The resulting enolate reacts with the aldehyde to form the desired product (Scheme 1.14).[45]

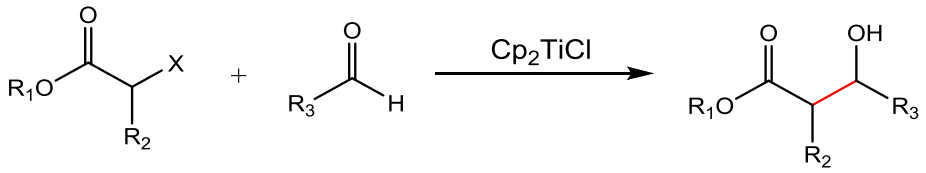

Scheme 1.13. Cp_2TiCl catalyzed Reformatsky addition reaction

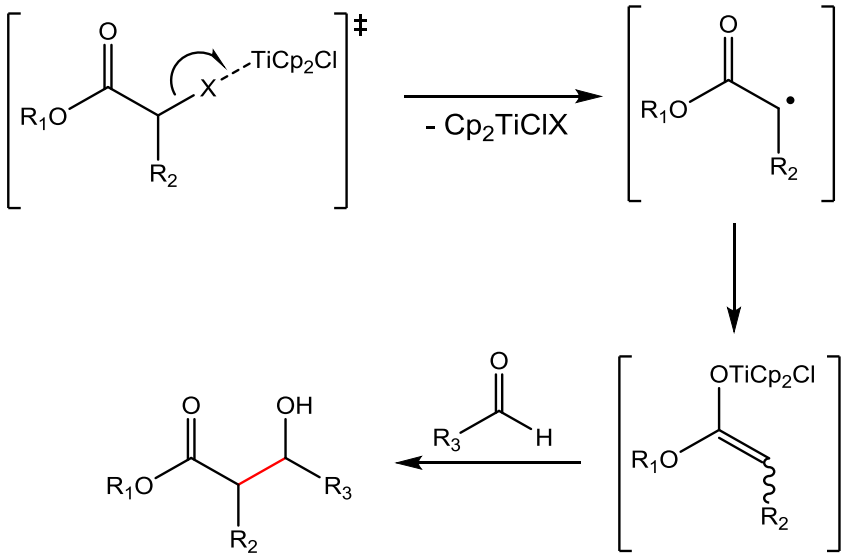

Scheme 1.14. Proposed reaction mechanism for Cp_2TiCl Reformatsky addition reaction

1.3.1.5 Pinacol and McMurry-type couplings

Gansäuer and coworkers reported a method for performing pinacol couplings with Cp_2TiCl. The advantage of using Cp_2TiCl was its ability facilitate the formation of highly diastereoselective pinacol products (Scheme 1.15).[46] Also, with the addition of a suitable proton source (Coll*HCl), only catalytic amounts of Cp_2TiCl were required for the reaction to proceed (Scheme 1.16).[46] Twelve years later, Barrero and coworkers showed that by replacing Coll*HCl with Me_3SiCl, a McMurry type carbonyl coupling product was formed (Scheme 1.17).[47] It was therefore proposed that Me_3SiCl did not facilitate the heterolytic cleavage of the Ti(IV)-O bond of the pinacol product and as a result, the Ti(IV) was reduced to Ti(III) to form a Ti(III)-O bond as shown in scheme 1.18. The titanocene(III) bound to the alkoxide facilitated the homolytic cleavage of the C-O bond to form $Cp_2Ti(IV)=O$ and the olefinic product.[47]

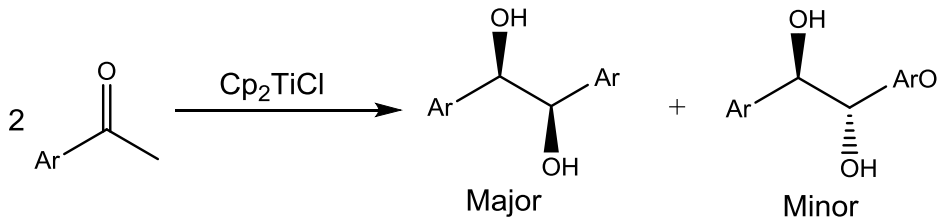

Scheme 1.15. Pinacol coupling by Cp_2TiCl

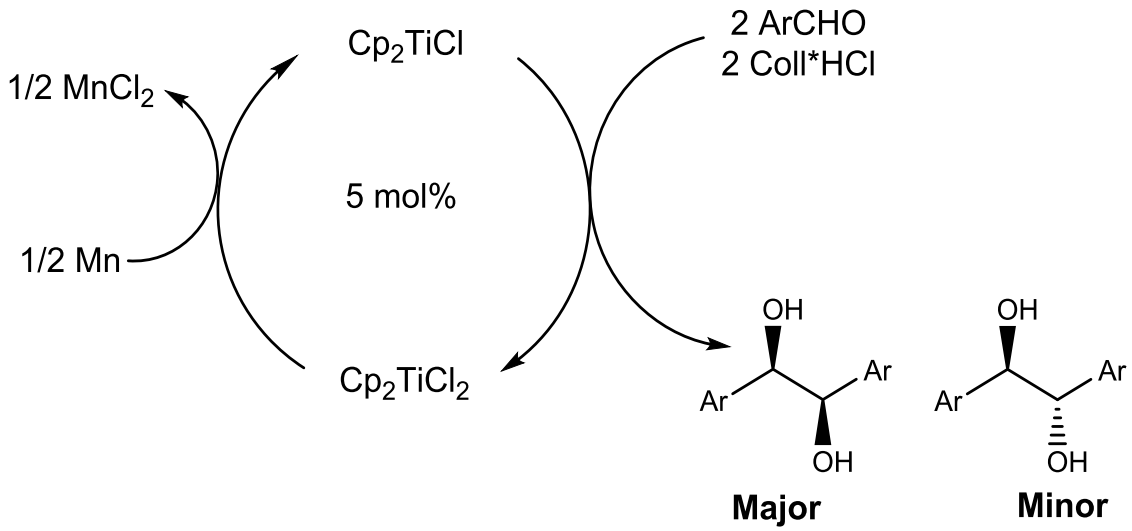

Scheme 1.16. Pinacol coupling catalyzed by Cp_2TiCl

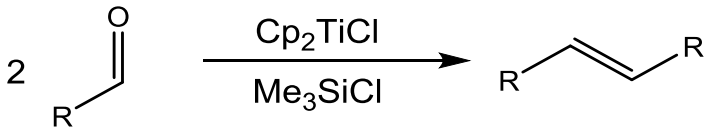

Scheme 1.17. McMurry-type couplings with Cp_2TiCl[47]

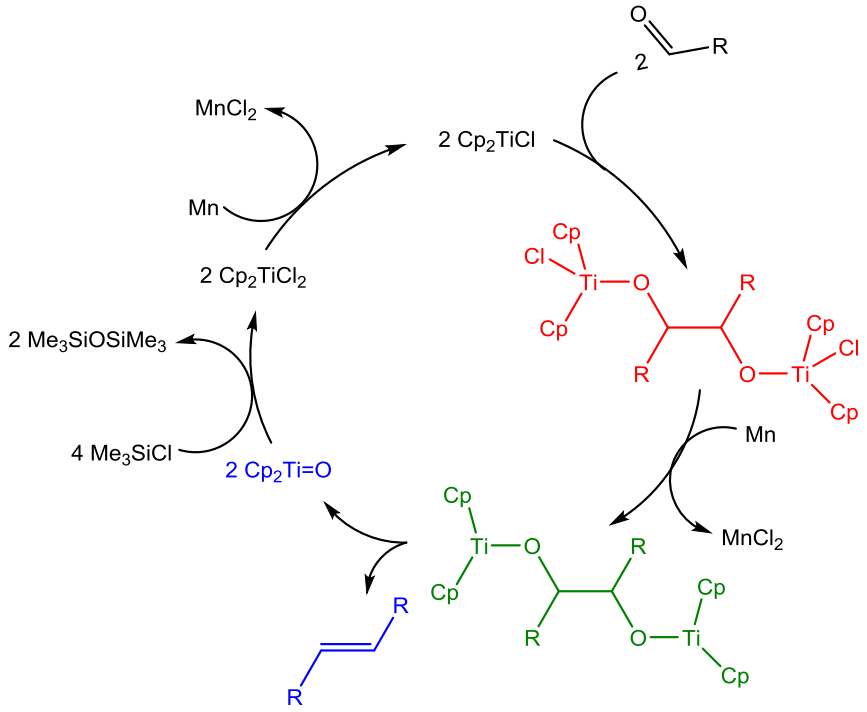

Scheme 1.18. McMurry-type couplings catalyzed by Cp_2TiCl[47]

1.3.1.6 Umpolung reactions

Cp_2TiCl has been shown to facilitate multiple umpolung-type reactions. Oltra and coworkers reported in 2006 the coupling of aldehydes with α, β-unsaturated aldehydes to form γ-lactols mediated by titanocene(III) chloride in the presence of water (Scheme 1.19).[48] It was proposed that the actual species involved in this process was a titanocene(III) aqua complex as shown in scheme 1.20. This complex reacts with the conjugated alkenal to form a titanoxy allyl radical, which attacks the carbonyl carbon of the aldehyde to form the intermediate **1** (Scheme 1.20). The desired product is formed in subsequent steps.[48]

Streuff and coworkers have developed novel Cp_2TiCl-catalyzed umpolung-type reactions whereby enones were coupled to acrylonitriles (Scheme 1.21).[49] Similar to the work reported by Oltra, the underlying principle for this process is that the radical

intermediate formed when Cp_2TiCl reacts with the enone, readily adds to the alkene moiety in the least sterically hindered position of the acrylonitrile. The desired product is formed in subsequent steps as shown in scheme 1.21.[49] Streuff and coworkers in 2015 also showed that α-hydroxy and α-amino ketones could be formed via a Cp_2TiCl catalyzed umpolung-type coupling of ketones or imines to nitriles (Scheme 1.22).[50–52]

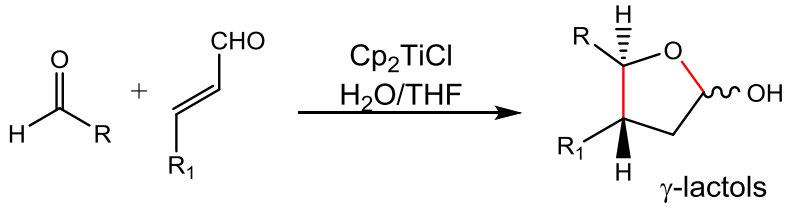

Scheme 1.19. Cp_2TiCl mediated formation of γ-lactols

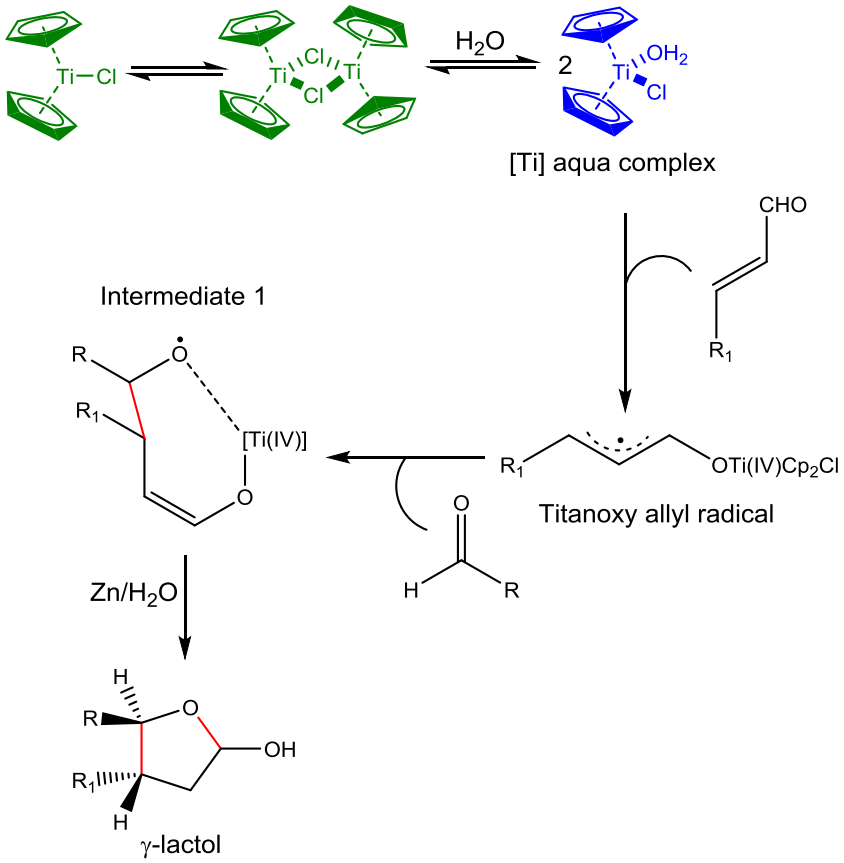

Scheme 1.20. Reaction mechanism Cp_2TiCl mediated formation of γ-lactols

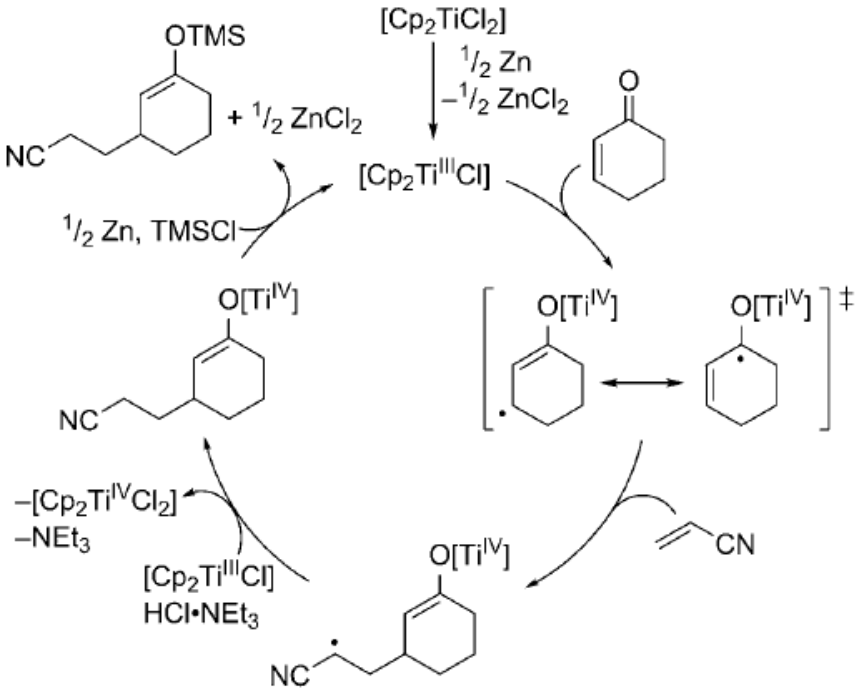

Scheme 1.21. Cp_2TiCl-catalyzed umpolung-type coupling of enones to acrylonitriles[49]

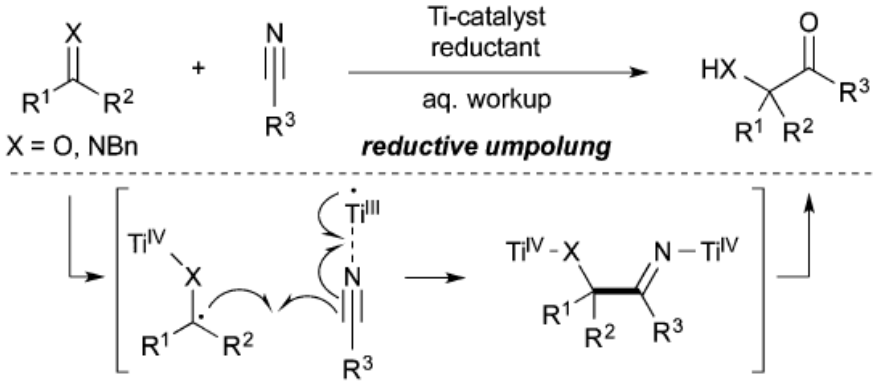

Scheme 1.22. Cp_2TiCl catalyzed umpolung-type coupling of ketones or imines to nitriles[51]

1.3.1.7 Barbier-type reactions

Titanocene(III) chloride has been shown to catalyze Barbier-type coupling reactions between organohalides and either ketones or aldehydes under mild and environmentally friendly conditions.[18] Barbier reaction protocols are advantageous because they facilitate one step C-C bond forming processes without the need of

synthesizing an organometallic reagent as is the case for Grignard processes. Barbier-type allylations, benzylations, and propargylations of aldehydes and ketones, catalyzed by Cp_2TiCl, were initially reported by Oltra, Cuerva and coworkers (Scheme 1.23).[53]

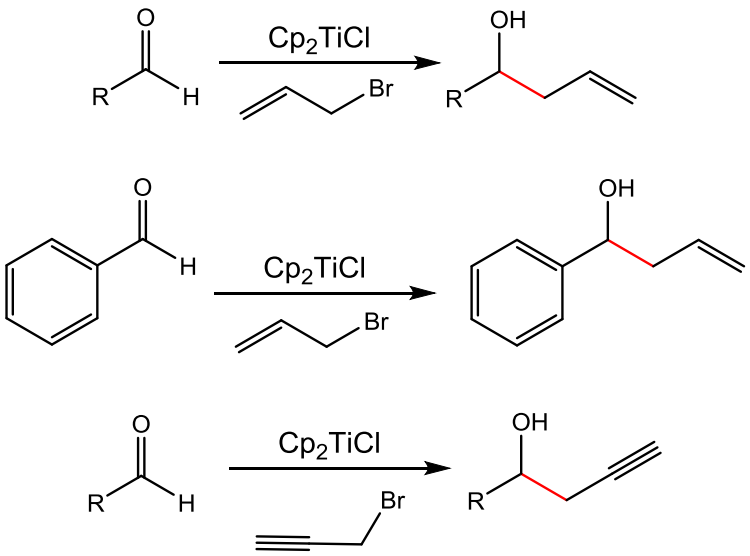

Scheme 1.23. Barbier-type allylations, benzylations, and propargylations catalyzed by Cp_2TiCl[53]

Since their initial report, many developments have been made on Barbier-type reactions mediated by Cp_2TiCl. For example, in the propargylation of ketones, it was later discovered that when unsubstituted propargyl halides were used, only homopropargylic alcohols were formed with no evidence of either allenic derivatives or pinacol products. This observation was attributed to the proposed preferential formation of an allenyl titanocene(IV) intermediate over a titanoxy radical intermediate, which is normally formed in the presence of a carbonyl compound. This allenyl titanocene(IV) species readily adds to the ketone or aldehyde resulting in the formation of the homopropargyl alcohol (Scheme 1.24).[54]

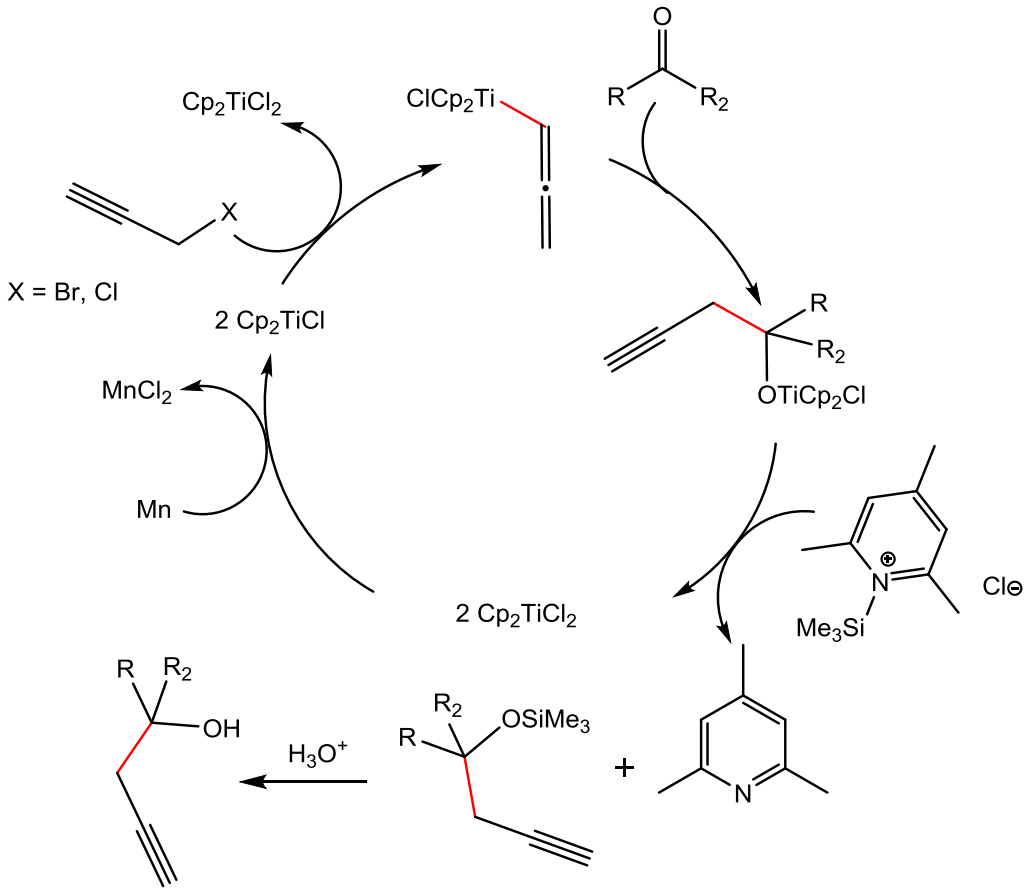

Scheme 1.24. Proposed cycle for Ti-catalyzed propargylation reactions[54]

However, with substituted propargyl halides, allenic products were mainly formed with aldehydes while homopropargylic alcohols were mainly observed with ketones (Scheme 1.25).[20,55] Oltra and coworkers proposed that with substituted propargyl halides, an equilibrium between a propargyl titanium and an allenyl titanium species was formed. The aldehyde preferentially attacked the propargyl titanium intermediate while the ketone preferentially attacked the allenyl titanium intermediate. Thus, resulting in the product selectivity as shown in scheme 1.25.[55]

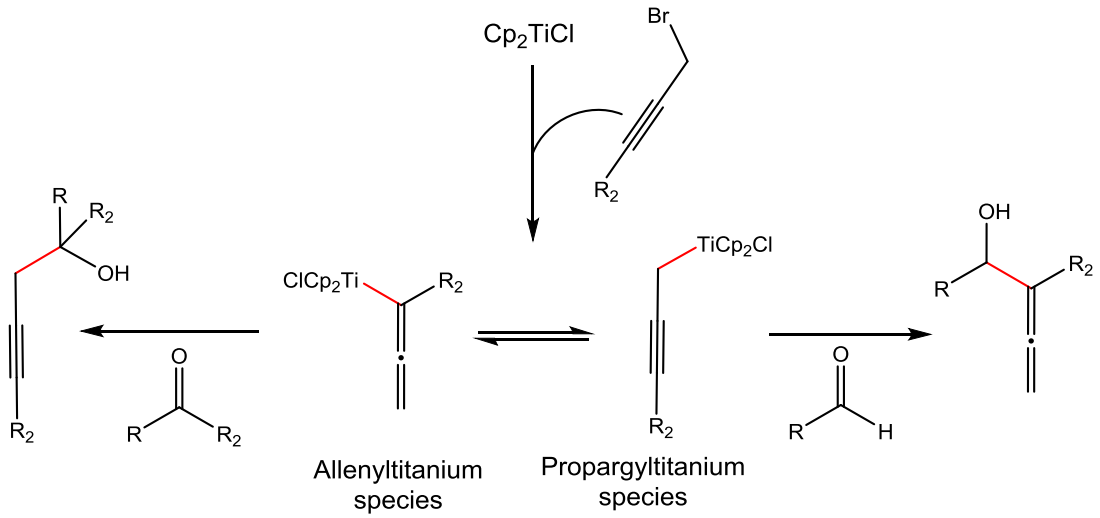

Scheme 1.25. Product selectivity for Ti-catalyzed propargylation reactions[55]

1.3.1.8 Additions catalyzed by Cp_2TiCl with other transition metal catalysts

Cuerva and coworkers have recently developed new methods for the allylation and propargylation of carbonyl compounds catalyzed by Cp_2TiCl in concert with palladium or nickel catalysts (Scheme 1.26).[56–58] One interesting feature for the Cp_2TiCl mediated carboxylate allylations was the product selectivity observed with either nickel or palladium as a catalyst. With a palladium catalyst, an allylic titanium(IV) intermediate is formed, which readily reacts with a carbonyl compound to form the corresponding allylation product. With a nickel catalyst however, a cyclization pathway is realized, which ultimately results in the formation carbocycles (Scheme 1.27).[59]

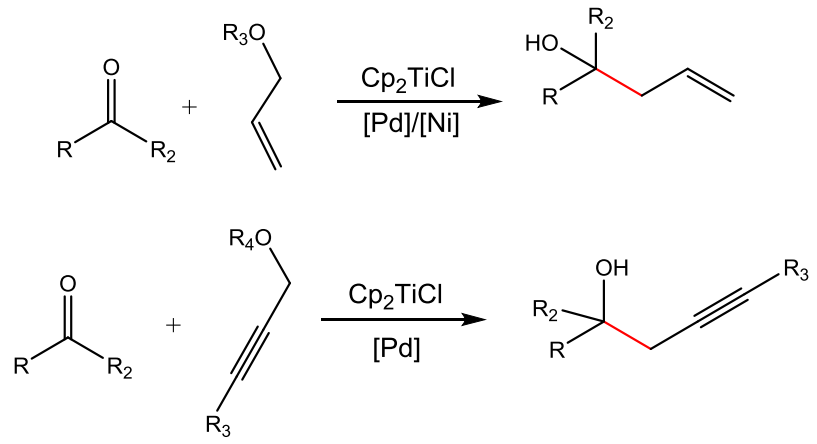

Scheme 1.26. Allylation and propargylation of carbonyl compounds by Cp_2TiCl with [Pd]/[Ni]

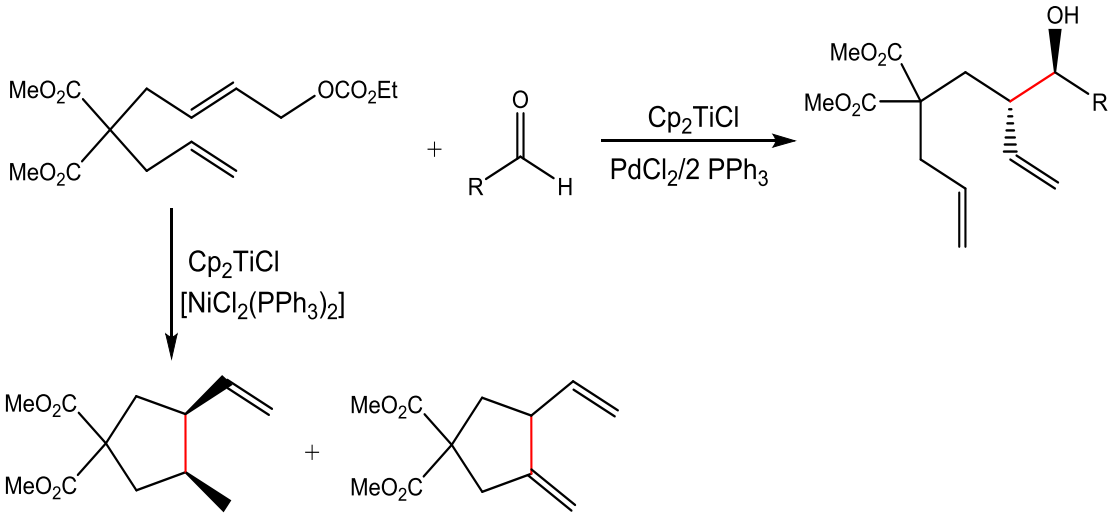

Scheme 1.27. Product selectivity observed with Cp_2TiCl mediated allylations with [Pd]/[Ni]

Cuerva and coworkers also studied other C-C bond forming reactions catalyzed by the combination of Cp_2TiCl and $NiCl_2$. From their studies, they discovered a Heck and reductive-type cyclization of alkyl iodides. The addition of water to this system was crucial for product selectivity as shown in scheme 1.28.[60] Cp_2TiCl has also been used in conjunction with $NiCl_2$ catalyst to facilitate direct intra and intermolecular conjugate addition of aryl and alkenyl halides to acrylates. Like Barbier type processes mediated by

Cp_2TiCl, this system bypasses the need for the formation an organometallic nucleophile (Scheme 1.29).[61]

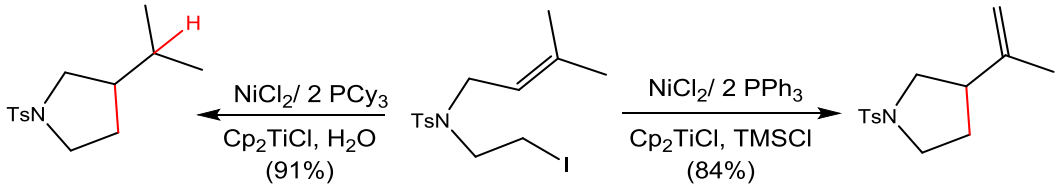

Scheme 1.28. Reductive-and Heck-type cyclization catalyzed Cp_2TiCl and $NiCl_2$[60]

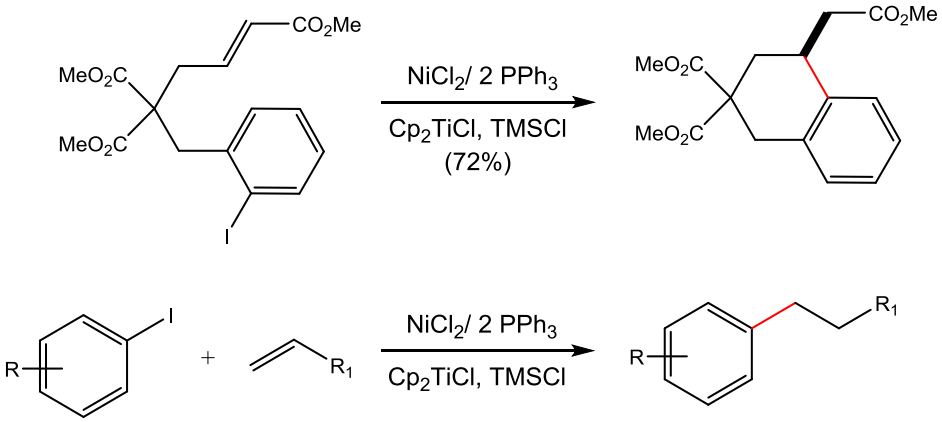

Scheme 1.29. Intra and intermolecular conjugate addition of aryl and alkenyl halides to acrylates[61]

1.4 Application of titanocene(III) complexes in sustainable chemistry

Sustainable chemistry, also known as green chemistry, is a branch of chemistry which primarily deals with the design and modification of established chemical processes to develop new protocols that are simple, environmentally safe, atom efficient, minimize the use of non-renewable raw materials, and minimize the generation of waste. For research chemists, the design of such systems depends heavily on the reagents vis-à-vis the catalysts and ligands employed to carry out such processes.

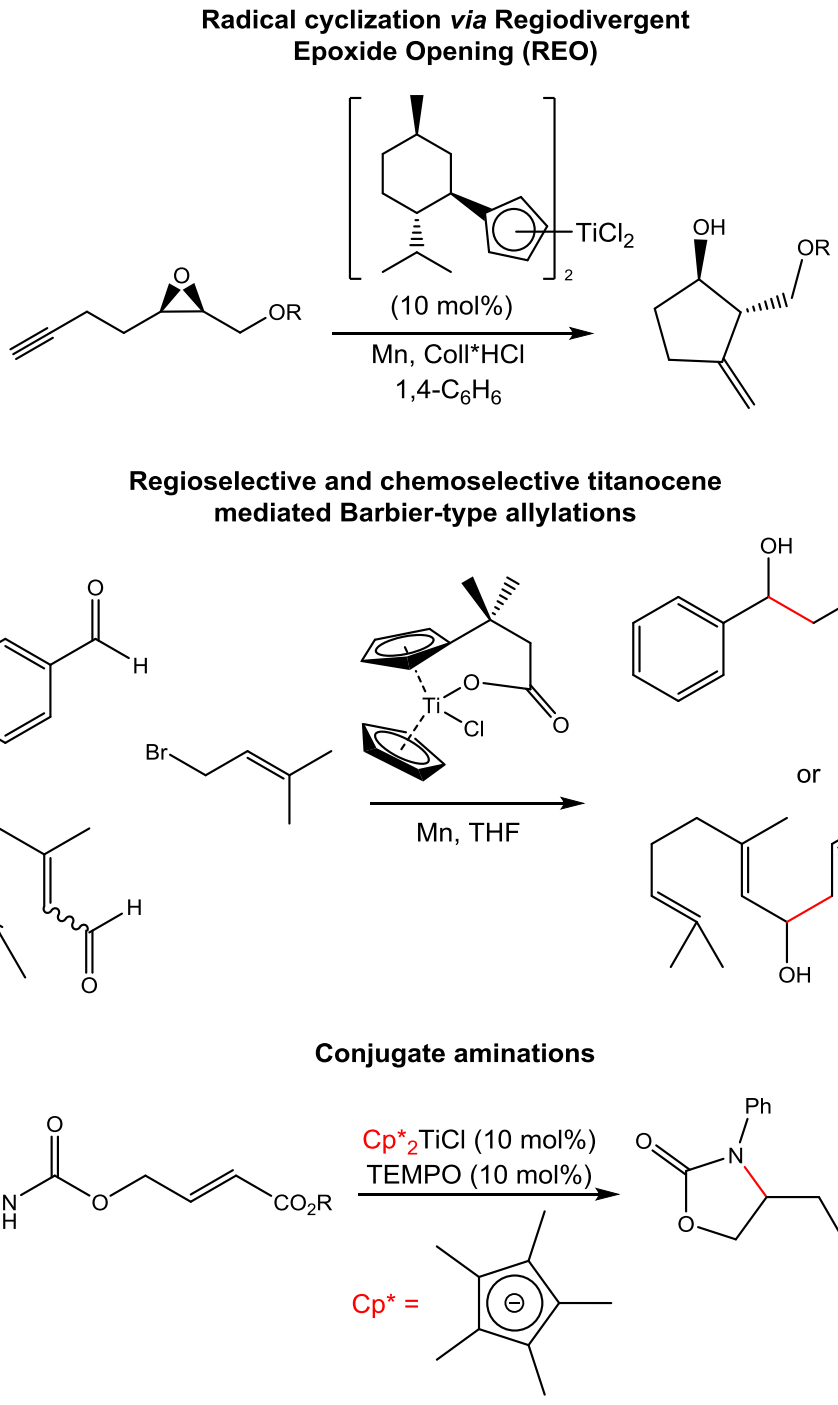

Scheme 1.30. Radical transformations catalyzed by titanocene(III) complexes.[62–64]

As shown in the previous sections of this chapter, titanium complexes most especially titanocene(III) chlorides are attractive in the design of sustainable chemical

processes because they are generated under mild conditions from readily available titanocene dichloride and can be manipulated to perform many chemical transformations. Another advantage of titanocene(III) chlorides is that they can be modified, to generate other titanocene(III) complexes that have improved reactivity and selectivity to catalyze transformations that were not possible with Cp_2TiCl alone (Scheme 1.30).[62–64]

1.5 Project goals

In this dissertation, the primary goal of developing titanocene(III) complexes that are capable of mediating sustainable chemical processes efficiently is discoursed. An atom-economical radical arylation of amino epoxides catalyzed by Ti(III) complexes to form indoline derivatives is studied in ensuing chapters of this dissertation.[65] The mechanistic studies performed to understand and propose a reasonable catalytic cycle for this process is ultimately presented.[23,66,67] Based on the proposed cycle, more efficient titanocene(III) complexes for the radical arylation of amino epoxides to form indoline derivatives were developed.[68] Finally, studies done to develop a procedurally simple, environmentally benign, and catalytic route for the reduction of carbonyl compounds to alcohols with titanocene(III) borohydride in concert with a suitable hydride source is presented.[69]

1.6 References

(1) Lide, D. R. *CRC Handbook of Chemistry and Physics*, 88th ed.; CRC Press: Boca Raton, FL, 2008.
(2) O'Neil, M. J. *The Merck index: an encyclopedia of chemicals, drugs, and biologicals*, 14th ed.; Merck & Co.,Inc.: Whitehouse Station, 2006.
(3) Ramon, D. J.; Yus, M. *Chem. Rev.* **2006**, *106* (6), 2126–2208.
(4) Gansäuer, A.; Rinker, B. *Titanium and Zirconium in Organic Synthesis*; Marek, I., Ed.; Wiley-VCH, 2000.
(5) Dai, Z.; Zhu, C.; Yang, M.; Zheng, Y.; Pan, Y. *Tetrahedron Asymmetry* **2005**, *16* (3), 605–608.
(6) Kataoka, T.; Iwama, T.; Tsujiyama, S.; Kanematsu, K.; Iwamura, T.; Watanabe, S. *Chemistry Letters*. 1999, pp 257–258.
(7) Braun, M.; Fleischer, R.; Mai, B.; Schneider, M. A.; Lachenicht, S. *Adv. Synth. Catal.* **2004**, *346* (4), 474–482.
(8) Qian, Y.; Huang, J.; Bala, M. D.; Lian, B.; Zhang, H.; Zhang, H. *Chem. Rev.* **2003**, *103*, 2633–2690.
(9) Rossi, B.; Prosperini, S.; Pastori, N.; Clerici, A.; Punta, C. *Molecules* **2012**, *17* (12), 14700–14732.
(10) Clerici, A.; Pastori, N.; Porta, O. *European J. Org. Chem.* **2001**, No. 12, 2235–2243.
(11) Fürstner, A.; Bogdanović, B. *Angew. Chemie Int. Ed. English* **1996**, *35* (21), 2442–2469.
(12) Fürstner, A.; Hupperts, A. *J. Am. Chem. Soc.* **1995**, *117* (16), 4468–4475.
(13) Fürstner, A.; Hupperts, A.; Ptock, A.; Janssen, E. *J. Org. Chem.* **1994**, *59* (18), 5215–5229.
(14) Gao, Y.; Klunder, J. M.; Hanson, R. M.; Masamune, H.; Ko, S. Y.; Sharpless, K. B. *J. Am. Chem. Soc.* **1987**, *109* (19), 5765–5780.
(15) Sharpless, K. B.; Katsuki, T. *J. Am. Chem. Soc.* **1980**, *102*, 5974–5976.
(16) Reding, M. T.; Buchwald, S. L. *J. Org. Chem.* **1995**, *60* (24), 7884–7890.
(17) RajanBabu, T.; Nugent, W. *J. Am. Chem. Soc.* **1994**, *116* (3), 986–997.
(18) Estevez, R. E.; Justicia, J.; Bazdi, B.; Fuentes, N.; Paradas, M.; Choquesillo-Lazarte, D.; Garcia-Ruiz, J. M.; Robles, R.; Gansäuer, A.; Cuerva, J. M.; Oltra, J. E. *Chem. - A Eur. J.* **2009**, *15* (12), 2774–2791.
(19) Nugent, W. a; Rajanbabu, T. V. *J. Am. Chem. Soc.* **1988**, *110* (9), 8561–8562.
(20) Rosales, A.; Rodríguez-García, I.; Muñoz-Bascõn, J.; Roldan-Molina, E.; Padial, N. M.; Morales, L. P.; García-Ocaña, M.; Oltra, J. E. *European J. Org. Chem.* **2015**, *2015* (21), 4567–4591.
(21) Gansäuer, A.; Lauterbach, T.; Narayan, S. *Angew. Chemie - Int. Ed.* **2003**, *42* (45), 5556–5573.
(22) Morcillo, S. P.; Miguel, D.; Campaña, A. G.; Álvarez de Cienfuegos, L.; Justicia, J.; Cuerva, J. M. *Org. Chem. Front.* **2014**, *1* (1), 15.
(23) Gansäuer, A.; Behlendorf, M.; Laufenberg, D. Von; Fleckhaus, A.; Kube, C.; Sadasivam, D. V; Flowers II, R. A. *Angew. Chem. Int. Ed.* **2012**, 4739–4742.
(24) Gansäuer, A.; Rinker, B. *Tetrahedron* **2002**, *58* (35), 7017–7026.

(25) Gansäuer, A.; Pierobon, M.; Bluhm, H. *Synthesis (Stuttg).* **2001**, *16*, 2500–2520.
(26) Gansäuer, A.; Pierobon, M.; Bluhm, H. *Angew. Chem. Int. Ed.* **1998**, *37*, 101–103.
(27) Gansauer, A.; Bluhm, H.; Pierobon, M. *J. Am. Chem. Soc.* **1998**, *120* (49), 12849–12859.
(28) Gansäuer, A.; Barchuk, A.; Keller, F.; Schmitt, M.; Grimme, S.; Gerenkamp, M.; Mück-Lichtenfeld, C.; Daasbjerg, K.; Svith, H. *J. Am. Chem. Soc.* **2007**, *129* (5), 1359–1371.
(29) Daasbjerg, K.; Svith, H.; Grimme, S.; Gerenkamp, M.; Mück-Lichtenfeld, C.; Gansäuer, A.; Barchuk, A.; Keller, F. *Angew. Chemie - Int. Ed.* **2006**, *45* (13), 2041–2044.
(30) Friedrich, J.; Dolg, M.; Gansäuer, A.; Geich-Gimbel, D.; Lauterbach, T. *J. Am. Chem. Soc.* **2005**, *127* (19), 7071–7077.
(31) Friedrich, J.; Walczak, K.; Dolg, M.; Piestert, F.; Lauterbach, T.; Worgull, D.; Gansäuer, A. *J. Am. Chem. Soc.* **2008**, *130* (5), 1788–1796.
(32) Justicia, J.; Rosales, A.; Bañuel, E.; Oller-López, J. L.; Valdivia, M.; Haïdour, A.; Oltra, J. E.; Barrero, A. F.; Cárdenas, D. J.; Cuerva, J. M. *Chem. - A Eur. J.* **2004**, *10* (7), 1778–1788.
(33) Justicia, J.; Álvarez de Cienfuegos, L.; Campaña, A. G.; Miguel, D.; Jakoby, V.; Gansäuer, A.; Cuerva, J. M. *Chem. Soc. Rev.* **2011**, *40* (7), 3525.
(34) Gansäuer, A.; Justicia, J.; Rosales, A.; Worgull, D.; Rinker, B.; Cuerva, J. M.; Oltra, J. E. *European J. Org. Chem.* **2006**, No. 18, 4115–4127.
(35) Morcillo, S. P.; Miguel, D.; Resa, S.; Martin-Lasanta, A.; Millan, A.; Choquesillo-Lazarte, D.; Garcia-Ruiz, J. M.; Mota, A. J.; Justicia, J.; Cuerva, J. M. *J. Am. Chem. Soc.* **2014**, *136* (19), 6943–6951.
(36) Cuerva, J.; Justicia, J.; Oller-López, J.; Oltra, J. *Radicals Synth. II* **2006**, No. December 2005, 63–91.
(37) Justicia, J.; Oller-López, J. L.; Campaña, A. G.; Oltra, J. E.; Cuerva, J. M.; Buñuel, E.; Cárdenas, D. J. *J. Am. Chem. Soc.* **2005**, *127* (42), 14911–14921.
(38) Hardouin, C.; Doris, E.; Rousseau, B.; Mioskowski, C. *J. Org. Chem.* **2002**, *67*, 6571–6574.
(39) Chakraborty, P.; Jana, S.; Saha, S.; Roy, S. C. *Tetrahedron Lett.* **2012**, *53* (48), 6584–6587.
(40) Doi, T.; Fuse, S.; Miyamoto, S.; Nakai, K.; Sasuga, D.; Takahashi, T. *Chem. - An Asian J.* **2006**, *1* (3), 370–383.
(41) Saha, S.; Roy, S. C. *Tetrahedron* **2010**, *66* (24), 4278–4283.
(42) Gansäuer, A.; Ndene, N.; Lauterbach, T.; Justicia, J.; Winkler, I.; Mück-Lichtenfeld, C.; Grimme, S. *Tetrahedron* **2008**, *64* (52), 11839–11845.
(43) Barrero, A. F.; Herrador, M. M.; Del Moral, J. F. Q.; Arteaga, P.; Arteaga, J. F.; Piedra, M.; Sánchez, E. M. *Org. Lett.* **2005**, *7* (12), 2301–2304.
(44) Shriner, R. L. *Org. React.* **1942**, *1*, 1–37.
(45) Parrish, J. D.; Shelton, D. R.; Little, R. D. *Org. Lett.* **2003**, *5* (20), 3615–3617.
(46) Gansäuer, A.; Bauer, D. *J. Org. Chem.* **1998**, *63* (7), 2070–2071.
(47) Dieguez, H.; López, A.; Domingo, V.; Arteaga, J. F.; Dobado, J. A.; Herrador, M. M.; Del Moral, J. F. Q.; Barrero, A. F. *J. Am. Chem. Soc.* **2010**, *132*, 254–259.

(48) Estévez, R. E.; Oller-Lopez, J. L.; Robles, R.; Melgarejo, C. R.; Gansäuer, A.; Cuerva, J. M.; Oltra, J. E. *Org. Lett.* **2006**, *8* (24), 5433–5436.
(49) Streuff, J. *Chem. - A Eur. J.* **2011**, *17* (20), 5507–5510.
(50) Frey, G.; Luu, H. T.; Bichovski, P.; Feurer, M.; Streuff, J. *Angew. Chemie - Int. Ed.* **2013**, *52* (28), 7131–7134.
(51) Feurer, M.; Frey, G.; Luu, H.-T.; Kratzert, D.; Streuff, J. *Chem. Commun.* **2014**, *50* (40), 5370–5372.
(52) Streuff, J.; Feurer, M.; Frey, G.; Steffani, A.; Kacprzak, S.; Weweler, J.; Leijendekker, L. H.; Kratzert, D.; Plattner, D. A. *J. Am. Chem. Soc.* **2015**, *137* (45), 14396–14405.
(53) Rosales, A.; Oller-lópez, J. L.; Gansäuer, A.; Oltra, J. E.; Cuerva, J. M. *Chem. Commun.* **2004**, 2628–2629.
(54) Justicia, J.; Sancho-Sanz, I.; Álvarez-Manzaneda, E.; Oltra, J. E.; Cuerva, J. M. *Adv. Synth. Catal.* **2009**, *351*, 2295–2300.
(55) Muñoz-Bascõn, J.; Sancho-Sanz, I.; Álvarez-Manzaneda, E.; Rosales, A.; Oltra, J. E. *Chem. - A Eur. J.* **2012**, *18*, 14479–14486.
(56) Millán, A.; Campaña, A. G.; Bazdi, B.; Miguel, D.; Álvarez De Cienfuegos, L.; Echavarren, A. M.; Cuerva, J. M. *Chem. - A Eur. J.* **2011**, *17* (14), 3985–3994.
(57) Millán, A.; De Cienfuegos, L. Á.; Martín-Lasanta, A.; Campaña, A. G.; Cuerva, J. M. *Adv. Synth. Catal.* **2011**, *353*, 73–78.
(58) Martínez-Peragón, Á.; Millán, A.; Campaña, A. G.; Rodríguez-Márquez, I.; Resa, S.; Miguel, D.; Álvarez De Cienfuegos, L.; Cuerva, J. M. *European J. Org. Chem.* **2012**, 1499–1503.
(59) Campaña, A. G.; Bazdi, B.; Fuentes, N.; Robles, R.; Cuerva, J. M.; Oltra, J. E.; Porcel, S.; Echavarren, A. M. *Angew. Chemie - Int. Ed.* **2008**, *47* (39), 7515–7519.
(60) Millán, A.; Álvarez De Cienfuegos, L.; Miguel, D.; Campaña, A. G.; Cuerva, J. M. *Org. Lett.* **2012**, *14* (23), 5984–5987.
(61) Márquez, I. R.; Miguel, D.; Millán, A.; Marcos, M. L.; De Cienfuegos, L. Á.; Campaña, A. G.; Cuerva, J. M. *J. Org. Chem.* **2014**, *79* (4), 1529–1541.
(62) Morcillo, S. P.; Martínez-Peragón, Á.; Jakoby, V.; Mota, A. J.; Kube, C.; Justicia, J.; Cuerva, J. M.; Gansäuer, A. *Chem. Commun. (Camb).* **2014**, *50* (17), 2211–2213.
(63) Gansäuer, A.; Shi, L.; Otte, M. *J. Am. Chem. Soc.* **2010**, *132* (34), 11858–11859.
(64) Tarantino, K. T.; Miller, D. C.; Callon, T. A.; Knowles, R. R. *J. Am. Chem. Soc.* **2015**, *137*, 6440.
(65) Wipf, P.; Maciejewski, J. P. *Org. Lett.* **2008**, *10* (19), 4383–4386.
(66) Gansäuer, A.; Kube, C.; Daasbjerg, K.; Sure, R.; Grimme, S.; Fianu, G. D.; Sadasivam, D. V.; Flowers, R. A. *J. Am. Chem. Soc.* **2014**, *136* (4), 1663–1671.
(67) Gansäuer, A.; Von Laufenberg, D.; Kube, C.; Dahmen, T.; Michelmann, A.; Behlendorf, M.; Sure, R.; Seddiqzai, M.; Grimme, S.; Sadasivam, D. V.; Fianu, G. D.; Flowers, R. A. *Chem. - A Eur. J.* **2015**, *21*, 280–289.
(68) Gansäuer, A.; Hildebrandt, S.; Michelmann, A.; Dahmen, T.; von Laufenberg, D.; Kube, C.; Fianu, G. D.; Flowers, R. A. *Angew. Chemie - Int. Ed.* **2015**, *54*, 7003–7006.
(69) Fianu, G. D.; Schipper, K. C.; Flowers, R. A. *Catal. Sci. Technol.* **2017**.

Chapter 2. Titanocene(III) complexes in the design of atom-economical processes: Mechanistic study and method development

2.1 Background and significance

2.1.1 Introduction to atom-economical processes

An atom-economical reaction is one where the maximum number of atoms of the reactants appears in the desired product. To many organic chemists, designing a reaction that is atom economic is just as important as designing a highly selective reaction, mainly because it is cost effective due to the efficient use of limited raw materials, decreased emission and waste disposal.[1–3] Classic examples of atom economical-reactions include cycloaddition reactions such as the Diels-Alder reaction, which is a 4+2 cycloaddition of a conjugated diene to an alkene or acetylene to form a cyclohexene derivative.[4,5] Other atom-economical reactions include several isomerization and cross coupling reactions where additional reagents are used in catalytic amounts.[1–3]

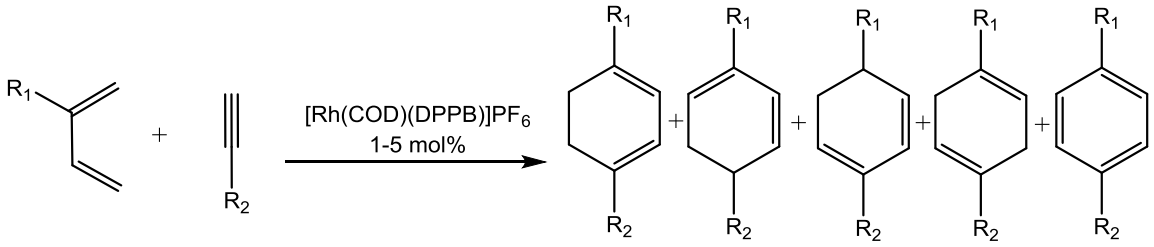

Scheme 2.1. Cycloaddition of 1,3-butadiene derivatives with non-activated terminal acetylenes catalyzed by Rh(1) complex[4]

When designing efficient atom-economical processes, the choice of reaction intermediates is crucial. To this end, radical intermediates are advantageous for designing efficient atom-economical processes because they are generated very easily under mild conditions, tolerate a wide range of functional groups, and easily add to unsaturated

hydrocarbons and arenes in a predictable manner.[6] Baran and coworkers in an elegant review on the potential of radical intermediates, have highlighted the intrinsic ability of radicals to facilitate tandem bond formations in highly selective and rapid fashions (Figure 2.1). Transformations mediated by radical intermediates could lead to the discovery of new and exciting complex structures of biological and synthetic utility that cannot be synthesized via a traditional two electron process.[7]

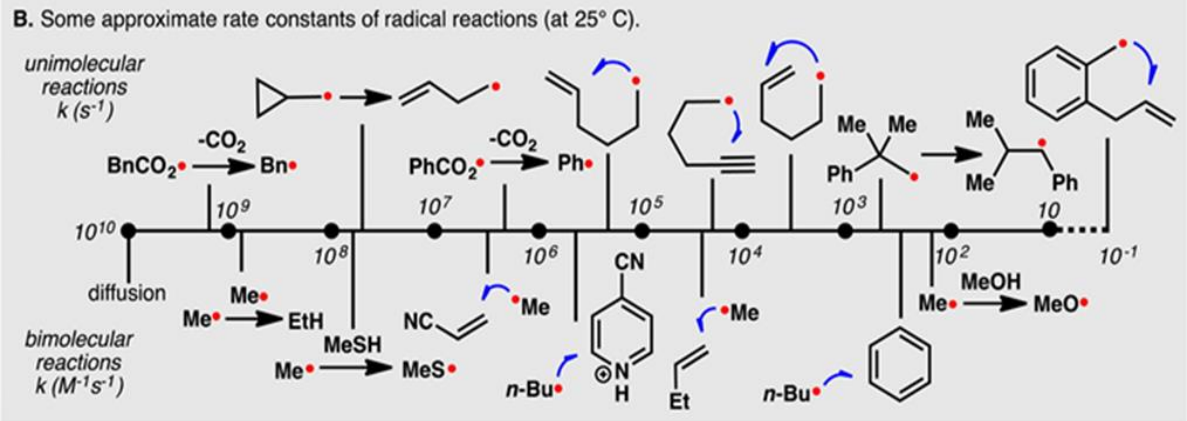

Figure 2.1. Approximate rate constants of radical reactions at 25ºC [7]

The choice of reagents is also crucial in the design of atom-economical processes. Any additional reagent used should ideally be added in catalytic amounts. These catalysts should be generated easily, reduce the substrate to form a radical intermediate from a low valent oxidation state and subsequently be involved in the oxidation of the intermediate radical σ-complex at its higher oxidation state.[2,3,8,9] The use of single electron oxidative additions and reductive eliminations in the design of efficient processes provides numerous possibilities for incorporating radical reactions that are related to classical organometallic catalysis.

There are a few atom-economical processes that meet the aforementioned criteria. One example is the work of Severin and coworkers in which a Ru(II) complex is employed to catalyze an atom transfer radical addition (ATRA) of organochlorides to olefins (Scheme 2.2). The active Ru(II) is generated from $Cp^*Ru(III)Cl_2(PPh_3)$, which is easily synthesized from commercially available reagents, and a cocatalyst azobis(isobutyronitrile) (AIBN).[10] The Ru(II) complex first abstracts a chloro atom from CCl_4 to give a Ru(III)−Cl complex and a CCl_3 radical. The organochloride radical adds to the olefin which then combines with the Ru(III)−Cl complex to give the addition product. The active catalyst is regenerated with AIBN.[10]

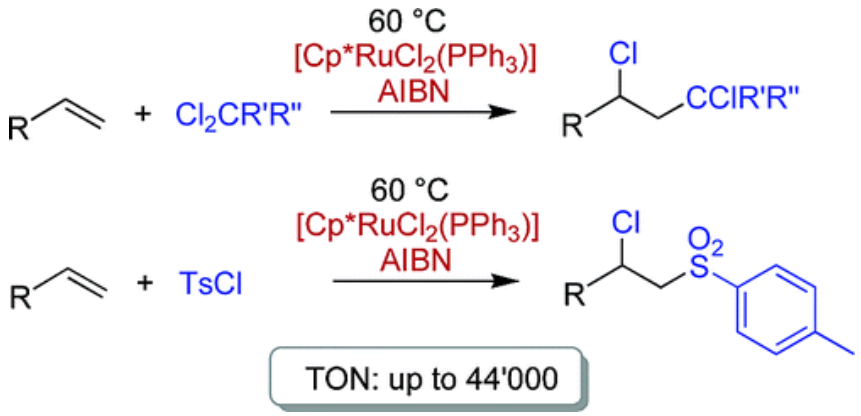

Scheme 2.2. Ru(II) catalyzed ATRA of organochlorides to olefins

Another example is work done by Norton and coworkers, which involves a hydrogen mediated chromium catalyzed radical cyclization of a 1,6-diene (Scheme 2.3).[11] The transfer of hydrogen atom from $CpCr(CO)_3H$ to the kinetically favored double bond of a 1, 6-diene is used to initiate a radical cyclization. The radical intermediate undergoes structural rearrangement to a chair-equatorial conformation as shown in scheme 2.4. This conformation facilitates the radical addition to the olefin to form the cyclized radical intermediate, which is presumably reduced by a hydrogen atom to release the product.

The $CpCr(CO)_3H$ is regenerated by hydrogen gas, making the reaction catalytic (Scheme 2.4).[11]

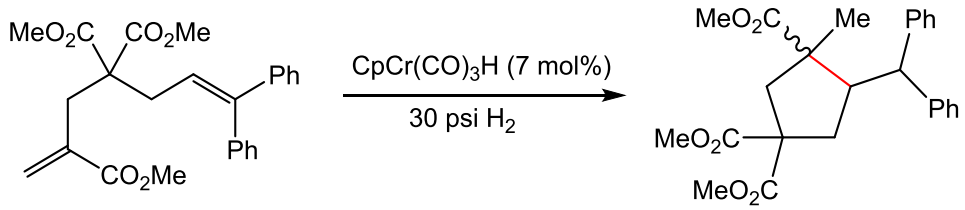

Scheme 2.3. Chromium catalyzed radical cyclization of 1,6 dienes

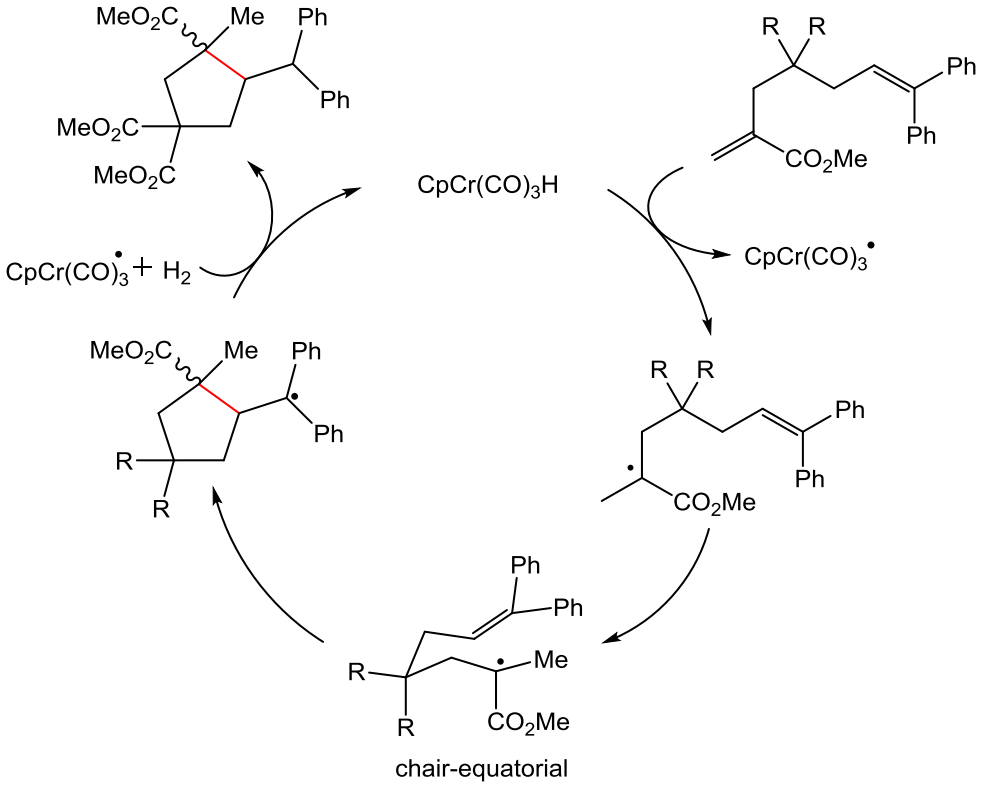

Scheme 2.4. Catalytic cycle for the chromium catalyzed radical cyclization of 1,6 dienes

2.1.2 Titanocene(III) chloride in the radical arylation of epoxides

Titanocene(III) chlorides have been used extensively by researchers and are known to readily open epoxides to form β-titanoxy radical intermediates that can undergo further transformations to generate complex molecules.[12–18] Doris and coworkers have

shown that titanocene(III) chloride (Cp_2TiCl) can be used in the synthesis of the antitumoral alkaloid Anhydrovinblastine from the selective deoxygenation of Leurosine (Scheme 2.5).[19] Trost and co-workers have also shown that titanocene(III) chloride can be used in the synthesis of Siccanin, a natural product possessing significant antifungal properties (Scheme 2.6).[20] Owing to their intrinsic property of easily interchanging between the +3 and +4 oxidation states, titanocene(III) chlorides have also been used in catalytic amounts for the synthesis of complex molecules such as terpenoids (Scheme 2.7)[21] and THF derivatives (Scheme 2.8).[22]

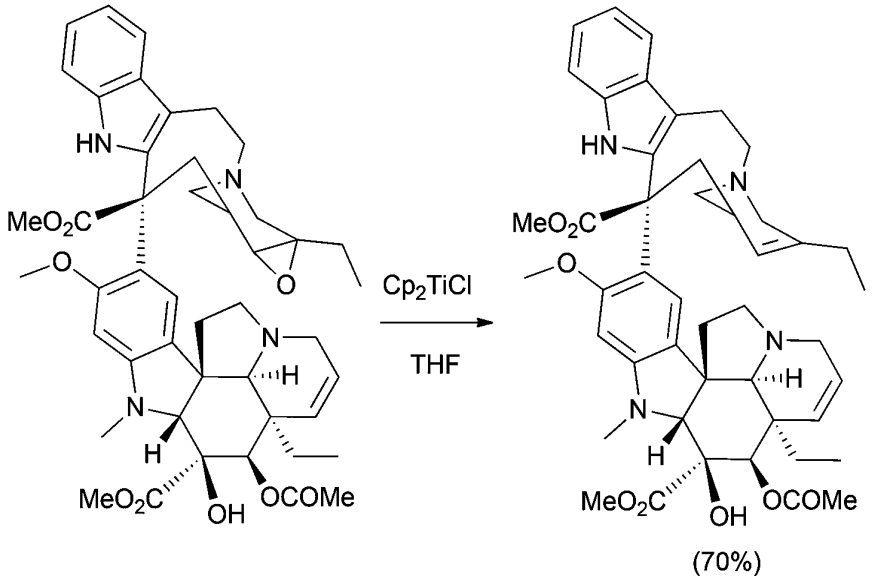

Scheme 2.5. Cp_2TiCl catalyzed synthesis of Anhydrovinblastine from Leurosine

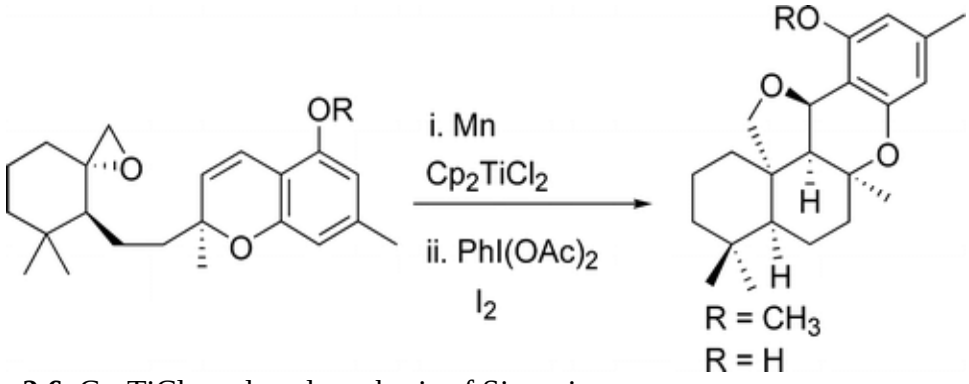

Scheme 2.6. Cp_2TiCl catalyzed synthesis of Siccanin

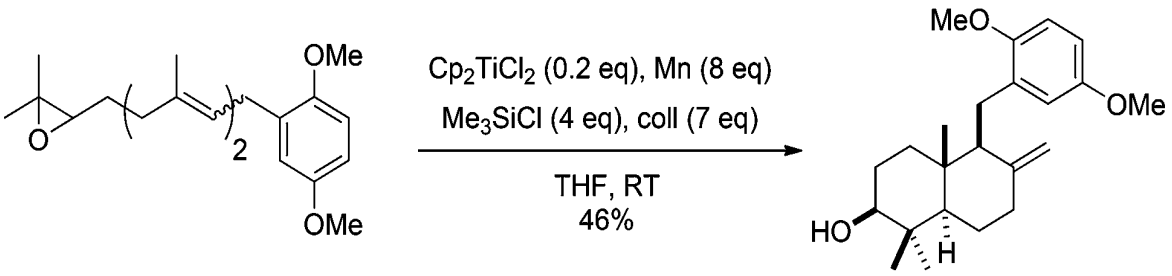

Scheme 2.7. Cp_2TiCl catalyzed synthesis of terpenoids

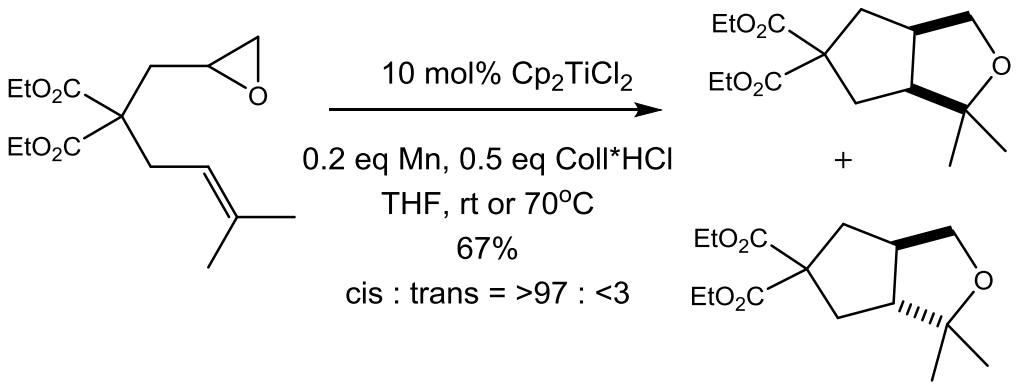

Scheme 2.8. Cp_2TiCl catalyzed synthesis of THF derivatives

2.1.3 Indoles

Indoles are important motifs in macromolecules of biological and synthetic significance (Figure 2.2).[23–26] Researchers have therefore developed many ways to effectively synthesize these basic structures.[27,28] The Fisher indole synthesis, an acid catalyzed sigmatropic rearrangement of a phenylhydrazone initially formed by reacting phenylhydrazine with a carbonyl compound, is one of the most widely used routes for making indoles (Scheme 2.9).[27,29] The Bartoli indole synthesis is another commonly utilized route to making indoles. Similar to the Fischer indole synthesis, this approach also takes advantage of a sigmatropic rearrangement of the intermediate formed by reacting nitro arenes with vinyl Grignard reagents (Scheme 2.10).[27,30]

Indoles have also been synthesized via single electron steps.[27] An example, shown in scheme 2.11, is the radical cyclization of iodo-substituted amides mediated by samarium diiodide.[31] The aryl radical formed by reacting the substrate with SmI_2 in the presence of HMPA, readily adds to the alkene to form the resulting spirooxindole product (Scheme 2.11).[31] Other reported methods for indole synthesis employ catalysts developed from a number of transition metals[27] including palladium (Pd) (Scheme 2.12),[32–36] rhodium (Rh) (Scheme 2.13),[37–39] and titanium (Ti) (Scheme 2.14).[40–42]

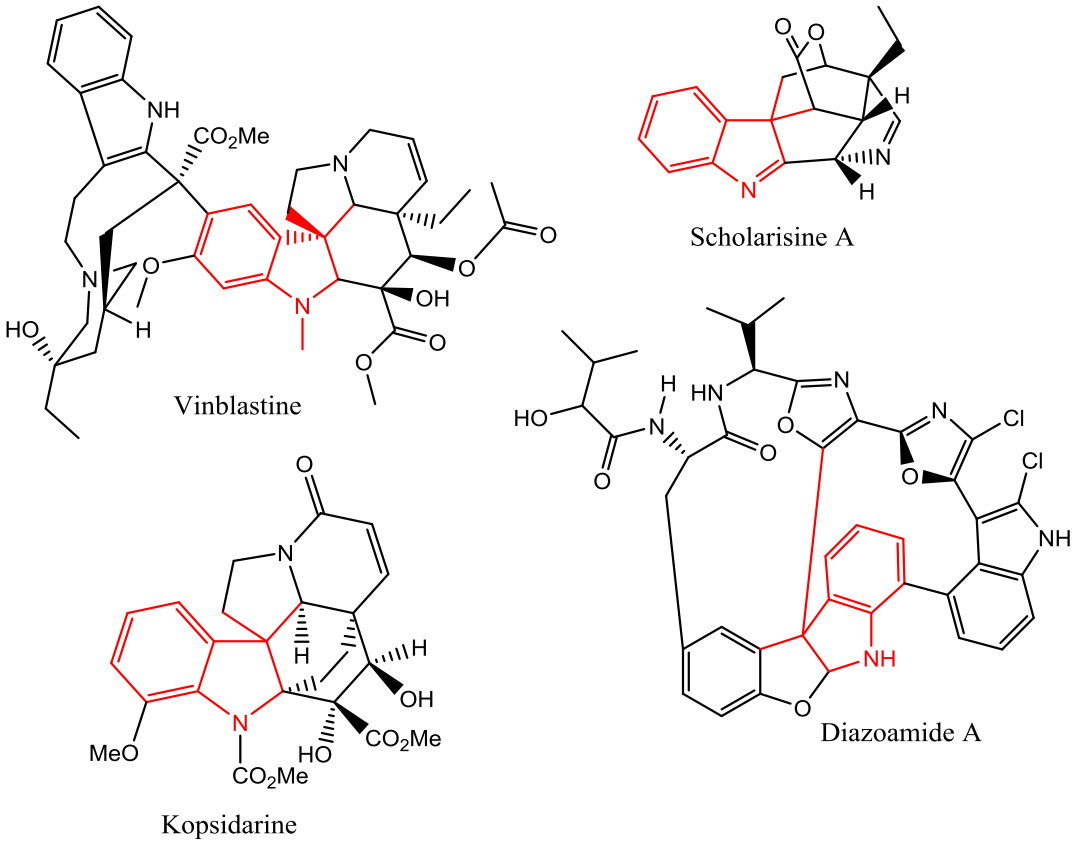

Figure 2.2. Complex molecules containing indoles as basic motifs

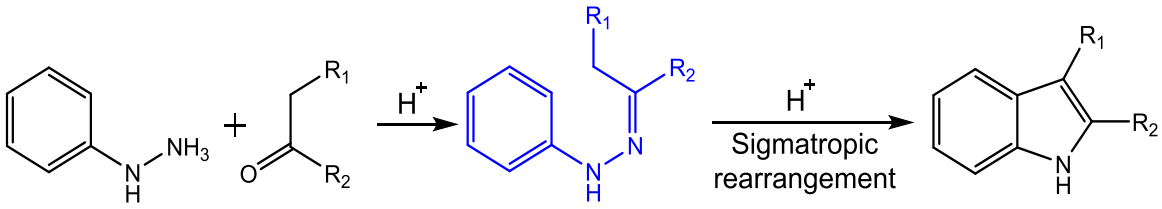

Scheme 2.9. Fischer indole synthesis

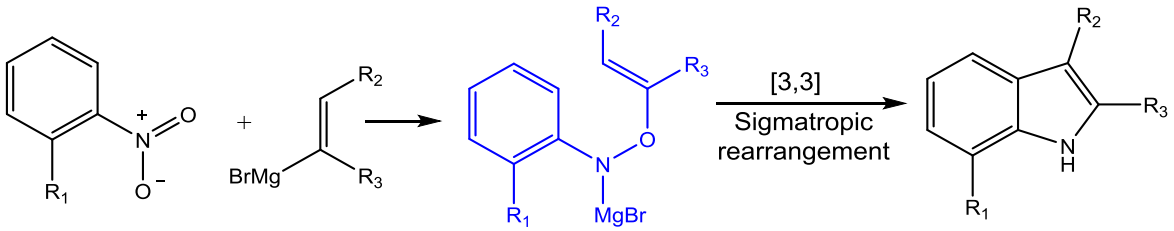

Scheme 2.10. Bartoli indole synthesis

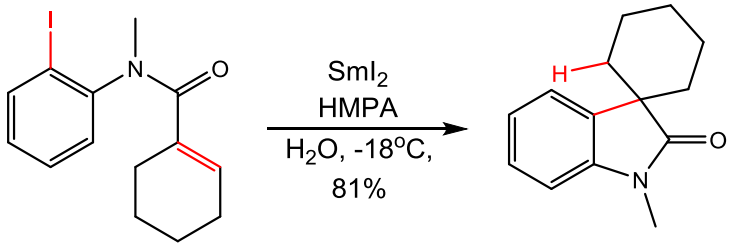

Scheme 2.11. Indole synthesis mediated by SmI_2

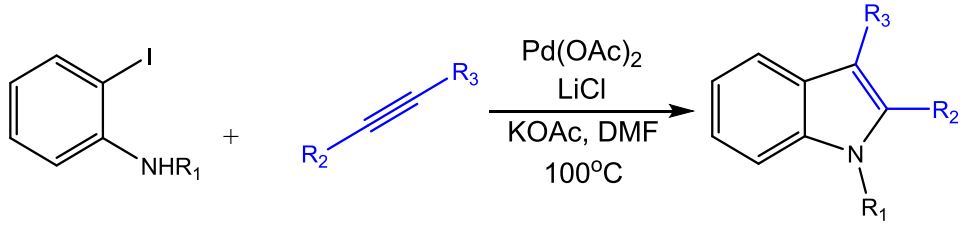

Scheme 2.12. Larock indole synthesis

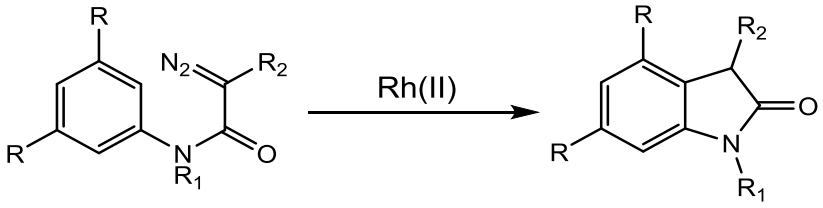

Scheme 2.13. Rhodium(II) catalyzed indole synthesis

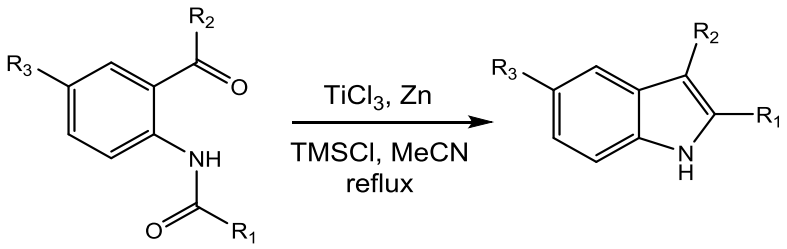

Scheme 2.14. Fürstner indole synthesis

2.1.4 Titanocene(III) catalyzed atom-economical radical arylation of amino epoxides to form indoline derivatives

The reaction under study is an elegant radical arylation of amino epoxides to form indoline derivatives developed by Peter Wipf from the University of Pittsburg (Scheme 2.15).[43] This is an atom-economical radical arylation process catalyzed by titanocene(III) chloride whose unique property of easily interchanging oxidation states from +4 to +3 makes it ideal. Manganese was used to initially activate the titanocene catalyst. The reaction was carried out under an inert atmosphere, in refluxing THF with Coll*HCl added as a proton source.[43] Under these reaction conditions, lower yields of desired products were obtained for electron deficient epoxides suggesting that the electronics of the substrates were impacting the reaction (Scheme 2.16).[43]

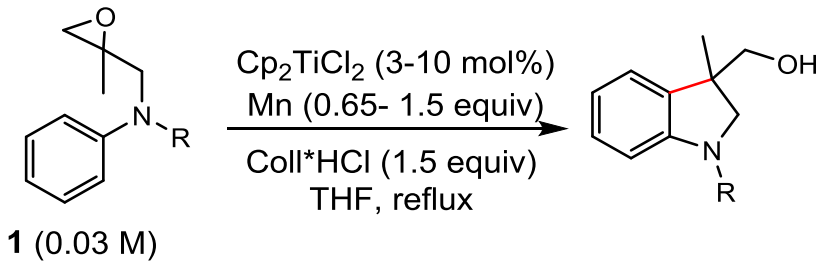

Scheme 2.15. Titanocene(III) catalyzed indole synthesis

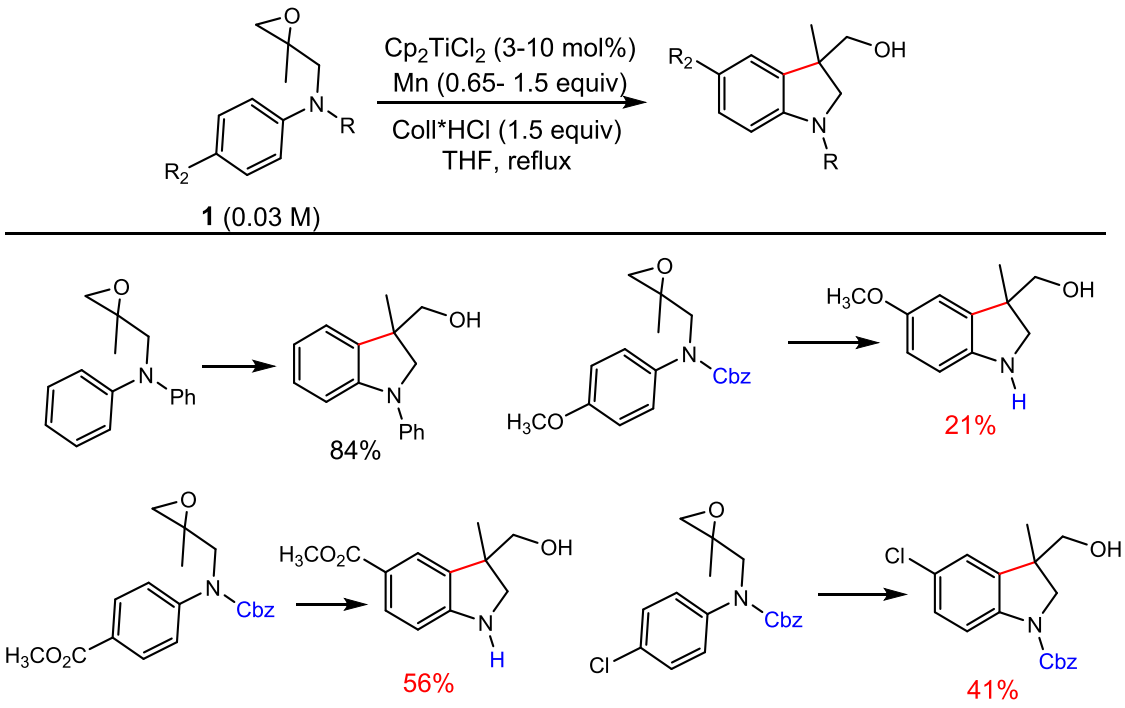

Scheme 2.16. Lower yields observed for electron deficient epoxides

The proposed catalytic cycle did not offer much insight into the cause of this phenomenon (Scheme 2.17). Moreover, in the proposed cycle, it was suggested that oxygen was involved in the final oxidation of the radical σ-complex. Titanocene(III) chloride is very sensitive to air and therefore reactions catalyzed by Cp_2TiCl are done under an inert atmosphere. As a result, it is highly unlikely that oxygen will be present in the system due to its ability to deactivate the catalyst. It was also proposed that excess Mn was used to prevent alkyl radical reformation.[43]

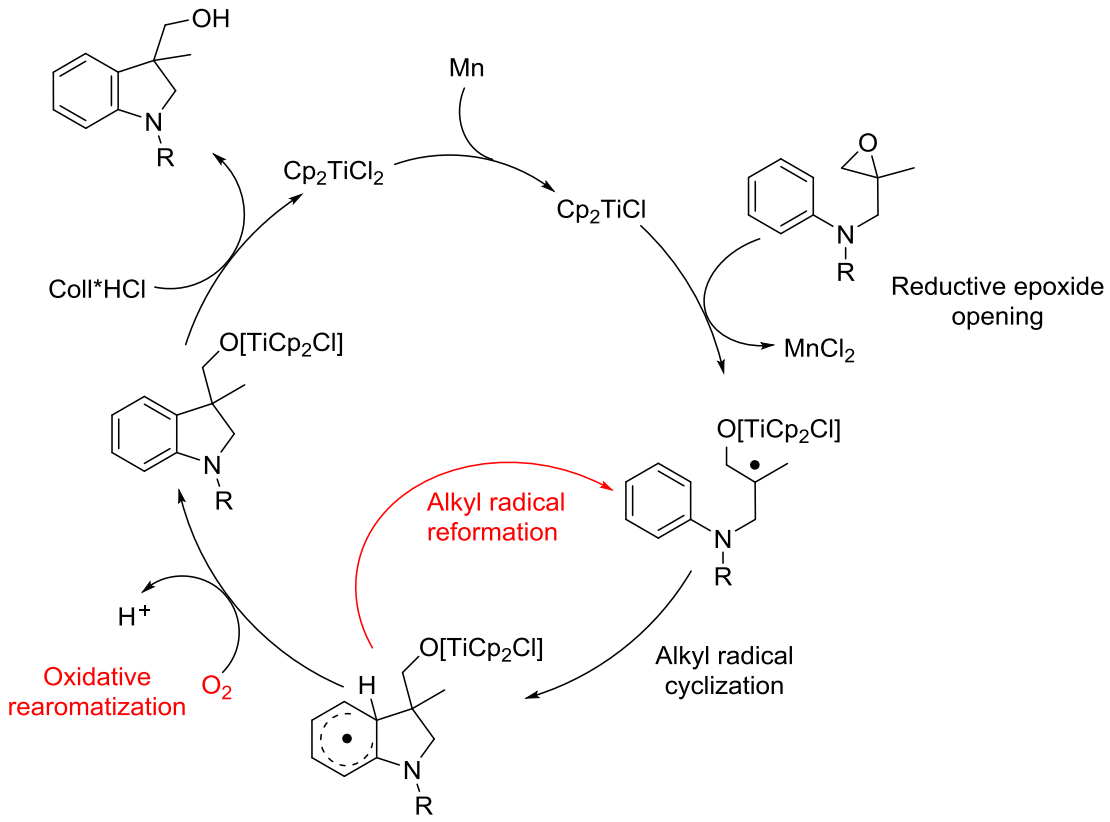

Scheme 2.17. Proposed catalytic cycle for the titanocene(III) catalyzed formation of indoles

2.1.5 Project goals

The incorporation of radical transformations in atom-economical C-C bond forming processes to form indoline derivatives is rare.[27,44] As a result, designing efficient atom-economical processes is a challenge because little is known about the mechanism of such processes, thus making it difficult to fine-tune these systems to cater for a wide range of substrates. In view of this, the Flowers lab, in collaboration with the Gansäuer lab, set out to perform an in-depth mechanistic study on the titanocene catalyzed radical arylation of amino epoxides to form indoles. We hoped to gain an understanding as to why low yields were obtained with electron deficient amino epoxides. We envisioned this information would help redesign this process to incorporate electron deficient epoxides.

With our studies, we wanted to verify the proposed role of oxygen in the system. We also wanted to examine the role of collidine hydrochloride (Coll*HCl), which was believed to act as a proton donor.

Furthermore, we wanted to test if manganese was playing an additional role other than the initial formation of the active catalyst. To perform a rigorous mechanistic study, we needed to test the stability of the catalyst under the reaction conditions. We also needed to know the orders of the reactants involved in the process and the turnover-limiting step of the reaction. Finally, a series of synthetic and computational experiments were done by Gansäuer and Grimme on this process to rule out the possibility of other competing reaction pathways.

2.2 Experimental

2.2.1 Materials and instrumentation

Unless otherwise stated, all reactions were carried out in a glove box and under argon atmosphere. An Innovative Technology solvent purification system was used to purify all the solvents used for experiments. All reagents and chemicals, mostly argon or nitrogen flushed, were purchased from reputable chemical vendors (Alfa Aesar, Acros, Sigma Aldrich, Beantown Chemical, and TCI) and used without further purification. Chemicals not flushed with an inert gas were degassed with argon and used without any additional purification protocols. ^{1}H-NMR spectra were measured on either a Bruker 500MHz or a Bruker 400MHz spectrometer in deuterated chloroform ($CDCl_3$). ^{13}C-NMR spectra were measured at either 126 MHz or at 101 MHz in $CDCl_3$.

GC-MS analyses were done with a Schimadzu GCMS-Q2010 series with a SHRX-5M (30m) column. Column chromatography was done using an automated CombiFlash® system from Teledyne Isco. Inc. Columns were prepacked with silica gel and product separations were performed with a gradient elution of hexanes and ethyl acetate. *In situ* IR experiments were done using Mettler-Toledo's ReactIR 15 fitted with DiComp probe and running iCIR software 4.3 SP1 or Mettler-Toledo's ReactIR 4000 fitted with SiComp probe and running iCIR software 4.2.26. Kinetic experiments were also performed with Venier SpectroVis Plus Spectrophotometer running Logger Lite software.

2.2.2 Methods

2.2.2.1 Procedure for synthesizing *N*-((2-methyloxiran-2-yl) methyl)-*N*-phenylaniline (1)

N-((2-methyloxiran-2-yl) methyl)-*N*-phenylaniline (**1**) was synthesized by following the procedure outlined in literature.[9] Sodium hydride (NaH, 1.10 equiv) was suspended in dry THF (1 mL per 1 mmol diphenylamine). Diphenylamine (1.00 equiv) was added to the suspension and stirred at room temperature for about 30 min. After 30 minutes 3-chloro-2-methylprop-1-ene (2.00 equiv) was added to the mixture and stirred overnight at reflux. Reaction mixture was cooled and ice was added to quench any unreacted NaH. Water and diethyl ether were added to the mixture. The aqueous layer was separated and extracted with diethyl ether three times. The organic layers were combined, washed with brine, and dried with $MgSO_4$. The solvents were removed under reduced pressure to obtain crude *N*-(2-methylallyl)-*N*-phenylaniline product.

N-(2-methylallyl)-*N*-phenylaniline (1.00 equiv) was dissolved in a 1:1:1 mixture of THF/acetone/water and a few drops of phosphate buffer (pH 7) was added. Osmium tetroxide (OsO_4, 0.01 equiv) and *N*-Morpholine-*N*-oxide hydrate (NMO, 1.50 equiv) were added to the mixture and stirred overnight at room temperature. The reaction was quenched by adding excess amounts of aqueous sodium hydrogen sulfite. Diethyl ether was added to the mixture and the aqueous layer was separated and extracted three times with diethyl ether. The combined organic layers were washed with brine and dried with $MgSO_4$. The solvents were removed under reduced pressure to obtain the crude 3-(diphenylamino)-2-methylpropane-1,2-diol product.

To a solution of 3-(diphenylamino)-2-methylpropane-1,2-diol (1.00 equiv) in dry THF, sodium hydride (2.00 equiv) was added slowly and stirred for 30 minutes. After stirring for 30 minutes, tosylchloride (p-TosCl, 1.50 equiv) was added and the mixture was stirred overnight. Ice was added to quench any unreacted NaH. Water and diethyl ether were added to the mixture. The aqueous layer was separated and extracted with diethyl ether three times. The organic layers were combined, washed with brine, and dried with $MgSO_4$. The solvents were removed under reduced pressure and the crude product was purified with flash column chromatography (Hexanes: Ethyl acetate = 70:30) to obtain **1**.

2.2.2.2 Procedure for radical arylation of epoxide (1) to form 2

An oven dried vial was charged with manganese, collidine hydrochloride (Coll*HCl), and catalyst in a glovebox under argon atmosphere. Dry degassed THF was added to the vial and stirred until a green colored solution was formed. The epoxide was

added to the mixture and left to stir for the given time. The reaction was quenched with saturated ammonium chloride solution (NH_4Cl). Diethyl ether was added and the phases were separated. The aqueous layer was extracted 3 times with diethyl ether, washed with brine and dried over $MgSO_4$. Evaporation of the solvent followed by flash chromatography gave the cyclized product (**2**).

2.2.2.3 Procedure for making 2-methyl-2-phenethyloxirane (7)

To a dried 250 mL round bottomed flask was added 50 ml of dry degassed THF under argon atmosphere. Sodium hydride (NaH, 1.20 equiv) was carefully measured into the flask containing THF. The mixture was sealed and taken out of the glove box and placed on a stirrer. Trimethylsulfoxonium iodide (1.40 equiv) was measured and quickly added to the mixture and left to stir for 30 minutes under argon. After 30 minutes, 4-phenylbutan-2-one (1.00 equiv) was measured and quickly added to the mixture and stirred overnight. Diethyl ether was added to the mixture followed by a drop of ice to react with any unreacted NaH. Water was added to the mixture and the organic layer was separated from the aqueous layer. The aqueous layer was washed two more times with diethyl ether and the separated organic layers were combined, washed with brine, dried with magnesium sulfate, and filtered. The organic solution was rotavaped to obtain crude product, which was purified with flash column chromatography (Hexanes: Ethyl acetate = 90:10) to obtain **7.**

2.2.2.4 Procedure for running experiments on ReactIR

2.2.2.4.1 General React IR 4000 procedure

Kinetic runs were carried out using Mettler-Toledo's ReactIR 4000 fitted with SiComp probe and running iCIR software 4.2.26. To a two-necked round bottom flask, Mn and Coll*HCl were added and attached to a reflux condenser inside the glove box. This was taken out and fixed to the ReactIR probe and flushed with argon. An air background (64 scans) was obtained and 11.5 mL of THF was added to the round bottom flask through a rubber septum and heated in an oil bath at 60.0 °C for 15 min. The iCIR software was initiated to obtain data. IR spectrum was collected every minute until the reaction was complete. The catalyst $(C_5H_4R)_2TiCl_2$ in 2.0 mL of THF was added after 4.0 - 5.0 minutes of starting the reaction and washed with 0.25 mL of THF. The reaction mixture was refluxed until the appearance of a green color indicative of formation of Ti(III). The epoxide in 1 mL of THF was added and washed with 0.25 mL THF. The reaction was left under reflux and monitored by ReactIR.

2.2.2.4.2 General ReactIR 15 procedure

Kinetic runs were carried out using a Mettler-Toledo's ReactIR 15 fitted with DiComp probe and running iCIR software 4.3 SP1. To a two-necked round bottom flask, Mn and the appropriate amount of Coll*HCl were added and attached to a reflux condenser inside the glove box. This was taken out, fixed to the ReactIR probe, and flushed with argon. An air background (256 scans) was obtained. Then 11.5 mL of THF was added through a rubber septum into the round bottom flask in an oil bath at 60.0 °C for 15 min. The iCIR software was initiated to obtain data. IR spectrum was collected

every minute until the completion of the reaction. The catalyst $(C_5H_4R)_2TiCl_2$ in 2.0 mL of THF was added after 4.0 - 5.0 minutes of starting the reaction and washed with 0.25 mL of THF. The reaction mixture was refluxed until the appearance of green color indicative of formation of Ti(III). The epoxide in 1 mL of THF was added and washed with 0.25 mL THF. The reaction was left under reflux and monitored by ReactIR.

2.2.2.5 General procedure for running experiments on SpectroVis

All solutions were prepared in an argon filled glove box. A Ti(III) solution was prepared by mixing $(C_5H_4R)_2TiCl_2$ and Mn dust in THF (25 mL). The solution was left to stir until a green colored solution was formed. A stock solution of epoxide and cyclohexadiene in THF was prepared for kinetic runs. The SpectroVis instrument was calibrated with THF. Each experiment was set to run for 500 seconds. For each run, 3 mL of a 2 mM filtered Ti(III) solution was measured into a cuvette containing a stirrer and sealed with an airtight cap. This cuvette was placed into the SpectroVis instrument. The experiment was started and left to run for about 50 seconds. The appropriate amount of epoxide (**7**) solution was added to the Ti(III) solution and the decay of Ti (III) was monitored at the appropriate wavelength (λ_{max}). All the Ti(III) complexes studied had a λ_{max} at 800 nm. The observed rate (k_{obs}) was obtained by fitting an exponential equation to the plot of absorbance versus time in seconds.

2.3 Results

2.3.1 Control and optimization experiments

A series of control and optimization experiments were performed in a completely air-free environment and the results are summarized in table 2.1. As shown, the reaction proceeded smoothly to form the desired indole product with catalytic amounts of Mn and

in the absence of Coll*HCl. The results from the experiment clearly suggest that oxygen was not involved in the oxidation of the radical σ-complex (see scheme 2.17), and that Coll*HCl, which was used as a proton source, was not necessary for reaction to proceed. Finally, only catalytic amounts of Mn were required to activate the catalyst, indicating that its proposed additional role of preventing a reversible alkyl radical formation from the radical σ-complex was highly unlikely.[9,43,45]

Table 2.1. Results from control and optimization experiments

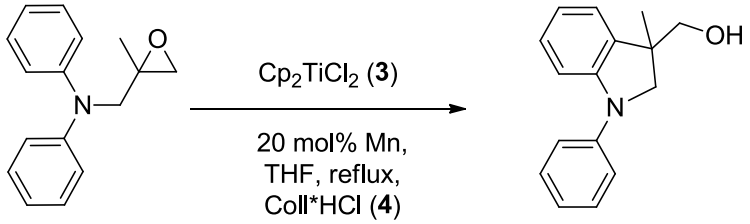

1 **2**

3 (mol%)	**4** (mol%)	Time	**1**:**2**	Yield (%)
10	-	30 min	0:100	98[a]
5	-	30 min	25:75[a]	-
5	10	30 min	0:100[a]	-
1[b]	5	2 h	0:100	96[c]

[a] 0.1 M. [b] 10 mol% Mn. [c] 0.5 M. All concentrations refer to **1**.[45]

Considering these new findings, Flowers and Gansäuer proposed an alternative mechanism for the radical arylation of **1** to **2** (Scheme 2.18). In this revised mechanism, the amino epoxide **1** is opened by titanocene(III) chloride ($Cp_2Ti(III)Cl$) to form the β-titanoxy radical **A** via a single-electron oxidation step. This radical readily adds to the arene to form the radical σ-complex **B**. Due to the intrinsic nature of titanocene(III) complexes to alternate between the +3 and +4 oxidation states, it was posited that this radical σ-complex **B** was oxidized by the pendant titanocene(IV) alkoxide moiety of the complex, resulting in the formation of a cationic intermediate **C**. The $Cp_2Ti(III)$-O bond

is subsequently cleaved upon protonation of the alkoxy moiety to release the active titanocene(III) catalyst into solution, with concomitant rearomatization of complex **C** to form the desired indole product (**2**).[9,45]

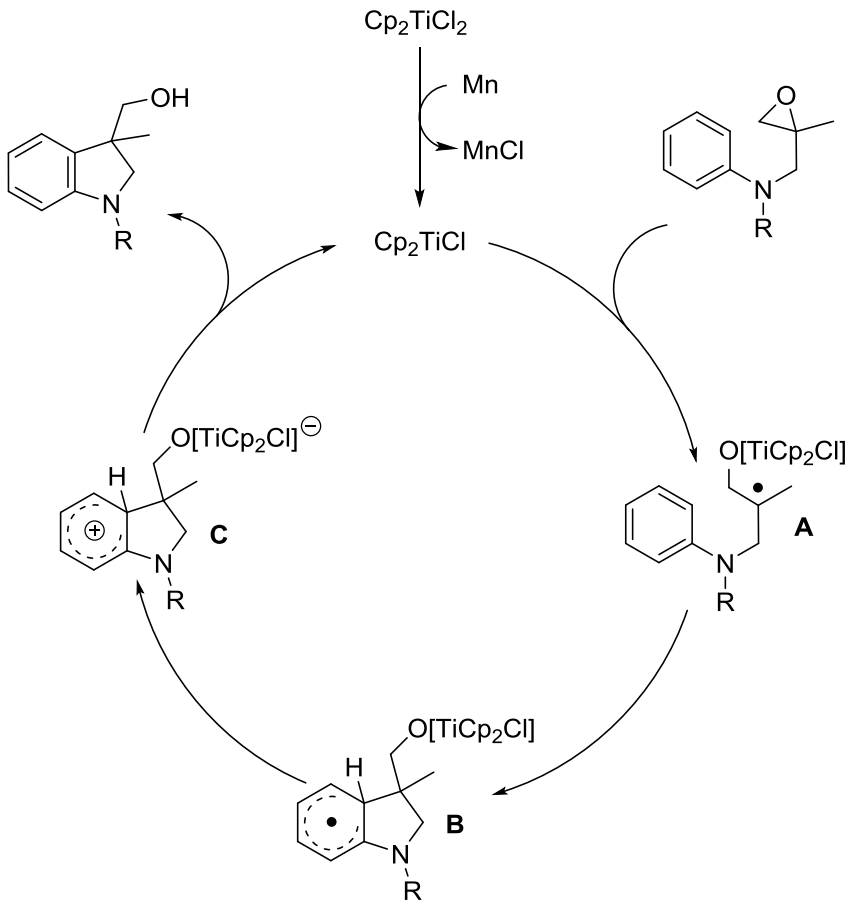

Scheme 2.18. Alternative cycle for the radical arylation of **1** to **2**

2.3.2 Catalyst stability tests

Catalyst stability tests were performed in the absence of Coll*HCl with Reaction Progress Kinetic Analysis.[46–48] In this technique, two separate reactions are carried out with the same catalyst under identical conditions, with the only difference being that one reaction starts with 50% of the reactant (Scheme 2.19). If the stoichiometry of the reactants during the reaction is known and there is no substrate or product inhibition, the

catalyst concentration is said to be constant or stable throughout the reaction when the rate of the first reaction at 50% conversion of the staring material is the same as the rate of the second reaction (Figure 2.3). In other words, a graphical overlay will be observed for a time-resolved plot of the reactant decay over time for both experiments if the catalyst is stable (Figure 2.5).[46–48]

$$[A] \xrightarrow{[M]} [B] \quad \text{(100\% Run)}$$

$$\frac{[A]}{2} \xrightarrow{[M]} \frac{[B]}{2} \quad \text{(50\% Run)}$$

Scheme 2.19. Catalyst stability test with RPKA

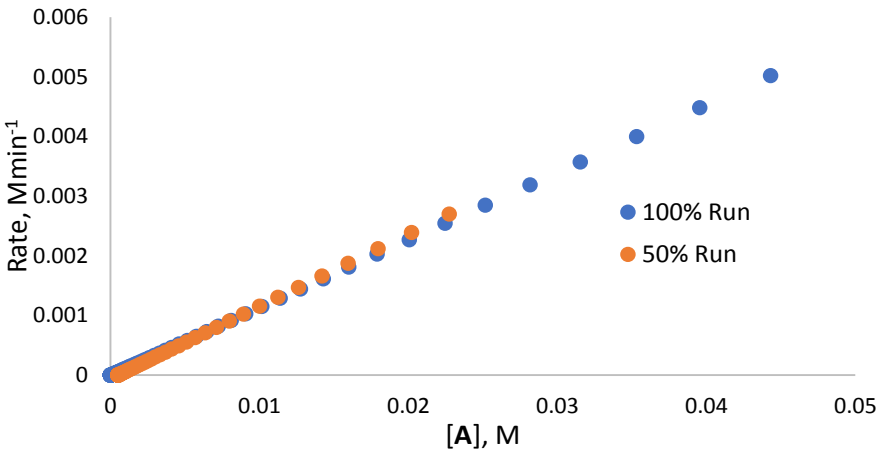

Figure 2.3. Plot of Rate vs. [A] for 100% and 50% experiments for catalyst stability test

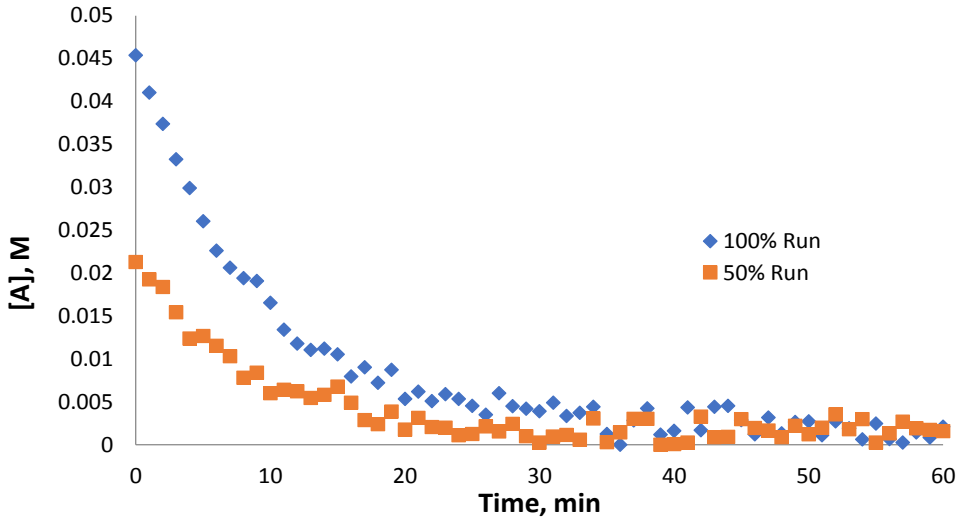

Figure 2.4. Decay plots of [A] over time for 100% and 50% runs

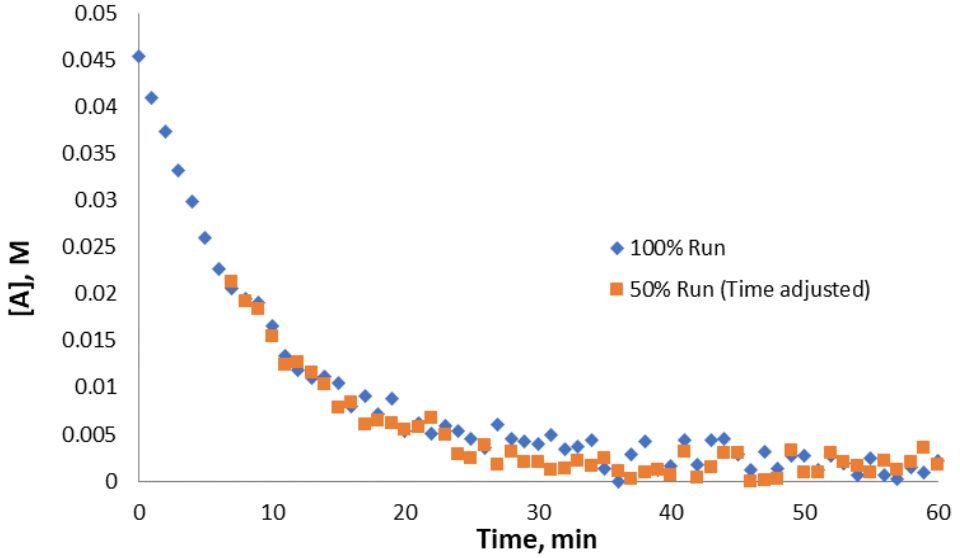

Figure 2.5. Time-resolved plots of [A] vs. time for 100% and 50% runs

Two separate experiments were performed under synthetically relevant conditions. The first experiment, which is labeled the 100% run, was carried out at the reaction conditions shown in table 2.2. The second experiment, labeled the 50% run, was

carried out under identical conditions as the 100% run. However, the initial concentration of the reactant in the 50% run is half that of the epoxide concentration in the 100% run.[9]

Table 2.2. Reaction conditions for catalyst stability tests

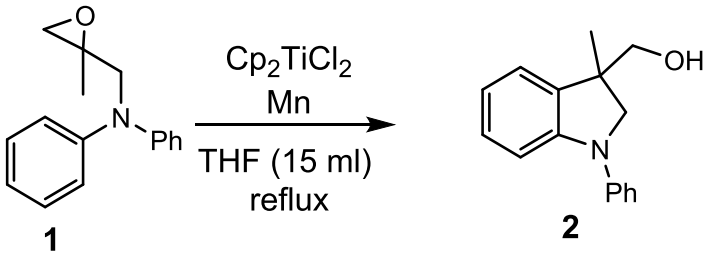

1 **2**

Run	[1], M	[Cp_2TiCl_2], M	[Mn], M	T °C
100 %	0.0550	0.0056	0.0407	60 ± 0.5
50 %	0.0275	0.0056	0.0407	60 ± 0.5

The ReactIR was used to monitor the growth of product *in situ* at 1386 cm^{-1} (Figure 2.6), which is absorption of the C-H wag of the C2 carbon of the indole product. A decay plot was derived for both experiments as shown in the figure 2.7. A time-resolved plot showed no overlay between the two decay plots (Figure 2.8), suggesting that the reaction was unstable under the new reaction conditions.[9]

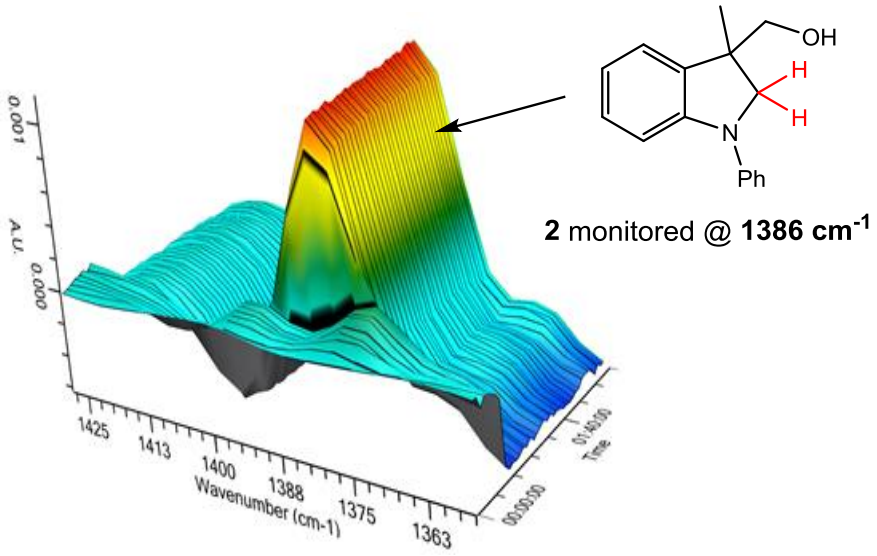

Figure 2.6. Product (**2**) monitored by ReactIR at 1386 cm^{-1}

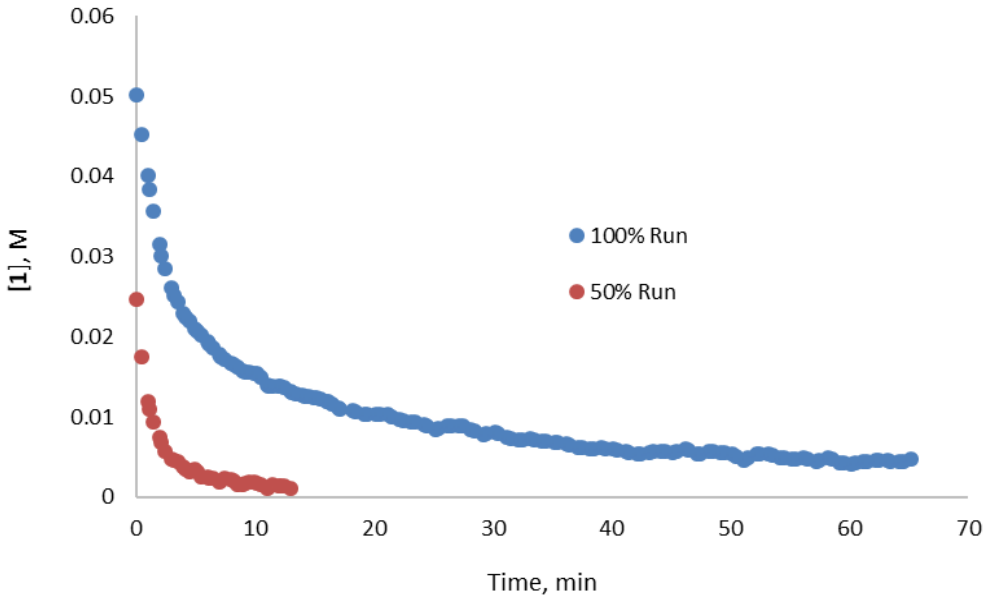

Figure 2.7. Decay plots for the radical arylation of **1** to **2** for 50% and 100% runs

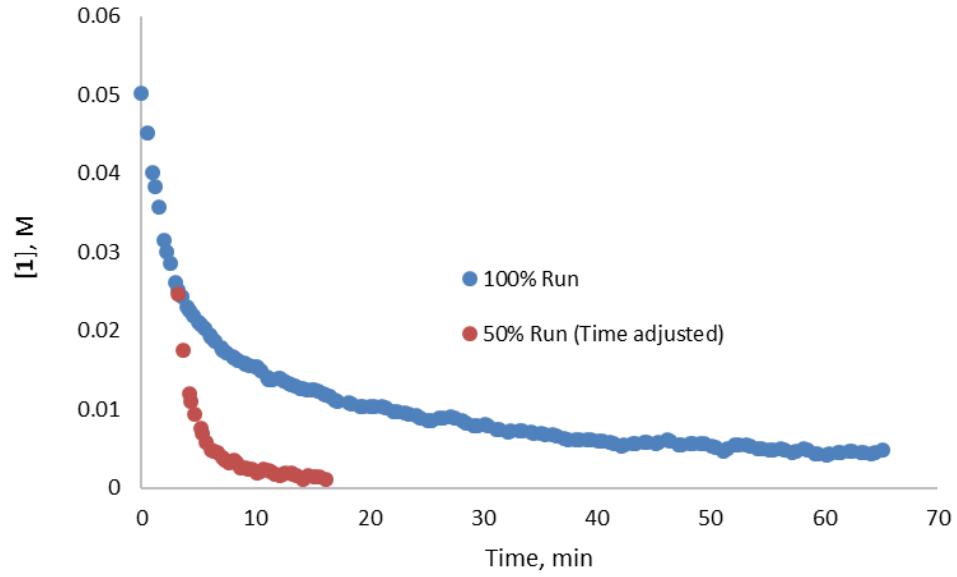

Figure 2.8. Time-resolved plots for the radical arylation of **1** to **2** for 50% and 100% runs

Based on these results, it was concluded that although the reaction proceeded smoothly to form products in the absence of Coll*HCl (**4**), the catalyst was deactivated

during the reaction. A second catalyst stability test was done but with the addition of Coll*HCl. The conditions are shown in table 2.3. A time-resolved plot showed that the catalyst remained stable throughout the reaction in the presence of Coll*HCl (Figure 2.10). Thus, Coll*HCl, which was initially added as a proton source, was very crucial in stabilizing the active catalyst.[9]

Table 2.3. Reaction conditions for catalyst stability tests in the presence of Coll*HCl

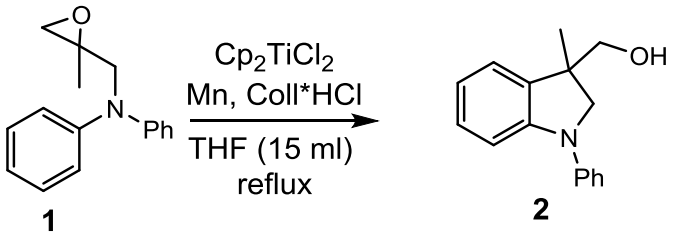

Run	[1], M	[Cp_2TiCl_2], M	[Mn], M	[Coll*HCl], M	T °C
100 %	0.0550	0.0056	0.0407	0.0132	60 ± 0.5
50 %	0.0275	0.0056	0.0407	0.0132	60 ± 0.5

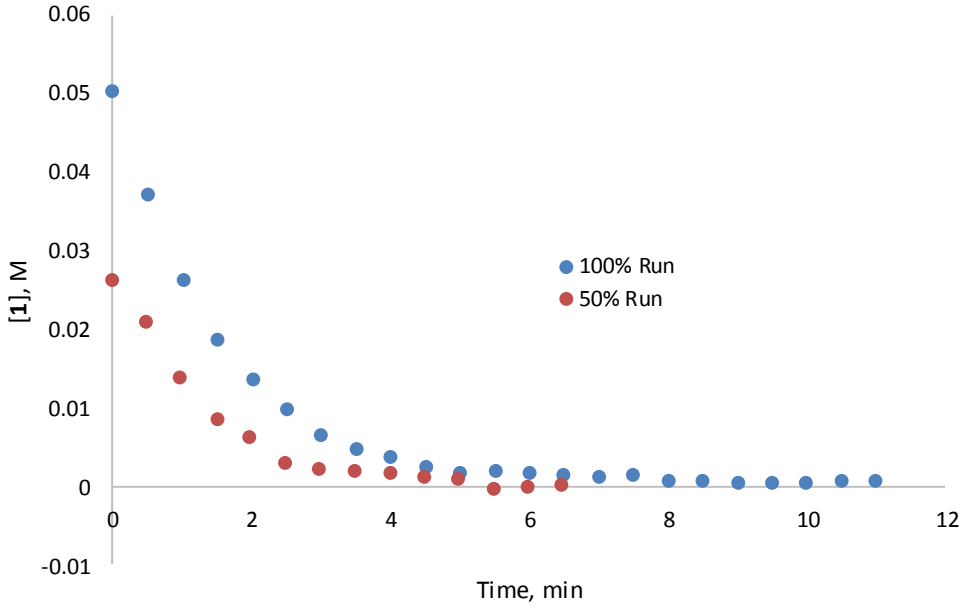

Figure 2.9. Decay plots for the radical arylation of **1** to **2** for 50% and 100% runs with Coll*HCl

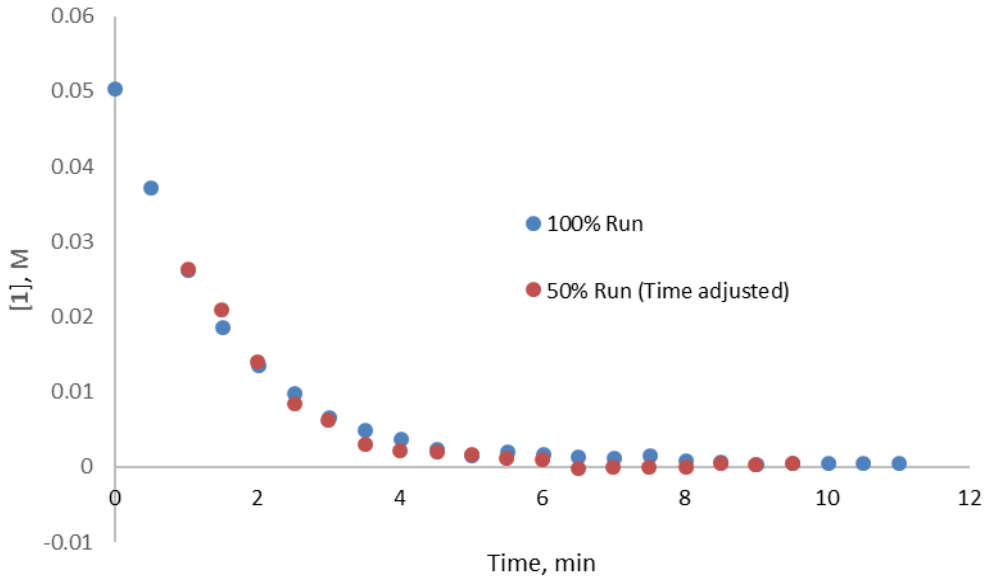

Figure 2.10. Time-resolved plots for the radical arylation of **1** to **2** for 50% and 100% runs with Coll*HCl

2.3.3 CV and computational studies

To further investigate the role of Coll*HCl, Gansäuer and coworkers performed cyclic voltammetry studies on the active catalyst (Cp_2TiCl), formed by reacting Cp_2TiCl_2 with Mn, in the presence of Coll*HCl. They observed that in addition to the expected titanocene peaks ($[Cp_2TiCl]_2$ and $[Cp_2TiCl]$), an extra peak corresponding to the formation of a titanocenium anion $[Cp_2TiCl_2]^-$ known to be unreactive towards epoxide opening, was also formed (Figure 2.11).[9,49,50] Flowers and coworkers performed computational studies to further investigate the interaction between Coll*HCl and the active titanocene catalyst. It was discovered that the active catalyst was forming a supramolecular complex with Coll*HCl (Figure 2.12).[9,51]

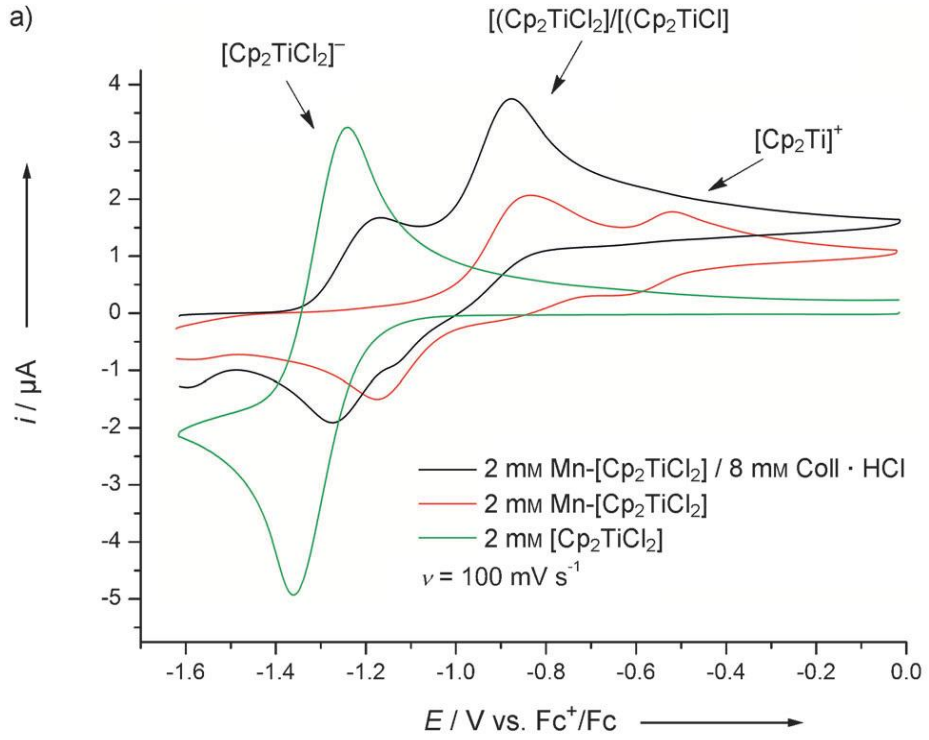

Figure 2.11. Cyclic voltammograms showing the impact of Coll*HCl on the identity of active titanocene complex

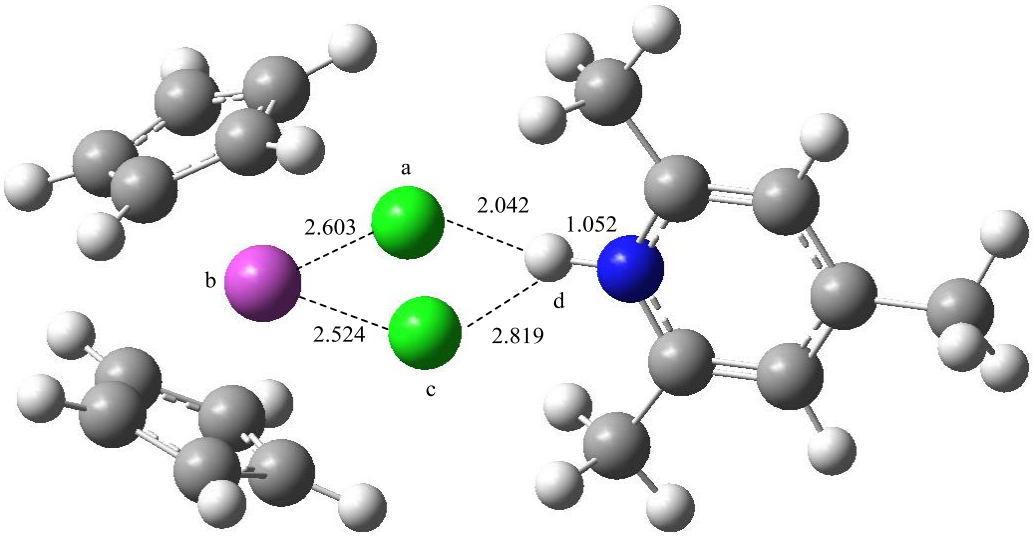

Figure 2.12. Calculated structure of supramolecular complex formed between active catalyst and Coll*HCl (Purple-Ti, green- Cl, blue- N, gray- C, white- H)

2.3.4 Kinetic studies

To understand how Coll*HCl was interacting with the catalyst, titanocene mediated epoxide opening experiments were carried out with 2-methyl-2-phenethyloxirane (**7**) as the model epoxide both with and without Coll*HCl. The rate constants obtained in both experiments were then compared (Scheme 2.20).

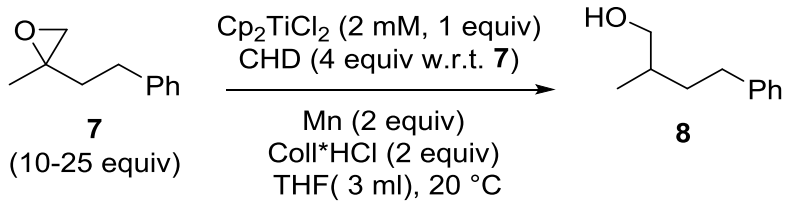

Scheme 2.20. Epoxide opening experiment

This epoxide opening experiment was done under pseudo first order conditions with a SpectroVis, which is a portable visible to near-IR spectrophotometer. This was done by monitoring the loss of the Ti(III) band for each of the manganese reduced titanocene complexes at 800 nm as described by Daasbjerg and co-workers (Figure 2.13).[13]

The decay plots were fitted to the appropriate exponential equation to derive the observed rate (k_{obs}) of the reaction (Figure 2.14).[45] This reaction was repeated at different concentrations of epoxide at least three times to ensure reproducibility of the data and the average k_{obs} were obtained at these concentrations. A graph of the observed rate (k_{obs}) versus epoxide concentration was plotted to obtain the rate constant (Figure 2.15). The order of the epoxide was also obtained by plotting the natural log of the observed rate versus the natural log of the concentration of the epoxide (Figure 2.16).[45]

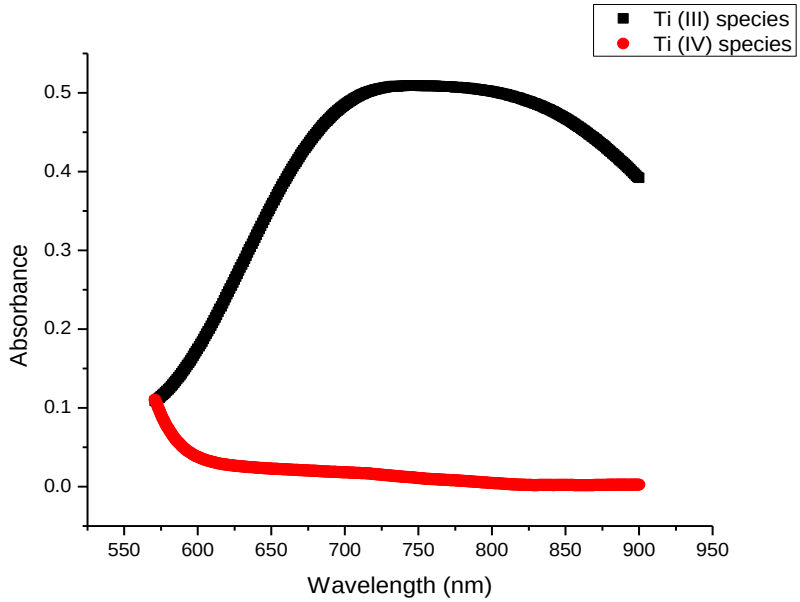

Figure 2.13. UV-Vis spectra of Ti(III)/(IV) species

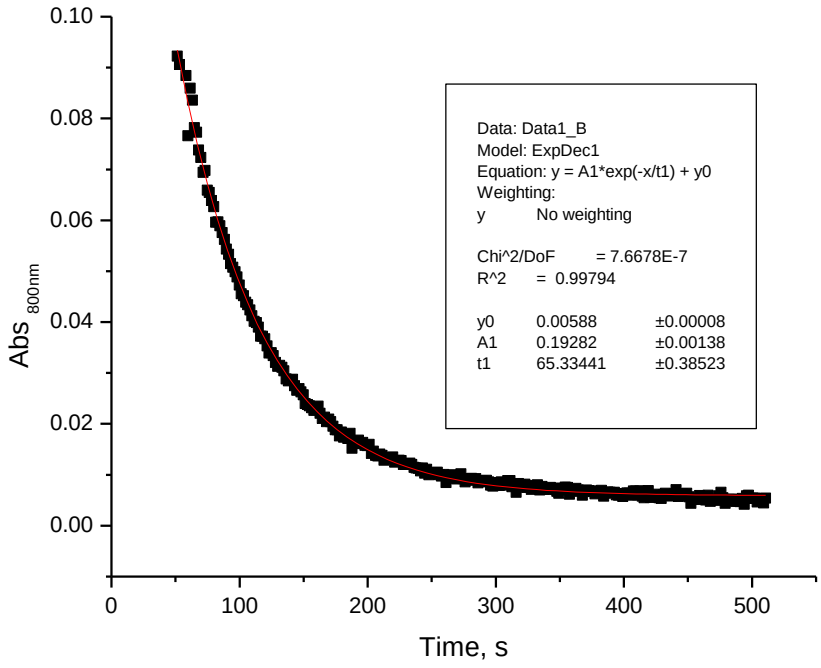

Figure 2.14. Plot of $Abs_{800\ nm}$ vs. time fitted to a single exponential equation

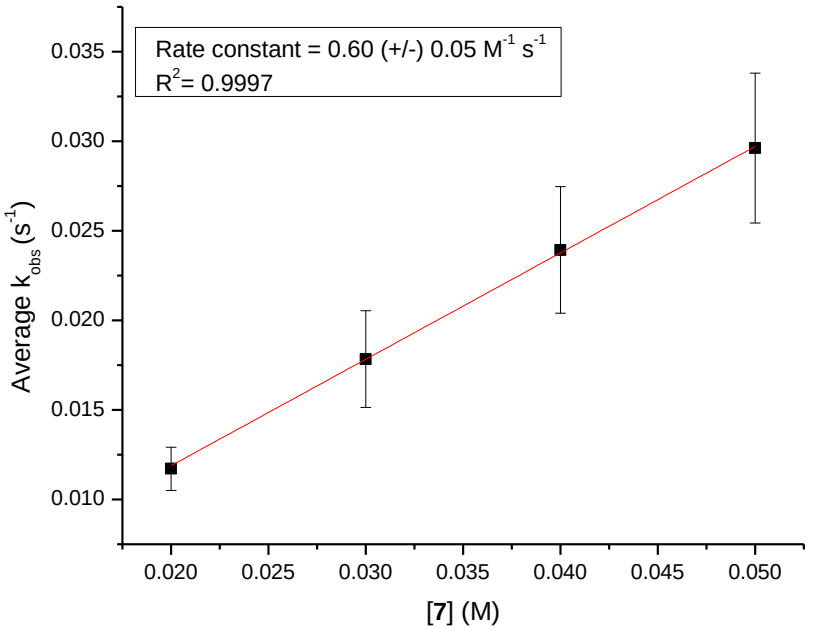

Figure 2.15. Plot of Average k_{obs} vs. [**7**]

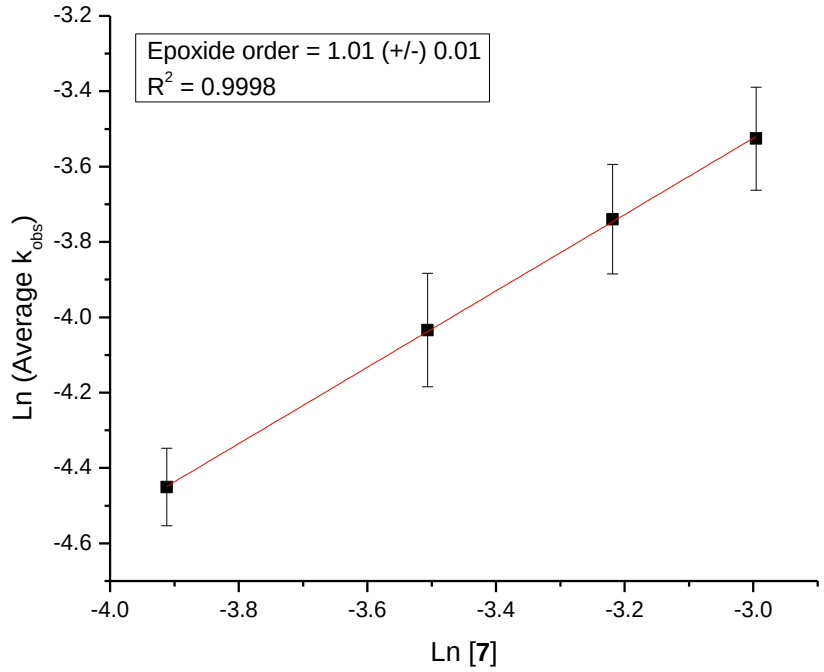

Figure 2.16. Plot of Ln (Average k_{obs}) Ln [**7**]

It was observed that in the absence of Coll*HCl, the decay plots fit better to a double exponential while in the presence of Coll*HCl, the plots fit better to a single exponential. As a result, the rate constants for opening the epoxide in the absence of Coll*HCl were 0.8 ± 0.1 $M^{-1}s^{-1}$ and 0.3 ± 0.1 $M^{-1}s^{-1}$ respectively. The rate constant obtained in the presence of Coll*HCl was 0.6 ± 0.1 $M^{-1}s^{-1}$. In the absence of Coll*HCl, it is known that titanocene(III) exists as a monomer and a dimer with the ratio of dimer to monomer being 1.5 and the dimer having a higher redox potential.[13] It was therefore hypothesized that in this system, both the open dimer and the monomer are involved in the epoxide opening process, which explains why the decay plots fit a double exponential. The dimer, due to its higher redox potential, reduced the epoxide faster than the monomer (Scheme 2.21).[45]

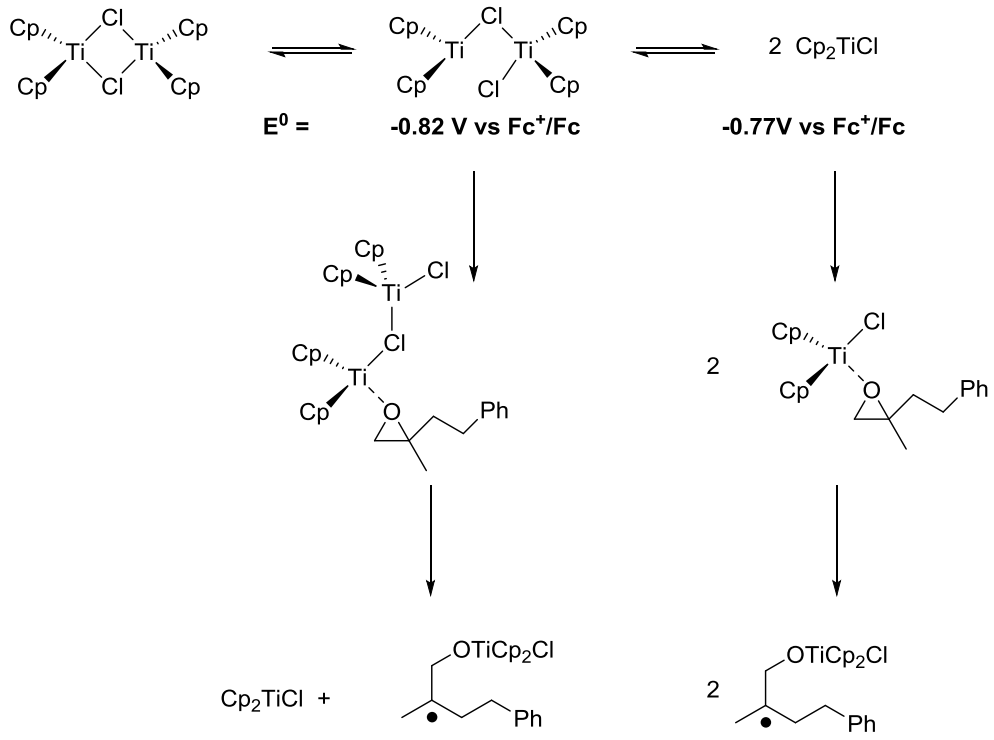

Scheme 2.21. Proposed mechanism for opening **7** in the absence of Coll*HCl

In the presence of Coll*HCl, only the supramolecular complex and the monomer could be detected and the dimer to monomer ratio was greatly reduced to <0.15. It was therefore posited that Coll*HCl disrupted the monomer dimer equilibrium by forming a supramolecular complex which is in equilibrium with the titanocene monomer and could be serving as the resting state for the active titanocene catalyst. Consequently, the titanocene catalyst in the monomer conformation reacts with the epoxide. This explains why in the epoxide opening experiment, the decay for the titanocene catalyst in the presence of Coll*HCl fits well to a single exponential equation (Scheme 2.22).[45]

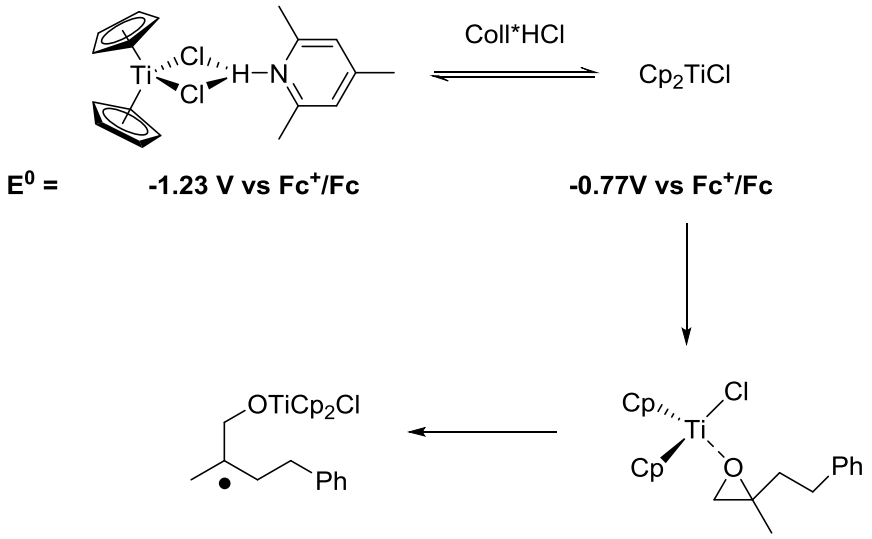

Scheme 2.22. Proposed mechanism for opening **7** in the presence of Coll*HCl

With these findings, the catalytic cycle proposed for the radical arylation of **1** was revised to incorporate the supramolecular complex in equilibrium with the active catalyst. This proposed revision offers insight as to why the catalyst remains stable in the presence of catalytic amounts of Coll*HCl.

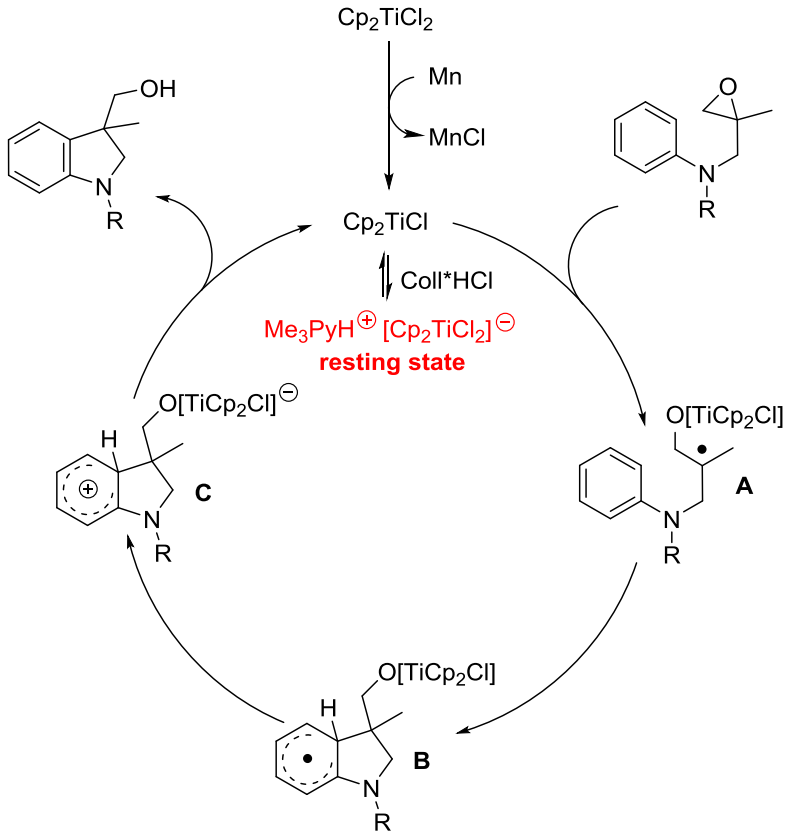

Scheme 2.23. Catalytic cycle for the arylation of **1** to **2** showing resting state of catalyst

2.3.5 Rate orders

The main components of this reaction are titanocene dichloride (Cp_2TiCl_2), epoxide (**1**), Coll*HCl (**4**), and Mn. Due to the sparingly soluble nature of Coll*HCl and Mn, it was not possible to determine their orders in the system. This leaves us with the titanocene dichloride and the epoxide (Scheme 2.24). The initial rates method was used to determine the orders of Cp_2TiCl_2 and **1**. With this method, reactions were carried out at synthetically relevant conditions and the reaction rate was determined by monitoring the initial decay or growth of product while still linear. A graph of change in concentration versus time was then plotted to obtain the initial rate of the reaction as shown in figure 2.17.

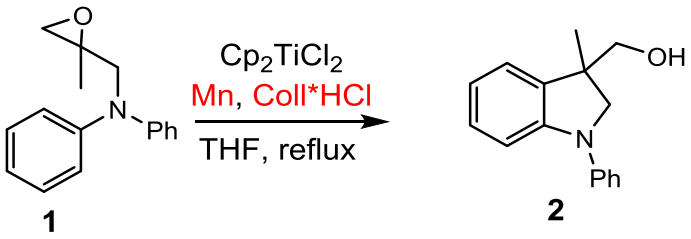

Rate = $k_{apparent}$ $[Cp_2TiCl_2]^x$ $[\mathbf{1}]^y$

Scheme 2.24. Rate expression dependent on only Cp_2TiCl_2 and epoxide

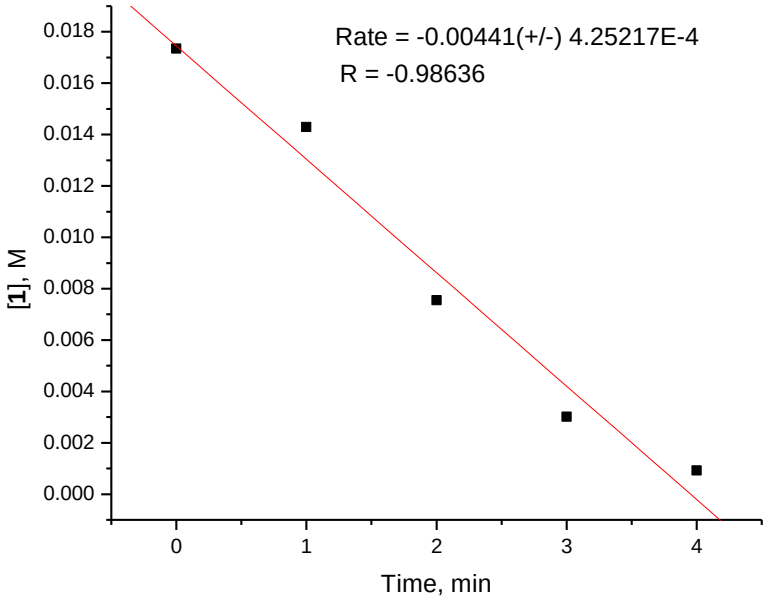

Figure 2.17. Sample initial rate plot

2.3.5.1 Order of epoxide (1)

To determine the order of the epoxide, a series of experiments were carried out with varying concentrations of epoxide while the other components were kept constant (Scheme 2.25). A plot of initial rates versus epoxide concentration was generated and with this information, the natural log of the rate versus the natural log of concentration of

epoxide was plotted. The slope of the obtained line was about 1, which is the order of epoxide (Figure 2.18).[45]

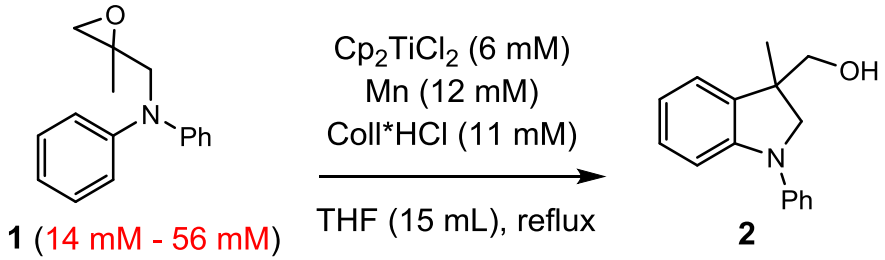

Scheme 2.25. Reaction conditions for order of epoxide (**1**)

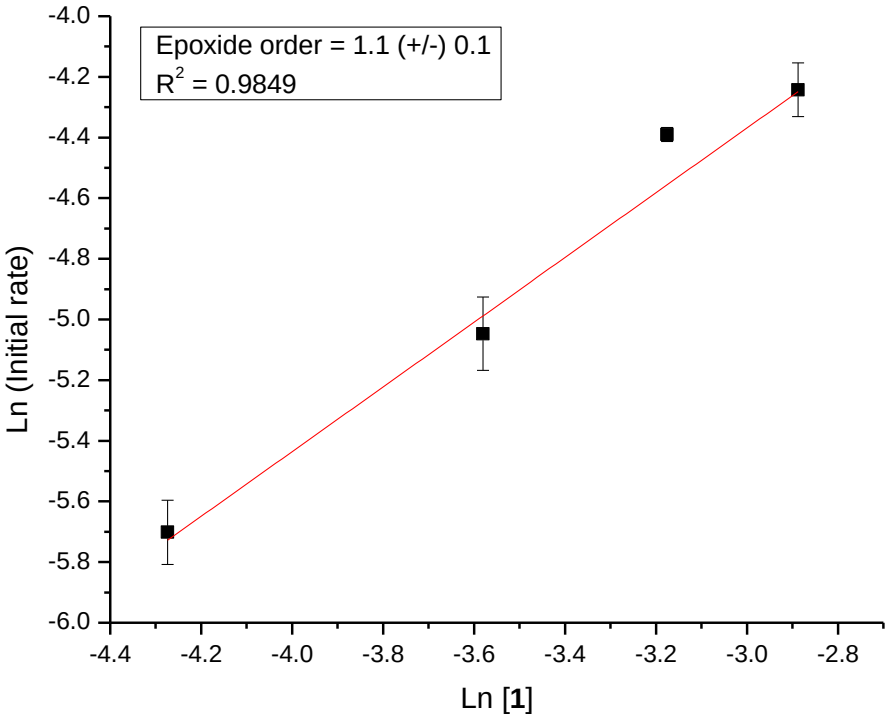

Figure 2.18. Plot of Ln(initial rate) vs. Ln[**1**]

2.3.5.2 Order of Cp_2TiCl_2

To determine the order of Cp_2TiCl_2, the concentrations of the other components in the reaction were kept constant while the concentration of Cp_2TiCl_2 was varied (Scheme 2.26). The order was calculated to be approximately 1 for Cp_2TiCl_2 (Figure 2.19).[45]

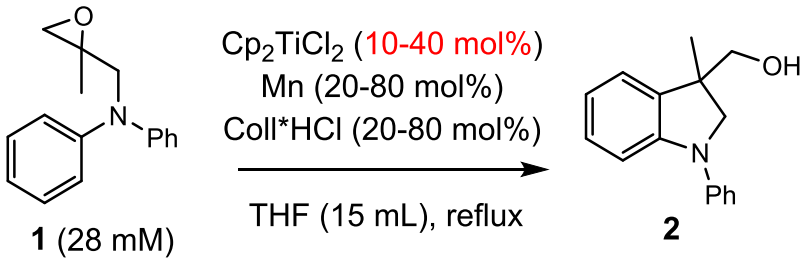

Scheme 2.26. Reaction conditions for order of Cp_2TiCl_2

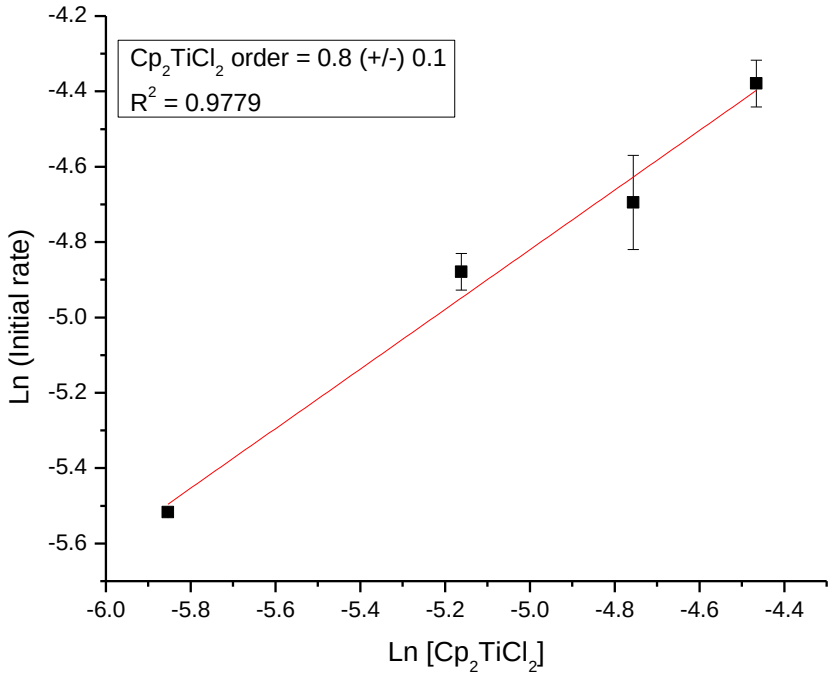

Figure 2.19. Plot of Ln(initial rate) vs. Ln[Cp_2TiCl_2]

2.3.6 Turnover-limiting step

There are four possible turnover limiting steps from the proposed mechanism shown in scheme 2.27: the epoxide opening step to form the β-titanoxy radical **A**, the radical addition to arene to form the radical σ-complex **B**, the back-electron transfer to the catalyst to form **C,** and the rearomatization with concomitant proton transfer and heterolytic cleavage to release product and close the cycle.

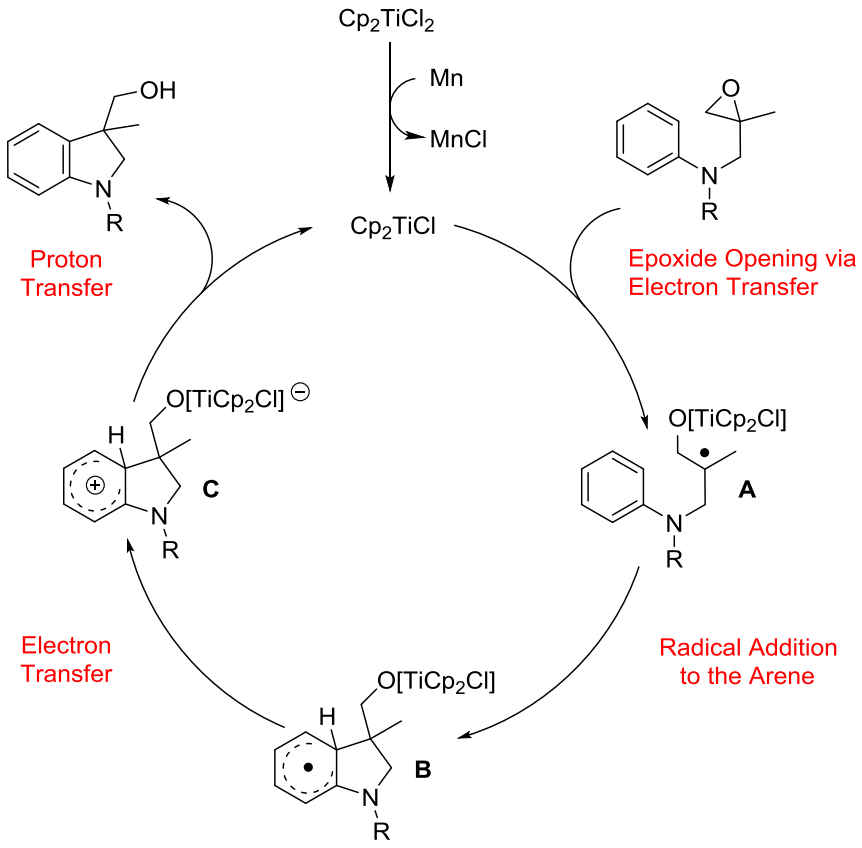

Scheme 2.27. Potential turnover-limiting steps in the radical arylation of **1** to **2**

2.3.6.1 Effects of electronics of catalyst on the radical arylation of epoxide (1)

Gansäuer and coworkers have shown that reaction rates and product yield can be manipulated by varying the electronics of the titanocene complex.[9] Mechanistic studies were therefore performed with Cp_2TiCl_2 (**3**), $(C_5H_4Me)_2TiCl_2$ (**5**), and $(C_5H_4Cl)_2TiCl_2$ (**6**)

with the last two being electron donating and electron withdrawing titanocene complexes respectively. The redox potentials of these titanocene complexes were determined by Gansäuer and coworkers and are summarized in the table 2.4.[45,49,50,52–54]

Table 2.4. Redox potentials of the titanocene(III) species generated during the CV of Mn- $C_5H_4X)_2TiCl_2$

[Ti]	E^0_1 [V][a]	E^0_2 [V][a]	E^0_3 [V][a]	E^0_4 [V][a]
Cp_2TiCl_2 (**3**)	-1.23	–0.83	-0.77	-0.77
$(C_5H_4Me)_2TiCl_2$ (**5**)	–1.31	–0.92	–0.95	–0.83
$(C_5H_4Cl)_2TiCl_2$ (**6**)	–1.08	–0.49	–0.58	–0.37

[a] Potentials are measured in V vs Fc^+/Fc and can be converted to SCE by adding 0.52 V. Catalysts were activated by reducing precatalyst with Mn. E^0_1 = Oxidation potential of $[(C_5H_4R)_2TiCl_2]^-$ in the presence of Coll*HCl (**4**). E^0_2 = Oxidation potential of dimer $[(C_5H_4R)_2TiCl]_2$ in the absence of Coll*HCl (**4**). E^0_3 = Oxidation potential of monomer $[(C_5H_4X)_2TiCl]$ in the presence of Coll*HCl (**4**). E^0_4 = Oxidation potential of monomer $[(C_5H_4X)_2TiCl]$ in the absence of Coll*HCl (**4**).

There are two steps where the reaction rate could be impacted by the electronics of the catalyst; the epoxide opening step and the back-electron transfer step (Scheme 2.27). The radical arylation of **1** to **2** was therefore performed with Mn-**3**, Mn-**5**, and Mn-**6** (Scheme 2.28) and the progress of the reaction was monitored by *in situ* IR. The rationale behind these experiments was that if the initial epoxide opening step was turnover-limiting, the entire reaction will occur at a faster rate with an electron rich titanocene complex. Conversely, if the back-electron transfer from the radical σ-complex was turnover-limiting, the entire reaction will occur at a faster rate with an electron deficient titanocene complex.

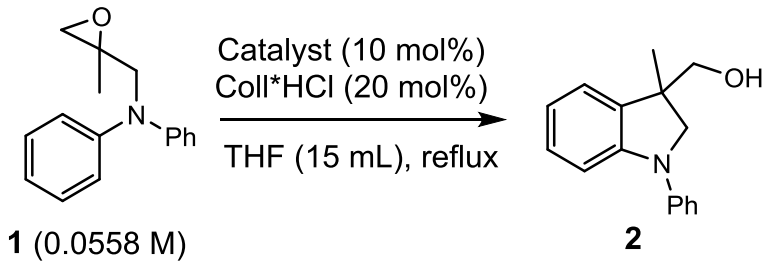

Scheme 2.28. The radical arylation of **1** to **2** with Mn-**3**, Mn-**5**, and Mn-**6**

As shown in figure 2.20, the reaction was slowest with the electron rich titanocene complex (Mn-**5**), while the reaction was fastest with the electron deficient titanocene complex (Mn-**6**). The decays were fitted to single exponential decay curve and the observed rates (k_{obs}) are summarized in table 2.5. It was evident that the back-electron transfer was impacting the entire reaction and could potentially be the turnover-limiting step.[45]

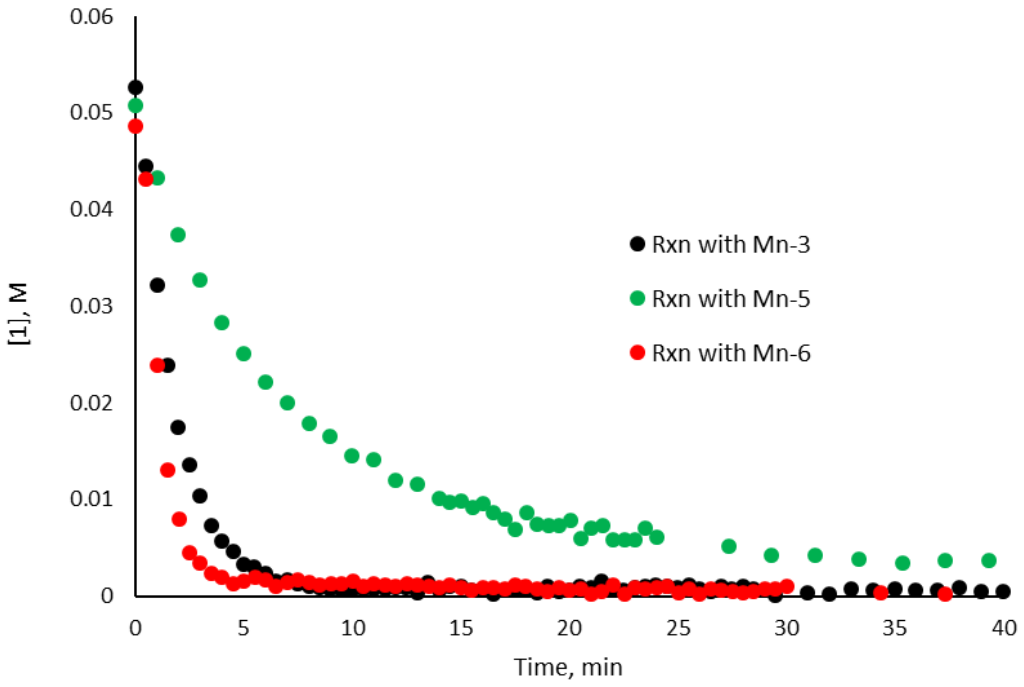

Figure 2.20. Decay plots for the arylation of **1** to **2** with Mn-**3**, Mn-**5**, and Mn-**6** (See scheme 2.28 for reaction conditions)

Table 2.5. k_{obs} for the arylation of **1** to **2** with Mn-**3**, Mn-**5**, and Mn-**6** (See scheme 2.28 for reaction conditions)

Catalyst	k_{obs}, min^{-1}
Cp_2TiCl_2 (**3**)	0.57 ± 0.02
$(C_5H_4Me)_2TiCl_2$ (**5**)	0.26 ± 0.01
$(C_5H_4Cl)_2TiCl_2$ (**6**)	0.85 ± 0.13

2.3.6.2 Epoxide opening experiment with Mn-3, Mn-5, and Mn-6

To confirm whether the rate of the radical arylation of **1** to **2** was solely based on the electronics of the titanocene complex and not the epoxide or any other contributing factor, an experiment was carried out where only epoxide opening was studied with the same titanocene complexes. In this experiment, the most electron rich titanocene complex should open the epoxide a lot faster while the most Lewis acidic titanocene complex should have the slowest rate of epoxide opening. Titanocene mediated epoxide opening experiments were done with 2-methyl-2-phenethyloxirane (**7**) as the model epoxide both with and without Coll*HCl (Scheme 2.29).

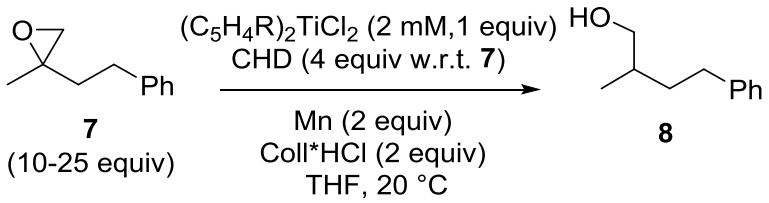

Scheme 2.29. Epoxide opening experiment with Mn-**3**, Mn-**5**, and Mn-**6**

The epoxide opening experiment (Scheme 2.29) was done under pseudo first order conditions with a SpectroVis, which is a portable visible to near-IR spectrophotometer. This was done by monitoring the loss of the Ti(III) band for each of the manganese reduced titanocene complexes at 800 nm as described by Daasbjerg and co-workers.[13] The decay plots were obtained and fitted to the appropriate exponential

equation to obtain the observed rates (k_{obs}) and the rate constants of the reactions which are summarized in table 2.6.

Table 2.6. Rate constants for opening **7** and observed rate for arylation of **1**

Catalyst	k_1, $M^{-1}s^{-1}$	k_2, $M^{-1}s^{-1}$	k, $M^{-1}s^{-1}$	k_{obs}, min^{-1}
Cp_2TiCl_2 (**3**)	0.8 ± 0.1	0.3 ± 0.1	0.6 ± 0.1[a]	0.57 ± 0.02[b]
$(C_5H_4Me)_2TiCl_2$ (**5**)	1.8 ± 0.3	0.6 ± 0.1	1.1 ± 0.2[a]	0.26 ± 0.01[b]
$(C_5H_4Cl)_2TiCl_2$ (**6**)	0.5 ± 0.1	0.13 ± 0.04	0.4 ± 0.1[a]	0.85 ± 0.13[b]

[a] Rate constant for opening 7 in in the presence of Coll*HCl (See scheme 2.29 for reaction details); [b] k_{obs} for the arylation of **1** to **2** (See scheme 2.28 for reaction conditions)

As expected, Mn-**6**, which is the most Lewis acidic, is the slowest at opening the epoxide (**7**) whereas the electron rich Mn-**5** is fastest at opening **7** both in the presence and absence of **4**, further suggesting that the radical arylation of **1** to **2** was influenced by the electronics of the titanocene complex and that the back-electron transfer was potentially turnover-limiting. Moreover, epoxide opening is substantially faster with reactions progressing over the range of several seconds at room temperature whereas the arylation takes place over the timeframe of several minutes in refluxing THF. Overall, this data is consistent with the back-electron transfer to the metal being turn-over-limiting and not the epoxide opening step. It should also be noted that in the absence of **4**, both the monomer and dimer of the Ti(III) complexes were involved in the epoxide opening process with the dimer being the most reactive (Table 2.6). However, in the presence of **4**, only the monomer was involved in the epoxide opening process for all three titanocene complexes studied (Table 2.6).[13,45,49,51–53]

The equilibrium constants derived from CV experiments showed that the monomer increased in the presence of **4** (Table 2.7). As a result, the rate constants of

epoxide opening by the monomers are slightly higher (by a factor of 2-3) in the presence of Coll*HCl (Table 2.6). The rate constants were obtained from total [Ti(III)] but since they are in the presence of **4**, *k* contains an equilibrium term for the complex of the titanocenes with Coll*HCl (**4**).[8]

Table 2.7. Dimer/monomer-ratio in 2 mM Mn-**3**, Mn-**5**, and Mn-**6** solutions in THF in the presence and absence of Coll*HCl

[Ti]	Dimer/Monomer [a]	Dimer/Monomer [b]	K (M^{-1}) [a]	K (M^{-1}) [b]
Cp_2TiCl_2 (**3**)	1.5	<0.15	3000	<100
$(C_5H_4CH_3)_2TiCl_2$ (**5**)	0.8	<0.15	1000	<100
$(C_5H_4Cl)_2TiCl_2$ (**6**)	0.4	<0.15	375	<100

[a] Values obtained in the absence of Coll*HCl. [b] Values obtained in the presence of Coll*HCl

2.3.6.3 Radical addition to arene

There are a limited number of studies done to determine the absolute rate constants of radical additions to arenes. These were mostly carried out for studying the Minisci reaction.[55,56] It was found that the butyl radical adds to benzene with a rate constant of about 4 x 10^2 M^{-1} s^{-1} at 79 °C.[55] The rate constants for radical addition to substituted anilines have been studied computationally by Gansäuer and Grimme and the values obtained ranged between 4 x 10^2 – 4 x 10^3 s^{-1},[57] which is about three orders of magnitude faster than the rate for epoxide opening and several orders of magnitude faster than the radical arylation process.[45] The radical additions were calculated to be exothermic by about 10 kcal mol^{-1}.[57]

2.3.6.4 Proton transfer

Finally, to explore the possibility of proton transfer to the alkoxide as being a potential turnover-limiting step, further kinetic studies were carried out with **1** containing

perdeuterated phenyl groups. If this step is turnover-limiting a substantial kinetic isotope effect would be expected. The k_H/k_D value obtained for this reaction is 1.1 ± 0.1 (Figure 2.21).[58] This finding strongly suggests that the final proton transfer leading to rearomatization is not turnover-limiting. Based on our mechanistic studies we were strongly convinced that the back-electron transfer was turnover-limiting for the radical arylation of the epoxide (**1**).[45]

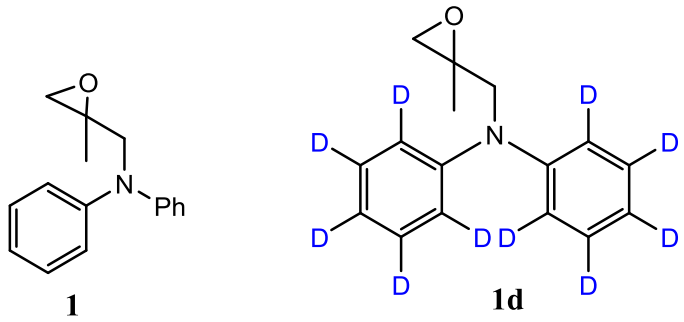
O
N
Ph
D
D
D

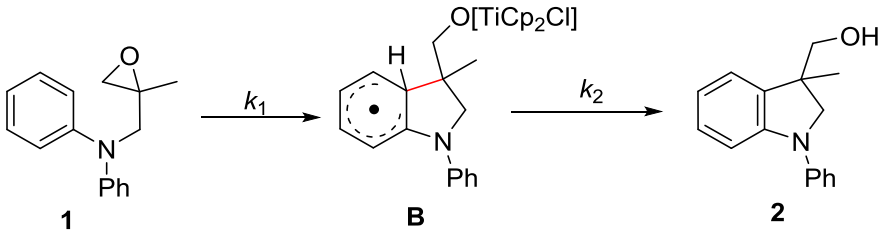

Scheme 2.30. Intermediate **B** in rate expression

At the start of the reaction [**1**] = [**1**]$_0$ (2.1), [**B**] = 0 (2.2), [**2**] = 0 (2.3)

At any point during the reaction process, the concentration of the epoxide, intermediate and product are equal to [**1**]$_0$.

$$[\mathbf{1}]_0 = [\mathbf{1}] + [\mathrm{B}] + [\mathbf{2}] \quad (2.4)$$

The rate expression for each step of the reaction is shown as follows:

$$\frac{d[\mathbf{1}]}{dt} = -k_1[\mathbf{1}] \quad (2.5)$$

$$\frac{d[\mathbf{B}]}{dt} = k_1[\mathbf{1}] - k_2[\mathbf{B}] \quad (2.6)$$

$$\frac{d[\mathbf{2}]}{dt} = k_2[\mathbf{B}] \quad (2.7)$$

Based on calculations performed in the late 1800s by Harcourt and Esson, the equations for the starting material (equation 2.8), intermediate (equation 2.10) and product (equation 2.11) were obtained via a series of integrations, differential equations, and substitution steps.[59–62]

Integration of equation (2.5)

$$[\mathbf{1}] = [\mathbf{1}]_0 e^{-k_1 t} \quad (2.8)$$

Sub [**1**] into equation (2.6)

$$\frac{d[\mathrm{B}]}{dt} = k_1[\mathbf{1}]_0 e^{-k_1 t} - k_2[\mathrm{B}] \quad (2.9)$$

Integration of equation (2.6)

$$[\mathrm{B}] = [\mathbf{1}]_0 \frac{k_1}{k_2 - k_1} (e^{-k_1 t} - e^{-k_2 t}) \quad (2.10)$$

Since

$$[\mathbf{1}]_0 = [\mathbf{1}] + [\mathrm{B}] + [\mathbf{2}]$$

Then

$$[\mathbf{2}] = [\mathbf{1}]_0 - [\mathbf{1}] - [\mathrm{B}]$$

$$[\mathbf{2}] = \frac{[\mathbf{1}]_0}{k_2 - k_1} [k_2(1 - e^{-k_1 t}) - k_1(1 - e^{-k_2 t})] \quad (2.11)$$

The kinetic equations shown above are obeyed frequently by nuclides undergoing radioactive decay.[63] Other examples are the thermal isomerizations of 1,1-dicyclopropylene and 1-cyclopropylcyclopentene.[64] For this system, the turnover-limiting step is the second step. As a result, the rate of reaction is dependent on k_2 and this simplifies the intermediate (2.10) and product (2.11) expressions to equations 2.12 and 2.13 respectively. The rate of the reaction is expressed in terms of k_2, k_1 and the initial epoxide concentration (equation 2.14).

Since $k_1 >> k_2$

$$\text{Rate} = \frac{d[\mathbf{2}]}{dt} = k_2[\mathrm{B}]$$

$$[\mathrm{B}] = (e^{-k_2 t} - e^{-k_1 t}) [\mathbf{1}]_0 \quad (2.12)$$

$$[\mathbf{2}] = (1 - e^{-k_2 t}) [\mathbf{1}]_0 \quad (2.13)$$

$$\text{Rate} = k_2(e^{-k_2 t} - e^{-k_1 t}) [\mathbf{1}]_0 \quad (2.14)$$

Since this constant expression is equal to an apparent constant (k_{app}) times the concentration of catalyst, the rate expression is simplified to equation 2.16, which agrees with the rate expression derived from the initial rates method.

$$k_2(e^{-k_2t} - e^{-k_1t}) = k_{app}[Cp_2TiCl_2] \quad (2.15)$$

$$\text{Rate} = k_{app}[Cp_2TiCl_2][\mathbf{1}]_0 \quad (2.16)$$

2.3.8 Homolytic vs. heterogenous cleavage of Ti-O bond

Gansäuer and co-workers have hypothesized the possibility of Ti-O homolysis in titanocene(III) catalysed tetrahydrofuran synthesis (Scheme 2.31).[22] In considering the radical arylation of **1** to **2** carefully, an alternative progression of events, Ti-O bond homolysis in the intermediate radical σ-complex and H-atom transfer to the O-centered radical (Scheme 2.32), might also be possible. Previous work by Waymouth and co-workers has shown that titanium oxygen bonds derived from TEMPO can be cleaved under the reaction conditions described herein, but more stable precursors derived from alkoxides could not.[65]

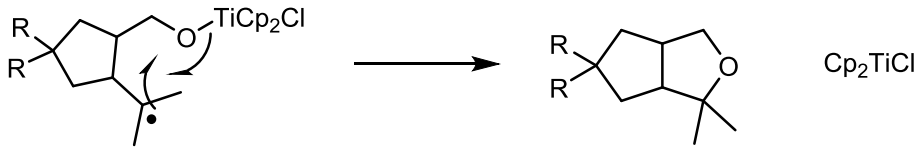

Scheme 2.31. Ti-O homolysis in THF synthesis

To determine whether homolytic cleavage of the Ti-O bond was possible under the conditions employed in this study, titanocene ethoxy chloride [Cp_2Ti(IV)Cl(OEt)] was prepared[66] and subjected to reaction conditions in the presence and absence of Coll*HCl. If Ti-O homolysis is occurring between the titanium alkoxide bond, then the active catalyst will be generated when [Cp_2Ti(IV)Cl(OEt)] is subjected to our reaction conditions. Previously, we found that the IR band of the C-H wag of the cyclopentadienyl ligand is sensitive to the oxidation state of Ti.

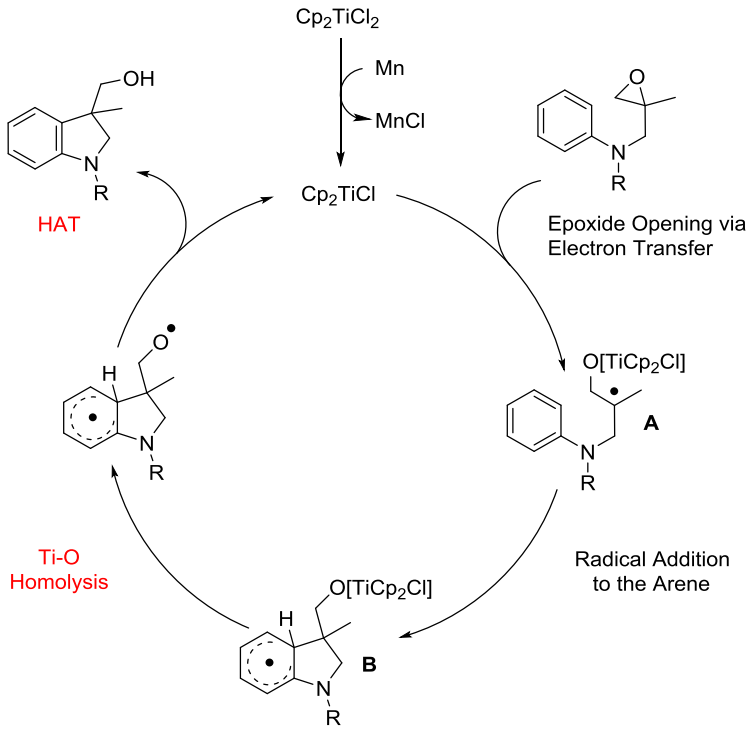

Scheme 2.32. Possible Ti-O homolysis in arylation of **1** to **2**

Therefore, the two different oxidation states of Ti can be distinguished experimentally. *In situ* monitoring of the reaction by IR spectroscopy enabled observation of the active catalyst Ti(III) at 798-800 cm^{-1}, the precatalyst Ti(IV) at 820-825cm^{-1}, and growth of the product at 1386 cm^{-1} (Figure 2.22 & Figure 2.23). When epoxide is added to the reaction mixture, the initial decay of [Ti(III)] is observed and, as the reaction progresses, the regeneration of [Ti(III)] can be followed (Figure 2.22). It is important to note that the regeneration of Ti(III) is concomitant with conversion of **1** to **2**, but its formation is not instantaneous (Figure 2.23).[45]

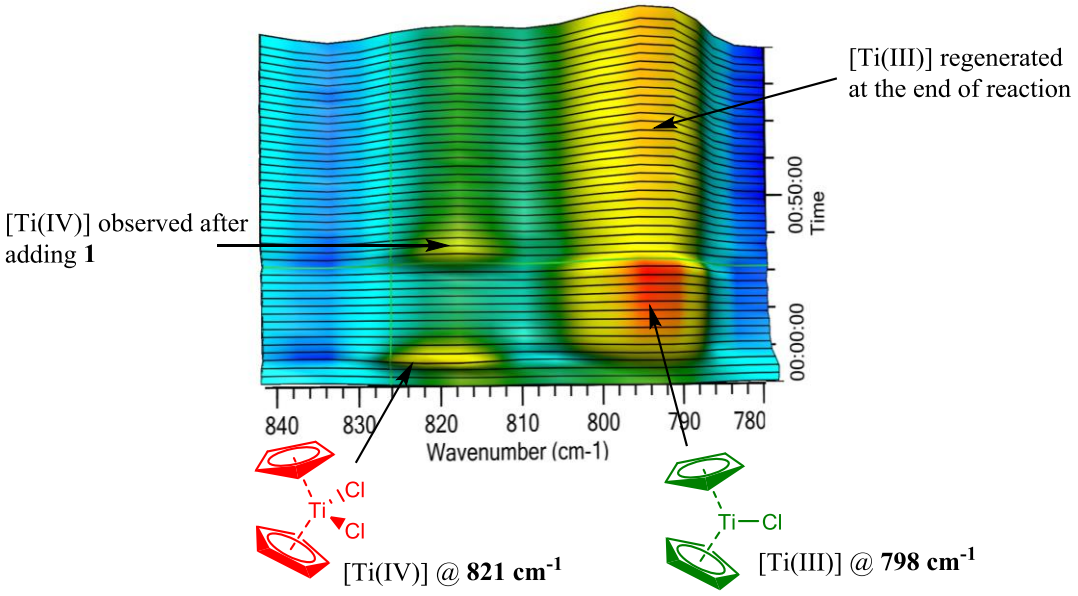

Figure 2.22. Monitoring Ti(IV)/(III) by ReactIR

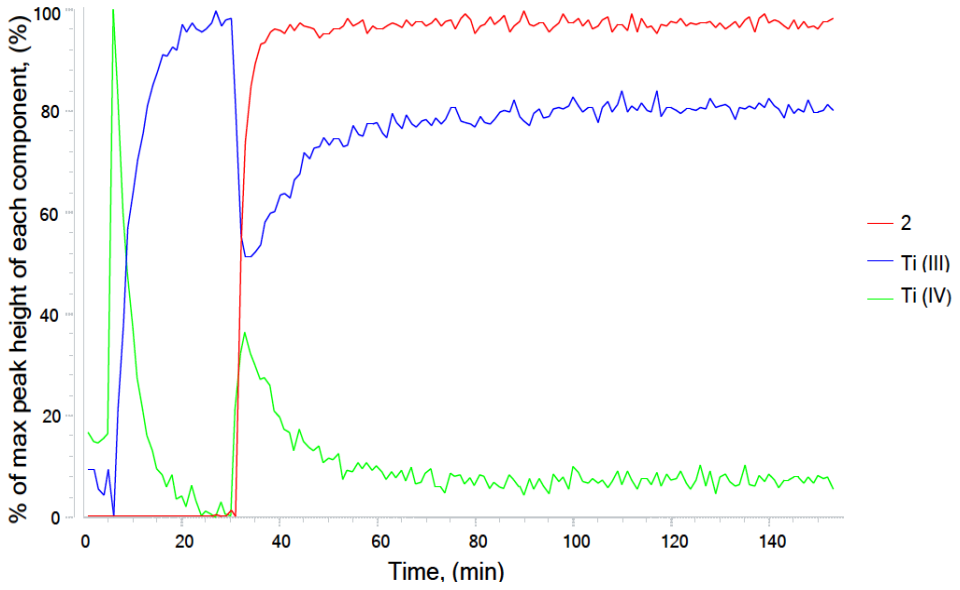

Figure 2.23. Conversion of **1** to **2** at 1386 cm^{-1} and regeneration of [Ti(III)] in THF at 60 °C followed by in-situ IR-monitoring. [**1**] = 28 mM; [**3**] = 5.7 mM; [**4**] = 11.5 mM. The C-H wag of the Cp ligand in the Ti(IV) precatalyst occurs at 821 cm^{-1} and for the Ti(III) catalyst occurs at 798 cm^{-1}. The loss of peak height in [Ti(III)] is a consequence of dilution upon addition of a solution of **1** to initiate the reaction**.**

After refluxing for up to 3 hours, no homolytic cleavage was observed (Scheme 2.33). This is consistent with Waymouth's observations that $Cp_2Ti(IV)$-O bonds derived from alkoxides are strong (90 $kcalmol^{-1}$)[65,67] and unlikely to homolytically cleave under our reaction conditions. One interesting feature that was determined from this study was the change in the intermediate formed upon the addition of Coll*HCl to $Cp_2TiCl(OEt)$. The C-H wag of this compound is observed at 808 cm^{-1}. Upon addition of Coll*HCl, there was an immediate shift to 820 cm^{-1}, an observation consistent with the formation of Cp_2TiCl_2. This finding shows that protonation and subsequent cleavage of the Ti-O bond is a rapid process (Scheme 2.33).[45]

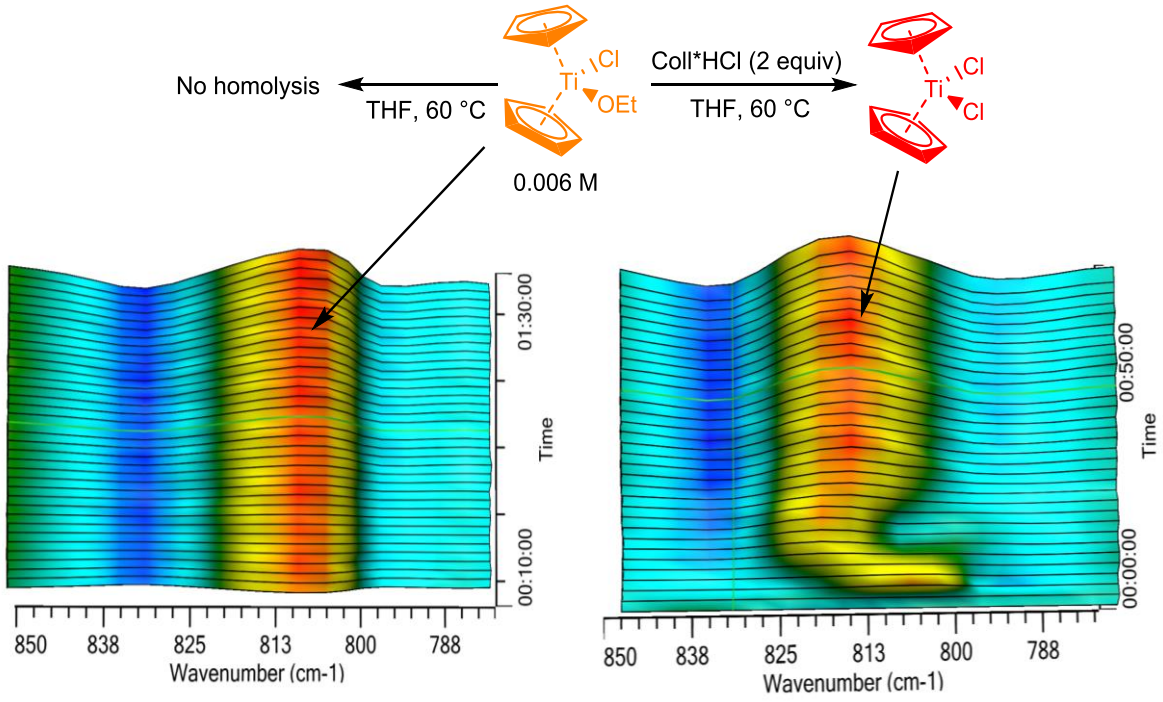

Scheme 2.33. Ti-O homolysis is an unlikely pathway for catalyst generation

2.3.9 Cationic intermediates before addition to the arene

To exclude the presence of cationic intermediates before addition to the arene in the arylation reaction and to provide experimental evidence for the rate of radical addition to anilines, Gansäuer and co-workers performed a series of experiments with **1** and **11** in the presence and absence of 1,4-cyclohexadiene and t-butyl acrylate.[68] These reagents have been used as radical traps in titanocene catalyzed epoxide openings.[69,70] The epoxide opening reactions however required excess amounts of Mn and Coll*HCl for complete conversion. As a result, Gansäuer and coworkers also subjected **1** and **11** to identical conditions without the radical traps to ensure comparability of the reactions. Their results are summarized in schemes 2.34 and 2.35.[45]

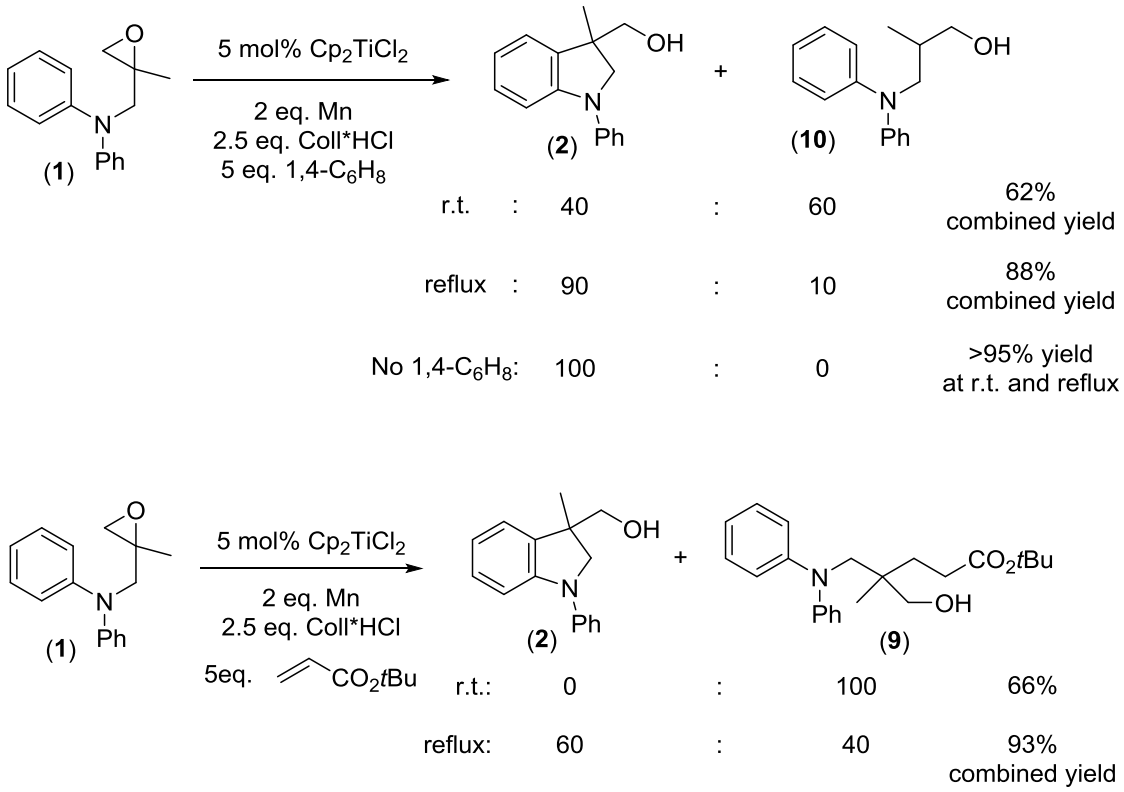

Scheme 2.34. Competition experiments with **1** between radical addition to the arene and radical trapping

Without CHD or acrylate, only **2** was formed in essentially quantitative yield (Scheme 2.34). Thus, excess amounts of Mn or Coll*HCl lead to essentially identical results as those obtained with catalytic amounts of Mn and Coll*HCl.[9] Therefore the conditions were ideally suited for the competition experiments.

At room temperature, only the acrylate addition product was detected and isolated. The entropically preferred intramolecular addition to the arene was the major product in refluxing THF (**2**:**9** = 60:40) (Scheme 2.34). It should be noted that the addition to the electron deficient acrylate is only possible for radicals and not for cations. Therefore, the generation of cationic intermediates through epoxide opening by Cp_2TiCl can be excluded. The experiments in the presence of CHD also confirmed the presence of radicals because **10** can only be formed through hydrogen atom abstraction by radical intermediates (Scheme 2.34). Based on their results, generation of cations from the epoxide-derived radical seemed highly unlikely, as no suitable oxidant was present in the reaction.[45]

The competition reactions of **11** with t-butyl acrylate and CHD are summarized in scheme 2.35. The use of excess amounts of Mn and **4** was of no consequence for the outcome of the arylation. Compared to the reactions of **1** (Scheme 2.34), it was posited that the radical arylation should be less competitive for **11** because of the methyl substituent on N.

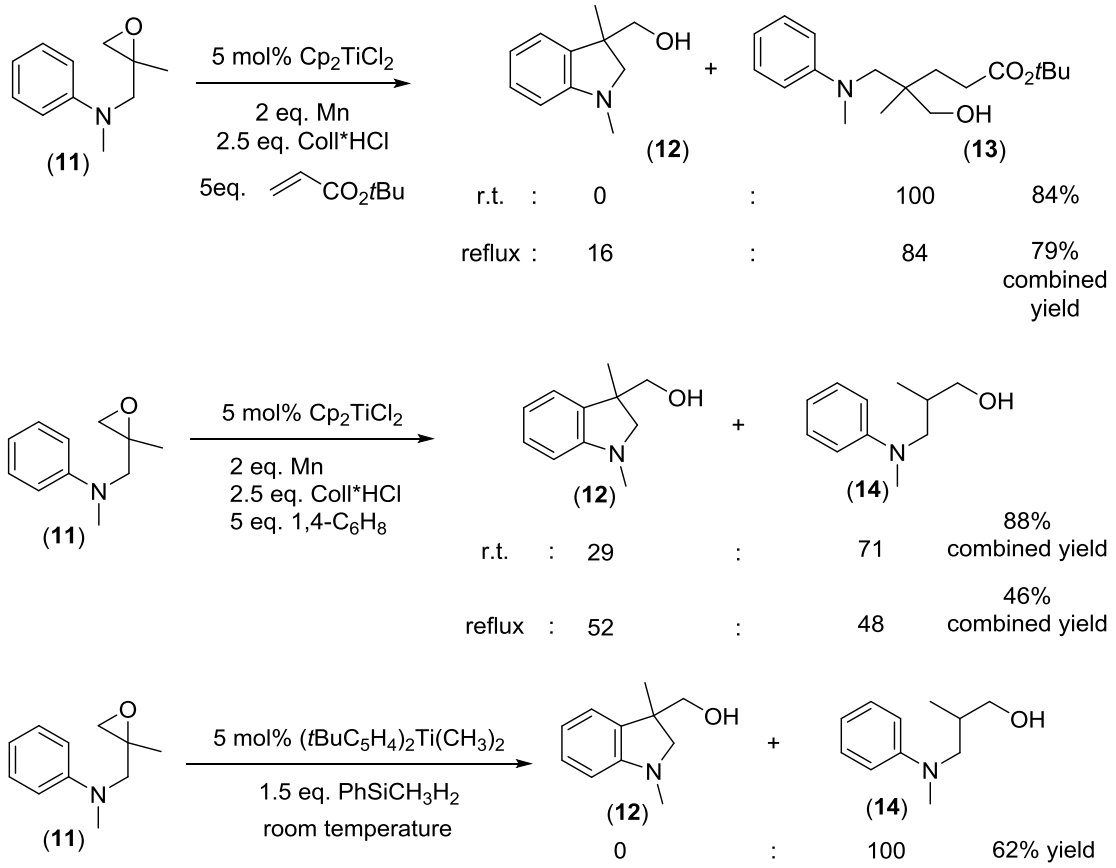

Scheme 2.35. Competition reactions with **11.**

This was indeed the case for the radical reduction and for the acrylate addition in refluxing THF (Scheme 2.35). They also showed that epoxide reduction via intramolecular HAT from a titanocene hydride generated with $PhSiCH_3H_2$ was much faster than arylation (Scheme 2.35).[71] For the same reasons previously discussed, the competition experiments with **11** demonstrate that cations are not formed under the reaction conditions.[45]

Finally, the competition between 5-exo cyclization and addition to the arene was investigated by Gansäuer with **15**. As highlighted in scheme 2.36, only **16** (47%), which is the product of the 5-exo cyclization, and **17** (28%) were isolated. The tetrahydrofuran

moiety of **17** was formed via a homolytic substitution at a Ti-O bond.[20,72,73] No radical arylation product was detected indicating that the 5-exo cyclization[74,75] is much faster than radical addition to the arene. Cationic intermediates would have resulted in the formation of piperidines via generation of tertiary carbenium ions via a 6-endo attack on the olefin.[45]

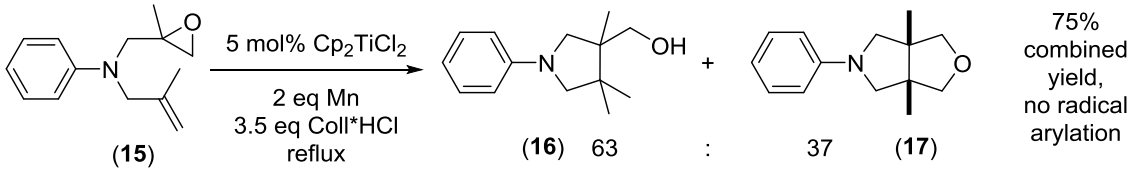

Scheme 2.36. Competition of radical arylation and 5-exo cyclization in THF

Based on their results, it was concluded that although the radical addition to anilines was substantially slower than 5-exo cyclizations or radical additions to acrylates, the addition could compete with the hydrogen atom abstraction of tertiary radicals from CHD. Their results suggest that the intramolecular addition of radicals to anilines has rate constants in the range of 10^2 – 10^4 s^{-1} at temperatures above 40 °C. Since the rate constants for epoxide opening is lower, radical addition can be ruled out as the potential turnover- limiting step as discussed earlier. The addition of radicals to aniline derivatives investigated here are likely as fast as titanocene catalyzed 4-exo and 3-exo cyclizations.[76–80] Moreover, the experiments exclude the formation of cationic intermediates under our reaction conditions.[45]

2.3.10 Computational study of the radical arylation of 1 to 2[45]

In collaboration with Stefan Grimme, a computational study on the radical arylation of **1** to **2** was carried out.[45]

2.3.10.1 Computational methods

All DFT calculations were performed with the TURBOMOLE 6.4 suite of programs.[81] The geometry optimizations were performed using the TPSS density functional[82] along with the polarized triple-zeta def2-TZVP basis set.[83] This choice avoids major basis set superposition errors (BSSE) without employing a counter-poise correction and gives theoretically consistent energies and structures.

Single point energies were obtained on the B3LYP,[84–86] PW6B95,[87] and M06-2X[88] level, together with the extended quadruple-zeta basis set def2-QZVP.[83] In all DFT calculations, the resolution-of-identity (RI) approximation for the Coulomb integrals[89] with matching default auxiliary basis sets[90] was applied. For integration of the exchange-correlation contribution the numerical quadrature grid m4 was employed. For all DFT calculations, the D3 dispersion correction scheme[91] applying the Becke-Johnson (BJ) damping[92–94] was used.

Computations of the harmonic vibrational frequencies were performed numerically using SNF version 2.2.1.[95] Thermal corrections from energy to free enthalpy were obtained via a coupled rigid-rotor-harmonic-oscillator approximation for each molecule in the gas phase.[96] For obtaining the vibrational entropy from the harmonic frequencies, low-lying modes below 100 cm^{-1} are treated within a rigid-rotor model to

reduce their error in the harmonic approximation; for additional details, see ref 94. The TPSS vibrational frequencies were used unscaled.

The COSMO-RS continuum solvation model[97,98] was used as implemented in COSMOtherm[99] to obtain all solvation free energies. Single point calculations employing the default BP86[100,101]/def-TZVP[102] level of theory were performed on the optimized gas phase geometries for each molecules. The solvation contribution was then added to the gas phase free energies.

2.3.10.2 Thermodynamics of radical arylation

To obtain the overall free energy of the radical arylation and the driving force of each step, we computationally investigated the Cp_2TiCl catalyzed reaction of **1** to **2** at 339 K. The overall reaction is highly exergonic at 339 K ($\Delta G_{overall}$ = -30.2 kcal mol^{-1}) because of the release of the epoxide's ring strain. Epoxide opening and radical addition together are exergonic by 7.6 kcal mol^{-1}. From these values the free energy of the rearomatization by electron and proton transfer, $\Delta G_{ET,PT}$, can be calculated as -22.6 kcal mol^{-1} (Scheme 2.37).

The calculations on the ET step gave largely varying results depending on the functionals employed. The discrepancies are a result of the inaccuracies in describing the electron transfer from the highly delocalized SOMO of the radical σ-complex to the localized d-orbital of titanium due to the so called self-interaction error in most contemporary functionals. Unfortunately, this implies that the intramolecular PT step can also not be treated computationally.[45] Nevertheless, the energy of the PT step can be estimated from the intermolecular model reaction shown in scheme 2.38.

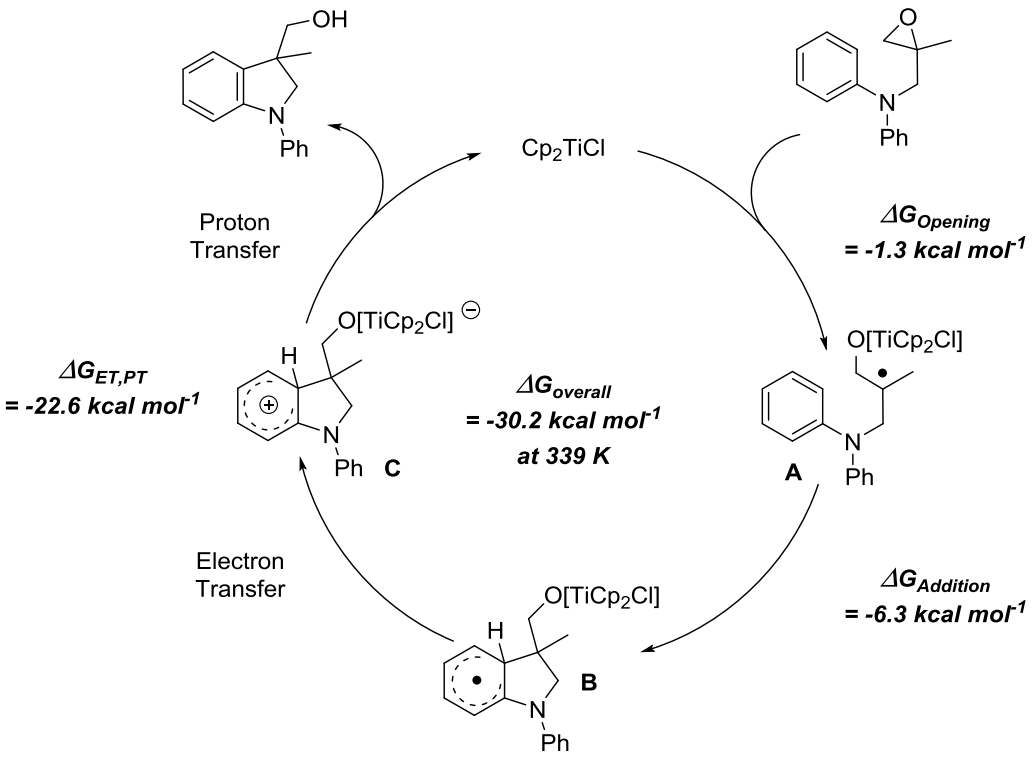

Scheme 2.37. Thermodynamics of the Cp_2TiCl catalyzed reaction of **1** to **2** at 339 K

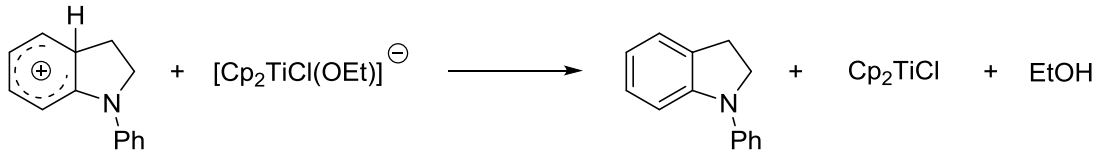

Method:	ΔG/ kcal mol^{-1}:
TPSS-D3/def2-TZVP	-41.6
B3LYP-D3/def2QZVP	-46.7

Scheme 2.38. Thermodynamics of the Cp_2TiCl catalyzed reaction of **1** to **2** at 339 K.

Based on these results, a value of -40 to -45 kcal mol^{-1} for ΔG_{PT} of the catalytic cycle (Scheme 2.37) can be assumed. ΔG_{ET} shown in Scheme 2.37 can then be estimated to be in the range of +17 - +22 kcal mol^{-1}. In agreement with the conclusion from the synthetic and kinetic studies, the computational analysis is consistent with a turnover-limiting ET step.

2.3.10.3 Mechanistic alternatives

As outlined above, the homolysis of the Ti-O bond in **B** (Scheme 2.32) is a potential alternative to rearomatization. To provide further evidence in addition to the experiment, the BDEs of the simple model titanocene complexes (Scheme 2.39) were calculated. The results demonstrate that the Ti-O bond in titanocene(IV) alkoxides is too strong for a homolytic cleavage at 60 °C, which is in agreement with the kinetic study. Therefore, the mechanism for rearomatization depicted in scheme 2.32 seems rather unlikely. In addition, the low BDE for the TEMPO derivative agrees with a previous study and highlights the quality of our calculations.

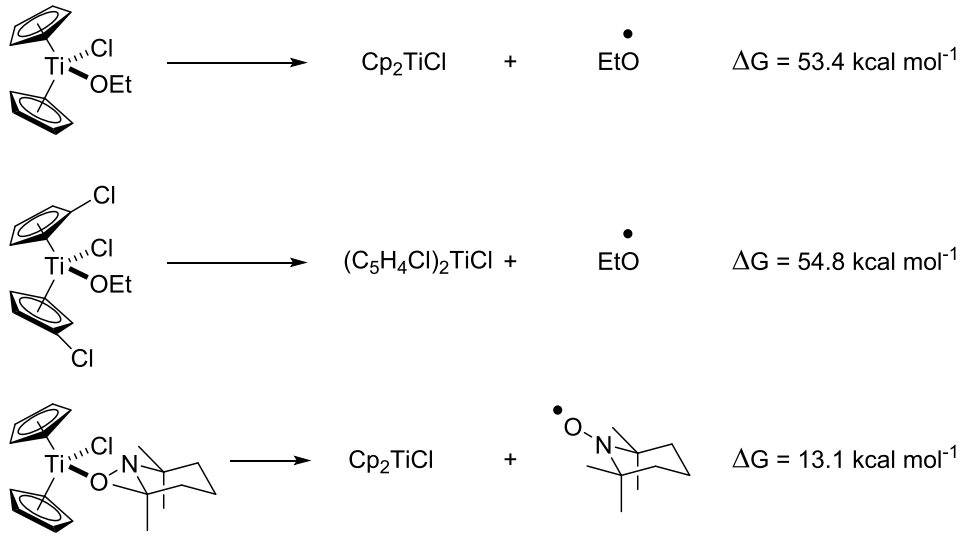

Scheme 2.39. Investigation of the BDE of Ti-O bonds at 339 K

Finally, a direct aryl titanation from radical **B** may also seem a mechanistic possibility. To this end the reactions of $Cp_2TiCl(OEt)$ with benzene and dimethyl aniline were investigated computationally as models (Scheme 2.40). The calculations indicate

that the aryl titanation is an unfavorable process. Certainly, it should not be able to compete with an intramolecular radical addition.

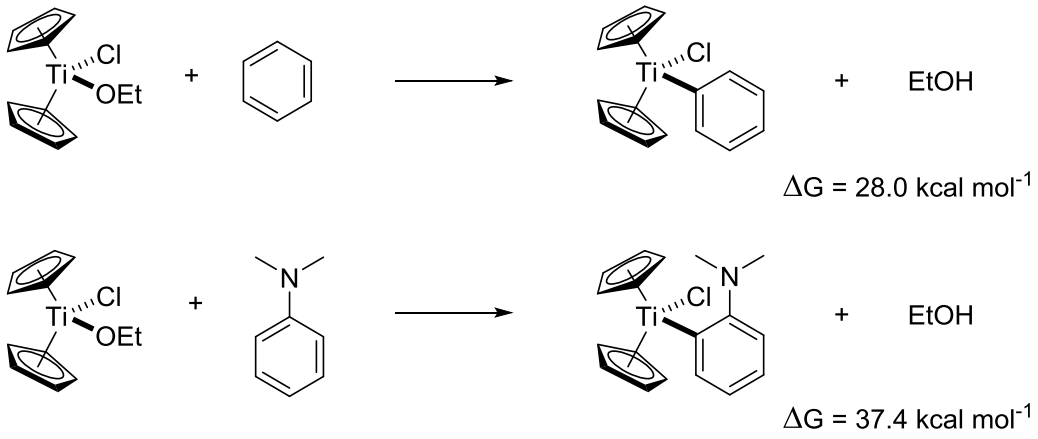

Scheme 2.40. Thermodynamics of aryl titanations at 339 K

2.3.11 Revised mechanism

Overall, the mechanistic studies (synthetic, kinetic, and computational studies) presented above in concert with previous work enables clarification of several key steps of the mechanism as shown in the catalytic cycle (Scheme 2.41). Reduction of Cp_2TiCl_2 leads to the formation of a monomer-dimer equilibrium of the low-valent titanocene. The presence of Coll*HCl disrupts the monomer-dimer equilibrium through the formation of an equilibrium mixture of monomeric titanocene and a complex between Coll*HCl and the titanocene which we propose to be the resting state. After radical generation through reductive electron transfer the radical σ-complex **B** is generated by intramolecular radical addition to the aniline. The intramolecular back-electron transfer from **B** to the pendant Ti(IV) leads to **C**, which is the turnover-limiting step. Proton transfer leads to product formation and regeneration of the active catalyst.[45]

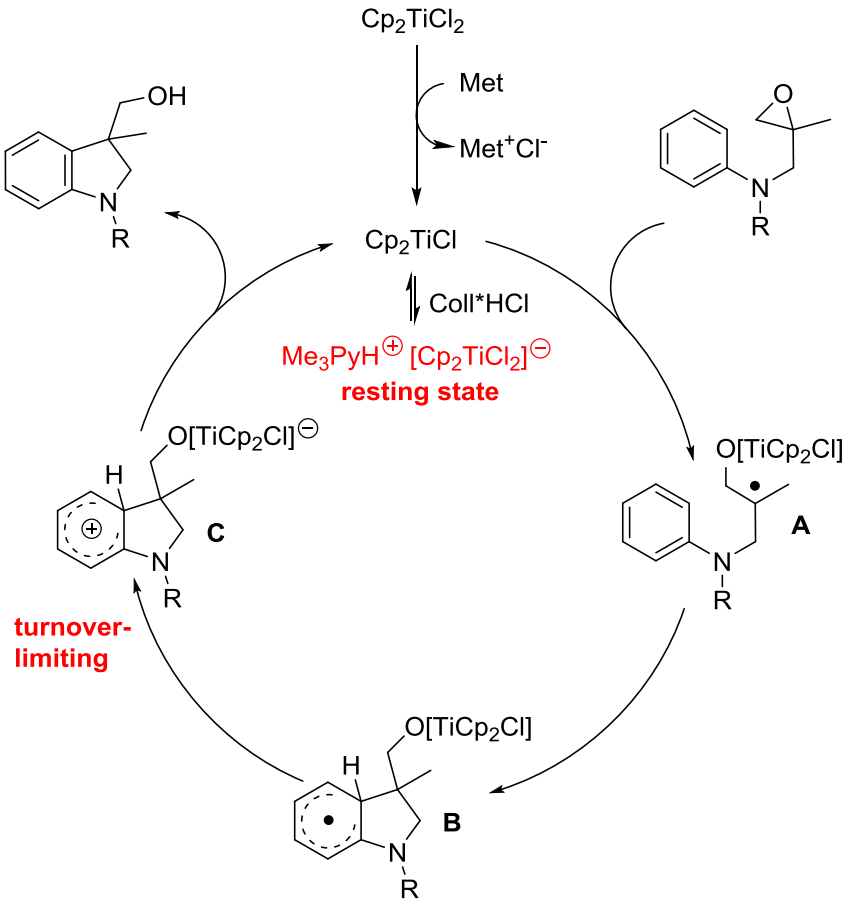

Scheme 2.41. Mechanism of the titanocene-catalyzed arylation of epoxide-derived radicals in the presence of Coll*HCl

2.3.12 Design of efficient systems based on insights from mechanistic studies

Since the oxidation of **B** is turn-over limiting, the use of titanocenes with electron withdrawing ligands, such as $(C_5H_4Cl)_2TiCl_2$ (**6**) (Table 2.8),[51] is essential for efficient reactions of electron deficient anilines,[9] such as carbamate protected substrates. Carbamate substituted anilines are especially interesting substrates because the free indoline can be obtained after deprotection. However, the oxidation of the radical σ–complex should be more difficult than for **1** due to the electron withdrawing nature of the carbamate group.

Gansäuer and coworkers performed a series of experiments with model epoxide **18** and it was found that in the absence of **4**, desired product **19** was only obtained in a disappointingly low yield of 18% because **18** readily decomposed to give **20** (Scheme 2.42). Optimization experiments were carried out to improve the performance of the reaction and results are summarized in table 2.9.[45]

Table 2.8. Redox potentials for titanocene complexes[51]

Compound	$E_{p,a}$ [1]
Kagan's complex	–0.82
$(C_5H_4tBu)CpTiCl_2$	–0.84
$(C_5H_4tBu)_2TiCl_2$	–0.74
Cp_2TiCl_2	–0.83
$(C_5H_4Cl)CpTiCl_2$	–0.71
$(C_5H_4COOMe)CpTiCl_2$	–0.58
$(C_5H_4Cl)_2TiCl_2$	–0.54
$(C_5H_4COOMe)_2TiCl_2$	–0.43
$(C_5H_4CN)CpTiCl_2$	–0.35

[1] Potentials were recorded at a glassy carbon disk electrode with $\nu = 0.1$ V s^{-1} in 0.2 M Bu_4NPF_6/THF; the values are given in V vs. Fc^+/Fc and can be converted to V vs. SCE by adding 0.52 V

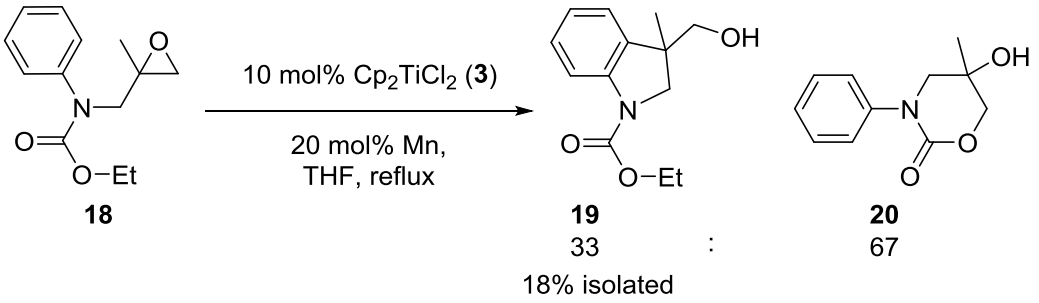

Scheme 2.42. Reaction of **18** in the absence of **4**

Table 2.9. Optimization of the reaction of **18**

[Ti], mol%	**4**, mol%	conv. %	**19**:**20**	**19**, %
3, 5	10	44	48:52	14
3, 5	20	53	75:25	30
3, 5	50	62	77:23	39
6, 10	20	95	>95:<5	70

These results highlight that Mn-**3** is not a suitable system for the clean transformation of **18** to **19**. While the addition of **4** improved conversion of **18**, the formation of **20** was not efficiently suppressed. Gratifyingly, the use of Mn-**6** resulted in an almost quantitative and highly selective formation of **19**. This clean reaction is attributed to the efficient oxidation of the intermediate radical σ–complex.[45]

The cleavage of ethyl carbamates requires harsh conditions,[103] thus, they are only rarely employed in synthetic applications. As a result, Gansäuer and coworkers also investigated benzyl carbamates as N-protecting group (Scheme 2.43).[103] Isolated yields of the protected indoline were high except for **22d**. In that case, the conversion was quantitative but the compound decomposed during SiO_2 purification. To obtain the free amines, the carbamate group was removed by catalytic hydrogenation (Scheme 2.44). Indolines **23a - 23c** were obtained in reasonable yields over two steps. The lower yield of **23d** is a consequence of its increased instability during SiO_2 chromatography.

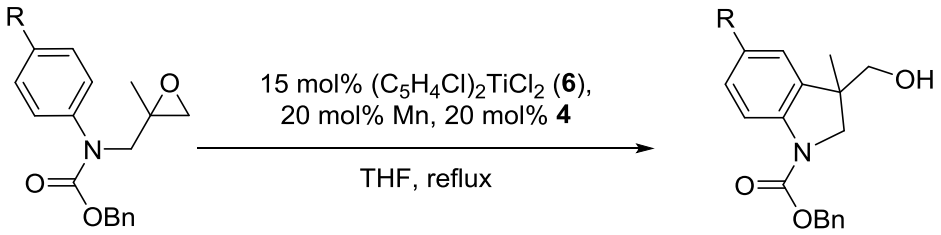

21 **22**

a: R = H 85%
b: R = CH_3 95%
c: R = CO_2CH_3 80%
d: R = OCH_3 69%

Scheme 2.43. Preparation of Z-protected indolines

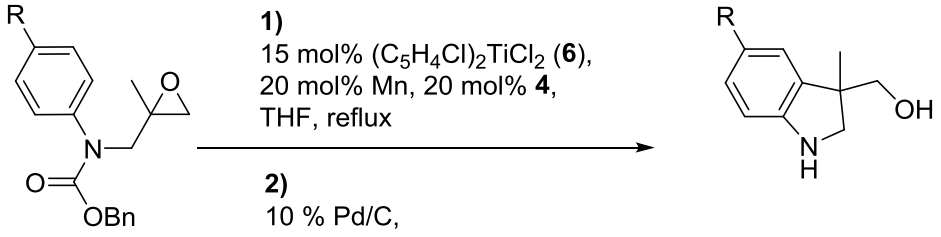

21 **23**

a: R = H 80%
b: R = CH_3 70%
c: R = CO_2CH_3 69%
d: R = OCH_3 56%

Scheme 2.44. Radical arylation and hydrogenative removal of the Z-protecting group.

2.4 Conclusions

In conclusion, an in-depth mechanistic study on the radical arylation of amino epoxides to form indoline products was presented. From results gleaned from synthetic, kinetic, and computational studies, it was proposed that the titanocene catalyst opens the epoxide to form the β-titanoxy radical, which readily adds to the arene to form the radical σ-complex **B**. A cationic species is then formed via a back-electron transfer from the σ-complex to the pendant titanocene moiety to regenerate the catalyst and product upon heterolytic cleavage. The back-electron transfer to the pendant titanocene moiety was

turnover-limiting. Furthermore, not only was Coll*HCl serving as a proton source, but it also stabilized the catalyst by forming a supramolecular complex, which is the resting state of the catalyst.

Based on the proposed mechanism, a more Lewis acidic titanocene complex was employed to facilitate the radical arylation of electron deficient epoxides. The use of cyclopentadienyl ligands with electron withdrawing substituents should also be of major importance for the design of efficient catalysts in enantioselective arylations via regiodivergent epoxide opening (REO).[16,17] Finally, our mechanistic studies have inspired research into efficient titanocene catalyzed radical arylation of pyrroloepoxides to form dihydropyrrolizines and tetrahydroindolizines, which are basic motifs found in many natural products of biological activity.[104]

2.5 References

(1) Trost, B. M. *Science (80-.).* **1983**, *219* (4582), 245–250.

(2) Trost, B. M. *Angew. Chem. Int. Ed.* **1995**, *34* (3), 256–281.

(3) Trost, B. M. *Science (80-.).* **1991**, *254* (5037), 1471–1477.

(4) Matsuda, I.; Shibata, M.; Sato, S.; Izumi, Y. *Tetrahedron Lett.* **1987**, *28* (29), 3361–3362.

(5) Schore, N. E. *Chem. Rev.* **1988**, *88*, 1081–1119.

(6) Heinrich, M. R.; Gansäuer, A. *Radicals in Synthesis III*; Springer, 2012; Vol. 7.

(7) Yan, M.; Lo, J. C.; Edwards, J. T.; Baran, P. S. **2016**.

(8) Gansäuer, A.; Von Laufenberg, D.; Kube, C.; Dahmen, T.; Michelmann, A.; Behlendorf, M.; Sure, R.; Seddiqzai, M.; Grimme, S.; Sadasivam, D. V.; Fianu, G. D.; Flowers, R. A. *Chem. - A Eur. J.* **2015**, *21*, 280–289.

(9) Gansäuer, A.; Behlendorf, M.; Laufenberg, D. Von; Fleckhaus, A.; Kube, C.; Sadasivam, D. V; Flowers II, R. A. *Angew. Chem. Int. Ed.* **2012**, 4739–4742.

(10) Quebatte, L.; Thommes, K.; Severin, K. *J. Am. Chem. Soc.* **2006**, *128*, 7440–7441.

(11) Smith, D. M.; Pulling, M. E.; Norton, J. R. *J. Am. Chem. Soc.* **2007**, *129* (4), 770–771.

(12) Morcillo, S. P.; Miguel, D.; Campaña, A. G.; Álvarez de Cienfuegos, L.; Justicia, J.; Cuerva, J. M. *Org. Chem. Front.* **2014**, *1* (1), 15.

(13) Daasbjerg, K.; Svith, H.; Grimme, S.; Gerenkamp, M.; Mück-Lichtenfeld, C.; Gansäuer, A.; Barchuk, A.; Keller, F. *Angew. Chemie - Int. Ed.* **2006**, *45* (13), 2041–2044.

(14) Cangönül, A.; Behlendorf, M.; Gansäuer, A.; Van Gastel, M. *Inorg. Chem.* **2013**, *52* (20), 11859–11866.

(15) Gansäuer, A.; Pierobon, M.; Bluhm, H. *Synthesis (Stuttg).* **2001**, *16*, 2500–2520.

(16) Gansäuer, A.; Fan, C. A.; Keller, F.; Karbaum, P. *Chem. - A Eur. J.* **2007**, *13* (29), 8084–8090.

(17) Gansäuer, A.; Shi, L.; Otte, M. *J. Am. Chem. Soc.* **2010**, *132* (34), 11858–11859.

(18) Gansäuer, A.; Rinker, B. *Titanium and Zirconium in Organic Synthesis*; Marek, I., Ed.; Wiley-VCH, 2000.

(19) Hardouin, C.; Doris, E.; Rousseau, B.; Mioskowski, C. *Org. Lett.* **2002**, *4* (7), 1151–1153.

(20) Trost, B. M.; Shen, H. C.; Surivet, J. P. *J. Am. Chem. Soc.* **2004**, *126* (39), 12565–12579.

(21) Gansäuer, A.; Justicia, J.; Rosales, A.; Worgull, D.; Rinker, B.; Cuerva, J. M.; Oltra, J. E. *European J. Org. Chem.* **2006**, No. 18, 4115–4127.

(22) Gansäuer, A.; Fleckhaus, A.; Lafont, M. A.; Okkel, A.; Kotsis, K.; Anoop, A.; Neese, F. *J. Am. Chem. Soc.* **2009**, *131* (46), 16989–16999.

(23) Gigant, B.; Wang, C.; Ravelli, R. B. G.; Roussi, F.; Steinmetz, M. O.; Curmi, P. a; Sobel, A.; Knossow, M. *Nature* **2005**, *435* (7041), 519–522.

(24) Lachia, M.; Moody, C. J. *Nat. Prod. Rep.* **2008**, *25*, 227.

(25) Subramaniam, G.; Kam, T. S. *Helv. Chim. Acta* **2008**, *91* (5), 930–937.

(26) Cai, X. H.; Tan, Q. G.; Liu, Y. P.; Feng, T.; Du, Z. Z.; Li, W. Q.; Luo, X. D. *Org. Lett.* **2008**, *10* (4), 577–580.

(27) Gribble, G. W. *J. Chem. Soc. Perkin Trans. 1* **2000**, *25* (7), 1045–1075.

(28) Van Order, R. B.; Lindwall, H. G. *Chemical Reviews*. 1942, pp 69–96.

(29) Robinson, B. *Chem. Rev.* **1969**, *69* (2), 227–250.

(30) Bartoli, G.; Palmieri, G.; Chimiche, S.; Mc, C.; Bosco, M.; Dalpozzo, R. *Tetrahedron Lett.* **1989**, *30* (scheme 1), 2129–2132.

(31) Cabri, W.; Candiani, I.; Colombo, M.; Franzoi, L.; Bedeschi, A. *Tetrahedron Lett.* **1995**, *36* (6), 949–952.

(32) Larock, R. C.; Kgun Yum, E. *J. Am. Chem. Soc.* **1991**, *113*, 6689–6690.

(33) Larock, R. C.; Yum, E. K.; Refvik, M. D. *J. Org. Chem.* **1998**, *63* (22), 7652–7662.

(34) Aoki, K.; Peat, A. J.; Buchwald, S. L. *J. Am. Chem. Soc.* **1998**, *120* (13), 3068–3073.

(35) Peat, A. J.; Buchwald, S. L. *J. Am. Chem. Soc.* **1996**, *118* (5), 1028–1030.

(36) Wagaw, S.; Rennels, R. A.; Buchwald, S. L. *J. Am. Chem. Soc.* **1997**, *119* (36), 8451–8458.

(37) Miah, S.; Slawin, A. M. Z.; Moody, C. J.; Sheehan, S. M.; Marino, J. P.; Semones, M. A.; Padwa, A.; Richards, I. C. *Tetrahedron* **1996**, *52* (7), 2489–2514.

(38) Brown, D. S.; Elliott, M. C.; Moody, C. J.; Mowlem, T. J.; Marino, J. P.; Padwa, A. *J. Org. Chem.* **1994**, *59*, 2447–2455.

(39) Moody, C. J.; Miah, S.; Slawin, A. M. Z.; Mansfield, D. J.; Richards, I. C. *Tetrahedron* **1998**, *54* (33), 9689–9700.

(40) Fürstner, A.; Hupperts, A. *J. Am. Chem. Soc.* **1995**, *117* (16), 4468–4475.

(41) Fürstner, A.; Hupperts, A.; Ptock, A.; Janssen, E. *J. Org. Chem.* **1994**, *59* (18), 5215–5229.

(42) Fürstner, A.; Bogdanović, B. *Angew. Chemie Int. Ed. English* **1996**, *35* (21), 2442–2469.

(43) Wipf, P.; Maciejewski, J. P. *Org. Lett.* **2008**, *10* (19), 4383–4386.

(44) Sortais, B.; Zard, S. Z.; Quiclet-Sire, B.; Ly, T.-M. *Tetrahedron Lett.* **1999**, *40*, 2533–2536.

(45) Gansäuer, A.; Von Laufenberg, D.; Kube, C.; Dahmen, T.; Michelmann, A.; Behlendorf, M.; Sure, R.; Seddiqzai, M.; Grimme, S.; Sadasivam, D. V.; Fianu, G. D.; Flowers, R. A. *Chem. - A Eur. J.* **2015**, *21* (1), 280–289.

(46) Blackmond, D. G. *Angew. Chemie - Int. Ed.* **2005**, *44* (28), 4302–4320.

(47) Baxter, R. D.; Sale, D.; Engle, K. M.; Yu, J. Q.; Blackmond, D. G. *J. Am. Chem. Soc.* **2012**, *134* (10), 4600–4606.

(48) Mathew, J. S.; Klussmann, M.; Iwamura, H.; Valera, F.; Futran, A.; Emanuelsson, E. A. C.; Blackmond, D. G. *J. Org. Chem.* **2006**, *71* (13), 4711–4722.

(49) Larsen, J.; Skrydstrup, T.; Daasbjerg, K. *Organometallics* **2004**, *23* (8), 1866–1874.

(50) Enemærke, R. J.; Larsen, J.; Skrydstrup, T.; Daasbjerg, K. *J. Am. Chem. Soc.* **2004**, *126* (25), 7853–7864.

(51) Gansäuer, A.; Kube, C.; Daasbjerg, K.; Sure, R.; Grimme, S.; Fianu, G. D.; Sadasivam, D. V.; Flowers, R. A. *J. Am. Chem. Soc.* **2014**, *136* (4), 1663–1671.

(52) Enemærke, R. J.; Hjøllund, G. H.; Daasbjerg, K.; Skrydstrup, T. *Comptes Rendus l'Academie des Sci. - Ser. IIc Chem.* **2001**, *4* (6), 435–438.

(53) Enemærke, R. J.; Larsen, J.; Hjøllund, G. H.; Skrydstrup, T.; Daasbjerg, K. *Organometallics* **2005**, *24* (6), 1252–1262.

(54) Larsen, J.; Enemarke, R. J.; Skrydstrup, T.; Daasbjerg, K. *Organometallics* **2006**, *25* (8), 2031–2036.

(55) Citterio, A.; Minisci, F.; Porta, O.; Sesana, G. *J. Am. Chem. Soc.* **1977**, *99* (24), 7960–7968.

(56) Citterio, A.; Arnoldi, A.; Minisci, F. *J. Org. Chem.* **1979**, *44* (15), 2674–2682.

(57) Gansäuer, A.; Seddiqzai, M.; Dahmen, T.; Sure, R.; Grimme, S. *Beilstein J. Org. Chem.* **2013**, *9*, 1620–1629.

(58) Simmons, E. M.; Hartwig, J. F. *Angew. Chemie - Int. Ed.* **2012**, *51* (13), 3066–3072.

(59) Laider, K. J. *Chemical Kinetics*, Third.; HarperCollinsPublishers, Inc., 1987.

(60) Harcourt, A. V.; Esson, W. *Philos. Trans.* **1867**, *157*, 117.

(61) Harcourt, A. V.; Esson, W. *Philos. Trans.* **1866**, *156*, 193.

(62) Harcourt, A. V.; Esson, W. *Proc. R. Soc. London* **1865**, *81*, 470.

(63) Rutherford, E.; Soddy, F. *J. Chem. Soc.* **1902**, *81* (321), 837.

(64) Branton, G. R.; Frey, H. M. *J. Chem. Soc.* **1966**, No. 1342.

(65) Huang, K.-W.; Han, J. H.; Cole, A. P.; Musgrave, C. B.; Waymouth, R. M. *J. Am. Chem. Soc.* **2005**, *127* (19), 3807.

(66) Huffman, J. C.; Moloy, K. G.; Marsella, J. A.; Caulton, K. G. *J. Am. Chem. Soc.* **1980**, *102* (9), 3009–3014.

(67) Domingos, A. M. T. S.; Simoes, M. J. A.; Teixeira, C.; Dias, A. R.; Carrondo, M.; Calhorda, M. J. *Organometallics* **1986**, *5* (4), 660–667.

(68) Newcomb, M.; Curran, D. P. *Acc. Chem. Res.* **1988**, *21* (5), 206–214.

(69) Gansäuer, A.; Pierobon, M.; Bluhm, H. *Angew. Chem. Int. Ed.* **1998**, *37*, 101–103.

(70) Gansauer, A.; Bluhm, H.; Pierobon, M. *J. Am. Chem. Soc.* **1998**, *120* (49), 12849–12859.

(71) Gansäuer, A.; Klatte, M.; Brändle, G. M.; Friedrich, J. *Angew. Chemie - Int. Ed.* **2012**, *51* (35), 8891–8894.

(72) Gansäuer, A.; Rinker, B.; Pierobon, M.; Grimme, S.; Gerenkamp, M.; Mück-Lichtenfeld, C. *Angew. Chemie - Int. Ed.* **2003**, *42* (31), 3687–3690.

(73) Gansäuer, A.; Rinker, B.; Ndene-Schiffer, N.; Pierobon, M.; Grimme, S.; Gerenkamp, M.; Muck-Lichtenfeld, C. *European J. Org. Chem.* **2004**, No. 11, 2337–2351.

(74) Gansäuer, A.; Lauterbach, T.; Narayan, S. *Angew. Chemie - Int. Ed.* **2003**, *42* (45), 5556–5573.

(75) RajanBabu, T.; Nugent, W. *J. Am. Chem. Soc.* **1994**, *116* (3), 986–997.

(76) Gansäuer, A.; Lauterbach, T.; Geich-Gimbel, D. *Chem. - A Eur. J.* **2004**, *10* (20), 4983–4990.

(77) Friedrich, J.; Dolg, M.; Gansäuer, A.; Geich-Gimbel, D.; Lauterbach, T. *J. Am. Chem. Soc.* **2005**, *127* (19), 7071–7077.

(78) Friedrich, J.; Walczak, K.; Dolg, M.; Piestert, F.; Lauterbach, T.; Worgull, D.; Gansäuer, A. *J. Am. Chem. Soc.* **2008**, *130* (5), 1788–1796.

(79) Gansäuer, A.; Worgull, D.; Knebel, K.; Huth, I.; Schnakenburg, G. *Angew. Chemie - Int. Ed.* **2009**, *48* (47), 8882–8885.

(80) Gansäuer, A.; Knebel, K.; Kube, C.; Van Gastel, M.; Cangönül, A.; Daasbjerg, K.;

Hangele, T.; Hulsen, M.; Dolg, M.; Friedrich, J. *Chem. - A Eur. J.* **2012**, *18* (9), 2591–2599.

(81) Ahlrichs, R.; Armbruster, M. K.; Bär, M.; Baron, H. P.; Bauernschmitt, R.; Crawford, N.; Deglmann, P.; Ehrig, M.; Eichkorn, K.; Elliott, S.; Furche, F.; Haase, F.; Häser, M.; Hättig, C.; Hellweg, A.; Horn, H.; Huber, C.; Huniar, U.; Kattannek, M.; Kölmel, C.; Kollwitz, M.; May, K.; Nava, P.; Ochsenfeld, C.; Öhm, H.; Patzelt, H.; Rappoport, D.; Rubner, O.; Schäfer, A.; Schneider, U.; Sierka, M.; Treutler, O.; Unterreiner, B.; von Arnim, M.; Weigend, F.; Weis, P.; Weiss, H. Universität Karlsruhe 2012.

(82) Tao, J.; Perdew, J. P.; Staroverov, V. N.; Scuseria, G. E. *Phys. Rev. Lett.* **2003**, *91* (14), 146401.

(83) Weigend, F.; Ahlrichs, R. *Phys. Chem. Chem. Phys.* **2005**, *7* (18), 3297–3305.

(84) Becke, A. D. *J. Chem. Phys.* **1993**, *98* (7), 5648.

(85) Lee, C.; Yang, W.; Parr, R. G. *Phys. Rev. B* **1988**, *37* (2), 785–789.

(86) Stephens, P. J.; Devlin, F. J.; Chabalowski, C. F.; Frisch, M. J. *J. Phys. Chem.* **1994**, *98* (45), 11623–11627.

(87) Zhao, Y.; Truhlar, D. G. *J. Phys. Chem. A* **2005**, *109* (25), 5656–5667.

(88) Zhao, Y.; Truhlar, D. G. *Theor. Chem. Acc.* **2008**, *120* (1–3), 215–241.

(89) Eichkorn, K.; Htiser, M.; Ahlrichs, R.; Eichkorn, K.; Treutler, O.; Marco, H.; Ahlrichs, R. *Chem. Phys. Lett.* **1995**, *240* (September), 283–290.

(90) Weigend, F. *Phys. Chem. Chem. Phys.* **2006**, *8* (9), 1057–1065.

(91) Grimme, S.; Antony, J.; Ehrlich, S.; Krieg, H. *J. Chem. Phys.* **2010**, *132* (15).

(92) Becke, A. D.; Johnson, E. R. *J. Chem. Phys.* **2005**, *123* (15).

(93) Johnson, E. R.; Becke, A. D. *J. Chem. Phys.* **2005**, *123* (2).

(94) Grimme, S.; Ehrlich, S.; Goerigk, L. *J. Comput. Chem.* **2011**, *32*, 1456–1465.

(95) Kind, C.; Reiher, M.; Neugebauer, J.; Hess, B. A. Universität Erlangen 2002.

(96) Grimme, S. *Chem. - A Eur. J.* **2012**, *18* (32), 9955–9964.

(97) Klamt, A. *J. Phys. Chem.* **1995**, *99* (7), 2224–2235.

(98) Eckert, F.; Klamt, A. *AIChE J.* **2002**, *48* (2), 369–385.

(99) Eckert, F.; Klamt, A. COSMOlogic GmbH & Co. KG: Leverkusen, Germany 2012.

(100) Becke, A. D. *Phys. Rev. A* **1988**, *38* (6), 3098–3100.

(101) Perdew, J. P. *Phys. Rev. B* **1986**, *33* (12), 8822–8824.

(102) Schäfer, A.; Huber, C.; Ahlrichs, R. *J. Chem. Phys.* **1994**, *100* (8), 5829.

(103) Wuts, P. G. M.; Greene, T. W. *Greene's Protective Groups in Organic Synthesis, 4th ed.*; John Wiley & Sons: Hoboken: New Jersey, 2007.

(104) Hildebrandt, S.; Gansäuer, A. *Angew. Chemie - Int. Ed.* **2016**, *128*, 1–5.

Chapter 3. The design of an efficient Ti(III) complex for catalysis in single-electron steps

3.1 Background and significance

The design of novel and efficient atom-economical transformations is a fundamental ideal in chemistry.[1–3] The incorporation of radical intermediates in the development of such processes offers attractive features such as ease of catalyst generation, high functional group tolerance, and the ability to add to unsaturated functional groups such as arene and alkenes.[4,5] Given these advantages, it is surprising that their potential as key intermediates in catalytic C-C bond formation is largely untapped. This could be attributed to the fact that very little is known about their reaction pathways, thus making it difficult to fine-tune such systems to make them more efficient and versatile. In chapter 2, a titanocene(III) catalyzed radical arylation of a diphenyl amino epoxide (**1**) to form an indoline derivative (**2**) was introduced (Scheme 3.1).[6–8]

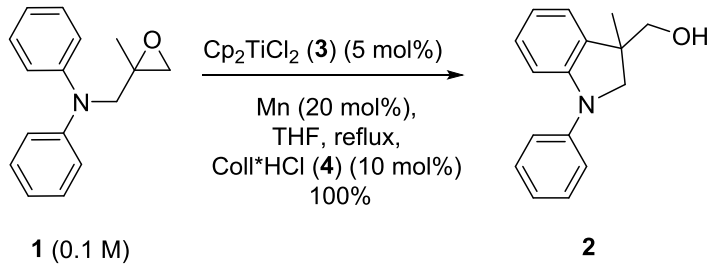

Scheme 3.1. Titanocene catalyzed radical arylation of **1** to **2**

Flowers, in collaboration with Gansäuer and co-workers, performed an in-depth mechanistic study on this system and they proposed that the titanocene catalyst opens the epoxide to form the β-titanoxy radical, which readily adds to the arene to form the radical σ-complex **B** (Scheme 3.2). A cationic species is then formed via a back-electron transfer

from the radical σ-complex to the pendant titanocene moiety to regenerate the catalyst and **2** upon heterolytic cleavage. The back-electron transfer to the pendant titanocene moiety was turnover-limiting. Furthermore, not only was Coll*HCl serving as a proton source, but it also stabilized the catalyst by forming a supramolecular complex, which is the resting state of the catalyst. Based on the proposed mechanism, the system was further fine-tuned by employing a more Lewis acidic titanocene complex to facilitate the radical arylation of electron deficient epoxides, which could not be realized when titanocene(III) dichloride was used as the catalyst (Scheme 3.3).[7,8]

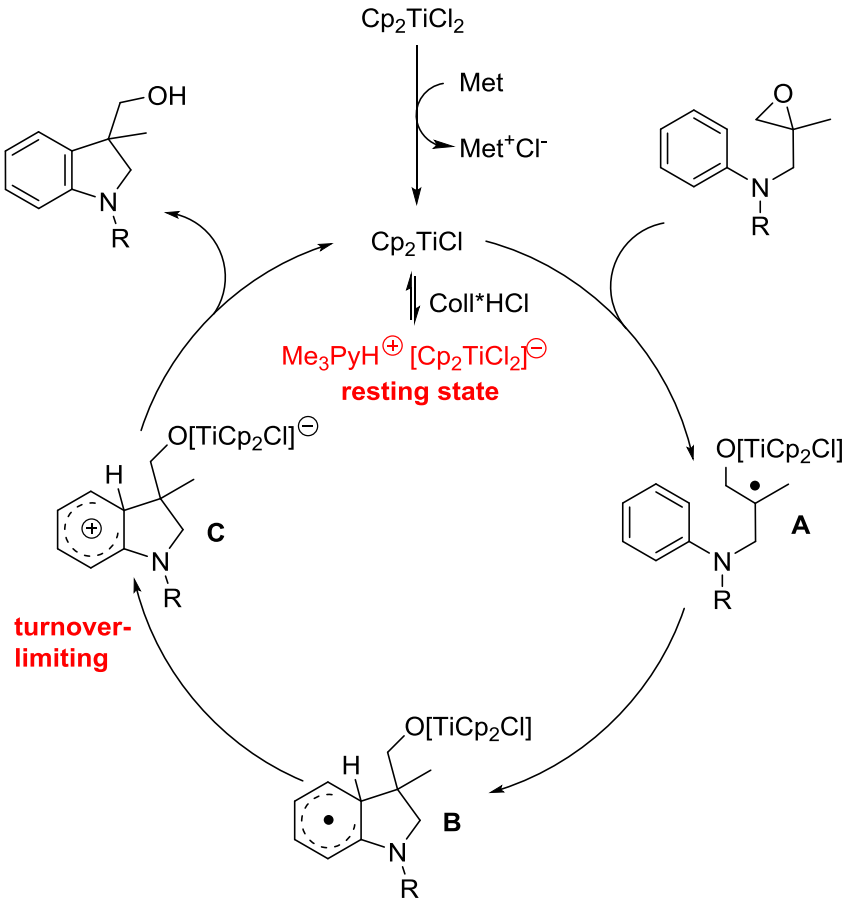

Scheme 3.2. Proposed catalytic cycle for the arylation of **1** to **2**

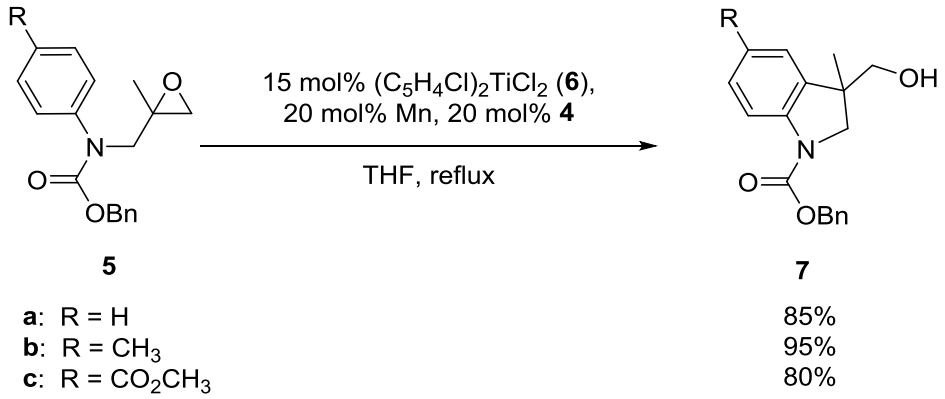

5

a: R = H
b: R = CH_3
c: R = CO_2CH_3

7

85%
95%
80%

Scheme 3.3. Preparation of Z-protected indolines[8]

As shown in scheme 3.2, the supramolecular complex is in equilibrium with the active titanocene catalyst and prevents catalyst deactivation making its use very crucial. We therefore questioned if this effect was solely based on the nature of the salt additive or if other salt additives could produce similar or better results. Flowers, in collaboration with Gansäuer and co-workers therefore performed cyclic voltammetry (CV), computational, and kinetic studies to investigate the nature of supramolecular complexes formed between titanocene(III) chloride and hydrochloride adducts. The impact of the concentration of salt additive on the radical arylation process was also studied.

THF has been extensively used as the solvent of choice for a number of reactions mediated by titanocene(III) complexes.[9–14] This is probably because it is readily available, facilitates the formation of the active titanocene(III) species, and loosely coordinates to the titanium metal.[15–17] We wanted to investigate the impact of other solvents on the radical arylation to form indoles. We particularly wanted to study the effect of solvents on the titanocene complex in terms of catalyst activation, identity, and activity in the radical arylation process. Finally, we wanted to study how ligands attached

to the titanocene complex also impacted the catalyst activation, identity, and activity in the radical arylation process.

By exploiting the effects of salt adducts, the effects of solvents, and the effects of anions on the titanium metal, we hoped to design a more efficient and robust catalytic system for the radical arylation of amino epoxides to form indoline derivatives. We also envisioned that the results gleaned from our studies would be extended to other titanocene mediated processes.

3.2 Experimental

3.2.1 Materials and instrumentation

Unless otherwise stated, all reactions were carried out in a glove box and under argon atmosphere. An Innovative Technology solvent purification system was used to purify all the solvents used for experiments. All reagents and chemicals, mostly argon or nitrogen flushed, were purchased from reputable chemical vendors (Alfa Aesar, Acros, Sigma Aldrich, Beantown Chemical, and TCI) and used without further purification. Chemicals not flushed with an inert gas were degassed with argon and used without any additional purification protocols. ^{1}H-NMR spectra were measured on either a Bruker 500MHz or a Bruker 400MHz spectrometer in deuterated chloroform ($CDCl_3$). ^{13}C-NMR spectra were measured at either 126 MHz or at 101 MHz in $CDCl_3$.

GC-MS analyses were done with a Schimadzu GCMS-Q2010 series with a SHRX-5M (30m) column. Column chromatography was done using an automated CombiFlash® system from Teledyne Isco. Inc. Columns were prepacked with silica gel and product separations were performed with a gradient elution of hexanes and ethyl acetate. *In situ* IR experiments were done using Mettler-Toledo's ReactIR 15 fitted with

DiComp probe and running iCIR software 4.3 SP1 or Mettler-Toledo's ReactIR 4000 fitted with SiComp probe and running iCIR software 4.2.26. Kinetic experiments were also performed with Vernier SpectroVis Plus Spectrophotometer running Logger Lite software.

3.2.2 Methods

3.2.2.1 Procedure for synthesizing *N*-((2-methyloxiran-2-yl) methyl)-*N*-phenylaniline (1)

N-((2-methyloxiran-2-yl) methyl)-*N*-phenylaniline (**1**) was synthesized by following the procedure outlined in the literature.[6] Sodium hydride (NaH, 1.10 equiv) was suspended in dry THF (1 mL per 1 mmol diphenylamine). Diphenylamine (1.00 equiv) was added to the suspension and stirred at room temperature for about 30 min. After 30 minutes 3-chloro-2-methylprop-1-ene (2.00 equiv) was added to the mixture and stirred overnight at reflux. Reaction mixture was cooled and ice was added to quench any unreacted NaH. Water and diethyl ether were added to the mixture. The aqueous layer was separated and extracted with diethyl ether three times. The organic layers were combined, washed with brine, and dried with $MgSO_4$. The solvents were removed under reduced pressure to obtain crude *N*-(2-methylallyl)-*N*-phenylaniline product.

N-(2-methylallyl)-*N*-phenylaniline (1.00 equiv) was dissolved in a 1:1:1 mixture of THF/acetone/water and a few drops of phosphate buffer (pH 7) was added. Osmium tetroxide (OsO_4, 0.01 equiv) and *N*-Morpholine-*N*-oxide hydrate (NMO, 1.50 equiv) were added to the mixture and stirred overnight at room temperature. The reaction was quenched by adding excess amounts of aqueous sodium hydrogen sulfite. Diethyl ether was added to the mixture and the aqueous layer was separated and extracted three times

with diethyl ether. The combined organic layers were washed with brine and dried with $MgSO_4$. The solvents were removed under reduced pressure to obtain the crude 3-(diphenylamino)-2-methylpropane-1,2-diol product.

To a solution of 3-(diphenylamino)-2-methylpropane-1,2-diol (1.00 equiv) in dry THF, sodium hydride (2.00 equiv) was added slowly and stirred for 30 minutes. After stirring for 30 minutes, tosylchloride (p-TosCl, 1.50 equiv) was added and the mixture was stirred overnight. Ice was added to quench any unreacted NaH. Water and diethyl ether were added to the mixture. The aqueous layer was separated and extracted with diethyl ether three times. The organic layers were combined, washed with brine, and dried with $MgSO_4$. The solvents were removed under reduced pressure and the crude product was purified with flash column chromatography (Hexanes: Ethyl acetate = 70:30) to obtain **1**.

3.2.2.2 Procedure for radical arylation of epoxide (1) to form 2

An oven dried vial was charged with an appropriate reductant, to this was added catalyst in a glovebox under argon atmosphere. Dry degassed solvent was added to the vial and stirred until the active catalyst was formed. The epoxide was added to the mixture and left to stir for the given time. The reaction was quenched with saturated ammonium chloride solution (NH_4Cl). Diethyl ether was added and the phases were separated. The aqueous layer was extracted 3 times with diethyl ether, washed with brine and dried over $MgSO_4$. Evaporation of the solvent followed by flash chromatography gave the final cyclized product (**2**).

3.2.2.3 Procedure for making 2-methyl-2-phenethyloxirane (14)

To a dried 250 mL round bottomed flask was added 50 mL of dry degassed THF under argon atmosphere. Sodium hydride (NaH, 1.20 equiv) was carefully measured into the flask containing THF. The mixture was sealed and taken out of the glove box then placed on a stirrer. Trimethylsulfoxonium iodide (1.40 equiv) was measured and quickly added to the mixture then left to stir for 30 minutes under argon. After 30 minutes, 4-phenylbutan-2-one (1.00 equiv) was measured and quickly added to the mixture and stirred overnight. Diethyl ether was added to the mixture followed by a drop of ice to react with any unreacted NaH. Water was added to the mixture and the organic layer was separated from the aqueous layer. The aqueous layer was washed two more times with diethyl ether and the separated organic layers were combined, washed with brine, dried with magnesium sulfate, and filtered. The organic solution was rotavaped to obtain crude product, which was purified with flash column chromatography (Hexanes: Ethyl acetate = 90:10) to obtain **14**.

3.2.2.4 Synthesis of hydrochloride salt (Coll*HCl, Py*HCl, and *n*Hex$_3$N*HCl)

The apparatus was set up accordingly, as can be seen in figure 3.1. The glassware was dried, purged with argon, and the joints were tightly sealed. About 10 equivalents of either sodium chloride (NaCl) or ammonium chloride (NH_4Cl) was measured into a three-necked round-bottomed flask. The base (1 equiv.) was dissolved in THF and set up as shown in figure 3.1 section B. About 10 equivalents of concentrated H_2SO_4 was added dropwise, via an addition funnel, to the salt while stirring. A violent evolution of HCl gas was observed bubbling through the solution containing the base, which resulted in the

formation of the hydrochloride salt as a precipitate. The bubbling was allowed to continue until no more gas was evolved. The solvent was evaporated to obtain the salt.

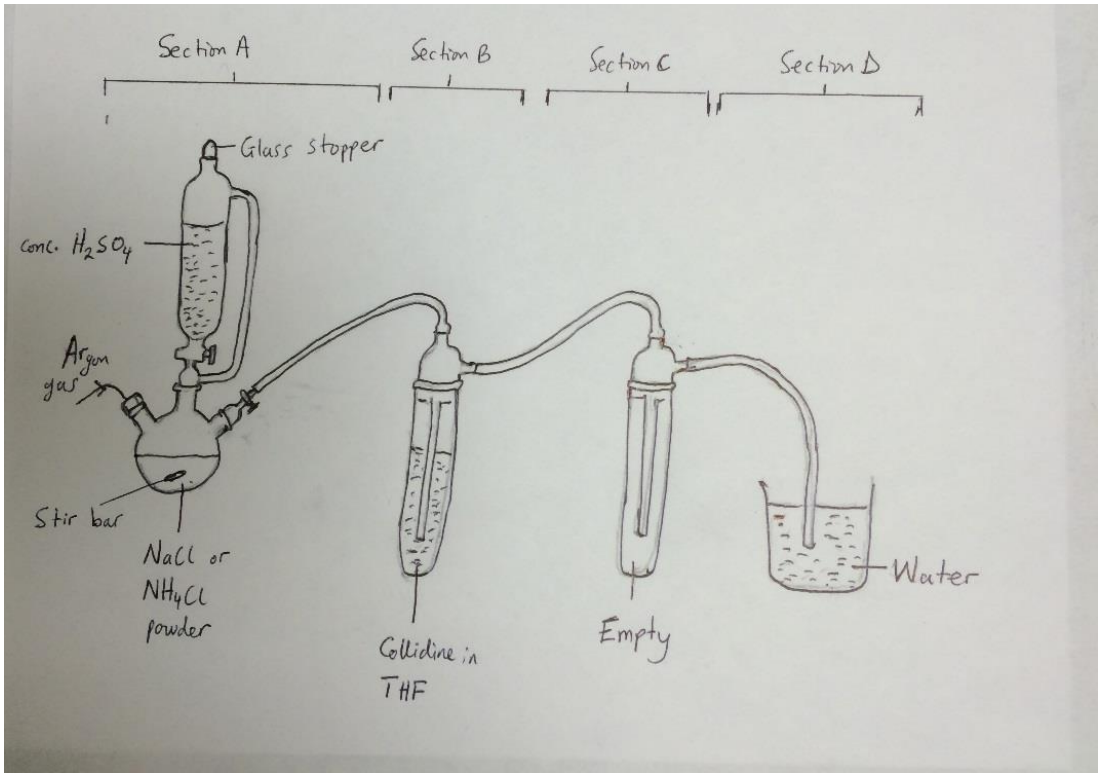

Figure 3.1. Set-up for the synthesis of Coll*HCl

3.2.2.5 Procedure for running experiments on ReactIR

3.2.2.5.1 General React IR 4000 procedure

Kinetic runs were carried out using Mettler-Toledo's ReactIR 4000 fitted with SiComp probe and running iCIR software 4.2.26. To a two-necked round bottom flask, a reductant and a salt additive were added and attached to a reflux condenser inside the glove box. This was taken out and fixed to the ReactIR probe and flushed with argon. An air background (64 scans) was obtained and 11.5 mL of solvent was added to the round bottom flask through a rubber septum and heated in an oil bath for 15 min. The iCIR

software was initiated to obtain data. An IR spectrum was collected every minute until the reaction was complete. The catalyst Cp_2TiX_2 in 2.0 mL of solvent was added after 4.0 - 5.0 minutes of starting the reaction and washed with 0.25 mL of solvent. The reaction mixture was refluxed until the active catalyst was formed. The epoxide in 1 mL of solvent was added and washed with 0.25 mL solvent. The reaction was left under reflux and monitored by ReactIR.

3.2.2.5.2 General ReactIR 15 procedure

Kinetic runs were carried out using a Mettler-Toledo's ReactIR 15 fitted with DiComp probe and running iCIR software 4.3 SP1. To a two-necked round bottom flask, a reductant and an appropriate amount of salt additive were added then attached to a reflux condenser inside a glove box. This was taken out, fixed to the ReactIR probe, and flushed with argon. An air background (256 scans) was obtained and 11.5 mL of solvent was added through a rubber septum into the round bottom flask and heated in an oil bath. The iCIR software was initiated to obtain data. IR spectrum was collected every minute until completion of the reaction. The catalyst Cp_2TiX_2 in 2.0 mL of solvent was added after 4.0 - 5.0 minutes of starting the reaction and washed with 0.25 mL of solvent. The reaction mixture was refluxed until the formation of active catalyst. The epoxide in 1 mL of solvent was added and washed with 0.25 mL solvent. The reaction was left under reflux and monitored by ReactIR.

3.2.2.6 General procedure for running experiments on the SpectroVis

All solutions were prepared in an argon filled glove box. A Ti(III) solution was prepared by mixing Cp_2TiX_2 and reductant in THF (25 mL). The solution was left to stir

until the active titanocene(III) catalyst was formed. A stock solution of epoxide and cyclohexadiene in THF was prepared for kinetic runs. The SpectroVis was calibrated with THF and each experiment was set to run until the reaction was completed. For each run, 3 mL of a 2 mM filtered Ti(III) solution was measured into a cuvette containing a stirrer and sealed with an airtight cap. This cuvette was placed into the SpectroVis instrument. The experiment was started and left to run for about 50 seconds. The appropriate amount of epoxide (**14**) solution was added to the Ti(III) solution and the decay of Ti(III) was monitored at the appropriate wavelength (λ_{max}). The observed rate (k_{obs}) was obtained by fitting an exponential equation to the plot of absorbance versus time in seconds.

3.3 Results

3.3.1 CV and computational analysis supramolecular complexes

To understand the impact of added chloride ions on the coordination sphere and the redox properties of titanocene(III) chlorides, Gansäuer and co-workers studied the cyclic voltammetric behavior of Zn-reduced Cp_2TiCl_2 in the presence of tri-n-hexylammonium chloride (Hex_3N*HCl), pyridine hydrochloride (Py*HCl), collidine hydrochloride (Coll*HCl), and guanidine hydrochloride (Gu*HCl). Figure 3.2 shows the cyclic voltammograms recorded for the selected chloride donors at a glassy carbon disk electrode using a sweep rate of 0.1 V s^{-1} in 0.2 M Bu_4NPF_6/THF.[18]

A common effect observed for all additives is that the oxidation wave for $[Cp_2TiCl_2]^-$ appears at low sweep rates. In the presence of Py*HCl, the voltammogram recorded is identical to those of electrochemically reduced Cp_2TiCl_2 in 0.2 M Bu_4NPF_6/THF. Essentially, only $[Cp_2TiCl_2]^-$ is detectable. This implies that the

association of chloride to either of Cp_2TiCl or $(Cp_2TiCl)_2$ cannot be outrun in the presence of these additives, at least for the sweep rates employed.[18]

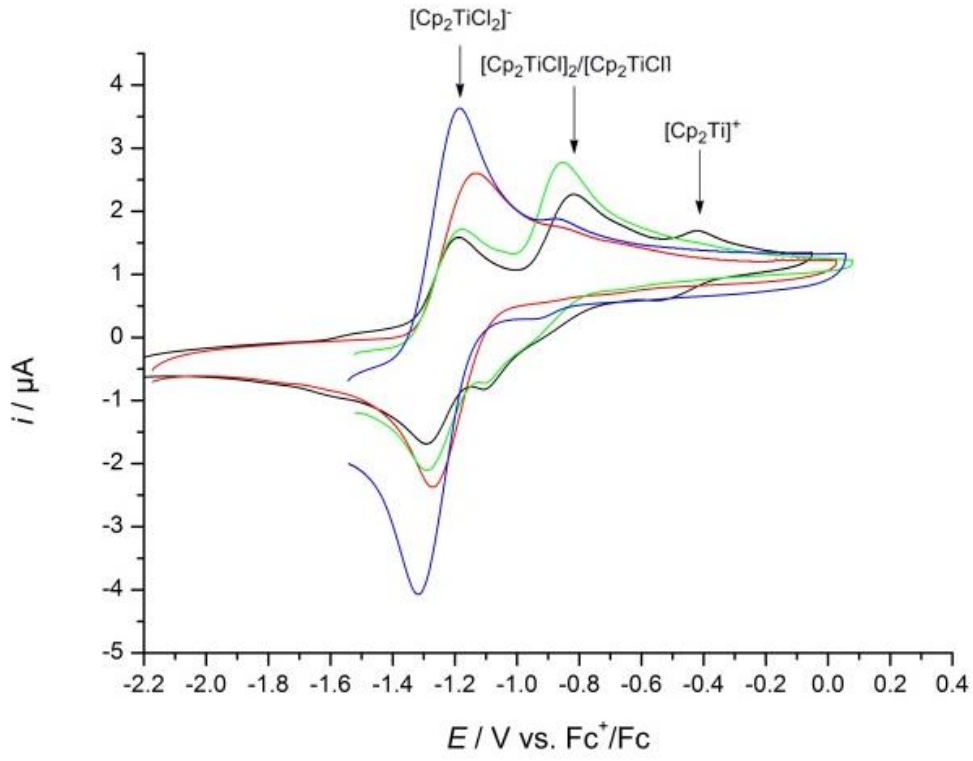

Figure 3.2. Cyclic voltammograms of 2 mM Zn-Cp_2TiCl_2 containing 2 equiv Gu*HCl (—), 2 equiv Hex_3N*HCl (—), 2 equiv Coll*HCl (—), and 2 equiv Py*HCl (—). Recordings were performed at a glassy carbon disk electrode using $\upsilon = 0.1$ V s^{-1} in 0.2 M Bu_4NPF_6/THF.[18]

The same observation mentioned above is seen for Hex_3N*HCl but the $Cp_2TiCl/(Cp_2TiCl)_2$ oxidation wave is dominant at high-sweep rates. The $Cp_2TiCl/(Cp_2TiCl)_2$ oxidation wave is high for Gu*HCl, showing that this hydrochloride is involved in relatively slower chloride transfer reactions that could be outrun by increasing the sweep rate. An oxidation wave pertaining to the highly Lewis acidic Cp_2Ti^+ species is also observed at low sweep rates in the presence of Gu*HCl. This could be due to the two modes of hydrogen bonding of the guanidium cation to $[Cp_2TiCl_2]^-$,

where the interconversion of the two isomers could be slow and outrun by the sweeping (Scheme 3.4).

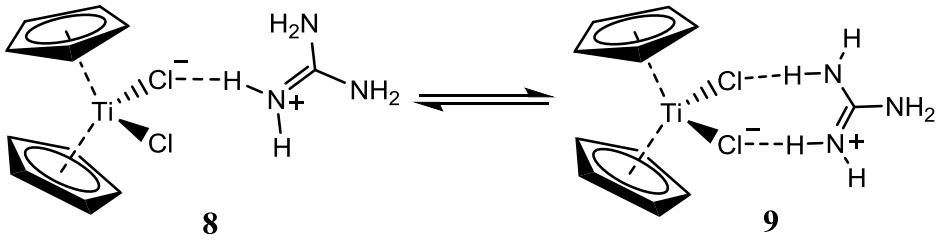

Scheme 3.4. Proposed two modes of hydrogen bonding of the guanidium cation to $[Cp_2TiCl_2]^-$

The oxidation wave of $[Cp_2TiCl_2]^-$ was observed in the presence of Coll*HCl and remained constant within sweep rates of 0.05–20 V s^{-1}. It was therefore inferred that the amount of $[Cp_2TiCl_2]^-$ was substantially stabilized under the experimental conditions in THF by Coll*H^+. As seen in figure 3.2, a lower amount of $[Cp_2TiCl_2]^-$ is formed in the presence of Coll*HCl whereas a higher amount of $[Cp_2TiCl_2]^-$ is formed with Py*HCl, which could be attributed to steric effects.

To further understand the interaction of the hydrochloride salts with titanocene(III) complexes on a molecular level, a computational study was performed by Flowers and co-workers using Gaussian09.[19] All DFT-structures were fully optimized at the UB3LYP/def2-TZVP level.[20–22] The combinations of Cp_2TiCl with Coll*HCl, Py*HCl, Et_3N*HCl and Gu*HCl were investigated. The DFT calculation identified stable adducts for all titanocenes with coordination of the additional chloride ion to titanium. The adducts are stabilized through hydrogen bonding between both chlorides and the N-H bond of the ammonium ions. However, the details of the structures revealed some differences (Figures 3.3 to 3.6).

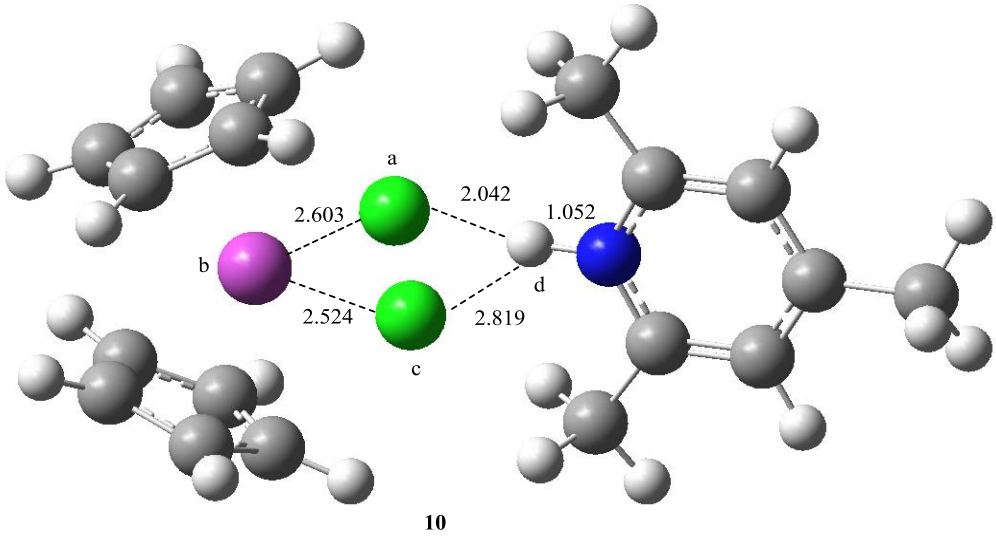

Figure 3.3. UB3LYP/def2-TZVP optimized structure of the adduct of Coll*HCl with Cp_2TiCl (Ti-Cyan, Cl-green, N-blue, C-grey, H-white)

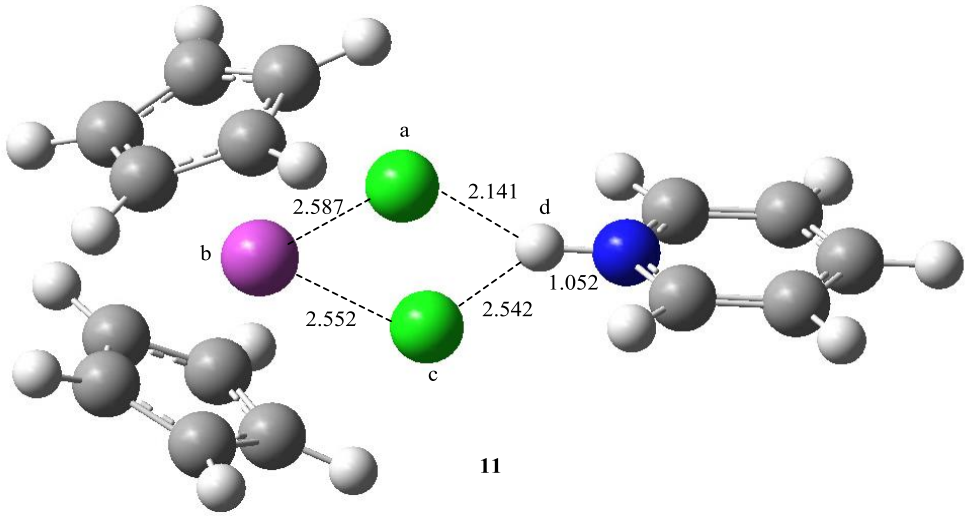

Figure 3.4. UB3LYP/def2-TZVP optimized structure of the adduct of Py*HCl with Cp_2TiCl (Ti-Cyan, Cl-green, N-blue, C-grey, H-white)

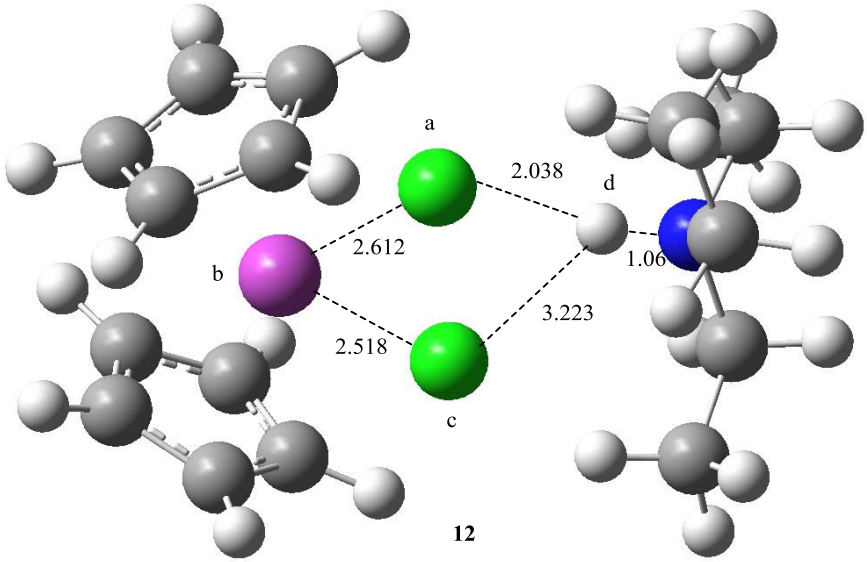

Figure 3.5. UB3LYP/def2-TZVP optimized structure of the adduct of Et_3N*HCl with Cp_2TiCl (Ti-Cyan, Cl-green, N-blue, C-grey, H-white)

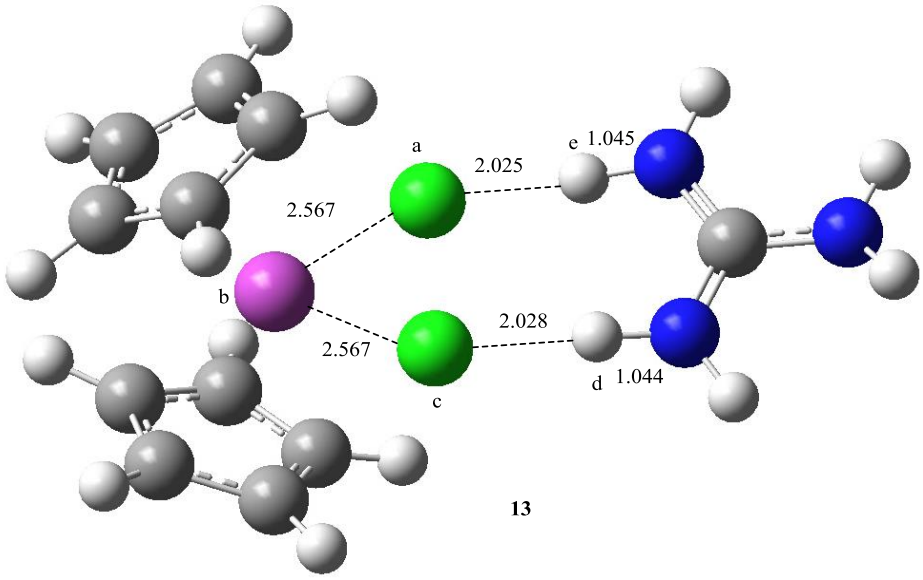

Figure 3.6. UB3LYP/def2-TZVP optimized structure of the adduct of Gu*HCl with Cp_2TiCl (Ti-Cyan, Cl-green, N-blue, C-grey, H-white).

Table 3.1. Selected structural data of **10**, **11**, and **12**

Complexes	N-H (Å)	H-Cl(a) (Å)	H-Cl(b) (Å)	Ti-Cl(a) (Å)	Ti-Cl(b) (Å)	Torsional angle, degrees
Cp_2TiCl-Coll*HCl (**10**)	1.052	2.042	2.819	2.603	2.524	84.06
Cp_2TiCl-Py*HCl (**11**)	1.052	2.141	2.542	2.587	2.552	-2.72
Cp_2TiCl-Et_3N*HCl (**12**)	1.06	2.038	3.223	2.038	2.518	-

The Py*HCl adduct **11** and Coll*HCl adduct **10** are distinguished by the orientation of the respective arenes. In **11,** the arene is almost in the plane containing both chlorides and Ti, whereas in **10,** the arene is nearly perpendicular to this plane. These results are consistent with unfavorable steric interactions between the 2,6-methyl groups of collidine and both chlorides disfavoring an in-plane orientation of the arene. The second significant difference between **10** and **11** is the mode of hydrogen bonding pattern. In **11**, the difference between both H-Cl distances (Δ(H-Cl) = 0.40 Å) is much shorter than for **10** (Δ(H-Cl) = 0.77 Å). It is proposed that the higher degree of dissymmetry in **11** is a consequence of the out-of-plane binding of Coll*H^+ to $[Cp_2TiCl_2]^-$. In case of a completely symmetric binding (Δ(H-Cl) = 0.0 Å) the 2,6-methyl groups of collidine would strongly interact with the Cp-ligands.

For the Et_3N*HCl adduct **12**, the hydrogen bonding is very similar to **10**. Therefore, Et_3N*H^+ is best regarded as a cation with a steric bulk like the collidinium ion. The adduct with Gu*HCl **13** has a symmetric hydrogen bonding pattern through a two-point interaction with the guanidinium cation. The Ti-Cl and H-Cl bonds are of equal length, respectively. In the gas phase, **11** is more stable than **10** for two reasons. First, the H-bonding pattern having a more symmetrical arrangement of both chlorides is more

favorable. Second, steric interactions between the pyridine and the cyclopentadienyl ligands are absent in **11** whereas in **10,** the two o-methyl groups disadvantageously interact with the titanocene. In solution, this repulsion results in a slower formation of **10** compared to **11** as judged by the CVs shown in figure 3.2.

For **10** and **12** the hydrogen bonding patterns are similar. However, the unfavorable steric interactions present in **10** are absent in **12**. Therefore, the formation of **12** should be more favorable and faster. Due to the very low solubility of Et_3N*HCl in THF, the experimental verification of this assumption was not possible. However, in agreement with the above analysis, the CV experiments with the more soluble and structurally related Hex_3N*HCl showed that adduct formation was much faster and more favorable than that for Coll*HCl.

The results obtained from the computational study done by Flowers and co-workers was further corroborated in a separate computational study performed by Stefan Grimme and co-workers (Figures 3.7 & 3.8).[18]

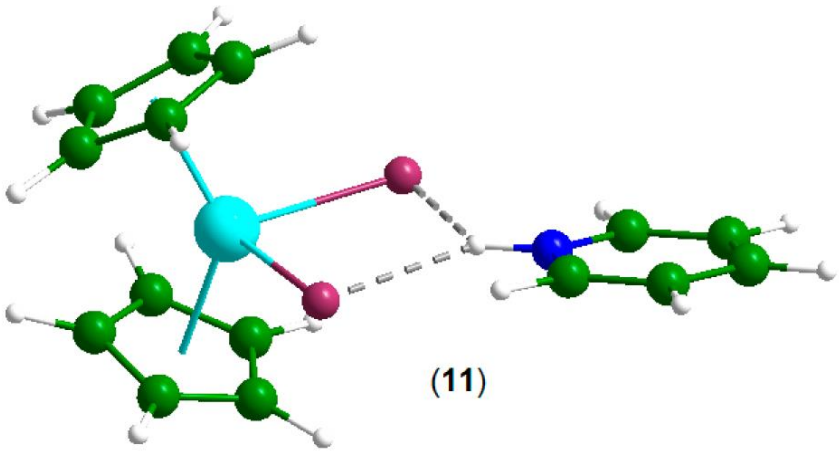

Figure 3.7. PW6B95-D3-COSMO-RS/def2-QZVP//TPSS-D3-COSMO/def2-TZVP-optimized structures of $[Cp_2TiCl_2]^-$*PyH^+ (**11**)[18]

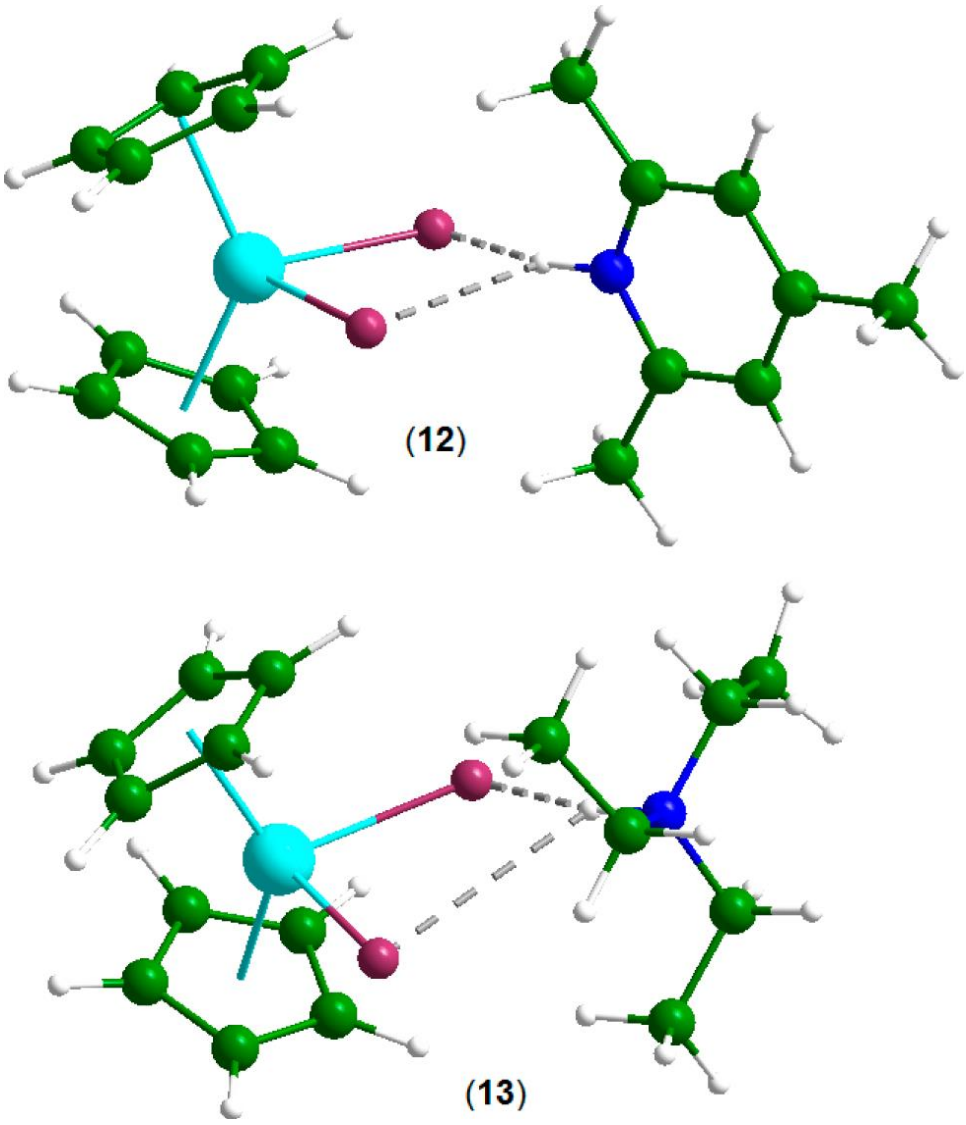

Figure 3.8. PW6B95-D3-COSMO-RS/def2-QZVP//TPSS-D3-COSMO/def2-TZVP-optimized structures of $[Cp_2TiCl_2]^-$*$CollH^+$ (**12**), and $[Cp_2TiCl_2]^-$*Et_3NH^+ (**13**)[18]

The CV and computational studies clearly show that addition of hydrochloride additives have a profound and unprecedented influence on the composition of metal reduced solutions of Cp_2TiCl_2 and its substituted derivatives. Besides Cp_2TiCl and $(Cp_2TiCl)_2$, adducts are formed that consist of the hydrogen bonded ion pairs of

[Cp_2TiCl_2] and the ammonium ion. The consequences of adduct formation on the performance of these reagents in catalysis is discussed in section 3.3.2.

3.3.2 Impact of salt additives on the rate of radical arylation of 1 to 2

The radical arylation of **1** to **2** was carried out in the presence of collidine hydrochloride (Coll*HCl), pyridine hydrochloride (Py*HCl), tri-n-hexylammonium chloride (Hex_3N*HCl), guanidinium chloride (Gu*HCl), lithium chloride (LiCl), and tetramethylammonium chloride ($(CH_3)_4NCl$). The ReactIR was used to monitor the growth of product *in situ* at 1386 cm^{-1} (Figure 2.9), which is the absorption of the C-H wag of the C2 carbon of the indole product. The observed rates (k_{obs}) for the reaction in the presence of the various salt adducts are summarized in the table 3.2.

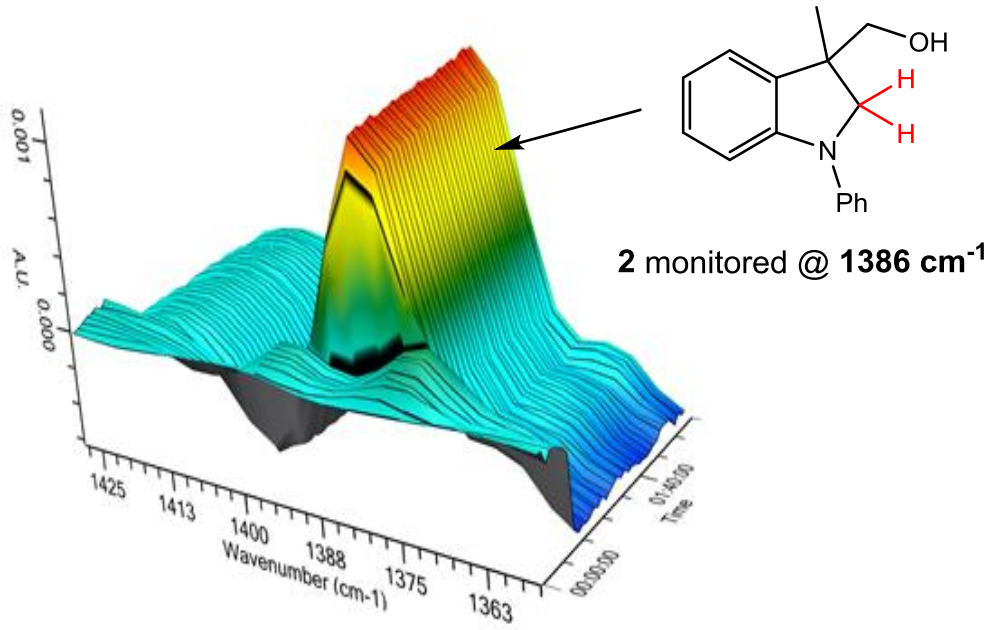

Figure 3.9. Product (**2**) monitored by ReactIR at 1386 cm^{-1}

Table 3.2. The observed rates (k_{obs}) for the arylation of **1** to **2** in the presence of salts

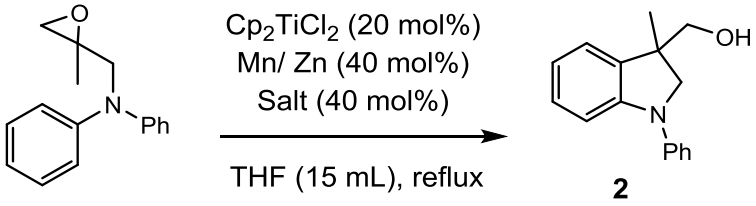

1 (0.0279 M, 1 equiv) **2**

Entry	Salt additive	k_1, min^{-1}	k_2, min^{-1}	k, min^{-1}	Metal
1	Coll*HCl	-	-	0.79 ± 0.09	Mn
2	Coll*HCl	-	-	1.1 ± 0.1	Zn
3	Py*HCl	-	-	0.67 ± 0.08	Mn
4	Hex_3N*HCl	-	-	0.57 ± 0.04	Mn
5	Gu*HCl	0.9 ± 0.2	0.060 ± 0.006	-	Mn
6	LiCl	0.5 ± 0.1	0.10 ± 0.01	-	Mn
7	$(CH_3)_4NCl$	0.7 ± 0.1	0.048 ± 0.007	-	Mn

The decay plots obtained for reactions done in the presence of Coll*HCl, Py*HCl, and Hex_3N*HCl fit to a single exponential, which is consistent with the hypothesis that in the presence of a salt additive, only the monomeric titanocene complex is involved in the radical arylation process. It was also observed that reactions done in the presence of Coll*HCl occurred at a much faster rate compared to Py*HCl, which is a much less sterically hindered hydrochloride salt. Suggesting that the resting state of the catalyst could be slightly favored in the presence of Py*HCl. The observed rate was also slightly improved in the presence of Coll*HCl when Zn was used in place of Mn as the metal reductant (Table 3.2. Entry 2).

Hex_3N*HCl, which is a more soluble salt than Coll*HCl and Py*HCl in THF, had the slowest observed rate for the radical arylation of **1** to **2**. The decay plots for the radical arylation of **1** to **2** in the presence of Gu*HCl surprisingly fit to a double

exponential, suggesting that there are possibly two titanocene complexes or other species involved in the radical arylation process. Similar trends were observed for reactions done in the presence of non-hydrochloride salts LiCl and $(CH_3)_4NCl$.

3.3.3 Impact on epoxide opening in the presence of different salt adducts

Titanocene(III) mediated epoxide opening experiments were carried out with 2-methyl-2-phenethyloxirane (**14**) as the model epoxide in the presence of Py*HCl and Hex_3N*HCl. The rate constants derived from both experiments were then compared to that obtained in the presence of Coll*HCl (Scheme 3.5).

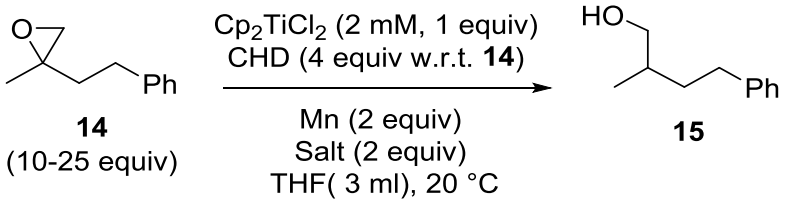

Scheme 3.5. Epoxide opening experiment

This epoxide opening experiment was done under pseudo first order conditions with a SpectroVis, which is a portable visible to near-IR spectrophotometer. This was done by monitoring the loss of the Ti(III) band for each of the manganese reduced titanocene complexes at 800 nm as described by Daasbjerg and co-workers (Figure 3.10).[23]

The decay plots were fitted to the appropriate exponential equation to derive the observed rate (k_{obs}) of the reaction (Figure 3.11).[8] This reaction was repeated at different concentrations of epoxide at least three times to ensure reproducibility of the data and the average k_{obs} were obtained at these concentrations. A graph of the observed rate (k_{obs}) versus epoxide concentration was plotted to obtain the rate constant (Figure 3.12). The order of the epoxide was also obtained by plotting the natural log of the observed rate

versus the natural log of the concentration of the epoxide (Figure 3.13).[8] The rate constants for opening **14** in the presence of the salt adducts are summarized in table 3.3.

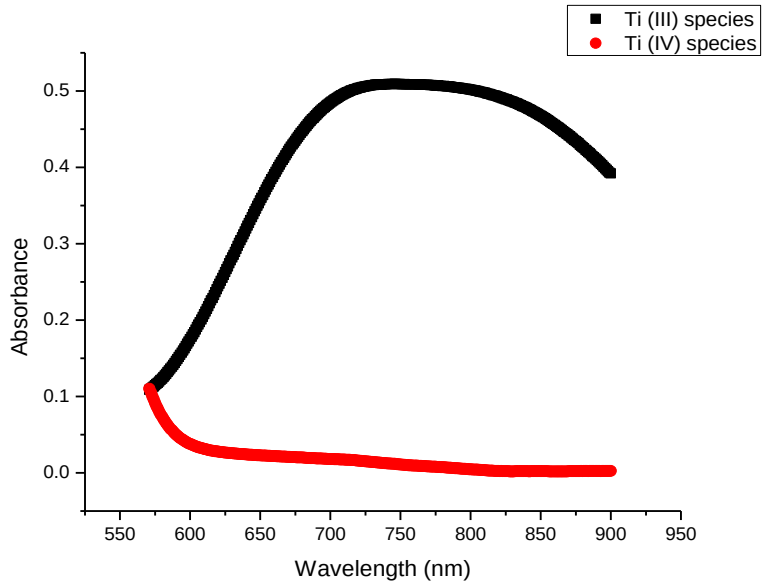

Figure 3.10. UV-Vis spectra of Ti(III)/(IV) species

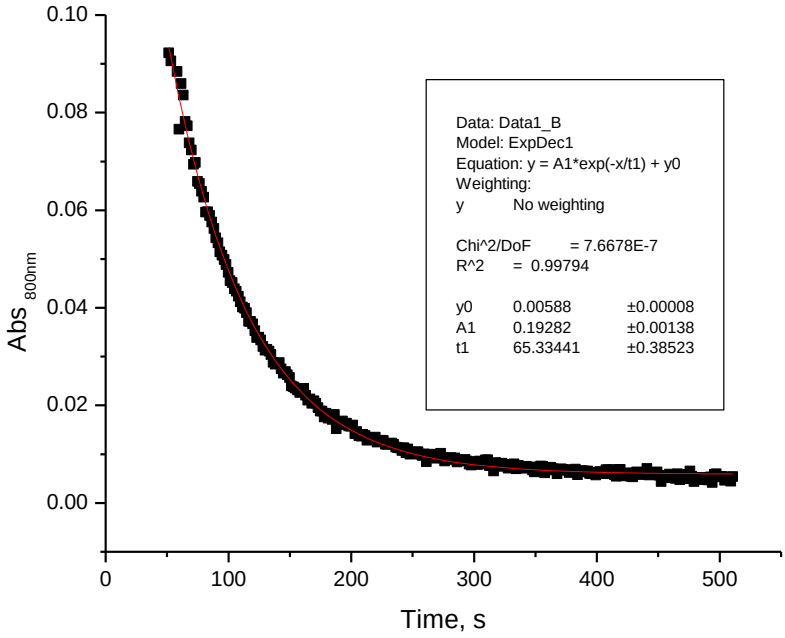

Figure 3.11. Plot of $Abs_{800\ nm}$ vs. time fitted to a single exponential equation

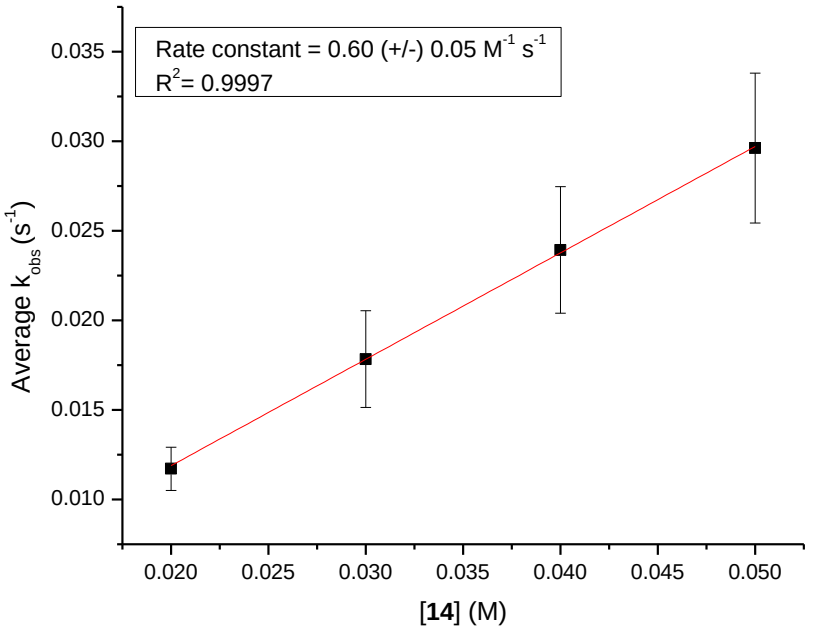

Figure 3.12. Plot of Average k_{obs} vs. [**14**] in the presence of Coll*HCl

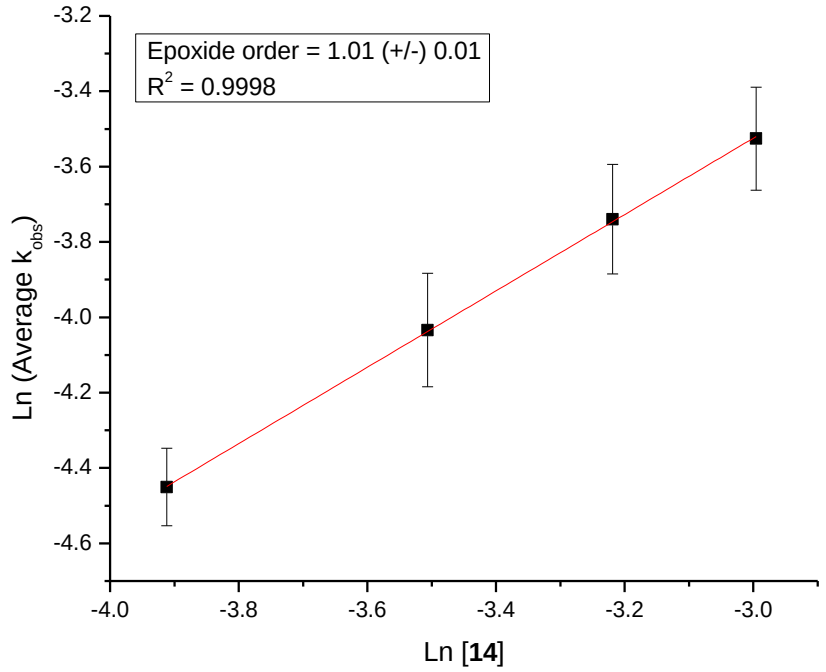

Figure 3.13. Plot of Ln (Average k_{obs}) Ln [**14**] in the presence of Coll*HCl

Table 3.3. Rate constants for opening **14** with Mn-Cp_2TiCl_2 in the presence of salts

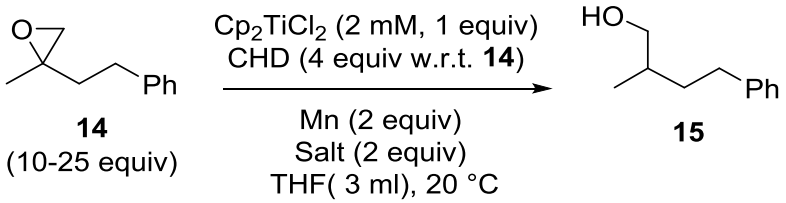

Salt additive	Rate constant, $M^{-1}s^{-1}$	Epoxide order
Coll*HCl	0.60 ± 0.05	1.01 ± 0.08
Py*HCl	0.31 ± 0.05	0.9 ± 0.2
Hex_3N*HCl	0.36 ± 0.14	0.8 ± 0.2

All the decay plots for Ti(III) fit to a single exponential (See appendix figures 6.79 to 6.90), which is indicative of only one titanocene(III) complex involved in the opening of the epoxide. The rate constants obtained from the epoxide opening experiment show that the reaction occurs at a much faster rate in the presence of Coll*HCl. Py*HCl and Hex_3N*HCl have slower and comparable rates constants. It could therefore be inferred, based on the results obtained from the CV, computational, and kinetic studies, that when the formation of the supramolecular complex between the titanocene(III) complex and salt additive is favored and more stable, the activity of titanocene(III) complex in reactions is slightly impeded. The impact of the concentration of the salt adduct on the activity of the titanocene complex in the radical arylation of 1 to 2 is discussed in the next section.

3.3.4 Impact of salt concentration on the arylation of 1 to 2

Based on the mechanistic study by the Flowers group on the arylation of epoxides by titanocene(III) complexes, it is known that the addition of a salt stabilizes the catalyst by forming a complex with the catalyst. The complex formed is known to be in equilibrium with the active catalyst.[6,8] It was therefore hypothesized that the rate of the

reaction could be altered if the equilibrium was shifted into one direction. According to principles of Le Chatelier, by increasing the concentration of the salt, the equilibrium should be shifted towards the formation of the supramolecular complex. This would reduce the active Ti(III) catalyst thereby reducing the rate of the reaction. Although Coll*HCl is the additive of choice in these reactions, Coll*HCl is sparingly soluble in THF. To avoid low solubility issues, the salt used for this reaction was tri-n-hexylammonium chloride salt (Hex_3N*HCl). This salt was used because it is completely soluble in THF, thus the correlation between salt concentration and rate could be measured more efficiently. The reaction was carried out as previous experiments with 40, 80 and 160 mol% Hex_3N*HCl salt (Scheme 3.6). The rate of product formation with respect to time was monitored on the React IR to obtain decay plots (Figure 3.14). The observed rates of reaction are summarized in table 3.4.[18]

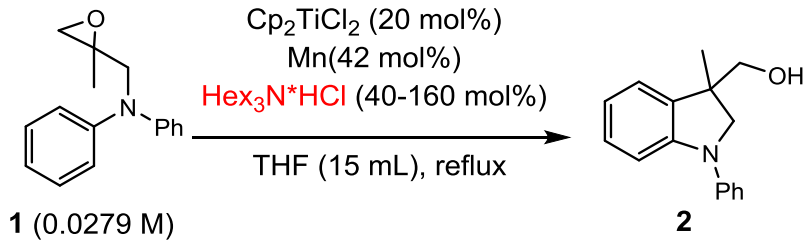

Scheme 3.6. Reaction conditions to test for impact of salt concentration on reaction

As expected, the rate of the reaction decreased with an increase in salt concentration. This is indicative of the equilibrium position shifting towards the supramolecular complex, thereby decreasing the concentration of active catalyst, which portends an inverse effect on the overall reaction (Figure 3.14).[18] It should however be noted that, in the case of Coll*HCl, this inverse effect is masked due to its low solubility in THF.

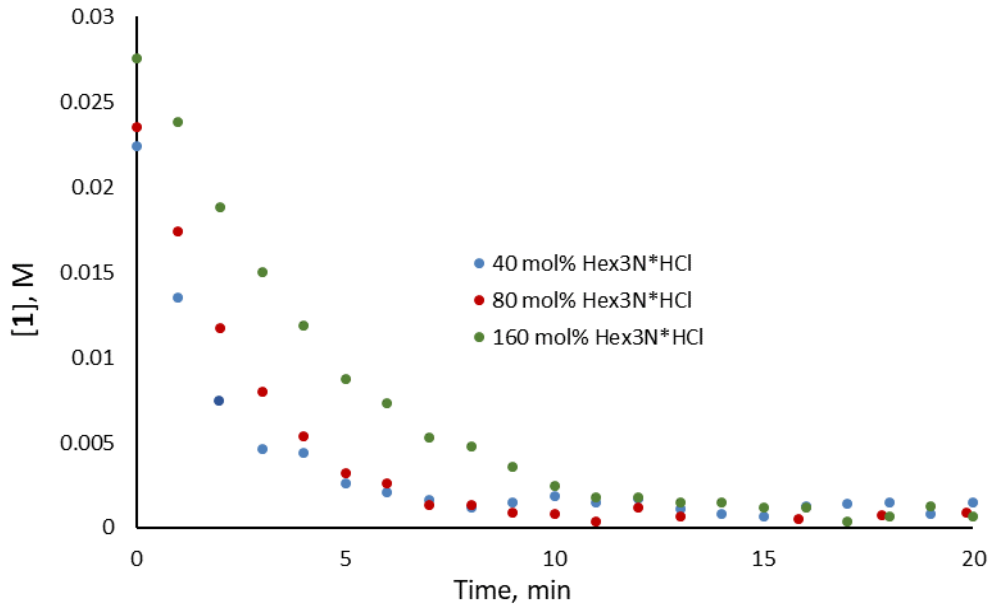

Figure 3.14. Impact of salt concentration on the arylation of **1** to **2**

Table 3.4. Impact of salt concentration on the arylation of **1** to **2** (Reaction conditions in scheme 3.6)

Hex_3N*HCl, mol%	k_{obs}, min^{-1}
40	0.57 ± 0.04
80	0.39 ± 0.01
160	0.24 ± 0.01

Also, the supramolecular complex formed with Coll*HCl is not as stable as the Hex_3N*HCl as shown by the CV and computational studies. A system where the catalyst will be stable without the need of a salt additive is ideal. To achieve this goal, the impact of the choice of solvent and the impact of the nature of the ligand attached to the titanocene complex were investigated.

3.3.5 Solvent effects

To test the impact of solvents, the radical arylation of **1** to **2** was carried out in a variety of solvents, the results are summarized in table 3.5. Cp_2TiCl_2 is not soluble in

diethyl ether and trifluorotoluene, and as a result, the active catalyst could not be formed (Table 3.5 entries 4 & 7). Conversely, Cp_2TiCl_2 dissolves in dichloromethane and toluene, however, when Mn was added, the active catalyst was not formed (Table 3.5 entries 3 & 5). The active titanocene catalyst was formed in dimethylformamide but was deactivated after 30 minutes to yield less than 50% of desired product (Table 3.5 entry 6). A change in color from green to blue black was observed (see Appendix figure 6.91). Thewalt and co-workers have shown that DMF strongly coordinates to $Cp^*_2Ti(III)Cl$ to form the structure shown in figure 3.15 B.[24] We therefore hypothesized that the deactivation of the active catalyst could be because of the formation of a stable titanocene complex due to the solvent strongly coordinating to the catalyst.

Table 3.5. Impact of solvent on the radical arylation of **1** to **2**

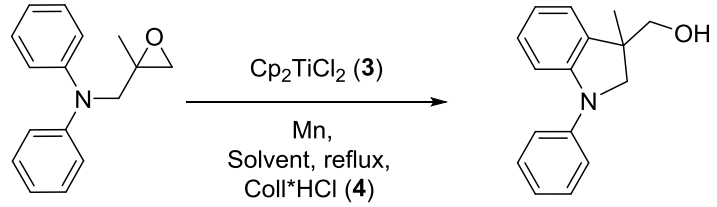

1 **2**

Entry	Solvent	**3** (mol%)	**4** (mol%)	Time (min)	**2** Conv	Yield (%)
1	THF	10[a]	-	30	100	98
2	THF	1[b]	5	120	100	96
3	Toluene	20[c]	-	2880	-	-
4	Trifluorotoluene	20[c]	-	1440	-	-
5	Dichloromethane	20[c]	-	1440	-	-
6	Dimethylformamide	20[d]	-	2160	<50	-
7	Diethyl ether	20[c]	-	1440	-	-
8	Dimethoxyethane	20[c]	-	170	100	89
9	Dimethoxyethane	20[c]	40	105	100	93
10	Acetonitrile	10[e]	-	120	100	91
11	Acetonitrile	10[e]	20	120	100	99

[a] [**1**] = 0.1 M; Mn = 20 mol%; THF = 5 mL; [b] [**1**] = 0.5 M; Mn = 10 mol%[25]; THF = 5 mL; [c] [**1**] = 0.028 M; Mn = 40 mol%; Solvent = 15 mL; [d] [**1**] = 0.1 M; Mn = 40 mol%; TLC analysis for conversion of **2**; DMF = 4 mL; [e] [**1**] = 0.1 M; Zn = 20 mol%; CH_3CN = 5 mL; All concentrations are with respect to **1**.

The active catalyst was formed in DME both in the presence and absence of Coll*HCl with the C-H wag of the cyclopentadienyl ligand having an absorbance at 802 cm^{-1} (Figures 5.16 & 5.18). The radical arylation in DME proceeded to give quantitative yield of product both with and without Coll*HCl (Table 3.5 entries 8 & 9). Reactions were monitored with ReactIR but rate studies could not be performed because the signals were too noisy (Appendix figures 6.92 to 6.94). It could however be observed that the reaction was faster in the presence of Coll*HCl (Table 3.5 entry 9). Unfortunately, the catalyst was not regenerated at the end of the reaction indicative of gradual catalyst deactivation even with Coll*HCl added (Figures 3.17 & 3.19).

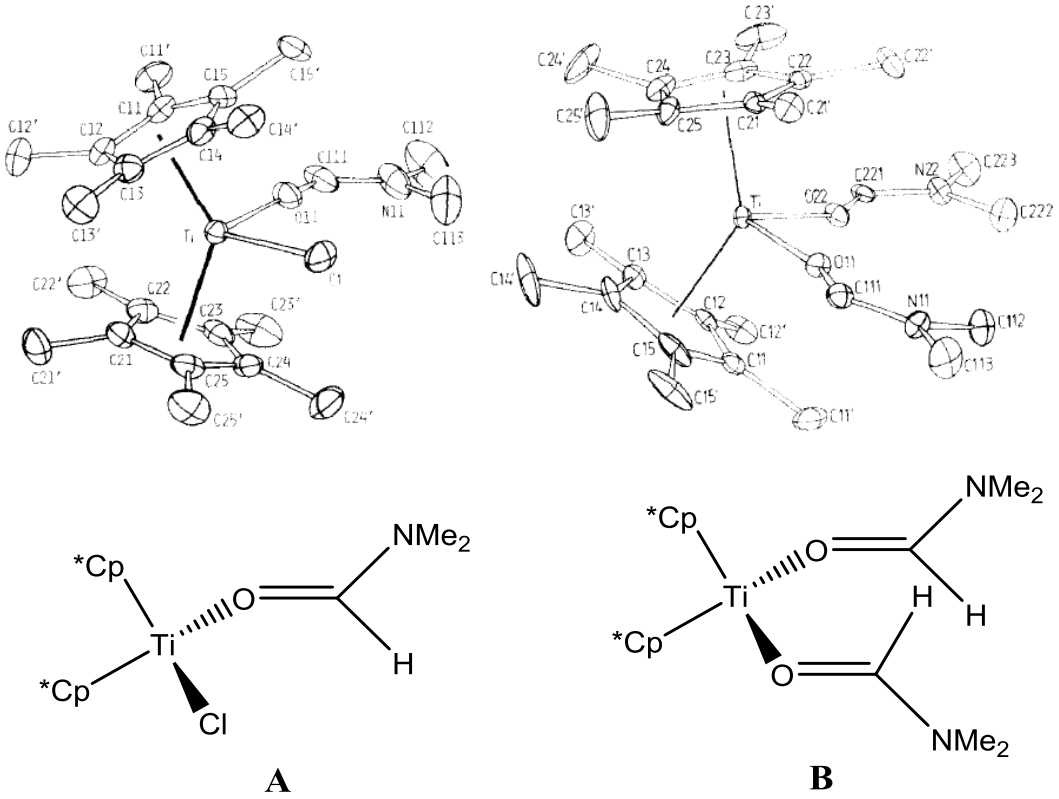

Figure 3.15. Crystal structures of titanium complexes in DMF[24]

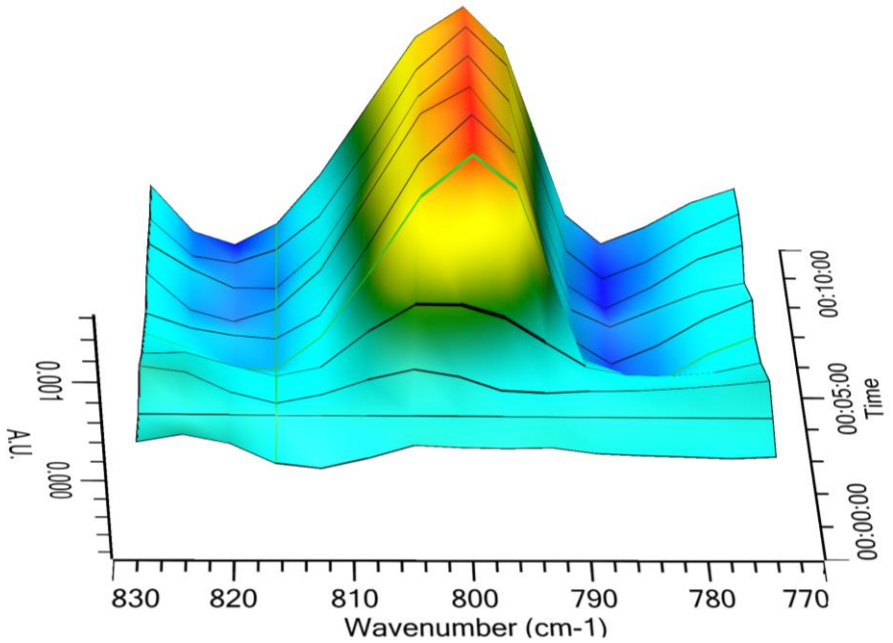

Figure 3.16. Active titanocene(III) catalyst in DME observed at 802 cm^{-1} without Coll*HCl

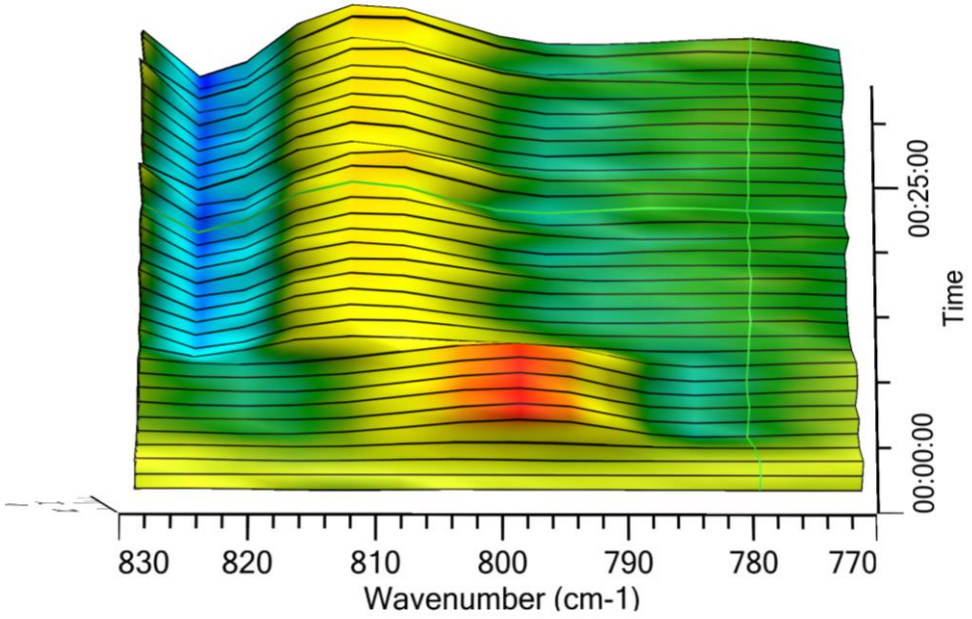

Figure 3.17. Catalyst deactivated in DME in the absence of Coll*HCl

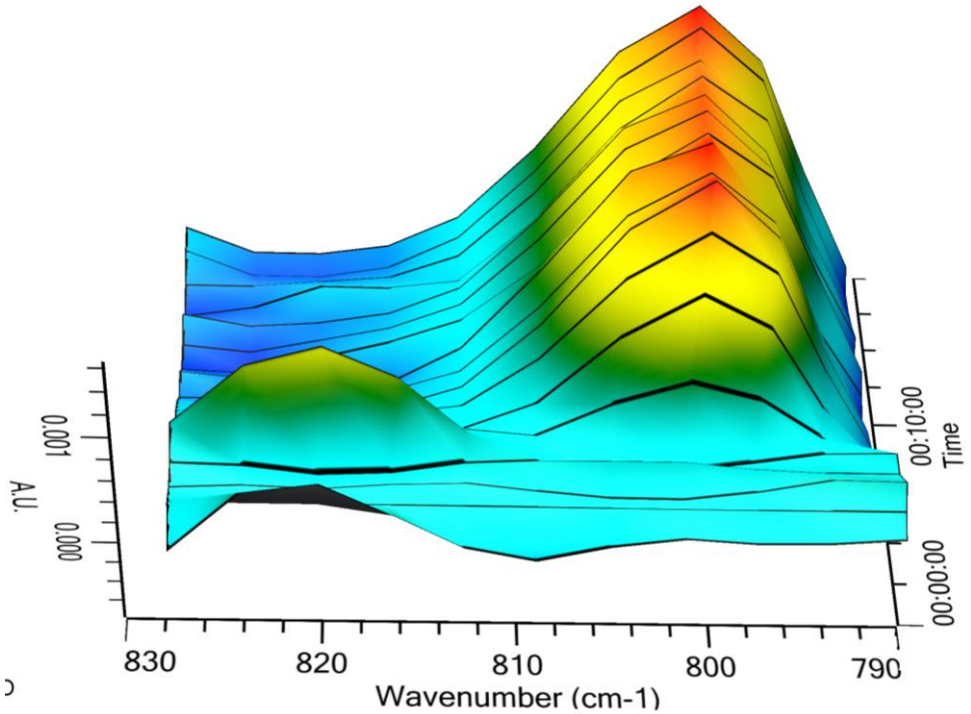

Figure 3.18. Active catalyst observed at 802 cm^{-1} in the presence of Coll*HCl in DME

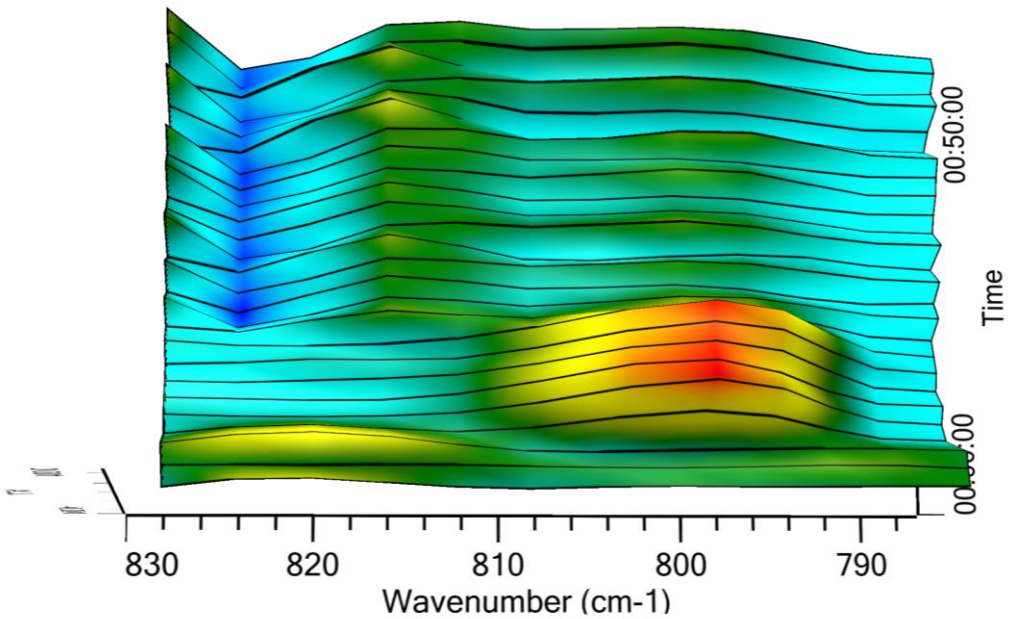

Figure 3.19. Catalyst deactivation in the presence of Coll*HCl in DME

In acetonitrile (CH_3CN), the radical arylation of **1** to **2** worked to produce good yields of **2** even in the absence of salt additive (Table 3.5 entries 10 & 11). In acetonitrile, a blue colored solution was observed instead of the green colored solution normally formed in THF (See Appendix figures 66B & 112A). Researchers have shown that a titanocenium cation is generated as the dominant species in acetonitrile and this species has a much lower redox potential as compared to the titanocene(III) chloride complex (Scheme 3.7, Figures 3.20 & 3.21).[26,27] We were also able to observe the growth of the active titanocene catalysts via *in situ* IR spectroscopy by monitoring the C-H wag of the cyclopentadienyl ligand of the titanocene complex. As shown in figure 3.22, the titanocenium complex is observed at 813 cm^{-1} as compared to the 798 cm^{-1} which is seen for the catalyst in THF (Figure 3.23).[27]

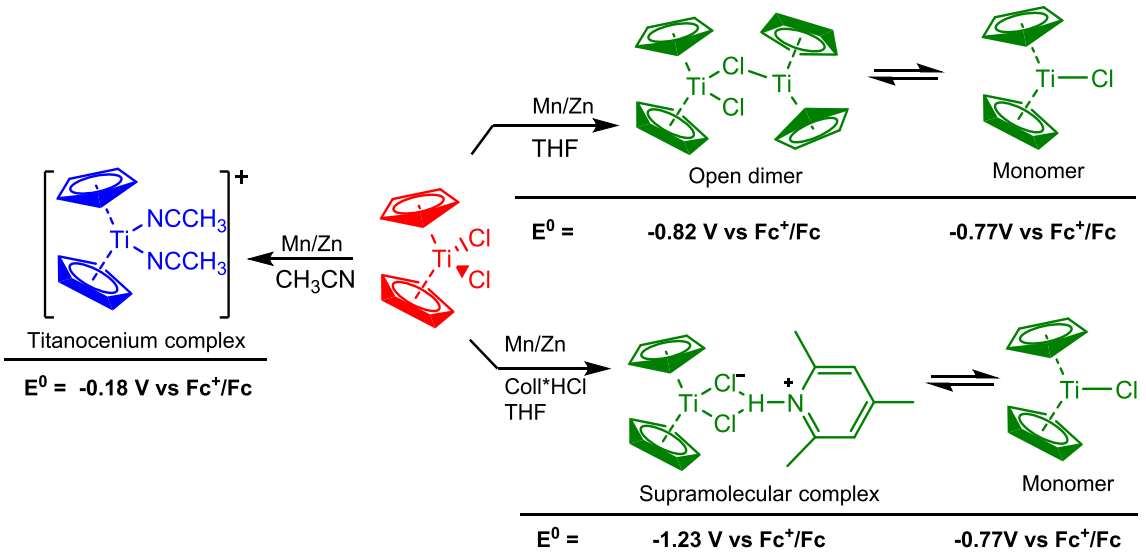

Scheme 3.7. Impact of CH_3CN on the identity and redox potential of titanocene complexes

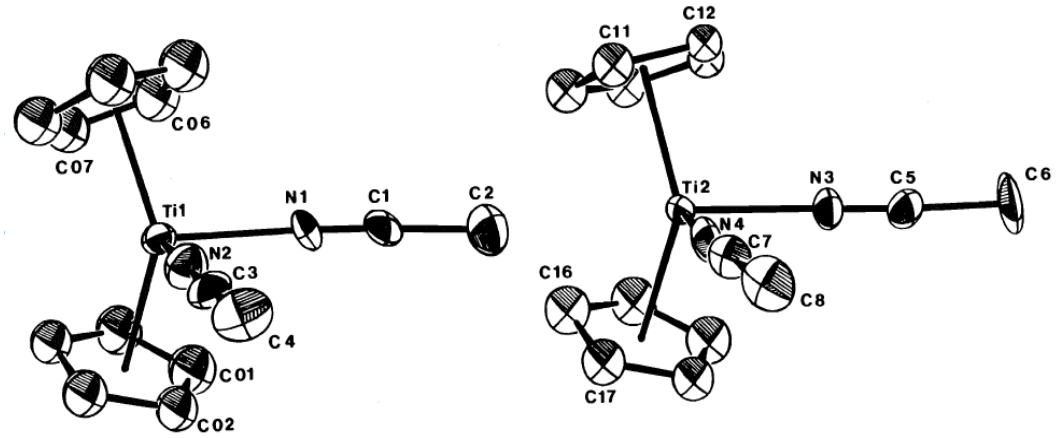

Figure 3.20. Crystal structure of titanocenium complex in CH_3CN[26]

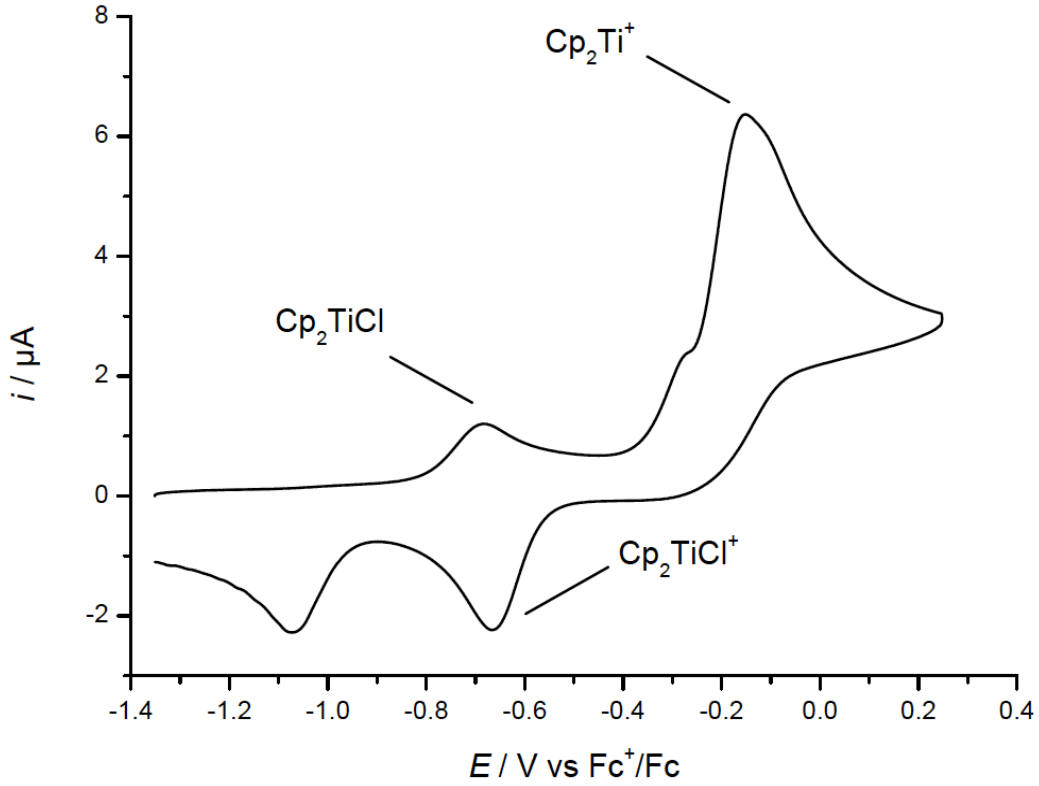

Figure 3.21. CV of 2 mM Zn-Cp_2TiCl_2 in 0.2 M Bu_4NPF_6/CH_3CN at υ = 0.2 Vs^{-1}

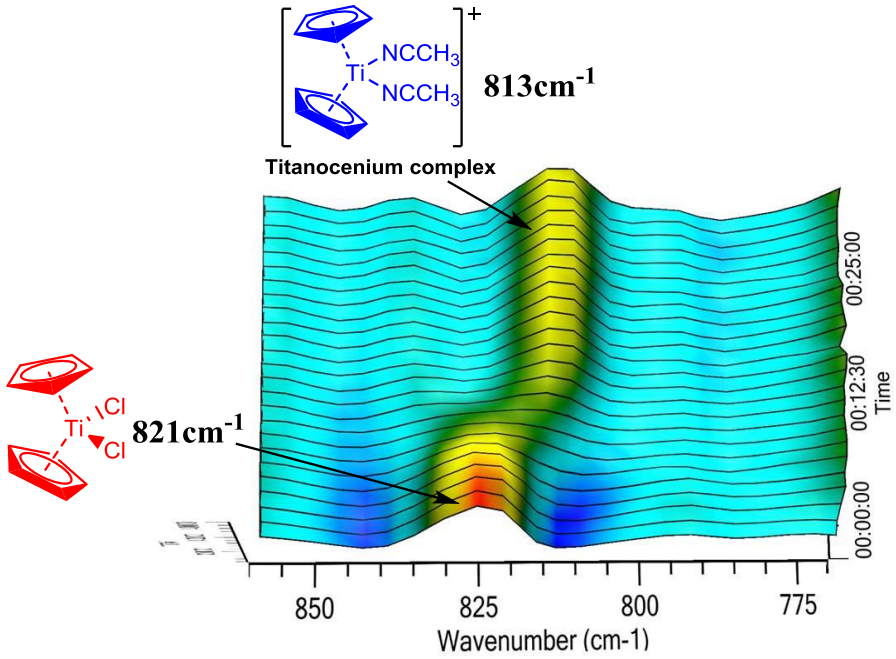

Figure 3.22. Titanocenium complex observed at 813 cm^{-1}

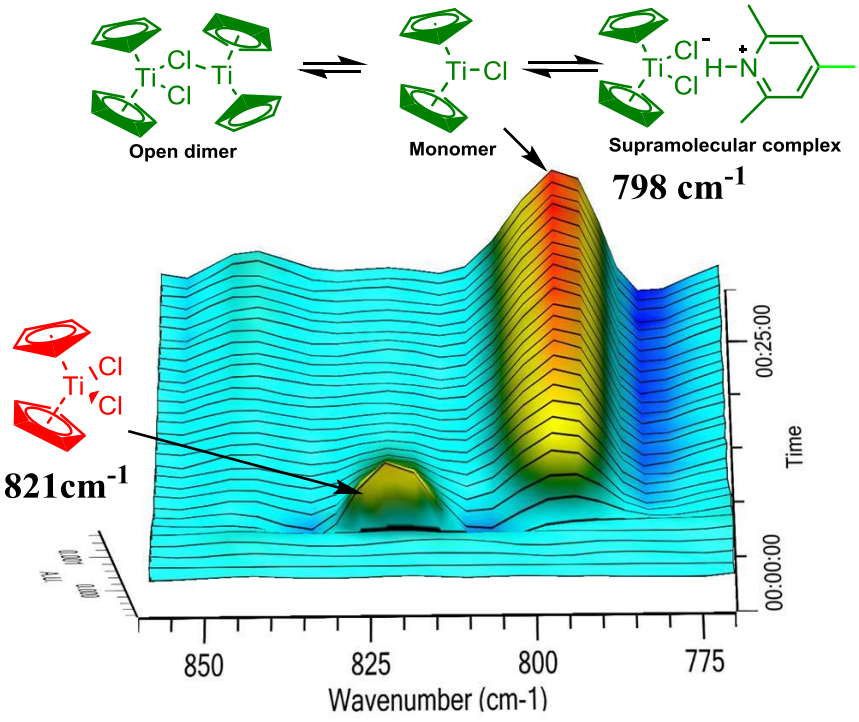

Figure 3.23. Titanocene(III) chloride observed at 798 cm^{-1}

3.3.5.1 Catalyst stability in CH_3CN

Catalyst stability tests were performed in the absence of Coll*HCl with Reaction Progress Kinetic Analysis.[28–30] In this technique, two separate reactions are carried out with the same catalyst under identical conditions, with the only difference being that one reaction starts with 50% of the reactant (Scheme 3.8). If the stoichiometry of the reactants during the reaction is known and there is no substrate or product inhibition, the catalyst concentration is said to be constant or stable throughout the reaction when the rate of the first reaction at 50% conversion of the staring material is the same as the rate of the second reaction (Figure 3.24). In other words, a graphical overlay will be observed for a time-resolved plot of the reactant decay over time for both experiments if the catalyst is stable (Figure 3.26).[28–30]

$$[A] \xrightarrow{[M]} [B] \quad \text{(100\% Run)}$$

$$\frac{[A]}{2} \xrightarrow{[M]} \frac{[B]}{2} \quad \text{(50\% Run)}$$

Scheme 3.8. Catalyst stability test with RPKA

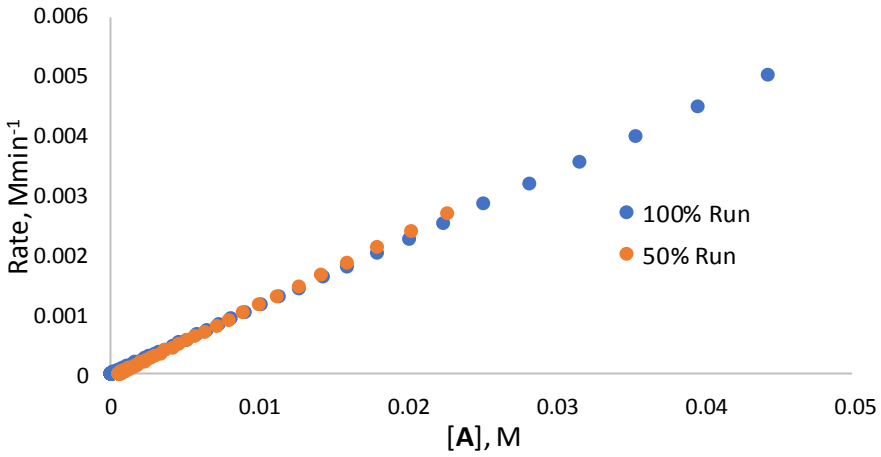

Figure 3.24. Plot of Rate vs. [A] for 100% and 50% experiments for catalyst stability test

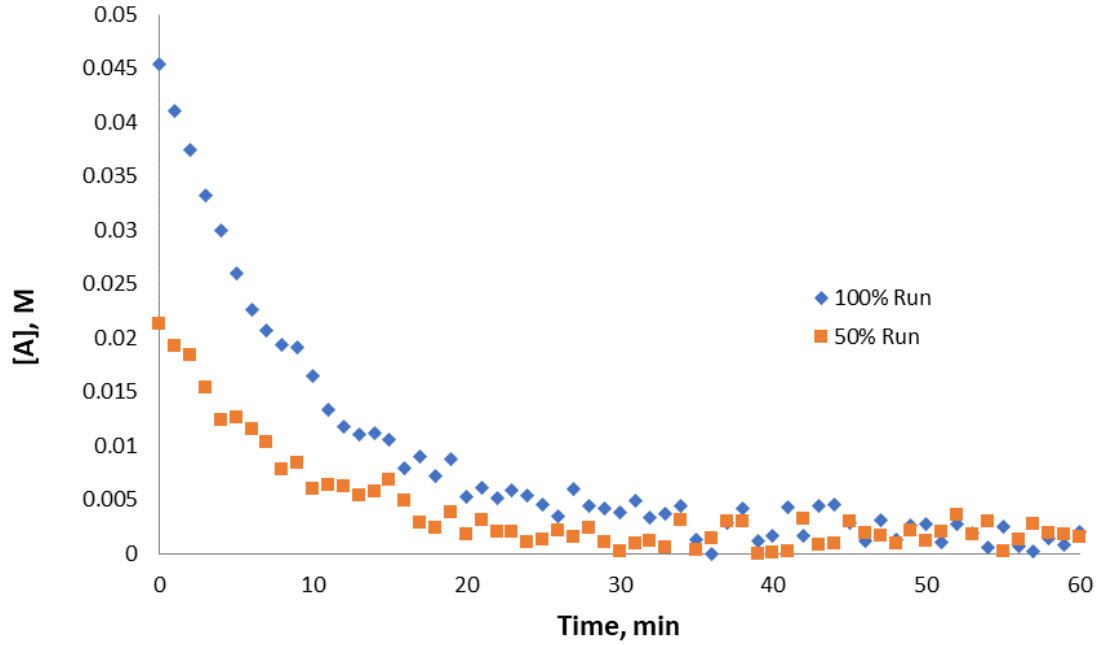

Figure 3.25. Decay plots of [A] over time for 100% and 50% runs

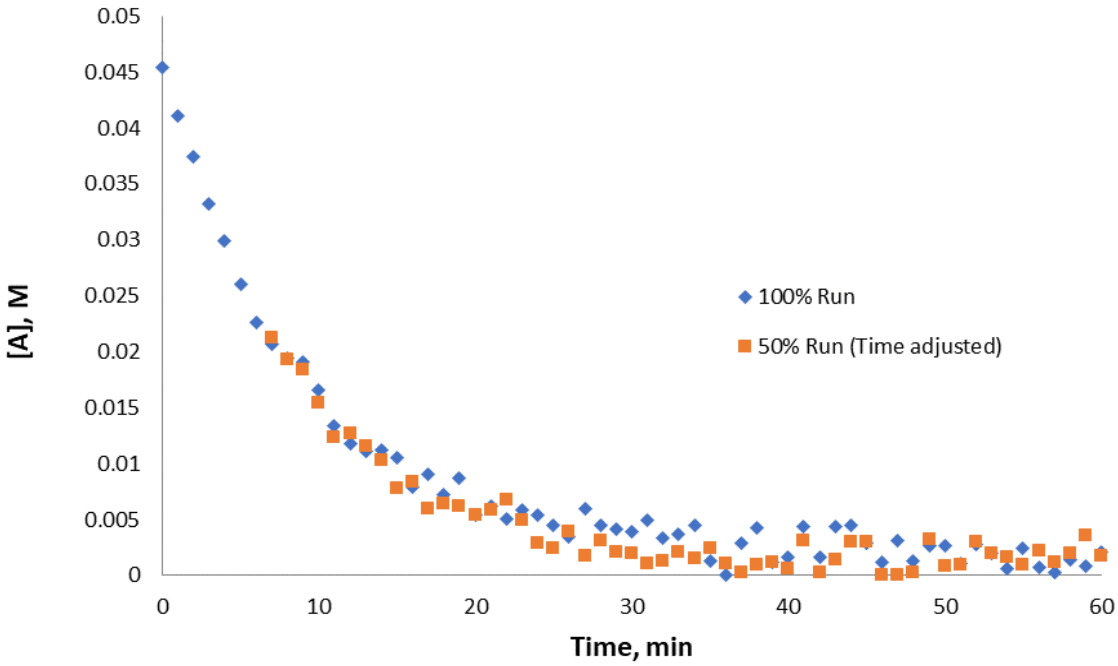

Figure 3.26. Time-resolved plots of [A] vs. time for 100% and 50% runs

Two separate experiments were performed under synthetically relevant conditions. The first experiment, which is labeled the 100% run, was carried out at the reaction conditions shown in table 3.6. The second experiment, labeled the 50% run, was carried out under identical conditions as the 100% run. However, the initial concentration of the reactant in the 50% run was half that of the epoxide concentration in the 100% run. Both experiments were monitored with *in-situ* IR spectroscopy by measuring the growth of the product at 1484 cm^{-1}, which is also the C-H wag of the C2 carbon of **2**. This wavenumber was chosen because CH_3CN has an absorbance at 1386 cm^{-1}, which overlaps the absorbance of the product. Decay plots were obtained for both experiments as shown in figure 3.27. Graphical overlay was observed for a time-resolved plot of the decay over time for both experiments indicating the catalyst remained stable in CH_3CN, even in the absence of Coll*HCl (Figure 3.28).

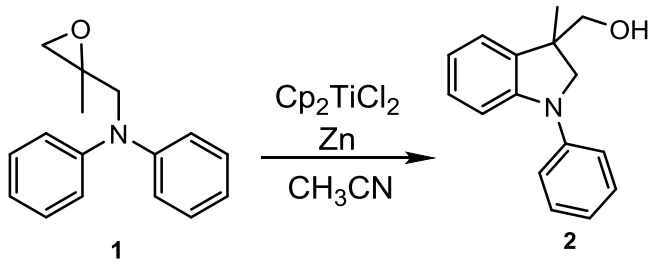

Scheme 3.9. Test for catalyst stability in CH_3CN

Table 3.6. Reaction conditions for catalyst stability test in CH_3CN

Run	[**1**], M	Cp_2TiCl_2, M	Zn, M	CH_3CN, mL	T^oC
100%	0.055	0.0055	0.011	15	90
50%	0.0275	0.0055	0.011	15	90

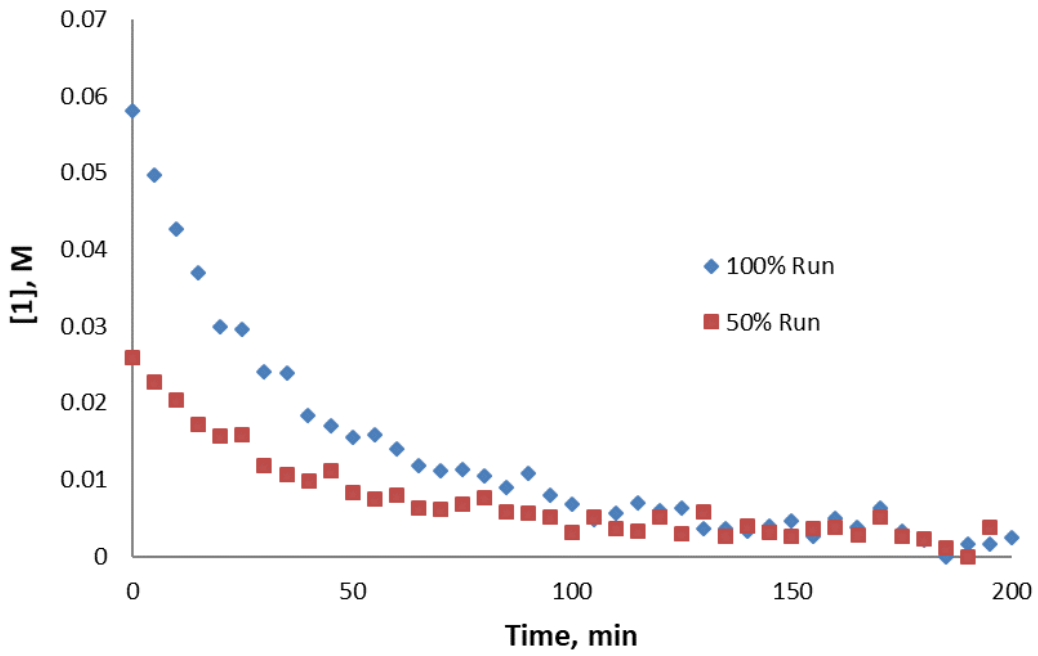

Figure 3.27. Decay plots for 50% and 100% runs (see table 3.6 for reaction conditions)

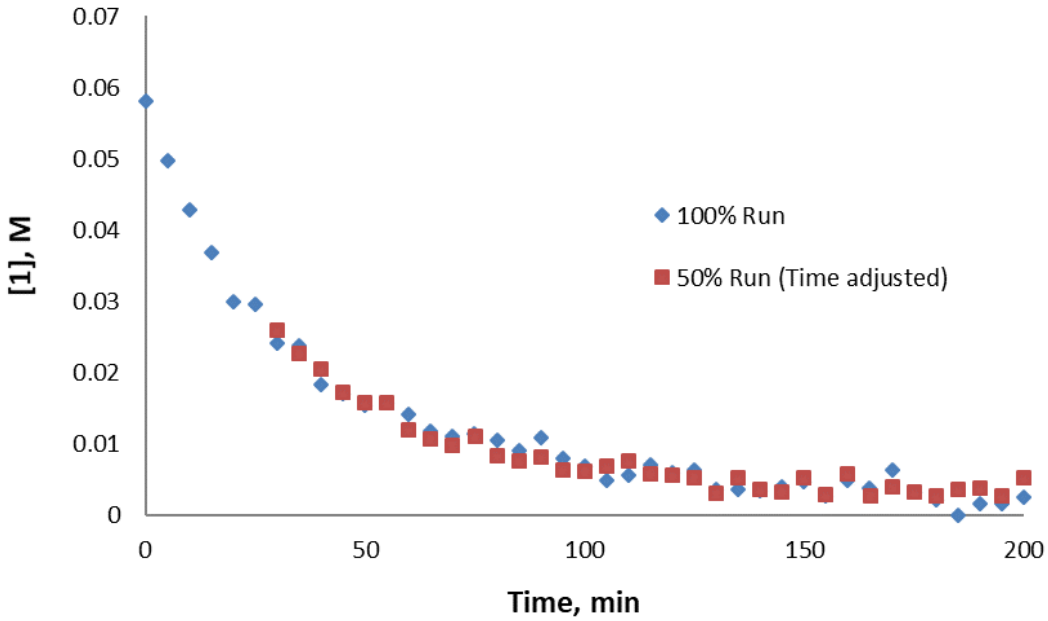

Figure 3.28. Time-resolved decay plots for 50% and 100% runs (see table 3.6 for reaction conditions)

3.3.5.2 Substrate scope and rate studies with CH_3CN as solvent

Gansäuer and co-workers performed a series of radical arylation experiments with a number of epoxides in acetonitrile and the results are summarized in scheme 3.10. It was observed that the system worked well with the epoxides tested including electron poor epoxides without needing an electron withdrawing substituent on the Cp ligand of the titanocene complex. It was however discovered that Coll*HCl was still needed to stabilize the catalyst for some epoxides. Also, moderate to low yields where observed for **21** and **22**.[27]

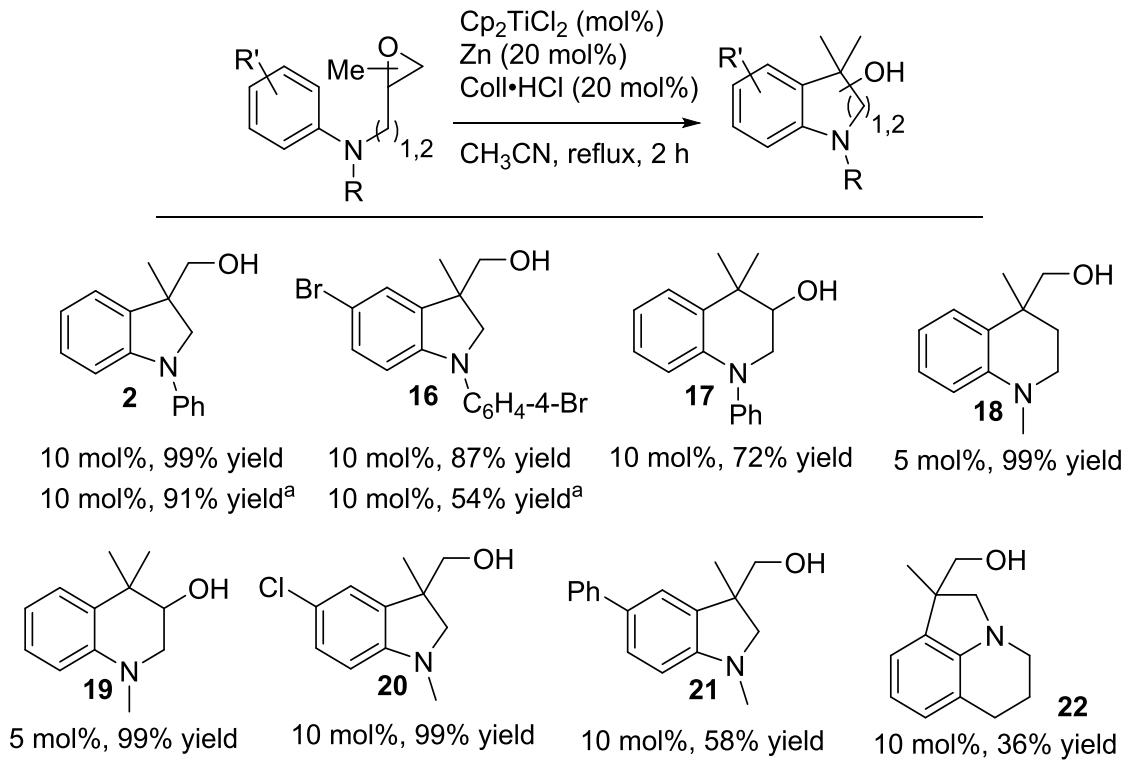

Scheme 3.10. Radical arylation of epoxides in CH_3CN; [a] Without Coll*HCl; [Epoxide] = 0.1 M; Zn = 20 mol%; CH_3CN = 5 mL

The rate of the radical arylation of **1** to **2** in acetonitrile was obtained and compared to the rate obtained in THF. It was observed that the rate for the radical arylation was much slower in CH_3CN (Table 3.7). This observation could be attributed to the strong coordination of acetonitrile to the titanocene which could negatively impact the transfer of electrons to and from the titanocene complex (Scheme 3.11). Acetonitrile is more polar than THF, as a result, the negative impact on rate in acetonitrile could also be because the radical σ- complex (**B**) is stabilized by the polar solvent, which slows down the back-electron transfer to the pendant titanocene moiety. It should however be noted that the presence of $Cp_2Ti(III)Cl$ as an active species in the radical arylation process cannot be ruled out in CH_3CN because its oxidation wave is also seen in the cyclic voltammogram shown in figure 3.21.

Table 3.7. Impact of solvent choice on rate of radical arylation

Catalyst	Additives	Solvent	T, ^oC	Reductant	kobs, min^{-1}
Cp_2TiCl_2	Coll*HCl	THF	60	Mn	0.79 ± 0.09
Cp_2TiCl_2		CH_3CN	90	Zn	0.032 ± 0.008

Reaction conditions: [**1**] = 28 mM; [Cp_2TiCl_2] = 5.6 mM; [Mn]/[Zn] = 11.2 mM; [Coll*HCl] = 11.2 mM

Although we found the titanocenium cation to be a promising reagent, being that it could successfully reduce electron poor epoxides, we were not satisfied with its impact on the rate observed and the need for Col*HCl to stabilize the catalyst in some cases. So, based on the limitations observed with acetonitrile as solvent, we wanted to synthesize the titanocenium complex in a less coordinating solvent, most preferably THF. To achieve this, we needed to understand the impact of ligands on the activity of titanocene complexes.

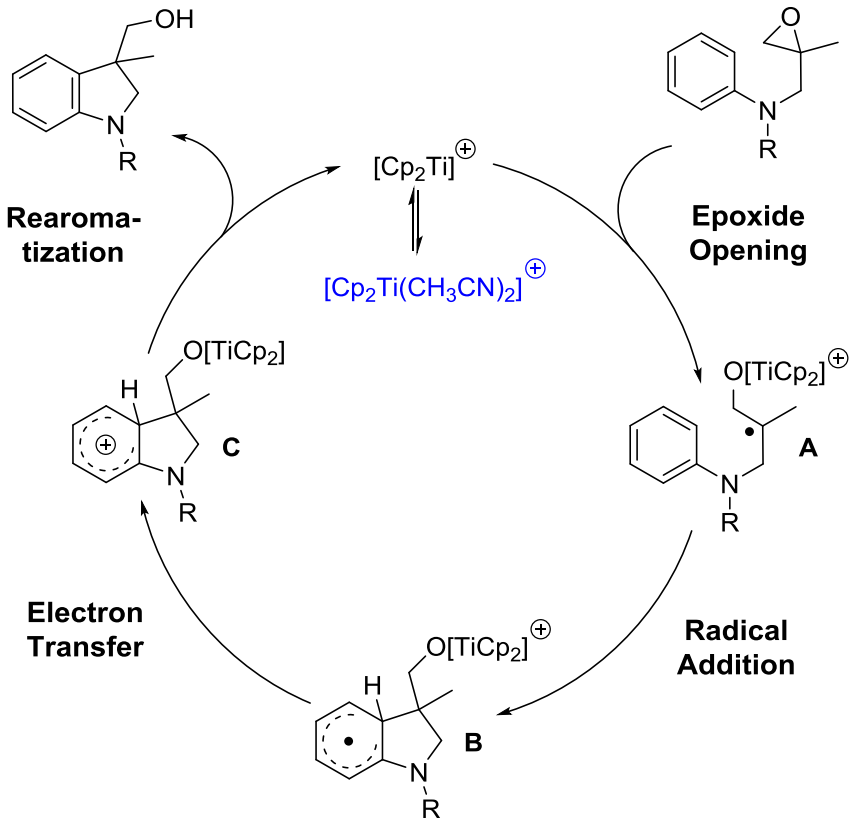

Scheme 3.11. Proposed catalytic cycle for radical arylation in CH_3CN

3.3.6 Ligand effects on the identity and activity of titanocene(III) complexes

The titanocenium cation could successfully be generated in THF by mixing equimolar amounts of sodium borohydride ($NaBH_4$) and titanocene ditriflate, which was synthesized based on the method outlined by Luinstra and co-workers (Scheme 3.12).[31] The crystal structure has been isolated by Thewalt and co-workers and it is shown to have one triflate anion coordinated to the titanocenium cation (Figure 3.29).[32] This complex has a redox potential like that measured in CH_3CN (Figure 3.30). It also forms a sky-blue colored solution (Appendix figure 6.112B) and has a C-H wag at 813 cm^{-1} like that seen in acetonitrile (Figure 3.31).[27]

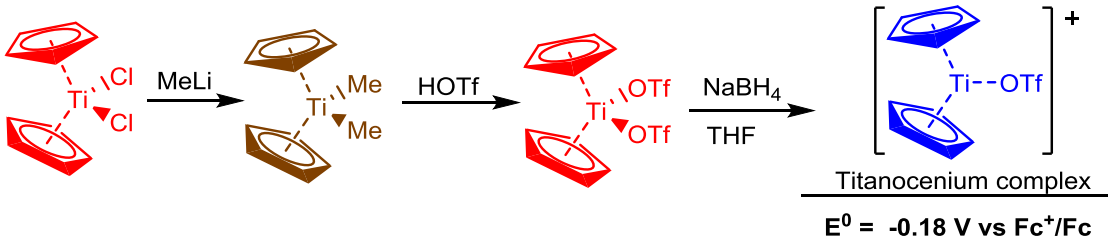

Scheme 3.12. Synthesis of titanocenium complex in THF from titanocene ditriflate[31]

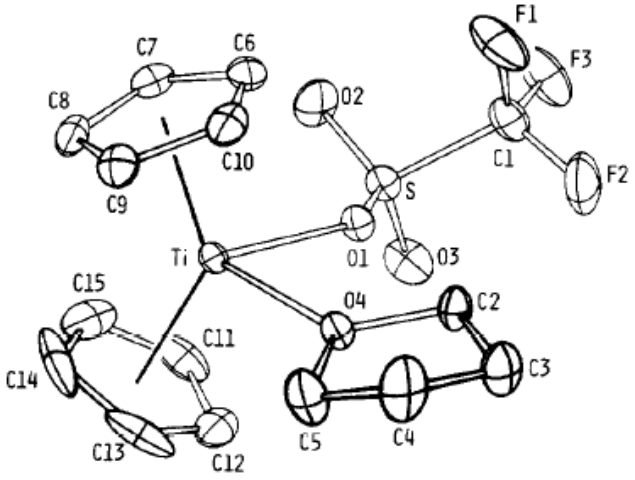

Figure 3.29. Titanocenium complex in THF[32]

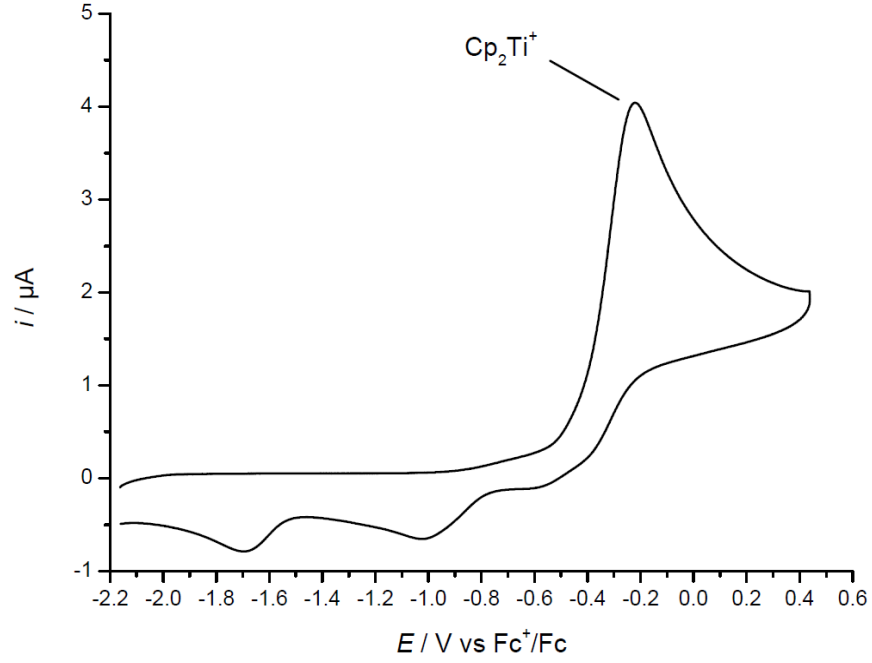

Figure 3.30. CV of 2 mM $NaBH_4$-$Cp_2Ti(OTf)_2$ in 0.2 M Bu_4NPF_6/THF at υ = 0.2 Vs^{-1}

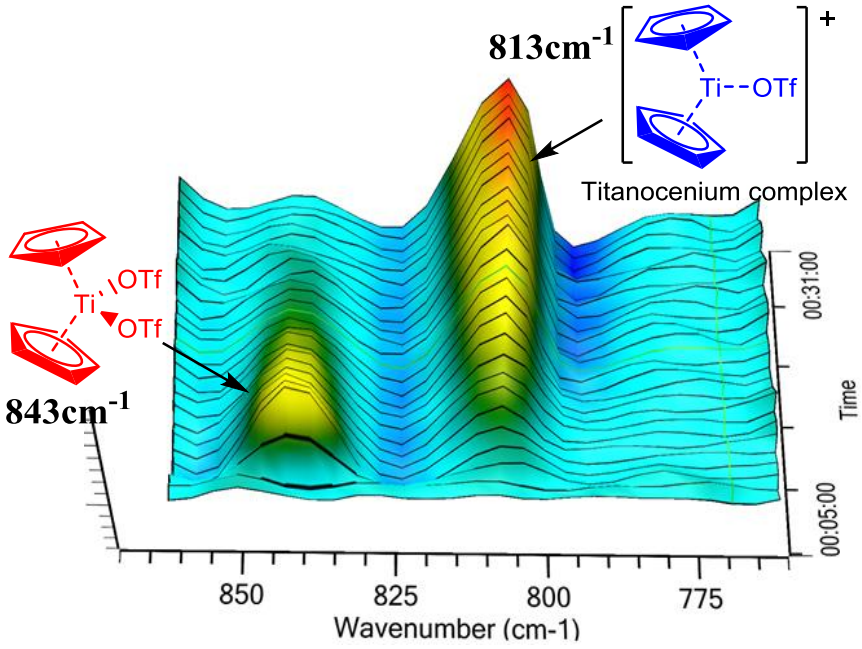

Figure 3.31. *In situ*-IR of $NaBH_4$-$Cp_2Ti(OTf)_2$ in THF

The radical arylation of **1** to **2** was performed with the titanocene triflate complex generated in THF and the reaction proceeded smoothly even at lower catalyst loadings (Scheme 3.13). The titanocene triflate was also stable under the reaction conditions as shown by the graphical overlay of the decay plots of the 50 and 100 % runs (Figure 3.32, **2** monitored at 1484 cm^{-1}).[27]

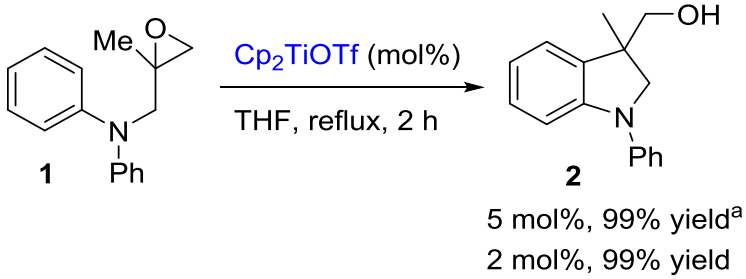

Scheme 3.13. Arylation of 1 to 2 with Cp_2Ti(III)OTf; a. 30 min; [1] = 0.1 M; [$NaBH_4$]: [$Cp_2Ti(OTf)_2$] = 1:1; THF = 5 mL

Table 3.8. Reaction conditions for catalyst stability test with $Cp_2Ti(OTf)_2$

Run	[**1**], M	$[Cp_2Ti(OTf)_2]$, M	$[NaBH_4]$, M	THF, mL	T, °C
100%	0.0556	0.0055	0.0058	15	60
50%	0.0279	0.0055	0.0058	15	60

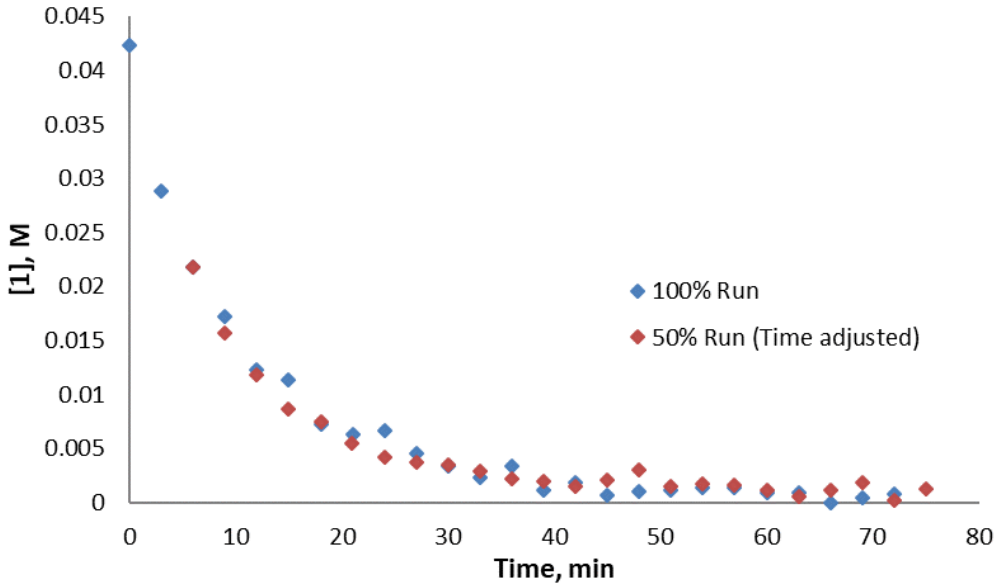

Figure 3.32. Catalyst stability test with $Cp_2Ti(III)(OTf)$

Kinetic studies showed that the radical arylation catalyzed by the titanocene(III) triflate in THF is much faster than in acetonitrile, supporting our initial hypothesis that acetonitrile is strongly coordinating to the titanium metal, thus negatively impacting the transfer of electrons to and from the catalyst.[27] Gansauer and co-workers also showed that a number of epoxides, including electron deficient epoxides worked well, even at lower catalyst loadings to produce good yields of products with titanocene triflate as catalyst without any addition of a salt additive (Scheme 3.14).[27]

Table 3.9. Impact of solvents and ligands on the activity of titanocene(III) complexes

Cp_2TiX_2	Solvent	T, °C	Reductant	E/V vs Fc+/Fc	k_{obs}, min^{-1}
Cp_2TiCl_2	THF	60	Mn	-0.77	0.79 ± 0.09[a]
Cp_2TiCl_2	CH_3CN	90	Zn	-0.18	0.032 ± 0.008
$Cp_2Ti(OTf)_2$	THF	60	$NaBH_4$	-0.18	0.12 ± 0.02

[a] 11.2 mM Coll*HCl added; [**1**] = 28 mM; [Cp_2TiX_2] = 5.6 mM; [Mn]/[Zn] = 11.2 mM; [$NaBH_4$] = 5.8 mM; Solvent = 15 mL

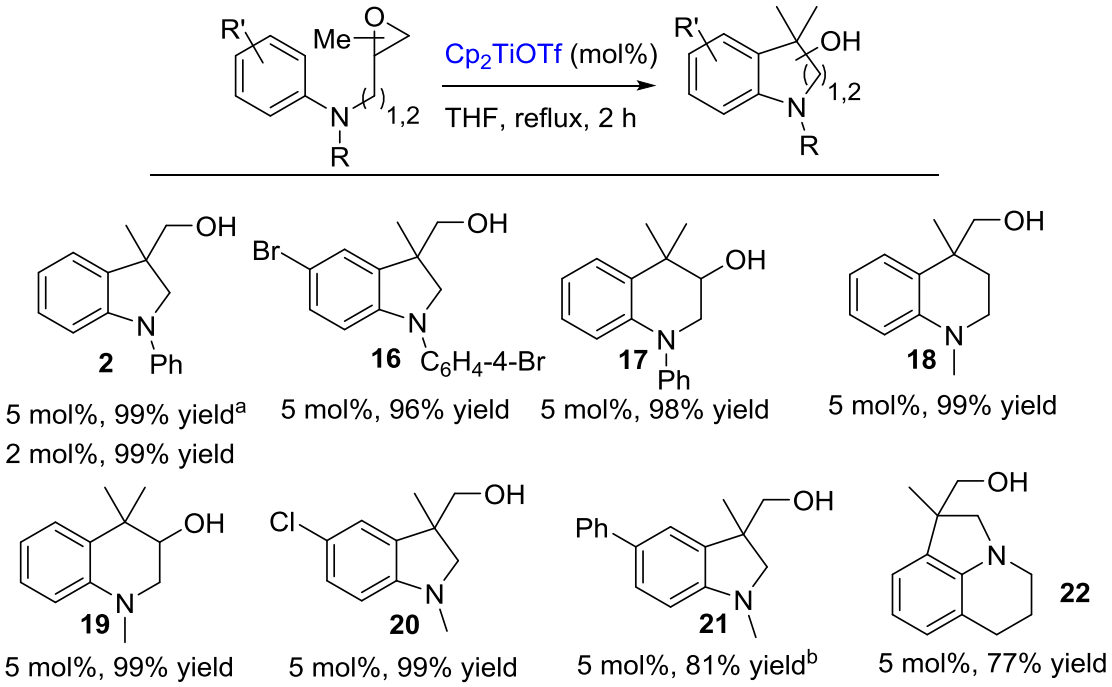

Scheme 3.14. Arylation of **1** to **2** with $Cp_2Ti(III)OTf$; a. 30 min; b. 1 h; [Epoxide] = 0.1 M; [$NaBH_4$]: [$Cp_2Ti(OTf)_2$] = 1:1; THF = 5 mL

3.3.7 The impact of acetonitrile on the radical arylation of epoxides in THF

From our studies, we know that acetonitrile strongly coordinates to titanocene(III) complexes thereby reducing their ability to transfer electrons via an inner sphere process. This was evident as the rate of the radical arylation of epoxides was significantly reduced when acetonitrile was used instead of THF as solvent (0.032 ± 0.008 min^{-1} in CH_3CN and 0.79 ± 0.09 min^{-1} in THF).[27] To further investigate the role acetonitrile plays on a

mechanistic level, an experiment was designed to measure the rate of the radical arylation of **1** to **2** in THF with increasing amounts of acetonitrile. From this experiment, the order of acetonitrile could be obtained. We could also determine to what extent the mixture of THF and acetonitrile hampered the activity of the titanocene catalyst. The radical arylation of **1** to **2** was carried out with $Cp_2Ti(III)Cl$ as catalyst in the presence and absence of Coll*HCl, and with $Cp_2Ti(III)OTf$ as catalyst.

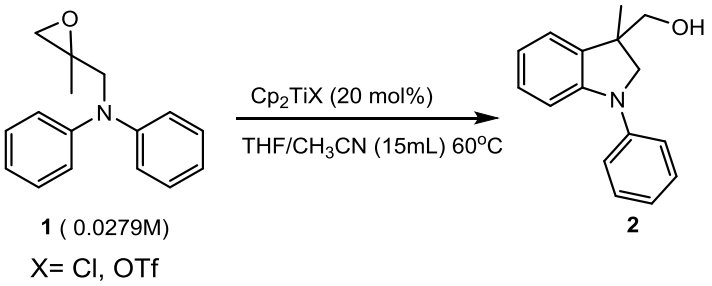

Scheme 3.15. Impact of CH_3CN on the radical arylation of **1** to **2** in THF

The initial rate of the radical arylation of the epoxide (**1**) was measured and a plot of initial rate vs. $[CH_3CN]$ was drawn as shown in figure 3.33. As expected, the initial rate was reduced with increasing amounts of acetonitrile. It was observed that the initial rate for the arylation process was about 4 times slower when $Cp_2Ti(III)OTf$, instead of $Cp_2Ti(III)Cl$, was used as the catalyst. This observation supports our work, which showed that the overall rate of reaction was slower when the titanocene triflate catalyst was used in place of titanocene chloride (0.11 ± 0.01 min^{-1} with Cp_2TiOTf and $0.79 \pm 0.09 min^{-1}$ with Cp_2TiCl). This is because the active catalyst formed in the former is a titanocenium cation, which is electron deficient and would open the epoxide a lot slower than the later catalyst.[27]

The relationships between the initial rates for the radical arylation of epoxide (**1**) with $Cp_2Ti(III)Cl$ with and without Coll*HCl were studied (Figure 3.34). It was observed that the initial rates for the arylation process were slightly slower, by about 10%, in the absence of Coll*HCl. This observation supports prior work that the rate for the overall radical arylation was enhanced by Coll*HCl.[33] It was also observed that the initial rate was not impacted until about 114 equivalents (with respect to the catalyst) of acetonitrile was added in the presence of Coll*HCl. This observation gives an insight into the stabilizing effect of Coll*HCl on the titanocene catalyst in this system. Conversely, it took about 45 equivalents (with respect to catalyst) of acetonitrile to impact the initial rate in the absence of Coll*HCl. From this information, one could infer that the active titanocene catalyst is about 3 times more stable with Coll*HCl as an additive.

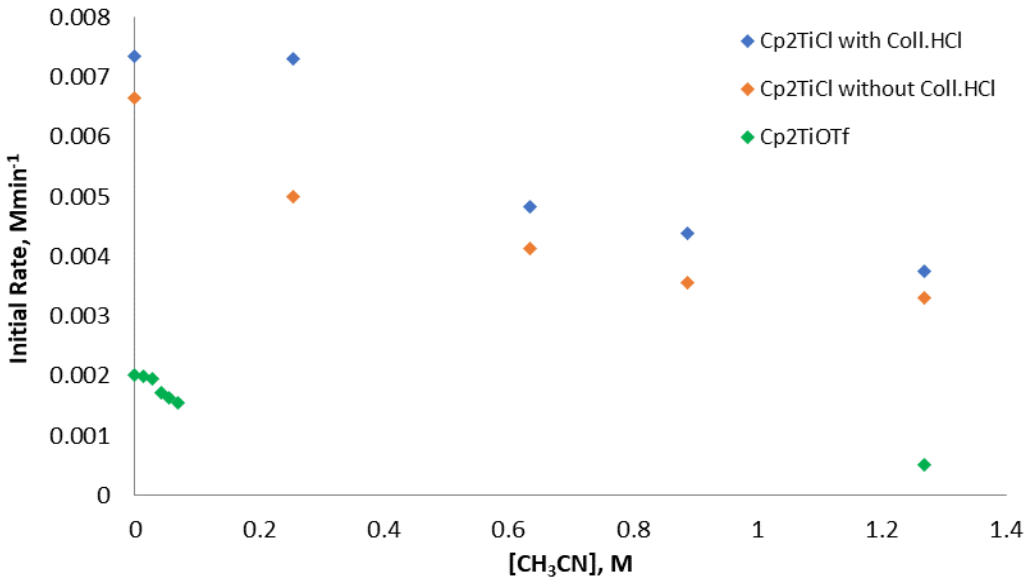

Figure 3.33. Plot of Initial rate vs. CH_3CN for three different experiments

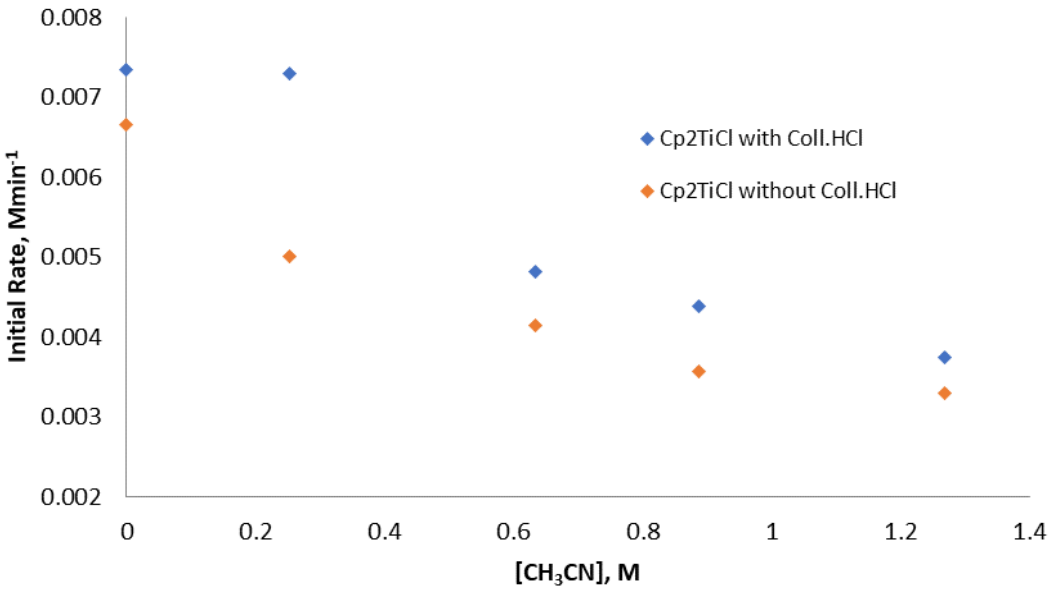

Figure 3.34. Plot of Initial rate vs. CH_3CN for experiments with Cp_2TiCl as catalysts with and without Coll*HCl

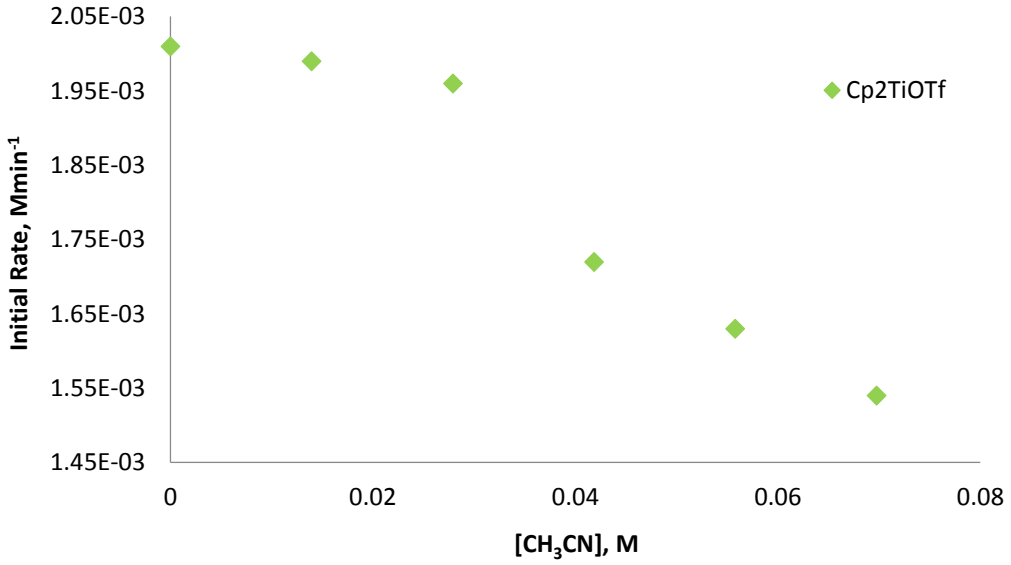

Figure 3.35. Plot of Initial rate vs. CH_3CN for experiments with Cp_2TiOTf

When $Cp_2Ti(III)OTf$ was used as the catalyst, it was observed that the initial rate for the reaction was not impacted until about 8 equivalents (with respect to the catalyst) of acetonitrile was added (Figure 3.35). In comparison to the results obtained when

Cp_2TiCl with Coll*HCl was used as catalyst, it is evident that the titanocene triflate catalyst is far less stable when acetonitrile is added. This could be attributed to the absence of the supramolecular complex, which is formed and serves as a resting state when Cp_2TiCl is used with Coll*HCl as an additive. The orders for acetonitrile were determined for the three experiments using the initial rates method. The results are summarized in the table 3.10.

Table 3.10. The orders of acetonitrile for the three experiments using the initial rates method

Cp_2TiX_2	Additive	Order of CH_3CN[a]
Cp_2TiCl_2	Coll*HCl	-0.48 ± 0.06
Cp_2TiCl_2	-	-0.29 ± 0.05
$Cp_2Ti(OTf)_2$	-	-0.26 ± 0.04[b]

a. [1] = 0.0280 M; $[Cp_2TiX_2]$ = 0.0056 M; [Mn] = 0.0112 M; $[NaBH_4]$ = 0.0058 M; [Coll*HCl] = 0.0112 M; $[CH_3CN]$ = 0.25 M – 1.27 M; b. $[CH_3CN]$ = 0.028 M – 0.070 M; Total solvent volume = 15 mL

As seen in table 3.10, an inverse order was obtained for acetonitrile in each experiment. It could be inferred from the calculated orders that acetonitrile negatively impacts the rate of the arylation process via a complex mechanistic pathway. Prior reasoning however suggests that acetonitrile coordinates to the titanocene complex and as a result, negatively impacts the inner-sphere electron transfer to and from the active catalyst. The orders for CH_3CN are similar in studies with Cp_2TiCl_2 in the absence of Coll*HCl and $Cp_2Ti(OTf)_2$ suggesting that the reaction pathways involving CH_3CN are similar in the absence of a salt adduct.

3.3.8 Alternative titanocene complexes in THF

3.3.8.1 Designing stable titanocene(III) complexes for radical arylations in THF

So far, a suitable catalyst for generating the titanocenium cation has been developed with the use of $Cp_2Ti(III)OTf$. This titanocenium complex efficiently catalyzes the radical arylation of epoxides at low catalyst loading and is stable without a salt additive. The method of catalyst activation can be problematic because it requires precisely equimolar amounts of $NaBH_4$ to generate the catalyst. Excess amounts of $NaBH_4$ leads to the formation of $Cp_2Ti(III)BH_4$, which is ineffective towards the arylation process. Also, titanocene ditriflate is prepared with triflic acid, which is an expensive super acid that can be hard to handle.[31]

As a corollary, alternative, milder acids, which we believe will form loosely coordinating ligands with the titanocene, have been used in place of triflic acid to synthesize new titanocene complexes (Scheme 3.16). With these new complexes, the active catalysts were easily activated with a metal reductant instead of $NaBH_4$. These titanocene(III) complexes efficiently catalyzed the radical arylation of **1** to **2**, and were stable without a salt additive as shown in the results obtained from the catalyst stability tests (Figures 3.36 to 3.39).

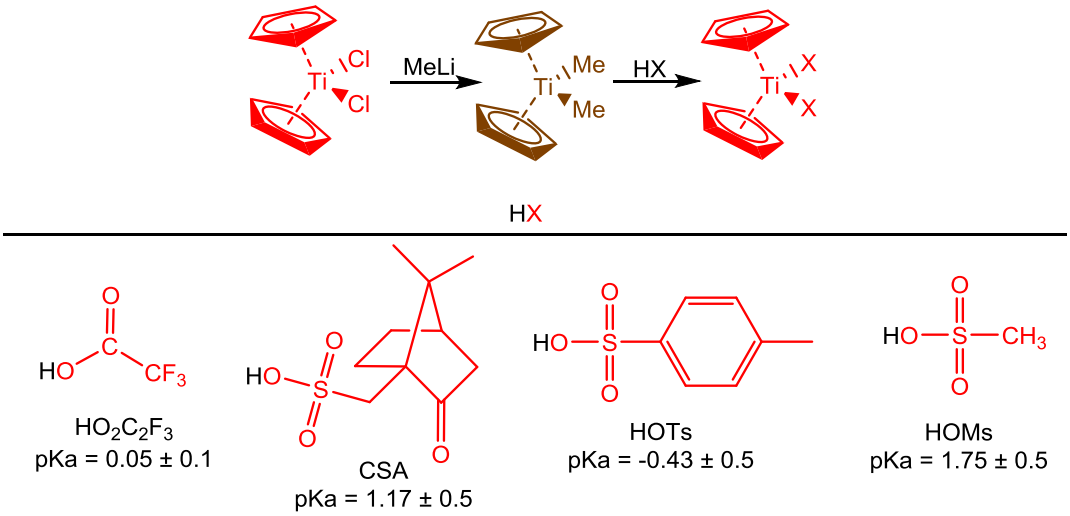

Scheme 3.16. Alternative milder acids for making titanocene complexes

Table 3.11. Conditions for the titanocene catalyst stability tests

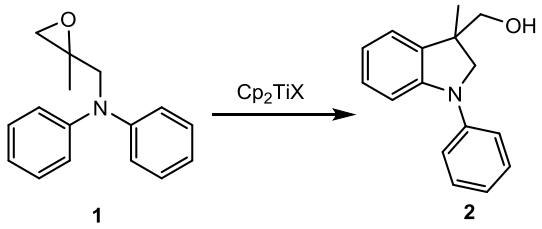

Run	Epoxide (M)	Cp_2TiX_2 (M)	Zn (M)	THF (mL)	T°C
100%	0.0557	0.0055	0.011	15	60
50%	0.0279	0.0055	0.011	15	60

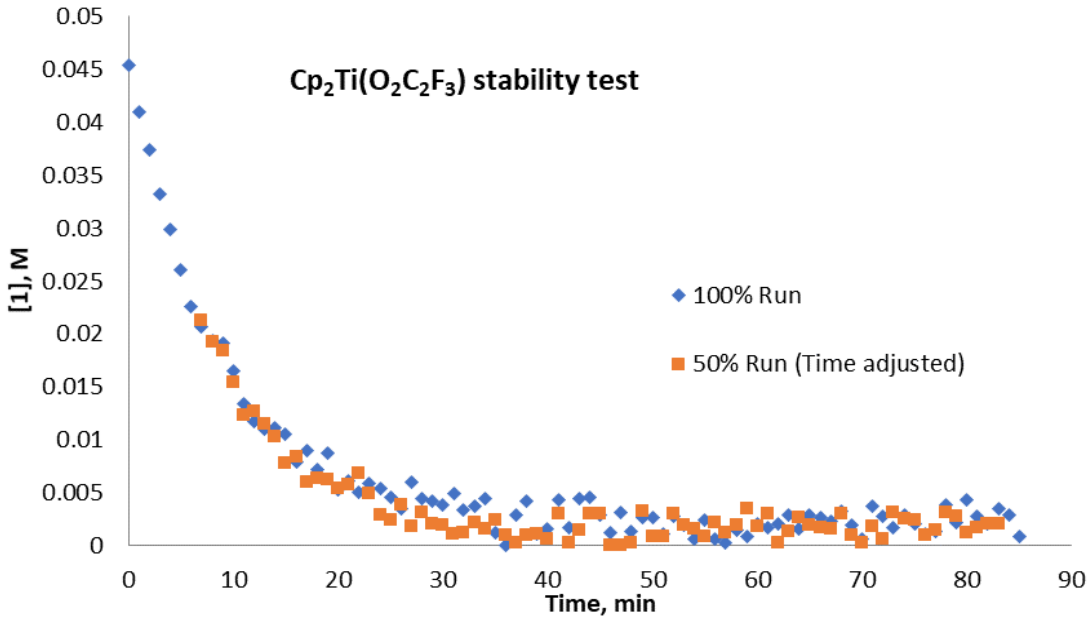

Figure 3.36. Time-adjusted decay plots for 100% and 50% runs with $Cp_2Ti(O_2C_2F_3)_2$ as catalyst

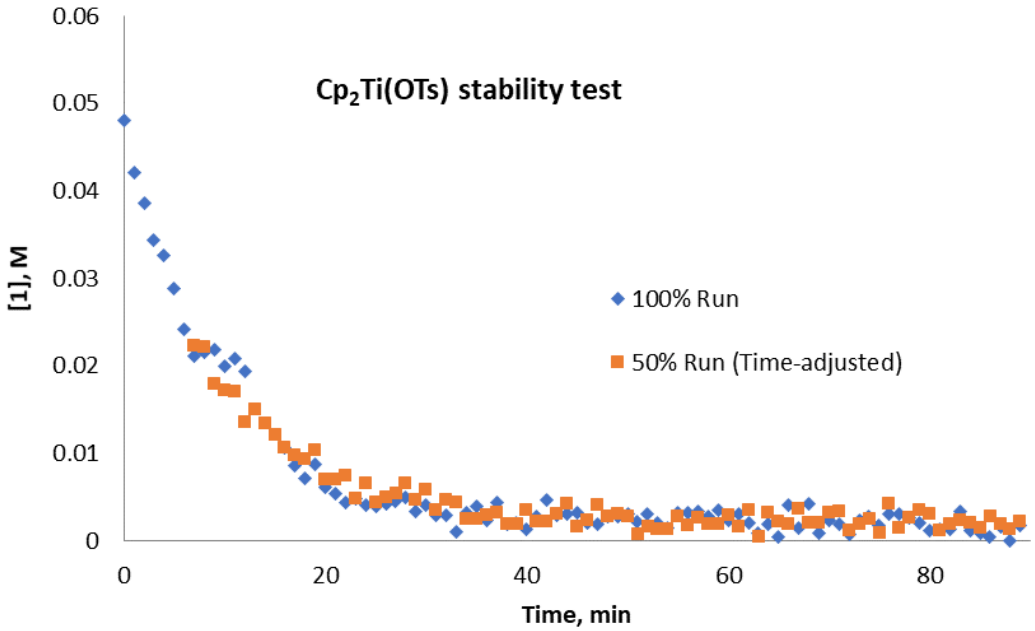

Figure 3.37. Time-adjusted decay plots for 100% and 50% runs with $Cp_2Ti(OTs)_2$ as catalyst

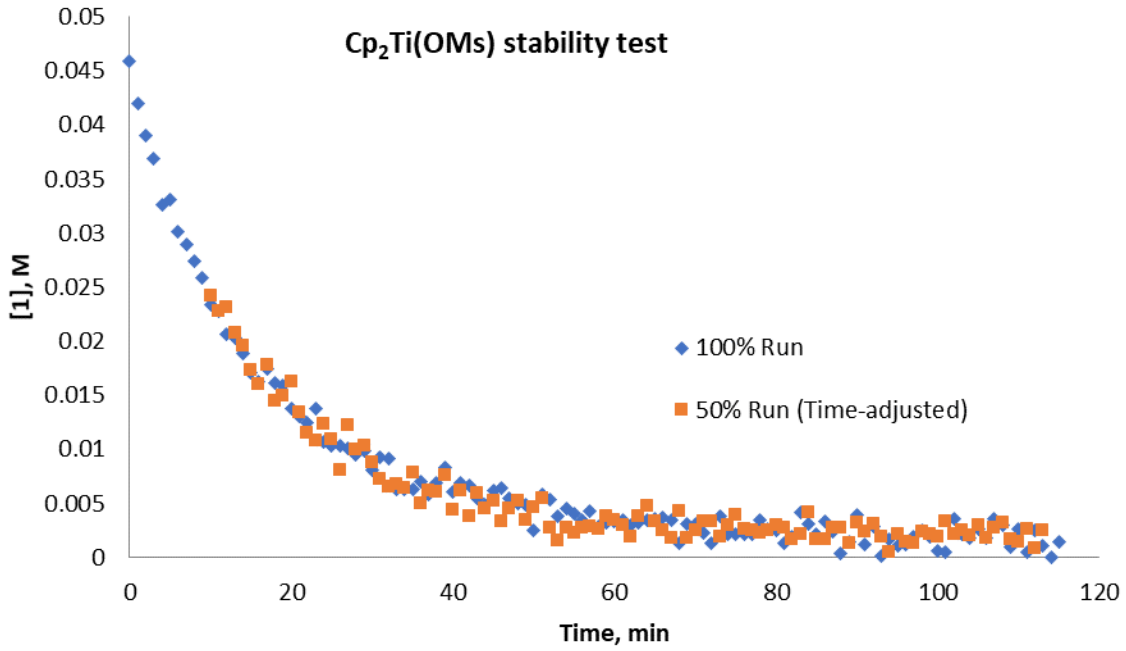

Figure 3.38. Time-adjusted decay plots for 100% and 50% runs with $Cp_2Ti(OMs)_2$ as catalyst

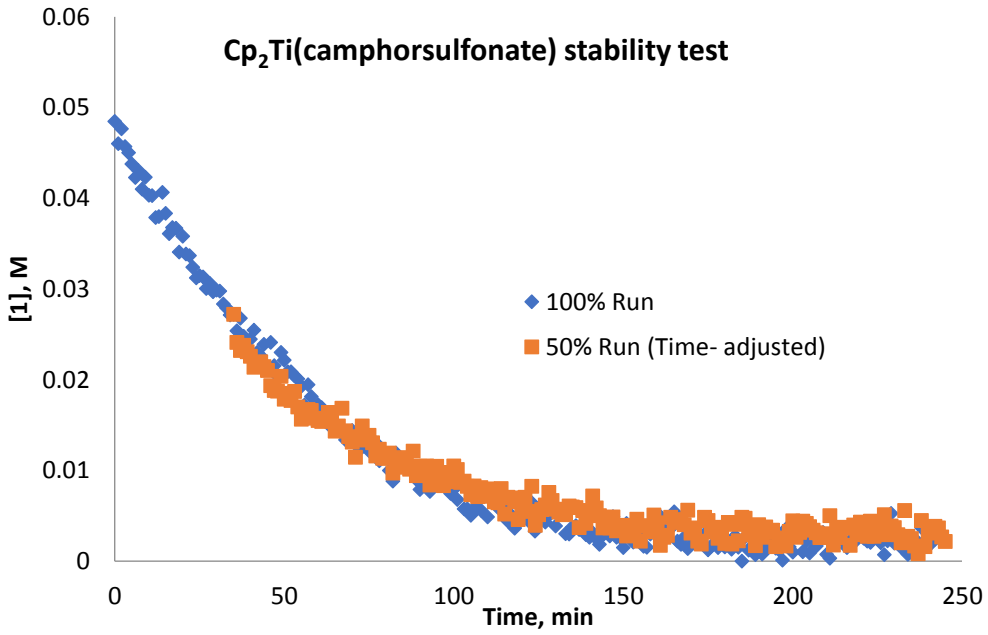

Figure 3.39. Time-adjusted decay plots for 100% and 50% runs with $Cp_2Ti(camphorsulfonate)_2$ as catalyst

The observed rate (k_{obs}) for the radical arylation of **1** to **2** with the titanocene(III) complexes were measured and the results are summarized in table 3.12. As seen in table 3.12, the radical arylation is fastest with Cp_2TiCl-Coll*HCl as catalyst.[8] The observed rates from the radical arylation are similar within experimental error for $Cp_2Ti(OTs)$, $Cp_2Ti(OMs)$, $Cp_2Ti(O_2C_2F_3)$, and $Cp_2Ti(OTf)$. The observed rate is much slower with Cp_2Ti(camphorsulfonate) even though the active titanocene species has a similar redox potential compared to $Cp_2Ti(OMs)$, $Cp_2Ti(O_2C_2F_3)$. A plausible explanation for this observation could be a result of steric effects due to the bulky camphorsulfonate ligand loosely coordinated to the titanocene complex potentially hindering the back-electron transfer, which in this case, is most likely the turnover-limiting step.

Table 3.12. k_{obs} for the radical arylation of **1** with Cp_2TiX_2

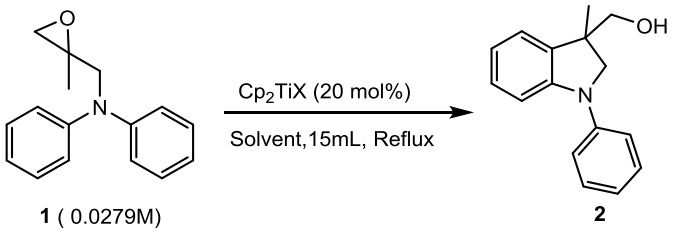

1 (0.0279M) **2**

Cp_2TiX_2	Solvent	T, °C	Reductant	E/V vs Fc+/Fc	k_{obs}, min^{-1}	**1** order	Cp_2TiX_2 order
Cp_2TiCl_2	THF	60	Mn	-0.77	0.79 ± 0.09	1.1 ± 0.1	0.8 ± 0.1
Cp_2TiCl_2	CH_3CN	90	Zn	-0.18	0.032 ± 0.008	1.11 ± 0.04	1.0 ± 0.1
$Cp_2Ti(OTf)_2$	THF	60	$NaBH_4$	-0.18	0.12 ± 0.02	1.0 ± 0.1	0.9 ± 0.1
Cp_2Ti(camphorsulfonate)$_2$	THF	60	Zn	-0.54	0.019 ± 0.002	1.1 ± 0.2	0.9 ± 0.1
$Cp_2Ti(OMs)_2$	THF	60	Zn	-0.57	0.06 ± 0.01	1.3 ± 0.3	1.0 ± 0.2
$Cp_2Ti(OTs)_2$	THF	60	Zn	-0.77	0.10 ± 0.01	1.1 ± 0.2	0.9 ± 0.1
$Cp_2Ti(O_2C_2F_3)_2$	THF	60	Zn	-0.51	0.12 ± 0.02	1.1 ± 0.2	0.9 ± 0.1

k_{obs} were obtained from an average of three separate experiments. [Mn]/[Zn]= 11 mM, [$NaBH_4$] = 5.8 mM, [Coll*HCl] = 11 mM

It should also be noted that these newly formed titanocene complexes have redox potentials ranging from -0.77V to -0.51V versus Fc+/Fc as internal standard. These potentials reported by Gansäuer and co-workers suggest that these ligands are not as loosely coordinated as compared to the triflate ligand, indicating that a different titanocene complex could be the active species in this system. ReactIR data also showed that the active catalysts have absorbances between $802cm^{-1}$ – $809cm^{-1}$ as compared to the $813cm^{-1}$ for the titanocenium cation. Further suggesting the formation of a different active titanocene complex (See appendix figure 6.118).

Based on these results, a suitable surrogate for $Cp_2Ti(OTf)$ can be found in $Cp_2Ti(OTs)$, $Cp_2Ti(OMs)$, $Cp_2Ti(O_2C_2F_3)$ without compromising the rate of reaction and catalyst stability. This is however based on the radical arylation of **1** to **2** and should not be generalized for other epoxides. Gansauer and co-workers further studied the activity of these titanocene(III) complexes with a variety of epoxides and the results are summarized in scheme 3.17.

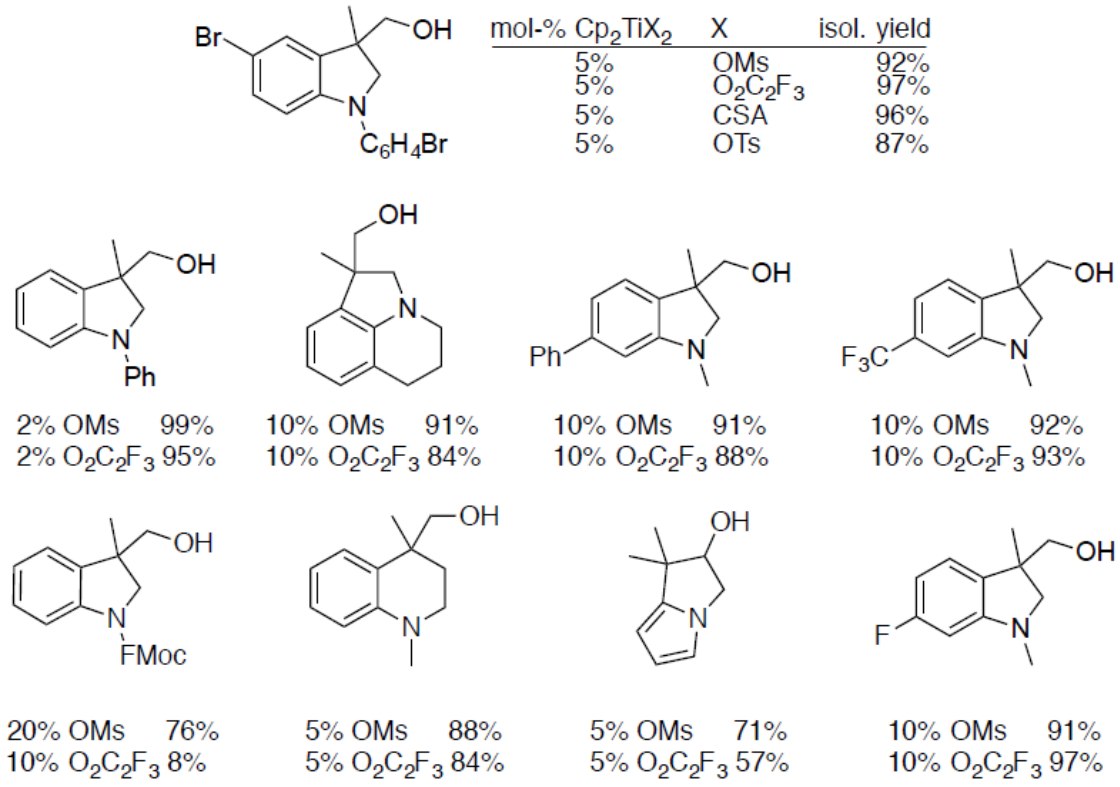

Scheme 3.17. Substrate scope to test the impact of ligands on catalyst activity. Fluorenylmethyloxycarbonyl (FMoc)

3.3.8.2 Epoxide opening with different catalysts

The impact of ligands on the activity of titanocene(III) complexes was further investigated by measuring the rate constants for opening epoxide **14**. The results are summarized in table 3.14. The epoxide opening experiment was performed under pseudo-first order conditions and the rate constants were obtained by monitoring the decay of the active titanocene(III) band with a SpectroVis, which is a portable visible to near-IR spectrophotometer.

Table 3.13. Rate constant for epoxide opening

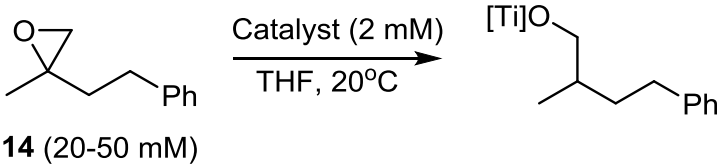

14 (20-50 mM)

Entry	Cp_2TiX_2	Rate Constant, $M^{-1}s^{-1}$	Epoxide order
1	Cp_2TiCl_2[a]	1.1 ± 0.1	1.0 ± 0.1
2	$Cp_2Ti(OTf)_2$[b]	0.0035 ± 0.0003	1.1 ± 0.1
3	$Cp_2Ti(Camphorsulfonate)_2$	0.019 ± 0.005	1.0 ± 0.3
4	$Cp_2Ti(OMs)_2$	0.013 ± 0.003	1.3 ± 0.2
5	$Cp_2Ti(OTs)_2$	0.022 ± 0.005	1.1 ± 0.2
6	$Cp_2Ti(O_2C_2F_3)_2$	0.019 ± 0.005	0.9 ± 0.2

$[Cp_2TiX_2]$ = 2 mM; [Zn] = 16 mM; THF = 3 mL; λ_{max} for [Ti(III)] is 675 nm; [Ti(III)] solutions were filtered before commencing runs; [a] 4 mM Coll*HCl added; [Mn] = 8 mM; λ_{max} for [Ti(III)] is 800 nm [b] [NaBH4] = 2 mM; 4-10 mM CHD added; λ_{max} for [Ti(III)] is 800 nm

The rate constants obtained from the epoxide opening experiment with the different titanocene complexes, except for $Cp_2Ti(III)Cl$ and $Cp_2Ti(III)OTf$, were similar within error uncertainty. The rate constant for opening **14** with $Cp_2Ti(III)OTf$ is much slower than the other titanocene(III) complexes because it has the lowest redox potential reported by Gansäuer and co-workers (Table 3.12). Further suggesting that the titanocene(III) complexes are not titanocenium(III) cations but are stable even in the absence of salt additives. This observation also indicates that although the titanocenium cation is very slow at opening epoxides it effectively facilitates the back-electron transfer in the arylation of **1** to **2**, which is turnover-limiting.[8,27]

3.4 Conclusion

The $Cp_2TiCl/(Cp_2TiCl)_2$ couple was introduced by Nugent and RajanBabu as a very mild and chemoselective reagent for the reductive opening of epoxides.[34–36] We have demonstrated that in the titanocene catalyzed atom-economical radical arylation of epoxides to form indoles, Coll*HCl prevents decomposition of titanocene(III) chloride by the reversible formation of a supramolecular complex that provides a resting state for the catalyst and is thermally more stable than the $Cp_2TiCl/(Cp_2TiCl)_2$ couple.[6,8,18]

Cyclic voltammetry, computational, and kinetic studies were performed to further investigate the composition and properties of a number of titanocene(III) chloride solutions in the presence of chloride additives. For all the hydrochloride salts used, $[Cp_2TiCl_2]^-$ was generated. The stability of the $[Cp_2TiCl_2]^-$ and the rate of its formation depended on the properties of the cation. The ammonium ions interact with $[Cp_2TiCl_2]^-$ through hydrogen bonding, which can be modulated by the choice of cation. Based on our studies, it was also concluded that stronger hydrogen bonding between the ammonium cation and the titanocenium anion, and more soluble salt additives, kinetically disfavour the radical arylation and epoxide opening processes.[18]

By employing solvent and anion effects, we have demonstrated that the titanocenium cation ($[Cp_2Ti]^+$) is a stable catalyst for radical arylation of epoxides proceeding through single-electron steps. For $[Cp_2Ti]^+$, THF is superior to the strongly coordinating CH_3CN, which inhibits epoxide binding. Solvent coordination to titanium affects the overall rate of electron transfer to substrate. By using loosely coordinating

ligands, we could easily generate Lewis acidic titanocene(III) complexes that are stable without the need of a salt additive and are capable of reducing a variety of epoxides.[27]

3.5 References

(1) Trost, B. M. *Science (80-.).* **1983**, *219* (4582), 245–250.

(2) Trost, B. M. *Angew. Chem. Int. Ed.* **1995**, *34* (3), 256–281.

(3) Trost, B. M. *Science (80-.).* **1991**, *254* (5037), 1471–1477.

(4) Heinrich, M. R.; Gansäuer, A. *Radicals in Synthesis III*; Springer, 2012; Vol. 7.

(5) Yan, M.; Lo, J. C.; Edwards, J. T.; Baran, P. S. **2016**.

(6) Gansäuer, A.; Behlendorf, M.; Laufenberg, D. Von; Fleckhaus, A.; Kube, C.; Sadasivam, D. V; Flowers II, R. A. *Angew. Chem. Int. Ed.* **2012**, 4739–4742.

(7) Wipf, P.; Maciejewski, J. P. *Org. Lett.* **2008**, *10* (19), 4383–4386.

(8) Gansäuer, A.; Von Laufenberg, D.; Kube, C.; Dahmen, T.; Michelmann, A.; Behlendorf, M.; Sure, R.; Seddiqzai, M.; Grimme, S.; Sadasivam, D. V.; Fianu, G. D.; Flowers, R. A. *Chem. - A Eur. J.* **2015**, *21* (1), 280–289.

(9) Friedrich, J.; Walczak, K.; Dolg, M.; Piestert, F.; Lauterbach, T.; Worgull, D.; Gansäuer, A. *J. Am. Chem. Soc.* **2008**, *130* (5), 1788–1796.

(10) Gansäuer, A.; Fan, C. A.; Keller, F.; Karbaum, P. *Chem. - A Eur. J.* **2007**, *13* (29), 8084–8090.

(11) Gansäuer, A.; Bauer, D. *J. Org. Chem.* **1998**, *63* (7), 2070–2071.

(12) Morcillo, S. P.; Martínez-Peragón, Á.; Jakoby, V.; Mota, A. J.; Kube, C.; Justicia, J.; Cuerva, J. M.; Gansäuer, A. *Chem. Commun. (Camb).* **2014**, *50* (17), 2211–2213.

(13) Cangönül, A.; Behlendorf, M.; Gansäuer, A.; Van Gastel, M. *Inorg. Chem.* **2013**, *52* (20), 11859–11866.

(14) Gansäuer, A.; Barchuk, A.; Keller, F.; Schmitt, M.; Grimme, S.; Gerenkamp, M.; Mück-Lichtenfeld, C.; Daasbjerg, K.; Svith, H. *J. Am. Chem. Soc.* **2007**, *129* (5), 1359–1371.

(15) Enemærke, R. J.; Larsen, J.; Skrydstrup, T.; Daasbjerg, K. *J. Am. Chem. Soc.* **2004**, *126* (25), 7853–7864.

(16) Daasbjerg, K.; Svith, H.; Grimme, S.; Gerenkamp, M.; Mück-Lichtenfeld, C.; Gansäuer, A.; Barchuk, A. *Top. Curr. Chem.* **2006**, *263* (December 2005), 39–69.

(17) Enemærke, R. J.; Larsen, J.; Hjøllund, G. H.; Skrydstrup, T.; Daasbjerg, K. *Organometallics* **2005**, *24* (6), 1252–1262.

(18) Gansäuer, A.; Kube, C.; Daasbjerg, K.; Sure, R.; Grimme, S.; Fianu, G. D.; Sadasivam, D. V.; Flowers, R. A. *J. Am. Chem. Soc.* **2014**, *136* (4), 1663–1671.

(19) Frisch, M. J. . et al. *Gaussian 09*. Gaussian, Inc: Wallingford 2010.

(20) Becke, A. D. *J. Chem. Phys.* **1993**, *98* (7), 5648.

(21) Lee, C.; Yang, W.; Parr, R. G. *Phys. Rev. B* **1988**, *37* (2), 785–789.

(22) Weigend, F.; Ahlrichs, R. *Phys. Chem. Chem. Phys.* **2005**, *7* (18), 3297–3305.

(23) Daasbjerg, K.; Svith, H.; Grimme, S.; Gerenkamp, M.; Mück-Lichtenfeld, C.; Gansäuer, A.; Barchuk, A.; Keller, F. *Angew. Chemie - Int. Ed.* **2006**, *45* (13), 2041–2044.

(24) Honold, B.; Thewalt, U. *J. Organomet. Chem.* **1986**, *316* (3), 291–300.

(25) Patel, N. R.; Flowers, R. A. *J. Org. Chem.* **2015**, *80* (11), 5834–5841.

(26) Seewald, P. A.; White, G. S.; Stephan, D. W. *Can. J. Chem.* **1988**, *66*, 1147–1152.

(27) Gansäuer, A.; Hildebrandt, S.; Michelmann, A.; Dahmen, T.; von Laufenberg, D.; Kube, C.; Fianu, G. D.; Flowers, R. A. *Angew. Chemie - Int. Ed.* **2015**, *54*, 7003–7006.

(28) Blackmond, D. G. *Angew. Chemie - Int. Ed.* **2005**, *44* (28), 4302–4320.

(29) Baxter, R. D.; Sale, D.; Engle, K. M.; Yu, J. Q.; Blackmond, D. G. *J. Am. Chem. Soc.* **2012**, *134* (10), 4600–4606.

(30) Mathew, J. S.; Klussmann, M.; Iwamura, H.; Valera, F.; Futran, A.; Emanuelsson, E. A. C.; Blackmond, D. G. *J. Org. Chem.* **2006**, *71* (13), 4711–4722.

(31) Luinstra, G. A. *J. Organomet. Chem.* **1996**, *517* (1–2), 209–215.

(32) Berhalter, K.; Thewalt, U. *J. Organomet. Chem.* **1991**, *420*, 53–56.

(33) Gansäuer, A.; Von Laufenberg, D.; Kube, C.; Dahmen, T.; Michelmann, A.; Behlendorf, M.; Sure, R.; Seddiqzai, M.; Grimme, S.; Sadasivam, D. V.; Fianu, G. D.; Flowers, R. A. *Chem. - A Eur. J.* **2015**, *21*, 280–289.

(34) Rosales, A.; Rodríguez-García, I.; Muñoz-Bascõn, J.; Roldan-Molina, E.; Padial, N. M.; Morales, L. P.; García-Ocaña, M.; Oltra, J. E. *European J. Org. Chem.* **2015**, *2015* (21), 4567–4591.

(35) RajanBabu, T.; Nugent, W. *J. Am. Chem. Soc.* **1994**, *116* (3), 986–997.

(36) Nugent, W. a; Rajanbabu, T. V. *J. Am. Chem. Soc.* **1988**, *110* (9), 8561–8562.

Chapter 4. Carbonyl reductions mediated by titanocene(III) complexes

4.1 Background and significance

Carbonyl reductions to alcohols are an important and fundamental reaction in organic chemistry. Synthetic organic chemists have routinely applied this transformation to form basic motifs in multi-step syntheses of complex organic molecules, of both biological and synthetic utility.[1–5] An example is the reduction of the cyclopentenone derivative shown in scheme 4.1 to form the corresponding alcohol, which is a preliminary step in the formation of the purine derivative MDL 201449A, a candidate for treating multiple anti-inflammatory diseases.[6] Another example, shown in scheme 4.2, is the reduction of the carbonyl on an indoline derivative to form the racemic alcohol, which is a preliminary step in the formation of fluvastatin, a drug used in the treatment of cardiovascular diseases.[1] Figure 4.1 shows other examples of biologically active compounds synthesized via multiple steps in which a carbonyl is reduced in one of its preliminary steps.[2,3,7]

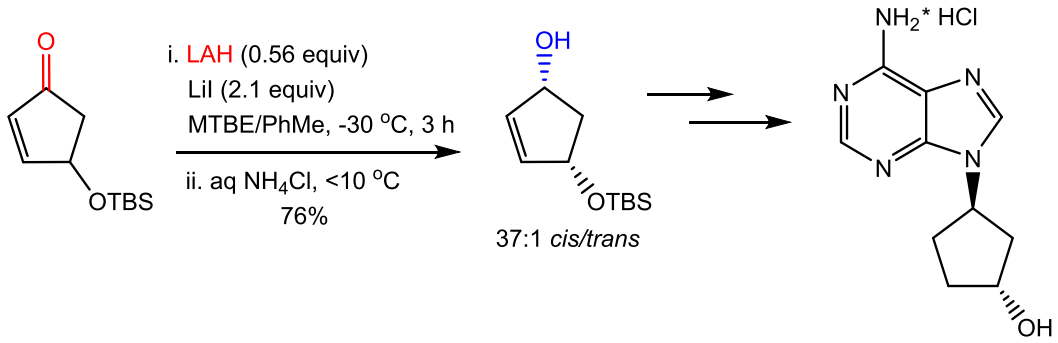

Scheme 4.1. Synthesis of MDL 201449A

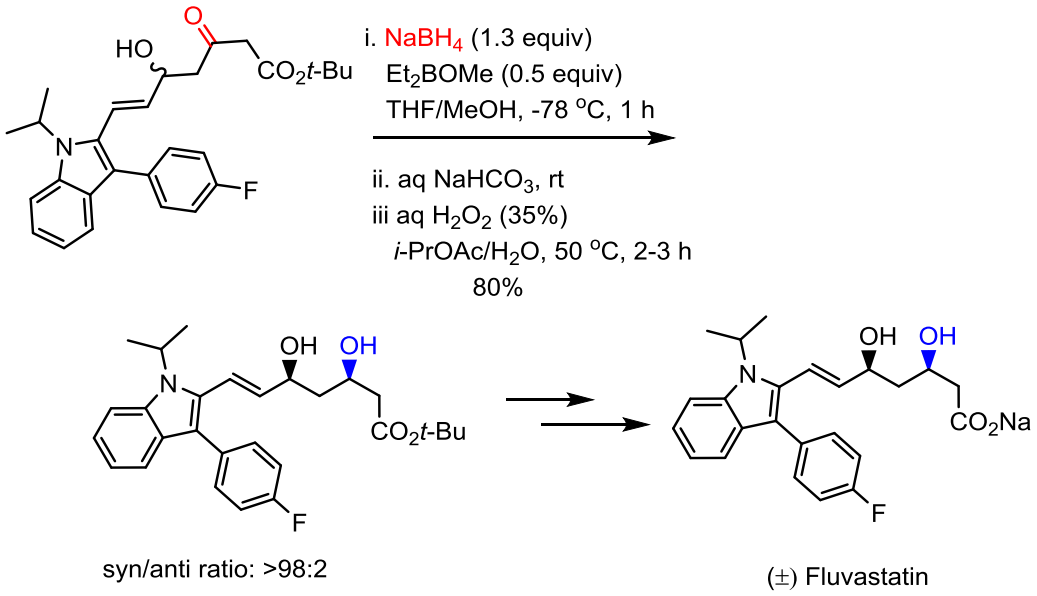

Scheme 4.2. Synthesis of fluvastatin

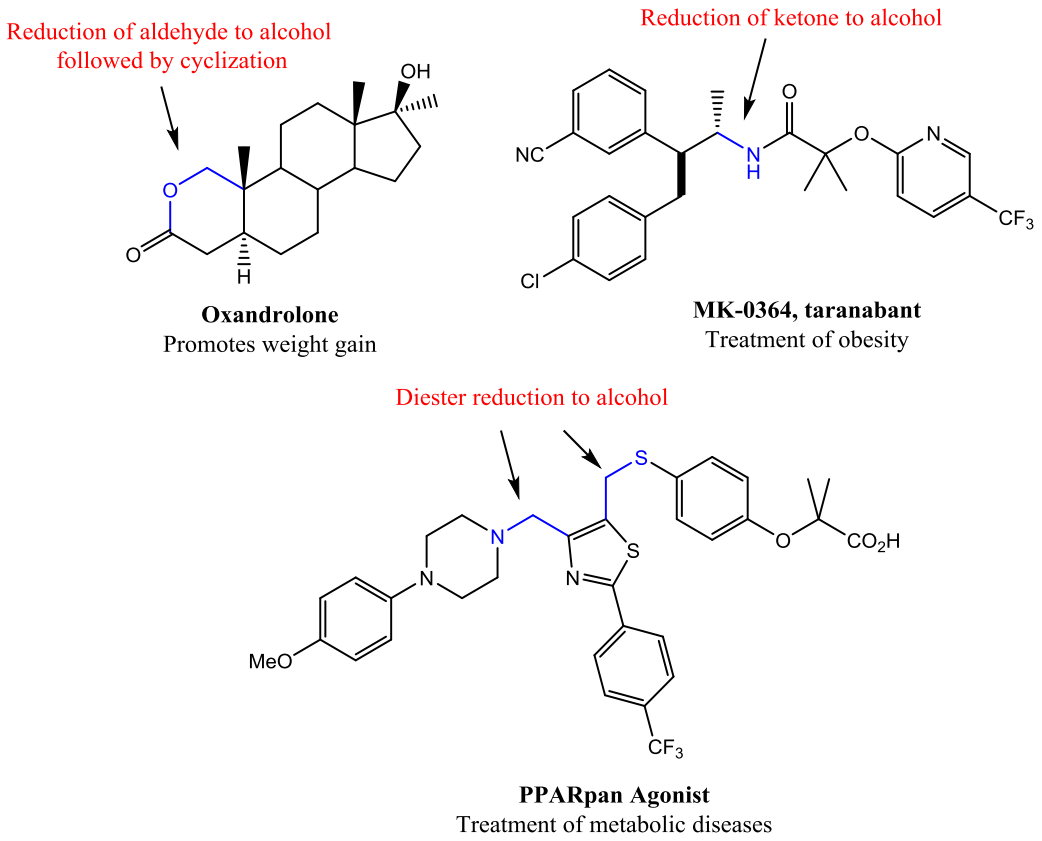

Figure 4.1. Carbonyl reductions in the formation of bioactive compounds[2,3,7]

In view of its significance, a large number of methods have been developed for carbonyl reductions to their respective alcohols. These methods include reductions mediated by enzymes,[8,9] hydride sources such as lithium aluminum hydride (LAH) and sodium borohydride ($NaBH_4$),[10] Meerwein-Ponndorf-Verley reductions,[11,12] samarium-mediated reductions,[13,14] catalytic hydrogenations,[15–17] and low-valent metal-catalyzed hydroborations or hydrosilylations (Scheme).[18–21]

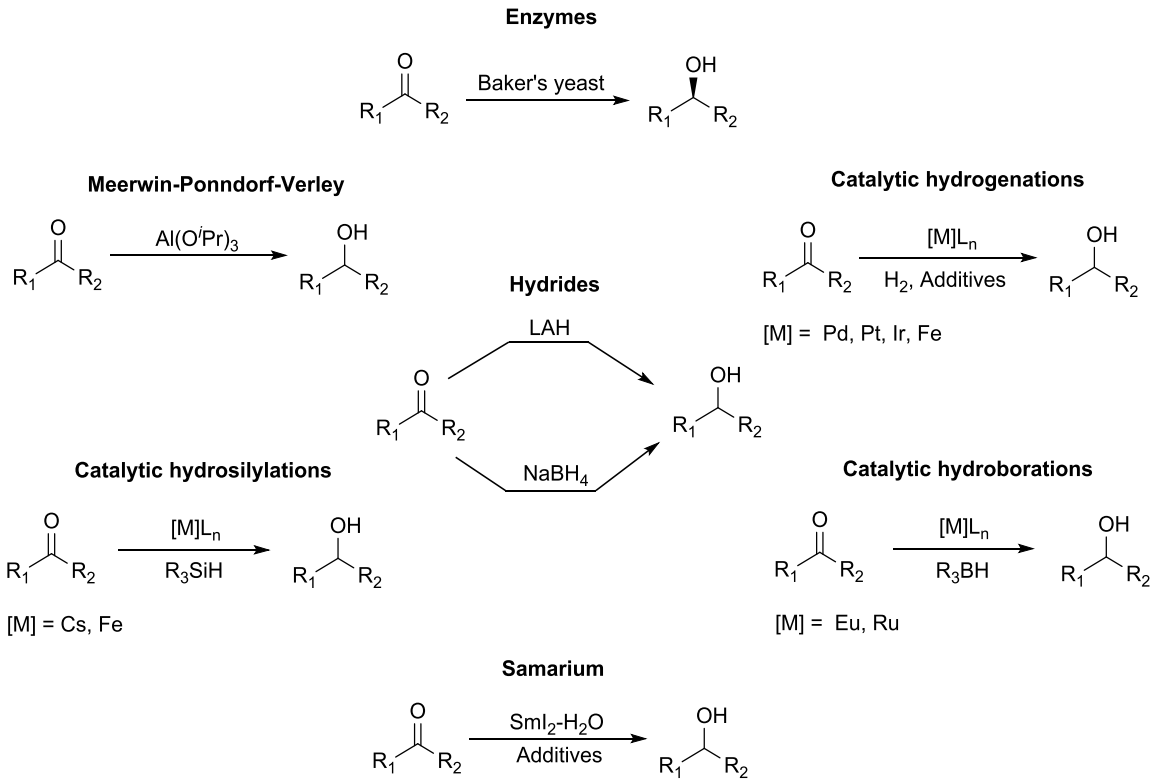

Scheme 4.3. Examples of methods for carbonyl reductions

4.1.1 Titanocene(III) mediated reduction of carbonyls

Reduction of carbonyls to their respective alcohols have also been facilitated with titanocene(III) complexes. Oltra and co-workers have reported a mild and inexpensive procedure for reducing aromatic ketones to their respective alcohols using a

titanocene(III) aqua complex (Scheme 4.4). As seen in scheme 4.4, water plays a key role in facilitating the formation of the alcohol instead of the pinacol product.[22,23] Based on their work, it has been proposed that the active catalyst reacts with the ketone to form the ketyl radical intermediate, which is trapped by a hydrogen atom donated from the titanocene aqua complex (Scheme 4.5). EPR and computational studies were done to identify the active species as a titanocenium cation bounded by two molecules of water.[24] The reduced product is obtained upon acid workup.[22]

Cuerva and co-coworkers performed further studies on the titanocene aqua complex and found that the coordination of H_2O to $Cp_2Ti(III)Cl$ significantly reduced the homolytic O-H bond dissociation by about 60 kcalmol^{-1}.[24–26] Thus making it an excellent hydrogen atom donor for epoxide opening and carbonyl reduction processes.[27–29]

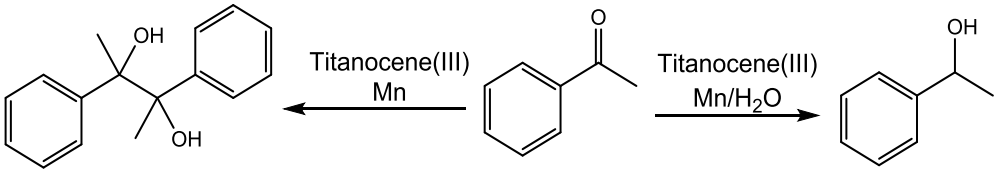

Scheme 4.4. Reduction of acetophenone with titanocene(III) aqua complex[23]

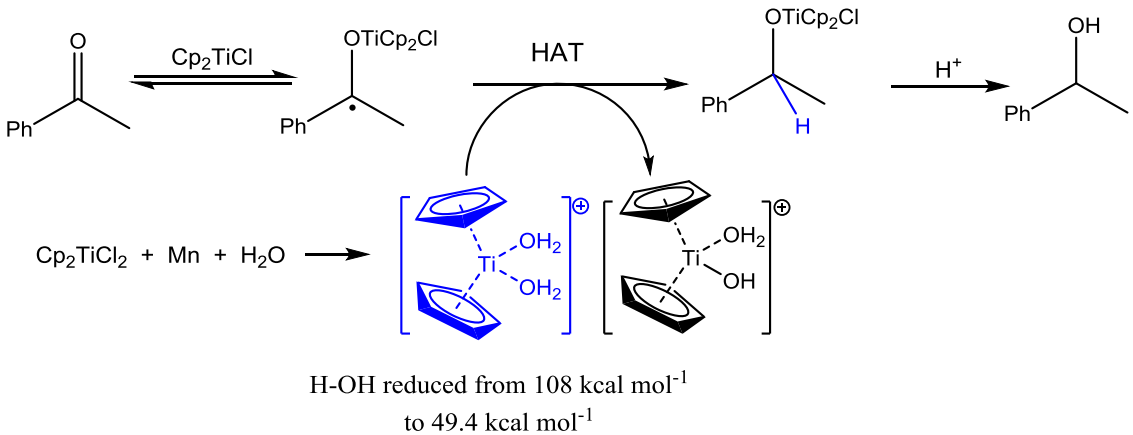

Scheme 4.5. Proposed mechanism for acetophenone reduction with titanocene aqua complex[26]

It should however be noted that Oltra and co-workers have reported an alternative mechanism for the reduction of acetophenone with titanocene aqua complexes where water is not serving as a hydrogen atom donor but is instead involved in hydrolyzing a proposed titanoxirane intermediate (**11**) (Scheme 4.6).[23] As a result, the conventionally free radical mechanism proposed for carbonyl reductions by titanocene(III) aqua complexes is still under debate.

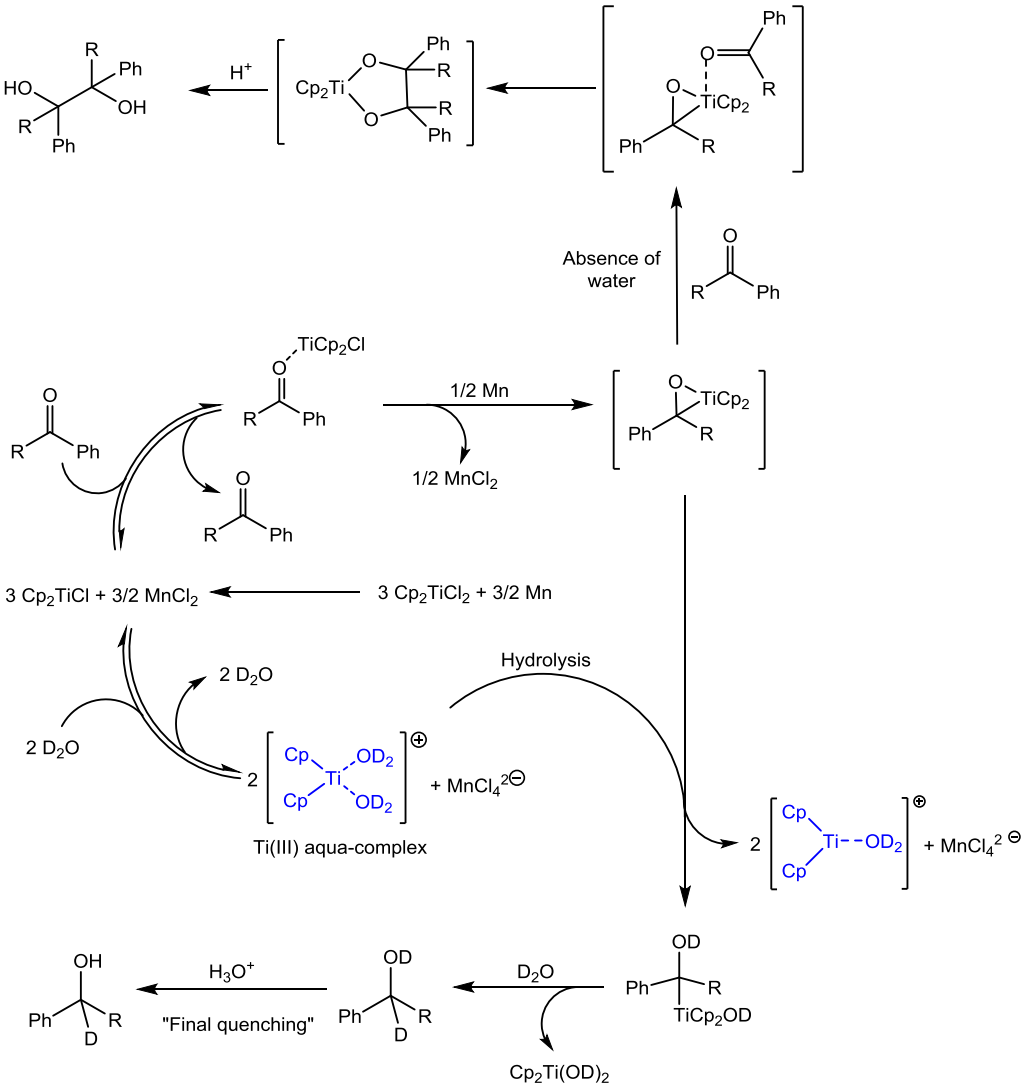

Scheme 4.6. Alternative mechanism for acetophenone reduction with titanocene aqua complex[23]

While the proposed mechanism for carbonyl reductions mediated by titanocene(III) aqua complexes is still uncertain, there are drawbacks with using titanocene aqua complexes: the reaction only works for aromatic ketones and not for aliphatic ketones, the reaction requires stoichiometric amounts of titanocene reagents and the reaction times are very long.[22,23] In view of these challenges, the development of a system that would reduce a wide variety of ketones including non-aromatic ketones with catalytic amounts of reductant, and at faster reaction times is highly sought.

Schwartz and coworkers developed a system whereby simple aromatic and aliphatic ketones were reduced to alcohols in aprotic media by titanocene(III) borohydride: a complex that is easily generated *in situ*, by mixing titanocene dichloride and $NaBH_4$ in dimethoxyethane (DME) (Scheme 4.7).[30] Although this method was simple, prepared from readily available reagents, and performed under mild conditions, it required stoichiometric amounts of titanocene borohydride. A catalytic approach to this process has not yet been developed.

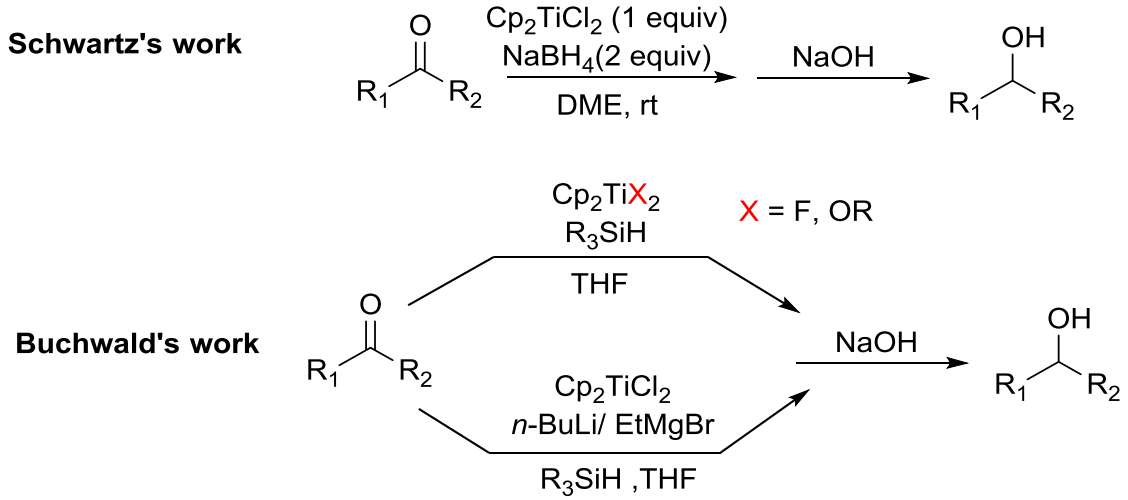

Scheme 4.7. Low-valent titanocene catalyzed reductions

Conversely, Buchwald and coworkers developed an elegant approach to carry out hydrosilylation of carbonyls with subsequent workup to produce alcohols with catalytic low-valent titanocene hydride complexes and an inexpensive siloxane polymer, poly(methylhydrosiloxane) (PMHS) as the stoichiometric reductant. In this approach, the active titanocene hydride species was either synthesized from a premade titanocene precatalyst or generated *in situ* at very low temperatures with reagents that required careful handing (Scheme 4.7).[31–34]

4.1.2 Project goals

In work done by Flowers and co-workers on carbonyl reductions mediated by a SmI_2-water system, it was discovered that the addition of an amine significantly improved the reducing the ability of SmI_2 and reduced the reaction time tremendously (Scheme 4.8).[13,35–37] In view of the challenges in reductions mediated by titanocene aqua complexes, experiments were carried out to develop a process that would reduce a wide variety of ketones primarily non-aromatic ketones with the titanocene(III) aqua complex at faster reaction times. It was our hope that this goal would be realized by the addition of an amine or any suitable base to the titanocene aqua complex.

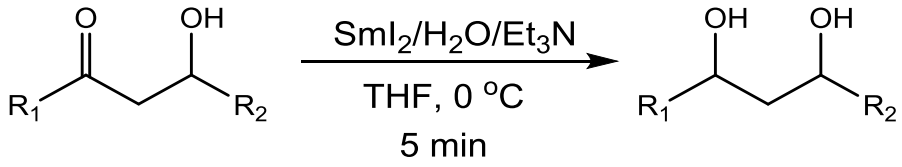

Scheme 4.8. Impact of amines on carbonyl reductions mediated by SmI_2-H_2O[13]

Based on the aforementioned titanocene mediated reductions developed by Schwartz and Buchwald, we also envisioned designing a system whereby carbonyls could

be reduced to their respective alcohols with catalytic amounts of titanocene(III) borohydride (Scheme 4.9). Ideally, this complex would be generated under mild conditions, from inexpensive, readily available titanocene dichloride and a hydride source as a stoichiometric reductant. Although catalytic approaches have been reported for reducing carbonyls to alcohols in refluxing diisopropylether (DIPE) using catalytic Zn(2-ethylhexanoate)$_2$ and $NaBH_4$ with PMHS as the stoichiometric reductant,[38] a similar approach with commercially available titanocene dichloride has not been reported.

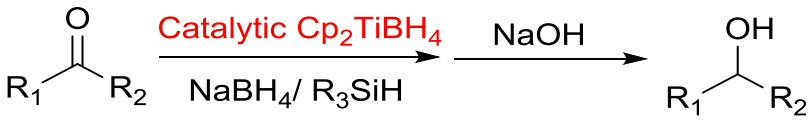

Scheme 4.9. Development of a new approach to carbonyl reductions with titanocene borohydride

4.2 Experimental

4.2.1 Materials and instrumentation

Unless otherwise stated, all reactions were carried out in a glove box and under argon atmosphere. An Innovative Technology solvent purification system was used to purify all the solvents used for experiments. All reagents and chemicals, mostly argon or nitrogen flushed, were purchased from reputable chemical vendors (Alfa Aesar, Acros, Sigma Aldrich, Beantown Chemical, and TCI) and used without further purification. Chemicals not flushed with an inert gas were degassed with argon and used without any additional purification protocols. ^{1}H-NMR spectra were measured on either a Bruker 500MHz or a Bruker 400MHz spectrometer in deuterated chloroform ($CDCl_3$). ^{13}C-NMR spectra were measured at either 126 MHz or at 101 MHz in $CDCl_3$. GC-MS analyses were done with a Schimadzu GCMS-Q2010 series with a SHRX-5M (30m)

column. Column chromatography was done using an automated CombiFlash® system from Teledyne Isco. Inc. Columns were prepacked with silica gel and product separations were performed with a gradient elution of hexanes and ethyl acetate. *In situ* IR experiments were done using Mettler-Toledo's ReactIR 15 fitted with DiComp probe and running iCIR software 4.3 SP1.

4.2.2 Methods

4.2.2.1 Procedure for reducing ketones with $Cp_2Ti(III)Cl$-Water-Base

An oven dried vial was charged with manganese and Cp_2TiCl_2 in a glovebox under argon atmosphere. Dry degassed THF was added to the vial and stirred until a green colored solution was formed. An appropriate amount of degassed H_2O was added to the solution and a change in color from green to blue was observed. The ketone was added to the mixture and the base was gradually added to the mixture. A blue-black solution was formed and left to stir for the given time. The reaction was quenched with saturated ammonium chloride solution (NH_4Cl). Diethyl ether was added and the phases were separated. The aqueous layer was extracted 3 times with diethyl ether, washed with brine and dried over $MgSO_4$. Evaporation of the solvent followed by flash chromatography gave the desired alcohol.

4.2.2.2 Procedure for reducing ketone with titanocene borohydride

All the reactions were carried out in the glove box under argon atmosphere. A 40-mL vial was charged with titanocene dichloride and sodium borohydride. To this 10 mL of dimethoxyethane (DME) was added and left to stir until a violet colored solution was formed, which was indicative of the formation of titanocene borohydride. The ketone was

added to the violet solution. The solution turned grey upon ketone addition. An aliquot (1 mL) was taken, exposed to air to quench the catalyst. 2 mL of ether was added followed by 2 mL H_2O to quench the excess $NaBH_4$. The organic layer was separated, biphenyl was then added and run through GCMS to evaluate progress of reaction and yield of product.

For experiments to generate titanocene borohydride with milder sodium borohydride sources, a vial was charged with titanocene dichloride and $NaBHX_3$. To this was added 10 mL of solvent and left to stir till a color change was observed, which was either green (Cp_2TiCl_2 and NaH_3CN in THF/DME) or yellow (Cp_2TiCl_2 and $NaH(OAc)_3$ in THF/DME). ketone was added to the resulting solution and stirred for the indicated time. The solutions were exposed to air, worked up, and analyzed by GCMS.

4.2.2.3 Procedure for carbonyl reduction with titanocene borohydride and PMHS

A 40-mL vial was charged with titanocene dichloride (Cp_2TiCl_2) (0.1 mmole, 25 mg) and sodium borohydride ($NaBH_4$) (0.2 mmole, 7.6 mg). To this 10 mL of dimethoxyethane (DME) was added and left to stir till a violet colored solution was formed, indicative of the formation of titanocene borohydride (Cp_2TiBH_4). Polymethylhydrosiloxane (PMHS) (3 mmole, 195 mg) was added to the solution. 2.0 mmole of either the aldehyde or the ketone was added to the violet solution. The solution turned grey upon ketone addition then gradually turned to a dirty green color. The solution was stirred for the appropriate time.

The solution was taken out of the glovebox and exposed to air to quench the catalyst. About 10 mL of diethyl ether was added followed by dropwise addition of 10

mL 1 M NaOH solution to quench the excess PMHS (Note: vigorous bubbling observed with NaOH addition). The mixture was stirred until bubbling stopped and clear layers were observed (Note: For good yields of alcohol products, the mixture was stirred overnight). Organic layer was separated and the aqueous layer was washed with 10 mL ether. Organic layers were combined and washed with 10 mL 1 M NaOH, followed by 10 mL brine solution then dried with $MgSO_4$. The solution was evaporated to dryness to obtain the isolated yield of clean product after NMR analysis.

4.2.2.4 Procedure for synthesizing 1-(2-phenylcyclopropyl) ethan-1-one (1-v)

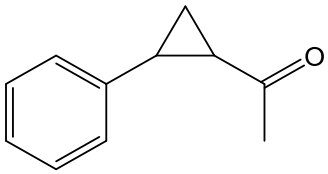

1-(2-phenylcyclopropyl) ethan-1-one **(1-v)** was synthesized using a variant of the Corey-Chaykovsky cyclopropanation reaction.[39] A 200 mL 3-necked round bottomed flask was charged with sodium hydride (NaH) (39.1 mmole, 1 g) under argon atmosphere. 20 mL of DMSO was then added to the mixture and stirred. Trimethylsulfoxonium iodide ($(CH_3)_3SOI$) (38 mmole, 8.3 g) was carefully and slowly added to the mixture. 40 mL of THF was added to the mixture and left to stir for about 30 minutes. Benzalacetone (34 mmole, 5 g) dissolved in 20 mL DMSO was added to the mixture, followed by 40 mL THF and stirred overnight. Ice was added to the mixture to quench excess NaH and rotavaped to remove THF. Excess distilled water (approximately 100 mL) was added to the mixture followed by 100 mL hexanes. The aqueous layer was separated and washed three more times with about 100 mL hexanes. The organic layers were combined and washed one more time with distilled water. The solution was

rotavaped and the compound was purified by flash chromatography (Hexanes: Ethyl acetate = 90:10) to obtain desired product **(1-v)**.

4.2.2.5 Procedure for reducing 2-octanone with titanocene difluoride[32,33]

A 40-mL vial was charged with titanocene difluoride (0.025 mmole, 5.4 mg). To this was added 10 mL tetrahydrofuran (THF) and either PMHS (1 mmole, 65 µL) or $PhSiH_3$ (1 mmole, 123 µL). The solution was stirred either at room temperature or at refluxing conditions until a green colored solution was formed. 2-octanone (0.5 mmole, 78 µL) was added to the solution and left to stir for an hour. An aliquot (1 mL) was taken and exposed to air to quench the catalyst. 2 mL of ether was added followed by 2 mL 1 M NaOH solution to quench the excess silane. The organic layer was separated, biphenyl was then added and run through GCMS to evaluate progress of reaction and yield of product.

4.2.2.6 Procedure for making esters

To a 100-mL round-bottomed flask was added the alcohol (R-OH, 1.5 equiv) and triethylamine (Et_3N, 2 equiv). 20 mL of dry THF was added to this solution followed by the slow addition of the acyl chloride (R-(CO)-Cl, 1 equiv). A white precipitate was formed and the mixture was stirred overnight. 20 mL of ethyl acetate was added to the mixture and allowed to stir for 15 minutes. 20 mL of 1 M HCl solution was added and the solution was transferred to a separatory funnel. The organic layer was separated and the aqueous layer was washed two more times with ethyl acetate. The organic layers were combined and washed with 20 mL of saturated sodium bicarbonate solution, sodium

chloride, and dried with magnesium sulfate ($MgSO_4$). Solution was rotavaped to obtain desired ester.

4.2.2.7 Procedure for running experiments on ReactIR 15

In situ IR experiments were done using Mettler-Toledo's ReactIR 15 fitted with DiComp probe and running iCIR software 4.3 SP1.

ReactIR Conditions

Reference Spectra **=** 00:01:53 (hh:mm:ss)

Background Replacement = Original

Baseline Correction = None

Spectrum Math = 2nd derivative (Subtle changes were observed when a 2nd derivative of the spectra was taken).

To a two-necked round bottom flask, sodium borohydride ($NaBH_4$) (0.2 mmole, 7.6 mg) was added and attached to a reflux condenser inside the glove box. This was taken out and fixed to the ReactIR probe and flushed with argon. An air background (256 scans) was obtained and 10 mL of DME was added to the round bottom flask through a rubber septum. The iCIR program was initiated to collect solvent background for 3 minutes (256 scans/minute). Titanocene dichloride (Cp_2TiCl_2) (0.1 mmole, 25 mg), dissolved in 2 mL DME, was added through the rubber septum, and rinsed with 0.5 mL DME. The mixture was left to stir until a violet solution was formed. To the violet solution, 2-octanone (2.0 mmole, 312 µL) dissolved in 1 mL DME was added and rinsed with 0.5 mL DME. The solution turned light blue upon ketone addition then gradually

turned to a dirty green color. After no further changes were observed, phenylsilane ($PhSiH_3$) (3.0 mmole, 195mg) in 1mL DME was added to the solution and the reaction progress was monitored on the ReactIR until completion of the reaction.

4.3 Results

4.3.1 Reductions with titanocene aqua complexes: Impact on system with the addition of base

Prior work done by Flowers and coworkers on samarium mediated reductions showed that ketone reductions proceeded at a much faster rate when a base was added.[13] The reduction of acetophenone with a titanocene(III) aqua complex was therefore repeated in the presence of a base. We hypothesized that by adding a suitable base, we would improve the reaction time. As shown in table 4.1 entry 2, acetophenone was reduced in an hour with the addition of pyrrolidine. Further studies showed that acetophenone was reduced with catalytic amounts of pyrrolidine (See appendix table 6.6, entry 3) and with MeOH as the hydrogen atom source. The reaction with MeOH as additive was however slower (See appendix table 6.6, entry 4).

The addition of base also made it possible to reduce 2-octanone, which generally does not undergo reductions with titanocene aqua systems (Table 4.1, entry 3). Our hypothesis is that the base abstracts a proton resulting in concomitant electron transfer from the titanocene to the ketone to form the ketyl radical intermediate that eventually forms the product in subsequent steps. The hydrochloride salt formed here crashes out of solution, which is observed at the end of the reaction (Scheme 4.10). Numerous attempts to reduce acetophenone or 2-octanone with catalytic amounts of Cp_2TiCl_2 were unsuccessful (See appendix table 6.6 & 6.7). Addition of excess amounts of hydrogen

atom source could be quenching the catalyst by forming titanocene alkoxide or titanocene hydroxide complexes.

Table 4.1. Reduction of ketones with $Cp_2TI(III)Cl$-H_2O-Base

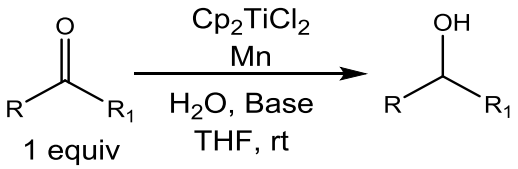

Entry	Ketone	Base	Time (h)	Yield (%)
1	Acetophenone	-	60	92[a]
2	Acetophenone	Pyrrolidine	1	100[b]
3	2-octanone	NaO^tBu (4equiv)	16	71[c]

Reaction conditions: Entry 1: [Ketone] = 0.033 M; [Cp_2TiCl_2] = 0.10 M (3 equiv); [Mn] = 0.27 M (8 equiv); [H_2O] = 3.33 M (100 equiv); THF = 30 mL; Entry 2: [Ketone] = 0.05 M; [Cp_2TiCl_2] = 0.11 M (2.2 equiv); [Mn] = 0.40 M (8 equiv); [H_2O] = 0.33 M (6.6 equiv); [Pyrrolidine] = 0.22 M (4.4 equiv); THF = 10 mL; Entry 3: [Ketone] = 0.05 M; [Cp_2TiCl_2] = 0.11 M (2.2 equiv); [Mn] = 0.40 M (8 equiv); [H_2O] = 0.33 M (6.6 equiv); THF = 10 mL; [NaO^tBu] = 0.20 M (4equiv); [a]Isolated yield; [b]Observed by TLC; [c]GC yield biphenyl as standard

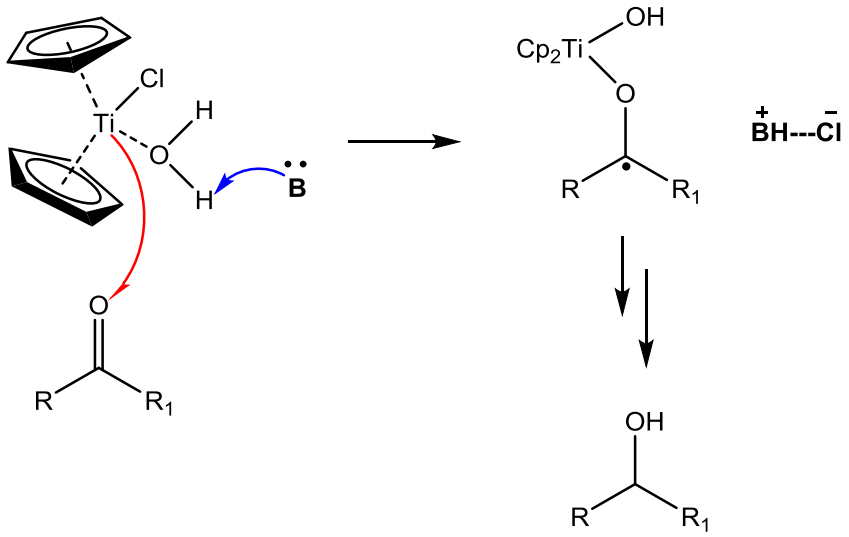

Scheme 4.10. Impact of base on the reduction of ketone with titanocene(III) aqua complexes

4.3.2 Carbonyl reductions mediated by titanocene borohydride

4.3.2.1 Optimizing reaction conditions

To optimize the reaction conditions for reducing carbonyls mediated by titanocene borohydride, a series of experiments were performed and the results are summarized in table 4.2. 2-octanone (**1**) was successfully reduced to 2-octanol (**2**) with up to 10 mol% catalyst and with $NaBH_4$ as the stoichiometric hydride source in DME (Table 4.2, entry 3). The reduction of **1** to **2** was ineffective in DME solvent with either only $NaBH_4$ as reductant or with the addition of 5 mol% catalyst (Table 4.2, entries 4 & 5). Complete reduction of **1** to **2** was achieved with 5 mol% catalyst and PMHS as stoichiometric reductant (Table 4.2, entry 6). Control experiments showed that the reaction was unsuccessful without the active titanocene catalyst (Table 4.2, entries 7 & 8).

Reductions were also performed in THF, which proceeded smoothly but relied on a very low catalyst to solvent ratio (6.25 mg (Cp_2TiCl_2):10 mL (THF) or 2.5 mM of catalyst). At higher catalyst to solvent ratios (25 mg (Cp_2TiCl_2):10 mL (THF) or 10 mM of catalyst), the active titanocene borohydride complex was not formed until after three days due to the poor solubility of $NaBH_4$ in THF, corroborating observations made by Schwartz and coworkers.[30] Attempts to form the active titanocene catalyst directly by mixing titanocene dichloride with PMHS were not successful.

In addition to $NaBH_4$, attempts to form the active titanocene borohydride intermediate with milder hydride sources including sodium cyanoborohydride ($NaBH_3CN$) and sodium triacetoxyborohydride ($NaBH(OAc)_3$), were not successful and provided only recovered starting material (Table 4.2, entries 9 to 16). With these control

studies in hand, further reactions were performed using DME as the solvent of choice because it provided the fastest preparation of the active catalyst.

Table 4.2. Results from control experiments for Cp_2TiBH_4 mediated reductions

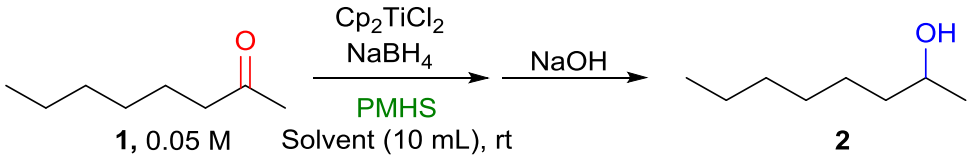

Entry	Cp_2TiCl_2 (mol%)	$NaBHX_3$	$NaBHX_3$ (mol%)	PMHS (mol%)	Solvent	Time (h)	Yield (%)[1]
1	20	$NaBH_4$	400	-	DME	1	100[2]
2	20	$NaBH_4$	200	-	DME	1	100[2]
3	10	$NaBH_4$	200	-	DME	4	95
4		$NaBH_4$	400	-	DME	96	41
5	5	$NaBH_4$	150	-	DME	4	57
6	5	$NaBH_4$	10	150	DME	1	100[2]
7	-	-	-	150	DME	24	-
8	-	$NaBH_4$	10	150	DME	24	13
9	-	$NaBH_3CN$	200	-	THF	24	-
10	5	$NaBH_3CN$	200	-	THF	6	-
11	-	$NaBH_3CN$	200	-	DME	24	-
12	5	$NaBH_3CN$	200	-	DME	6	-
13	-	$NaBH(OAc)_3$	200	-	THF	24	-
14	5	$NaBH(OAc)_3$	200	-	THF	6	-
15	-	$NaBH(OAc)_3$	200	-	DME	24	-
16	5	$NaBH(OAc)_3$	200	-	DME	6	-

[1]GC yields with biphenyl as internal standard. [2] Only product observed by GC.

4.3.2.2 Substrate scope

To further investigate the breadth of this approach, we probed the reduction of a variety of aldehydes and ketones with different steric and electronic properties. Our findings are summarized in scheme 4.11. All the aldehydes and ketones examined were successfully reduced to alcohols irrespective of their structural features. Under the reaction conditions, the *cis*-isomer was preferred to the *trans*- isomer for ketones **2-l** & **2-n,** suggesting that the hydride preferentially attacks the carbonyl carbon at the least sterically hindered position. Nardi and coworkers observed similar trends in their $Er(OTf)_3/NaBH_4$ catalyzed reductions of α,β-unsaturated ketones.[19]

Like Luche reductions,[40,41] α,β-unsaturated ketones **2-l** and **2-u** favorably reduced via 1,2 addition under the reaction conditions. This approach serves as a compliment to titanocene(III) catalyzed reductions of α,β-unsaturated ketones to ketones.[42] 1-(2-phenylcyclopropyl) ethan-1-one (**1-v**) was successfully reduced to 1-(2-phenylcyclopropyl) ethan-1-ol (**2-v**) without any evidence of ring opening. This observation suggests that this reaction proceeds via a hydride transfer as opposed to a hydrogen atom transfer (HAT). Heterocycles with pendant carbonyls (**1-w** & **1-x**) were also effectively reduced to their respective alcohols (**2-w** & **2-x**).

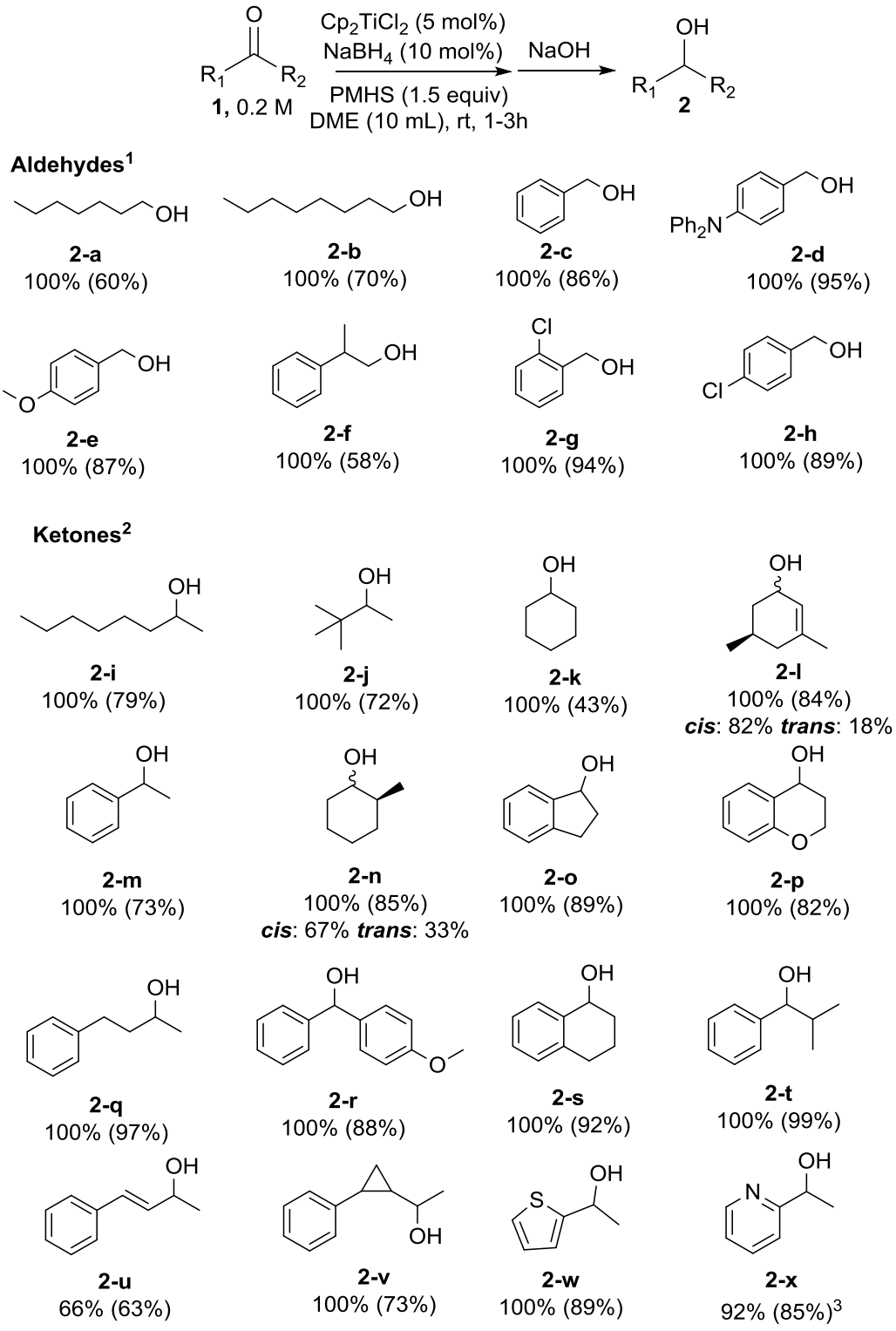

Scheme 4.11. Reduction of aldehydes and ketones Cp_2TiCl_2/$NaBH_4$/PMHS in DME. Conversion to alcohol based on NMR analysis & Isolated yields in parenthesis; [1]Reaction time was 1 hour; [2]Reaction time was 1-3 hours; [3]Reaction stirred overnight.

4.3.2.3 Mechanistic study

4.3.2.3.1 Reduction of 2-octanone monitored by ReactIR

In situ IR experiments were done using Mettler-Toledo's ReactIR 15 fitted with a DiComp probe and running iCIR software 4.3 SP1. From a mechanistic standpoint, we hypothesized that the carbonyl was being reduced via a hydrosilylation instead of a hydrogen atom transfer (*vide supra*). To further study the process, the model reaction shown in scheme 4.12 was performed and monitored by ReactIR. The C-H wag of the Cp ligand is known to be sensitive to the oxidation state of the titanocene complex as well as the nature of the ligands coordinated to the titanium metal.[43,44] Additionally, *in situ* monitoring also enabled us to follow carbonyl reduction and conversion of the Si-H bond to an Si-O bond. Since PMHS has an absorption that interferes with the C-H wag of the Cp ligand of the titanocene, we employed phenylsilane ($PhSiH_3$) as there was no interference from this terminal reductant.

The titanocene borohydride complex whose X-ray structure is known,[45] was generated by the addition of sodium borohydride to titanocene(IV) dichloride. Reduction of Ti(IV) to Ti(III) and formation of the titanocene borohydride was demonstrated by the shift of the C-H wag of the Cp ligand (Figure 4.2) from 820 cm^{-1} to 809 cm^{-1} and a change in color from red to violet was observed. Once this conversion was complete, ketone **1** was added to the solution and the C-H absorption of the Cp shifted from 809 cm^{-1} to 799 cm^{-1} (Figure 4.3) and a change in color from violet to green was observed.

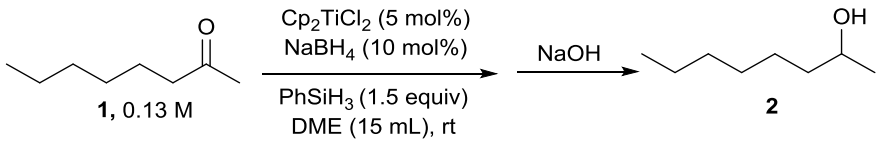

Scheme 4.12. Reaction conditions for ReactIR studies

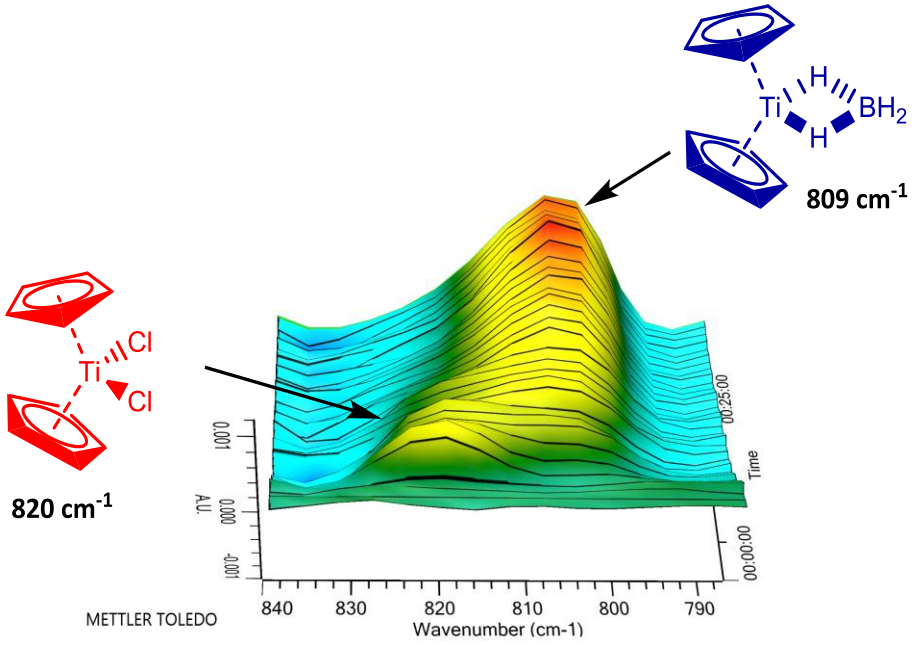

Figure 4.2. Formation of titanocene borohydride monitored by ReactIR

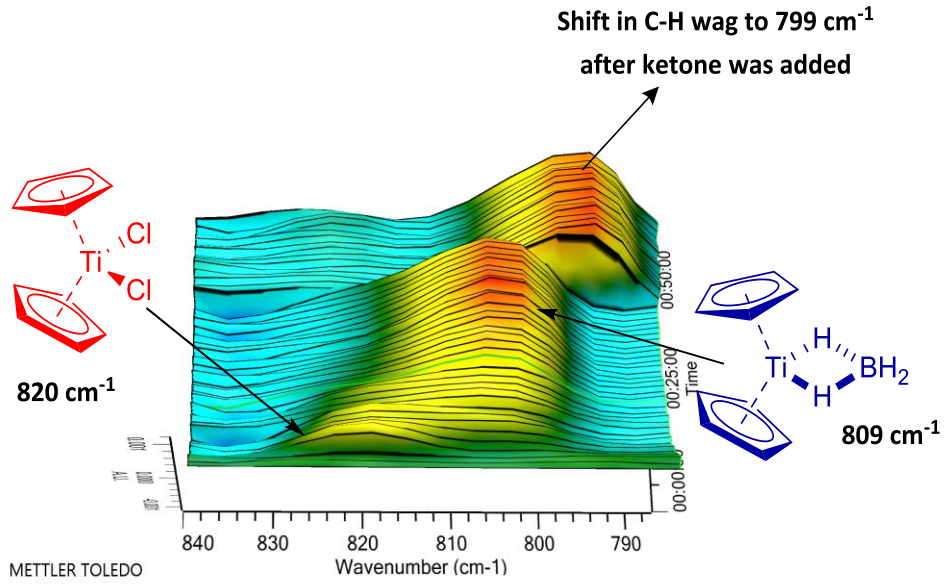

Figure 4.3. Shift in C-H wag upon ketone addition

Figure 4.4 contains a plot of the change in absorption over time for the C-H wag for the Cp of titanocene borohydride before and after addition of ketone **1**. Upon addition of the ketone, the absorption at 1719 cm^{-1} was observed. Concurrently there was a disappearance of the C-H wag absorption for titanocene borohydride at 809 cm^{-1}, and the subsequent growth of another absorption at 799 cm^{-1} consistent with the C-H wag of a Cp_2Ti-O interaction.[43,44] The initial growth of ketone observed at 1719 cm^{-1} was followed by a minor drop in the absorption consistent with initial reduction of 2-octanone by titanocene borohydride (Figure 4.4). Furthermore, the C-H wag absorption at 799 cm^{-1} characteristic of Cp_2Ti(III) complexes indicates that the titanocene catalyst remains in the +3 oxidation state bound to the alkoxide.[30,46,47]

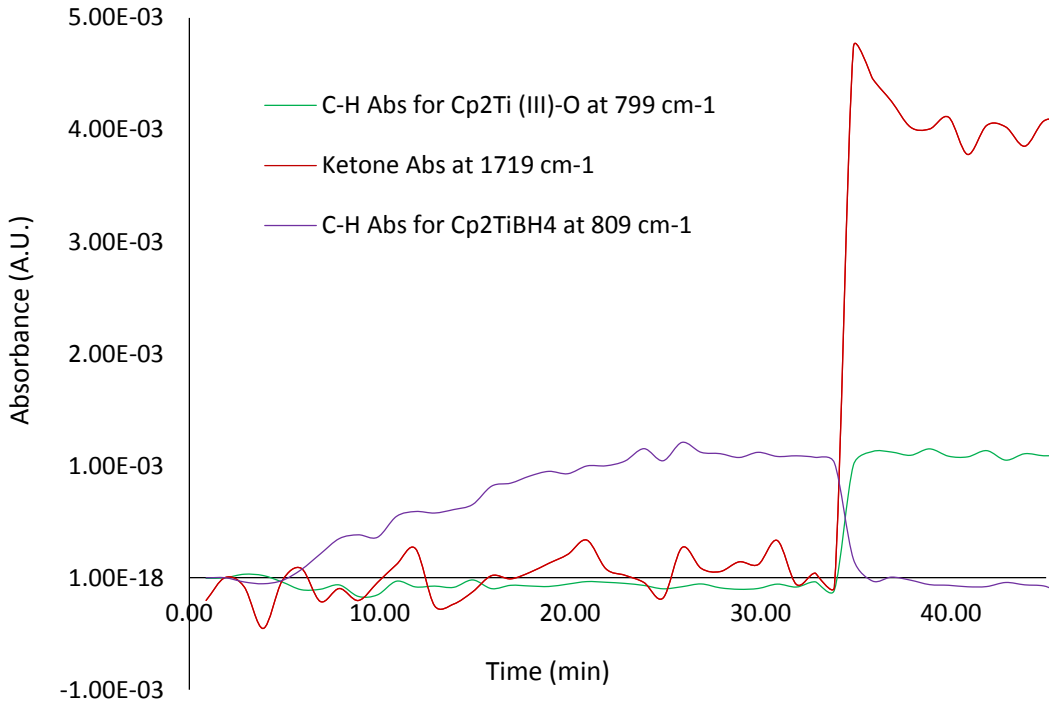

Figure 4.4. Trend observed on ReactIR for 2-octanone and catalyst

Once no further changes were observed, phenylsilane was added to the solution to initiate the reaction. The ketone absorption at 1719 cm^{-1} decayed over the course of approximately 100 minutes until the reaction was complete (Figure 4.5). The Si-H stretch of phenylsilane was observed at 705 cm^{-1}. The phenylsilane peak decreased with concomitant development of another absorption at 835 cm^{-1}, which is attributed to the OSi-H stretch due to silylation of the Ti(III)-bound alkoxide (Figure 4.5). Interestingly, the C-H wag absorbance for titanocene at 799 cm^{-1} remains after ketone reduction, indicating the presence of either Ti(III)-O species or an active titanocene hydride intermediate (Figure 4.6). At this point, the reaction was exposed to air and worked up with 1 M NaOH, and provided a nearly quantitative yield of the carbinol product.

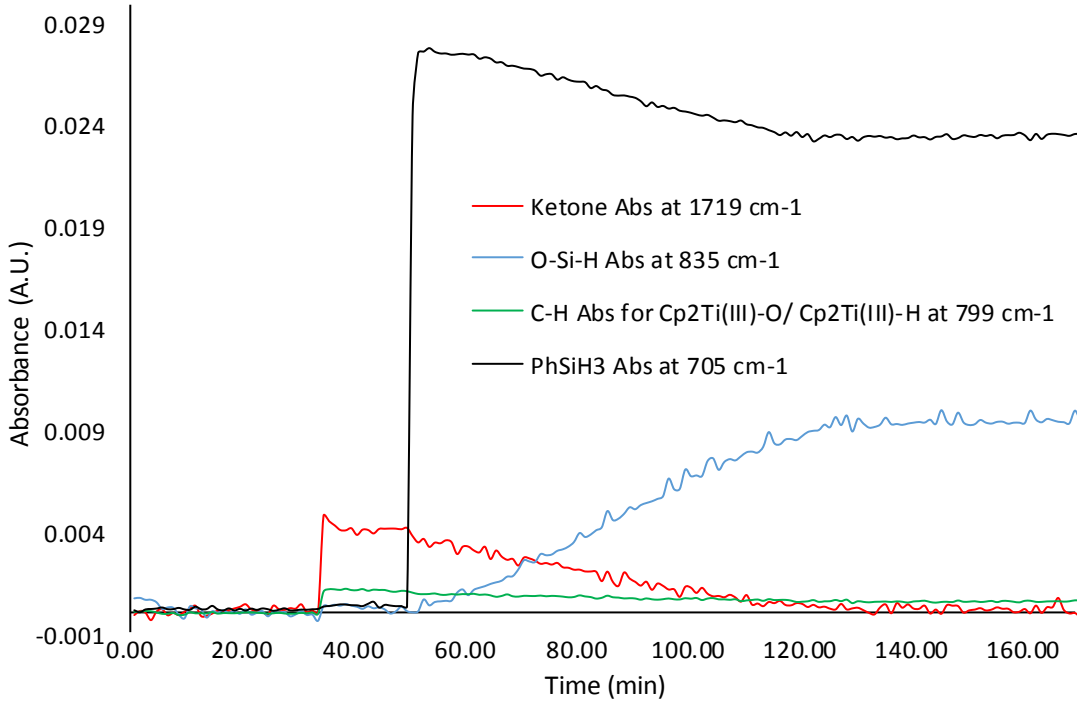

Figure 4.5. Monitoring the progress of the reaction after the addition of phenylsilane

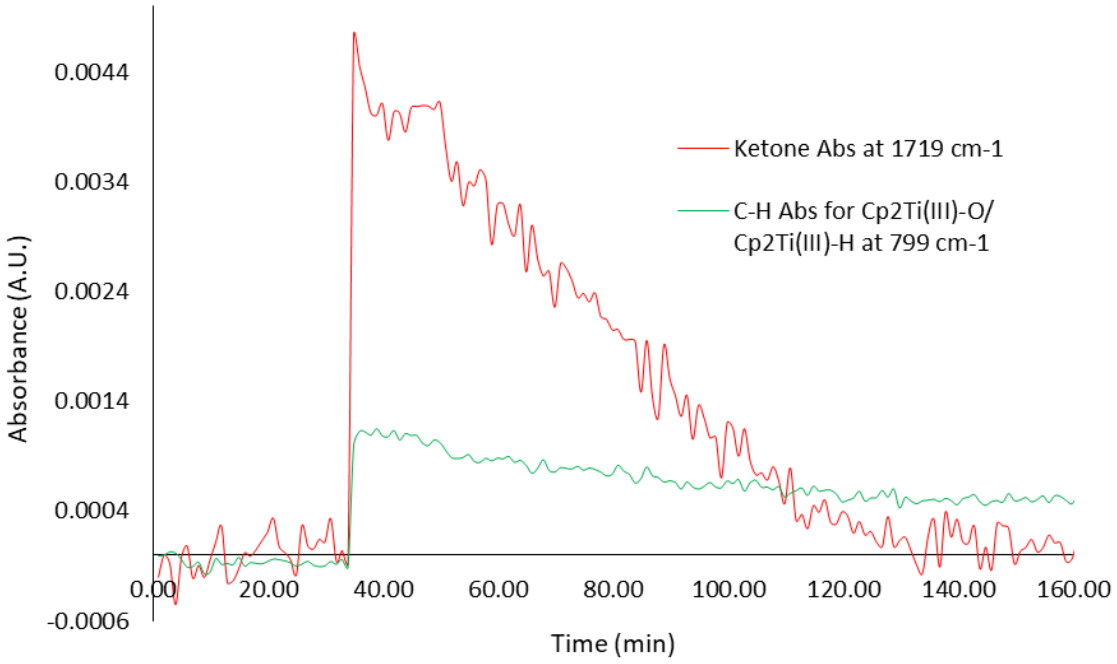

Figure 4.6. Persistence of the C-H wag absorbance at 799 cm^{-1} after complete ketone reduction

4.3.2.3.2 Identity of titanocene catalyst formed *in situ*

To verify the intermediacy of a Ti(III) hydride species, a titanocene hydride complex was generated via the approach described by Buchwald[32–34] and monitored by ReactIR. In this experiment, titanocene difluoride was mixed with phenylsilane in refluxing THF. The formation of a titanocene(III) hydride species was demonstrated by the shift in the C-H wag of the Cp ligand of titanocene from 813 cm^{-1} to 799 cm^{-1} and a change in color from yellow to green was observed (Figure 4.7). The C-H wag absorbance at 799 cm^{-1} suggests that a Ti(III) hydride complex is formed as an intermediate in the reduction process with titanocene(III) borohydride and PMHS as the stoichiometric reductant.

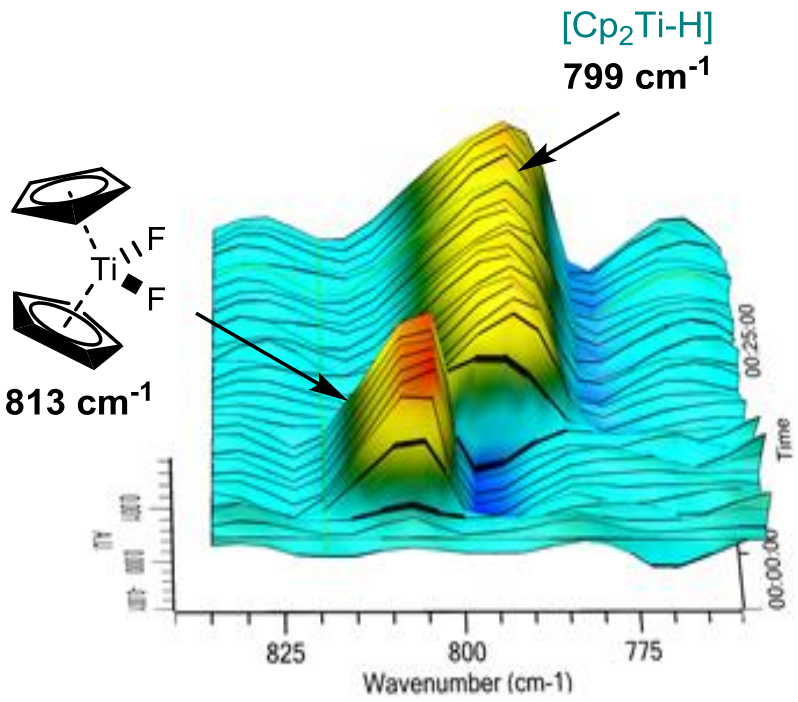

Figure 4.7. Formation of titanocene(III) hydride monitored by ReactIR

To determine if the titanocene hydride intermediate in our approach is the same as the one generated by Buchwald, the reduction of 2-octanone to 2-octanol was performed via the method described by Buchwald and coworkers[32–34] and the results are summarized in table 4.3. Reactions were monitored after an hour and it was observed that the reduction of 2-octanone only proceeded under refluxing conditions. Product yield was improved when the active catalyst was prepared with 20 mol% $PhSiH_3$ (Table 4.3, entry 5). With our optimized reaction conditions however, full conversion to product was realized within an hour and at room temperature (*vide supra*).

Table 4.3. Reduction of **1** to **2** with Cp_2TiF_2

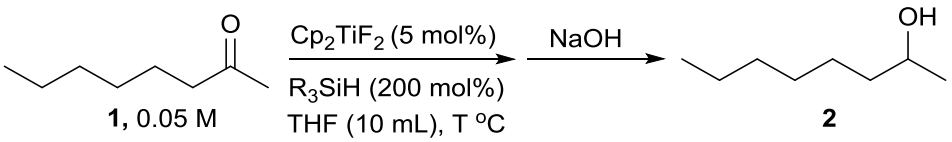

Entry	R_3SiH	T (^oC)	Yield (%)[1]
1	$PhSiH_3$	r.t.	-
2	PMHS	r.t.	-
3	PMHS[2]	r.t.	-
4	PMHS	60	45
5	PMHS[2]	60	91

[1]GC yields after 1 h with biphenyl as internal standard. [2] Active catalyst formed with 20 mol% $PhSiH_3$ under reflux.

Further studies on the identity of the titanocene(III) hydride complex generated by our method were done by reducing **1-v** via Buchwald's method[32–34] and comparing the results to the reduction performed with the titanocene borohydride PMHS system. The results are summarized in table 4.4. For entry 1, the titanocene(III) hydride complex activated with 20 mol% $PhSiH_3$, 20 mol% MeOH, and 20 mol% pyrrolidine under reflux. PMHS and **1-v** were added sequentially at room temperature. About 7 equiv of MeOH was slowly added over 4 hours via a syringe pump and only starting material was recovered.[32] Reaction was repeated with 7 equiv of MeOH added slowly over 20 h via a syringe pump and left to stir for 96 hours and still no product formed.

Table 4.4. Results from the reduction of **1-v** with titanocene(III) hydride complexes[1]

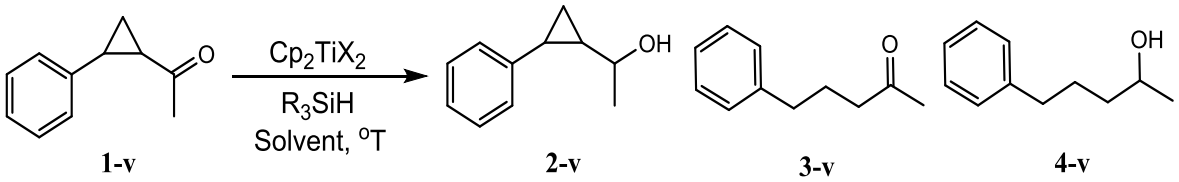

1-v **2-v** **3-v** **4-v**

Entry	Cp_2TiX_2 (5 mol%)	R_3SiH (mol%)	T (°C)	Time (h)	**2-v** (%)	**3-v** (%)	**4-v** (%)
1	Cp_2TiF_2	PMHS (400)[a]	r.t.	24	-	-	-
2	Cp_2TiF_2	PMHS (400)[b]	60	5	55	15	-
3	Cp_2TiF_2	$PhSiH_3$ (200)[c]	60	48	45	55	-
4	-	PMHS (400)[d]	60	24	-	-	-

1. Yields determined by NMR analysis.

a. [**1-v**] = 33 mM; [Cp_2TiF_2] = 1.7 mM; [$PhSiH_3$] = 6.6 mM; [MeOH] = 6.6 mM; [Pyrrolidine] = 6.6 mM; [PMHS] = 132 mM; [MeOH] = 218 mM; THF = 15 ml; [**1-v**] = 50 mM.

b. [Cp_2TiF_2] = 2.5 mM; [$PhSiH_3$] = 10 mM; [PMHS] = 200 mM; THF = 10 ml; 70% conversion to alcohol.

c. [**1-v**] = 50 mM; [Cp_2TiF_2] = 2.5 mM; [$PhSiH_3$] = 100 mM; THF = 10 ml.

d. Control experiment; [**1-v**] = 50 mM; [$PhSiH_3$] = 10 mM; [PMHS] = 200 mM; THF = 10 ml; **1-v** added at reflux.

For entry 2, the titanocene(III) hydride complex was activated with 20 mol% $PhSiH_3$ under reflux. PMHS and **1-v** were added sequentially at reflux. About 70% of the starting material was converted to product with evidence of ring opened product **3-v**. Interestingly, when $PhSiH_3$ instead of PMHS was used as the stoichiometric reductant, the ring opened product **3-v** was slightly higher than **2-v**. Conversely, no evidence of ring opened product was observed when reductions were mediated by the titanocene borohydride-PMHS system (Scheme 4.11). These results indicate that the titanocene hydride generated *in situ* with our approach is not identical to that generated in the system developed by Buchwald and coworkers.

Attempts to isolate and crystallize the intermediate generated using our approach has not been successful thus far. Nonetheless, it is useful to examine other protocols developed in the literature for generating titanocene(III) hydride complexes. To this end, we looked at the studies on titanocene(III) hydride complexes done independently by Harrod[48] and Brintzinger.[49,50] Brintzinger studied titanocene hydride complexes generated with either hydrogen gas, organolithiums or Grignard reagents.[49,50] Harrod, however, studied titanocene(III) hydride complexes generated by reacting dimethyltitanocene with phenylsilane.[48]

We therefore hypothesized that the titanocene hydride intermediate generated in our system would be similar but not necessarily identical to that generated by Harrod (Figure 4.8). Complex **b** (Figure 4.9) was prepared by reacting stoichiometric amounts of dimethyltitanocene (1:1 mole ratio) with phenylsilane while complex **c** (Figure 4.10) was prepared by reacting catalytic amounts of dimethyltitanocene with phenylsilane. They observed that **c** decomposed to **b**, which eventually decomposed to **a**. Intermediate **a** was observed by ESR spectroscopy. All the intermediates were found to be reactive in polymerizing silanes with concomitant evolution of H_2 gas.[48]

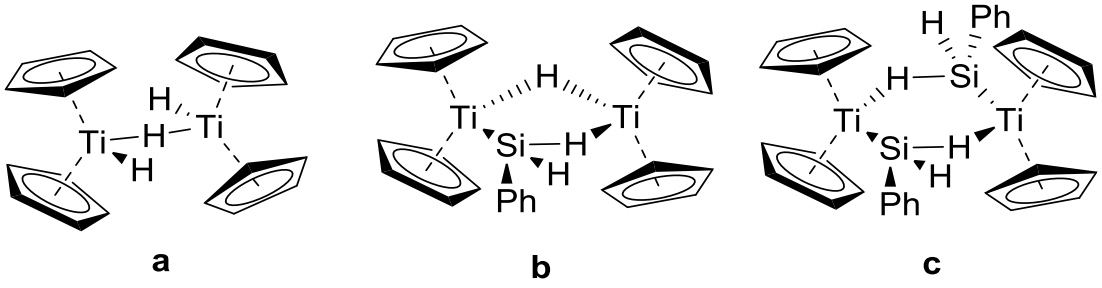

Figure 4.8. Titanocene(III) hydride complexes proposed by Harrod[48]

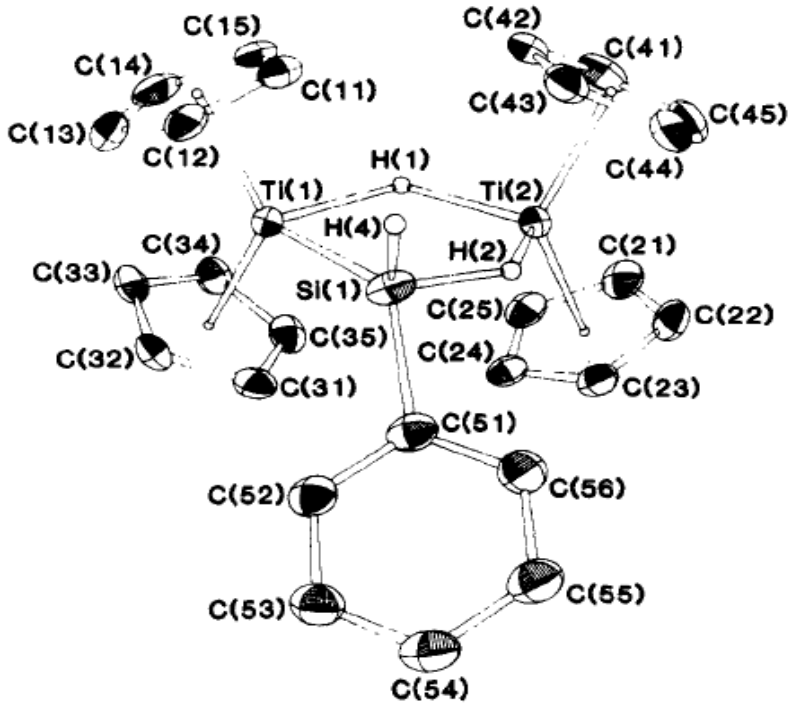

Figure 4.9. Crystal structure for complex **b**[48]

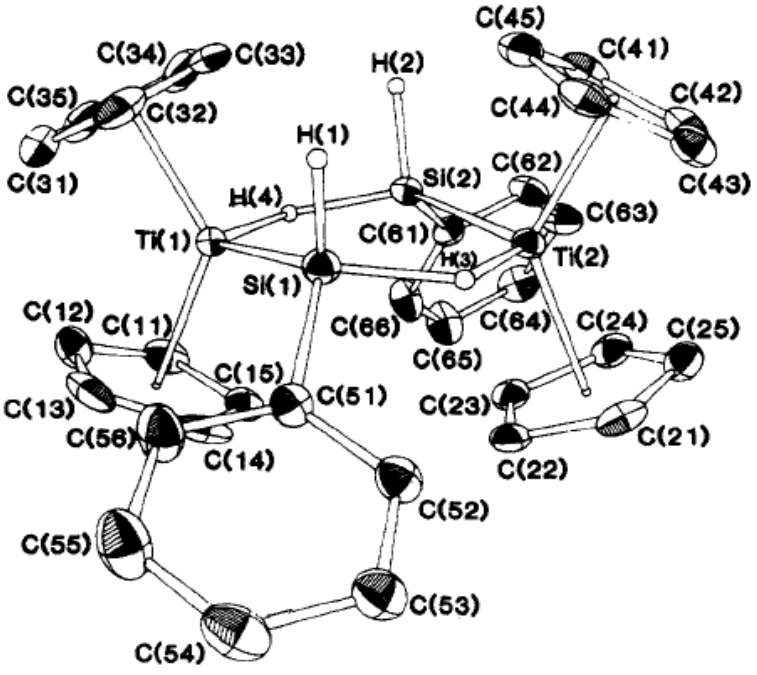

Figure 4.10. Crystal structure for complex **c**[48]

It is therefore possible that for our system, the reduction could be mediated by either one or more titanocene hydride complexes generated *in situ*, which may have varying reactivity towards carbonyl reductions. This could explain the discrepancies observed between the reductions performed via our titanocene borohydride-PMHS system and the approach outlined by Buchwald. It should also be noted that the presence of a Ti(III)-bound alkoxide cannot be ruled out as a possible intermediate since its Cp ligand has the same C-H wag absorption at 799 cm^{-1}.

Based on the results obtained from monitoring this process via *in situ* IR spectroscopy, a catalytic cycle was proposed as shown in scheme 4.13. In the proposed cycle, the titanocene borohydride, formed via the method described in the literature,[30,51] reduces the carbonyl to form the titanium(III) alkoxide.[30,46,47] It is then posited that the titanium alkoxide reacts with the silane, via a method similar to that proposed by Buchwald and coworkers,[32,33,52] leading to the formation of silylated product and a titanocene(III) hydride intermediate, whose structural identity at the moment is unknown. This intermediate presumably reacts with another carbonyl to complete the cycle.

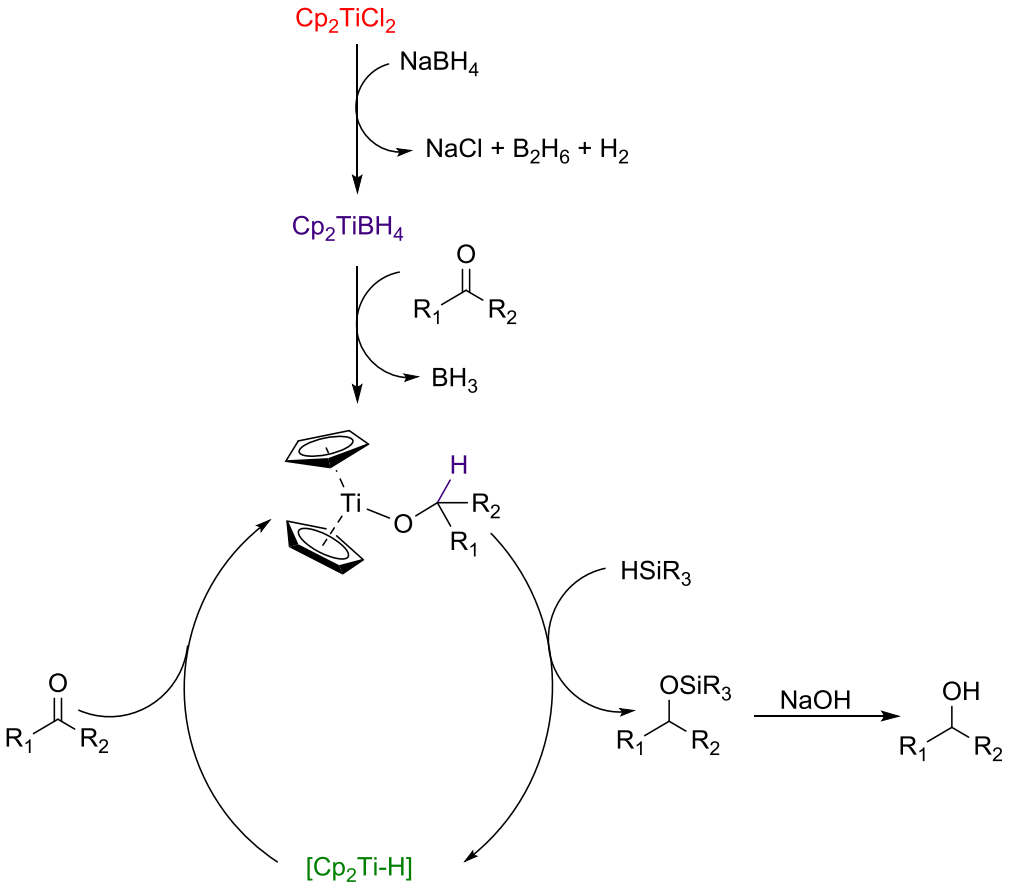

Scheme 4.13. Proposed catalytic cycle for carbonyl reduction

4.3.2.4 Limitations of Cp_2TiBH_4-PMHS system

The reduction of 1,2-diones and 1,3-diones to alcohols were unsuccessful under the reaction conditions (Scheme 4.14). Partial reductions were however observed with 1,4 diones. These observations suggest that the catalyst might be quenched by forming a titanocene bounded to the two carbonyls as shown in scheme 4.14. Esters could not be reduced with the titanocene borohydride PMHS system (Scheme 4.14, **4-e**). This is because the initial reduction of the carbonyl by titanocene borohydride does not occur with esters.

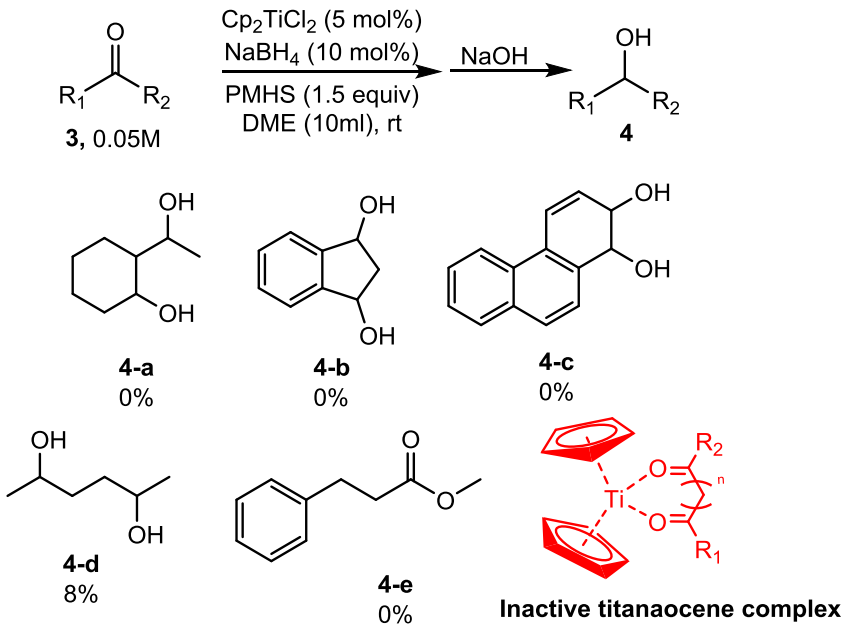

Scheme 4.14. Test for the reduction of diols under the titanocene borohydride-PMHS system

4.3.2.5 Reactivity of the titanocene hydride formed *in situ* towards esters

Based on our results from the mechanistic studies on carbonyl reductions by titanocene borohydride-PMHS, it is known that an active titanocene hydride is formed *in situ* after the initial carbonyl reduction by titanocene borohydride. We therefore wanted to test if this titanocene hydride formed *in situ* was reactive towards esters. To test the reactivity of the titanocene hydride formed *in situ*, titanocene borohydride was first reacted with acetone to form the proposed titanocene alkoxide complex. PMHS was then added to generate this titanocene hydride complex. To this solution was added the ester **3** and the reaction was monitored via *in situ* IR spectroscopy (Scheme 4.15).

As shown in figure 4.11, the ester was reduced within 15 minutes by the titanocene hydride formed *in situ*. We also discovered that the titanocene(III) alkoxide

moiety could also be generated by adding NaO^{t}Bu instead of acetone. As a result, a series of esters were reduced where the titanocene alkoxide was formed with either acetone or NaO^{t}Bu and the results are summarized in table 4.5.

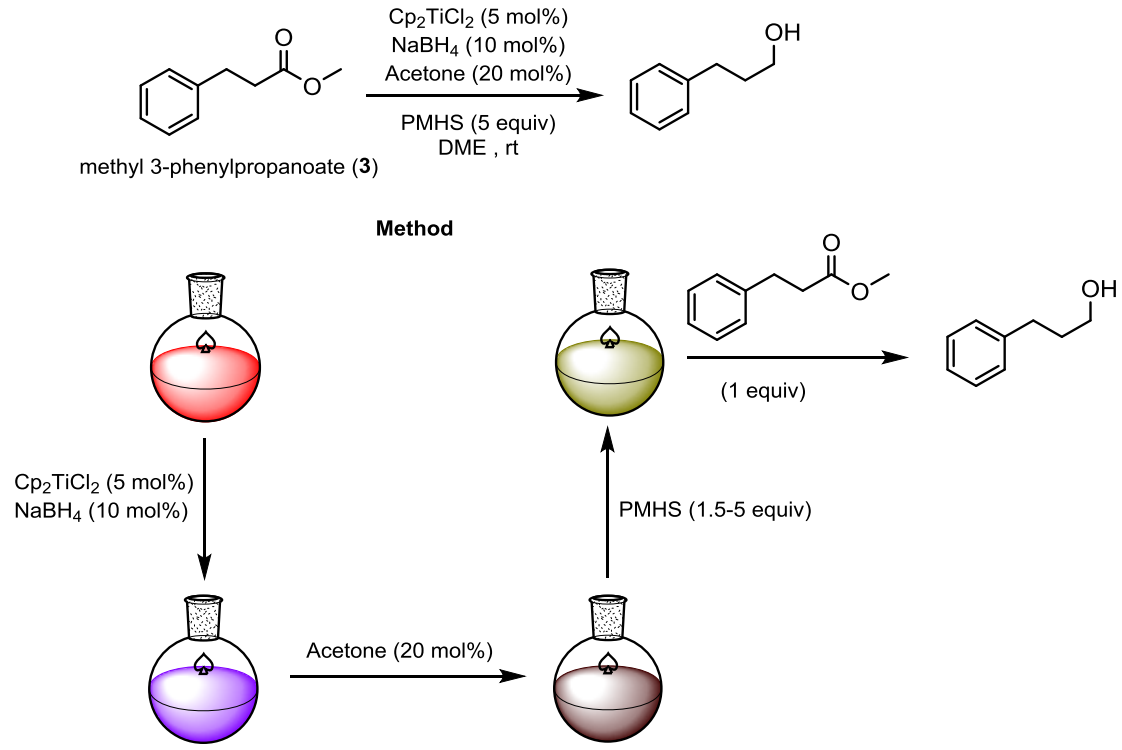

Scheme 4.15. Reactivity of titanocene(III) hydride formed *in situ* towards esters

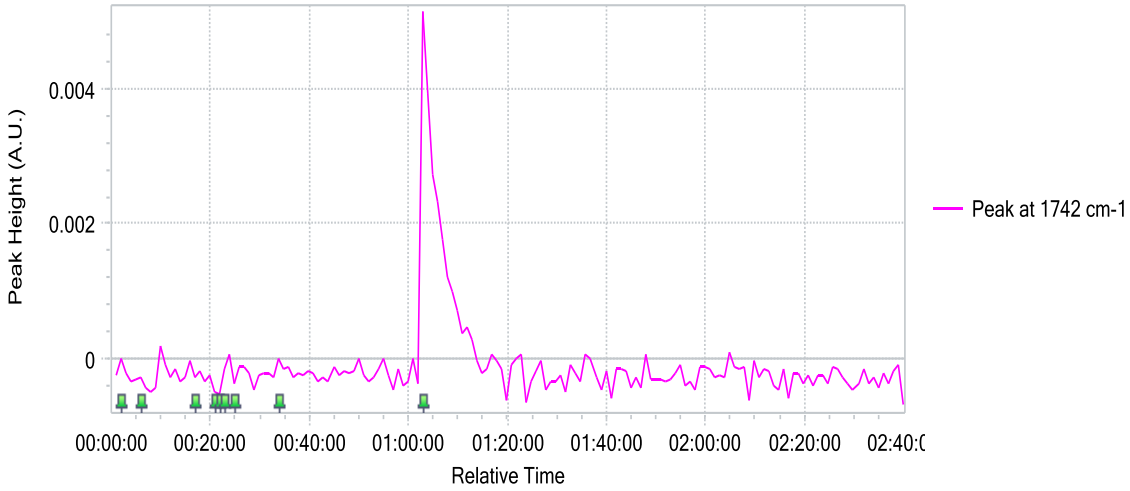

Figure 4.11. Ester reduced by the titanocene hydride formed *in situ*. Decay of C=O peak at 1742 cm^{-1}

Table 4.5. Substrate scope for ester reductions with Cp_2TiBH_4/Additive/PMHS

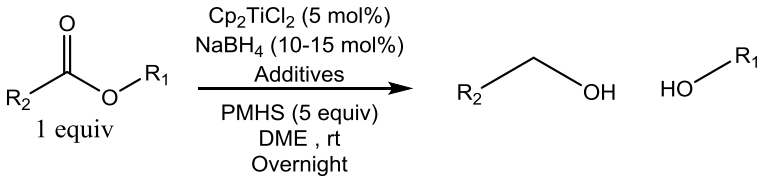

Entry	Ester	Product	Additive	Conv. (%)[1]
1	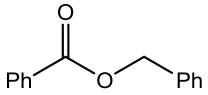	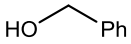	Acetone	91
2	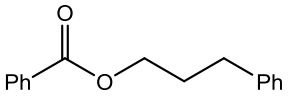	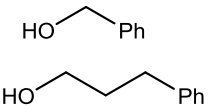	NaO^tBu	100
3	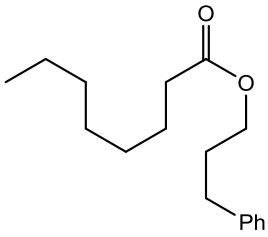	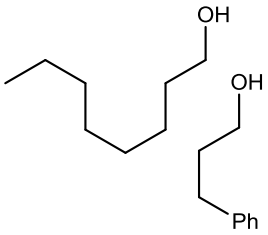	NaO^tBu	100
4	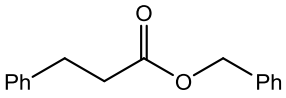	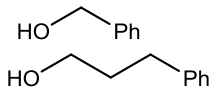	NaO^tBu	100
5	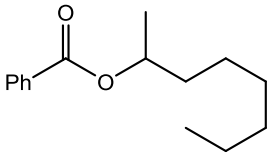	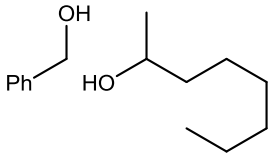	NaO^tBu	81
6	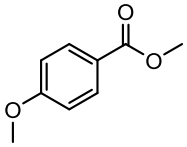	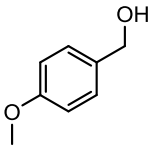	Acetone NaO^tBu	97 94
7	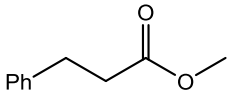	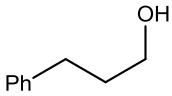	Acetone	100[2]

[1] Conversion to alcohol products by NMR analysis; [Ester] = 0.1 M; [Cp_2TiCl_2] = 0.005 M; [$NaBH_4$] = 0.01 M; [Acetone] = 0.04 M; [NaO^tBu] = 0.007 M; DME = 10 mL; [2] [Ester] = 0.1 M; [Cp2TiCl2] = 0.005 M; [NaBH4] = 0.01 M; [Acetone] = 0.04 M; DME = 20 mL; Reaction time was 15 min (Monitored by ReactIR)

4.4 Conclusion

In conclusion, the development of an efficient procedure for the reduction of aromatic and aliphatic ketones by a titanocene(III) aqua complex in the presence of an appropriate base was demonstrated. Although reaction time was improved for the reduction of ketones with the addition of a base, attempts to make the system catalytic were unsuccessful. Regeneration of the active titanocene complex proved to be more challenging than anticipated and more work needs to be done to better understand this system on a mechanistic level.

Work was therefore focused on developing an efficient method for reducing carbonyls catalyzed by titanocene hydride complexes. From our studies, a procedurally straightforward, inexpensive, and mild approach for the reduction of aldehydes and ketones with a titanocene borohydride-PMHS system was developed. This method was used to successfully reduce a wide range of aldehydes and ketones. Preliminary mechanistic studies suggest that the reaction was mediated by a reactive titanocene hydride complex formed *in situ*. Results from our studies also demonstrate that the titanocene complex remains in the +3-oxidation state throughout the reaction. Esters could not be reduced with titanocene borohydride, however, the titanocene hydride formed *in situ* by the addition of acetone or NaO^{t}Bu to titanocene borohydride, was found to be reactive towards the reduction of esters.

Future endeavors will focus on asymmetric carbonyl reductions[15,16,32,53] catalyzed by titanocene borohydride. We are optimistic that this potentially has direct application to the synthesis of complex organic compounds. Future endeavors will also focus on

extending this system to reduce other related functional groups including amides, imines, and nitriles.

4.5 References

(1) Fuenfschilling, P. C.; Hoehn, P.; Mutz, J. P. *Org. Process Res. Dev.* **2007**, *11* (1), 13–18.

(2) Chen, C. Y.; Frey, L. F.; Shultz, S.; Wallace, D. J.; Marcantonio, K.; Payack, J. F.; Vazquez, E.; Springfield, S. A.; Zhou, G.; Liu, P.; Kieczykowski, G. R.; Chen, A. M.; Phenix, B. D.; Singh, U.; Strine, J.; Izzo, B.; Krska, S. W. *Org. Process Res. Dev.* **2007**, *11* (3), 616–623.

(3) Cabaj, J. E.; Kairys, D.; Benson, T. R. *Org. Process Res. Dev.* **2007**, *11* (3), 378–388.

(4) Ikemoto, T.; Ito, T.; Hashimoto, H.; Kawarasaki, T.; Nishiguchi, A.; Mitsudera, H.; Wakimasu, M.; Tomimatsu, K. *Org. Process Res. Dev.* **2000**, *4* (6), 520–525.

(5) Hett, R.; Fang, Q. K.; Gao, Y.; Wald, S. A.; Senanayake, C. H. *Org. Process Res. Dev.* **1998**, *2* (2), 96–99.

(6) Watson, T. J. N.; Curran, T. T.; Hay, D. A.; Shah, R. S.; Wenstrup, D. L.; Webster, M. E. *Org. Process Res. Dev.* **1998**, *2* (6), 357–365.

(7) Guo, J.; Erickson, G. A.; Fitzgerald, R. N.; Matsuoka, R. T.; Rafferty, S. W.; Sharp, M. J.; Sickles, B. R.; Wisowaty, J. C. *J. Org. Chem.* **2006**, *71* (21), 8302–8305.

(8) Zhou, B.; Gopalan, A. S.; VanMiddlesworth, F.; Shieh, W.-R.; Sih, C. J. *J. Am. Chem. Soc.* **1983**, *105*, 5925–5926.

(9) Ahluwalia, V. K.; Parashar, R. K. *Organic Reaction Mechanisms*, 4th Ed.; Alpha Science International Ltd, 2011.

(10) Magano, J.; Dunetz, J. R. *Org. Process Res. Dev.* **2012**, *16* (6), 1156–1184.

(11) Sharma, P. K.; Kolchinski, A.; Shea, A.; Nair, J. J.; Gou, Y.; Romanczyk, L. J.; Schmitz, H. H.; Company, I.; Street, H.; Street, E. *Org. Process Res. Dev.* **2007**, *11* (3), 422–430.

(12) Cha, J. S. *Org. Process Res. Dev.* **2006**, *10* (5), 1032–1053.

(13) Davis, T. A.; Chopade, P. R.; Hilmersson, G.; Flowers, R. A. *Org. Lett.* **2005**, *7* (1), 119–122.

(14) Chciuk, T. V.; Anderson, W. R.; Flowers, R. A. *J. Am. Chem. Soc.* **2016**, *138* (28), 8738–8741.

(15) Li, Y.; Yu, S.; Wu, X.; Xiao, J.; Shen, W.; Dong, Z.; Gao, J. *J. Am. Chem. Soc.* **2014**, *136*, 4031–4039.

(16) Wu, W.; Liu, S.; Duan, M.; Tan, X.; Chen, C.; Xie, Y.; Lan, Y.; Dong, X. Q.; Zhang, X. *Org. Lett.* **2016**, *18* (12), 2938–2941.

(17) Connolly, T. J.; Matchett, M.; Mcgarry, P.; Sukhtankar, S.; Zhu, J. *Org. Process*

Res. Dev. **2004**, *8* (4), 624–627.

(18) Zhao, M.; Xie, W.; Cui, C. *Chem. - A Eur. J.* **2014**, *20*, 9259–9262.

(19) Nardi, M.; Sindona, G.; Costanzo, P.; Oliverio, M.; Procopio, A. *Tetrahedron* **2015**, *71*, 1132–1135.

(20) Wekesa, F. S.; Arias-Ugarte, R.; Kong, L.; Sumner, Z.; McGovern, G. P.; Findlater, M. *Organometallics* **2015**, *34*, 5051–5056.

(21) Kaithal, A.; Chatterjee, B.; Gunanathan, C. *Org. Lett.* **2015**, *17*, 4790–4793.

(22) Barrero, A. F.; Rosales, A.; Cuerva, J. M.; Gansäuer, A.; Oltra, J. E. *Tetrahedron Lett.* **2003**, *44* (5), 1079–1082.

(23) Rosales, A.; Muñoz-Bascón, J.; Roldan-Molina, E.; Castañeda, M. A.; Padial, N. M.; Gansäuer, A.; Rodríguez-García, I.; Oltra, J. E. *J. Org. Chem.* **2014**, *79* (16), 7672–7676.

(24) Gansäuer, A.; Behlendorf, M.; Cangönül, A.; Kube, C.; Cuerva, J. M.; Friedrich, J.; Van Gastel, M. *Angew. Chemie - Int. Ed.* **2012**, *51* (13), 3266–3270.

(25) Paradas, M.; Campaña, A. G.; Marcos, M. L.; Justicia, J.; Haidour, A.; Robles, R.; Cárdenas, D. J.; Oltra, J. E.; Cuerva, J. M. *Dalt. Trans.* **2010**, *39*, 8796–8800.

(26) Paradas, M.; Campaña, A. G.; Jiménez, T.; Robles, R.; Oltra, J. E.; Buñuel, E.; Justicia, J.; Cárdenas, D. J.; Cuerva, J. M. *J. Am. Chem. Soc.* **2010**, *132* (36), 12748–12756.

(27) Cuerva, J. M.; Campaña, A. G.; Justicia, J.; Rosales, A.; Oller-López, J. L.; Robles, R.; Cárdenas, D. J.; Buñuel, E.; Oltra, J. E. *Angew. Chemie - Int. Ed.* **2006**, *45* (33), 5522–5526.

(28) Estévez, R. E.; Oller-Lopez, J. L.; Robles, R.; Melgarejo, C. R.; Gansäuer, A.; Cuerva, J. M.; Oltra, J. E. *Org. Lett.* **2006**, *8* (24), 5433–5436.

(29) Jimenez, T.; Campana, A. G.; Bazdi, B.; Paradas, M.; Arraez-Roman, D.; Segura-Carretero, A.; Fernandez-Gutierrez, A.; Oltra, J. E.; Robles, R.; Justicia, J.; Cuerva, J. M. *European J. Org. Chem.* **2010**, No. 22, 4288–4295.

(30) Barden, M.; Schwartz, J. *J. Org. Chem.* **1995**, *60* (18), 5963–5965.

(31) Barr, K. J.; Berk, S. C.; Buchwald, S. L. *J. Org. Chem.* **1994**, *59* (15), 4323–4326.

(32) Yun, J.; Buchwald, S. L. *J. Am. Chem. Soc.* **1999**, *121* (24), 5640–5644.

(33) Verdaguer, X.; Hansen, M. C.; Berk, S. C.; Buchwald, S. L. *J. Org. Chem.* **1997**, *62* (24), 8522–8528.

(34) Verdaguer, X.; Lange, U. E. W.; Reding, M. T.; Buchwald, S. L. *J. Am. Chem. Soc.* **1996**, *118* (c), 6784–6785.

(35) Szostak, M.; Spain, M.; Eberhart, A. J.; Procter, D. J. *J. Org. Chem.* **2014**, *79*

(24), 11988–12003.

(36) An, J.; Work, D. N.; Kenyon, C.; Procter, D. J. *J. Org. Chem.* **2014**, *79*, 6743–6747.

(37) Szostak, M.; Spain, M.; Procter, D. J. *Org. Lett.* **2012**, *14* (3), 840–843.

(38) Mimoun, H. *J. Org. Chem.* **1999**, *64* (7), 2582–2589.

(39) Corey, Elias, J.; Chaykovsky, M. *J. Am. Chem. Soc.* **1965**, *87* (6), 1353–1364.

(40) Luche, J.-L. *J. Am. Chem. Soc.* **1978**, *100* (7), 2226–2227.

(41) Luche, J. L.; Rodriguez-Hahn, L.; Crabbe, P. *J. Chem. Soc. Chem. Commun.* **1978**, *326* (14), 601–602.

(42) Kosal, A. D.; Ashfeld, B. L. *Org. Lett.* **2010**, *12* (1), 44–47.

(43) Gansäuer, A.; Von Laufenberg, D.; Kube, C.; Dahmen, T.; Michelmann, A.; Behlendorf, M.; Sure, R.; Seddiqzai, M.; Grimme, S.; Sadasivam, D. V.; Fianu, G. D.; Flowers, R. A. *Chem. - A Eur. J.* **2015**, *21* (1), 280–289.

(44) Gansäuer, A.; Hildebrandt, S.; Michelmann, A.; Dahmen, T.; von Laufenberg, D.; Kube, C.; Fianu, G. D.; Flowers, R. A. *Angew. Chemie - Int. Ed.* **2015**, *54*, 7003–7006.

(45) Lippard, S. J.; Coucouvanis, D.; Melmed, K. M. *Inorg. Chem.* **1973**, *12* (1), 232–236.

(46) Matsubara, K.; Niibayashi, S.; Nagashima, H. *Organomet.* **2003**, *22*, 1376–1382.

(47) Niibayashi, S.; Mitsui, K.; Motoyama, Y.; Nagashima, H. *J. Organomet. Chem.* **2005**, *690*, 276–285.

(48) Aitken, C. T.; Harrod, J. F.; Samuel, E. *J. Am. Chem. Soc.* **1986**, *108* (14), 4059–4066.

(49) Brintzinger, H. *J. Am. Chem. Soc.* **1967**, *89* (26), 6871–6877.

(50) Bercaw, J. E.; Marvich, R. H.; Bell, L. G.; Brintzinger, H. H. *J. Am. Chem. Soc.* **1972**, *94* (4), 1219–1238.

(51) Lucas, C. R. *Inorg. Synth* **1977**, *17*, 91–94.

(52) Reding, M. T.; Buchwald, S. L. *J. Org. Chem.* **1995**, *60* (24), 7884–7890.

(53) Xin, S.; Harrod, J. *Can. J. Chem.* **1995**, *73*, 999–1002.

Chapter 5. Conclusion & outlook

In conclusion, the potential of titanocene(III) complexes in the design of sustainable chemical transformations have been presented in this dissertation. The ability to tune the reactivity of titanocene(III) complexes with different additives make them versatile reagents for carrying out a variety of reactions. The Intrinsic property of titanocene(III) complexes to shuttle between the +3/+4 redox couple make them powerful catalysts for single electron transformations including C-C bond forming reactions and carbonyl reductions.

A titanocene(III) catalyzed atom-economical radical arylation of amino epoxides to form indoline derivatives was introduced in chapter 2. A thorough mechanistic study of this system led to two major discoveries. The first discovery was that Coll*HCl, the salt additive, was stabilizing the active titanocene catalyst by forming a supramolecular complex, which was in equilibrium with the catalyst. The second major discovery was that the turnover limiting step for this radical arylation process was the back-electron transfer from the radical σ-complex to the titanium metal.

Based on the proposed mechanism, a more Lewis acidic titanocene complex was employed to facilitate the radical arylation of electron deficient epoxides, which were once recalcitrant toward the arylation process. Our findings from the mechanistic study have inspired the development of a sustainable atom-economical radical arylation of pyrroloepoxides to form dihydropyrrolizines and tetrahydroindolizines, which are basic motifs found in many natural products of biological activity. A fundamental understanding of titanocene catalyzed radical arylation of epoxides to form indoles and other cyclized products provides a platform for developing other atom-economical

processes with different functional groups such as carbonyls and nitriles. Also, the use of cyclopentadienyl ligands with electron withdrawing substituents would be of major importance for the design of efficient catalysts in enantioselective arylations *via* regiodivergent epoxide opening (REO).

In chapter 3, the effects of salts, solvents, and ligands on the identity and activity of titanocene(III) complexes in the radical arylation of amino epoxides was investigated. From our studies, it was found that the stability of the supramolecular complex impacts the activity of the titanocene catalyst. It was also discovered that the solubility of the salt negatively impacts the activity of the active catalyst.

Moreover, we found that the choice of solvent also impacts the nature and activity of the catalyst. In acetonitrile, the more Lewis acidic titanocenium cation was formed, which facilitated the radical arylation of electron deficient epoxides. However, due to the strong coordination and polarity of the solvent, the reaction rate was drastically reduced. The titanocenium complex could however be generated in THF with titanocene triflate. Other titanocene complexes with loosely coordinating ligands were also developed and were found to be stable and active towards the radical arylation epoxides.

Titanocene(III) complexes are efficient in opening epoxides to form β-titanoxy radicals that readily add to arenes or olefins in simple intramolecular processes. However, the potential for titanocene catalyzed intermolecular radical additions to protonated electron deficient heterocycles or arenes is largely untapped. With adequate insight into the general mechanism for the radical arylation of epoxides and with ample knowledge on the design of efficient titanocene(III) complexes for various reactions,

work to investigate the viability of intermolecular radical processes, catalyzed by low-valent titanocene(III) complexes, would be interesting. The success of this endeavor will ultimately lead to the development of an effective method to add radicals derived from epoxides to benzene derivatives in a mild and highly selective manner. The products obtained could serve as intermediates and the backbone in the total synthesis of many biological and pharmaceutical compounds like ibuprofen and ketoprofen.

In chapter 4, the development of an efficient procedure for the reduction of aromatic and aliphatic ketones by a titanocene(III) aqua complex in the presence of an appropriate base was demonstrated. Future work will focus on performing mechanistic studies and ultimately developing a catalytic process for this system. Furthermore, a procedurally straightforward and simple way to reduce aldehydes, ketones, and esters with catalytic titanocene(III) borohydride-PMHS was also developed. Preliminary mechanistic studies have shown that the titanium remains in the +3-oxidation state throughout the reaction and that a titanocene hydride species is formed *in situ*. Future studies will focus on other functional groups such as nitriles, amides, and imines. Future endeavors will also focus on asymmetric carbonyl reductions catalyzed by titanocene borohydride.

Organofluoride compounds are widely used in the pharmaceutical industry mainly due to their stable nature in biological systems. As a result, a lot of work has been done to develop ways to add fluorides to organic compounds. However, efficient defluorination protocols for removing excess organofluorides from the environment have not been developed. Since titanium fluoride or silyl fluoride bonds are very strong, we are

optimistic that we can develop new ways to remove fluorides from organofluorides *via* a titanocene borohydride-PMHS system.

In this dissertation, we have shown how titanocene(III) complexes developed from readily available and inexpensive Cp_2TiCl_2 are attractive in the development of sustainable chemical processes. Depending on the activation protocols, the nature of additives, and the choice of solvent, the nature and activity of the titanocene(III) complex can be manipulated to carry out interesting transformations *via* either single electron catalysis or a 2-electron process. The work presented herein highlights the latent potential of titanocene(III) complexes and future studies will focus on pushing the boundaries of our understanding of titanocene(III) complexes on a molecular level to discover new and exciting chemistry.

Chapter 6. Appendix

6.1 Incorporation of Ti(III) complexes in the design of atom economical processes

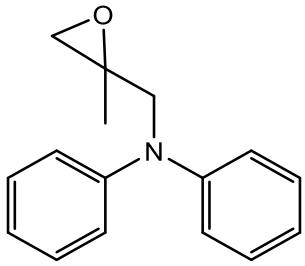

***N*-((2-methyloxiran-2-yl) methyl)-*N*-phenylaniline (1)**

^{1}H NMR (500 MHz, $CDCl_3$) δ 7.35 (t, *J* = 7.8 Hz, 5H), 7.13 (t, *J* = 8.9 Hz, 5H), 7.05 (t, *J* = 7.3 Hz, 2H), 4.00 (s, 2H), 2.78 (d, *J* = 4.6 Hz, 1H), 2.66 (d, *J* = 4.7 Hz, 1H), 1.48 (s, 3H). ^{13}C NMR (126 MHz, $CDCl_3$) δ 148.53, 129.42, 121.72, 121.09, 121.02, 117.87, 77.48, 77.23, 76.98, 56.88, 56.67, 52.56, 19.85.

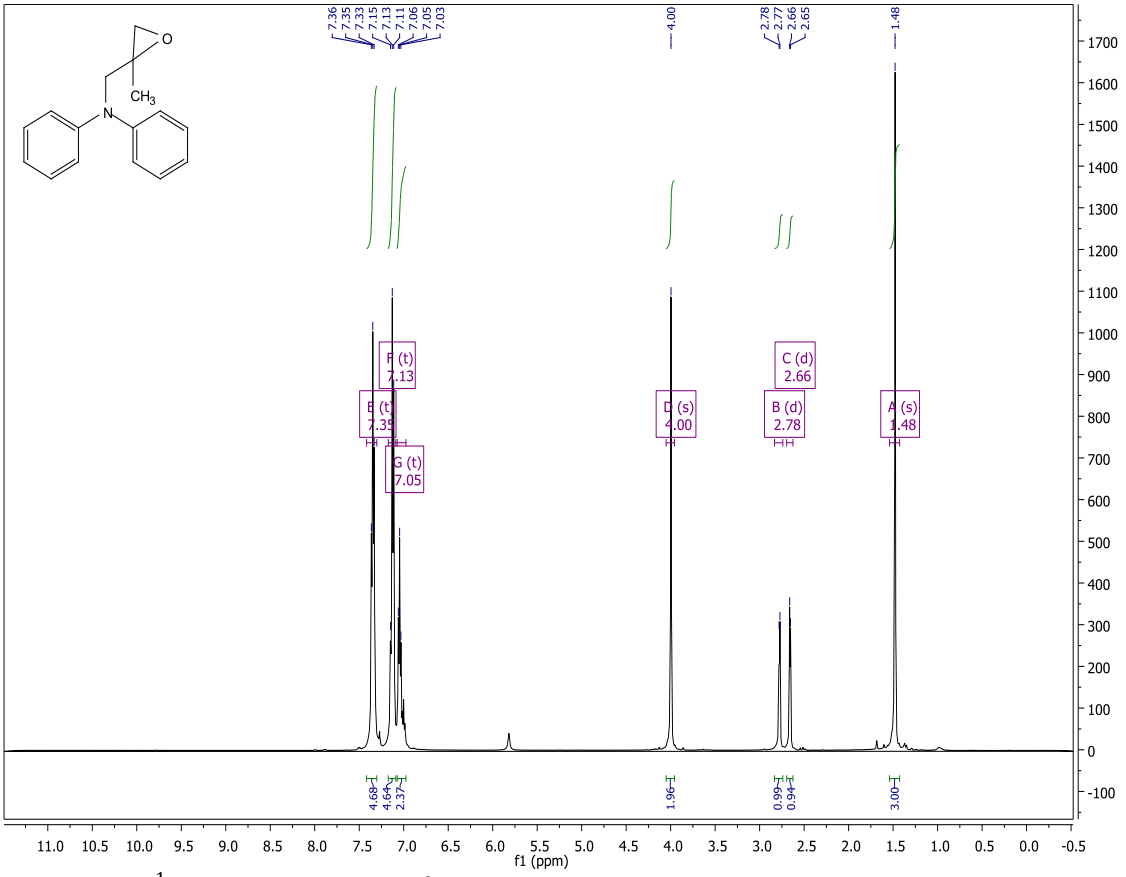

Figure 6.1. ^{1}H NMR spectrum of **1**

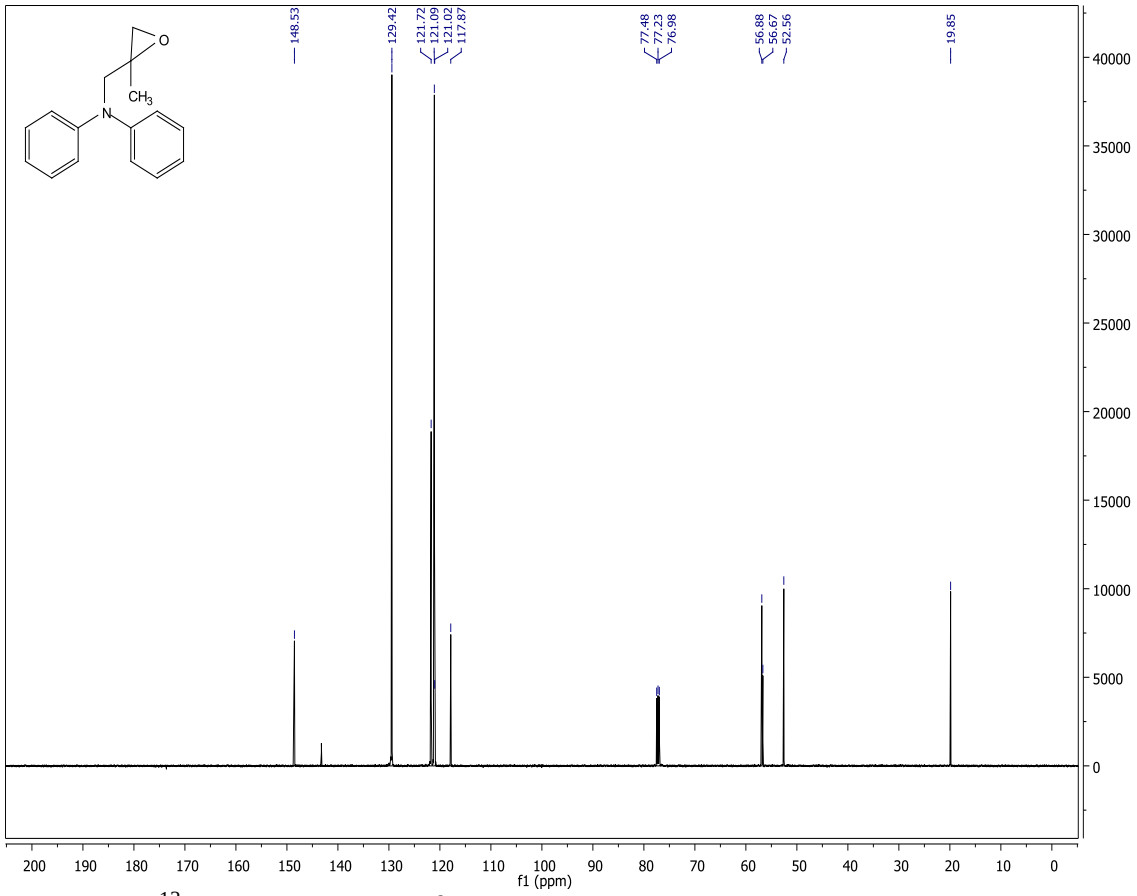

Figure 6.2. ^{13}C NMR spectrum of **1**

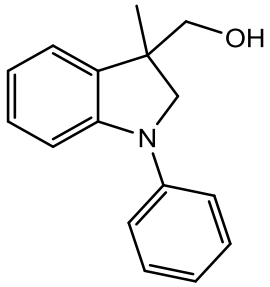

(3-methyl-1-phenylindolin-3-yl) methanol (2)

^{1}H NMR (500 MHz, CDCl3) δ 7.40 – 7.35 (m, 2H), 7.27 (d, J = 7.7 Hz, 2H), 7.21 (d, J = 7.5 Hz, 1H), 7.16 (t, J = 7.2 Hz, 2H), 7.00 (t, J = 7.3 Hz, 1H), 6.83 (td, J = 7.3, 0.9 Hz, 1H), 3.97 (d, J = 9.3 Hz, 1H), 3.71 (dd, J = 13.9, 10.1 Hz, 2H), 3.62 (d, J = 10.8 Hz, 1H), 1.69 (s, 1H), 1.43 (s, 3H).^{13}C NMR (126 MHz, $CDCl_3$) δ 146.77, 143.87, 135.43, 129.23, 128.11, 123.30, 121.07, 119.00, 117.62, 108.53, 77.35, 77.10, 76.84, 68.99, 61.62, 45.52, 22.33.

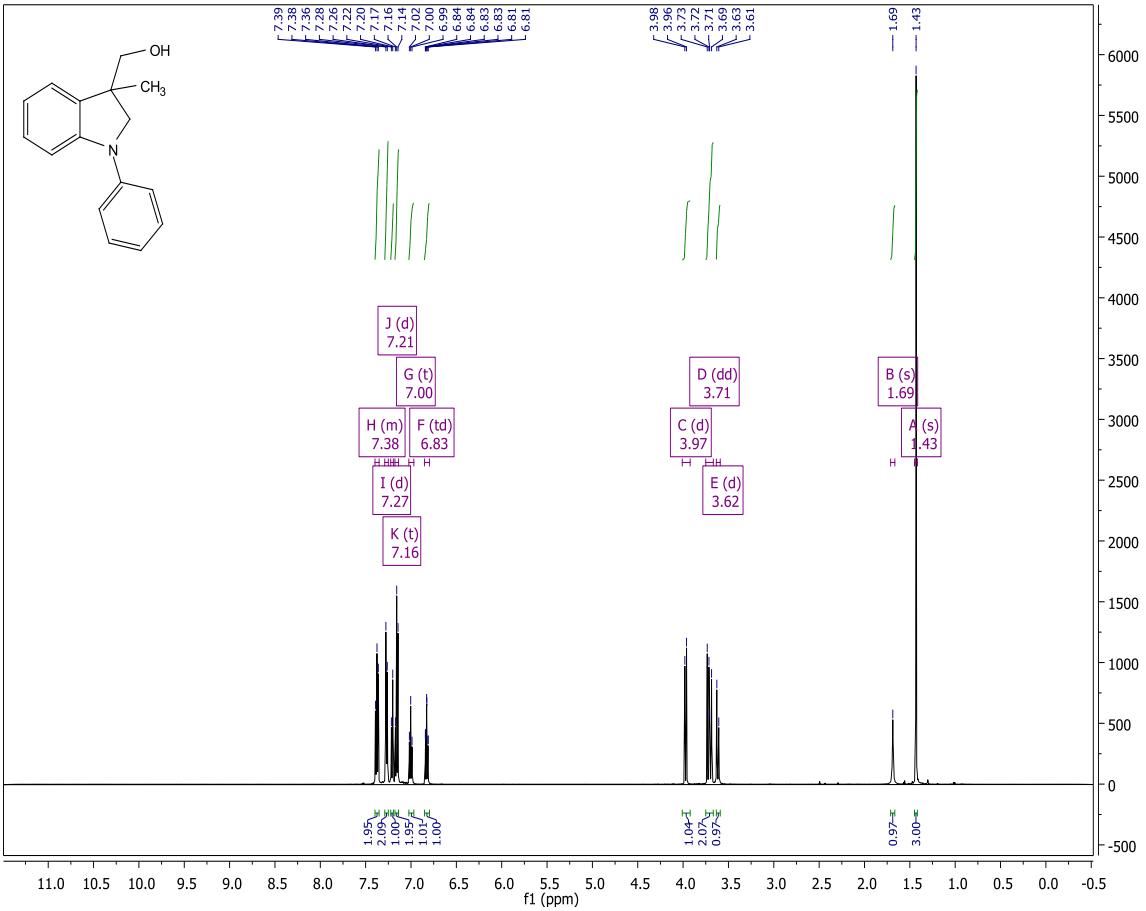

Figure 6.3. ^{1}H NMR spectrum of **2**

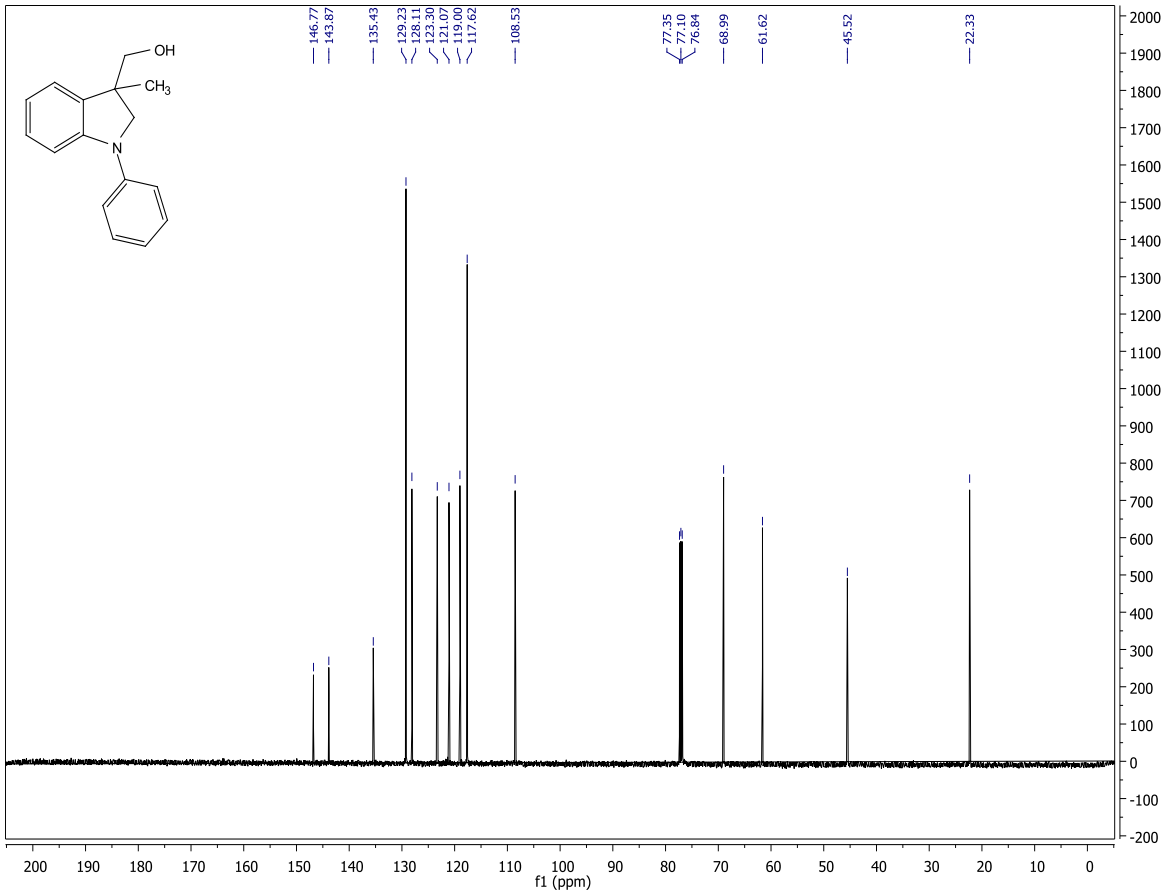

Figure 6.4. ^{13}C NMR spectrum of **2**

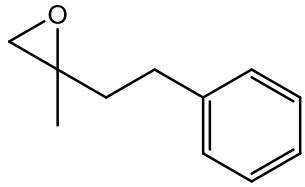

2-methyl-2-phenethyloxirane (7 or **14** in Chapter 3)

^{1}H NMR (400 MHz, $CDCl_3$) δ 7.31 – 7.25 (m, 2H), 7.19 (dddd, *J* = 6.3, 2.3, 1.0, 0.4 Hz, 3H), 2.77 – 2.65 (m, 2H), 2.58 (qd, *J* = 4.8, 0.5 Hz, 2H), 1.88 (dddd, *J* = 20.9, 13.9, 9.1, 7.9 Hz, 2H), 1.37 (s, 3H). ^{13}C NMR (101 MHz, $CDCl_3$) δ 141.63, 128.47, 128.31, 126.00, 77.43, 77.11, 76.79, 56.74, 53.97, 38.60, 31.47, 21.08.

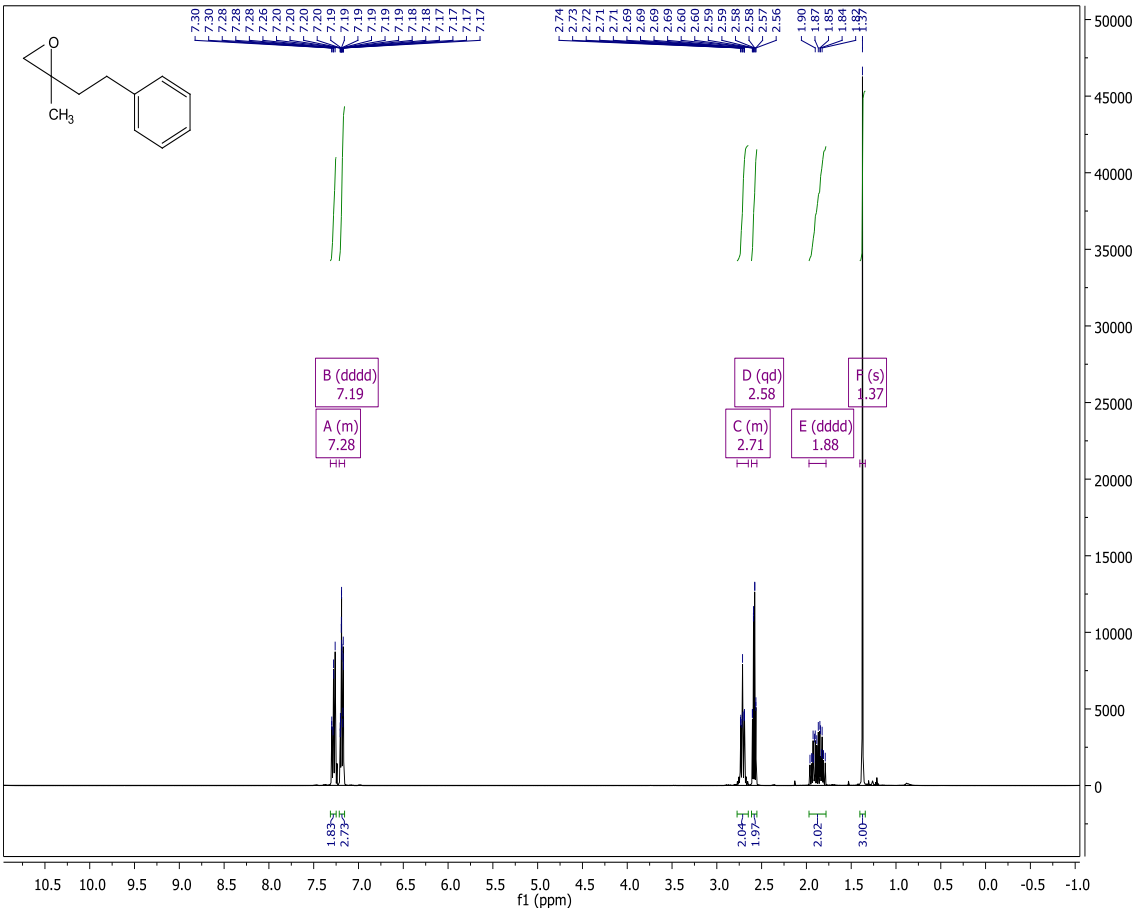

Figure 6.5. ^{1}H NMR spectrum of **7** or **14** (Chapter 3)

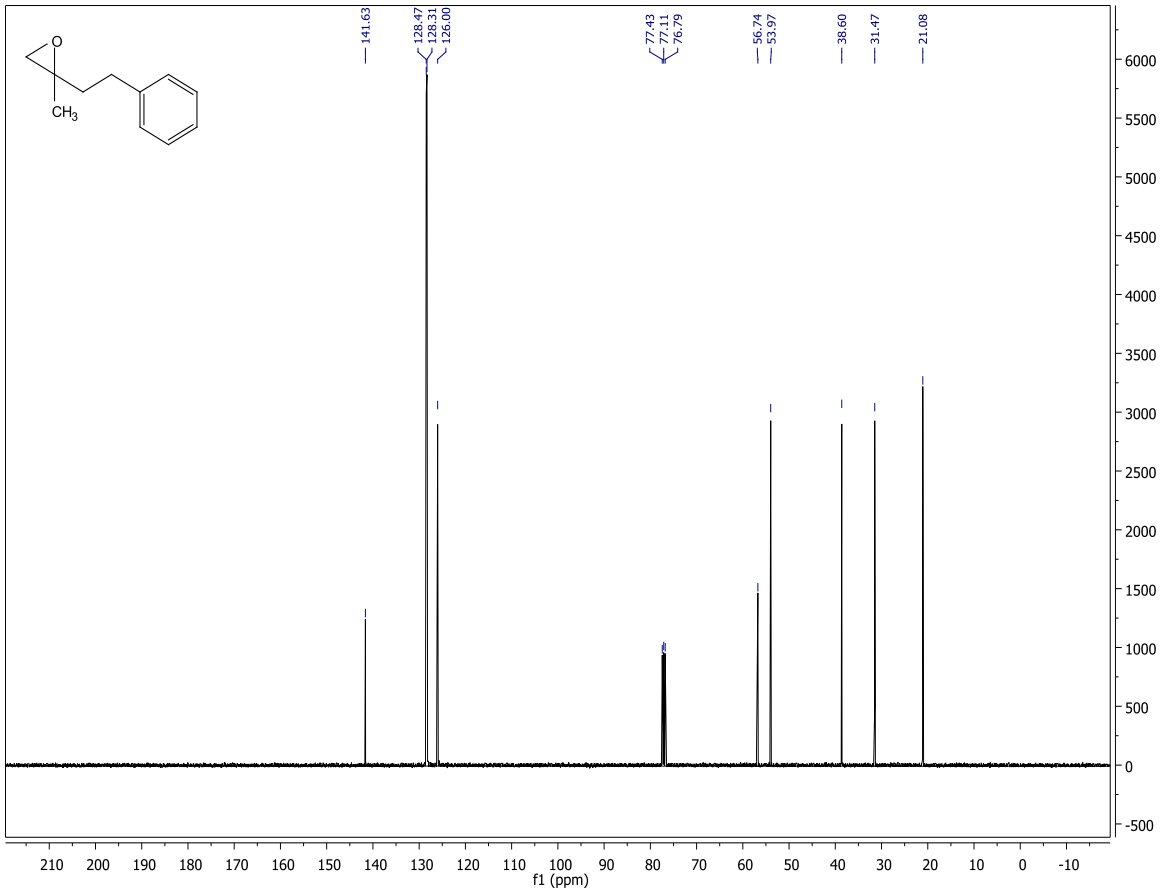

Figure 6.6. ^{13}C NMR spectrum of **7**

Figure 6.7. Set up for ReactIR 15

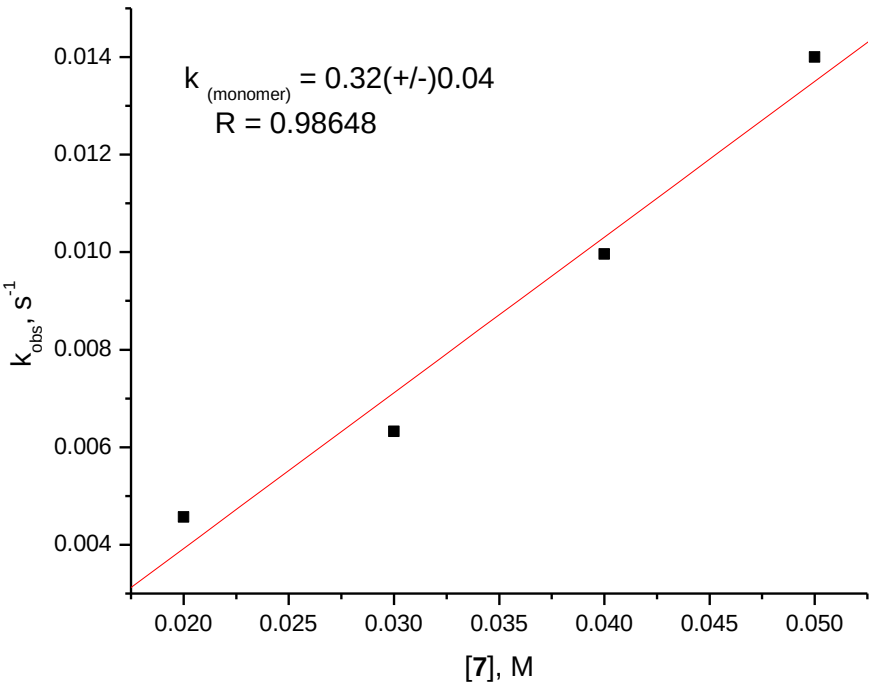

Figure 6.8. Rate constant for opening **7** by Mn-**3** in the monomer conformation

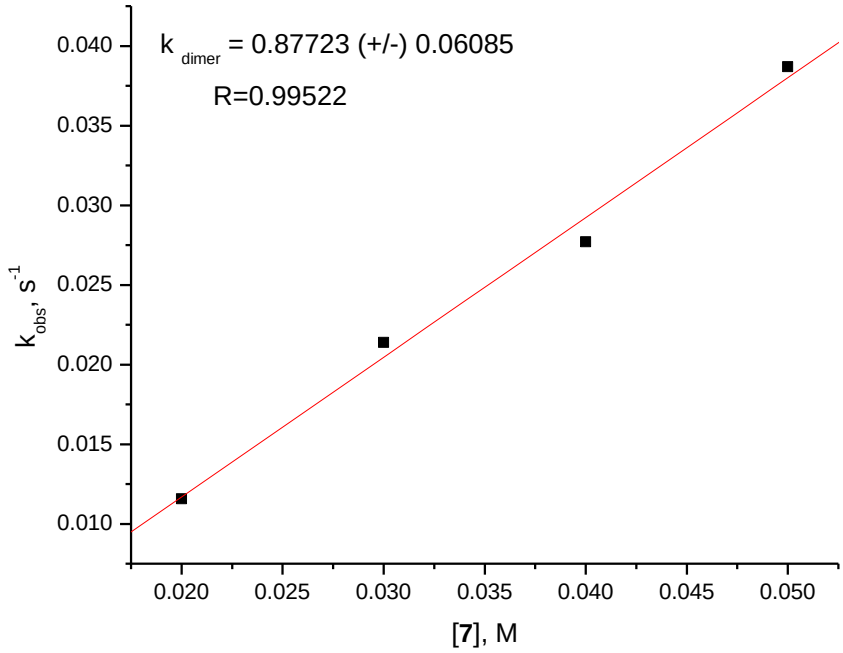

Figure 6.9. Rate constant for opening **7** by Mn-**3** in the dimer conformation

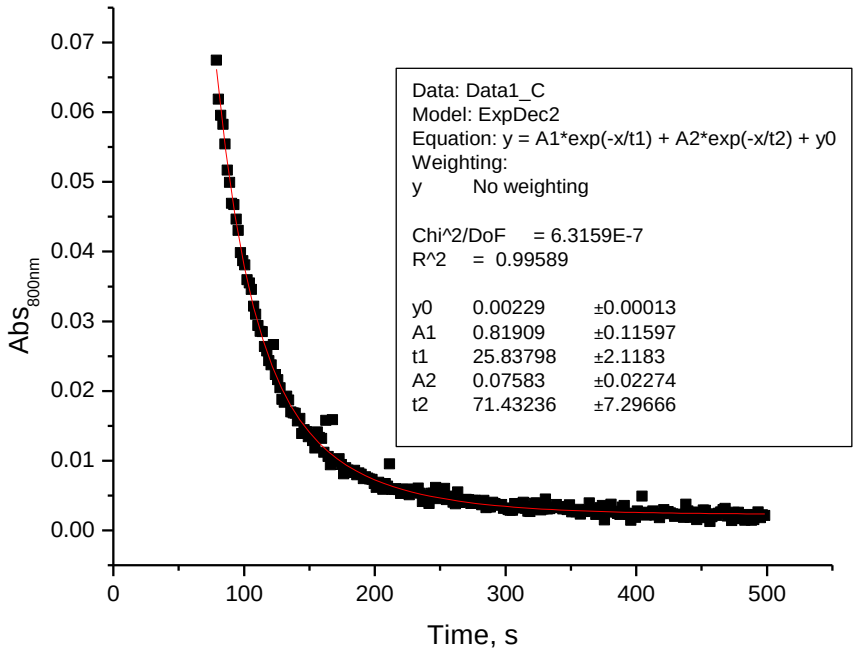

Figure 6.10. Decay of Mn-**3** at 800 nm after adding 50 mM of **7**

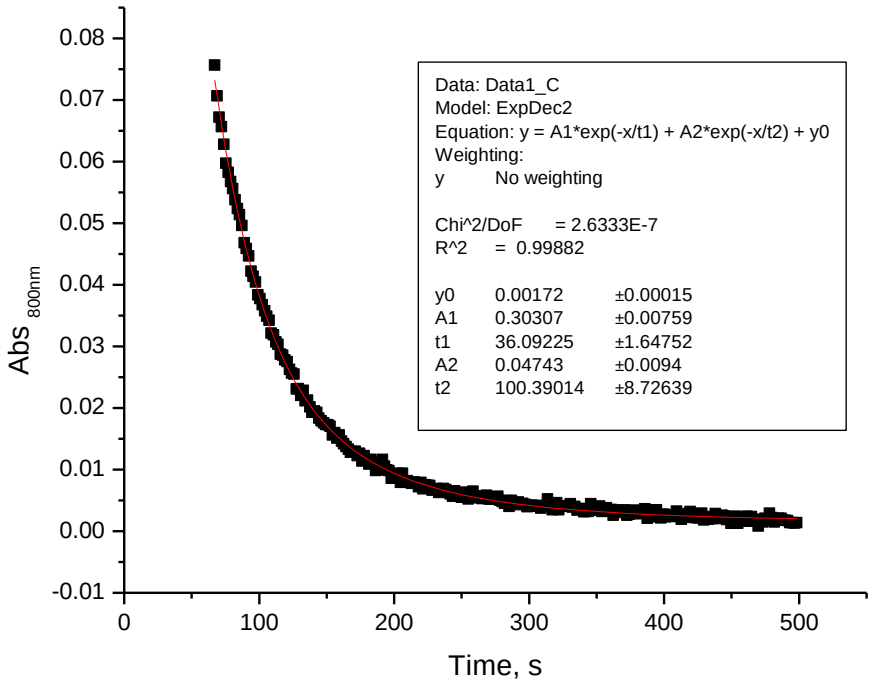

Figure 6.11. Decay of Mn-**3** at 800 nm after adding 40 mM of **7**

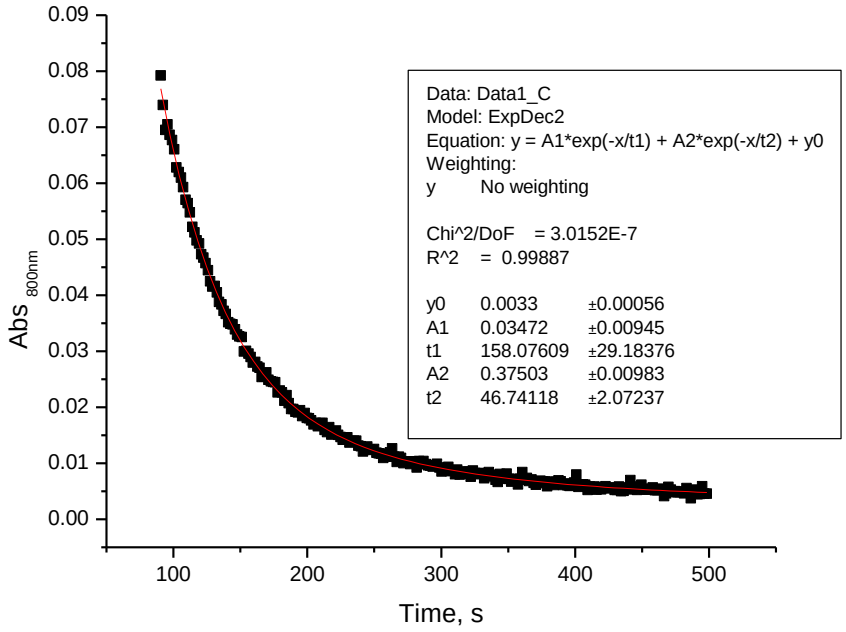

Figure 6.12. Decay of Mn-**3** at 800 nm after adding 30 mM of **7**

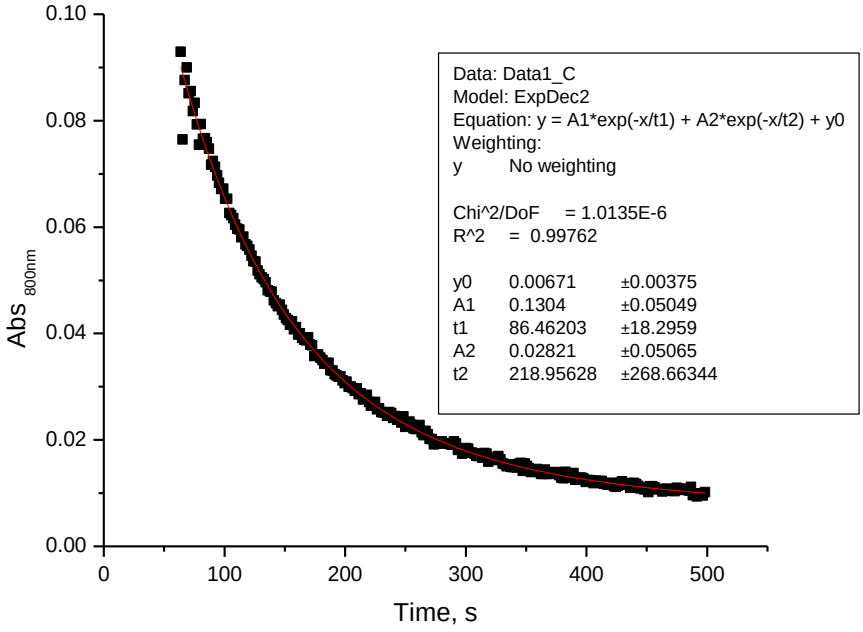

Figure 6.13. Decay of Mn-**3** at 800 nm after adding 20 mM of **7**

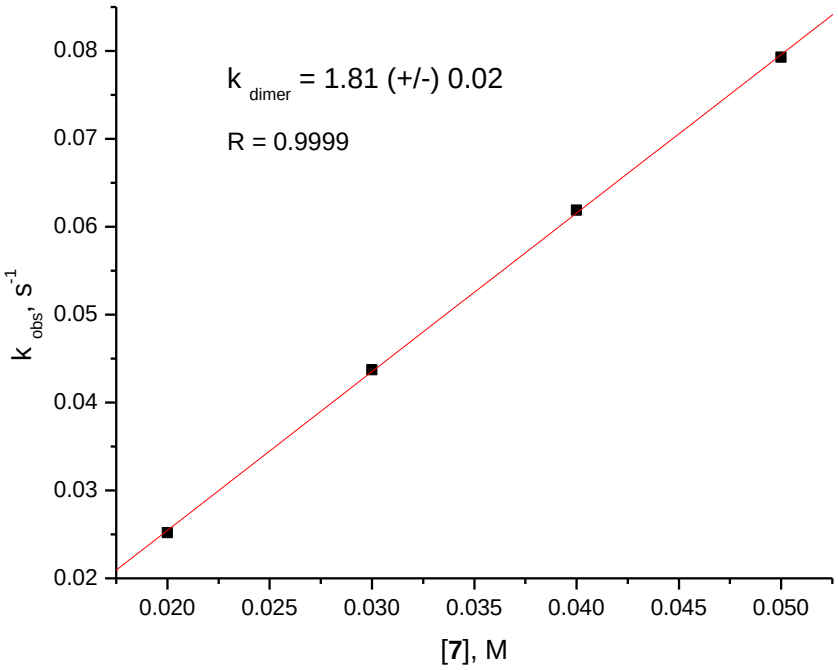

Figure 6.14. Rate constant for opening **7** by Mn-**5** in the dimer conformation

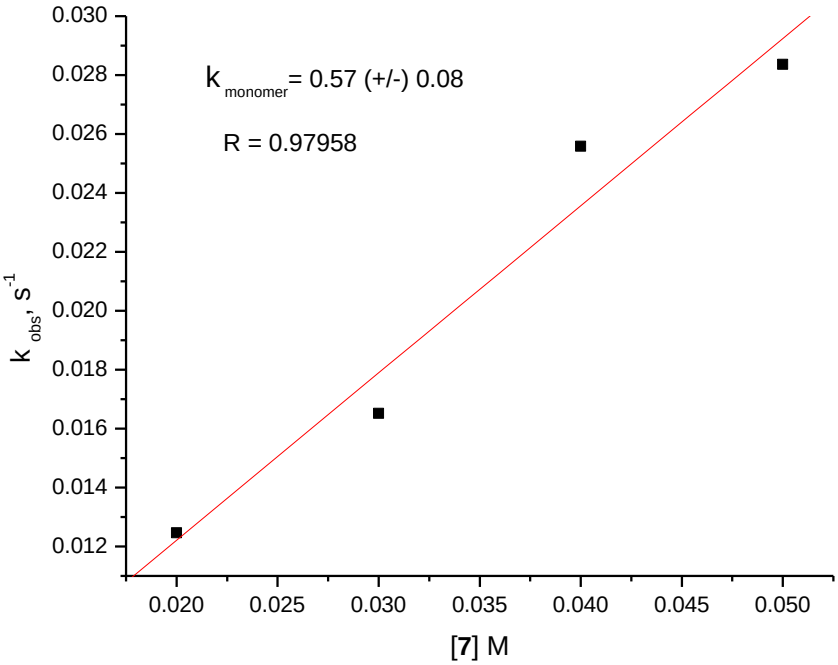

Figure 6.15. Rate constant for opening **7** by Mn-**5** in the monomer conformation

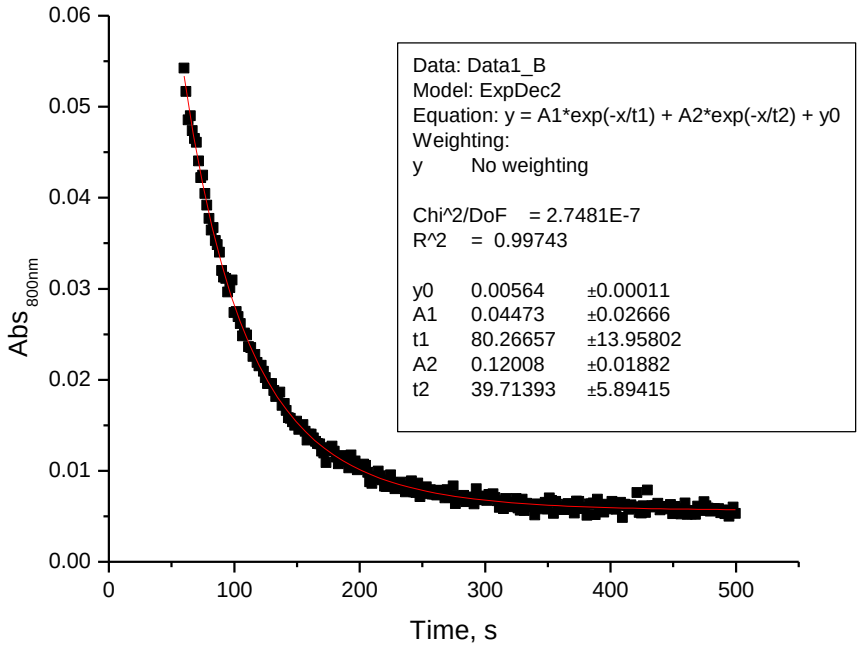

Figure 6.16. Decay of Mn-**5** at 800 nm after adding 20 mM of **7**

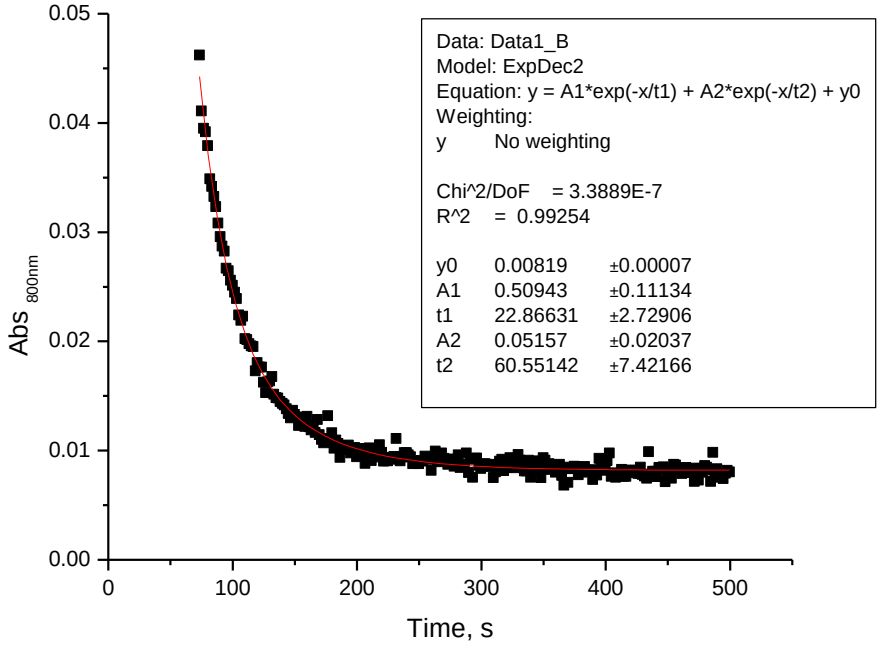

Figure 6.17. Decay of Mn-**5** at 800 nm after adding 30 mM of **7**

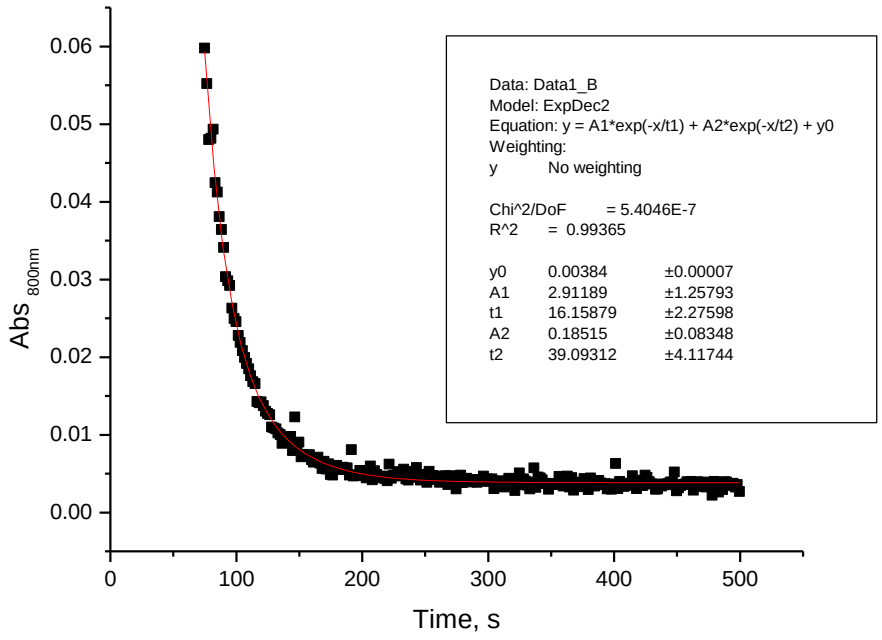

Figure 6.18. Decay of Mn-**5** at 800 nm after adding 40 mM of **7**

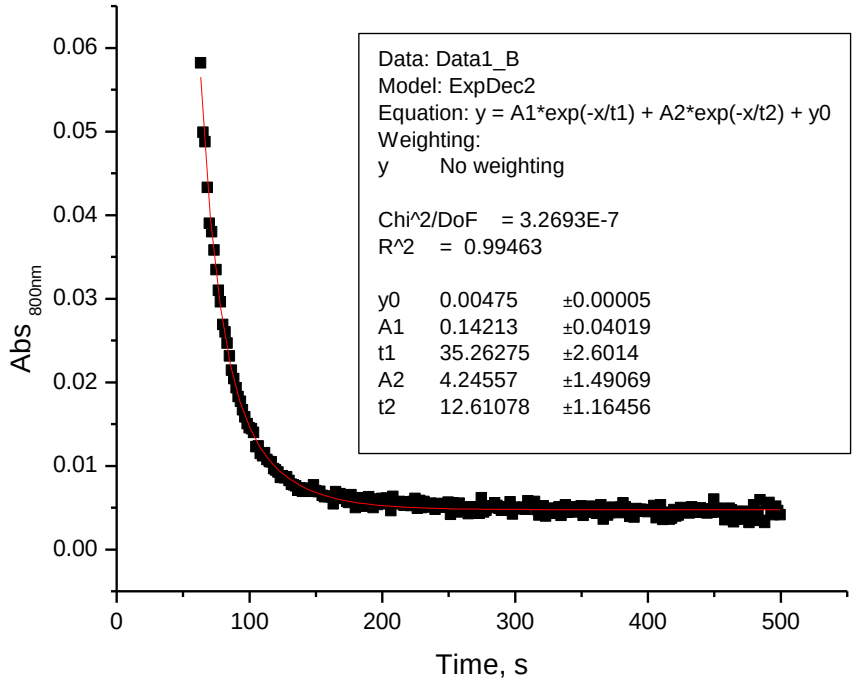

Figure 6.19. Decay of Mn-**5** at 800 nm after adding 50 mM of **7**

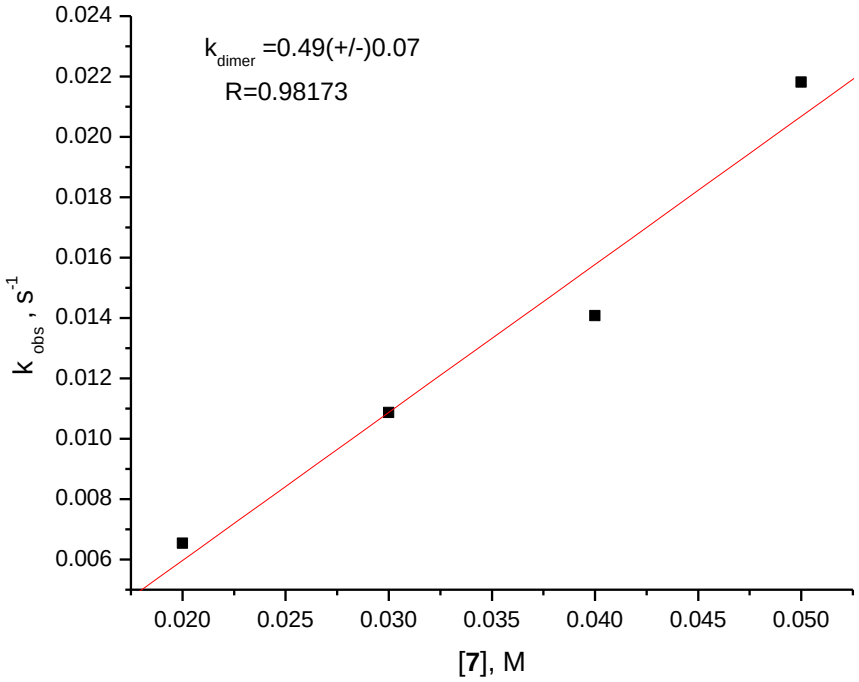

Figure 6.20. Rate constant for opening **7** by Mn-**6** in the dimer conformation

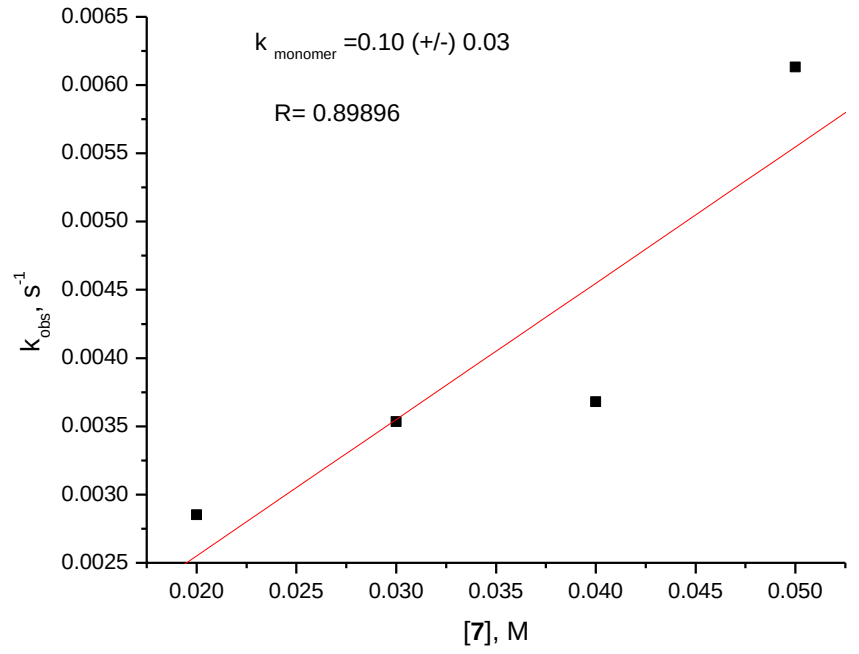

Figure 6.21. Rate constant for opening **7** by Mn-**6** in the monomer conformation

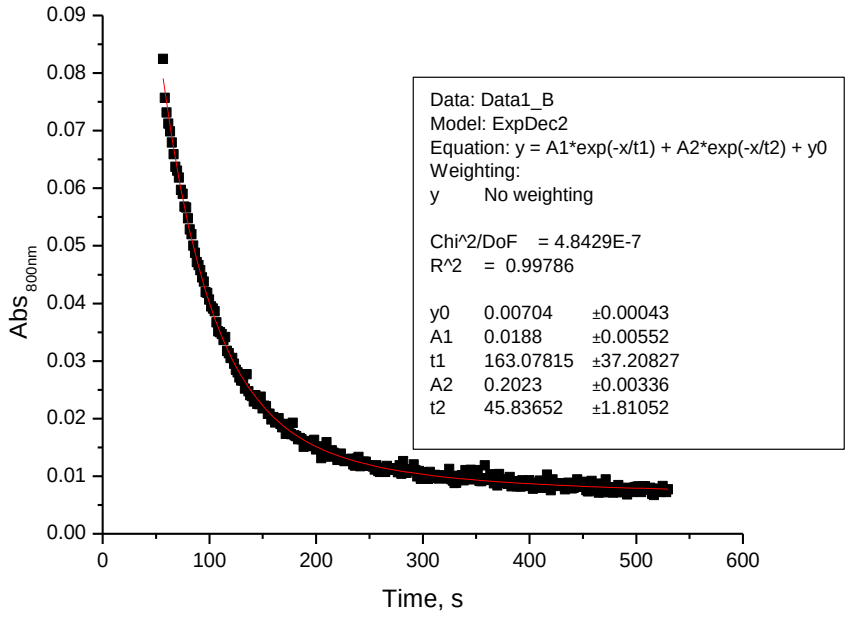

Figure 6.22. Decay of Mn-**6** at 800 nm after adding 50 mM of **7**

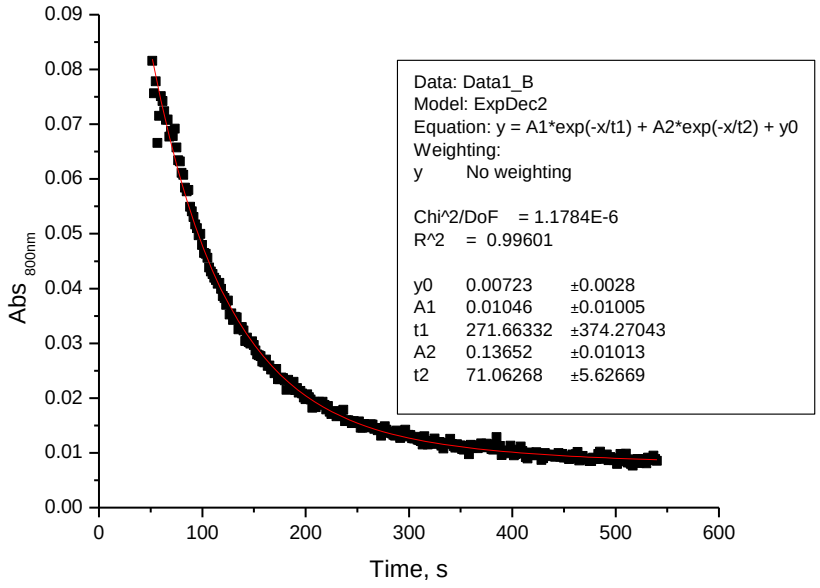

Figure 6.23. Decay of Mn-**6** at 800 nm after adding 40 mM of **7**

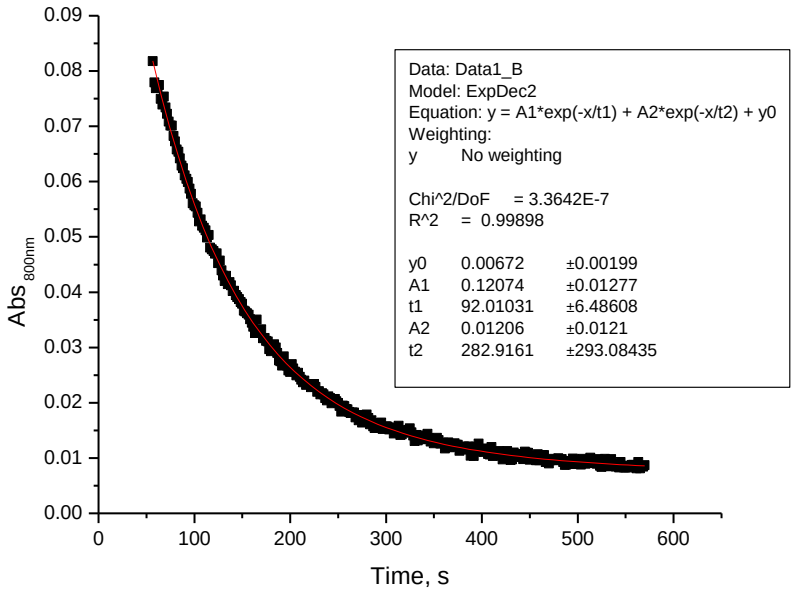

Figure 6.24. Decay of Mn-**6** at 800 nm after adding 30 mM of **7**

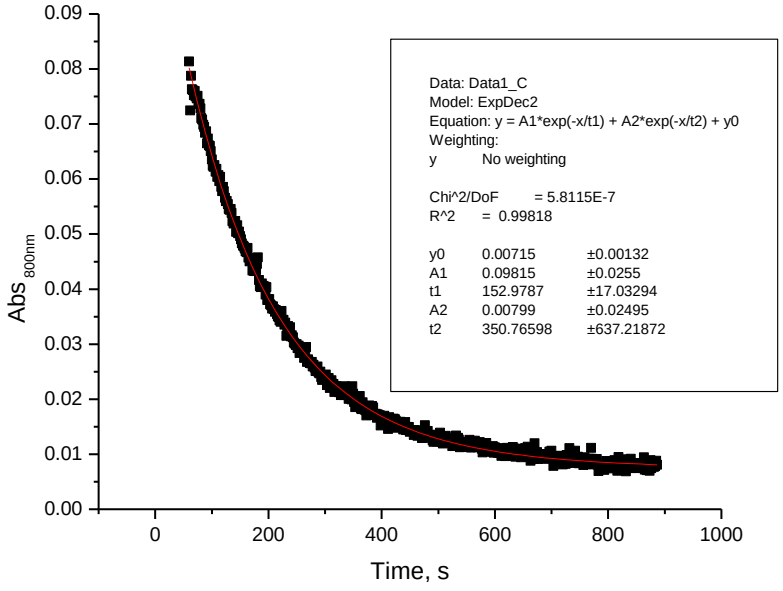

Figure 6.25. Decay of Mn-**6** at 800 nm after adding 20 mM of **7**

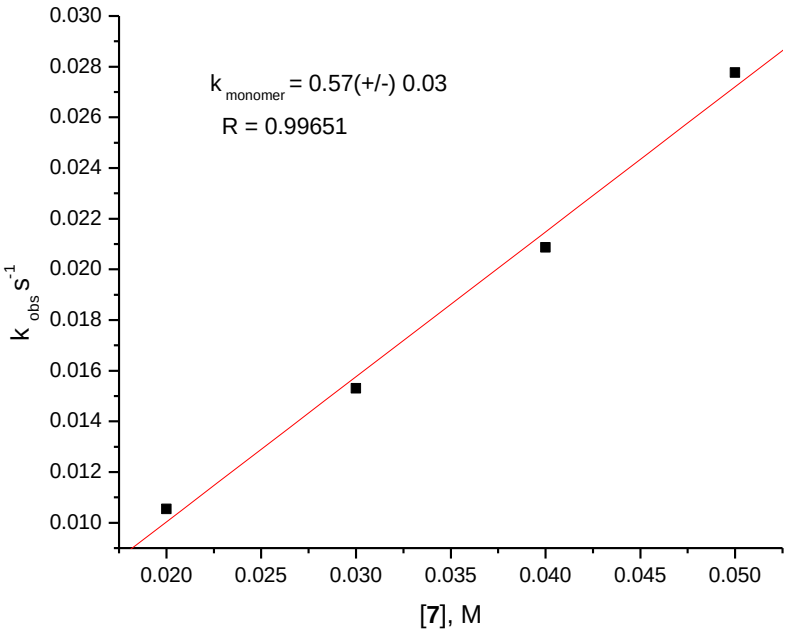

Figure 6.26. Rate constant for opening **7** by Mn-**3** in the presence of 2 eq. of Coll*HCl

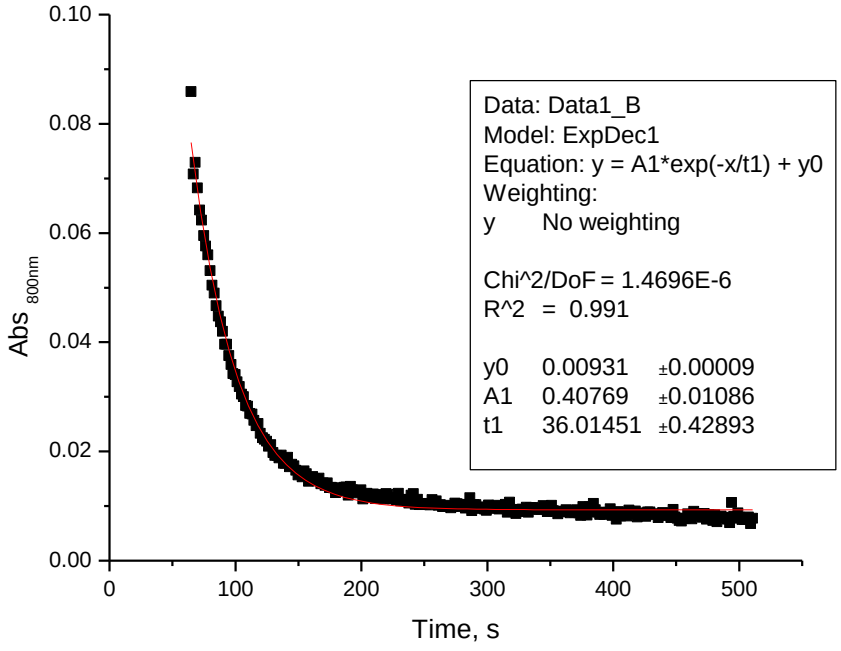

Figure 6.27. Decay of Mn-**3** at 800 nm after adding 50 mM of **7** in the presence of 2 eq. of Coll*HCl

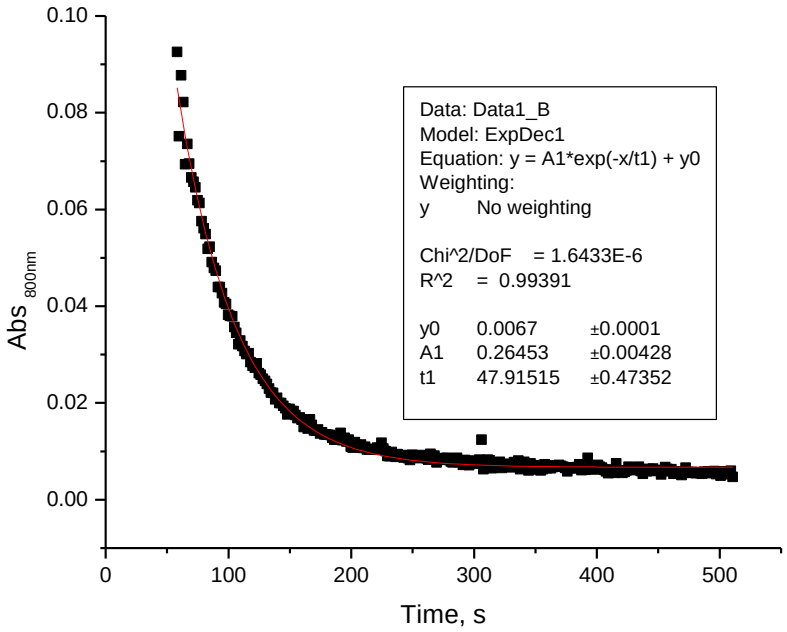

Figure 6.28. Decay of Mn-**3** at 800 nm after adding 40 mM of **7** in the presence of 2 eq. of Coll*HCl

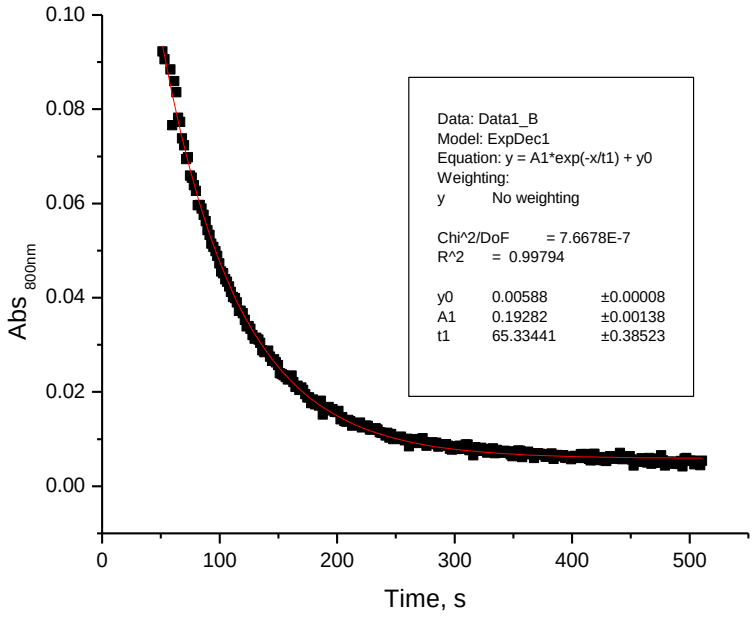

Figure 6.29. Decay of Mn-**3** at 800 nm after adding 30 mM of **7** in the presence of 2 eq. of Coll*HCl

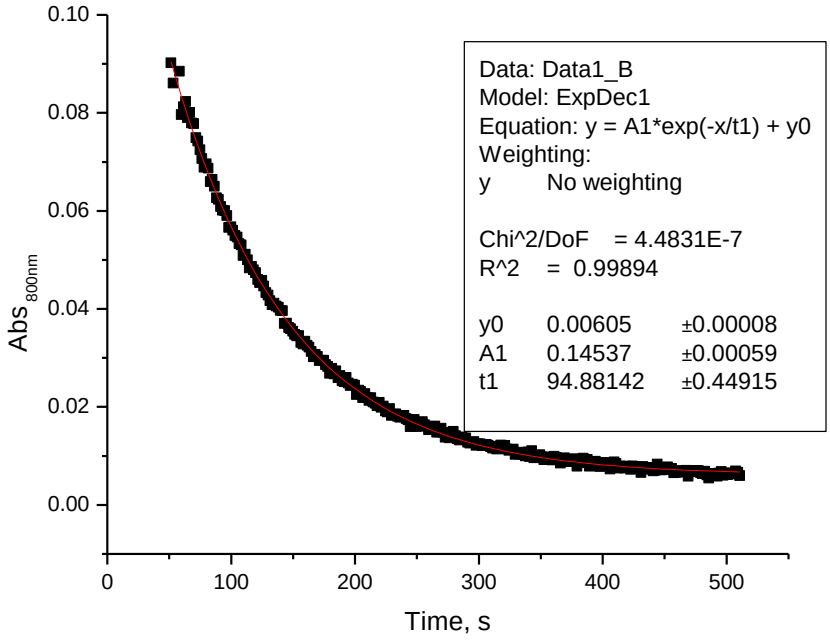

Figure 6.30. Decay of Mn-**3** at 800 nm after adding 20 mM of **7** in the presence of 2 eq. of Coll*HCl

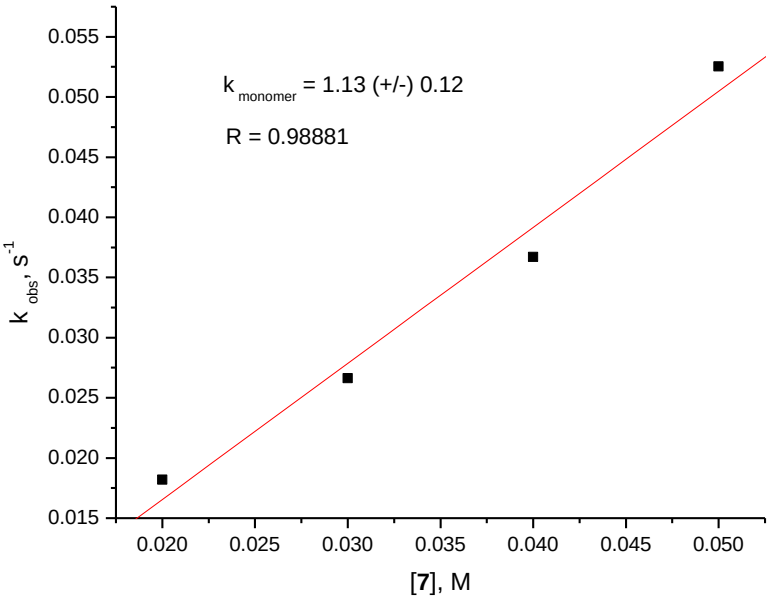

Figure 6.31. Rate constant for opening **7** by Mn-**5** in the presence of 2 eq. of Coll*HCl

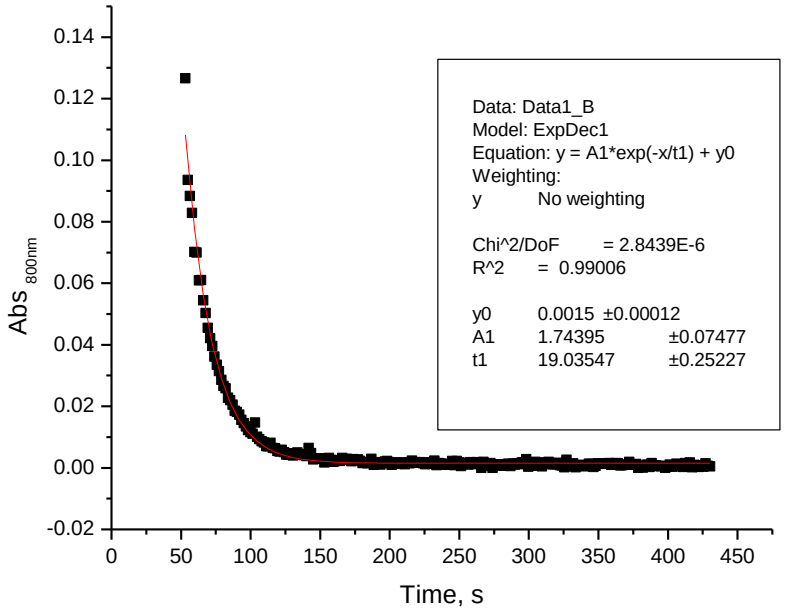

Figure 6.32. Decay of Mn-**5** at 800 nm after adding 50 mM of **7** in the presence of 2 eq. of Coll*HCl

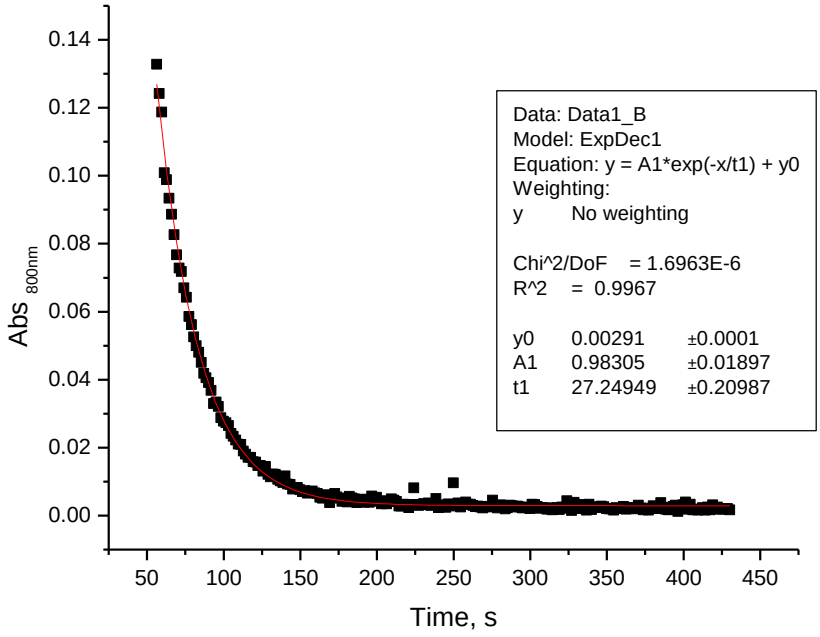

Figure 6.33. Decay of Mn-**5** at 800 nm after adding 40 mM of **7** in the presence of 2 eq. of Coll*HCl

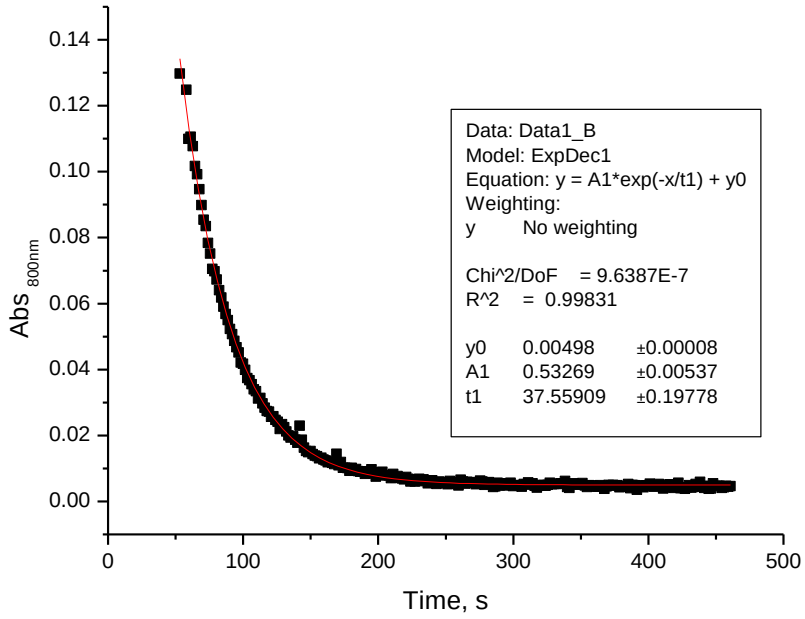

Figure 6.34. Decay of Mn-**5** at 800 nm after adding 30 mM of **7** in the presence of 2 eq. of Coll*HCl

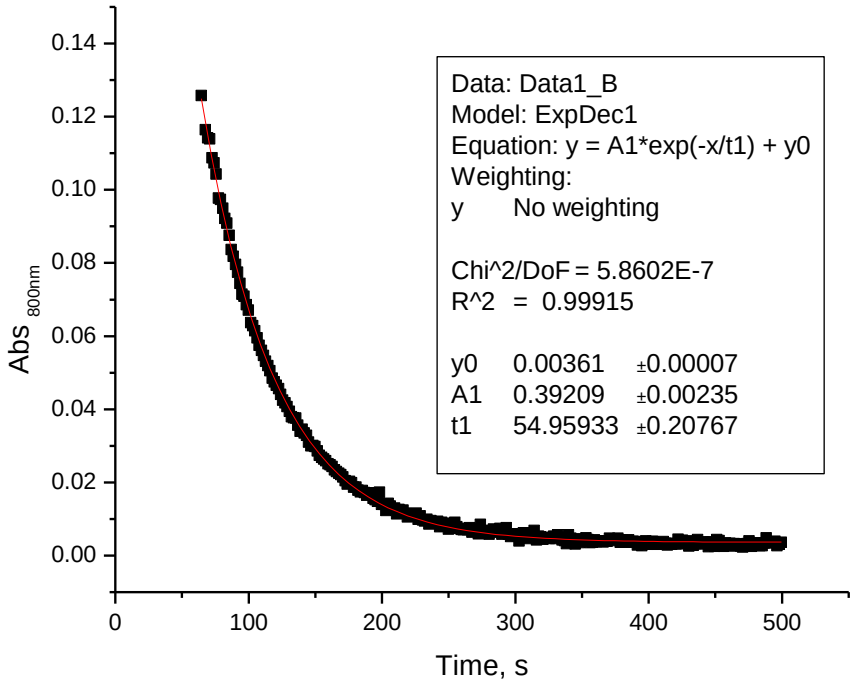

Figure 6.35. Decay of Mn-**5** at 800 nm after adding 20 mM of **7** in the presence of 2 eq. of Coll*HCl

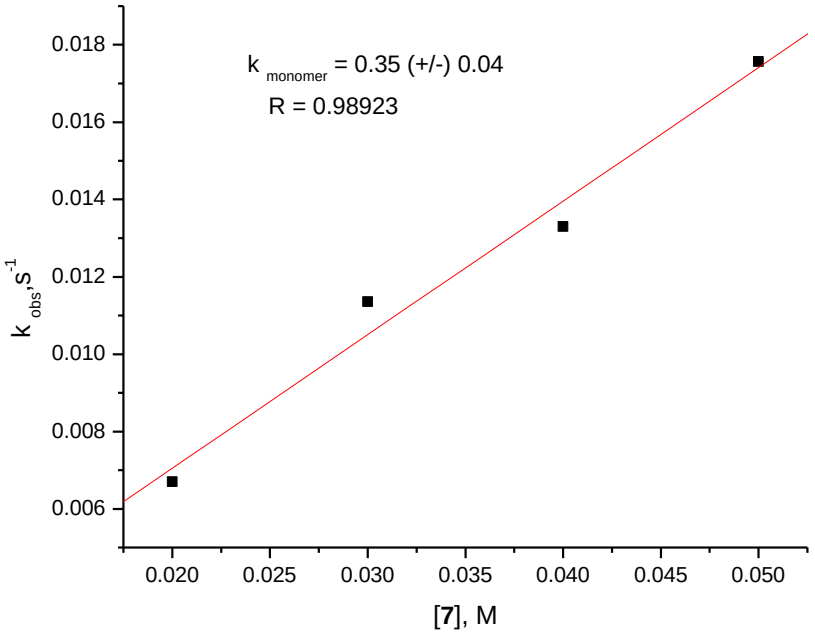

Figure 6.36. Rate constant for opening **7** by Mn-**6** in the presence of 2 eq. of Coll*HCl

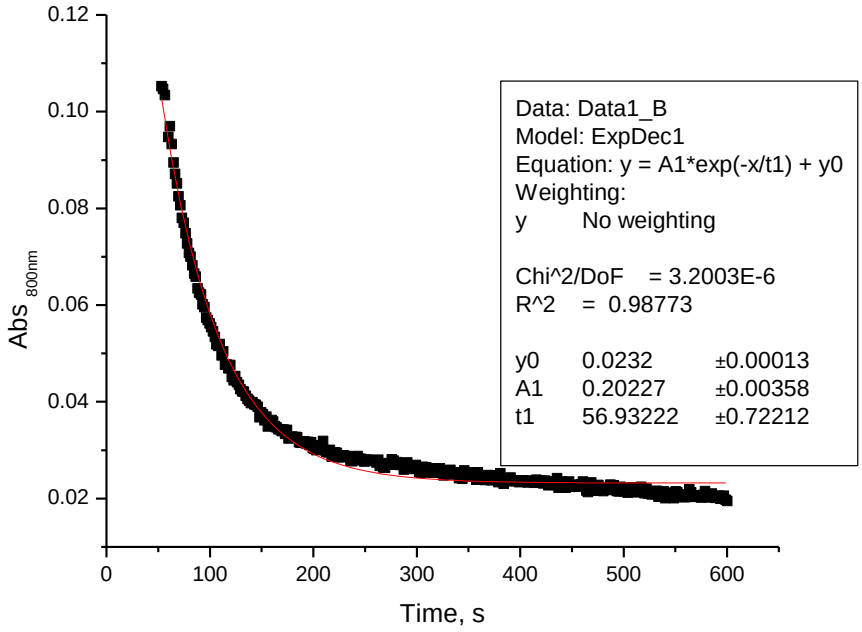

Figure 6.37. Decay of Mn-**6** at 800 nm after adding 50 mM of **7** in the presence of 2 eq. of Coll*HCl

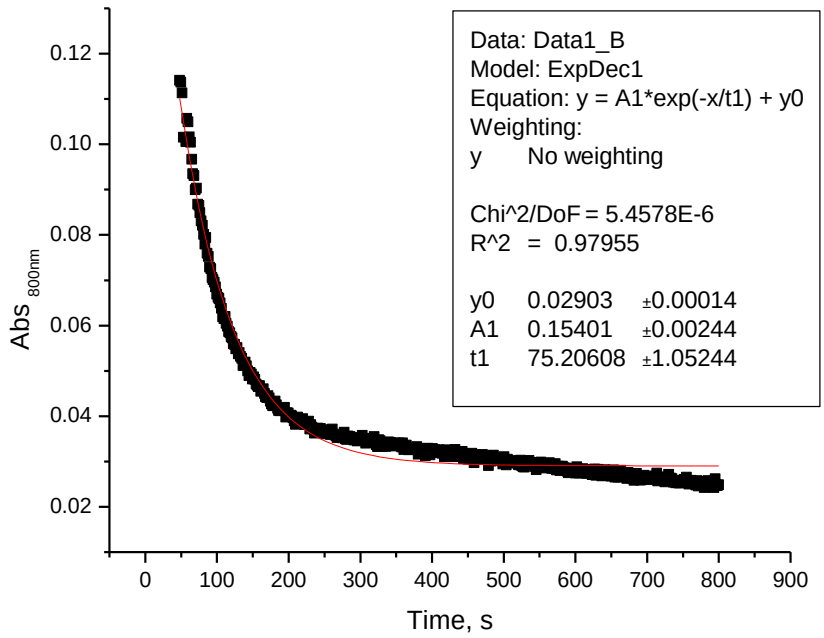

Figure 6.38. Decay of Mn-**6** at 800 nm after adding 40 mM of **7** in the presence of 2 eq. of Coll*HCl

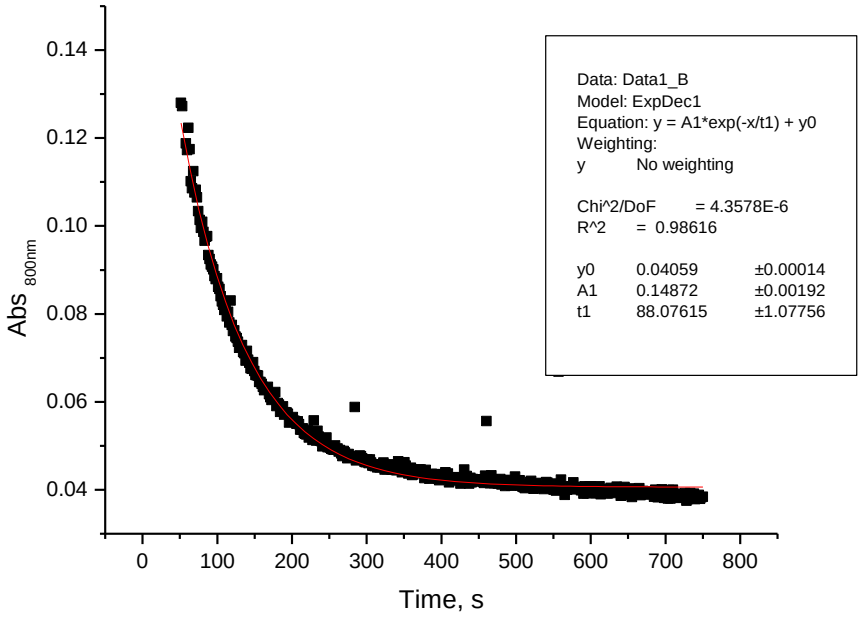

Figure 6.39. Decay of Mn-**6** at 800 nm after adding 30 mM of **7** in the presence of 2 eq. of Coll*HCl

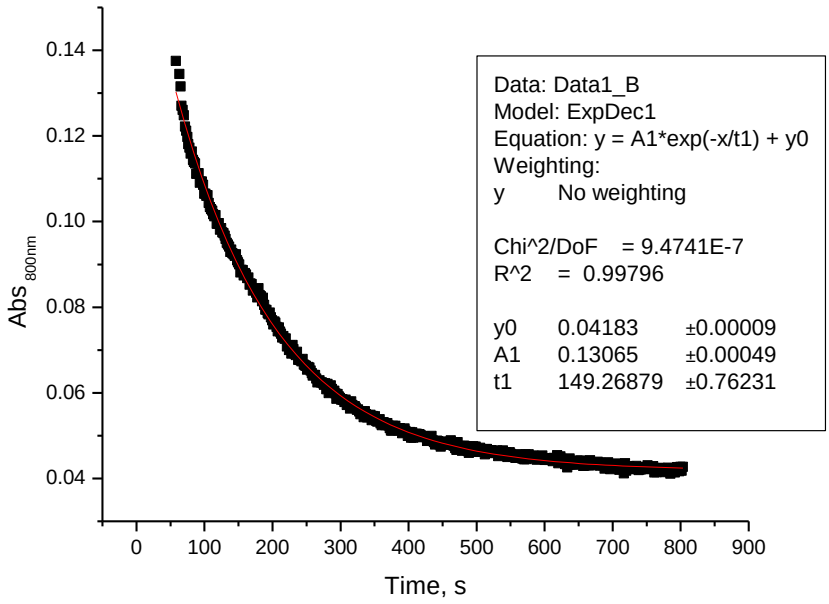

Figure 6.40. Decay of Mn-**6** at 800 nm after adding 20 mM of **7** in the presence of 2 eq. of Coll*HCl

It is important to note that all the traces obtained for the decay of Mn-**3**, Mn-**6** and Mn-**5** in the presence of 2equiv. of Coll*HCl, approximately fit well to both single and double exponential fits (R^2 is approximately 0.99 for all fits). However, as shown in figures 6.41, 6.43, and 6.45, there is little or no correlation observed when the k_{obs1} obtained when double exponential fits are plotted against the epoxide (**7**). As a result, it was hypothesized that the addition of salt disrupts the monomer-dimer complex of the catalyst and shifts it more to the monomer-salt conformation. However, the possibility of the presence of catalyst in the dimer conformation cannot be ruled out, but based on computational work, it is known that the monomer-salt complex is stable under the reaction conditions and serves as the resting state for active catalyst. Also, some of the absorbance at 800nm for the epoxide opening experiment did not go to zero. This was so because not all the reactions were fully completed after about 500 seconds. We only need

a minimum of three half-lives (75% complete) for the decay of catalyst to accurately calculate k_{obs}.

Table 6.1. k_{obs} obtained from the double exponential fits for the decay of Mn-**3** in the presence of 2 equiv. of Coll*HCl

[7], M	**k_{obs1}, s^{-1}**	**k_{obs2}, s^{-1}**
0.02	0.005625318	0.011839884
0.03	0.005146161	0.017142852
0.04	0.006095111	0.02509307
0.05	0.011070134	0.040699743

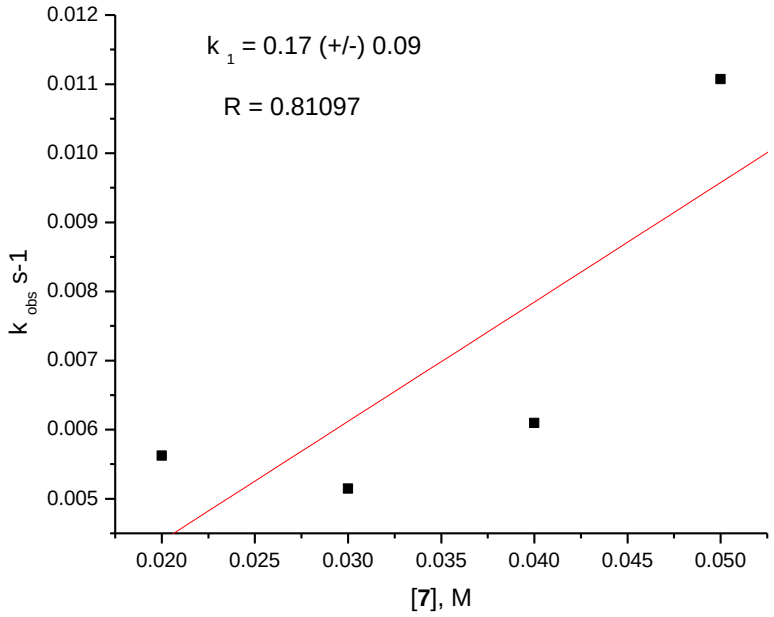

Figure 6.41. Plot of k_{obs1} vs. [**7**]

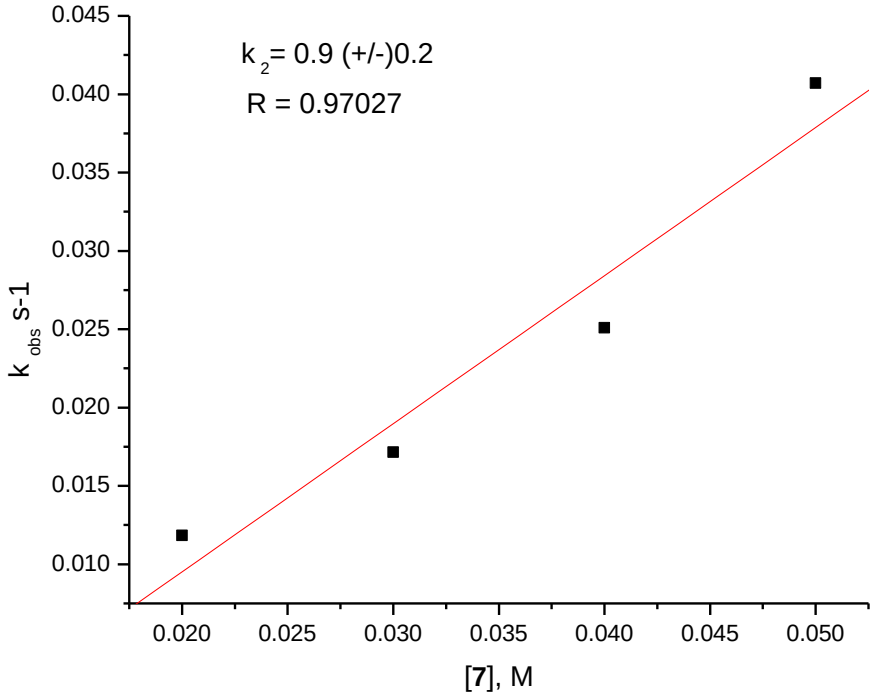

Figure 6.42. Plot of k_{obs2} vs. [**7**]

Table 6.2. *k_{obs}* obtained from the double exponential fits for the decay of Mn-**6** in the presence of 2 equiv. of Coll*HCl

[7], M	**k_{obs1}, s^{-1}**	**k_{obs2}, s^{-1}**
0.02	0.005179137	0.00708332
0.03	0.002278396	0.014722701
0.04	0.00014111	0.018573707
0.05	0.001618081	0.023925483

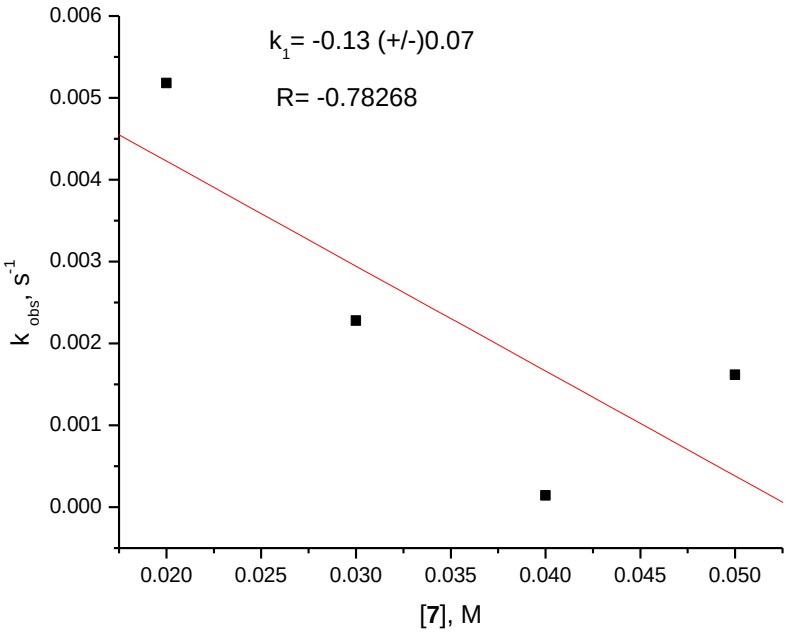

Figure 6.43. Plot of k_{obs1} vs. [**7**]

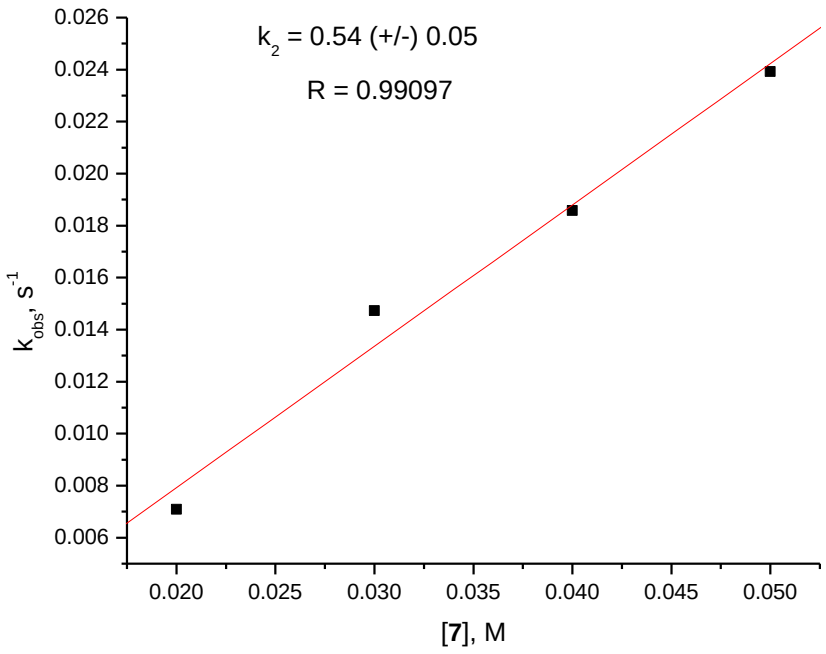

Figure 6.44. Plot of k_{obs2} vs. [**7**]

Table 6.3. k_{obs} obtained from the double exponential fits for the decay of Mn-**5** in the presence of 2 equiv. of Coll*HCl

[7], M	k_{obs1}, s^{-1}	k_{obs2}, s^{-1}
0.02	0.011787410	0.021557634
0.03	0.006842562	0.028007525
0.04	0.036697921	0.036697935
0.05	0.065355206	0.065355206

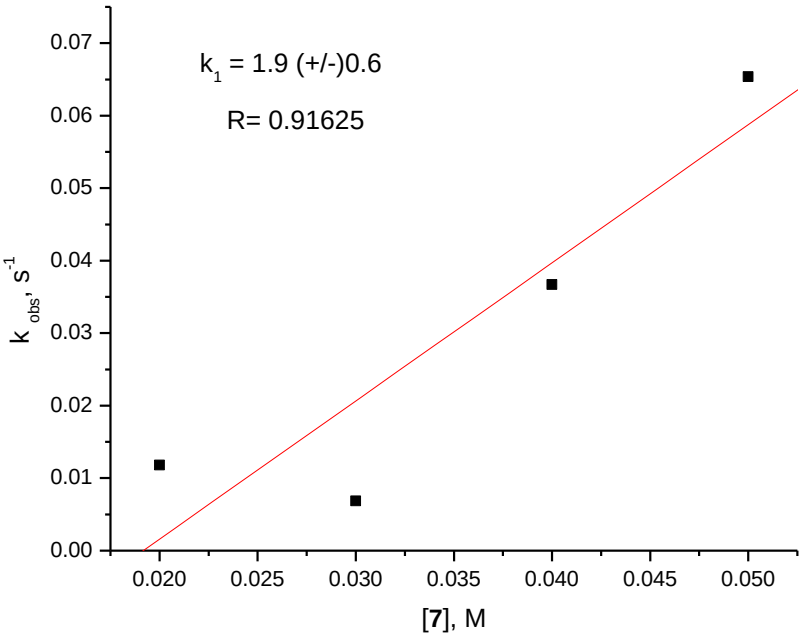

Figure 6.45. Plot of k_{obs1} vs. [**7**]

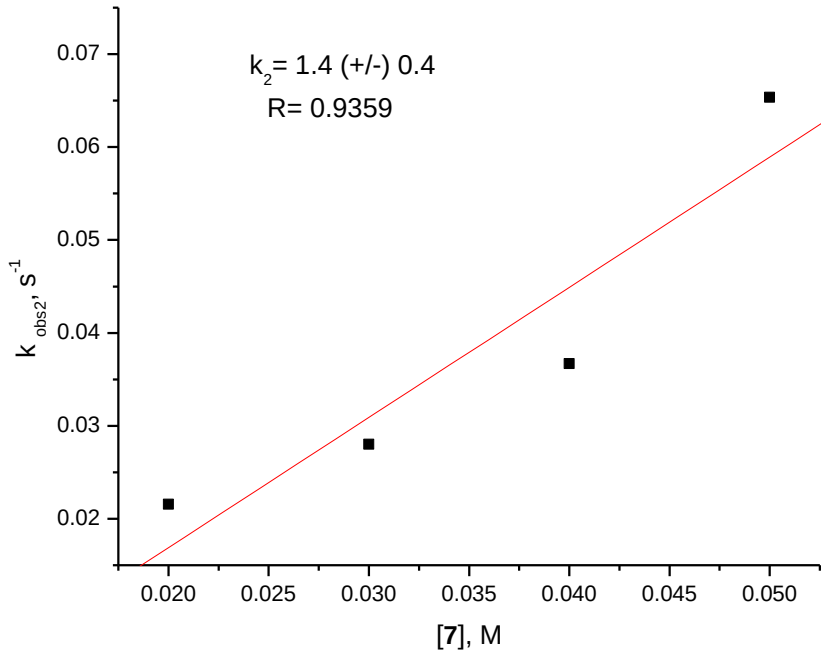

Figure 6.46. Plot of k_{obs2} vs. [**7**]

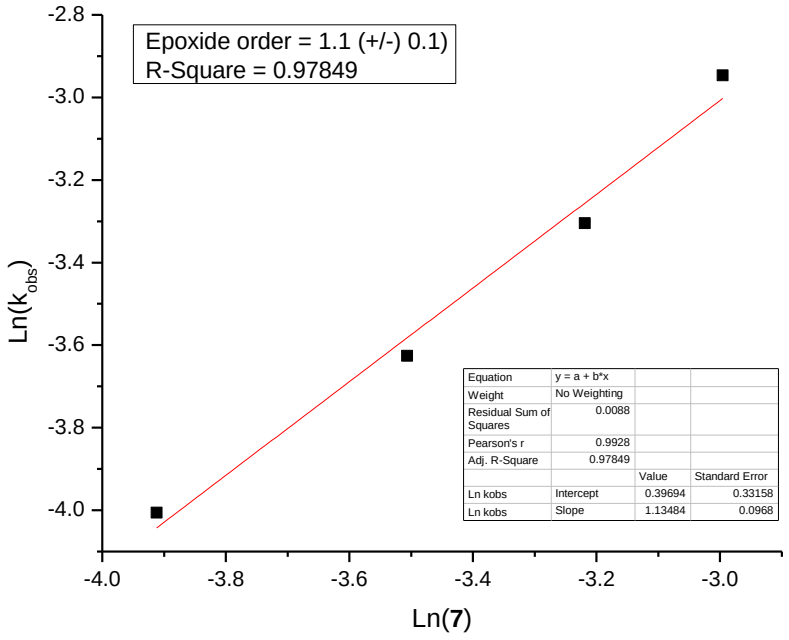

Figure 6.47. Epoxide (**7**) order with Mn-**5** as catalyst

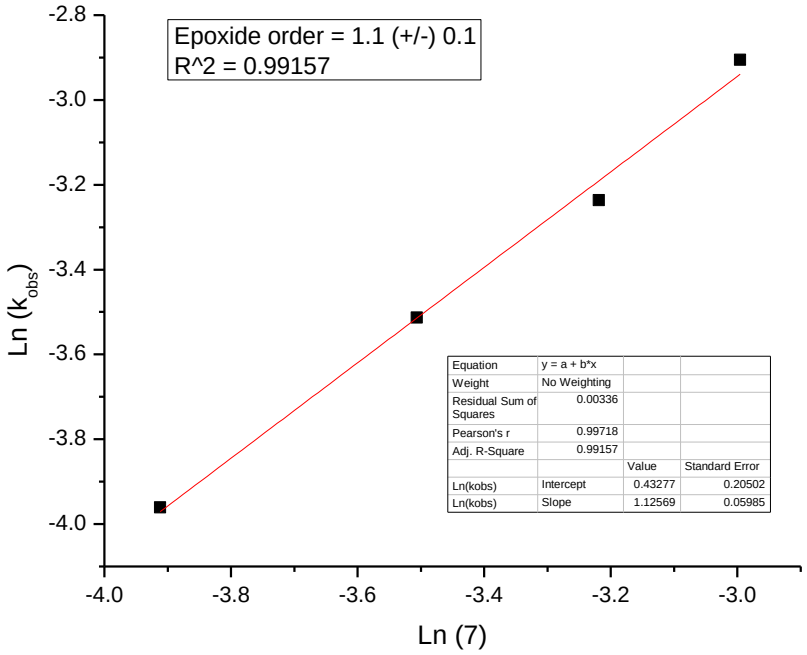

Figure 6.48. Epoxide (**7**) order with Mn-**5** as catalyst (repeat)

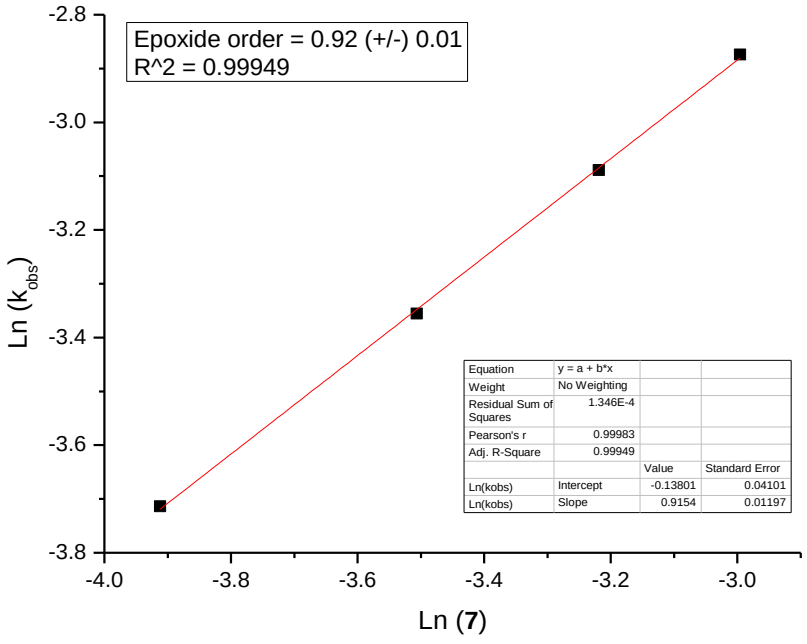

Figure 6.49. Epoxide (**7**) order with Mn-**5** as catalyst (repeat 2)

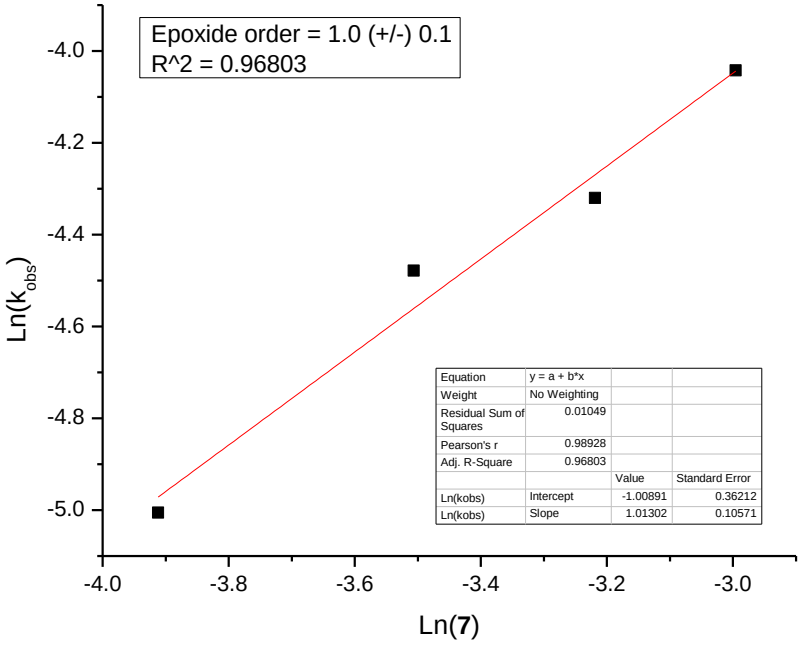

Figure 6.50. Epoxide (**7**) order with Mn-**6** as catalyst

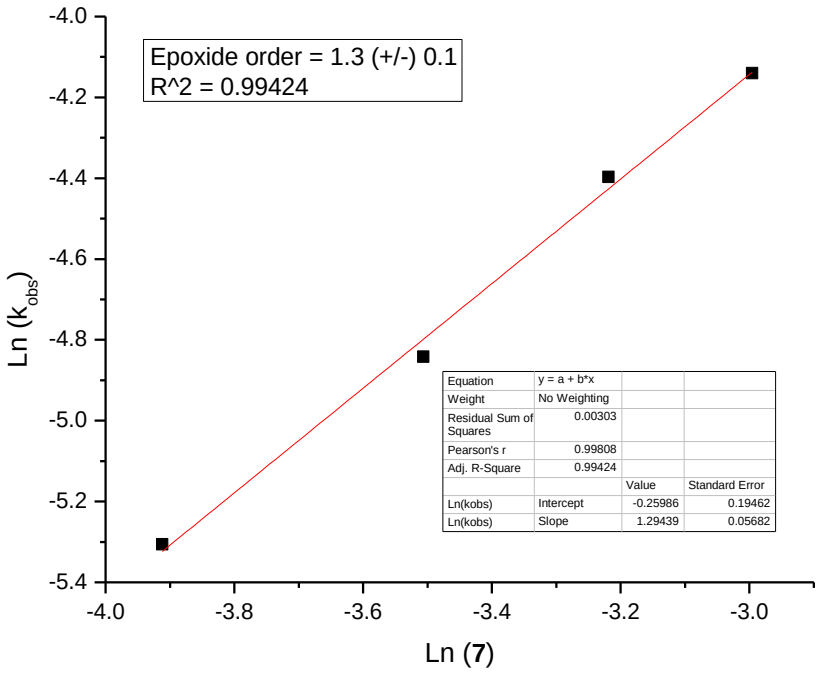

Figure 6.51. Epoxide (**7**) order with Mn-**6** as catalyst (repeat)

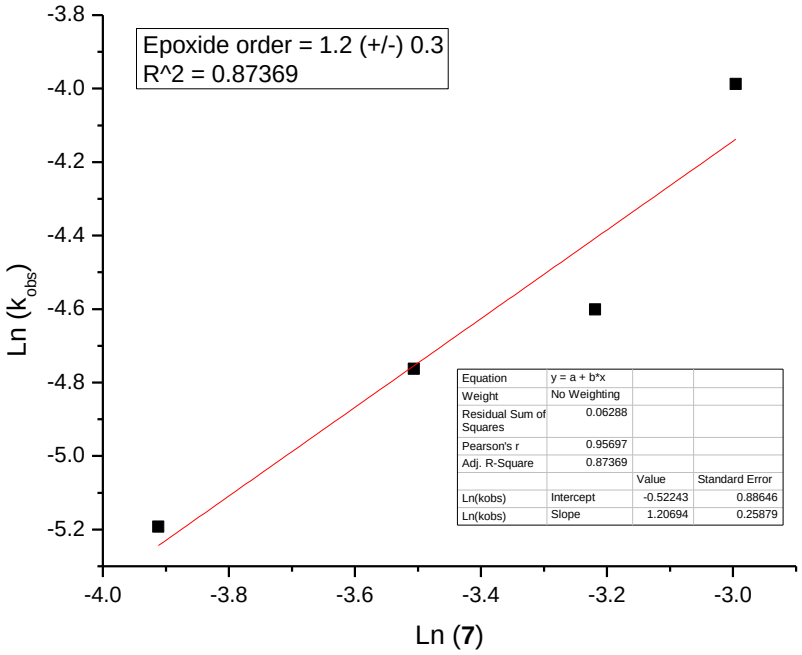

Figure 6.52. Epoxide (**7**) order with Mn-**6** as catalyst (repeat 2)

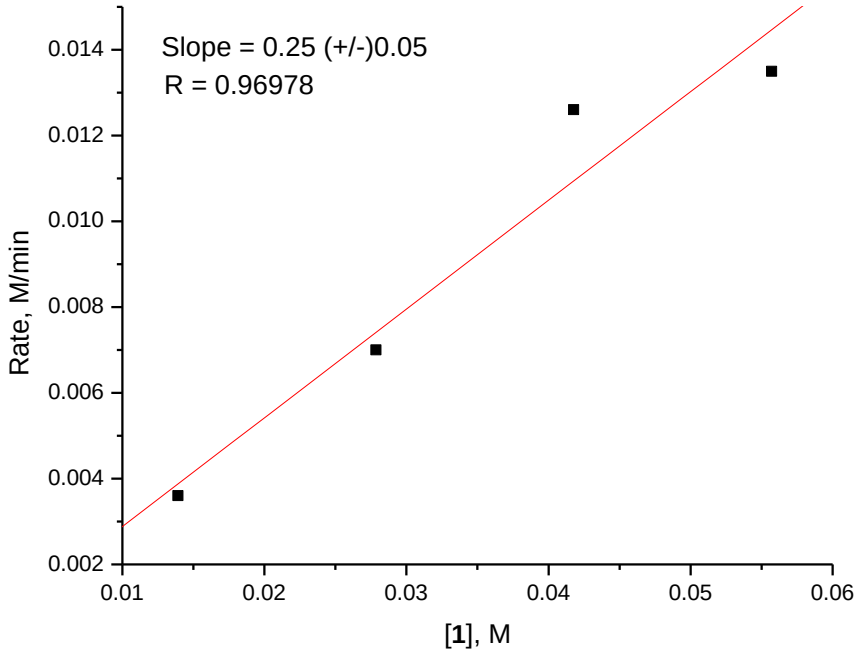

Figure 6.53. Plot of initial rate vs. **1**

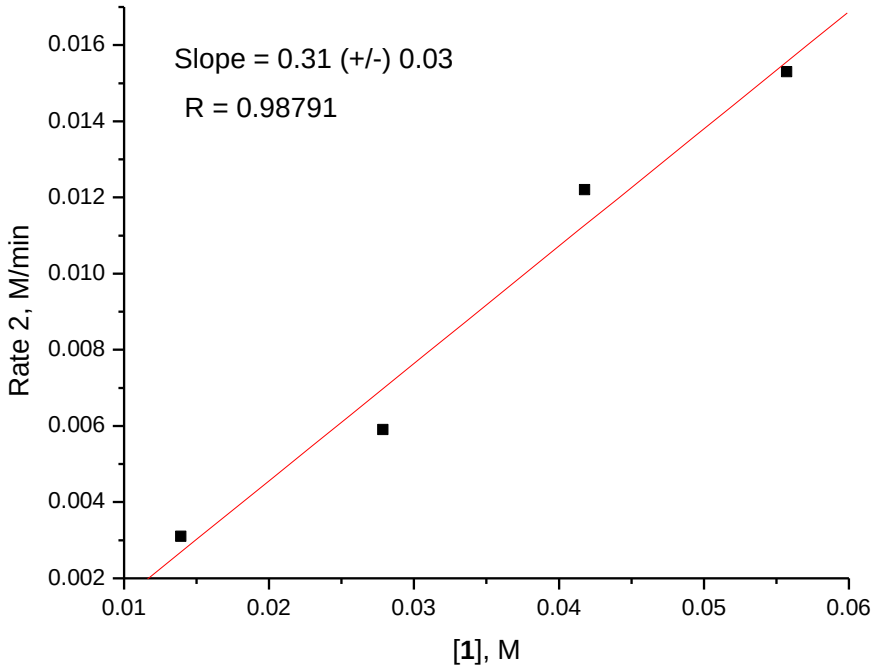

Figure 6.54. Plot of initial rate vs. **1**

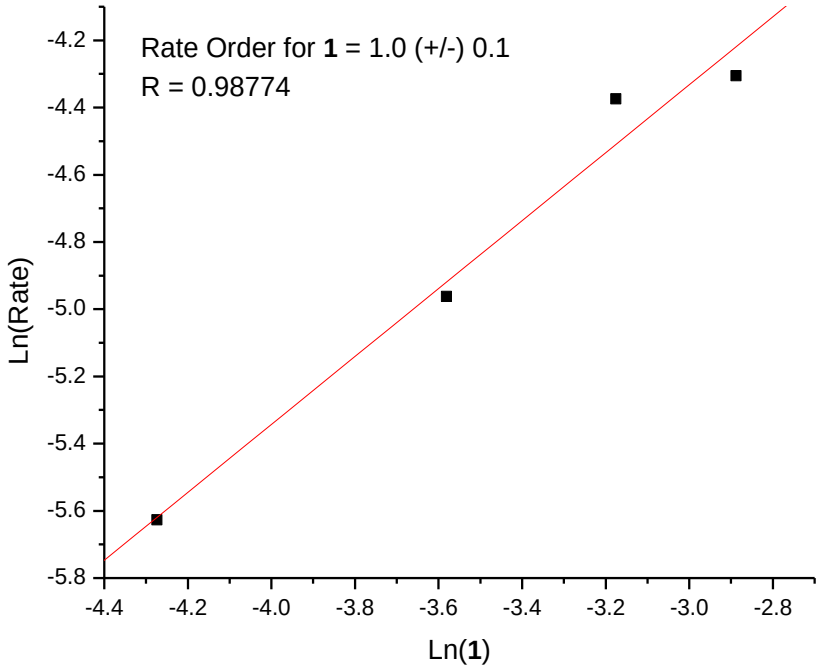

Figure 6.55. Plot of Ln (initial rate) vs. Ln (**1**)

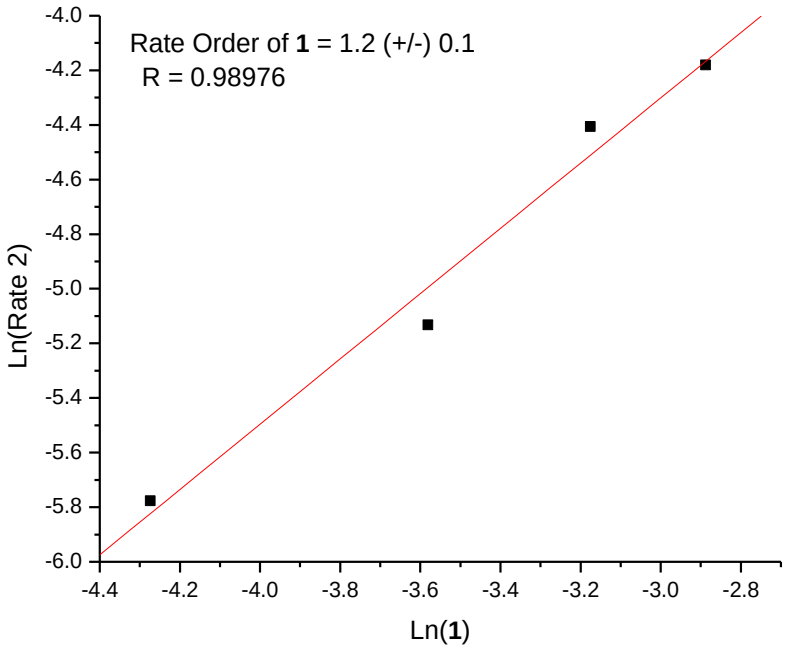

Figure 6.56. Plot of Ln (initial rate) vs. Ln (**1**)

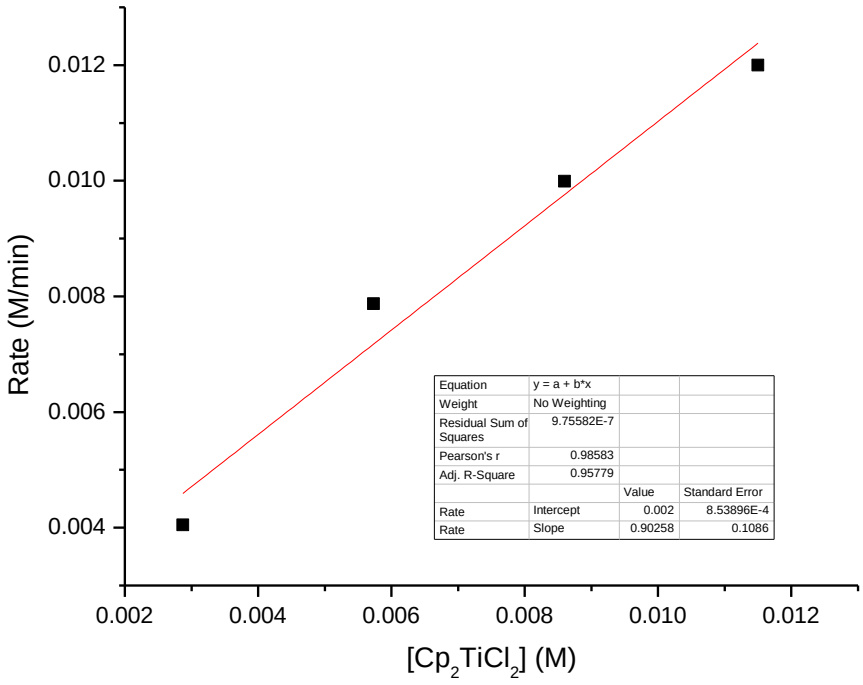

Figure 6.57. Plot of initial rate vs. [Cp_2TiCl_2]

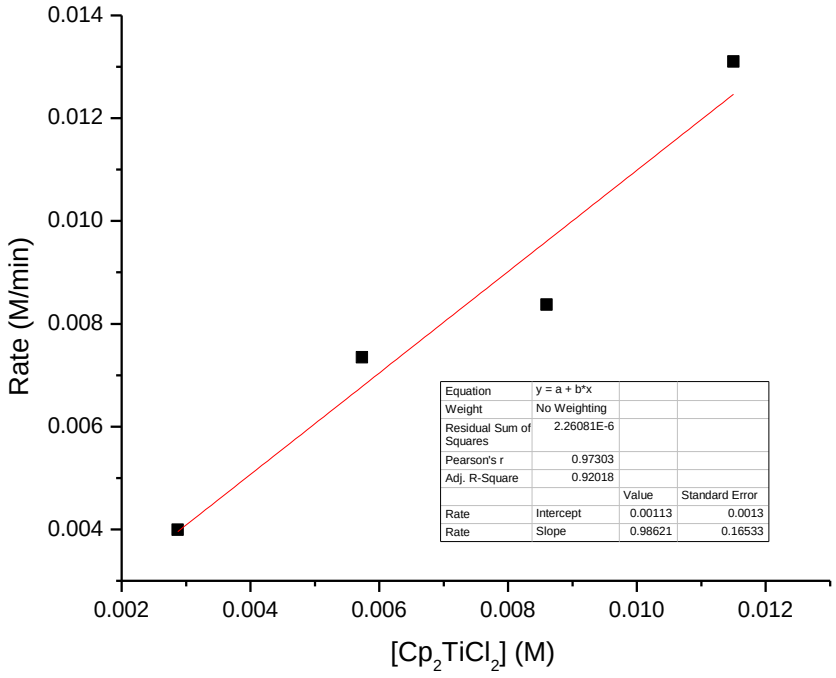

Figure 6.58. Plot of initial rate vs. [Cp_2TiCl_2] repeat

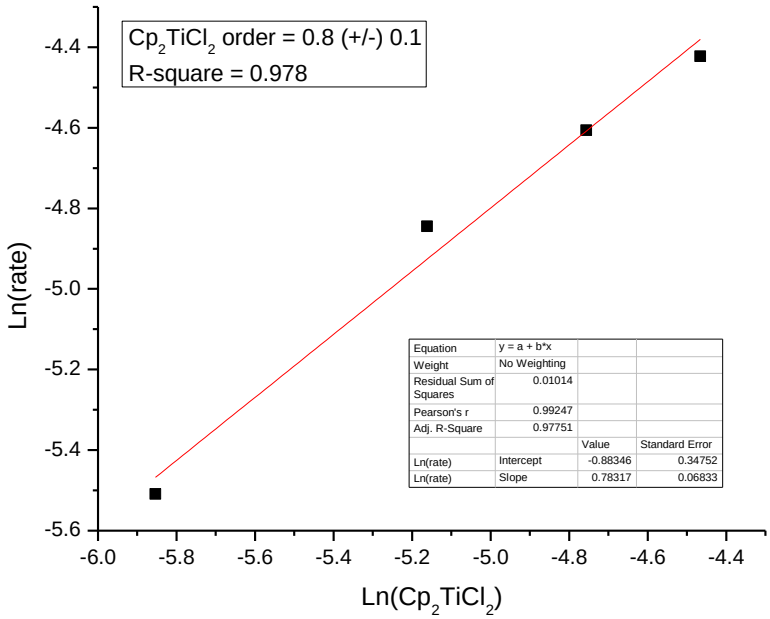

Figure 6.59. Plot of Ln (initial rate) vs. Ln [Cp_2TiCl_2]

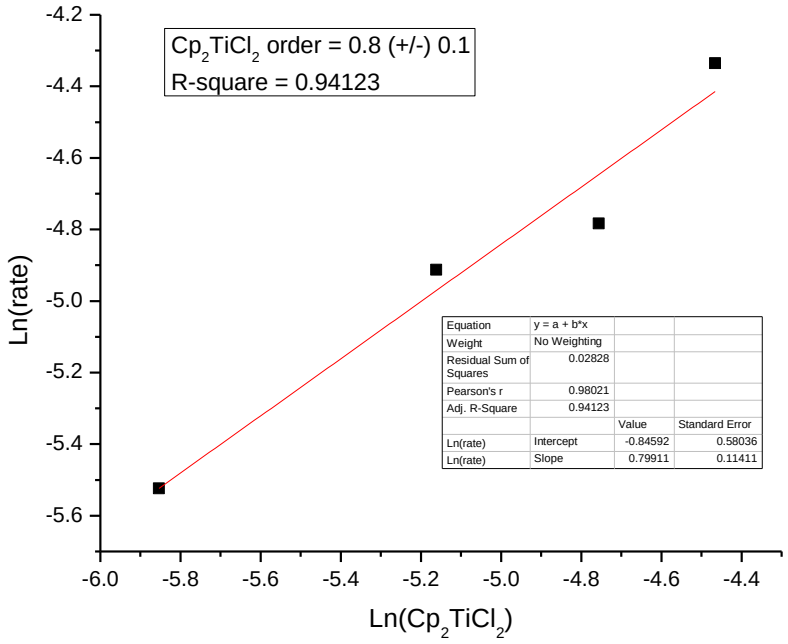

Figure 6.60. Plot of Ln (initial rate) vs. Ln [Cp_2TiCl_2]

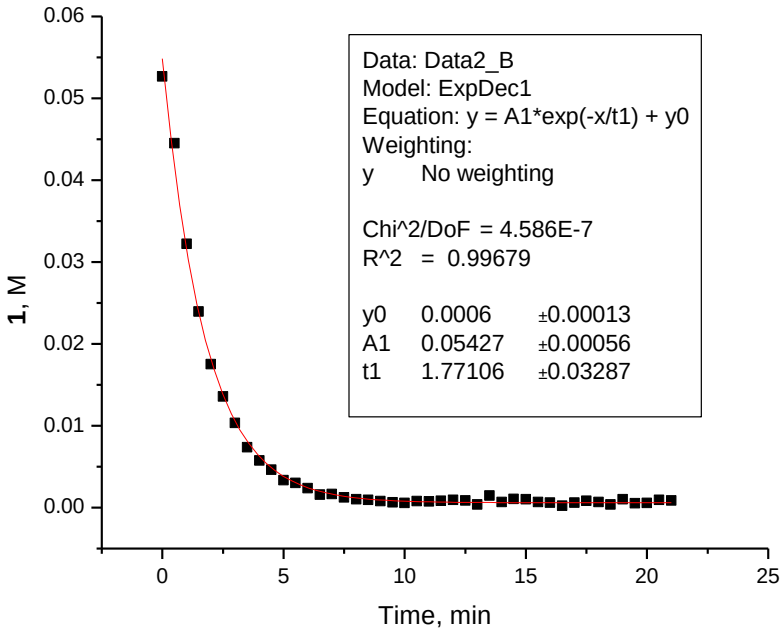

Figure 6.61. Decay of **1** by Mn-**3**

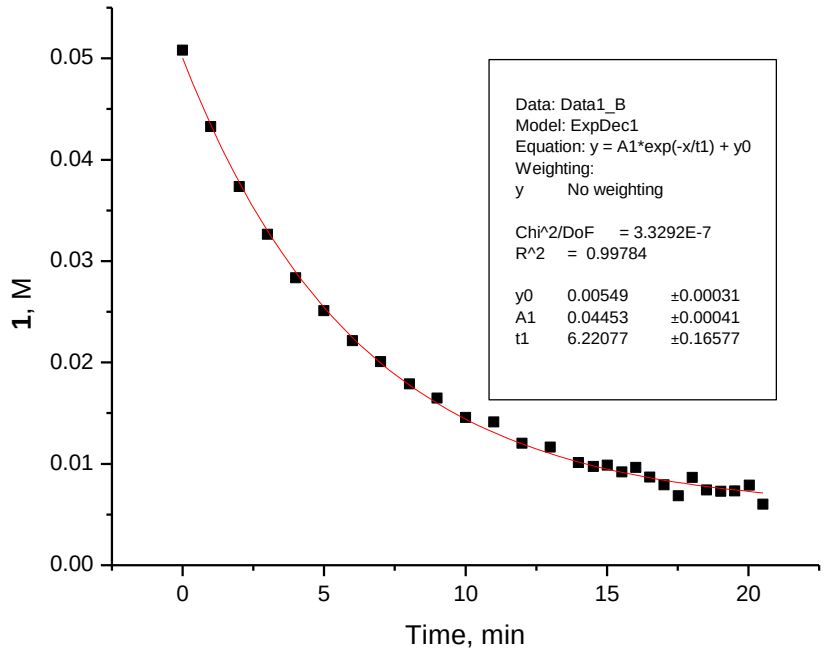

Figure 6.62. Decay of **1** by Mn-**5**

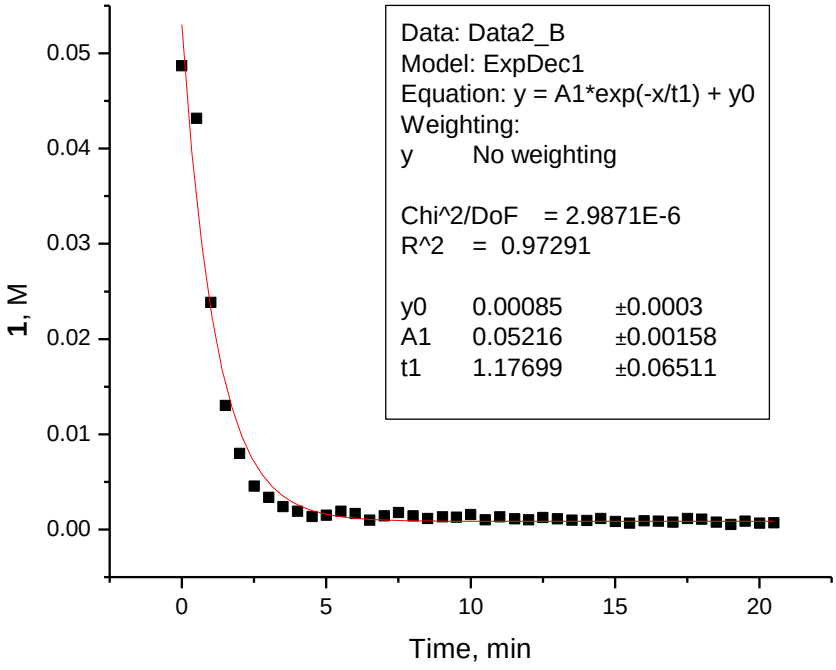

Figure 6.63. Decay of **1** by Mn-**6**

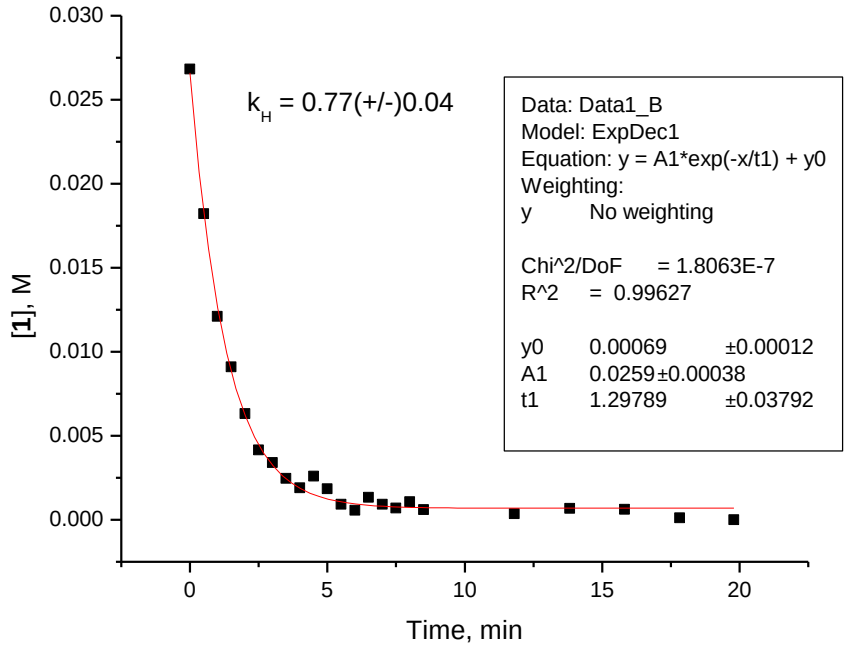

Figure 6.64. Decay of **1** by 20 mol% Mn-**3** to obtain k_H

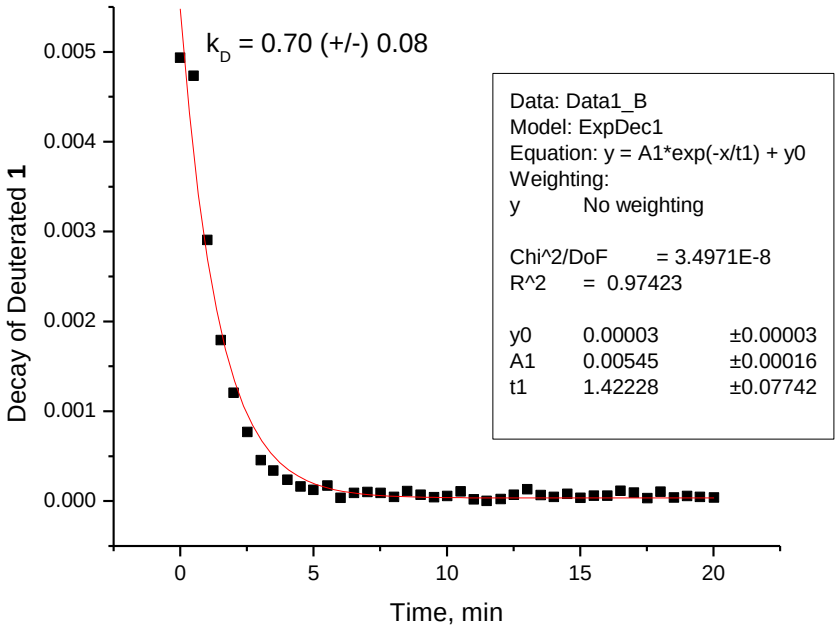

Figure 6.65. Decay of deuterated **1** by 20 mol% Mn-**3** to obtain k_D

A.  **B.** 

Figure 6.66. A. Cp_2TiCl_2 in THF (Red); **B.** Cp_2TiCl in THF

A. 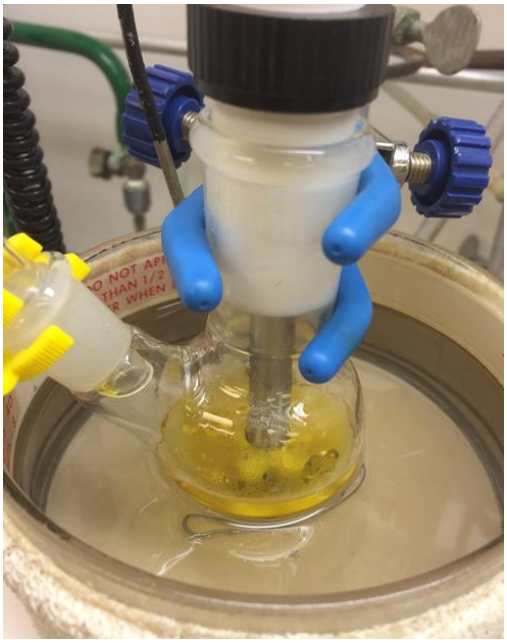 **B.** 

Figure 6.67. Ti-O Homolysis test; **A.** Cp2TiCl(OEt) in THF at 60^{o}Cat the start of reaction (yellow); **B.** Change in color from yellow to orange after 3 hours.

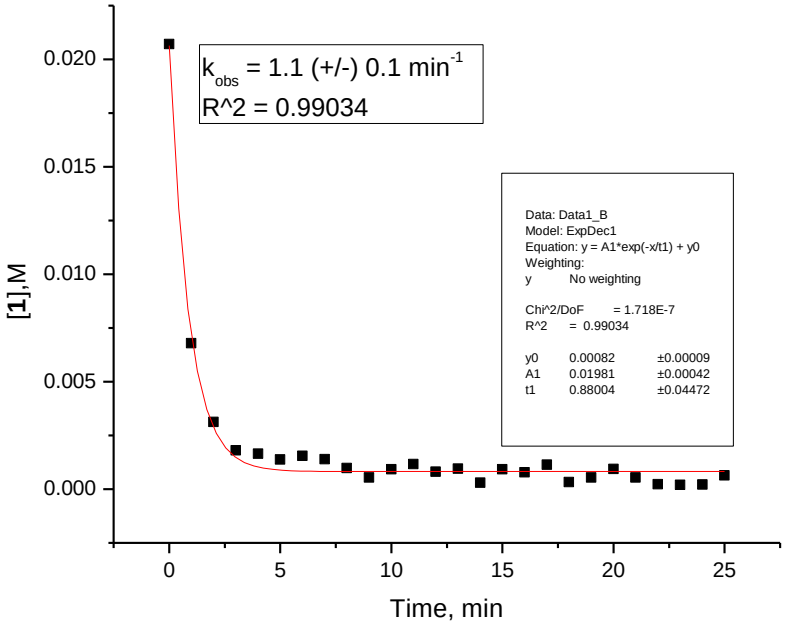

Figure 6.68. Decay plot for **1** with 20 mol% Zn-**3** in the presence of 40 mol% Coll*HCl

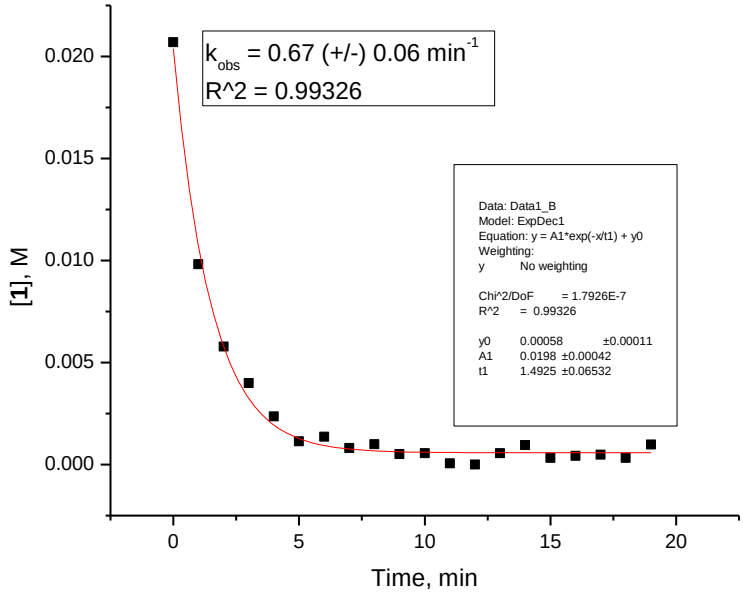

Figure 6.69. Decay plot for **1** with 20 mol% Mn-**3** in the presence of 40 mol% Pyr*HCl

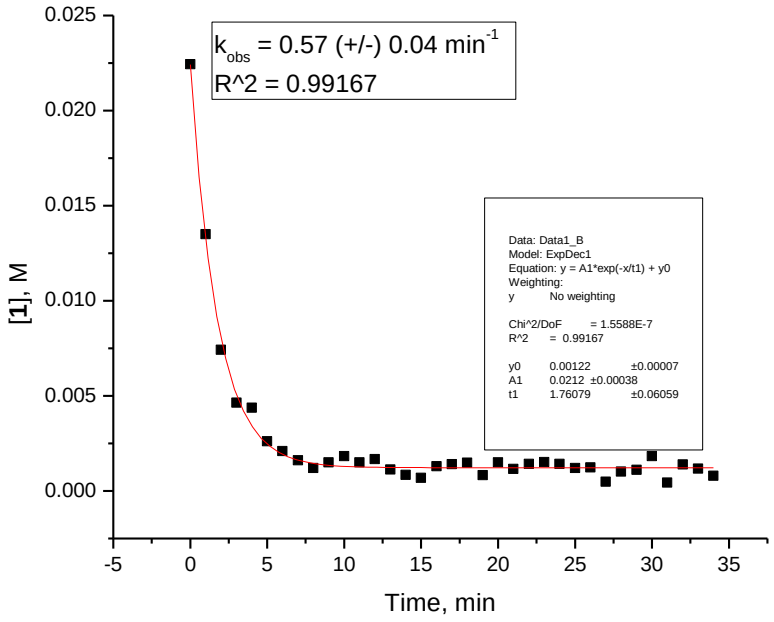

Figure 6.70. Decay plot for **1** with 20 mol% Mn-**3** in the presence of 40 mol% Hex_3N*HCl

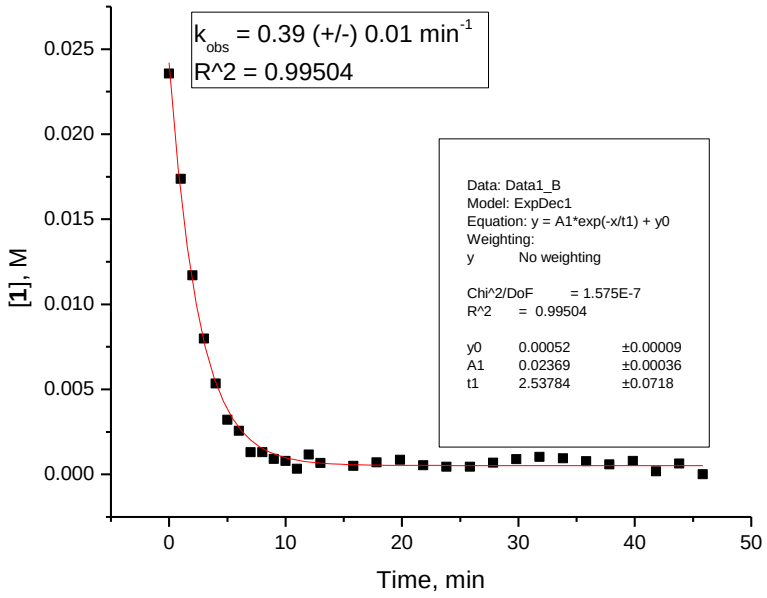

Figure 6.71. Decay plot for **1** with 20 mol% Mn-**3** in the presence of 80 mol% Hex_3N*HCl

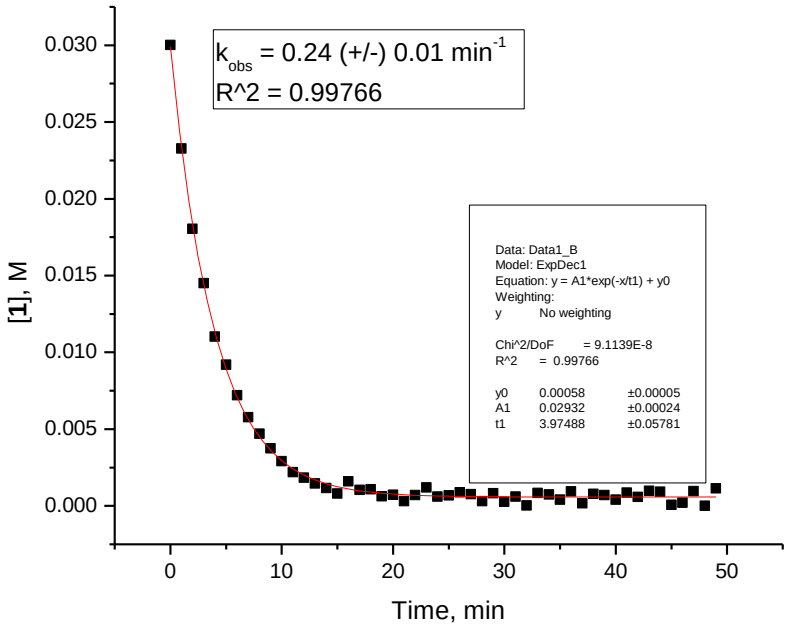

Figure 6.72. Decay plot for **1** with 20 mol% Mn-**3** in the presence of 160 mol% Hex_3N*HCl

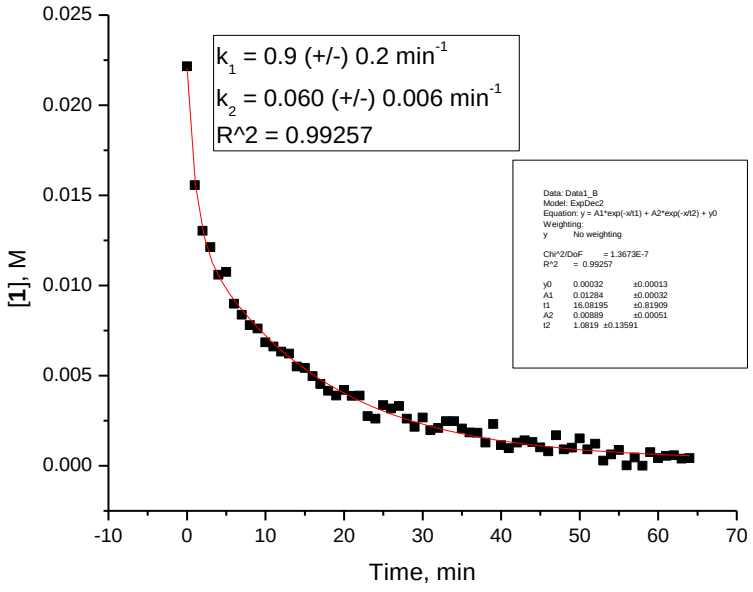

Figure 6.73. Decay plot for **1** with 20 mol% Mn-**3** in the presence of 40 mol% Gu*HCl

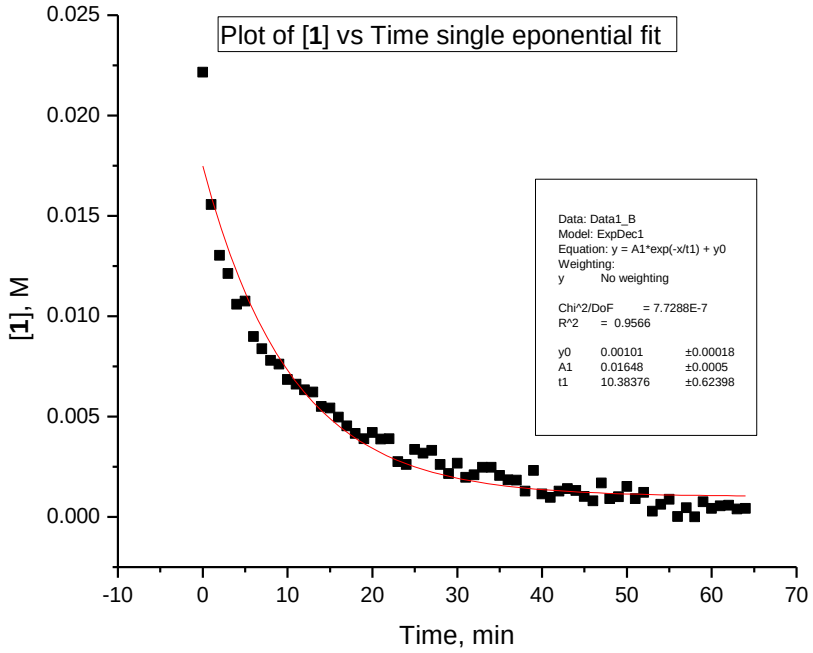

Figure 6.74. Decay plot for **1** with 20 mol% Mn-**3** in the presence of 40 mol% Gu*HCl

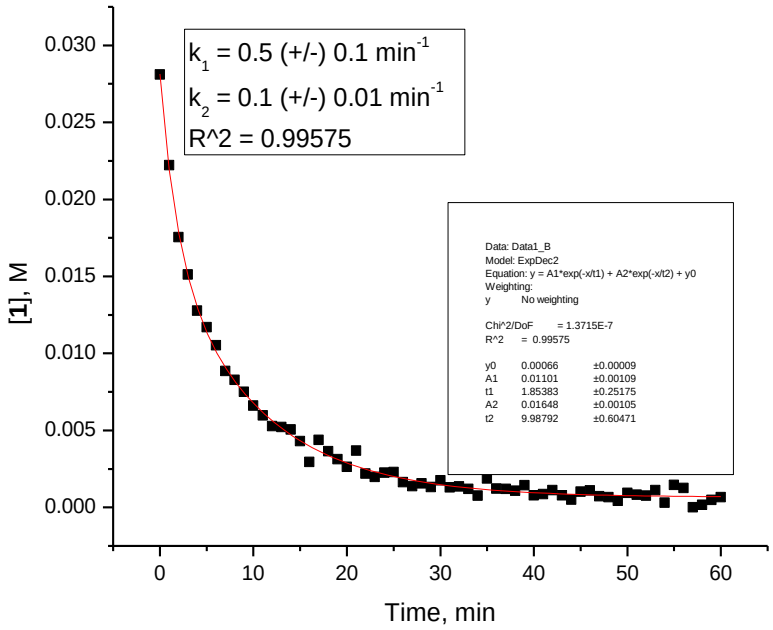

Figure 6.75. Decay plot for **1** with 20 mol% Mn-**3** in the presence of 40 mol% LiCl

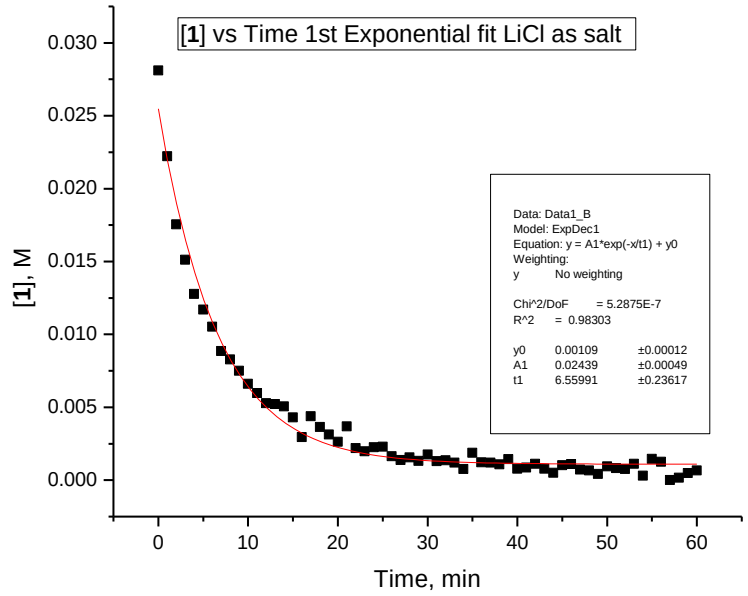

Figure 6.76. Decay plot for **1** with 20 mol% Mn-**3** in the presence of 40 mol% LiCl

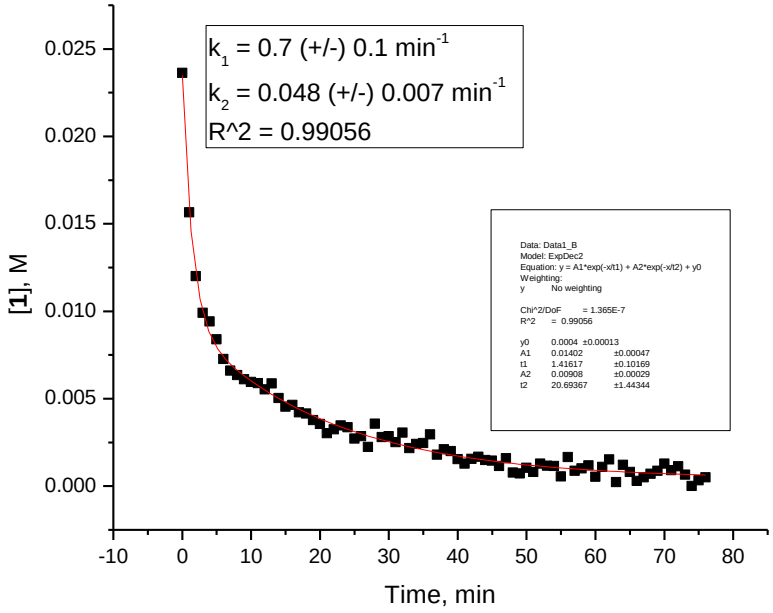

Figure 6.77. Decay plot for **1** with 20 mol% Mn-**3** in the presence of 40 mol% $(CH_3)_4NCl$

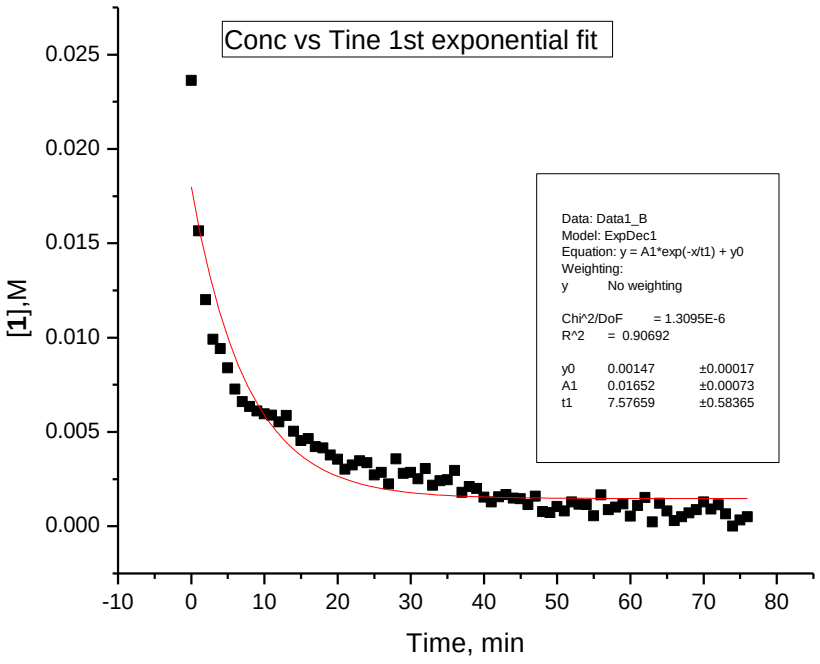

Figure 6.78. Decay plot for **1** with 20 mol% Mn-**3** in the presence of 40 mol% $(CH_3)_4NCl$

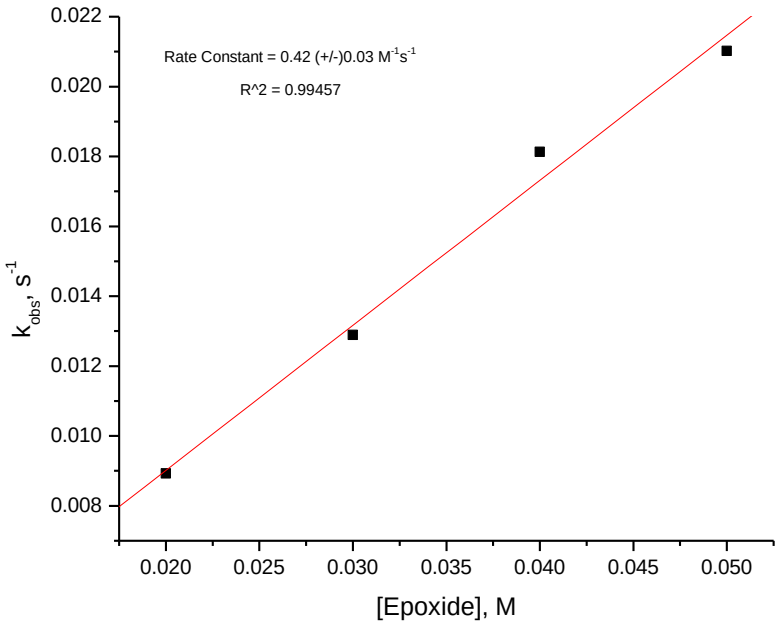

Figure 6.79. Plot of k_{obs} vs. [**14**] with 2 equiv Pyr*HCl

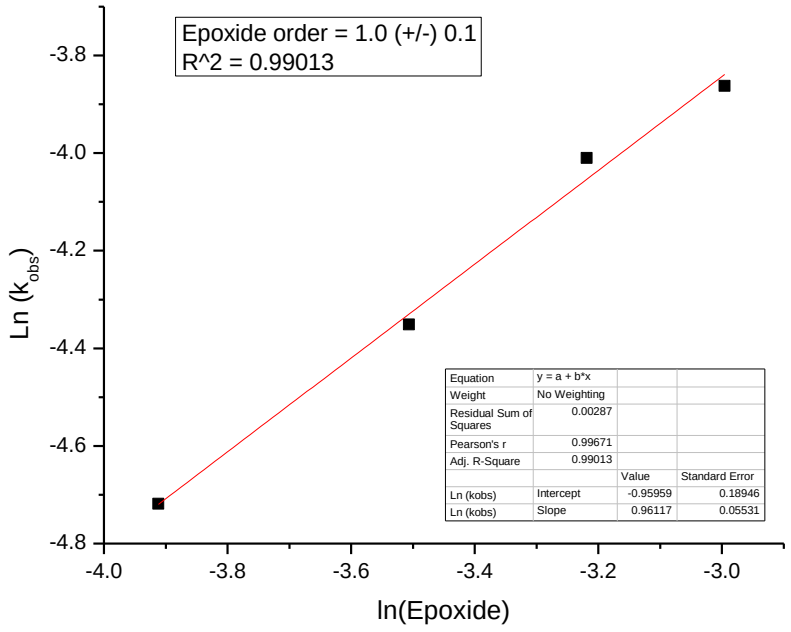

Figure 6.80. Plot of Ln(k_{obs}) vs. Ln (**14**) with 2 equiv Pyr*HCl

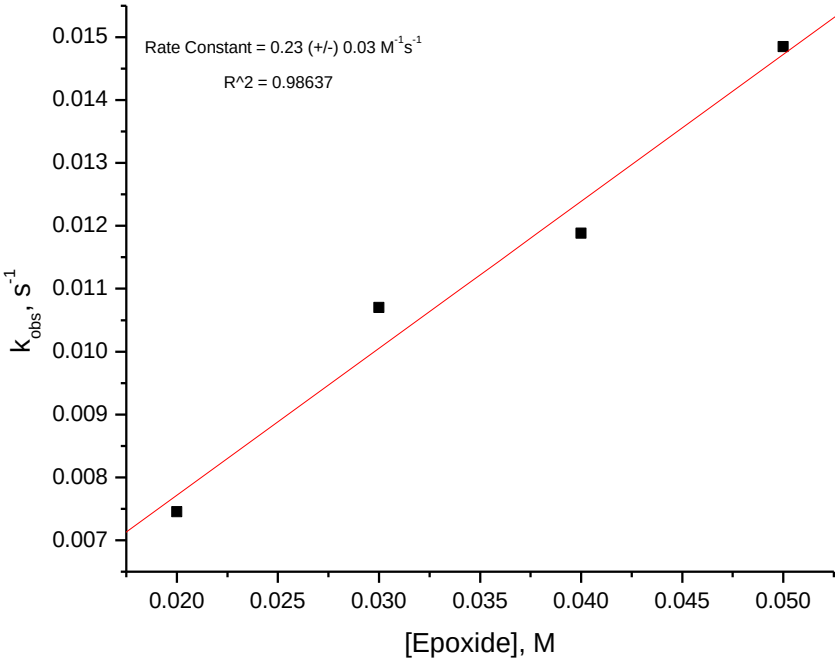

Figure 6.81. Plot of k_{obs} vs. [**14**] with 2 equiv Pyr*HCl (Repeat)

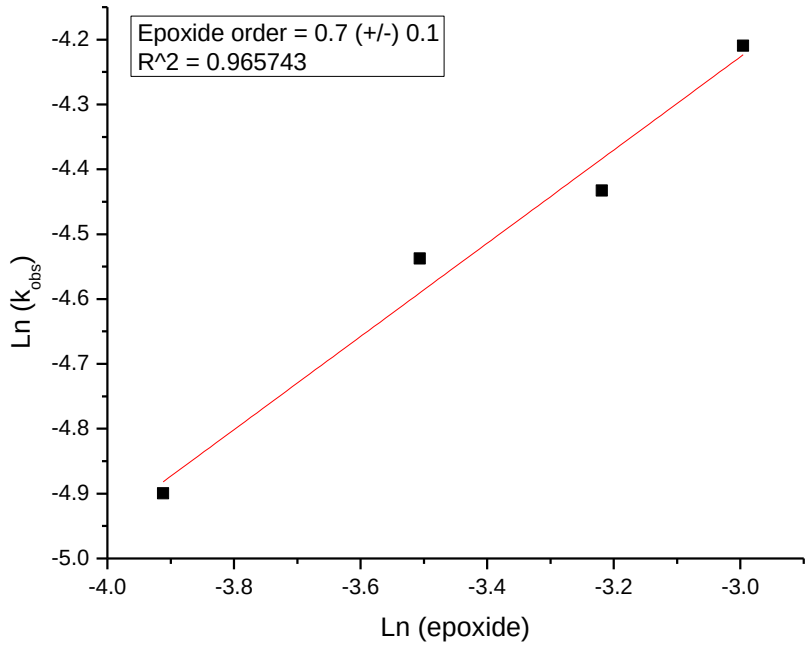

Figure 6.82. Plot of Ln (k_{obs}) vs. Ln (**14**) with 2 equiv Pyr*HCl (Repeat)

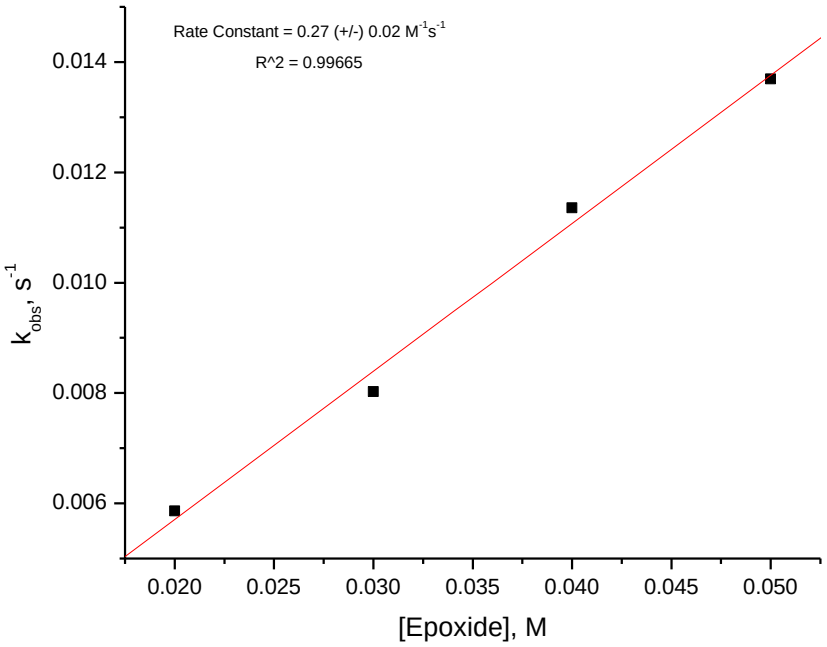

Figure 6.83. Plot of k_{obs} vs. [**14**] with 2 equiv Pyr*HCl (2nd Repeat)

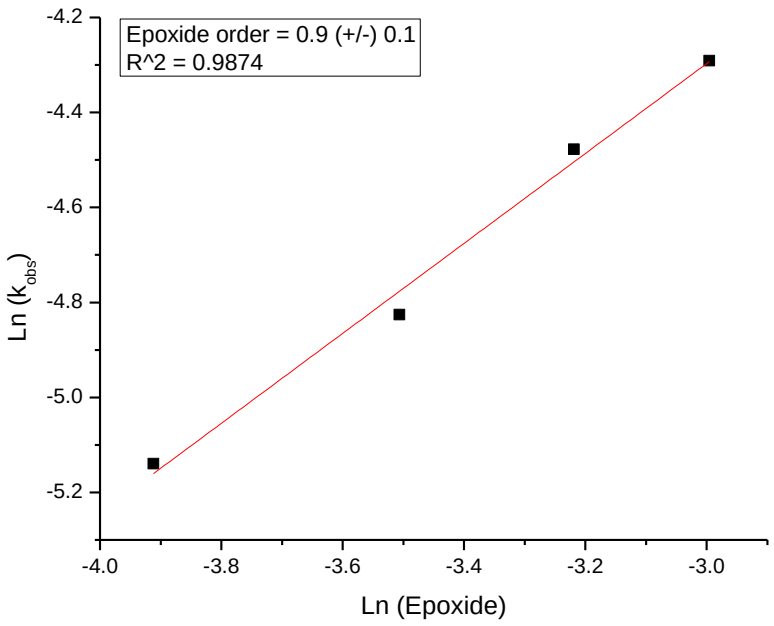

Figure 6.84. Plot of Ln (k_{obs}) vs. Ln (**14**) with 2 equiv Pyr*HCl (2nd Repeat)

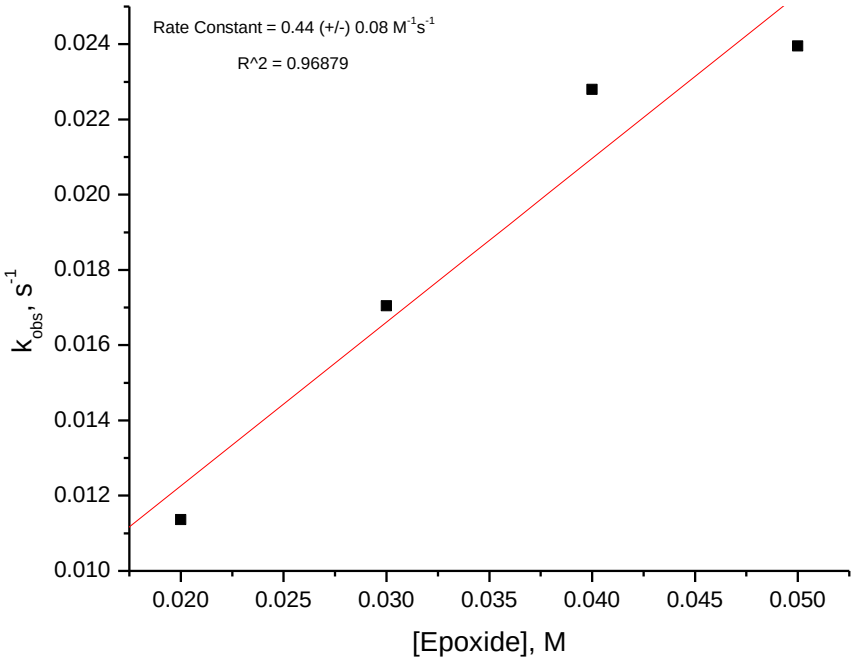

Figure 6.85. Plot of k_{obs} vs. [**14**] with 2 equiv Hex_3*HCl

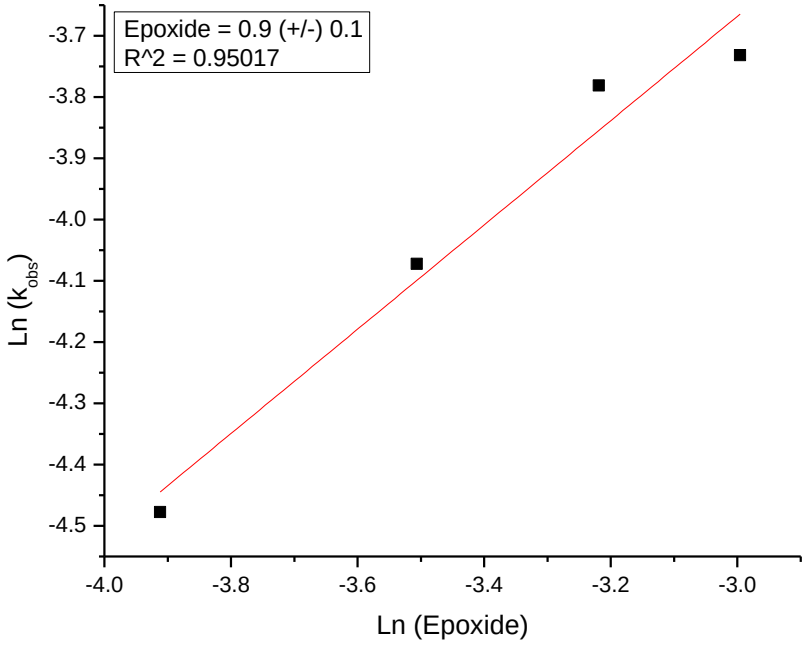

Figure 6.86. Plot of Ln (k_{obs}) vs. Ln (**14**) with 2 equiv Hex_3*HCl

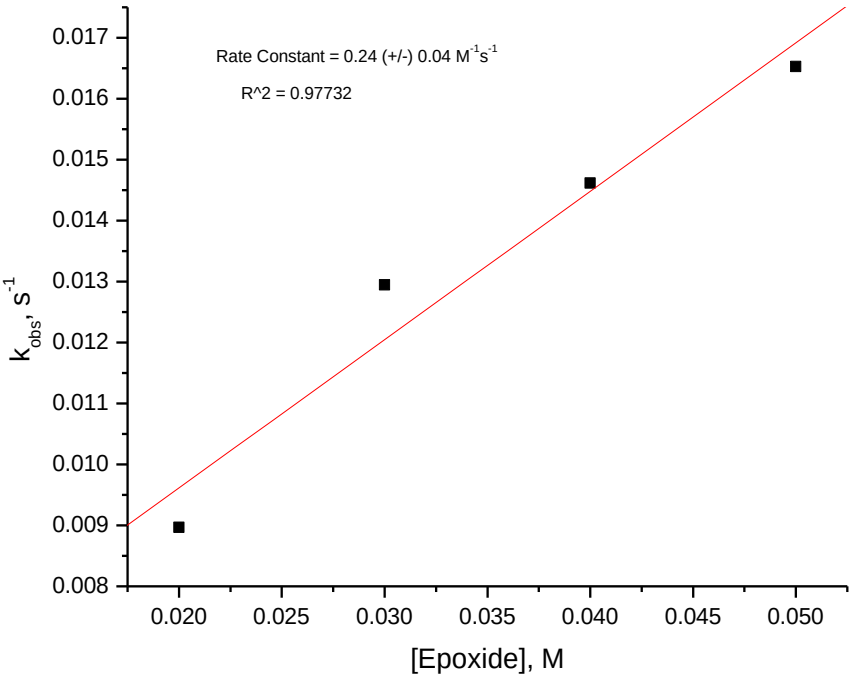

Figure 6.87. Plot of k_{obs} vs. [**14**] with 2 equiv Hex_3*HCl (Repeat)

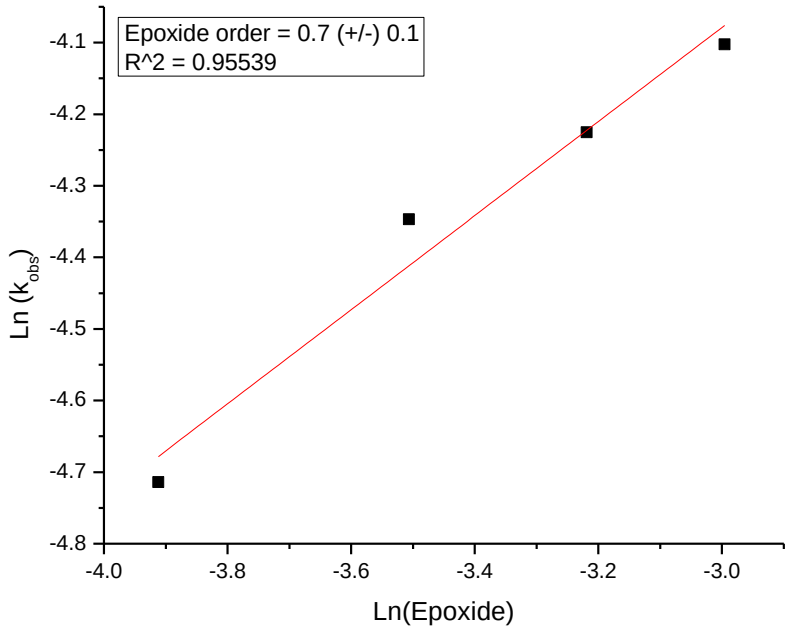

Figure 6.88. Plot of Ln (k_{obs}) vs. Ln (**14**) with 2 equiv Hex_3*HCl (Repeat)

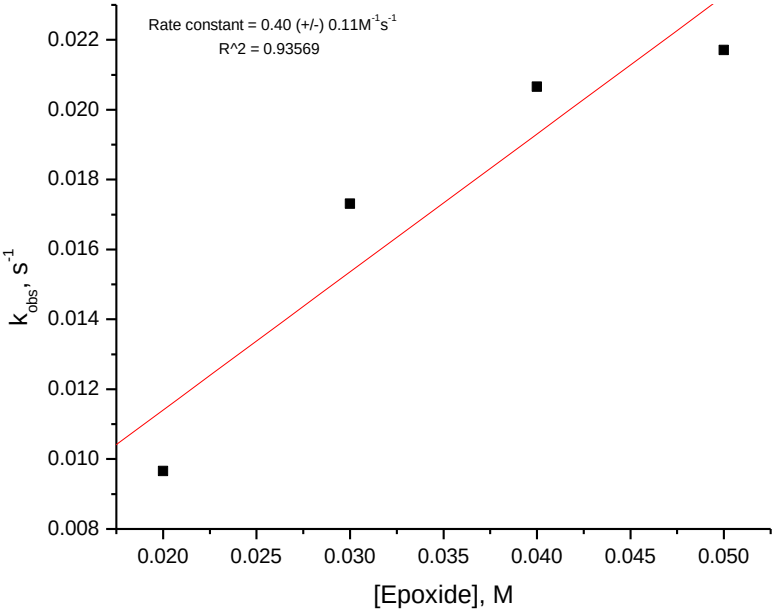

Figure 6.89. Plot of k_{obs} vs. [**14**] with 2 equiv Hex_3*HCl (2^{nd} Repeat)

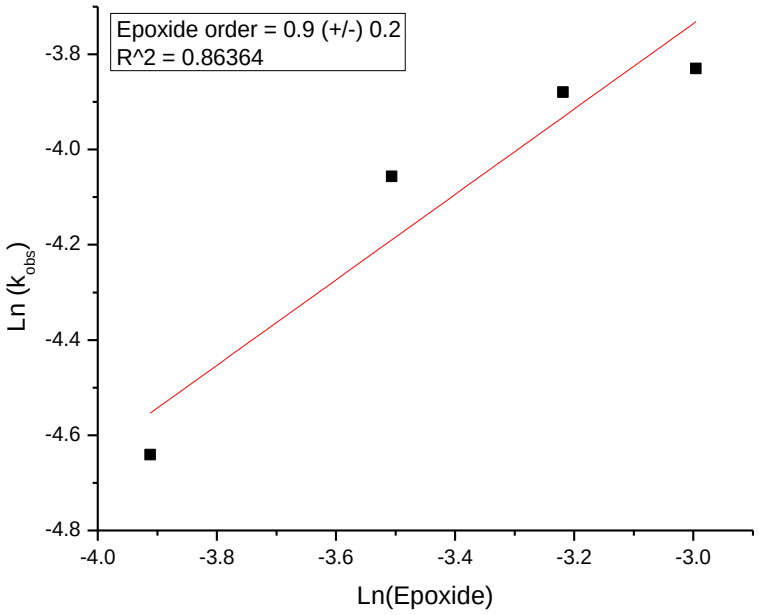

Figure 6.90. Plot of Ln (k_{obs}) vs. Ln (**14**) with 2 equiv Hex_3*HCl (2^{nd} Repeat)

A. 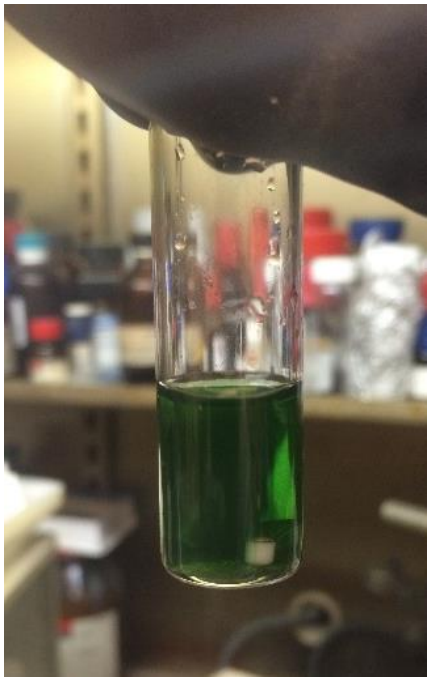 **B.** 

Figure 6.91. Radical arylation of 1 to 2 in DMF at rt; Reaction conditions: [**1**] = 28 mM; [Cp_2TiCl_2] = 5.6 mM; [Mn] = 11.2 mM; DMF = 4 mL; **A.** reaction after 30 min; **B.** reaction after 2 hours

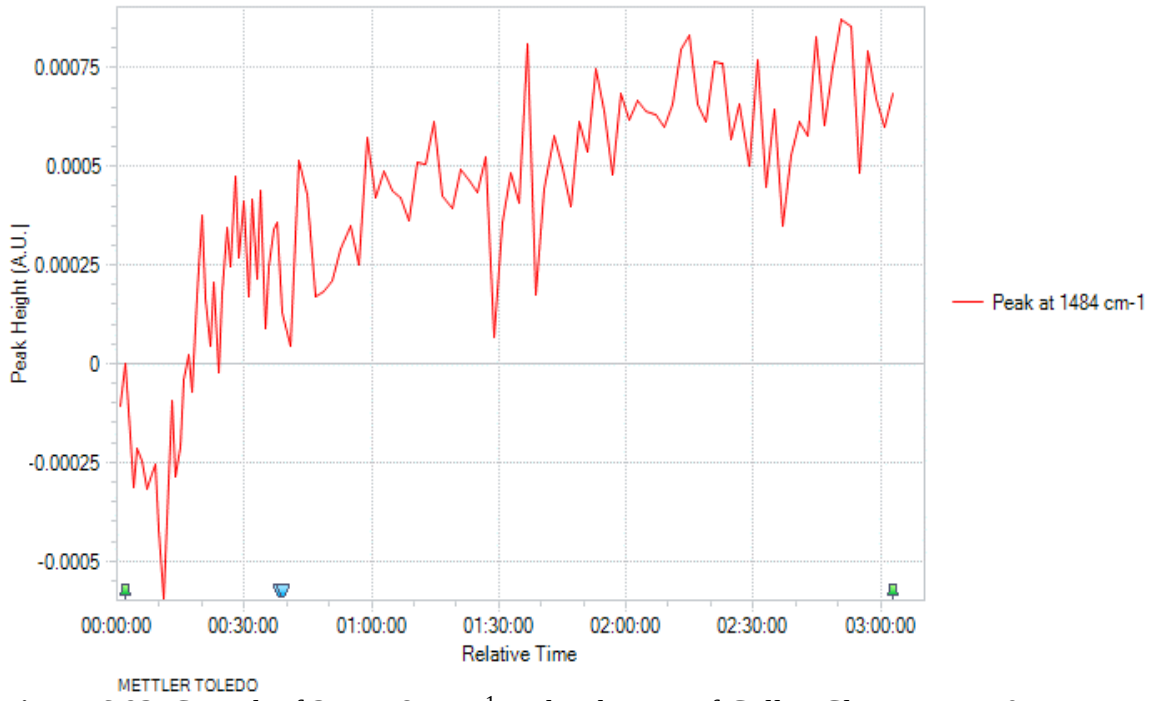

Figure 6.92. Growth of **2** at 1484 cm^{-1} in the absence of Coll*HCl in DME 170 min

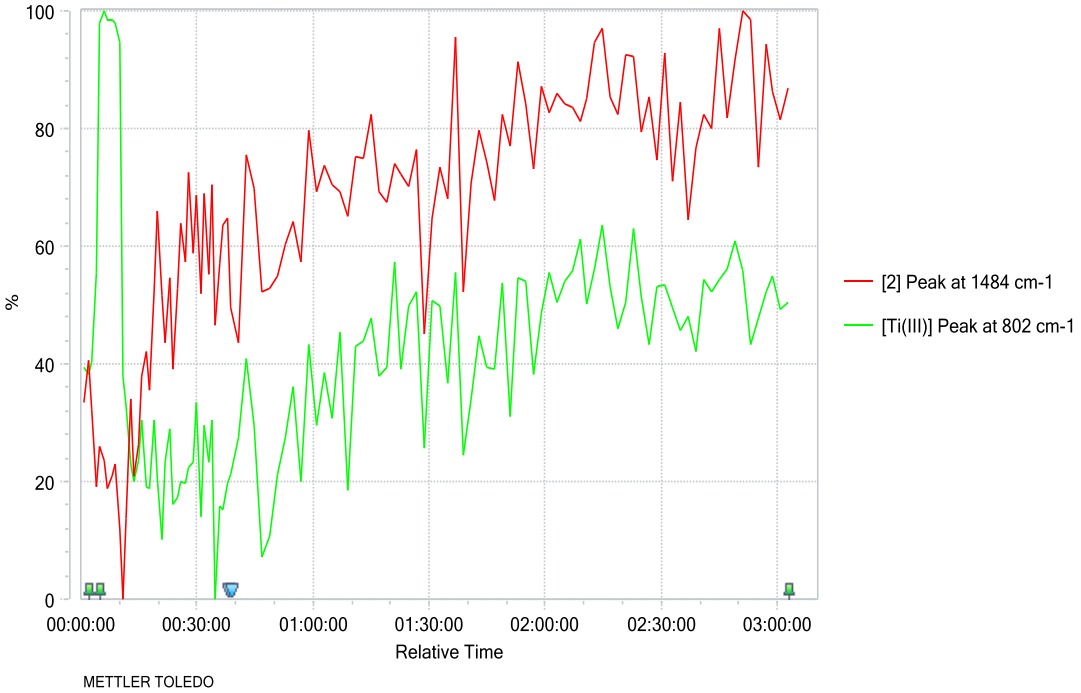

Figure 6.93. Monitoring product growth and catalyst deactivation in DME in the absence of Coll*HCl

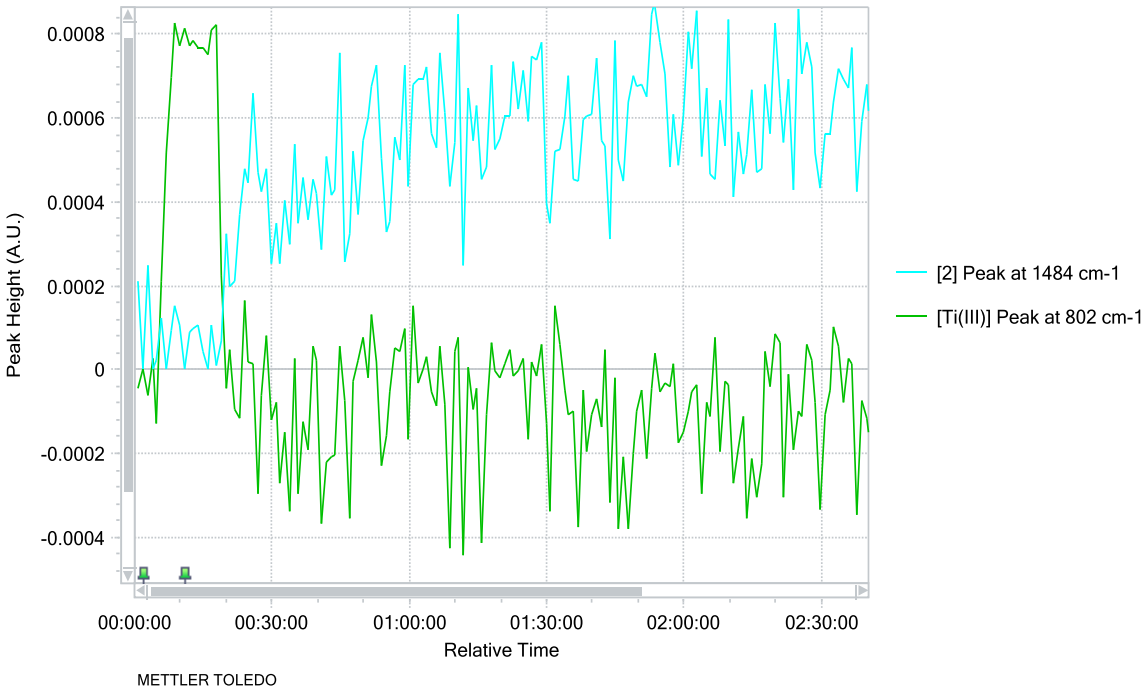

Figure 6.94. Monitoring product growth and catalyst deactivation in DME in the presence of Coll*HCl

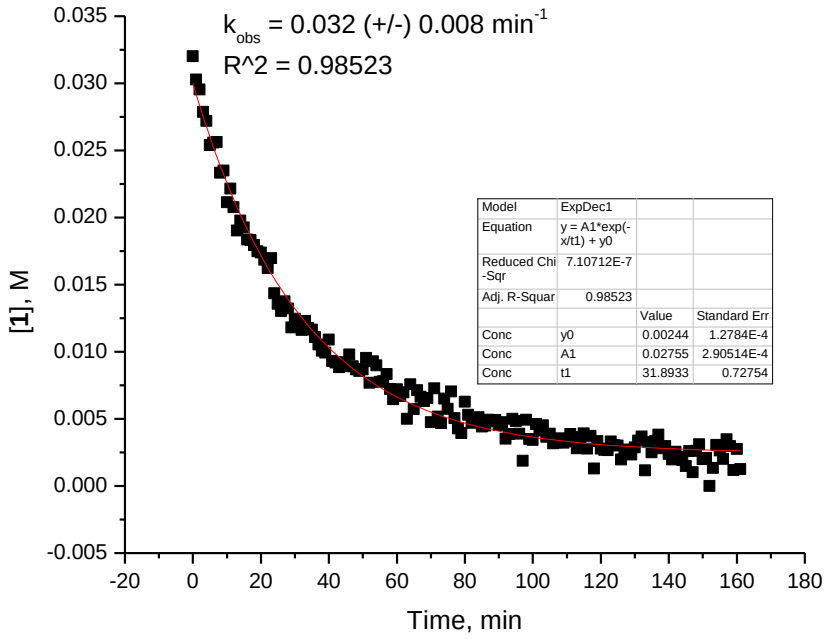

Figure 6.95. Decay of epoxide (**1**) by 20 mol% of Zn-Cp_2TiCl_2 (Zn-**3**) in CH_3CN

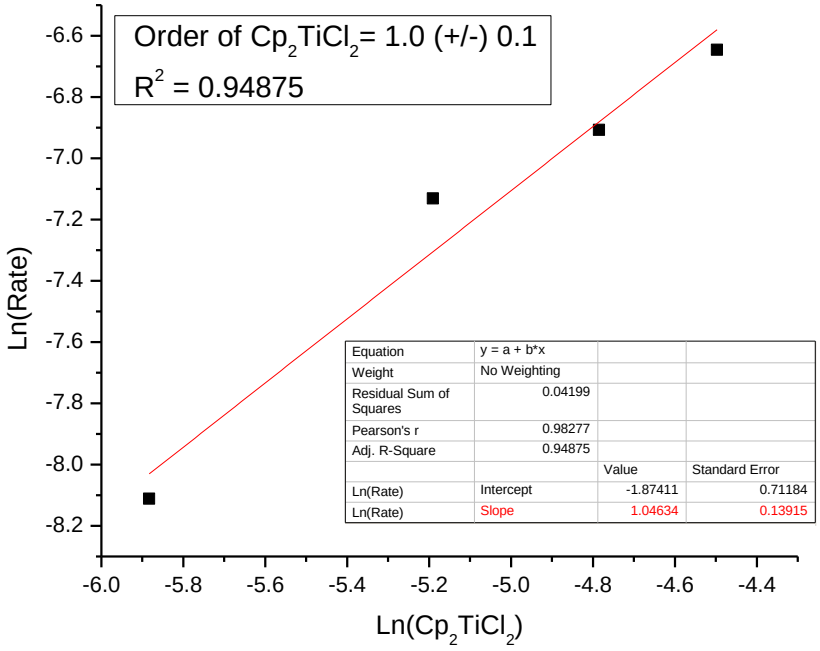

Equation	y = a + b*x		
Weight	No Weighting		
Residual Sum of Squares	0.04199		
Pearson's r	0.98277		
Adj. R-Square	0.94875		
		Value	Standard Error
Ln(Rate)	Intercept	-1.87411	0.71184
Ln(Rate)	Slope	1.04634	0.13915

Figure 6.96. Order for Zn-**3** in MeCN

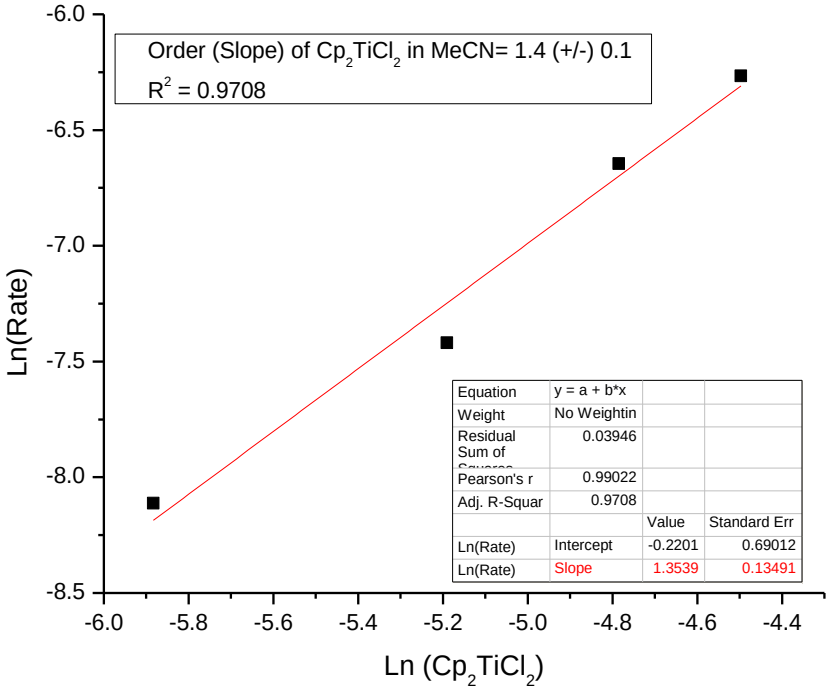

Equation	y = a + b*x		
Weight	No Weightin		
Residual Sum of	0.03946		
Pearson's r	0.99022		
Adj. R-Squar	0.9708		
		Value	Standard Err
Ln(Rate)	Intercept	-0.2201	0.69012
Ln(Rate)	Slope	1.3539	0.13491

Figure 6.97. Order for Mn-**3** in MeCN

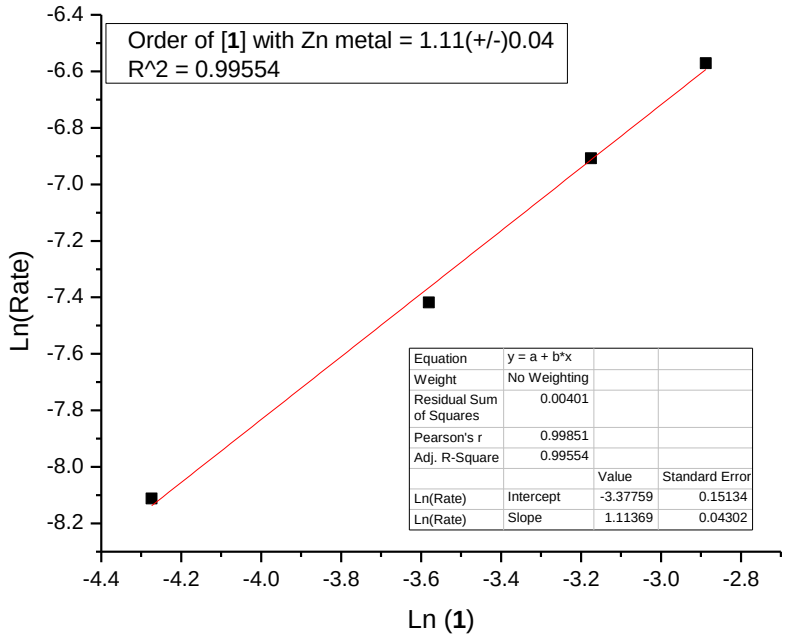

Figure 6.98. Order for **1** in MeCN with Zn-**3**

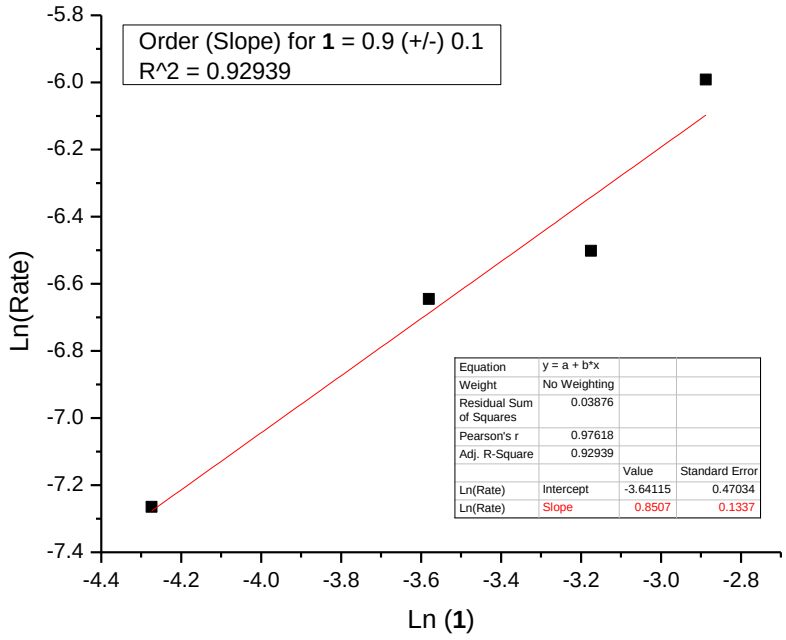

Figure 6.99. Order for **1** in MeCN with Mn-**3**

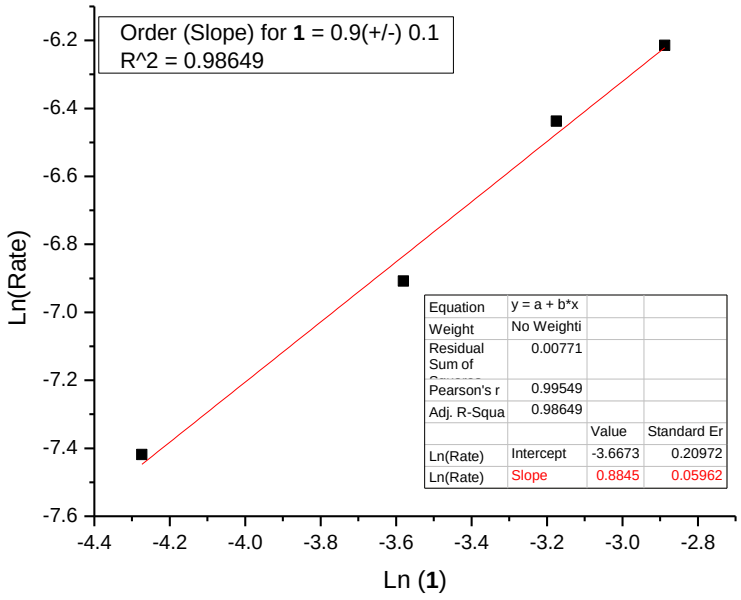

Figure 6.100. Order for **1** in MeCN with Mn-**3** (Repeat)

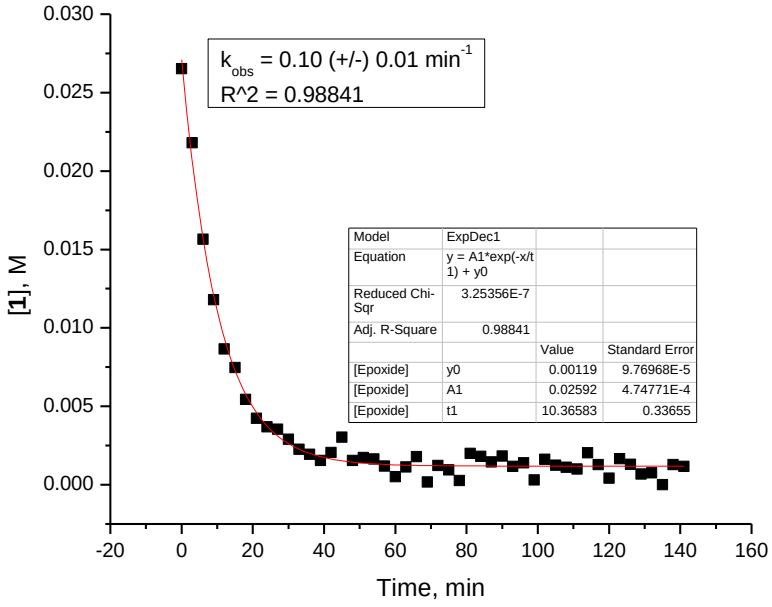

Figure 6.101. Decay of epoxide (**1**) by 20 mol% of NaBH4-$Cp_2Ti(OTf)_2$ in THF

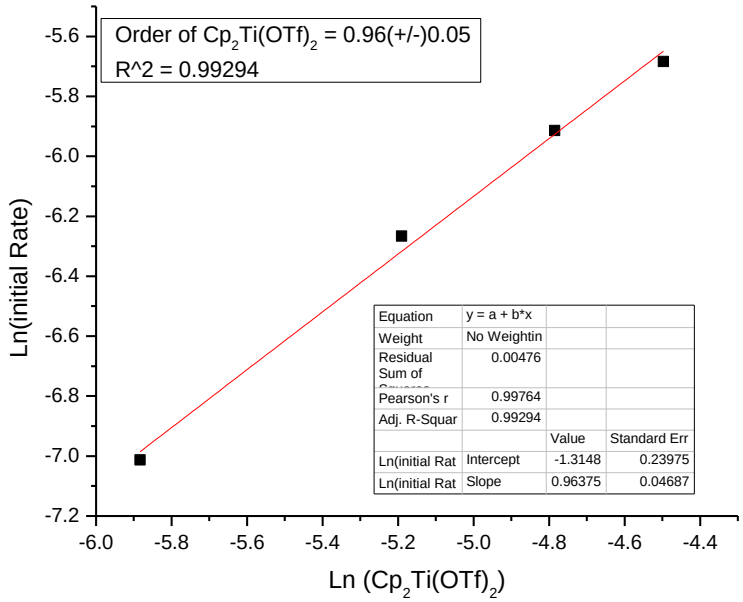

Figure 6.102. Order of $Cp_2Ti(OTf)_2$ for arylation of **1** in THF

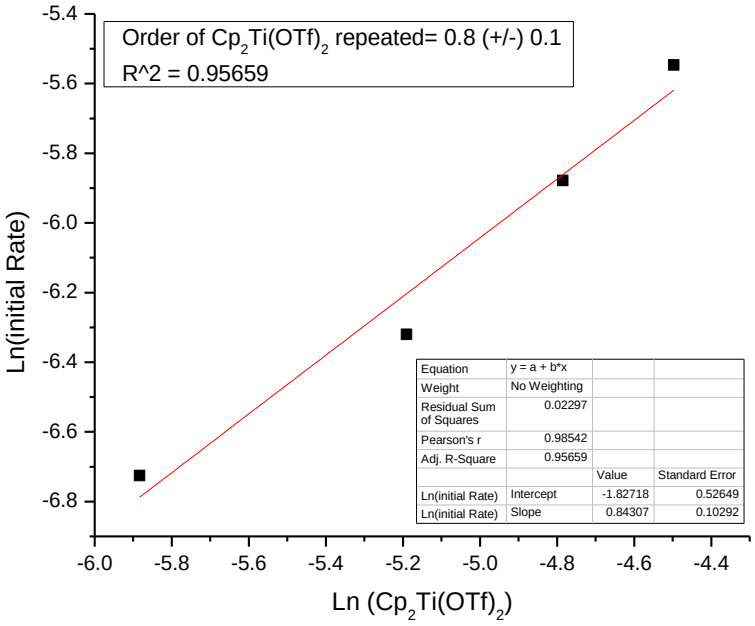

Figure 6.103. Order of $Cp_2Ti(OTf)_2$ for arylation of **1** in THF (repeat)

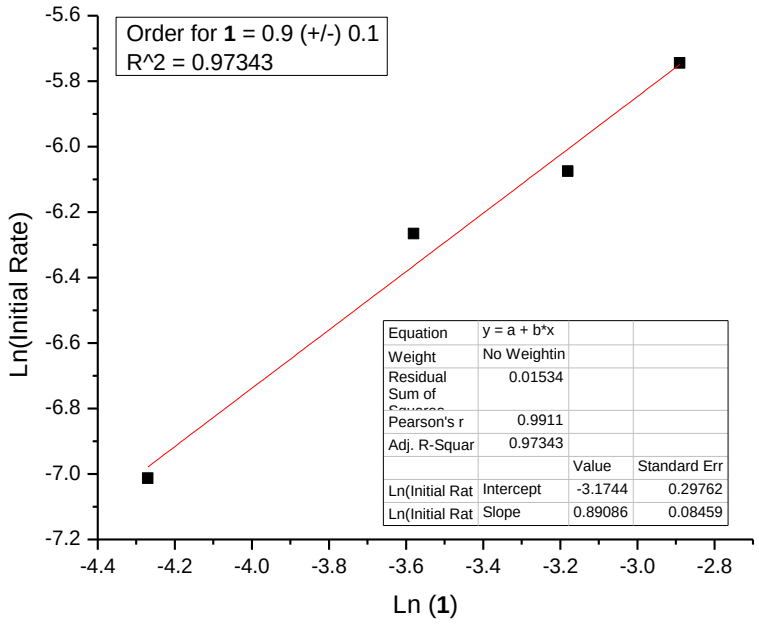

Figure 6.104. Order for **1** in THF with $Cp_2Ti(OTf)_2$

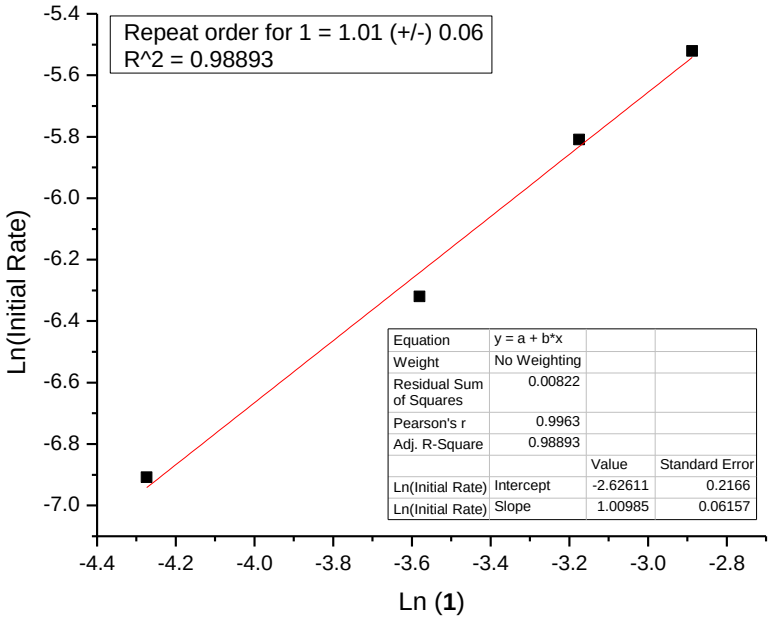

Figure 6.105. Order for **1** in THF with $Cp_2Ti(OTf)_2$ (Repeat)

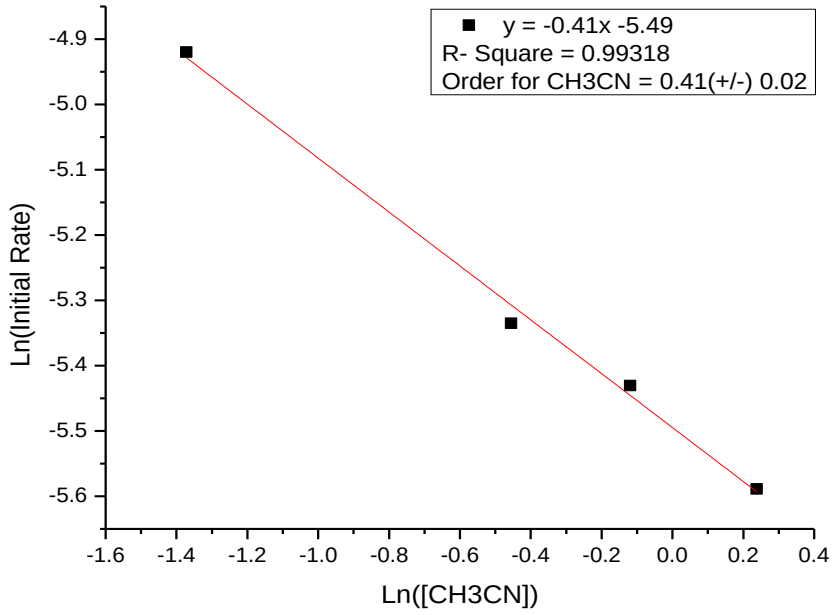

Figure 6.106. Plot of Ln(CH_3CN) vs. Ln (Rate) Mn-**3** with Coll*HCl (Values range from 0.25M to 1.27M of CH_3CN)

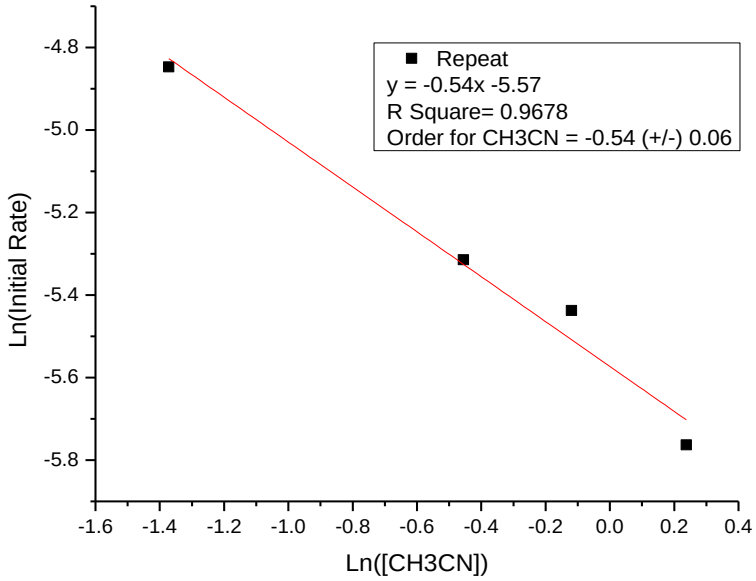

Figure 6.107. Repeat of plot of Ln(CH_3CN) vs. Ln (Rate) Mn-**3** with Coll*HCl (Values range from 0.25M to 1.27M of CH_3CN)

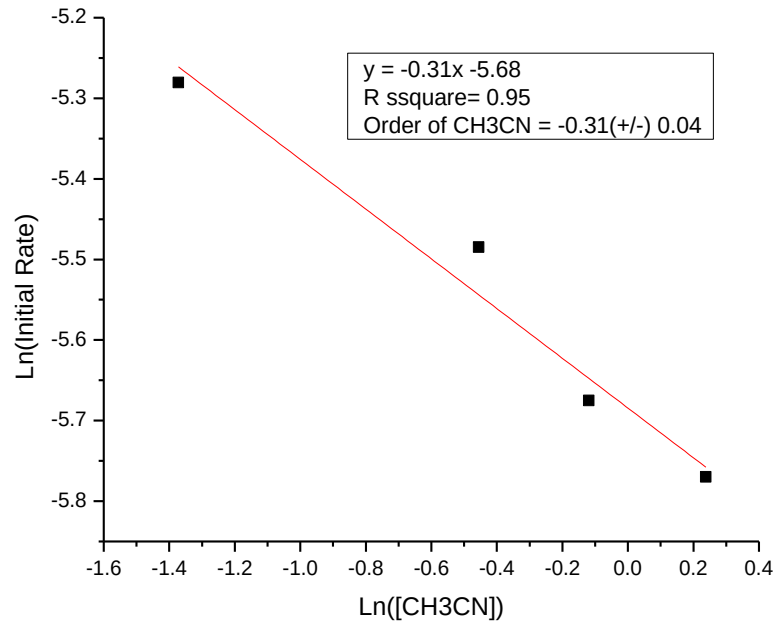

Figure 6.108. Plot of Ln(CH_3CN) vs. Ln (Rate) Mn-**3** without Coll*HCl (Values range from 0.25M to 1.27M of CH_3CN)

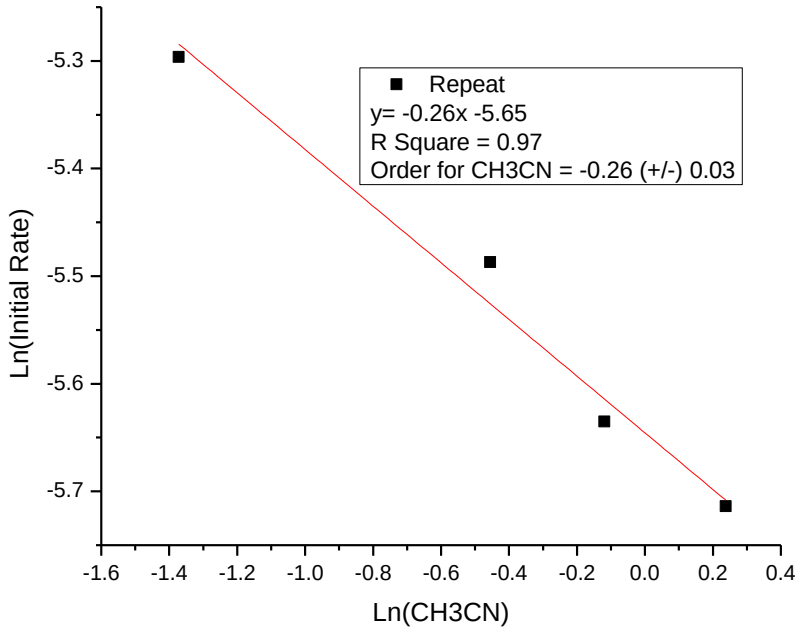

Figure 6.109. Repeat of Plot of Ln(CH_3CN) vs. Ln (Rate) Mn-**3** without Coll*HCl (Values range from 0.25M to 1.27M of CH_3CN)

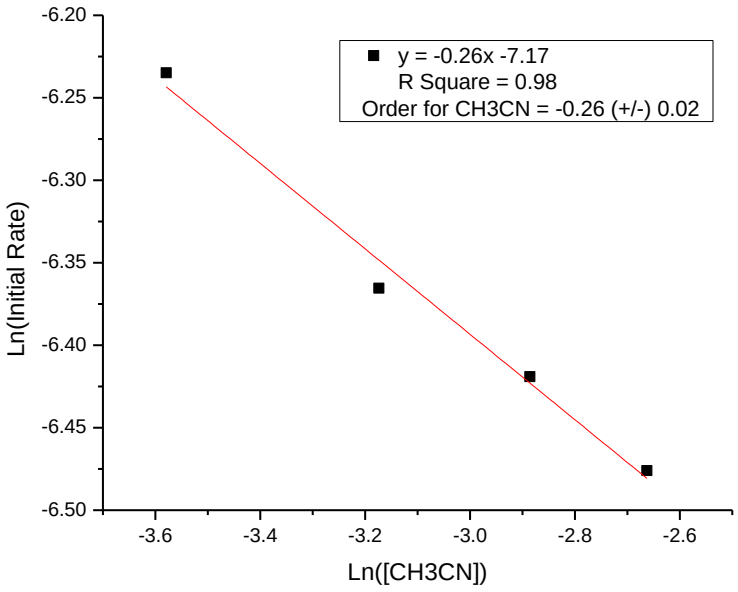

Figure 6.110. Plot of Ln(CH_3CN) vs. Ln (Rate) with $NaBH_4$-$Cp_2Ti(OTf)_2$ (Values range from 0.028M to 0.070M of CH_3CN)

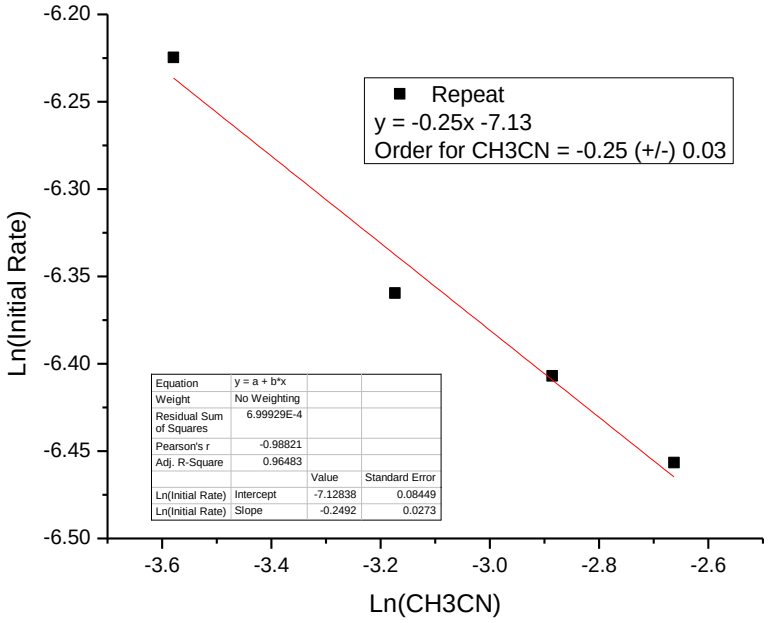

Figure 6.111. Repeat for plot of Ln(CH_3CN) vs. Ln (Rate) with $NaBH_4$-$Cp_2Ti(OTf)_2$ (Values range from 0.028M to 0.070M of CH_3CN)

A. 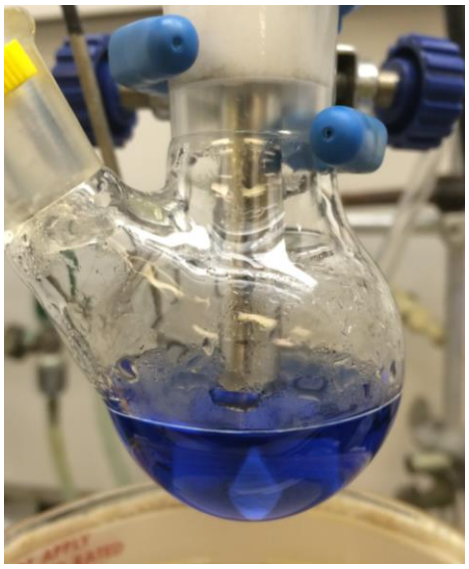 **B.** 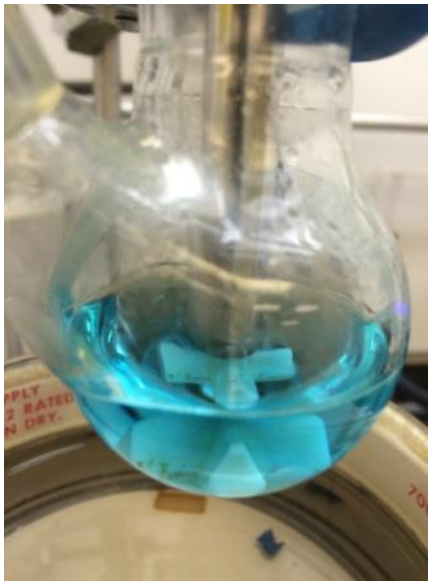

Figure 6.112. A. Zn reduced Cp_2TiCl_2 in CH_3CN; **B.** $NaBH_4$ reduced $Cp_2Ti(OTf)_2$ in THF

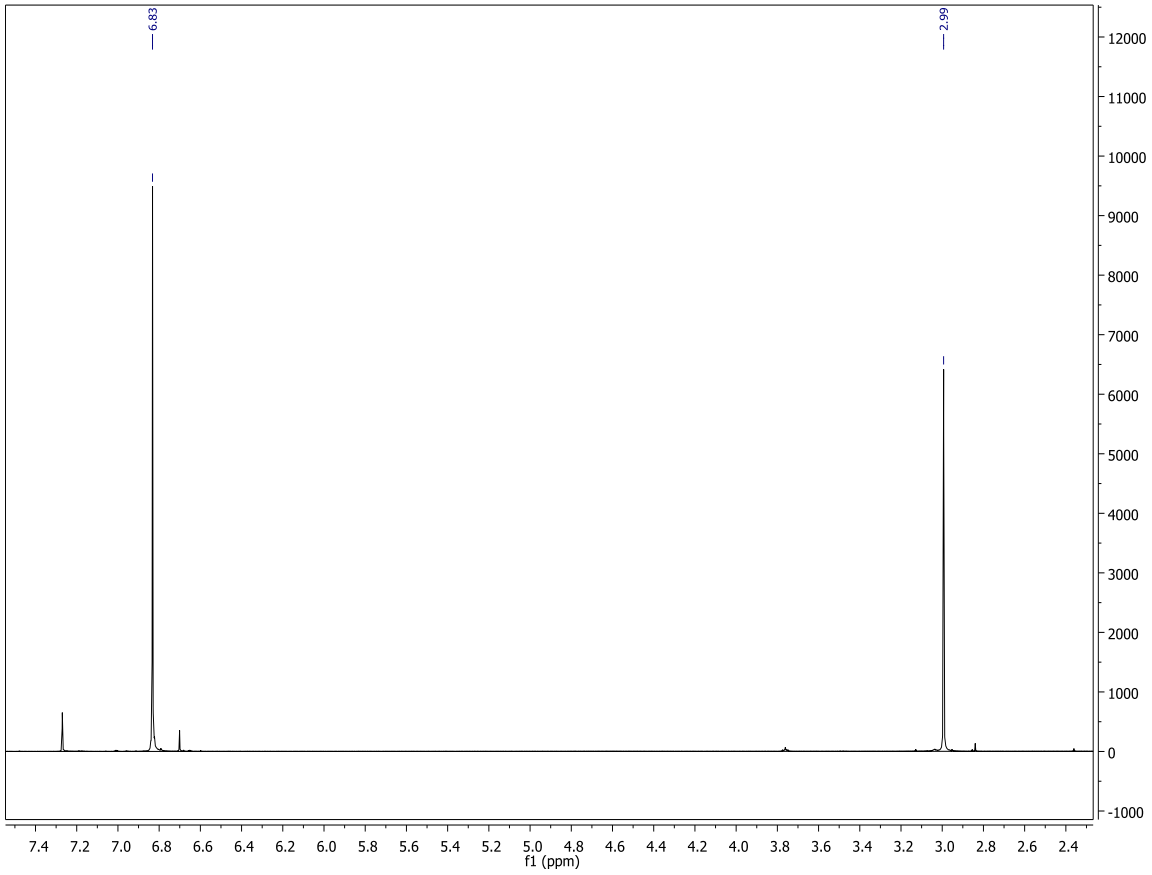

Figure 6.113. ^1H NMR spectrum of $Cp_2Ti(OMs)_2$

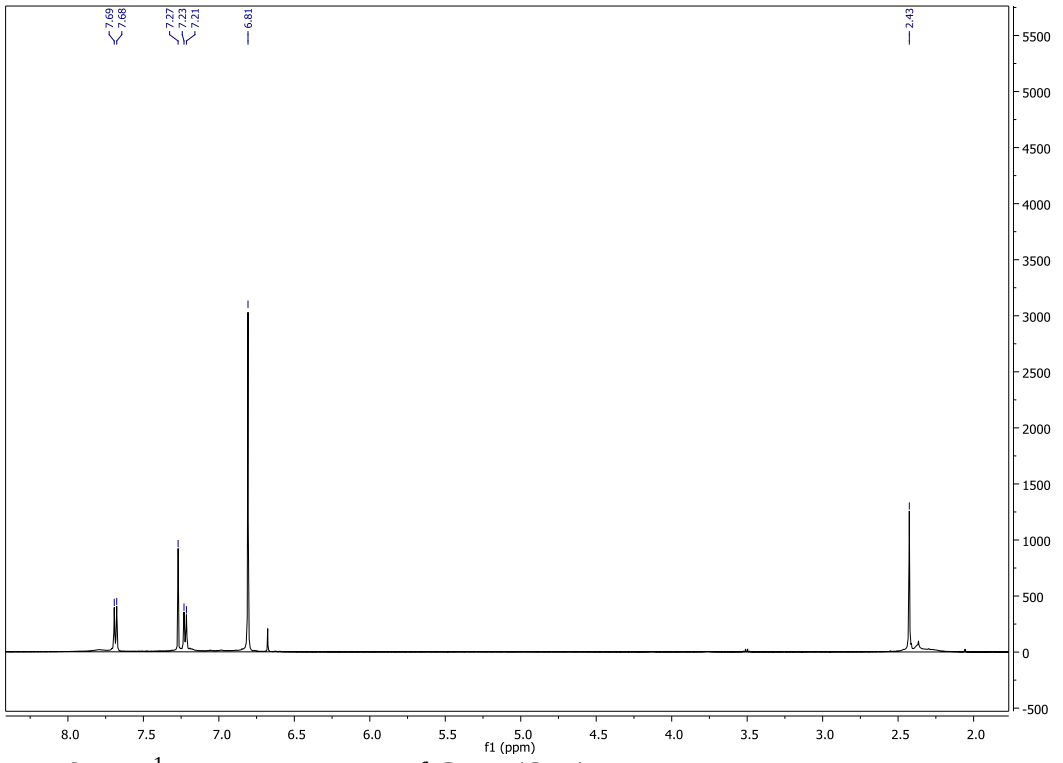

Figure 6.114. ^{1}H NMR spectrum of $Cp_2Ti(OTs)_2$

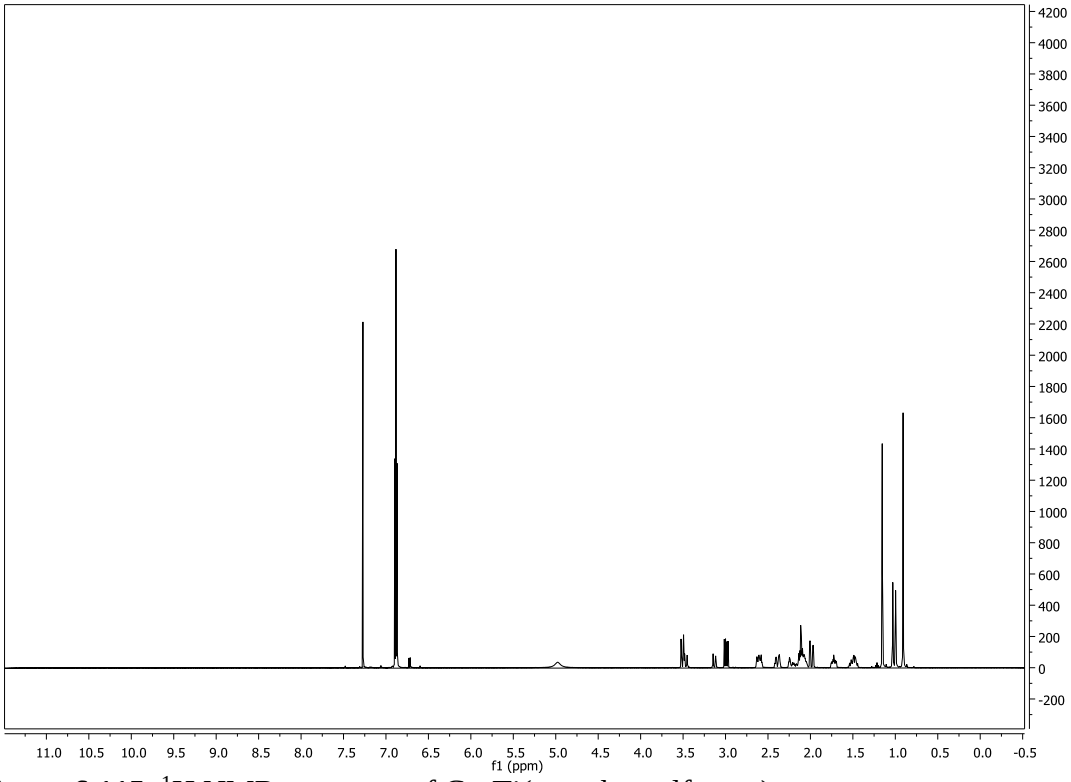

Figure 6.115. ^{1}H NMR spectrum of $Cp_2Ti(camphorsulfonate)_2$

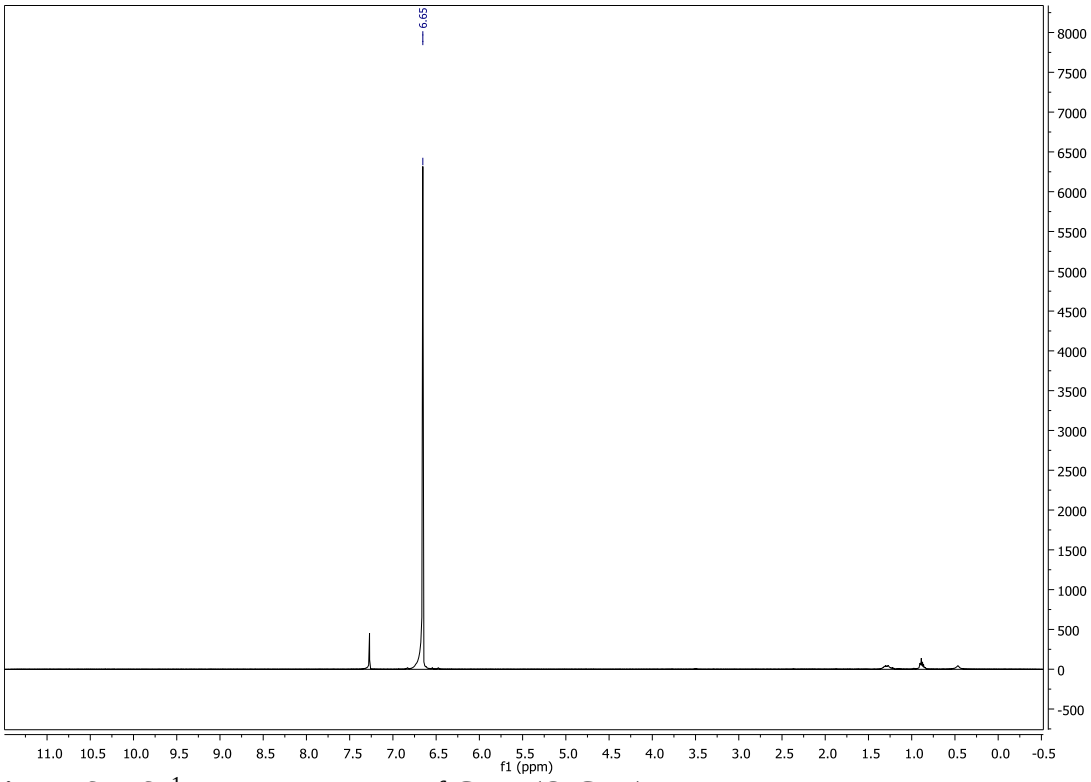

Figure 6.116. ^{1}H NMR spectrum of $Cp_2Ti(O_2C_2F_3)_2$

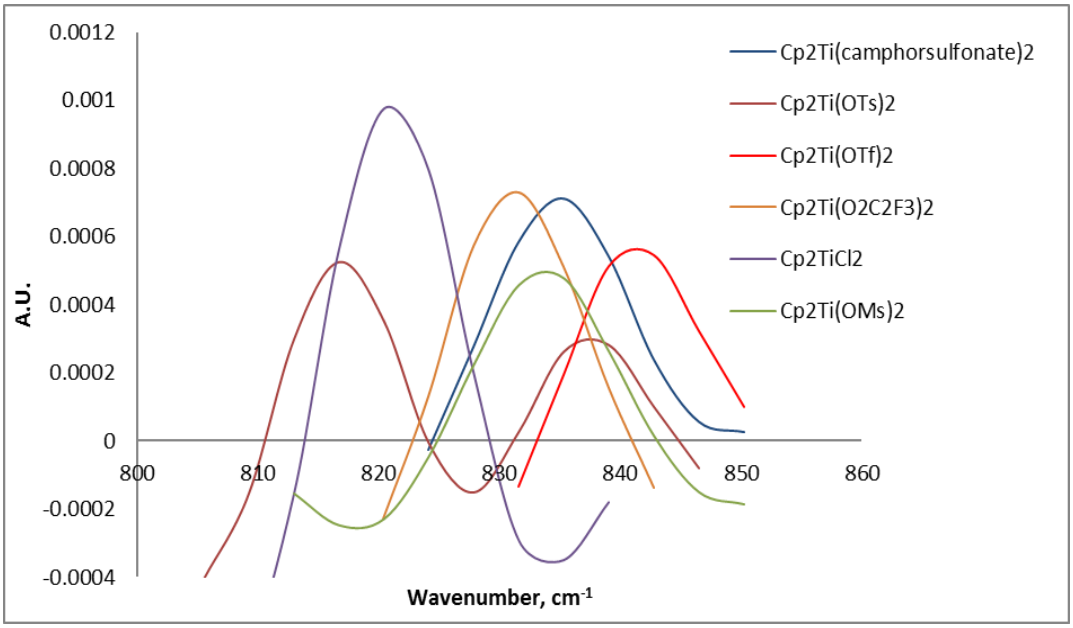

Figure 6.117. Observed peaks on ReactIR for C-H wag of Cp ligands of Cp_2TiX_2

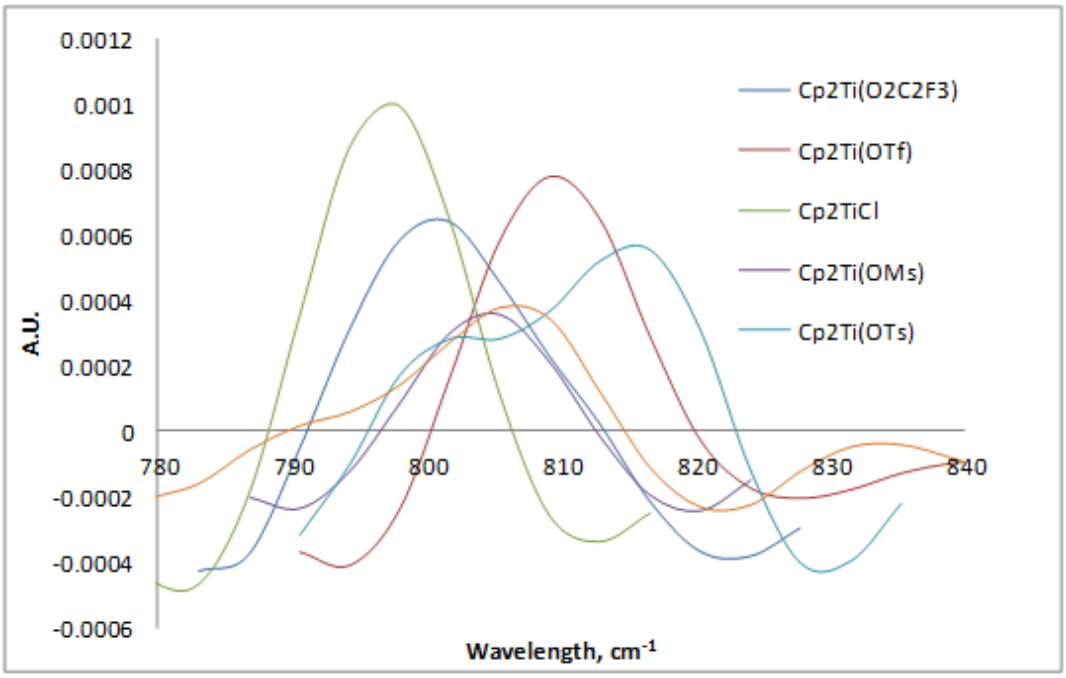

Figure 6.118. Observed peaks on ReactIR for C-H wag of Cp ligands of Cp_2TiX

Table 6.4. Observed peaks on ReactIR for C-H wag of Cp ligands of titanocene complexes in +4 and +3 oxidation states

Cp_2TiX_2	Cp_2TiX_2 (cm^{-1})	Cp_2TiX (cm^{-1})
Cp_2TiCl_2	821	798
Cp_2Ti(camphorsulfonate)$_2$	836	809
$Cp_2Ti(O_2C_2F_3)_2$	830	802
$Cp_2Ti(OTs)_2$	839 & 817	817 & 802
$Cp_2Ti(OTf)_2$	843	813
$Cp_2Ti(OMs)_2$	831	805

A

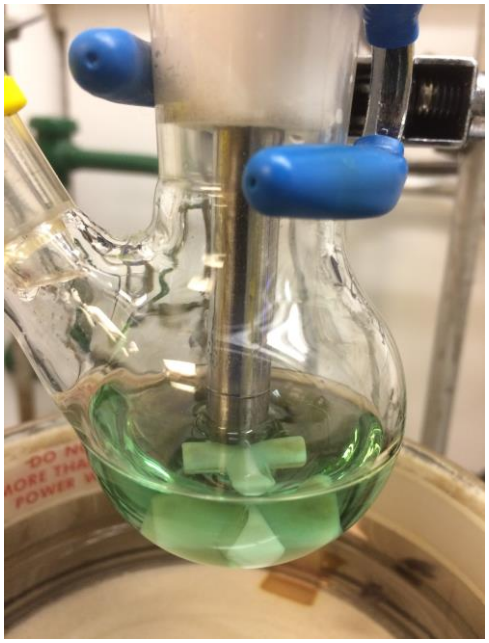

B

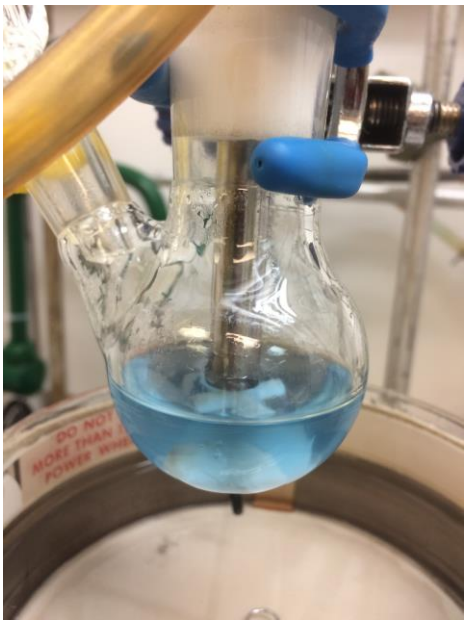

C

D

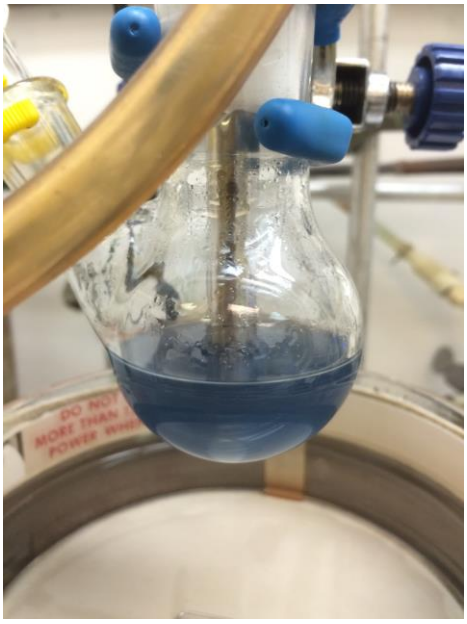

Figure 6.119. A. Cp_2Ti(camphorsulfonate) in THF **B.** Cp_2Ti(OMs) in THF **C.** $Cp_2Ti(O_2C_2F_3)$ in THF **D.** Cp_2Ti(OTs) in THF

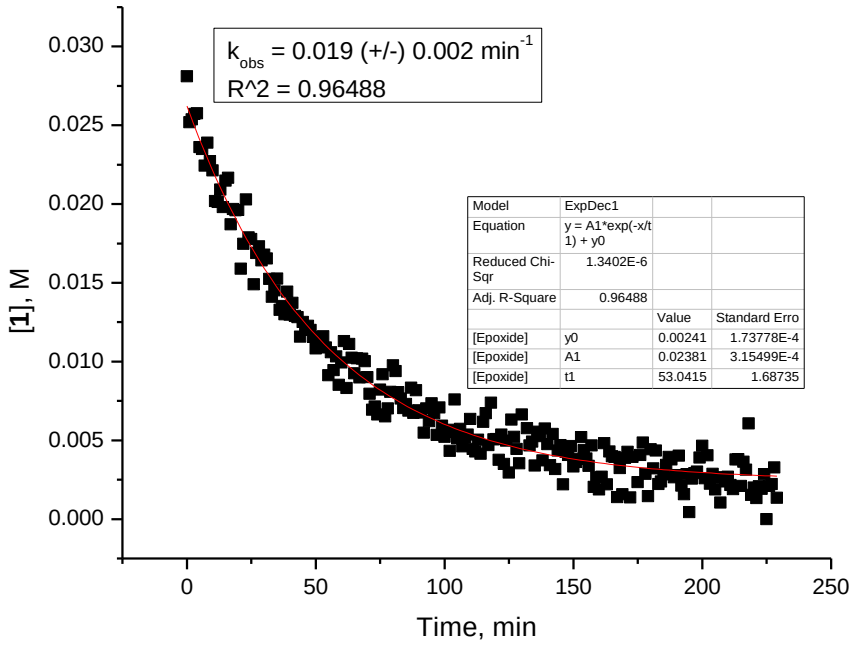

Figure 6.120. Decay of **1** with 20 mol% Zn-$Cp_2Ti(camphorsulfonate)_2$

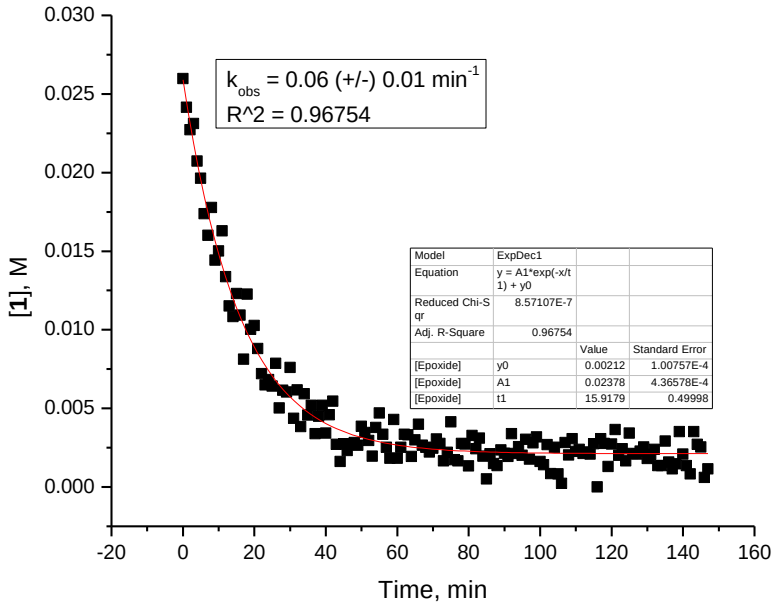

Figure 6.121. Decay of **1** with 20 mol% Zn-$Cp_2Ti(OMs)_2$

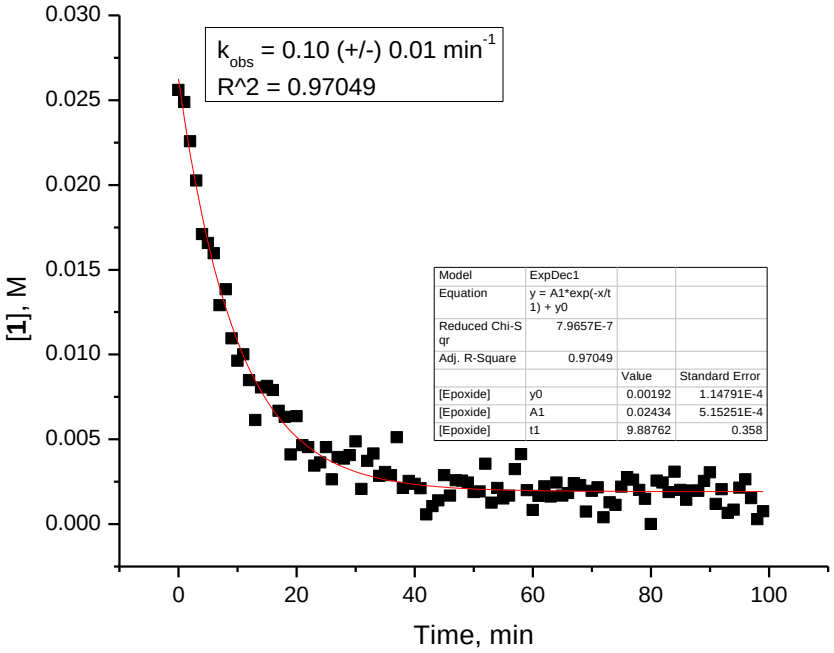

Figure 6.122. Decay of **1** with 20 mol% Zn-$Cp_2Ti(OTs)_2$

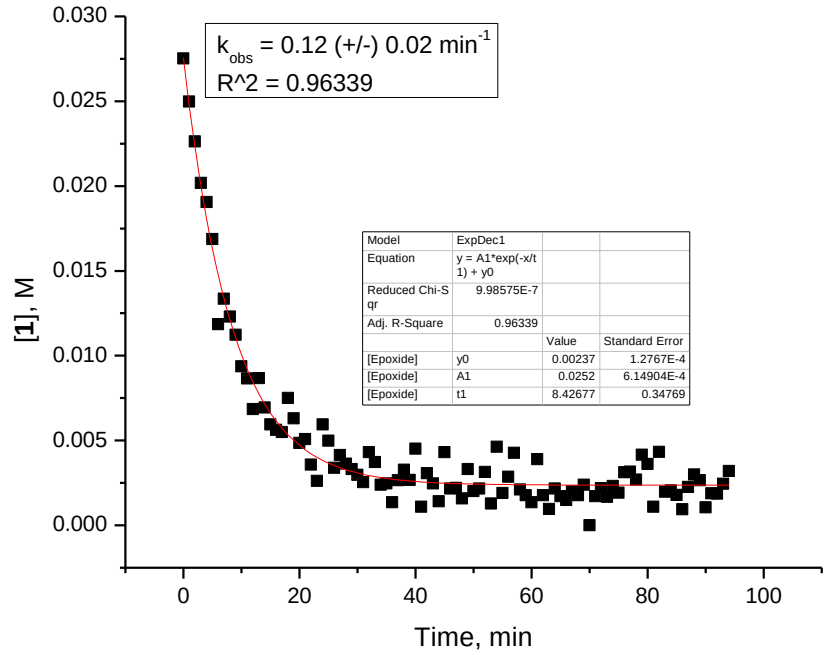

Figure 6.123. Decay of **1** with 20 mol% Zn-$Cp_2Ti(O_2C_2F_3)_2$

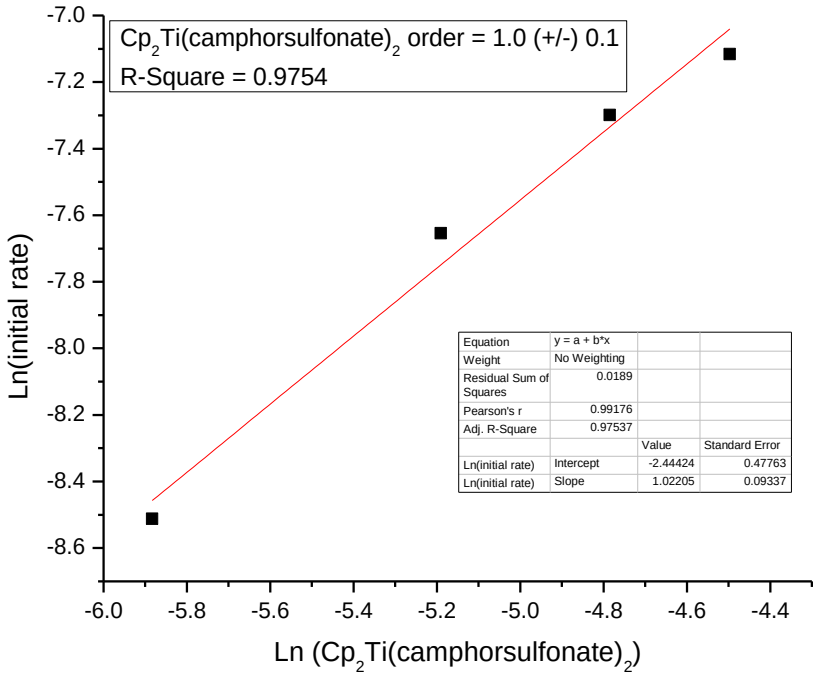

Figure 6.124. Plot of Ln (Initial rate) vs. Ln ($Cp_2Ti(camphorsulfonate)_2$)

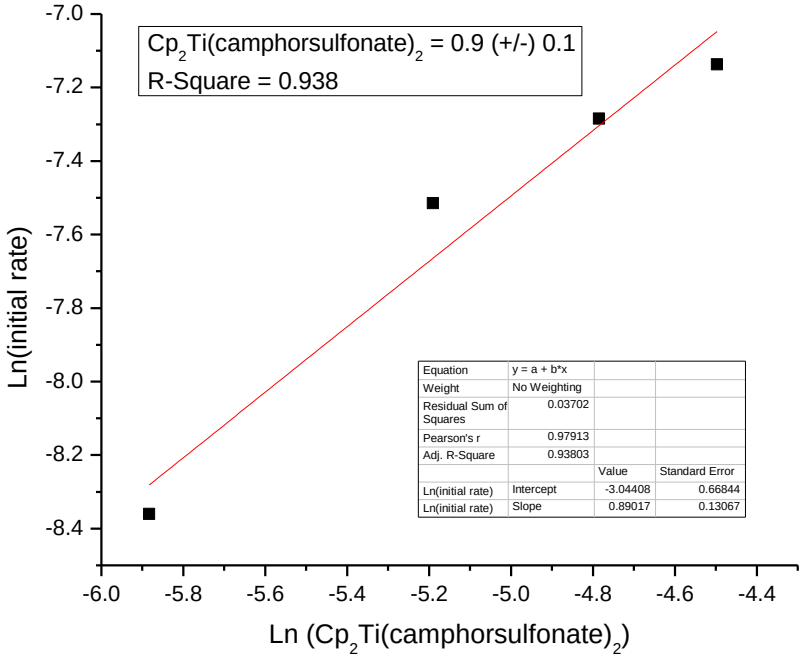

Figure 6.125. Plot of Ln (Initial rate) vs. Ln ($Cp_2Ti(camphorsulfonate)_2$) (Repeat)

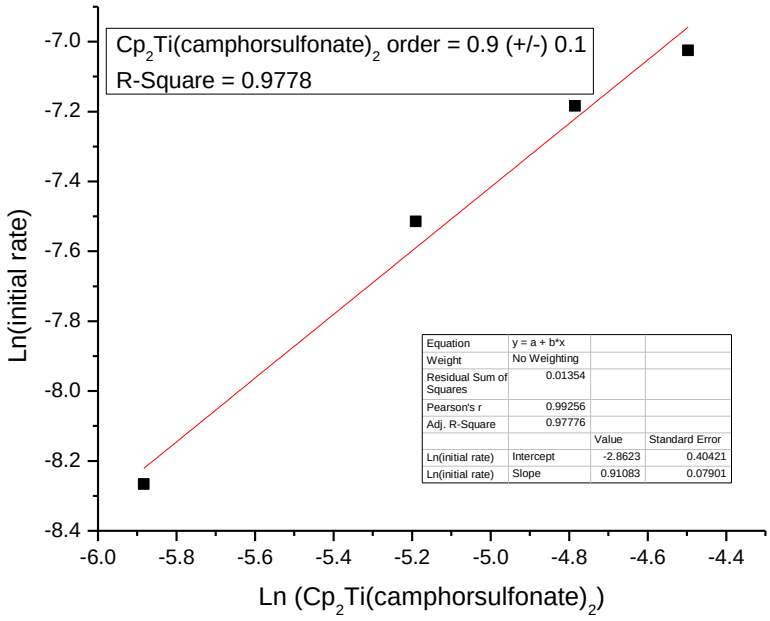

Figure 6.126. Plot of Ln (Initial rate) vs. Ln ($Cp_2Ti(camphorsulfonate)_2$) (2nd Repeat)

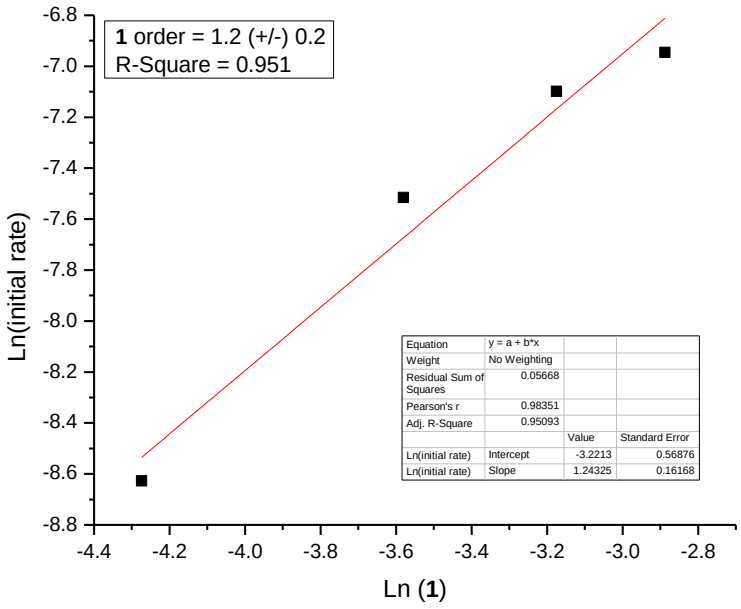

Figure 6.127. Plot of Ln (Initial rate) vs. Ln (**1**) with Zn-$Cp_2Ti(camphorsulfonate)_2$

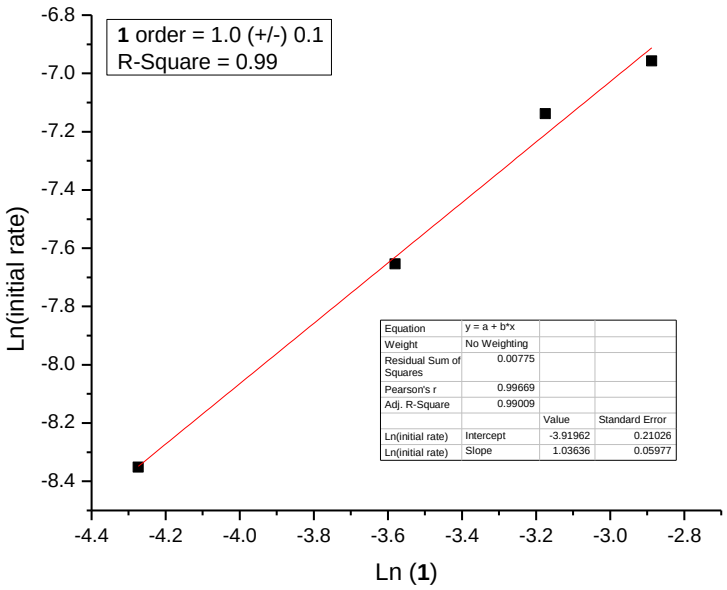

Figure 6.128. Plot of Ln (Initial rate) vs. Ln (**1**) with Zn-$Cp_2Ti(camphorsulfonate)_2$ (Repeat)

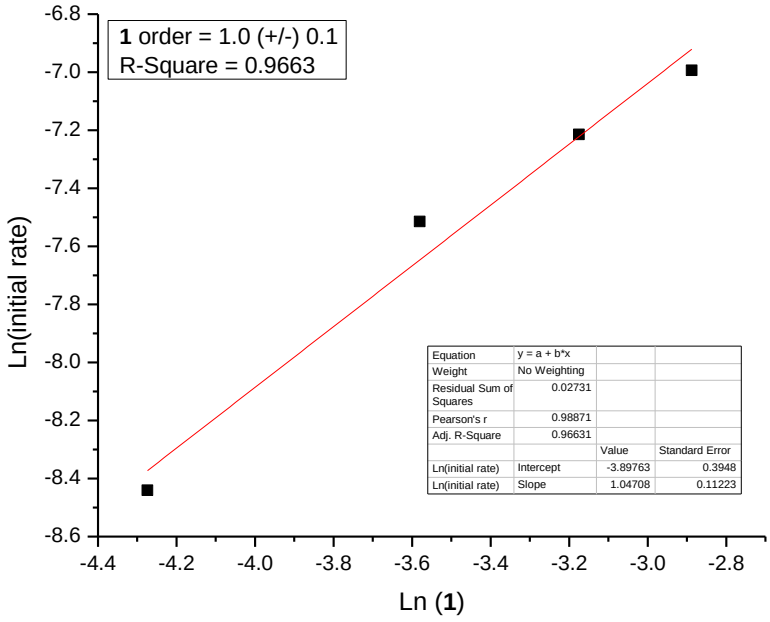

Figure 6.129. Plot of Ln (Initial rate) vs. Ln (**1**) with Zn-$Cp_2Ti(camphorsulfonate)_2$ (2^{nd} Repeat)

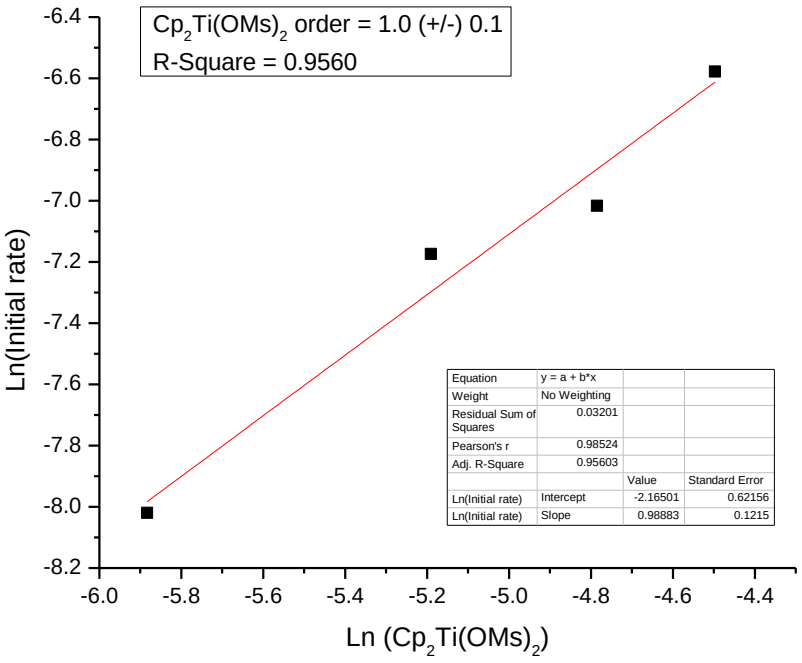

Equation	y = a + b*x		
Weight	No Weighting		
Residual Sum of Squares	0.03201		
Pearson's r	0.98524		
Adj. R-Square	0.95603		
		Value	Standard Error
Ln(Initial rate)	Intercept	-2.16501	0.62156
Ln(Initial rate)	Slope	0.98883	0.1215

Figure 6.130. Plot of Ln (Initial rate) vs. Ln ($Cp_2Ti(OMs)_2$)

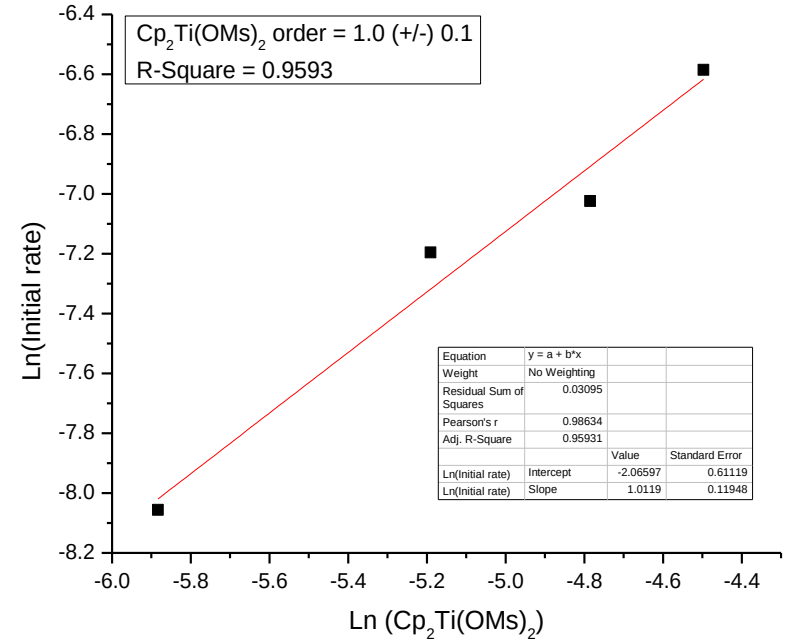

Equation	y = a + b*x		
Weight	No Weighting		
Residual Sum of Squares	0.03095		
Pearson's r	0.98634		
Adj. R-Square	0.95931		
		Value	Standard Error
Ln(Initial rate)	Intercept	-2.06597	0.61119
Ln(Initial rate)	Slope	1.0119	0.11948

Figure 6.131. Plot of Ln (Initial rate) vs. Ln ($Cp_2Ti(OMs)_2$) (Repeat)

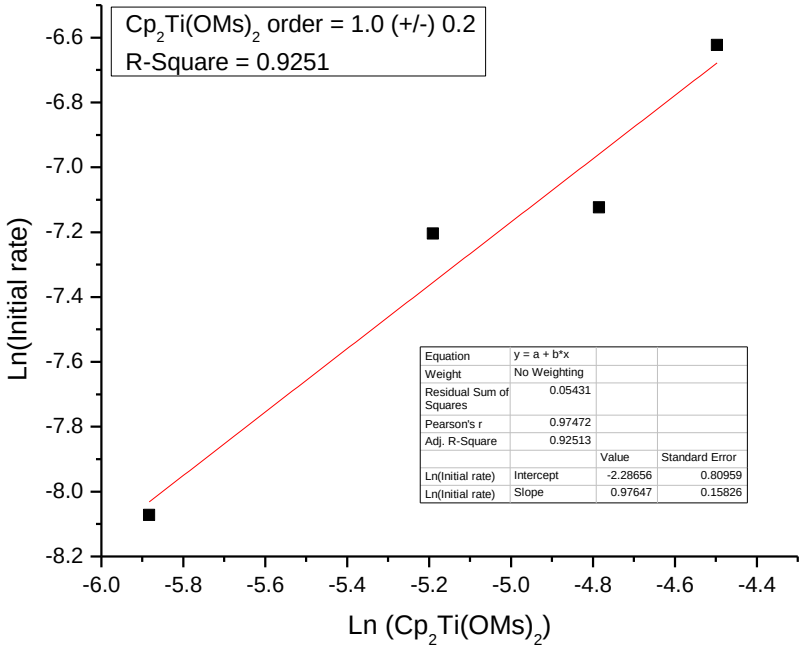

Figure 6.132. Plot of Ln (Initial rate) vs. Ln ($Cp_2Ti(OMs)_2$) (2nd Repeat)

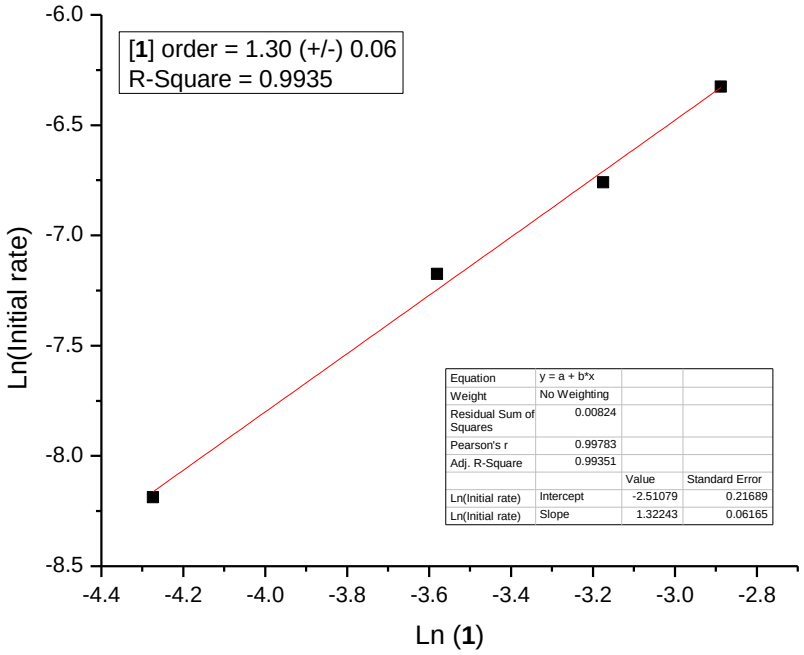

Figure 6.133. Plot of Ln (Initial rate) vs. Ln (**1**) with Zn-$Cp_2Ti(OMs)_2$

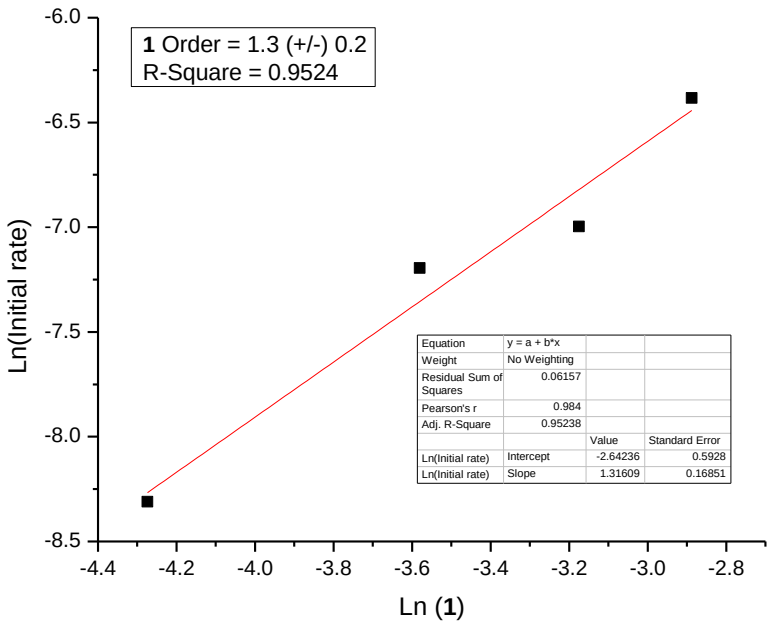

Figure 6.134. Plot of Ln (Initial rate) vs. Ln (**1**) with Zn-$Cp_2Ti(OMs)_2$ (Repeat)

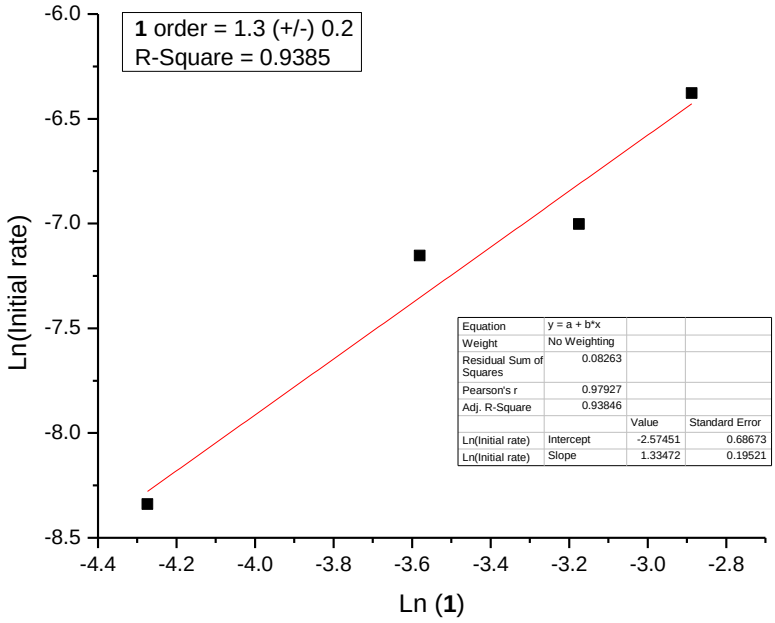

Figure 6.135. Plot of Ln (Initial rate) vs. Ln (**1**) with Zn-$Cp_2Ti(OMs)_2$ (2^{nd} Repeat)

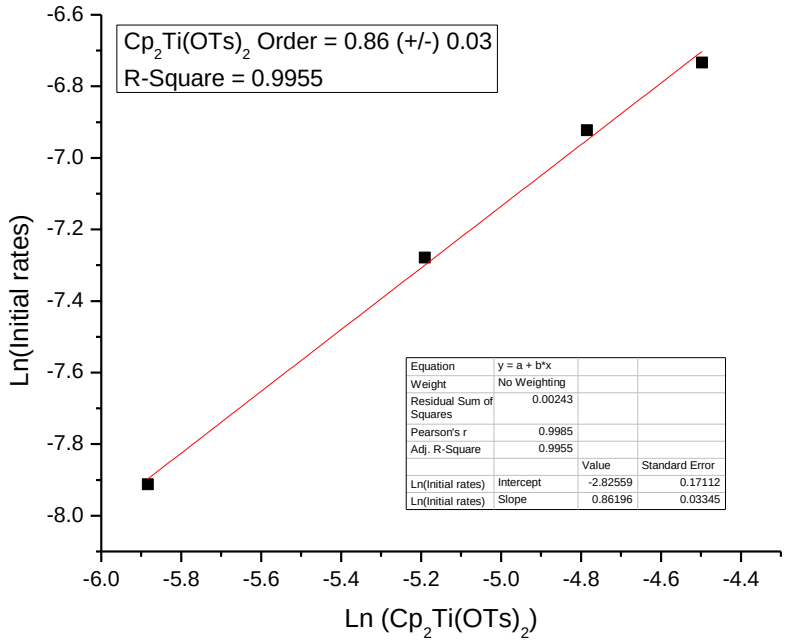

Figure 6.136. Plot of Ln (Initial rate) vs. Ln ($Cp_2Ti(OTs)_2$)

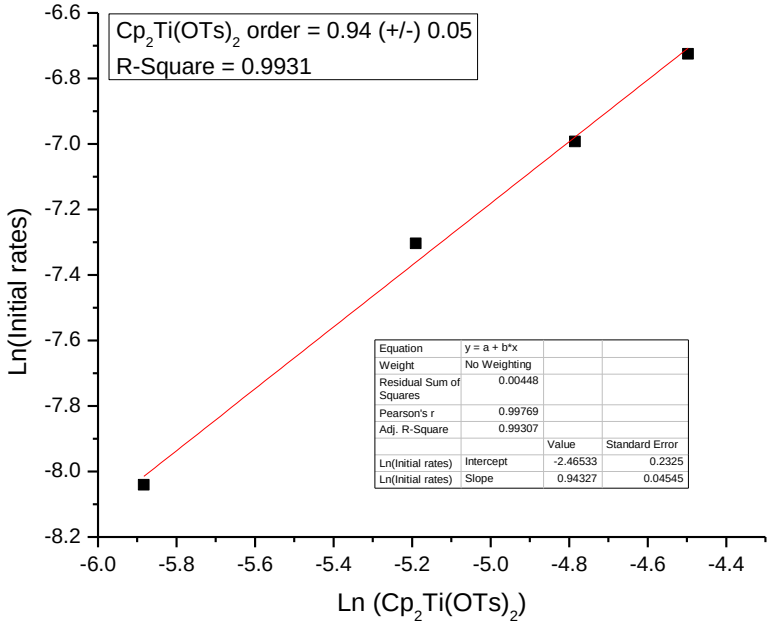

Figure 6.137. Plot of Ln (Initial rate) vs. Ln ($Cp_2Ti(OTs)_2$) (Repeat)

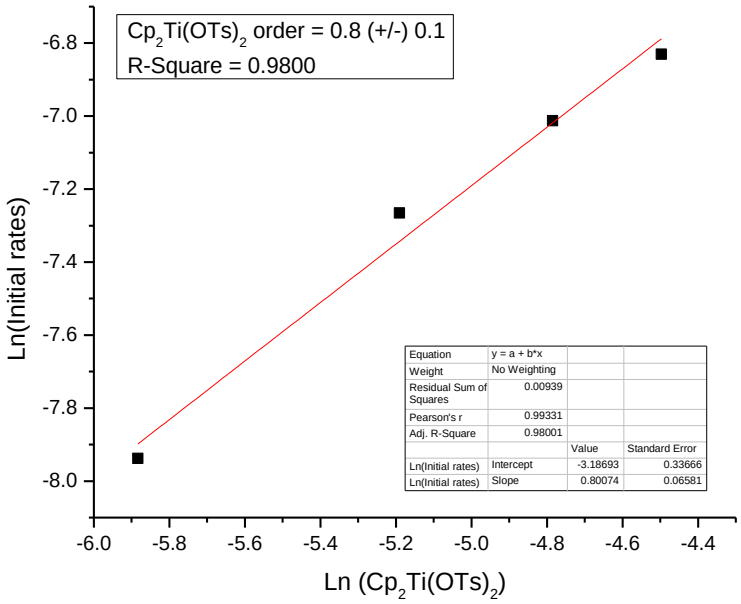

Figure 6.138. Plot of Ln (Initial rate) vs. Ln ($Cp_2Ti(OTs)_2$) (2nd Repeat)

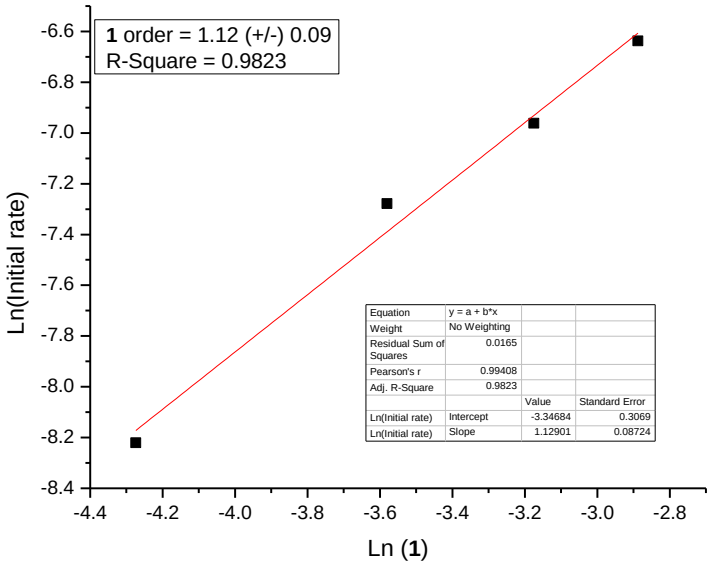

Figure 6.139. Plot of Ln (Initial rate) vs. Ln (**1**) with Zn-$Cp_2Ti(OTs)_2$

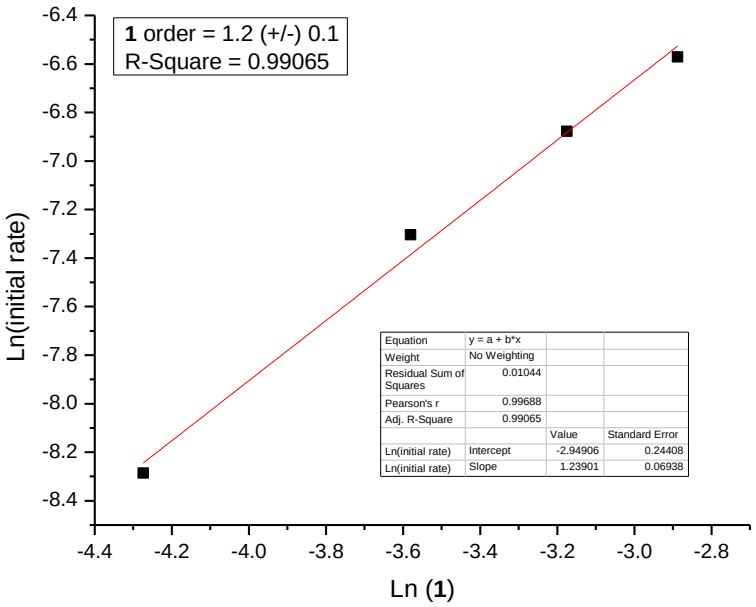

Figure 6.140. Plot of Ln (Initial rate) vs. Ln (**1**) with Zn-$Cp_2Ti(OTs)_2$ (Repeat)

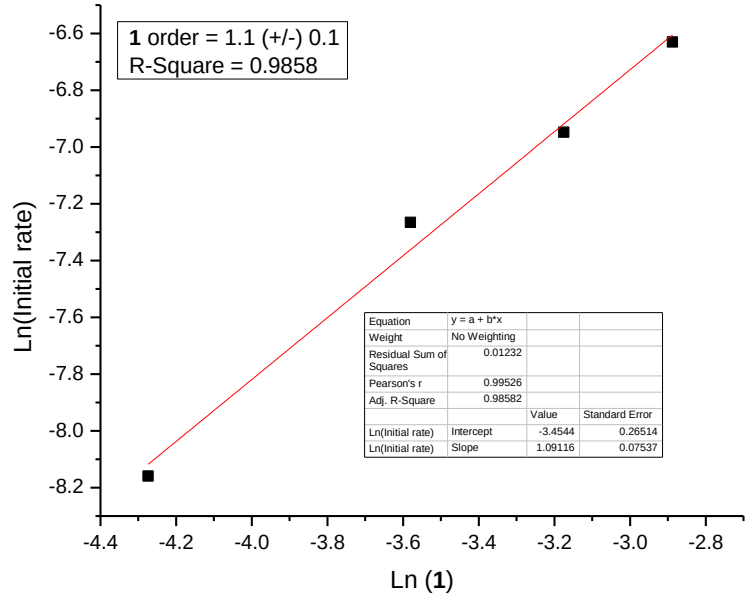

Figure 6.141. Plot of Ln (Initial rate) vs. Ln (**1**) with Zn-$Cp_2Ti(OTs)_2$ (2^{nd} Repeat)

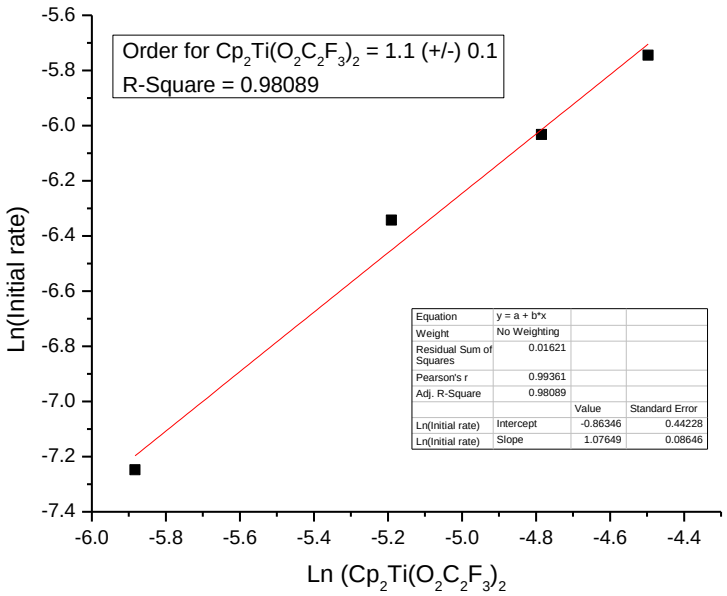

Figure 6.142. Plot of Ln (Initial rate) vs. Ln ($Cp_2Ti(O_2C_2F_3)_2$)

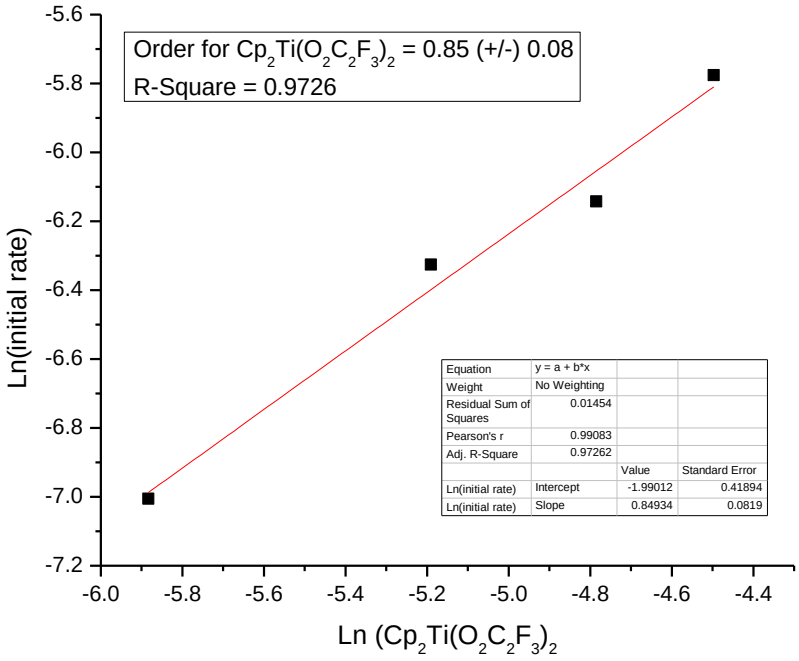

Figure 6.143. Plot of Ln (Initial rate) vs. Ln ($Cp_2Ti(O_2C_2F_3)_2$) (Repeat)

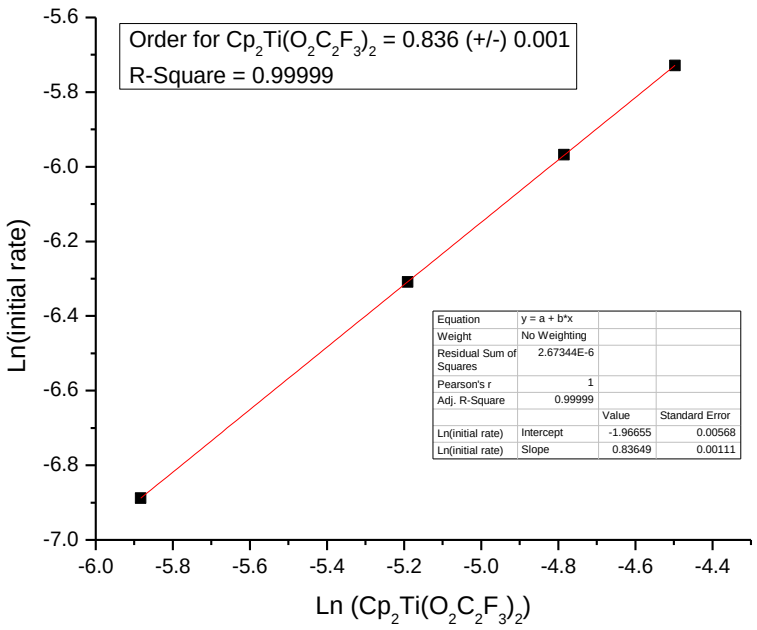

Figure 6.144. Plot of Ln (Initial rate) vs. Ln ($Cp_2Ti(O_2C_2F_3)_2$) (2nd Repeat)

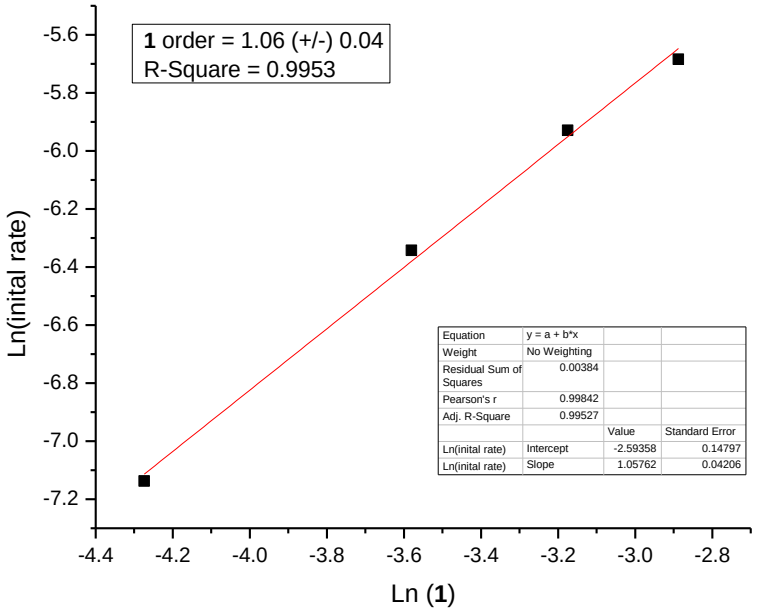

Figure 6.145. Plot of Ln (Initial rate) vs. Ln (**1**) with Zn-$Cp_2Ti(O_2C_2F_3)_2$

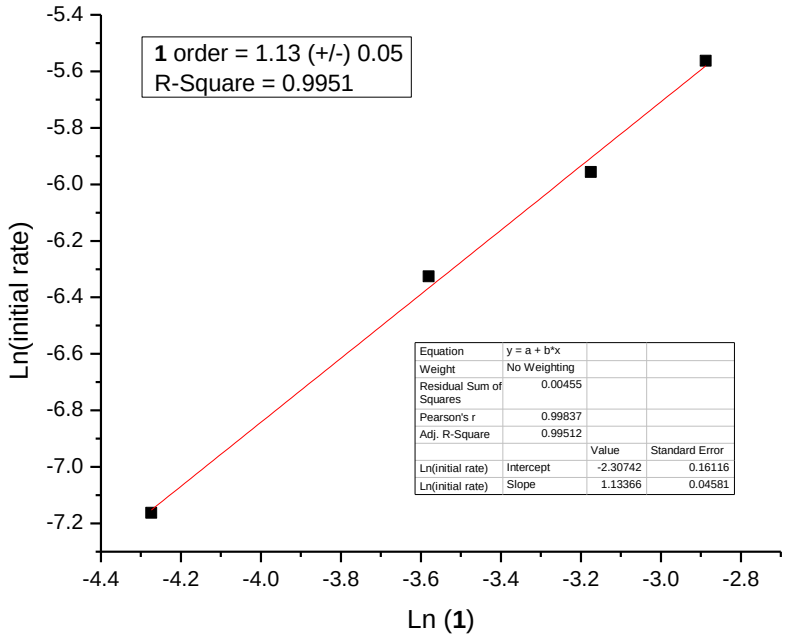

Figure 6.146. Plot of Ln (Initial rate) vs. Ln (**1**) with Zn-$Cp_2Ti(O_2C_2F_3)_2$ (Repeat)

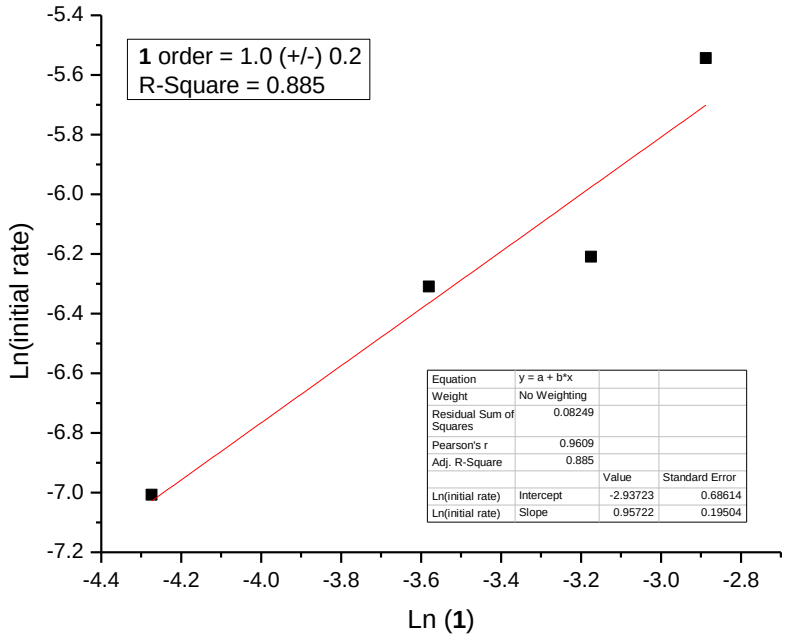

Figure 6.147. Plot of Ln (Initial rate) vs. Ln (**1**) with Zn-$Cp_2Ti(O_2C_2F_3)_2$ (2nd Repeat)

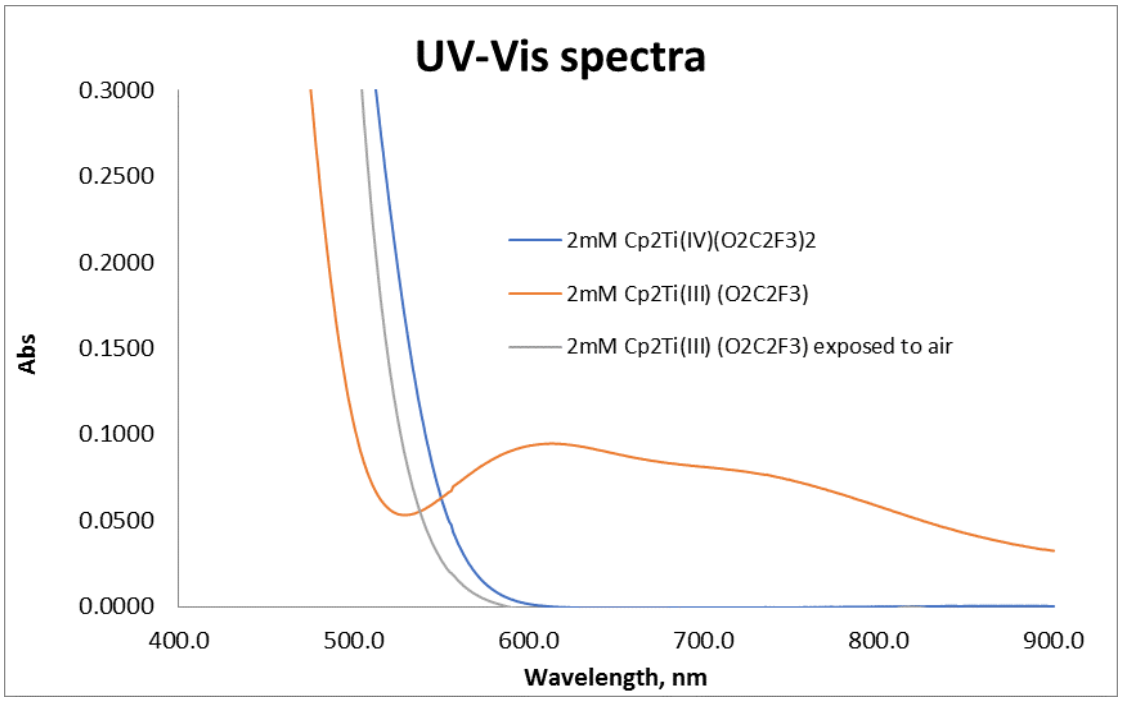

Figure 6.148. UV-Vis spectra for $Cp_2Ti(O_2C_2F_3)_2$, $Cp_2Ti(O_2C_2F_3)$, $Cp_2Ti(O_2C_2F_3)$ exposed to air

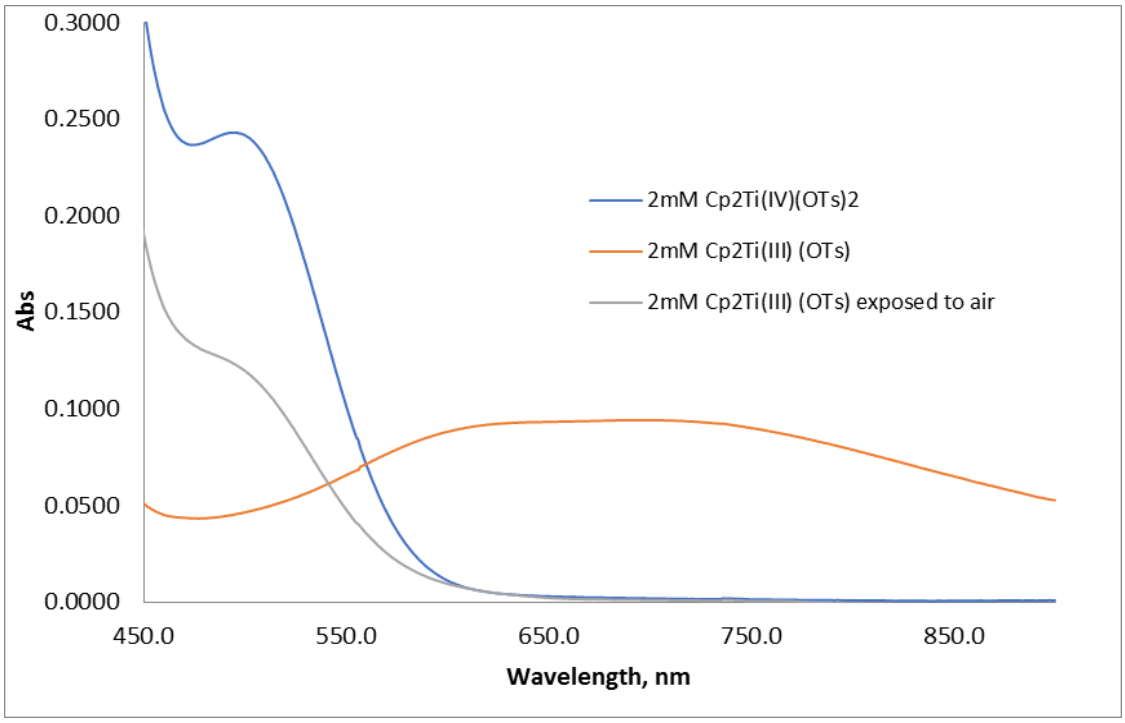

Figure 6.149. UV-Vis spectra for $Cp_2Ti(OTs)_2$, Cp_2Ti (OTs), Cp_2Ti (OTs) exposed to air

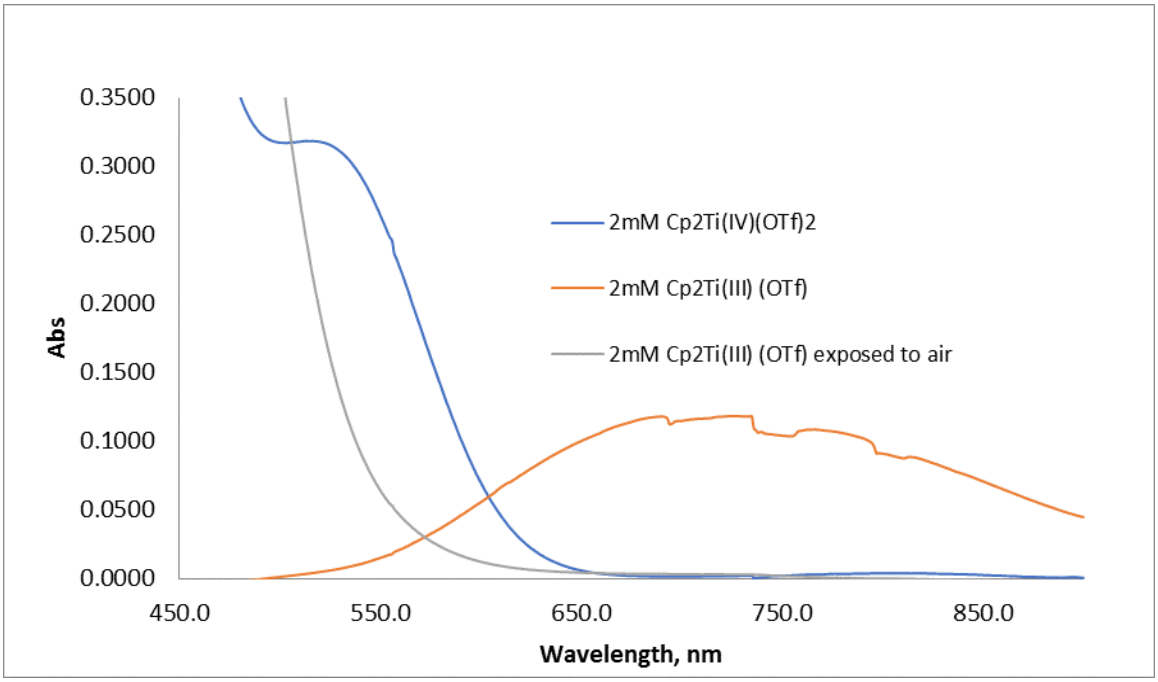

Figure 6.150. UV-Vis spectra for $Cp_2Ti(OTf)_2$, Cp_2Ti (OTf), Cp_2Ti(OTf) exposed to air

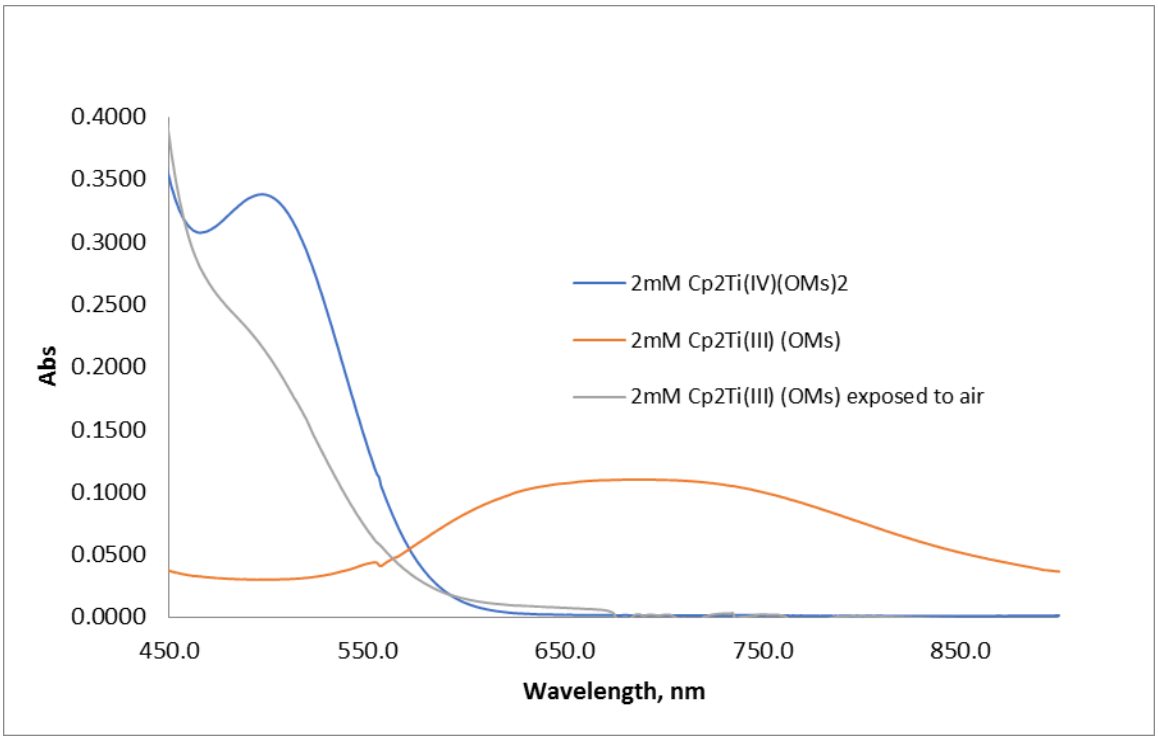

Figure 6.151. UV-Vis spectra for $Cp_2Ti(OMs)_2$, Cp_2Ti(OMs), Cp_2Ti(OMs) exposed to air

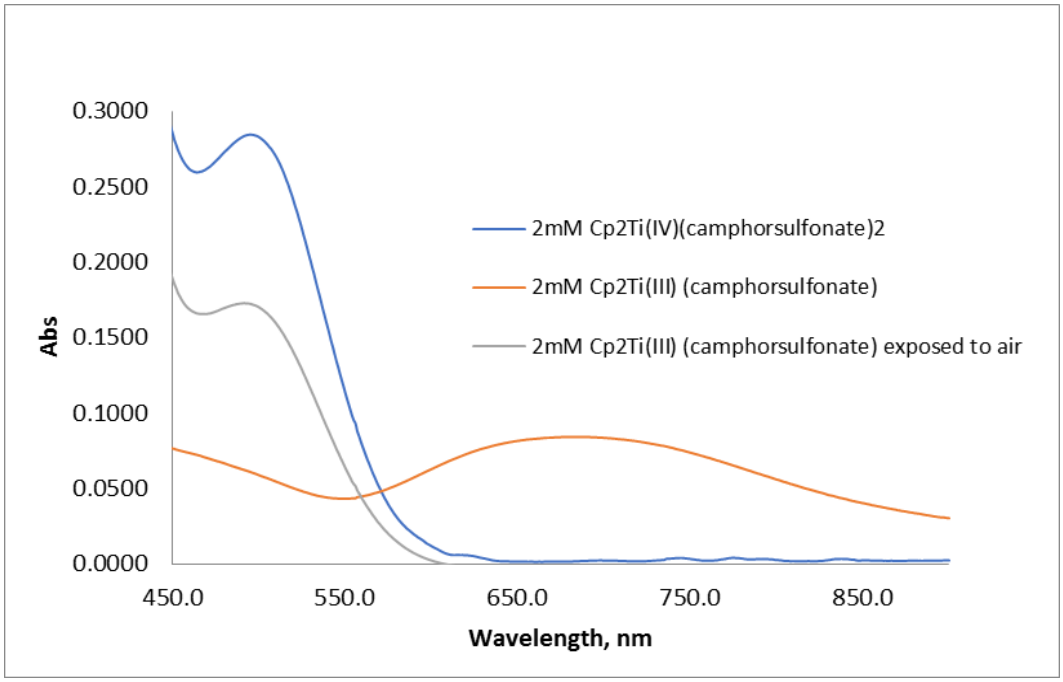

Figure 6.152. UV-Vis spectra for $Cp_2Ti(camphorsulfonate)_2$, Cp_2Ti (camphorsulfonate), Cp_2Ti (camphorsulfonate) exposed to air

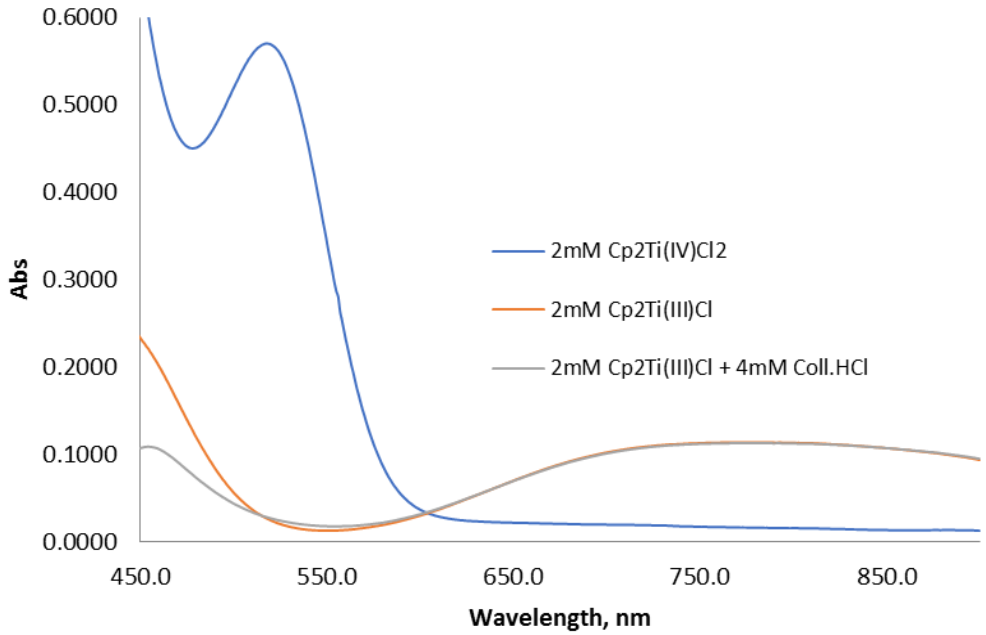

Figure 6.153. UV-Vis spectra for Cp_2TiCl_2, Cp_2TiCl, Cp_2TiCl + Coll*HCl

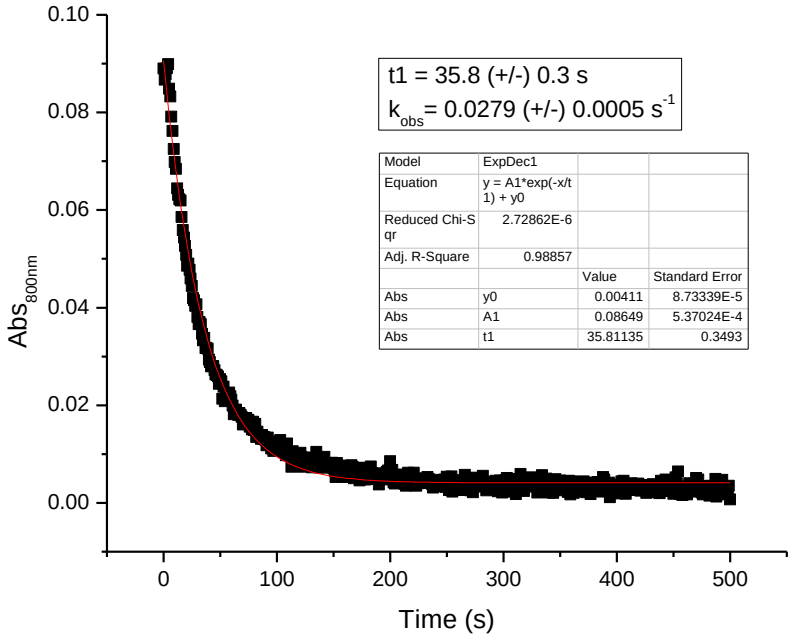

Figure 6.154. Decay of Cp_2TiCl when 50µL (20 mM) **14** is added

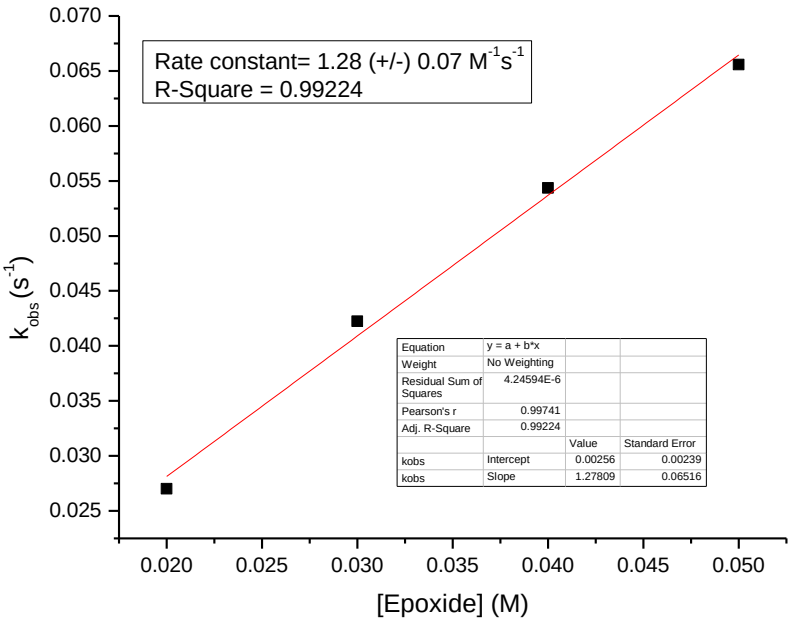

Figure 6.155. Plot of k_{obs} versus [**17**] for Cp_2TiCl with Coll*HCl as additive

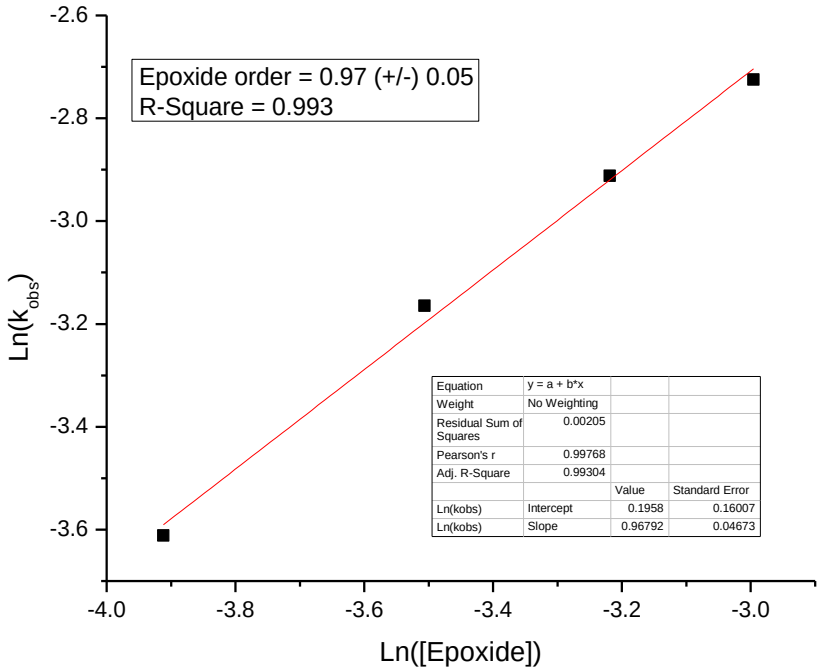

Figure 6.156. Plot of Ln(k_{obs}) versus Ln ([**14**]) for Cp_2TiCl with Coll*HCl

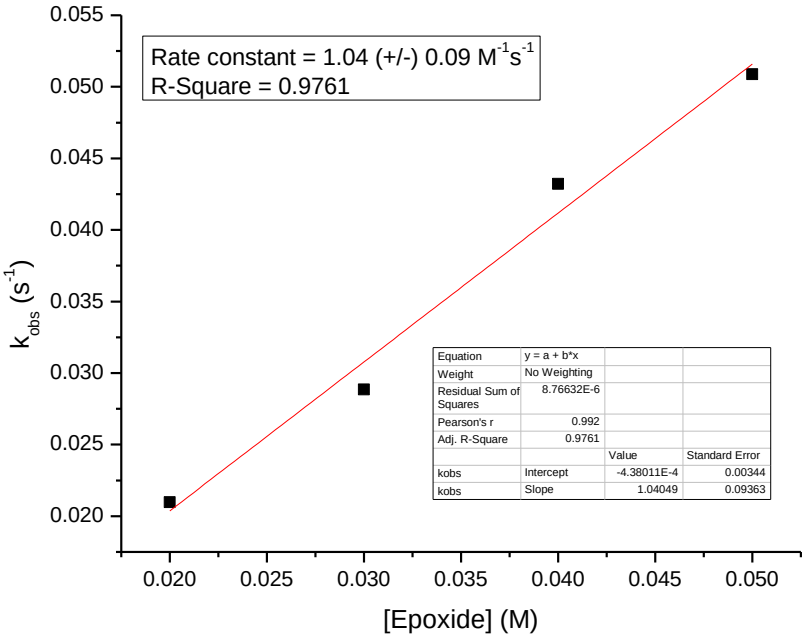

Figure 6.157. Repeat for plot of k_{obs} versus [**14**] for Cp_2TiCl with Coll*HCl as additive

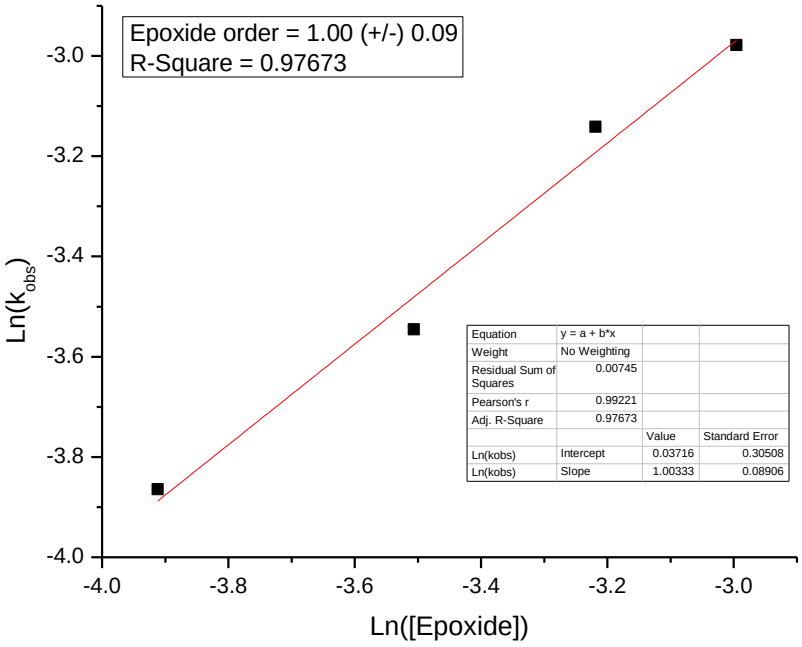

Figure 6.158. Repeat plot of Ln(k_{obs}) versus Ln ([**14**]) for $Cp_2Ti(Cl)$ with Coll*HCl

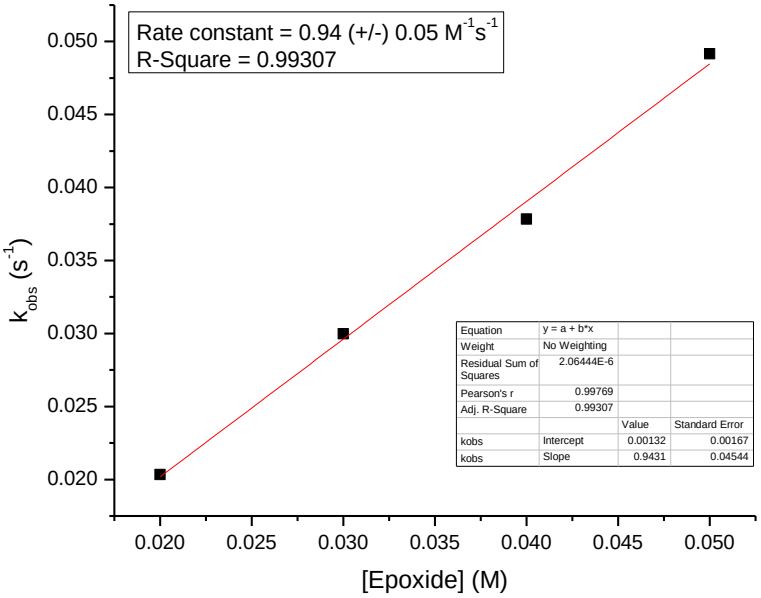

Figure 6.159. Repeat 2 for the plot of k_{obs} versus [**14**] for $Cp_2Ti(Cl)$ with Coll*HCl as additive

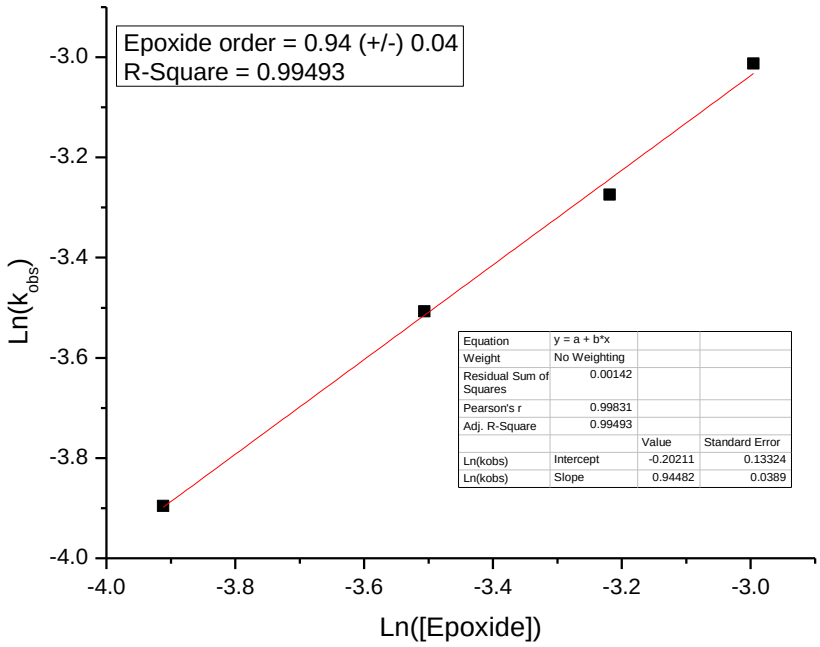

Figure 6.160. Repeat 2 plot of Ln(k_{obs}) versus Ln ([**14**]) for $Cp_2Ti(Cl)$ with Coll*HCl

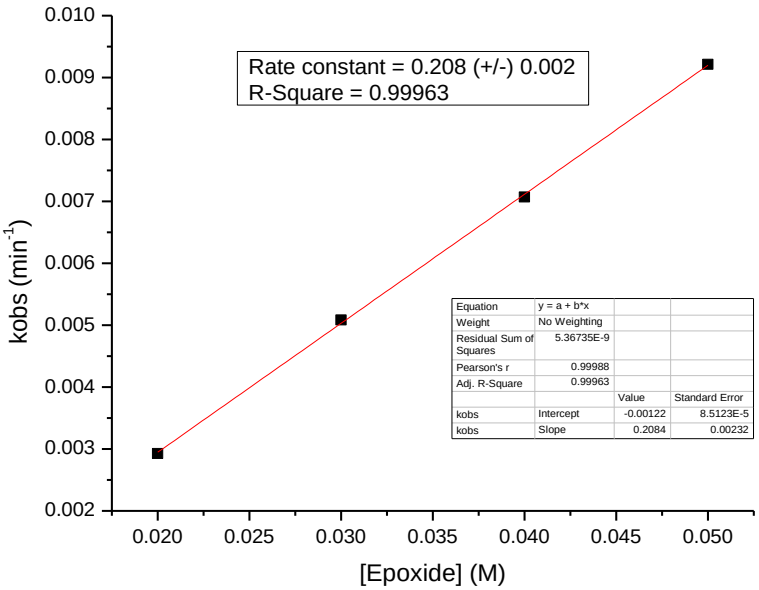

Figure 6.161. Plot of k_{obs} versus [**14**] for $Cp_2Ti(OTf)$ with 1,4-cyclohexadiene (CHD) as additive

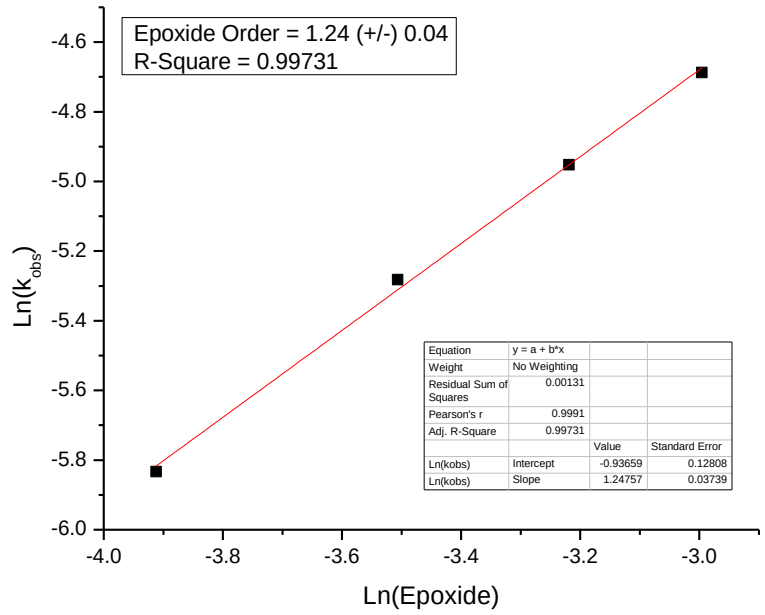

Figure 6.162. Plot of Ln(k_{obs}) versus Ln ([**14**]) for $Cp_2Ti(OTf)$ with 1,4-cyclohexadiene (CHD) as additive

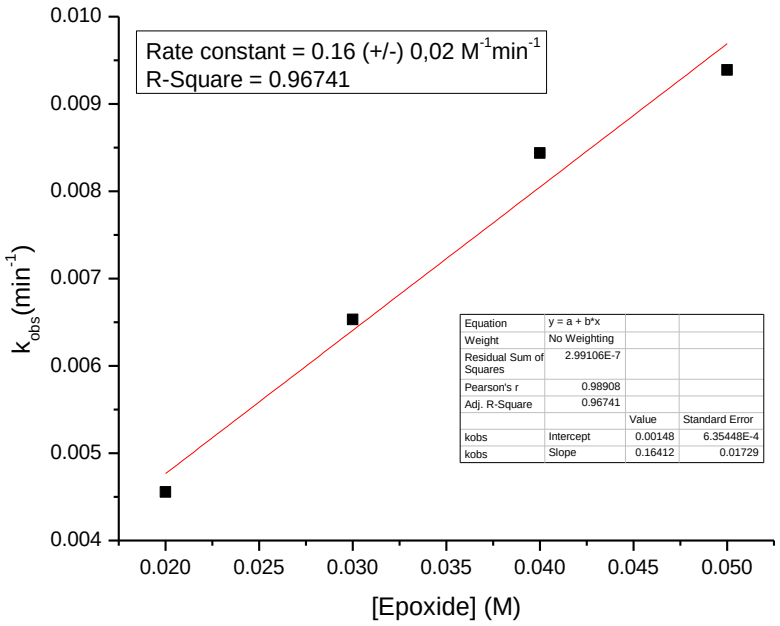

Figure 6.163. Repeat plot of k_{obs} versus [**14**] for $Cp_2Ti(OTf)$ with 1,4-cyclohexadiene (CHD) as additive

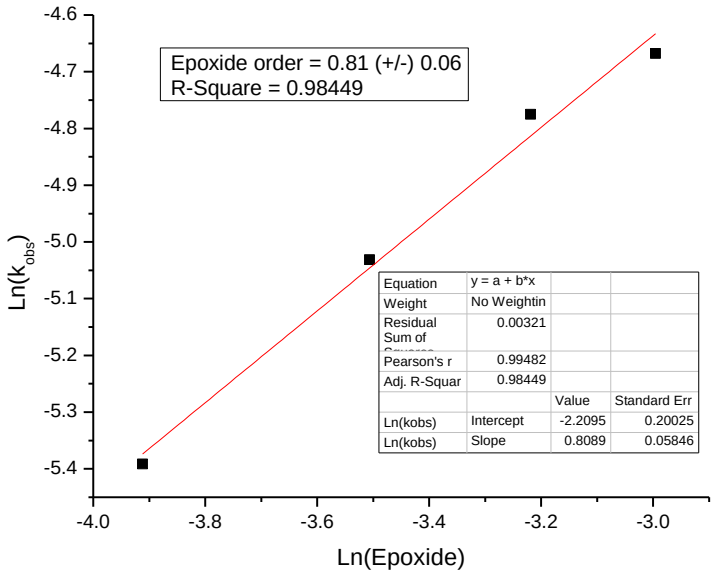

Figure 6.164. Repeat of plot of Ln(k_{obs}) versus Ln ([**14**]) for $Cp_2Ti(OTf)$

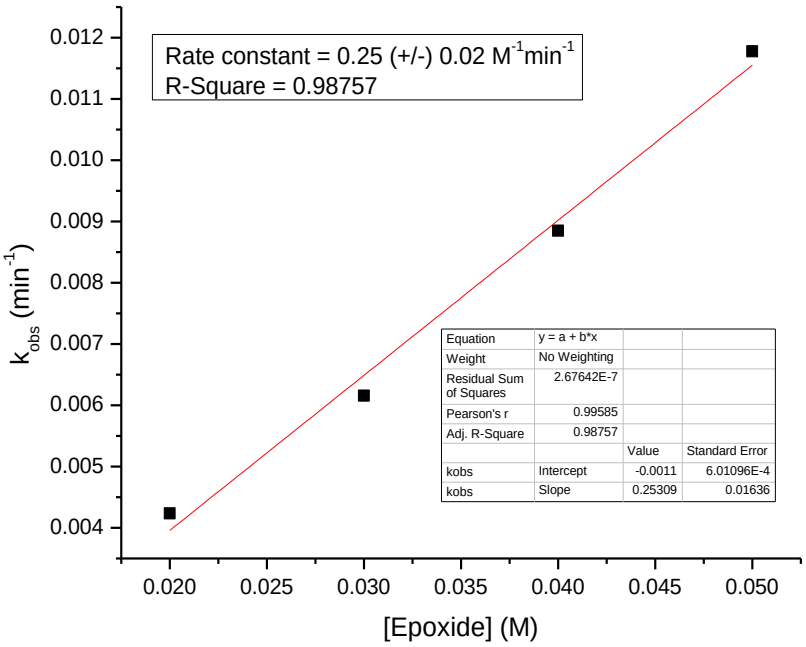

Figure 6.165. Repeat 2 plot of k_{obs} versus [**14**] for $Cp_2Ti(OTf)$ with 1,4-cyclohexadiene (CHD) as additive

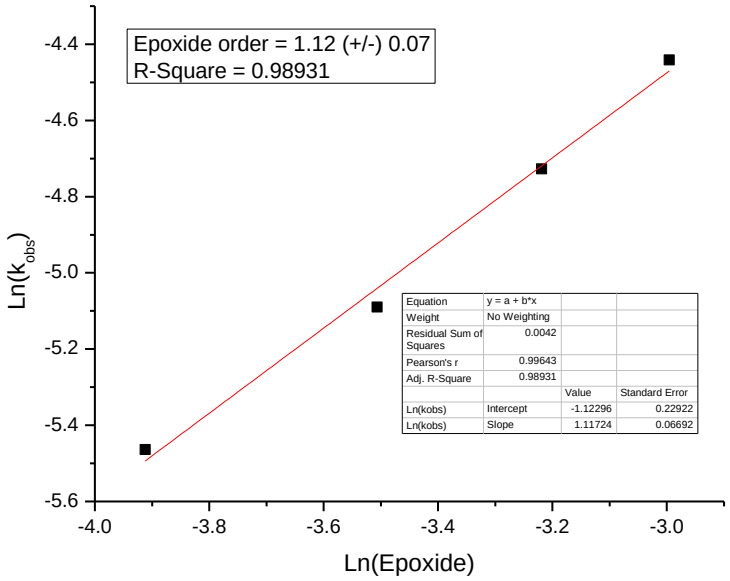

Figure 6.166. Repeat 2 of plot of Ln(k_{obs}) versus Ln ([**14**]) for $Cp_2Ti(OTf)$ with Coll*HCl

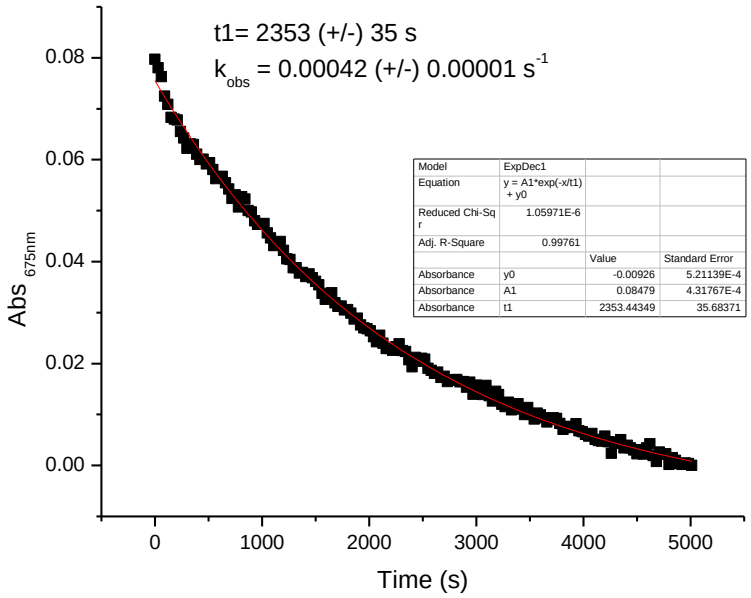

Figure 6.167. Decay of Cp_2Ti(camphorsulfonate) when 50µL (20mM) epoxide **14** is added

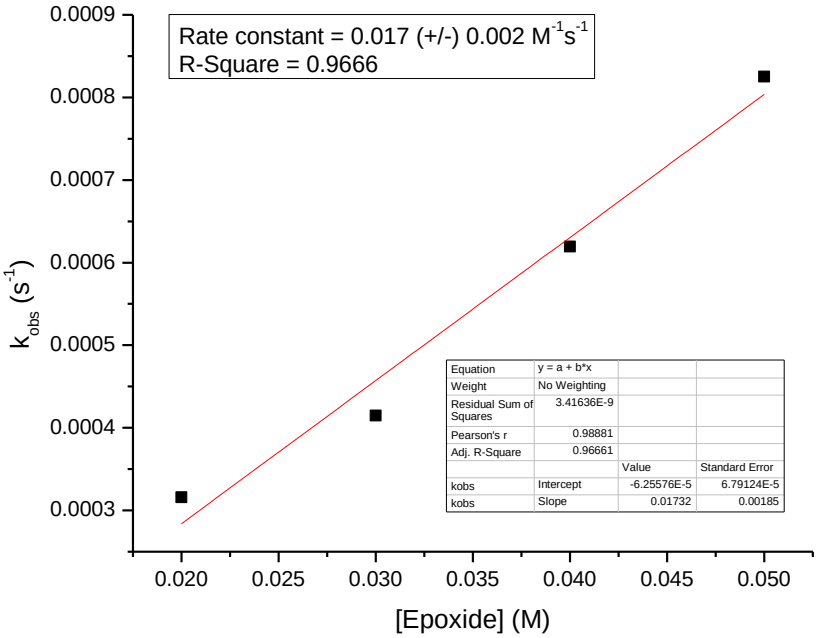

Figure 6.168. Plot of k_{obs} versus [**14**] for Cp_2Ti(camphorsulfonate)

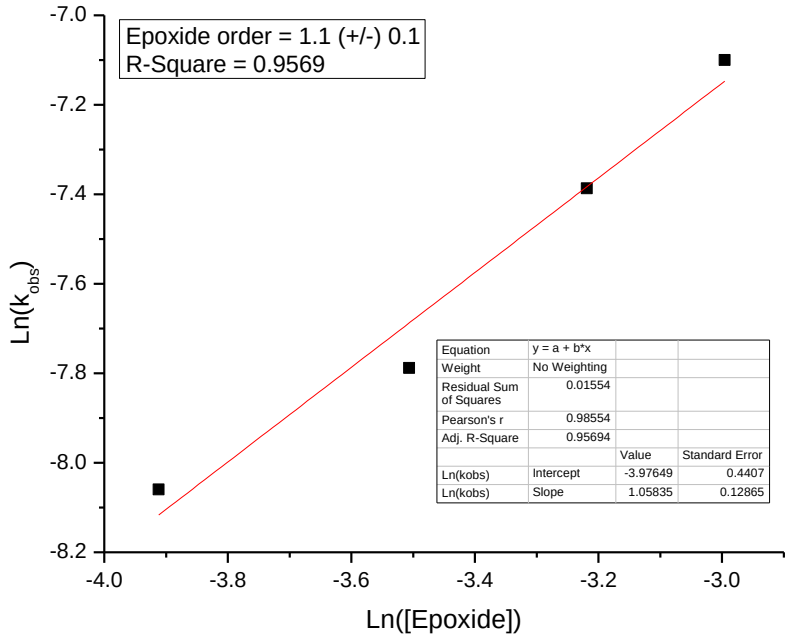

Figure 6.169. Plot of Ln(k_{obs}) versus Ln ([**14**]) for Cp_2Ti(camphorsulfonate)

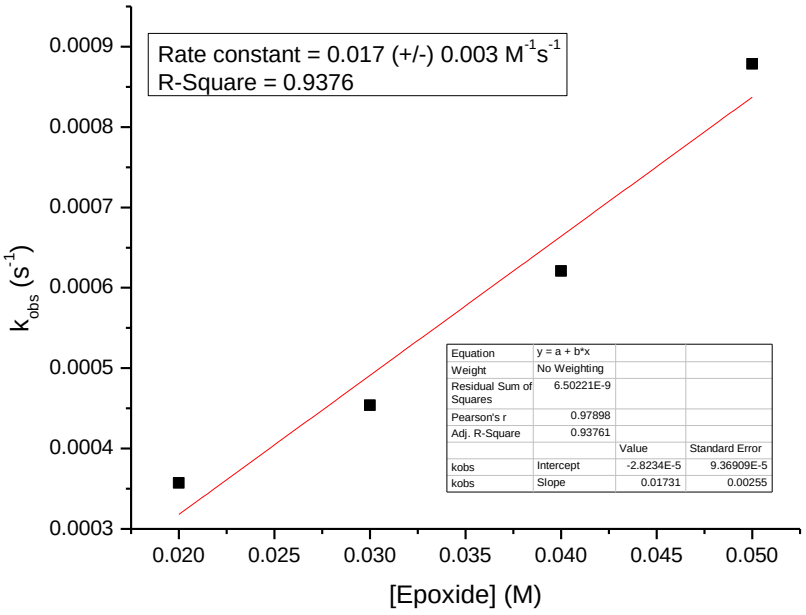

Figure 6.170. Repeat for plot of k_{obs} versus [**14**] for Cp_2Ti(camphorsulfonate)

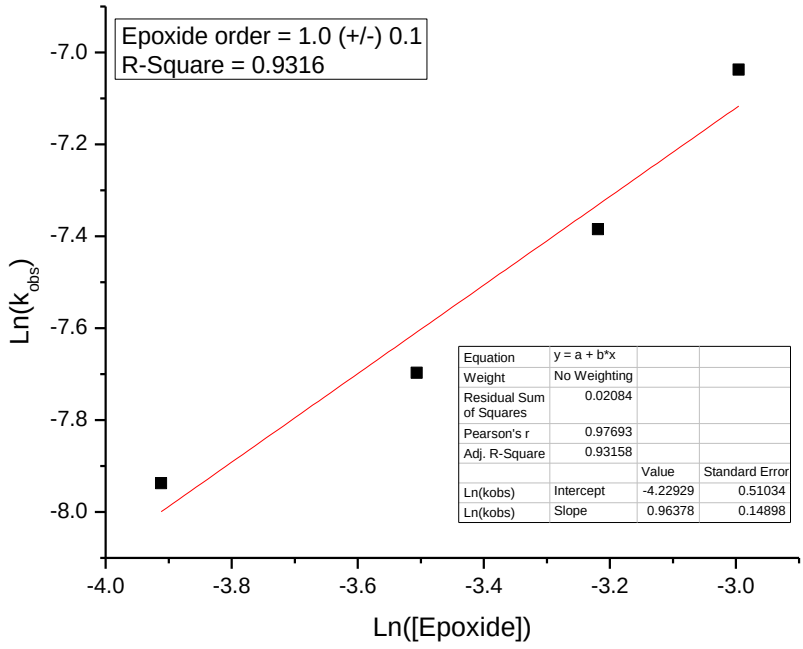

Figure 6.171. Repeat for plot of Ln(k_{obs}) versus Ln ([**14**]) for Cp_2Ti(camphorsulfonate)

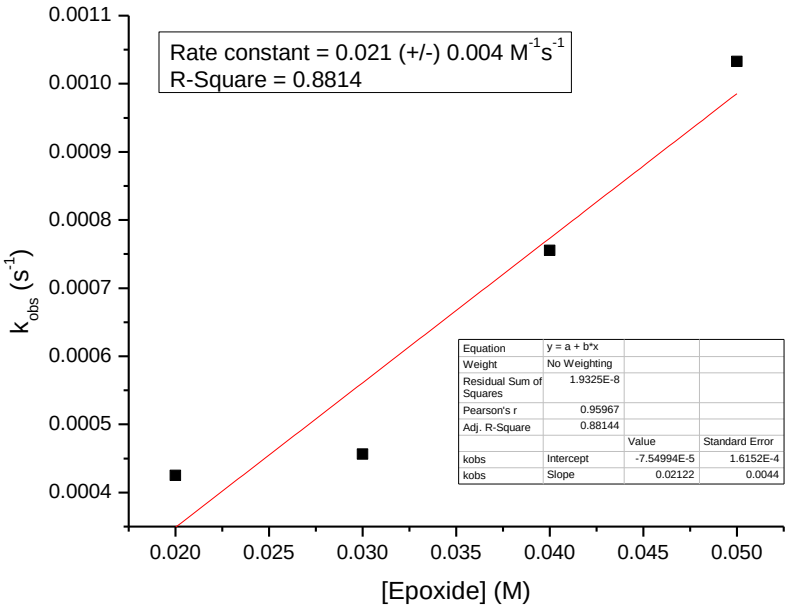

Figure 6.172. Repeat 2 for plot of k_{obs} versus [**14**] for Cp_2Ti (camphorsulfonate)

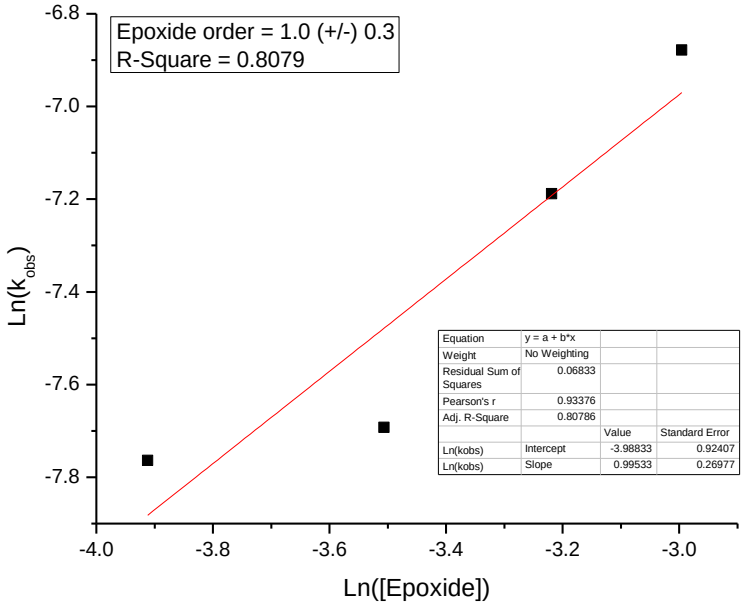

Figure 6.173. Repeat 2 for plot of Ln(k_{obs}) versus Ln ([**14**]) for Cp_2Ti (camphorsulfonate)

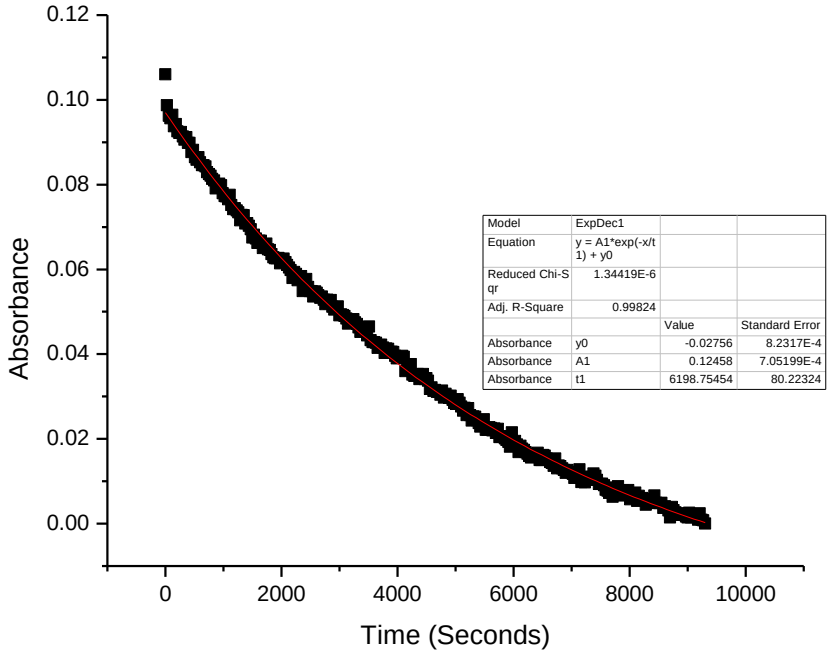

Figure 6.174. Decay of Cp_2Ti(OMS) in THF after addition of 20mM (50µL) of **14**

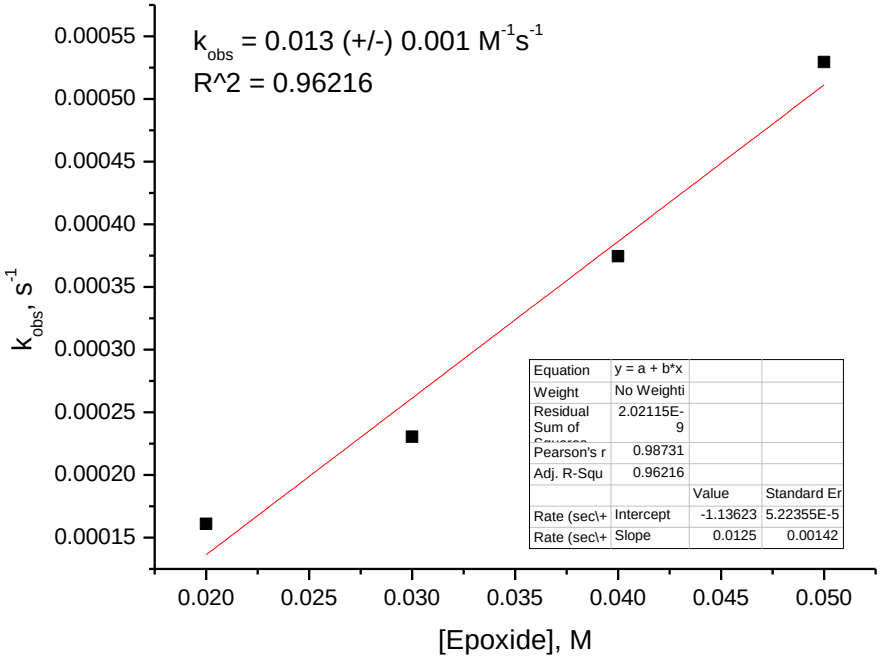

Figure 6.175. Plot of k_{obs} versus [**14**] for Cp_2Ti (OMs)

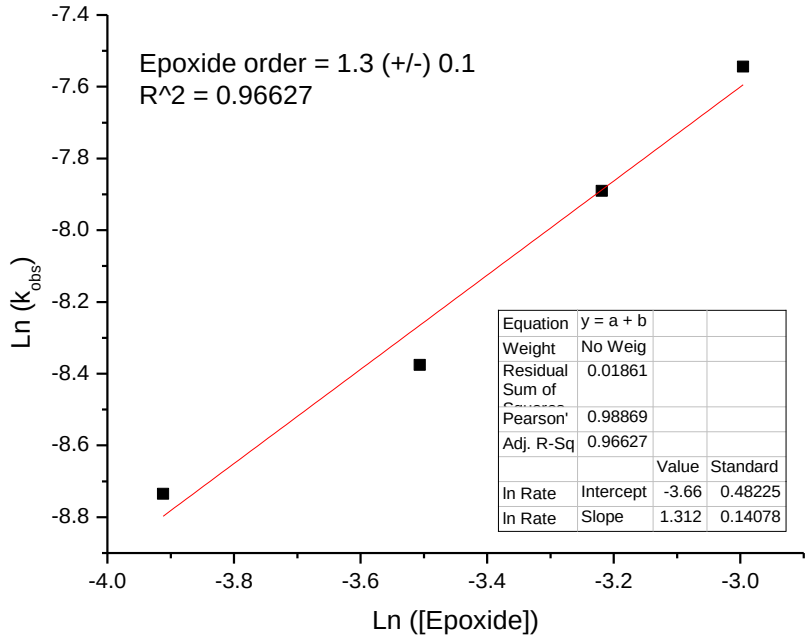

Figure 6.176. Plot of Ln(k_{obs}) versus Ln ([**14**]) for Cp_2Ti (OMs)

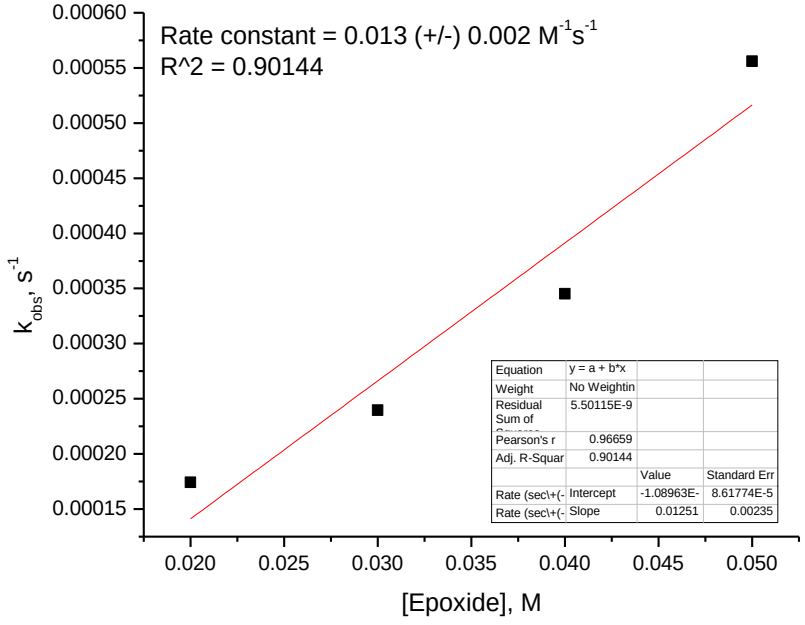

Figure 6.177. Plot of k_{obs} versus [**14**] for Cp_2Ti(OMs) (Repeat)

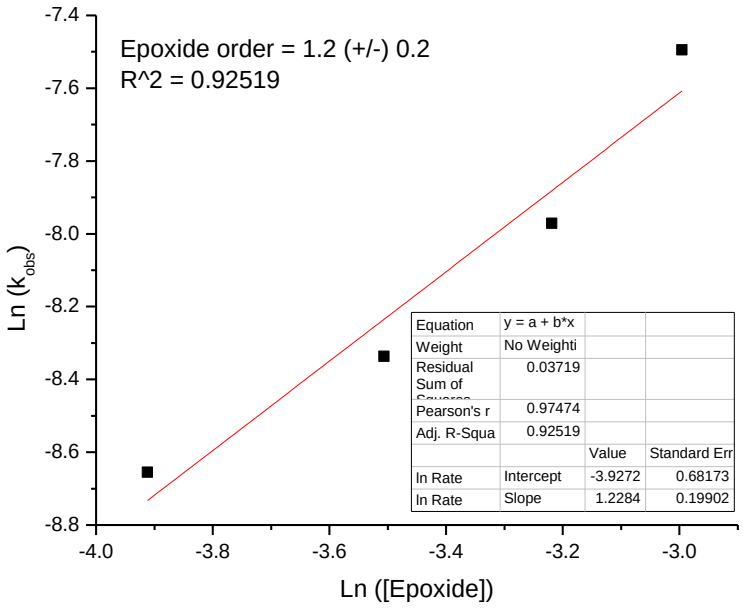

Figure 6.178. Plot of Ln(k_{obs}) versus Ln ([**14**]) for Cp_2Ti (OMs) (Repeat)

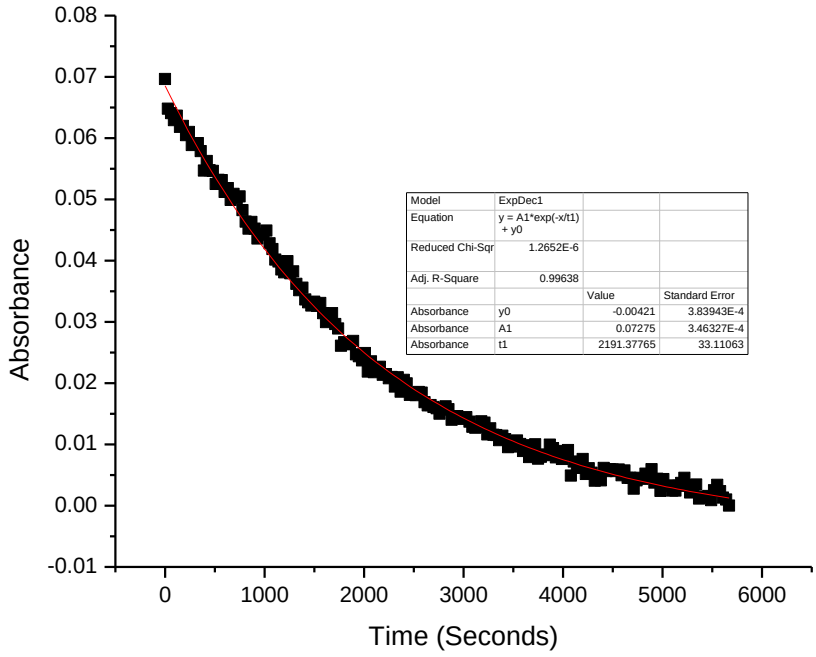

Figure 6.179. Decay of $Cp_2Ti(O_2C_2F_3)$ in THF after addition of 20mM (50µL) of **14**

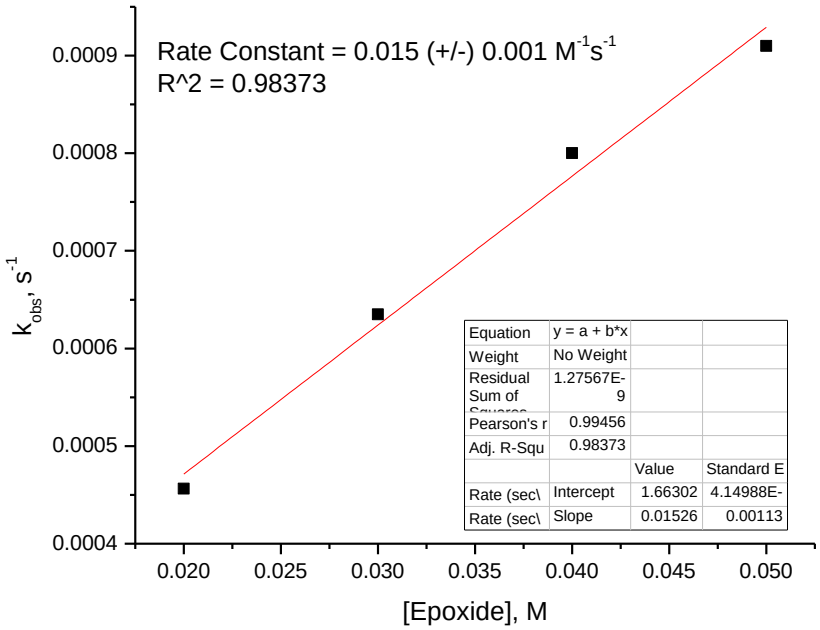

Figure 6.180. Plot of k_{obs} versus [**14**] for $Cp_2Ti(O_2C_2F_3)$

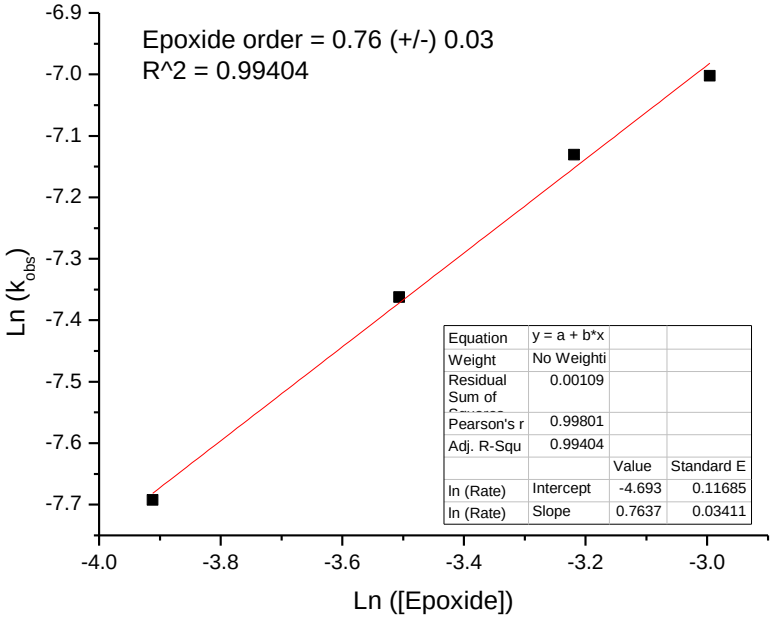

Figure 6.181. Plot of Ln (k_{obs}) versus Ln ([**14**]) for $Cp_2Ti(O_2C_2F_3)$

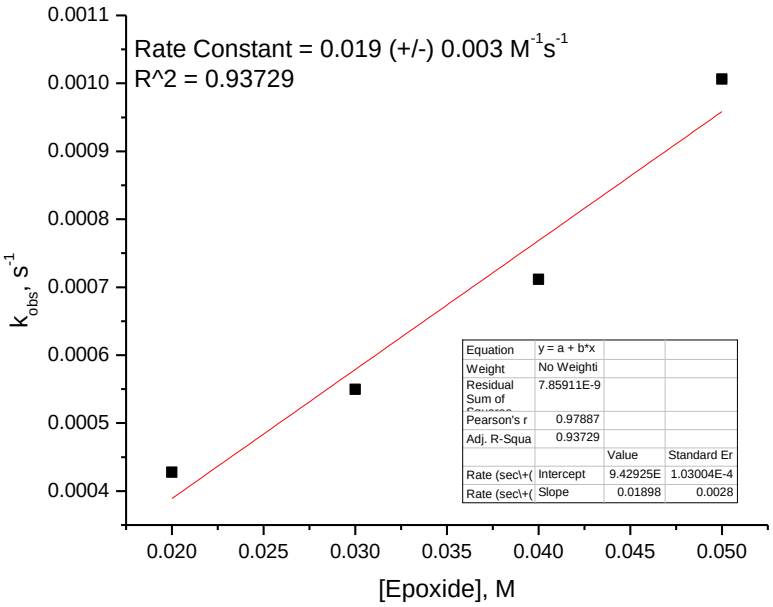

Figure 6.182. Plot of k_{obs} versus [**14**] for $Cp_2Ti(O_2C_2F_3)$ (Repeat)

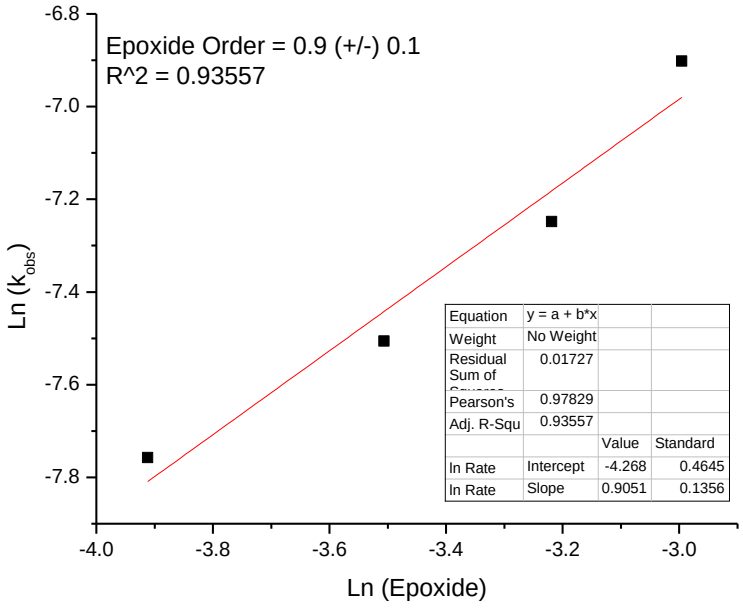

Figure 6.183. Plot of Ln (k_{obs}) versus Ln ([**14**]) for $Cp_2Ti(O_2C_2F_3)$ (Repeat)

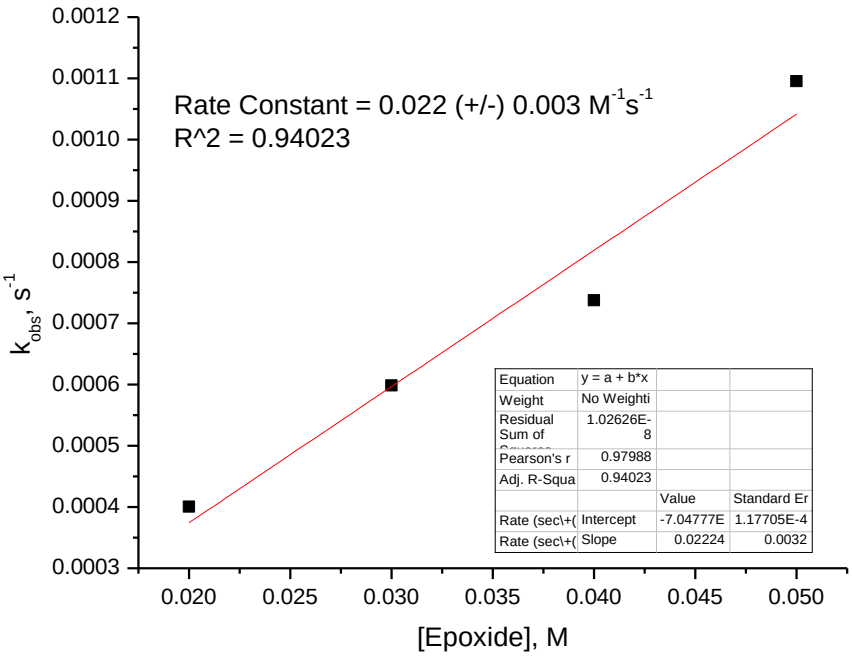

Figure 6.184. Plot of k_{obs} versus [**14**] for $Cp_2Ti(O_2C_2F_3)$ (2nd Repeat)

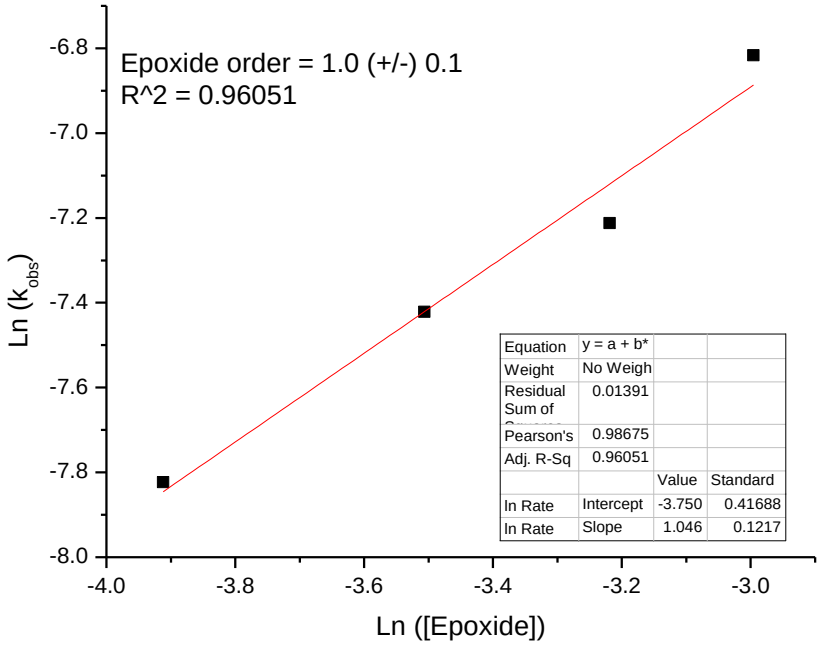

Figure 6.185. Plot of Ln (k_{obs}) versus Ln ([**14**]) for $Cp_2Ti(O_2C_2F_3)$ (2nd Repeat)

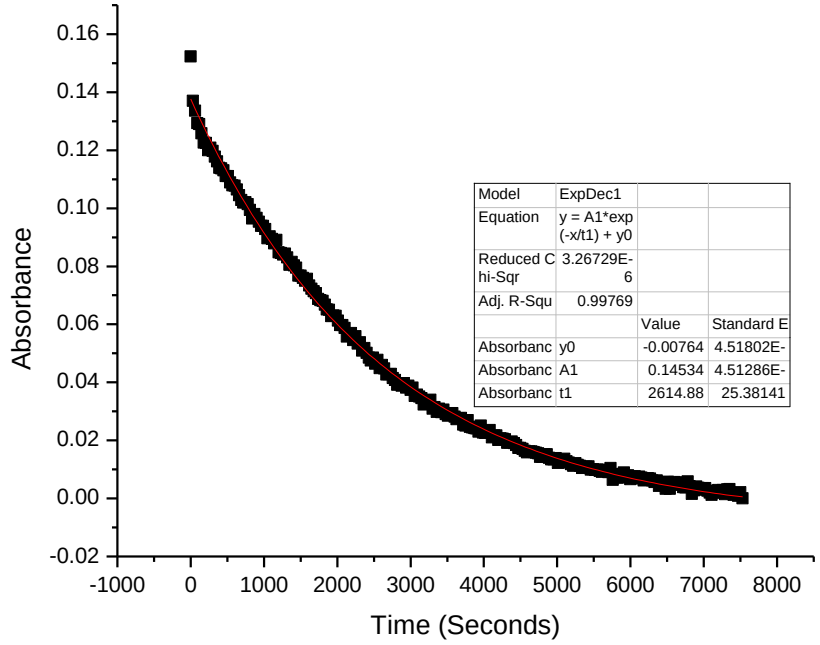

Figure 6.186. Decay of $Cp_2Ti(OTs)$ in THF after addition of 20mM (50µL) of **14**

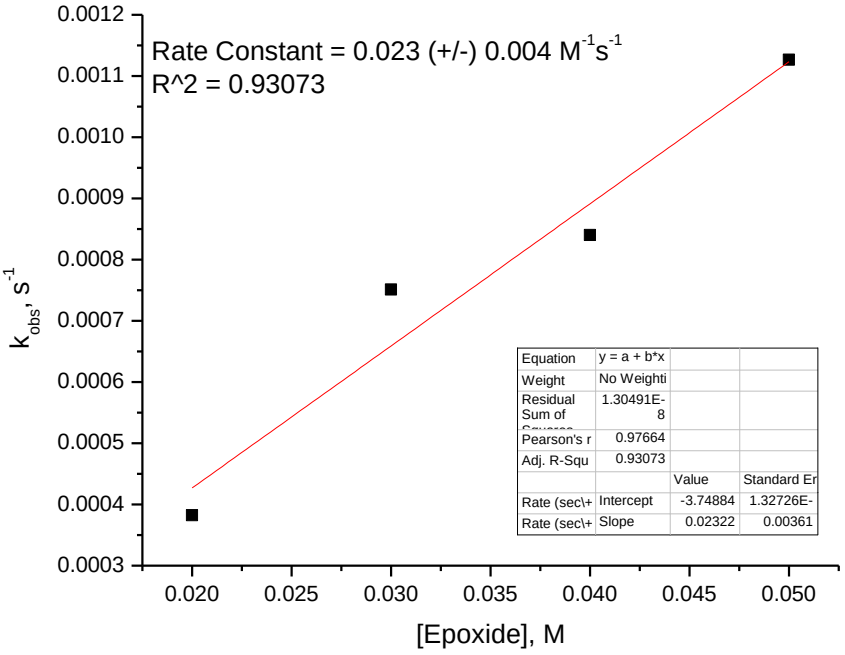

Figure 6.187. Plot of k_{obs} versus [**14**] for Cp_2Ti (OTs)

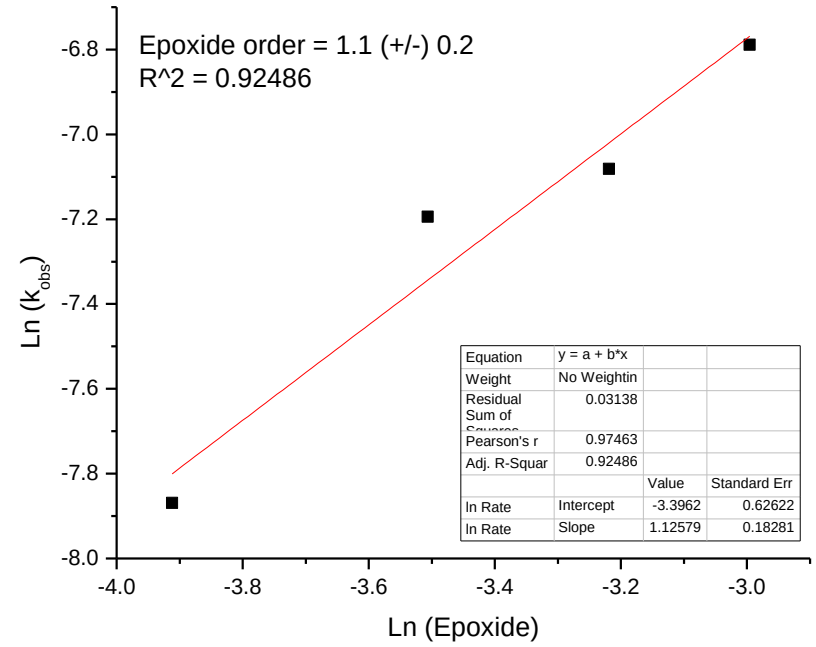

Figure 6.188. Plot of Ln (k_{obs}) versus Ln ([**14**]) for Cp_2Ti (OTs)

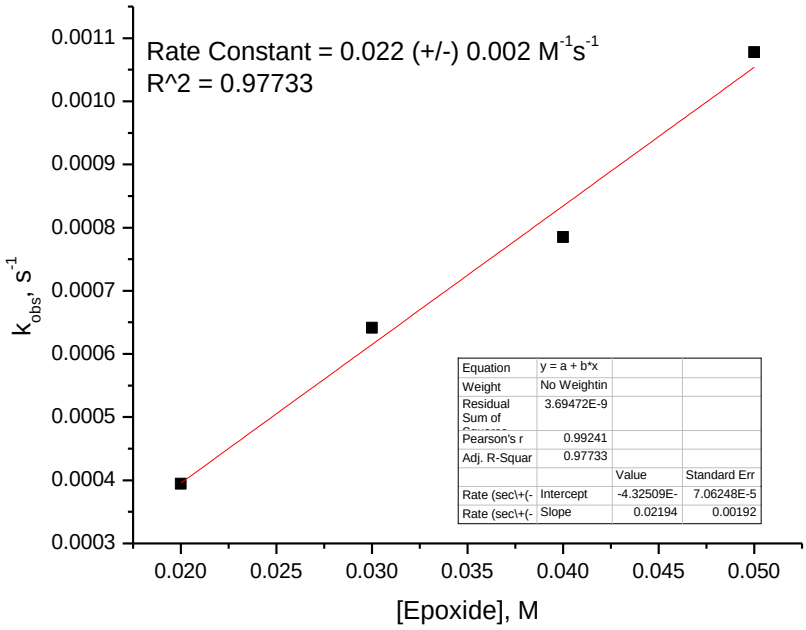

Figure 6.189. Plot of k_{obs} versus [**14**] for Cp_2Ti (OTs) (Repeat)

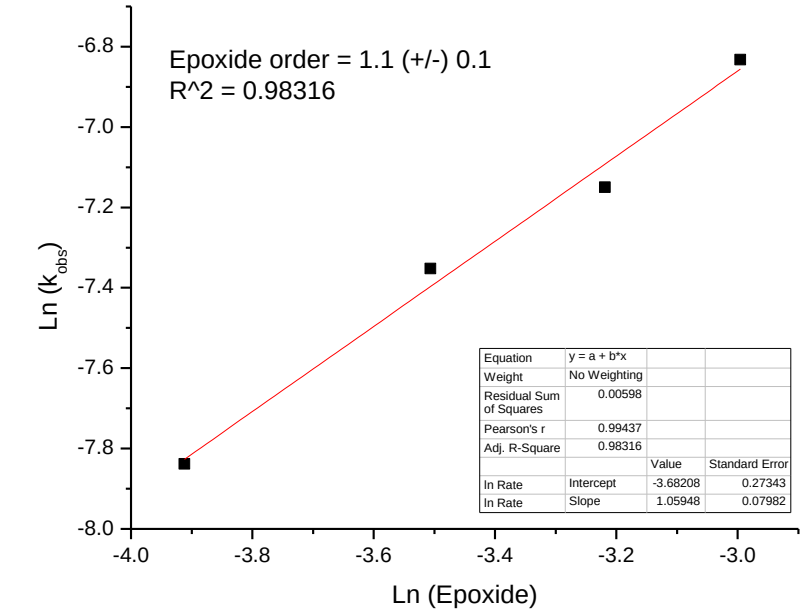

Figure 6.190. Plot of Ln (k_{obs}) versus Ln ([**14**]) for Cp_2Ti (OTs) (Repeat)

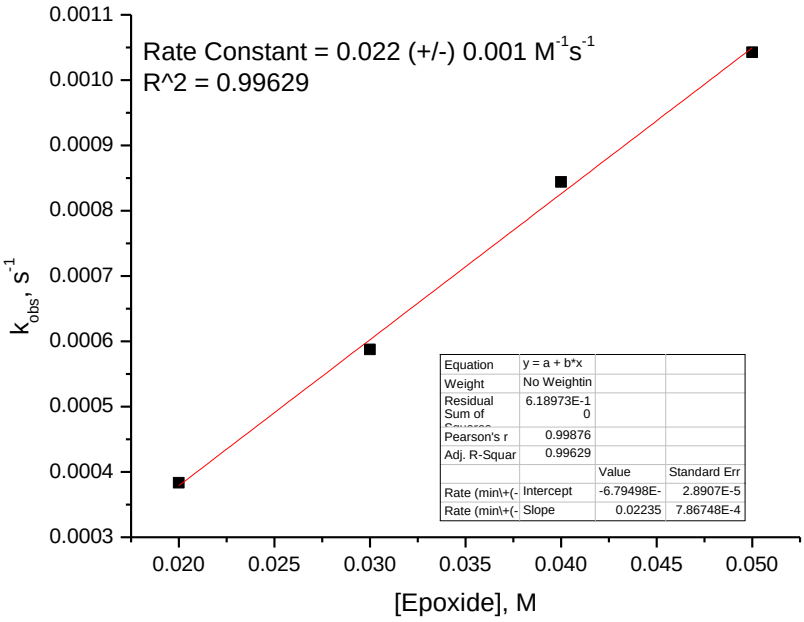

Figure 6.191. Plot of k_{obs} versus [**14**] for Cp_2Ti (OTs) (2nd Repeat)

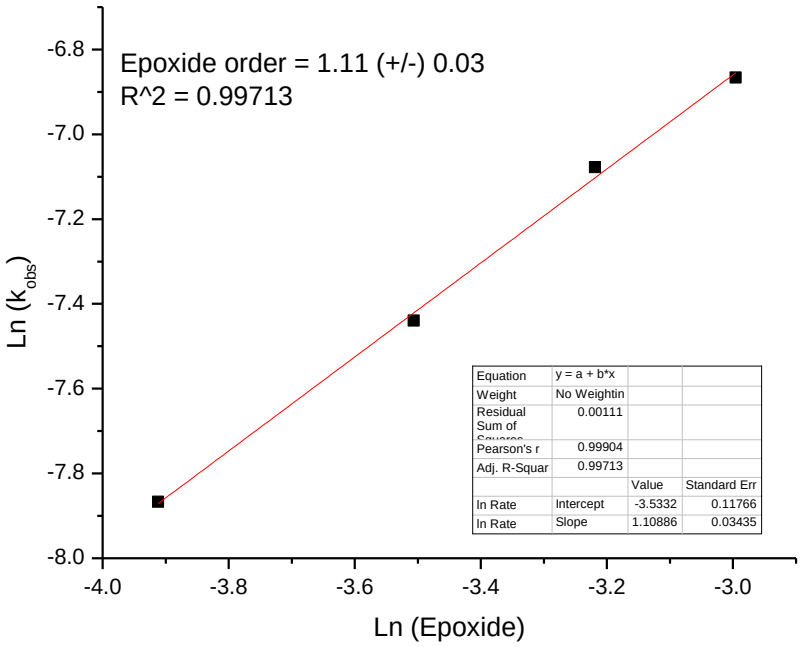

Figure 6.192. Plot of Ln (k_{obs}) versus Ln ([**14**]) for Cp_2Ti (OTs) (2nd Repeat

6.3 Carbonyl reductions mediated by titanocene(III) complexes

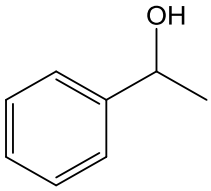

1-phenylethan-1-ol

^{1}H NMR (500 MHz, $CDCl_3$) δ 7.40 – 7.26 (m, 5H), 4.87 (q, *J* = 6.2 Hz, 1H), 2.41 (s, 1H), 1.49 (dd, *J* = 6.5, 1.1 Hz, 3H).

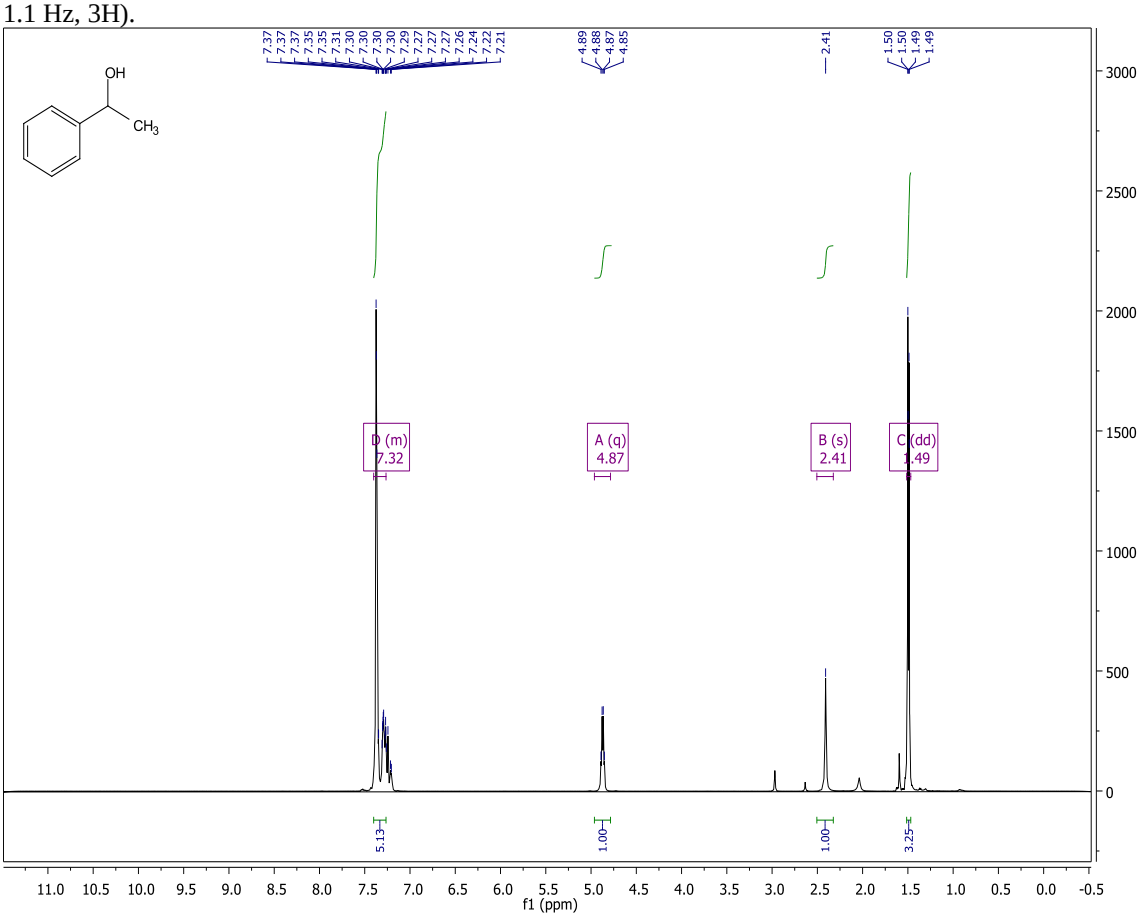

Figure 6.193. ^{1}H NMR for 1-phenylethan-1-ol (reduction with Cp_2TiCl with H_2O)

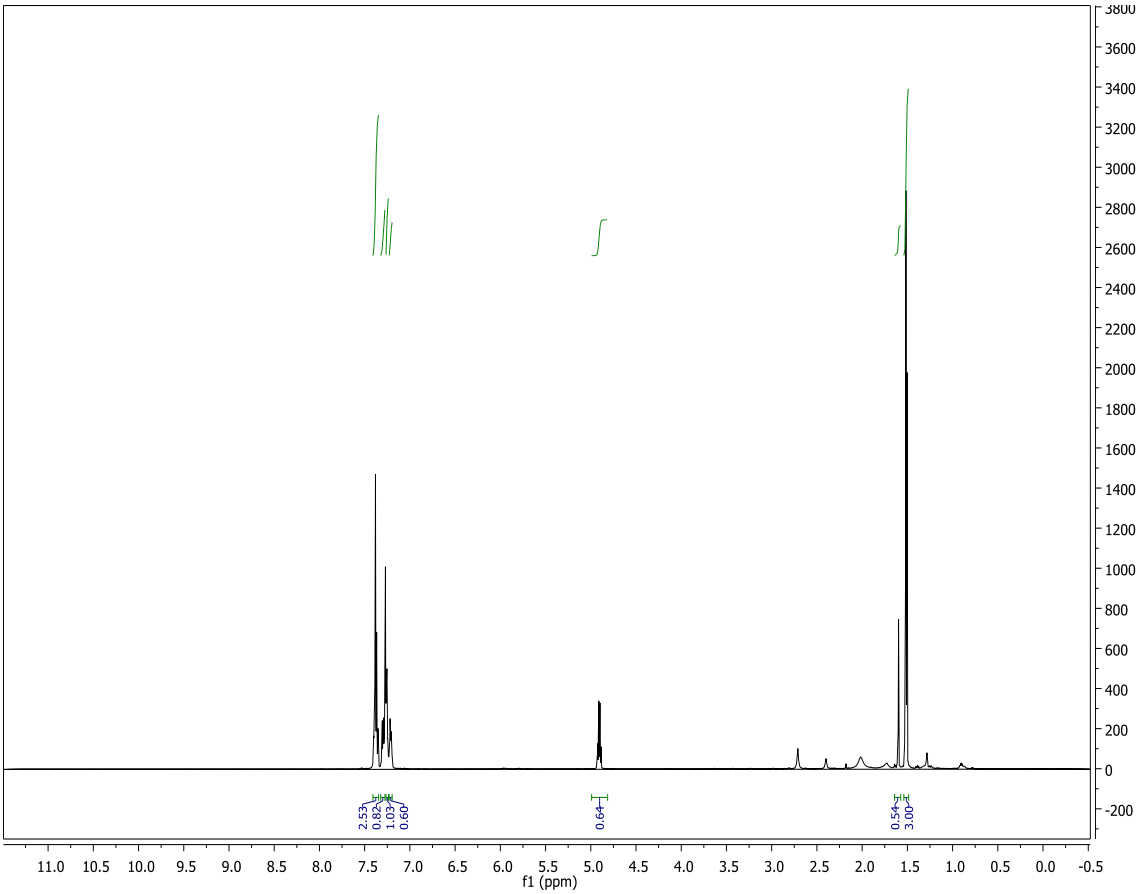

Figure 6.194. ^{1}H NMR for 1-phenylethan-1-ol (reduction with Cp_2TiCl with H_2O and pyrrolidine)

Table 6.5. GC yield for 2-octanol with biphenyl as internal standard

Peak#	Ret. Time	Start Time	End Time	m/z	Area	Area%	Name	mass (g)	% Yield
1	3.652	3.628	3.692	TIC	2087990	13.96	2-Octanone	0.01628	29.34
2	3.72	3.698	3.768	TIC	6079618	40.64	2-Octanol	0.03922	70.66
3	6.147	6.122	6.195	TIC	6793725	45.4	Biphenyl	0.0606	
Average response factors									
2-octanone	1.1437								
2-octanol	1.3825								

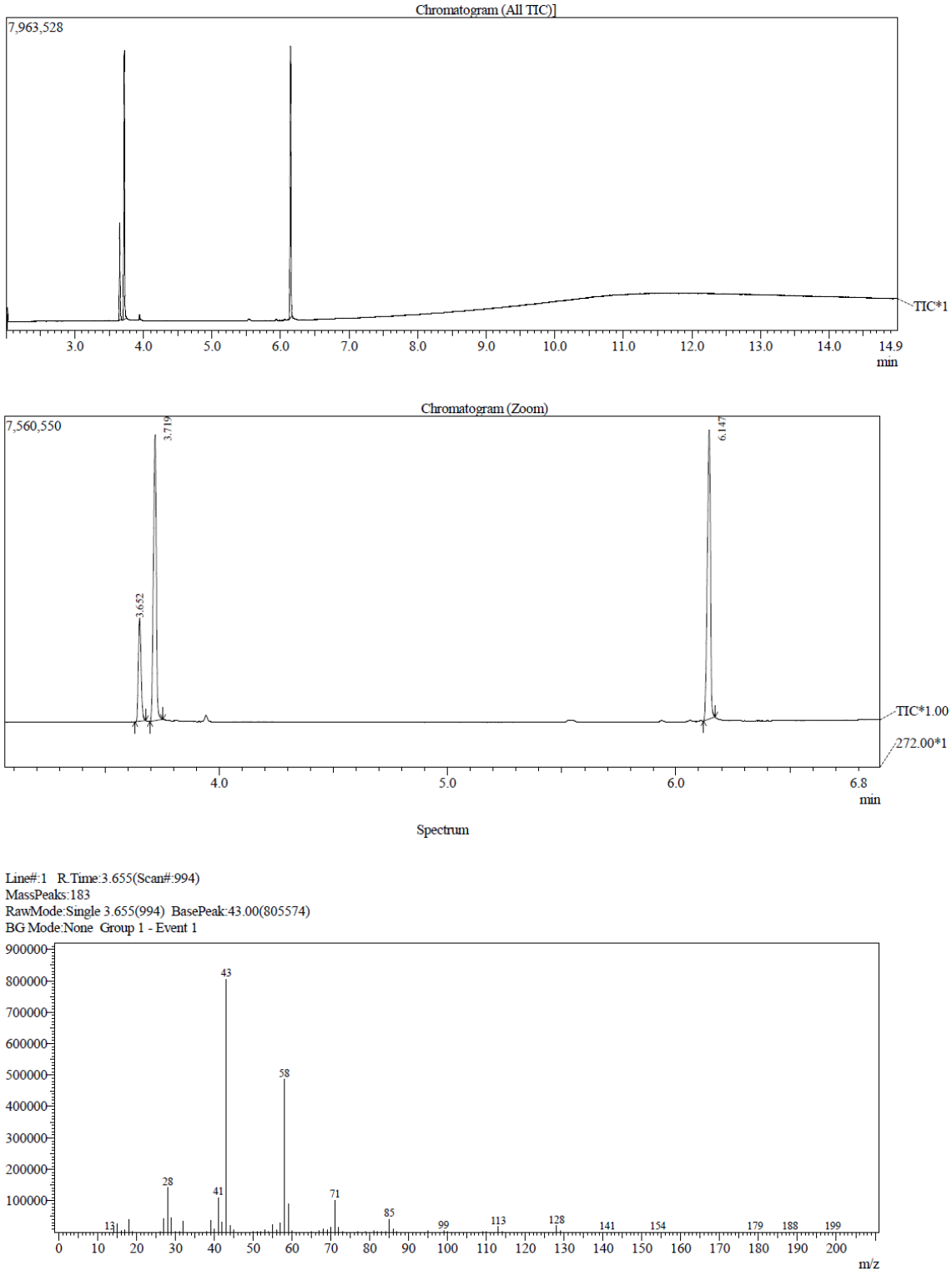

Figure 6.195. Chromatogram for 2-octanone reduction and MS for 2-octanone

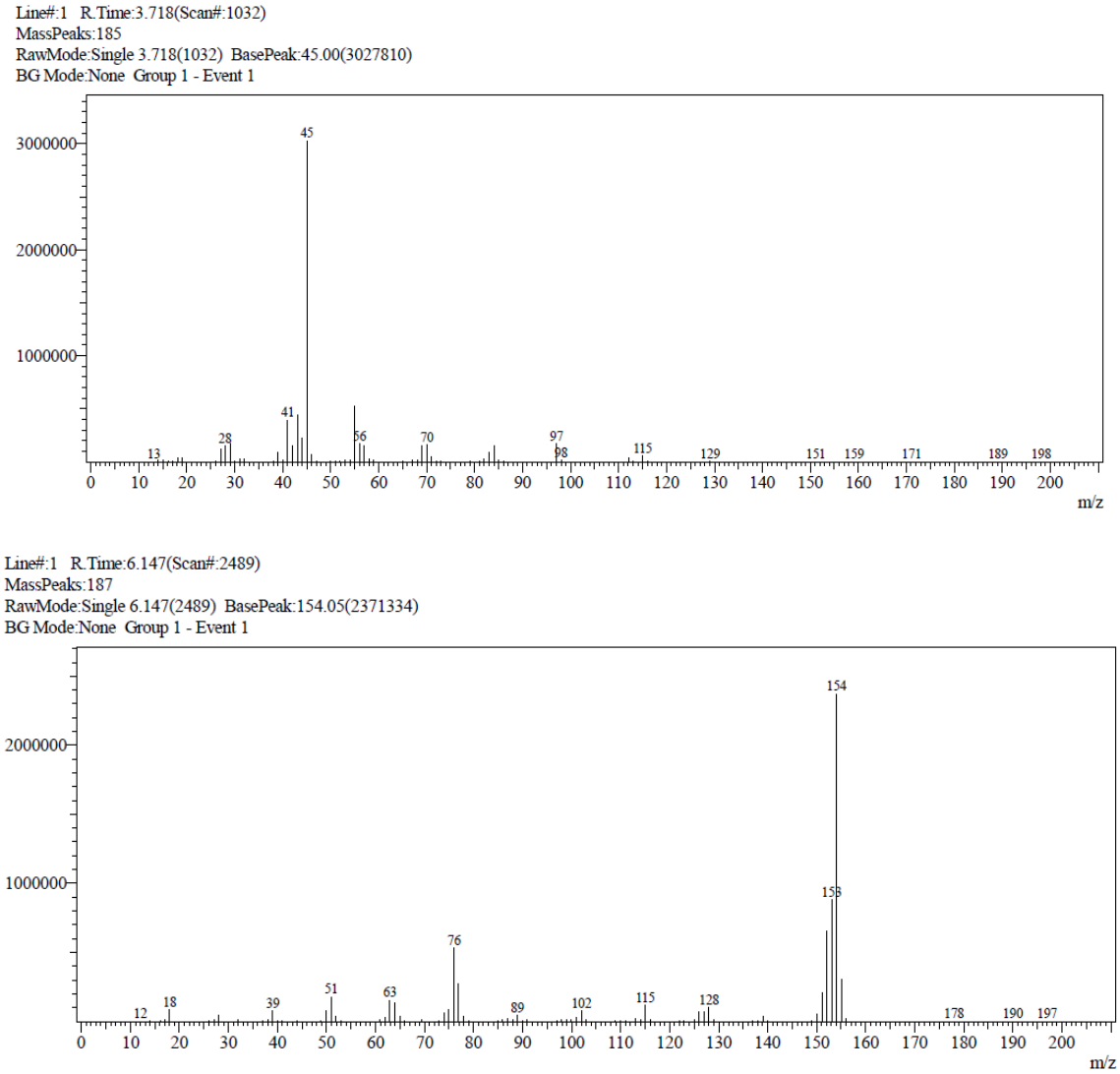

Figure 6.196. MS for 2-octanol and biphenyl

Table 6.6. Reduction of acetophenone by Cp_2TiCl

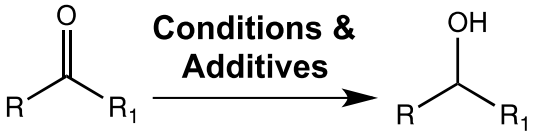

Entry	Conditions	Ketone	Additive	Time (h)	Conversion to alcohol (%)
1	Cp_2TiCl_2 (2.2equiv) Mn (8equiv) THF (10ml), rt	Acetophenone (0.5mmole, 62µL)	H_2O (6.6equiv) Pyrrolidine (4.4equiv)	1	100 (TLC, NMR)
2	Cp_2TiCl_2 (10mol%) Mn (8equiv) THF (10ml), rt		H_2O (6.6equiv) Pyrrolidine (4.4equiv)	48	0 (TLC)
3	Cp_2TiCl_2 (2.2equiv) Mn (8equiv) THF (10ml), rt		H_2O (6.6equiv) Pyrrolidine (20mol%)	2	100 (TLC, NMR)
4	Cp_2TiCl_2 (2.2equiv) Mn (8equiv) THF (10ml), rt		MeOH (6.6equiv) Pyrrolidine (4.4equiv)	6	100 (TLC, NMR)
5	Cp_2TiCl_2 (20mol%) Mn (8equiv) THF (10ml), rt		Coll*HCl (1.5equiv) Pyrrolidine (20mol%) MeOH (40mol%)	3.5	Alcohol formed but dimer also formed (GC/MS)
6	Cp_2TiCl_2 (20mol%) Mn (8equiv) THF (12ml), 60°C		Coll*HCl (1.5equiv) Pyrrolidine (20mol%) MeOH (40mol%)	5.5	Alcohol formed but ketone also seen (NMR, GC/MS)
7	Cp_2TiCl_2 (20mol%) Mn (8 equiv) THF (10ml), rt		Pyrrolidine (20mol%) MeOH (40mol%)	17	0 (TLC)
8	Cp_2TiCl_2 (20mol%) Mn (8equiv) THF (12ml), 60°C		Pyrrolidine (20mol%) MeOH (40mol%)		0 (TLC)

Table 6.7. Reduction of 2-octanone by Cp_2 TiCl

Entry	Conditions	Ketone	Additive	Time (h)	Conversion to alcohol (%)
1	Cp_2TiCl_2 (2.2equiv) Mn (8equiv) THF (10ml), rt	2-Octanone (0.5mmole, 78µL)	H_2O (6.6equiv) Pyrrolidine (4.4 equiv)	19	Unknown product formed (TLC, NMR)
2	Cp_2TiCl_2 (10 mol%) Mn (8equiv) THF (10ml), rt		H_2O (6.6 equiv) Pyrrolidine (4.4 equiv)	2 to 48	0 (TLC)
3	Cp_2TiCl_2 (10mol%) Mn (8equiv) THF (20ml), rt		MeOH (6.6equiv) Pyrrolidine (20mol%) Added over 100min	15	0 (TLC)
4	Cp_2TiCl_2 (10mol%) Mn (4equiv) THF (20ml), rt		MeOH (6.6equiv) Pyrrolidine (20mol%) Added over 100 min Coll*HCl (1equiv)	17	0 (TLC)
5	Cp_2TiCl_2 (10mol%) Mn (4equiv) THF (20ml), 60ºC		MeOH (6.6equiv) Pyrrolidine (20mol%) Added over 100 min Coll*HCl (1equiv)	17	0 (TLC)
6	Cp_2TiCl_2 (10mol%) Mn (4equiv) THF (20ml), rt		MeOH (6.6equiv) Pyrrolidine (20mol%) Added over 100min Coll*HCl (1equiv) CHD (4equiv)	17	0 (TLC)
7	Cp_2TiCl_2 (10mol%) Mn (2equiv) THF (20ml), rt		MeOH (6.6equiv) Pyrrolidine (20mol%) Added over 100min Coll*HCl (1equiv) $PhSiH_3$ (1.5equiv)	17	0 (TLC)
8	Cp_2TiCl_2 (10mol%) Mn (4equiv)		Coll.HCl (1equiv) $PhSiH_3$ (1.5equiv)	17	0 (TLC)

	THF (10ml), rt			
9	THF (10ml), rt	Coll*HCl (1equiv) $PhSiH_3$ (1.5equiv)	17	0 (TLC)
10	Cp_2TiCl_2 (20mol%) Mn (8equiv) THF (10ml), rt	Coll*HCl (1.5equiv) Pyrrolidine (20mol%) MeOH (40mol%)	17	0 (TLC)
11	Cp_2TiCl_2 (20mol%) Mn (8equiv) THF (12ml), 60°C	Coll*HCl (1.5equiv) Pyrrolidine (20mol%) MeOH (40mol%)	8	11 (TLC, GC yield)
12	Cp_2TiCl_2 (20mol%) Mn (8equiv) THF (10ml), rt	Coll*HCl (1.5equiv) Pyrrolidine (20mol%) H_2O (40mol%)	13.75	0 (TLC)
13	Cp_2TiCl_2 (20mol%) Mn (8equiv) THF (12ml), 60°C	Coll*HCl (1.5equiv) Pyrrolidine (20mol%) H_2O (40mol%)	9.5	5.8 (GC yield)
14	Cp_2TiCl_2 (20mol%) Mn (8equiv) THF (12ml), 60°C	Hex_3N*HCl (2equiv) Pyrrolidine (20mol%) MeOH (40mol%)	6	0 (TLC)

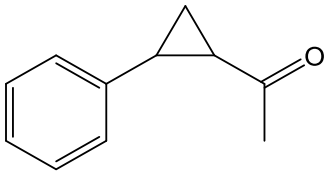

1-(2-phenylcyclopropyl) ethan-1-one (1-v)

^{1}H NMR (500 MHz, $CDCl_3$) δ 7.31 (dd, *J* = 10.4, 4.6 Hz, 2H), 7.23 (dt, *J* = 9.2, 4.2 Hz, 1H), 7.11 (dd, *J* = 8.1, 0.9 Hz, 2H), 2.57 – 2.50 (m, 1H), 2.32 (s, 3H), 2.26 – 2.20 (m, 1H), 1.69 (ddd, *J* = 9.3, 5.2, 4.3 Hz, 1H), 1.40 (ddd, *J* = 8.1, 6.6, 4.2 Hz, 1H). ^{13}C NMR (126 MHz, $CDCl_3$) δ 140.35, 128.54, 126.56, 126.04, 77.37, 77.12, 76.86, 32.93, 30.90, 29.07, 19.19.

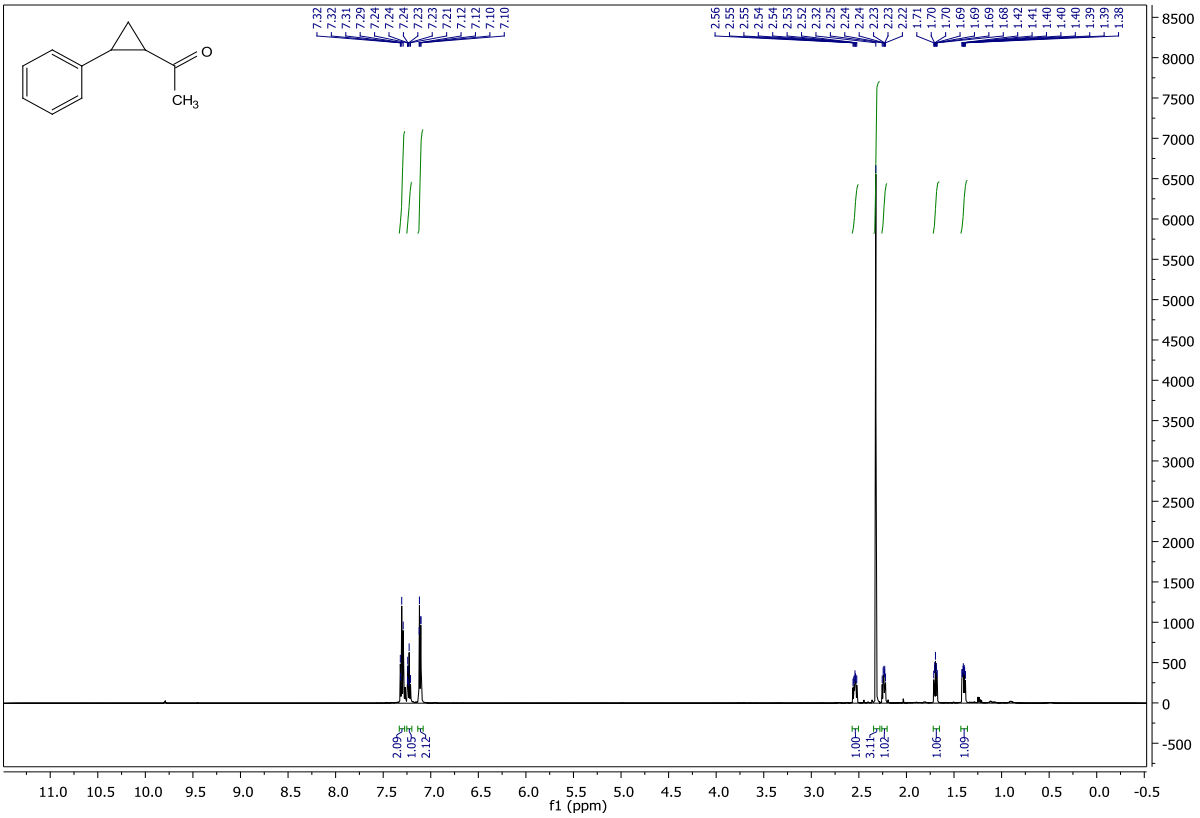

Figure 6.197. ^{1}H NMR for **1-v**

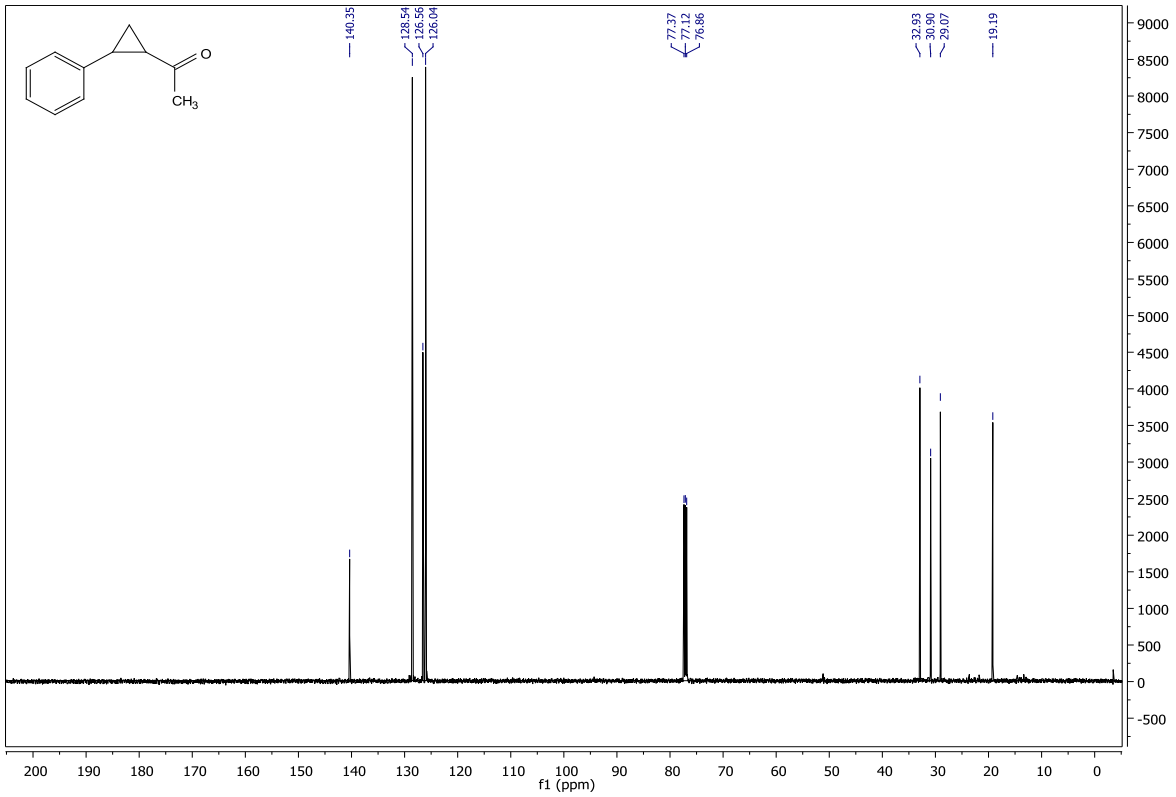

Figure 6.198. ^{13}C NMR for **1-v**

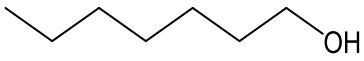

1-Heptanol (2-a)

1-heptanol (**2-a**) was prepared from heptanal (**1-a**) by the procedure outlined in chapter 4. NMR analysis showed 100% conversion in 1 hour. 60% isolated yield of alcohol product was obtained after complete workup and flash chromatography (Hex: EtOAc = 70:30). ^{1}H NMR (400 MHz, $CDCl_3$) δ 3.53 (t, *J* = 6.8 Hz, 2H), 2.78 (s, 1H), 1.53 – 1.43 (m, 2H), 1.31 – 1.14 (m, 8H), 0.81 (t, *J* = 6.9 Hz, 3H). ^{13}C NMR (101 MHz, $CDCl_3$) δ 77.40, 77.09, 76.77, 62.70, 32.68, 31.83, 29.13, 25.72, 22.60, 14.03.

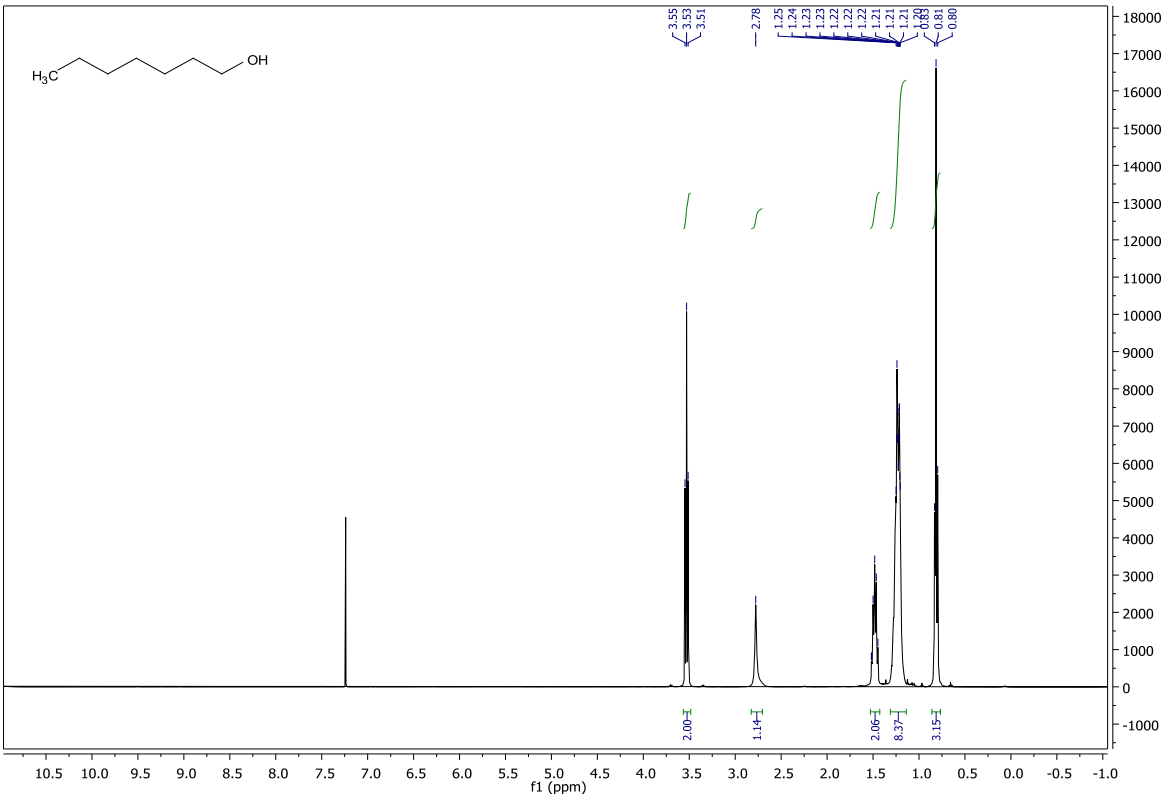

Figure 6.199. ^{1}H NMR for **2-a**

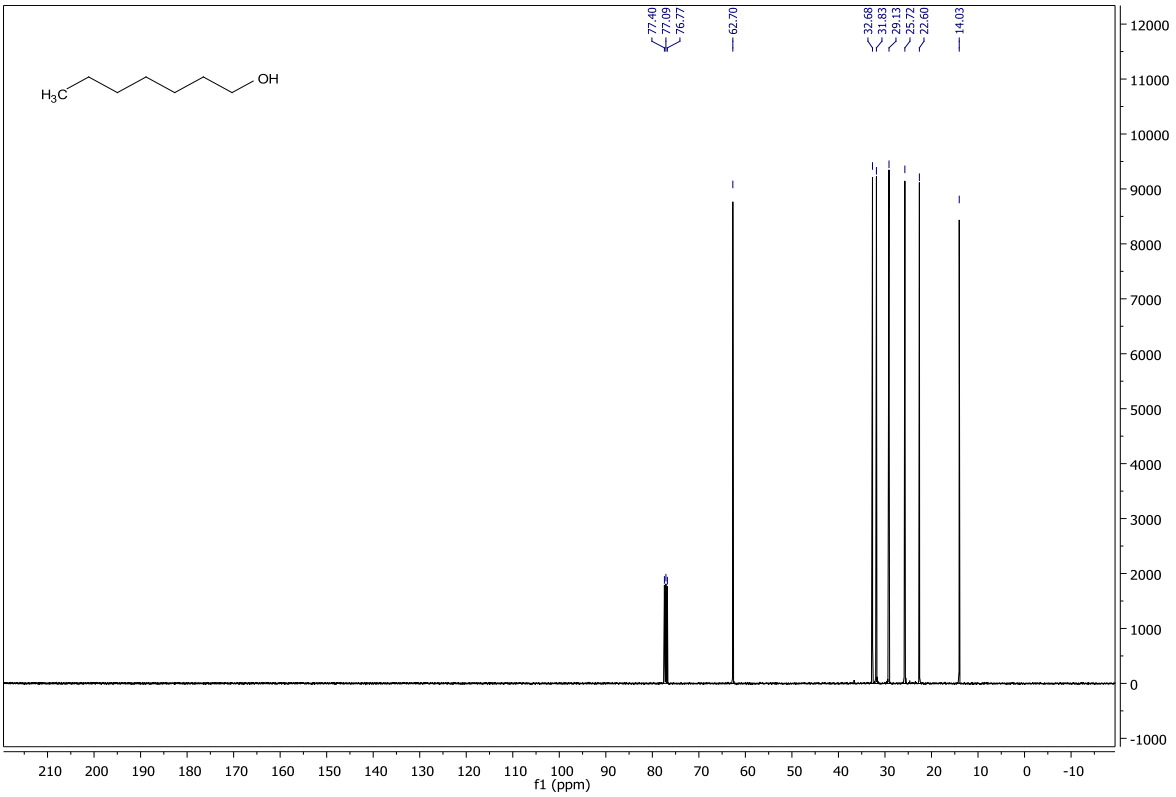

Figure 6.200. ^{13}C NMR for **2-a**

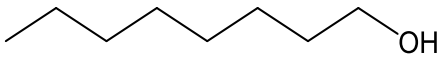

1-Octanol (2-b)

1-octanol (**2-b**) was prepared from octantal (**1-b**) by the procedure outlined in chapter 4. NMR analysis showed 100% conversion in 1 hour. 70% isolated yield of alcohol product was obtained after complete workup and flash chromatography (Hex: EtOAc = 70:30). ^{1}H NMR (400 MHz, $CDCl_3$) δ 3.54 (t, *J* = 6.7 Hz, 2H), 2.57 (s, 1H), 1.50 (dq, *J* = 13.8, 6.7 Hz, 2H), 1.31 – 1.16 (m, 10H), 0.82 (t, *J* = 6.9 Hz, 3H). ^{13}C NMR (101 MHz, $CDCl_3$) δ 77.40, 77.08, 76.76, 62.77, 32.70, 31.83, 29.43, 29.30, 25.77, 22.65, 14.07.

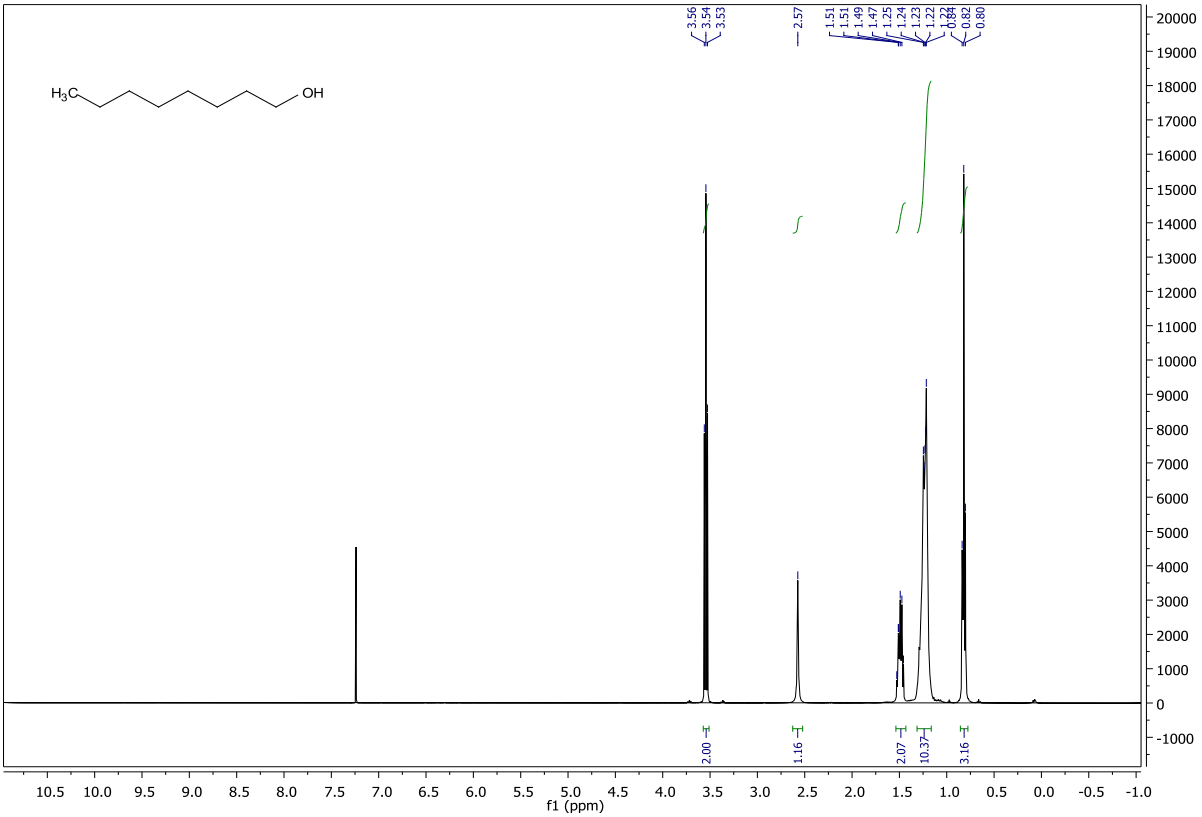

Figure 6.201. ^{1}H NMR for **2-b**

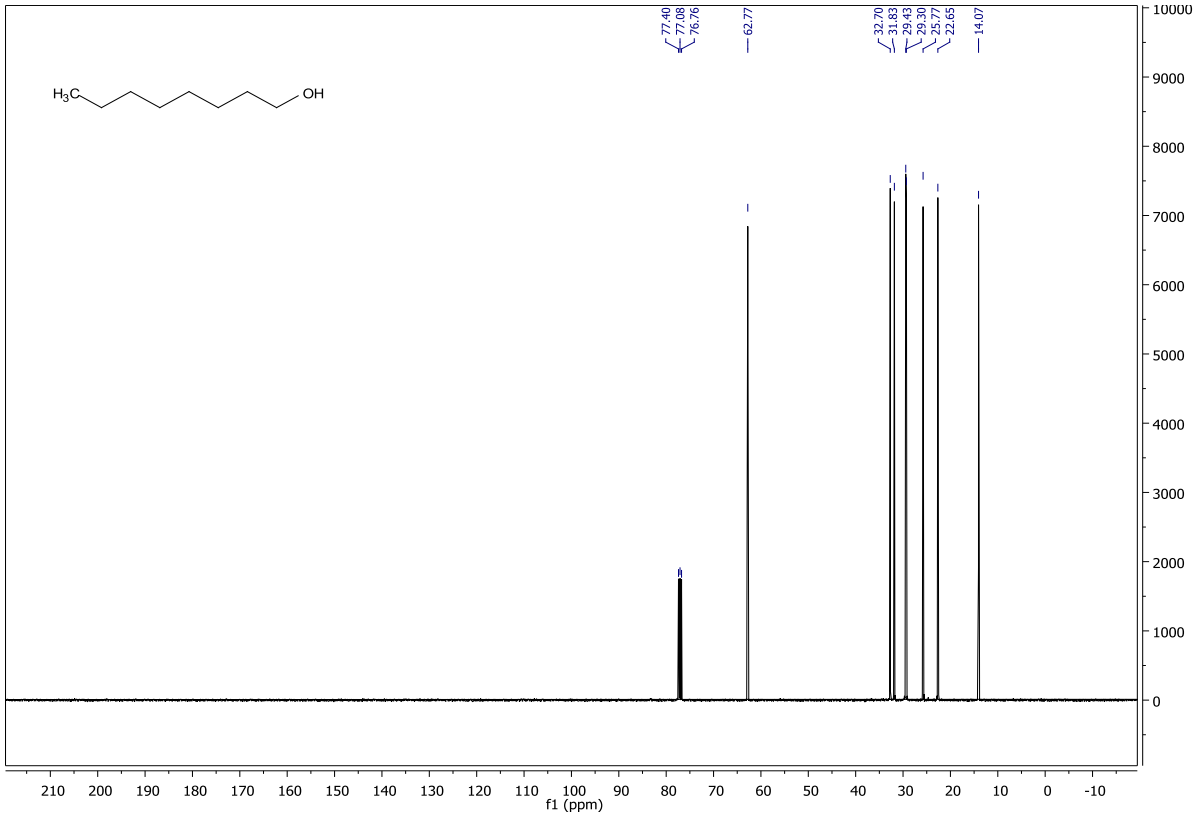

Figure 6.202. ^{13}C NMR for **2-b**

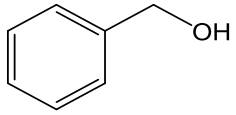

Phenyl methanol (2-c)

Phenyl methanol (**2-c**) was prepared from benzaldehyde (**1-c**) by the procedure outlined in chapter 4. NMR analysis showed 100% conversion in 1 hour. 86% isolated yield of alcohol product was obtained after complete workup. ^{1}H NMR (400 MHz, $CDCl_3$) δ 7.37 – 7.26 (m, 5H), 4.59 (s, 2H), 2.99 (s, 1H). ^{13}C NMR (101 MHz, $CDCl_3$) δ 140.92, 128.56, 127.60, 127.07, 77.52, 77.20, 76.88, 65.04.

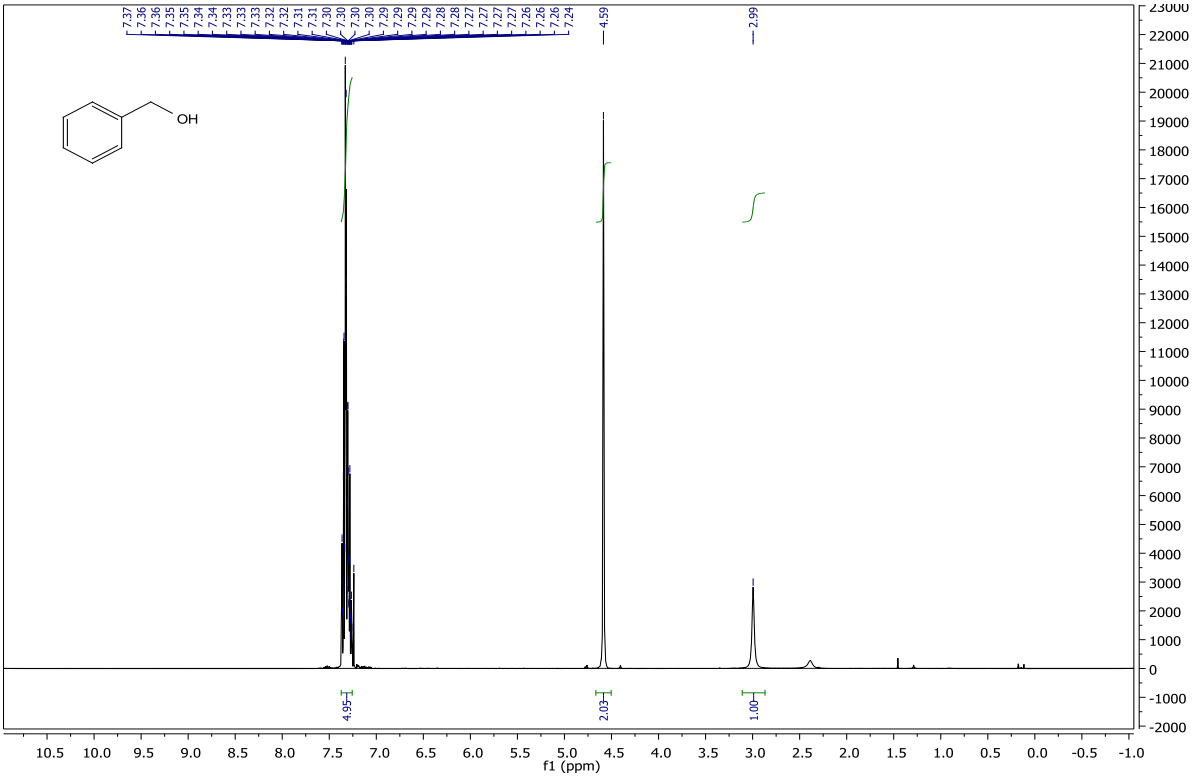

Figure 6.203. ^{1}H NMR for **2-c**

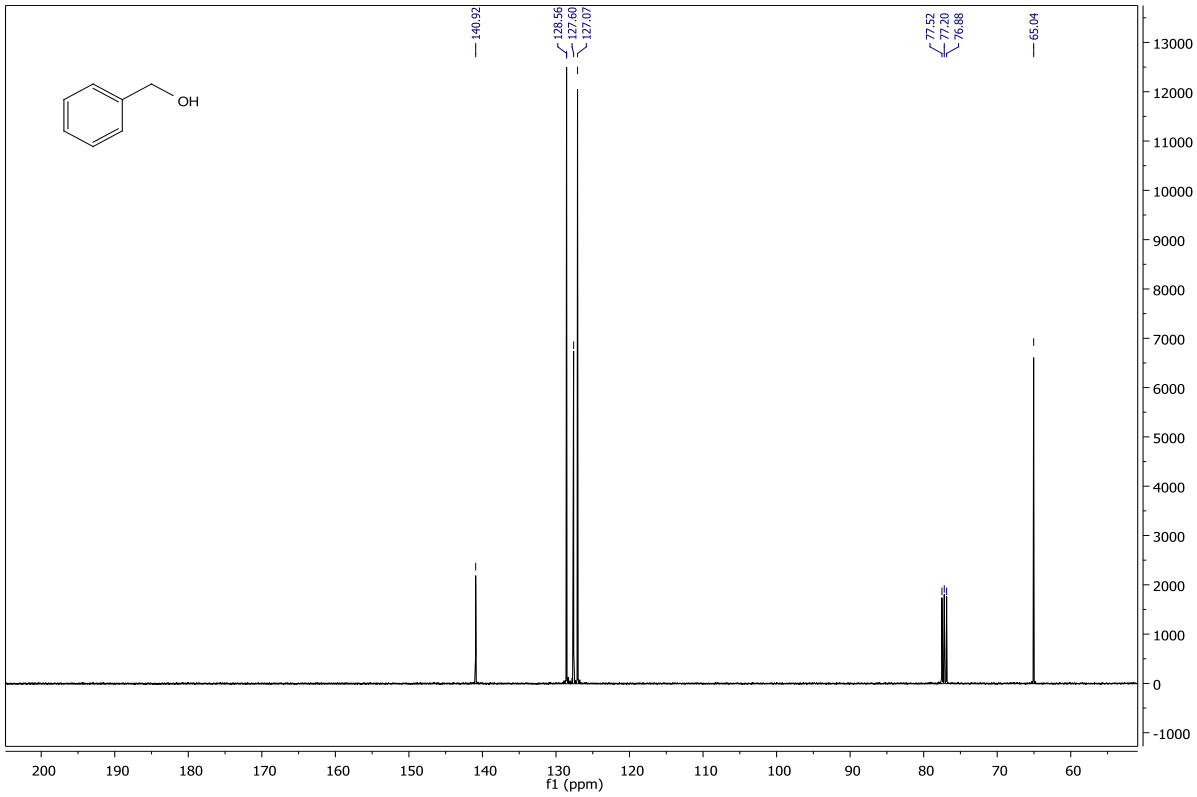

Figure 6.204. ^{13}C NMR for **2-c**

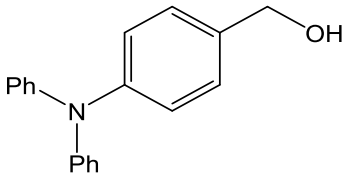

(4-(diphenylamino) phenyl) methanol (2-d)

(4-(diphenylamino) phenyl) methanol (**2-d**) was prepared from 4-(diphenylamino) benzaldehyde (**1-d**) by the procedure outlined in chapter 4. NMR analysis showed 100% conversion in 1 hour. 95% isolated yield of alcohol product was obtained after complete workup. ^{1}H NMR (400 MHz, $CDCl_3$) δ 7.24 (ddt, *J* = 7.2, 4.1, 2.1 Hz, 6H), 7.13 – 7.07 (m, 6H), 7.05 – 6.98 (m, 2H), 4.60 (s, 2H), 2.33 (s, 1H). ^{13}C NMR (101 MHz, $CDCl_3$) δ 147.82, 147.47, 135.09, 129.34, 128.39, 124.28, 124.11, 122.88, 77.52, 77.20, 76.88, 64.97.

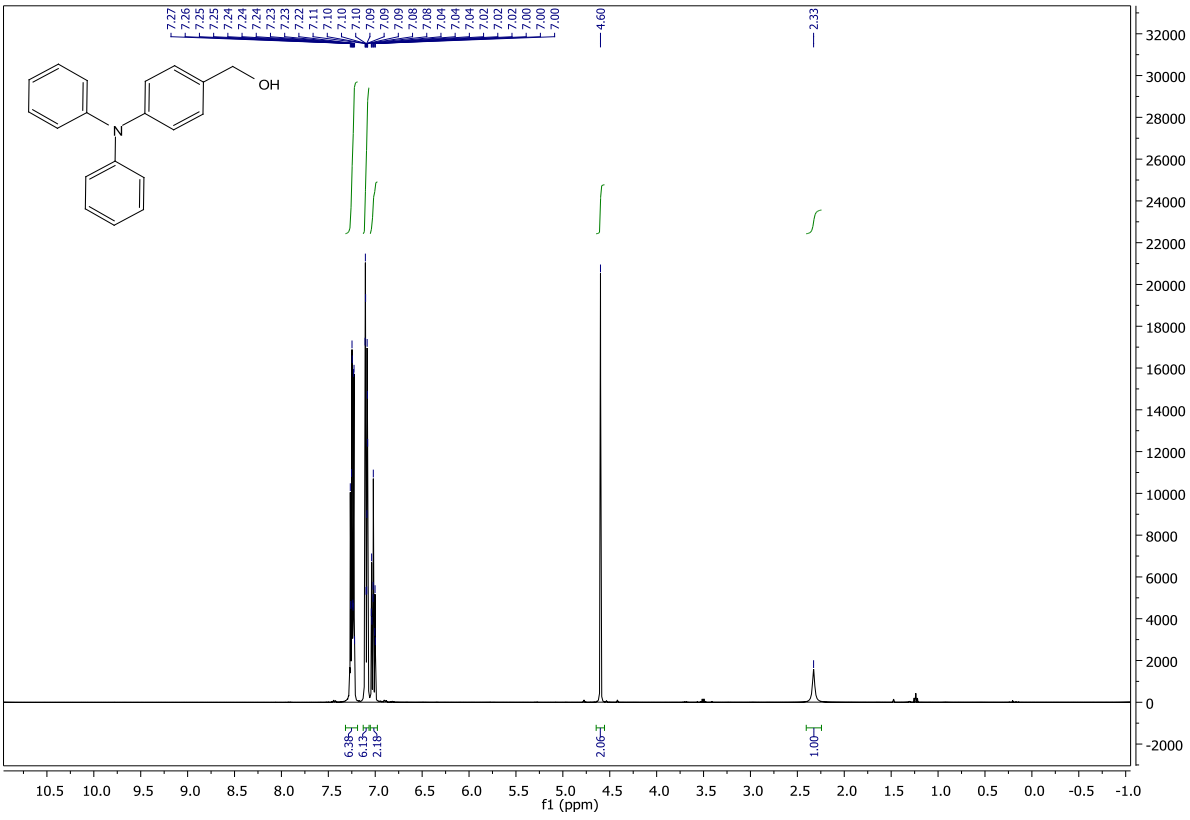

Figure 6.205. ^{1}H NMR for **2-d**

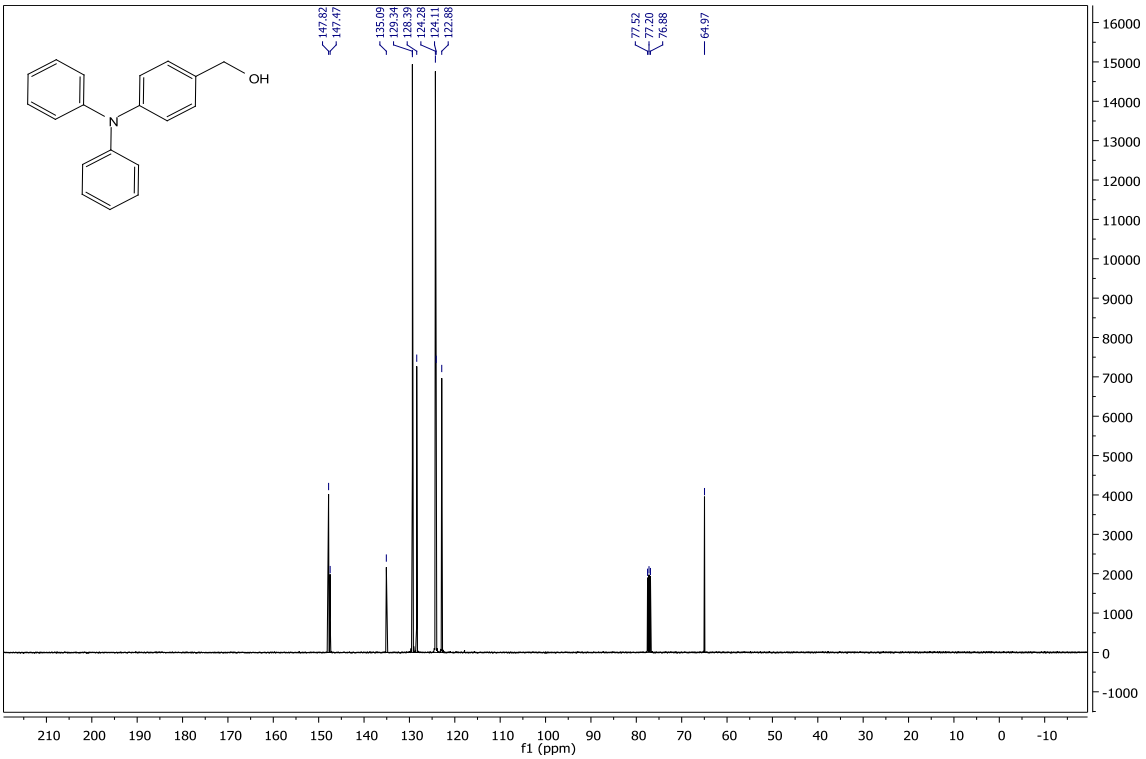

Figure 6.206. ^{13}C NMR for **2-d**

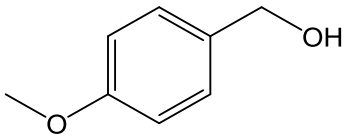

(4-methoxyphenyl) methanol (2-e)

(4-methoxyphenyl) methanol **(2-e)** was prepared from 4-methoxybenzaldehyde **(1-e)** by the procedure outlined in chapter 4. NMR analysis showed 100% conversion in 1 hour. 87% isolated yield of alcohol product was obtained after complete workup. ^{1}H NMR (400 MHz, $CDCl_3$) δ 7.26 – 7.16 (m, 2H), 6.88 – 6.78 (m, 2H), 4.49 (s, 2H), 3.75 (s, 3H), 2.92 (s, 1H). ^{13}C NMR (101 MHz, $CDCl_3$) δ 159.03, 133.22, 128.67, 113.87, 77.53, 77.22, 76.90, 64.63, 55.29.

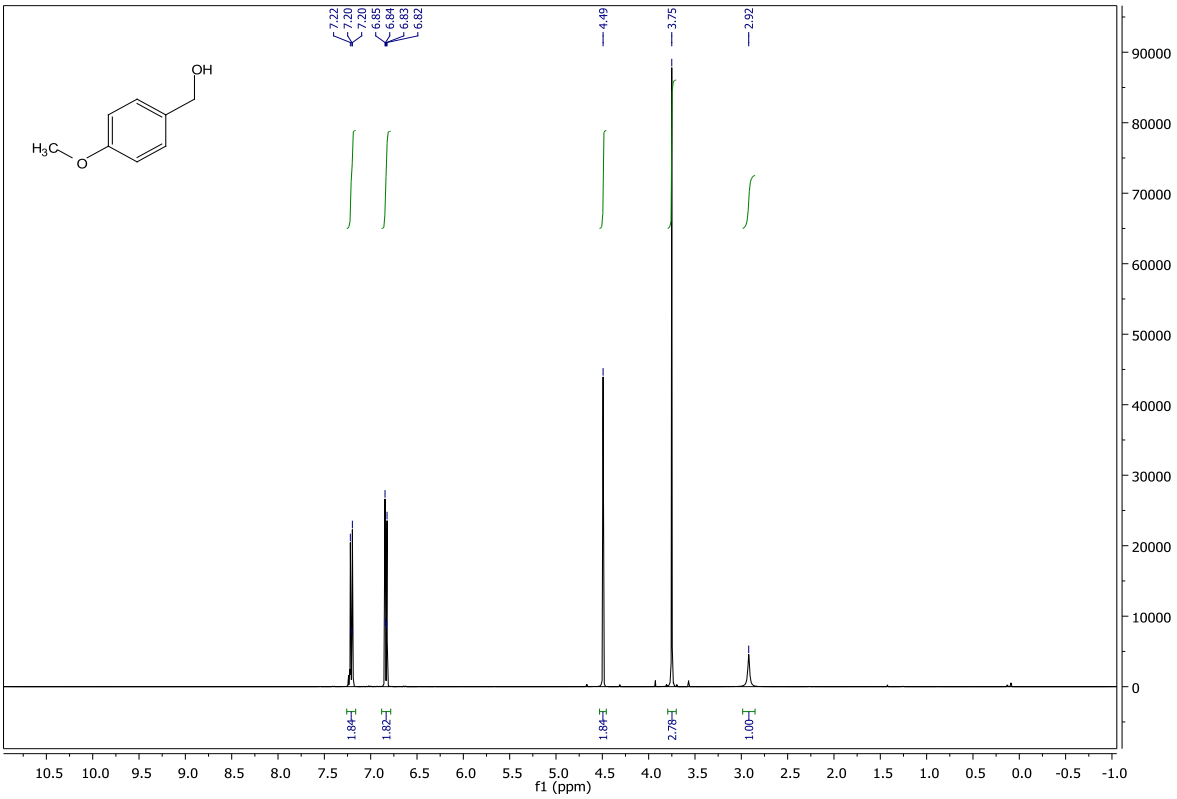

Figure 6.207. ^{1}H NMR for **2-e**

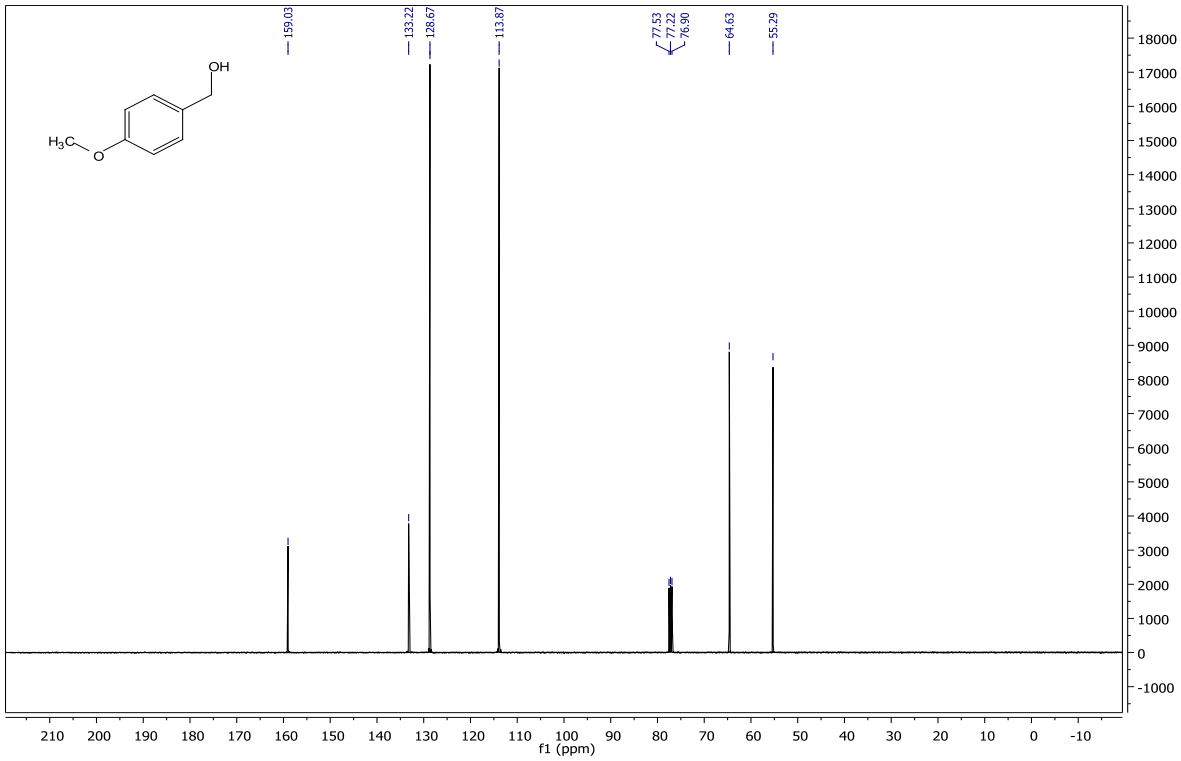

Figure 6.208. ^{13}C NMR for **2-e**

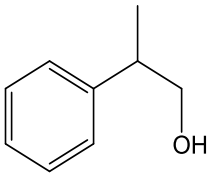

2-phenylpropan-1-ol (2-f)

2-phenylpropan-1-ol **(2-f)** was prepared from 2-phenylpropanal **(1-f)** by the procedure outlined in chapter 4. NMR analysis showed 100% conversion in 1 hour. 58% isolated yield of alcohol product was obtained after complete workup and flash chromatography (Hex: EtOAc = 70:30). ^{1}H NMR (400 MHz, $CDCl_3$) δ 7.36 – 7.30 (m, 2H), 7.26 – 7.21 (m, 3H), 3.71 – 3.59 (m, 2H), 2.98 – 2.86 (m, 1H), 2.04 (s, 1H), 1.27 (d, *J* = 7.0 Hz, 3H). ^{13}C NMR (101 MHz, $CDCl_3$) δ 143.88, 128.64, 127.57, 126.67, 77.52, 77.20, 76.88, 68.64, 42.45, 17.69.

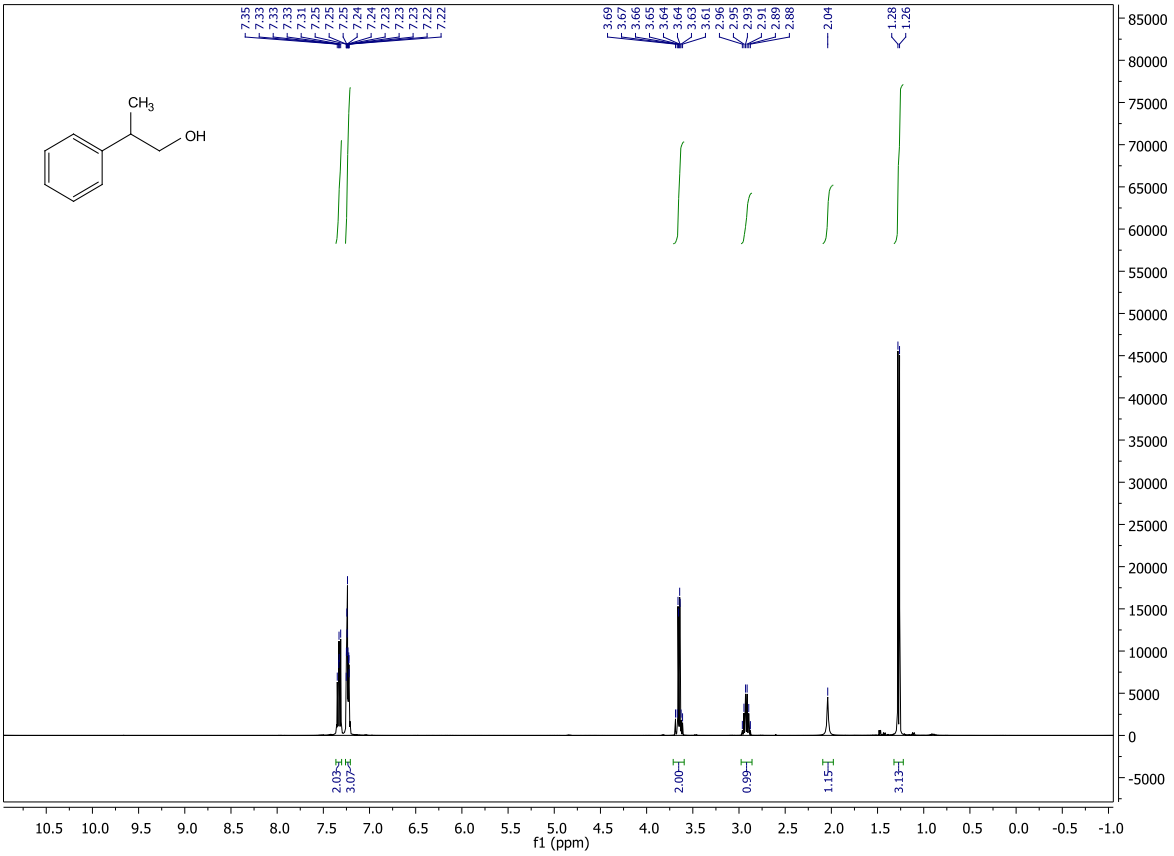

Figure 6.209. ^{1}H NMR for **2-f**

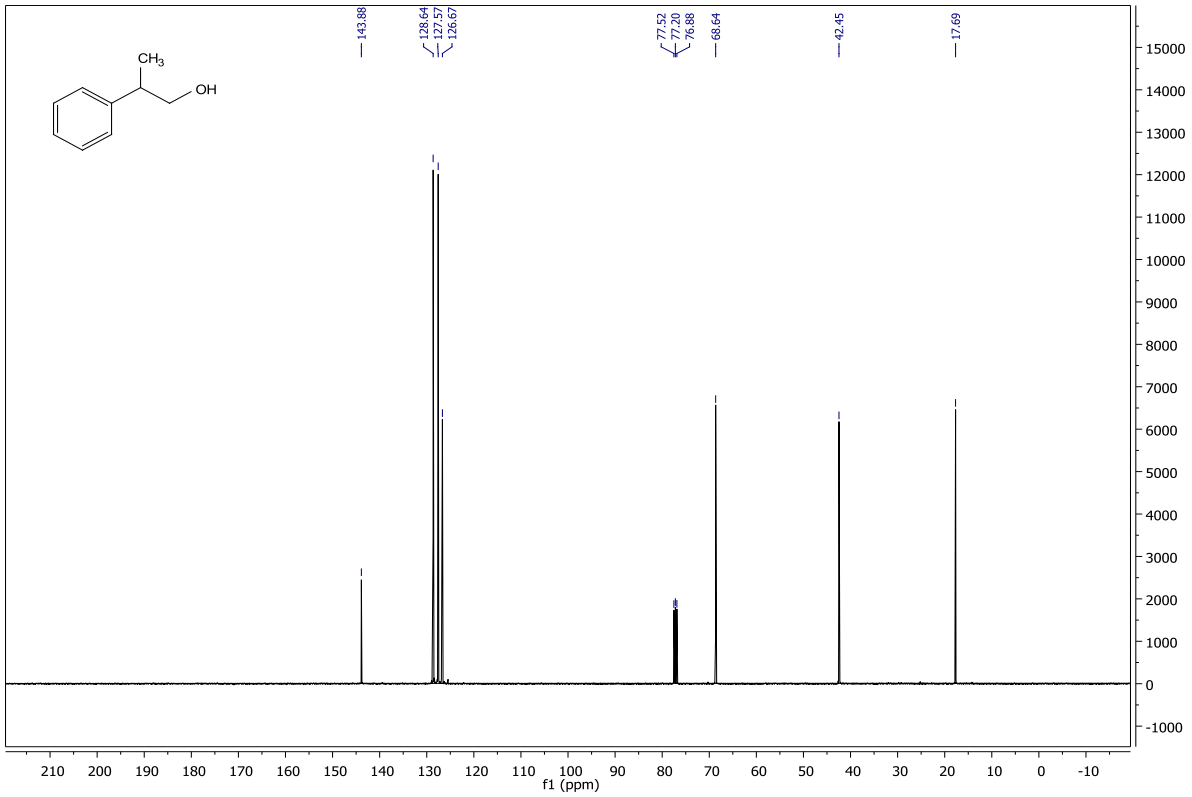

Figure 6.210. ^{13}C NMR for **2-f**

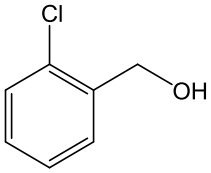

(2-chlorophenyl) methanol (2-g)

(2-chlorophenyl) methanol **(2-g)** was prepared from 2-chlorobenzaldehyde **(1-g)** by the procedure outlined in chapter 4. NMR analysis showed 100% conversion in 1 hour. 94% isolated yield of alcohol product was obtained after complete workup. ^{1}H NMR (400 MHz, $CDCl_3$) δ 7.41 (ddd, *J* = 7.1, 1.6, 0.5 Hz, 1H), 7.31 (dd, *J* = 7.6, 1.6 Hz, 1H), 7.25 – 7.13 (m, 2H), 4.68 (d, *J* = 5.2 Hz, 2H), 3.20 (t, *J* = 5.6 Hz, 1H). ^{13}C NMR (101 MHz, $CDCl_3$) δ 138.17, 132.58, 129.29, 128.74, 128.56, 127.01, 77.51, 77.19, 76.87, 62.49.

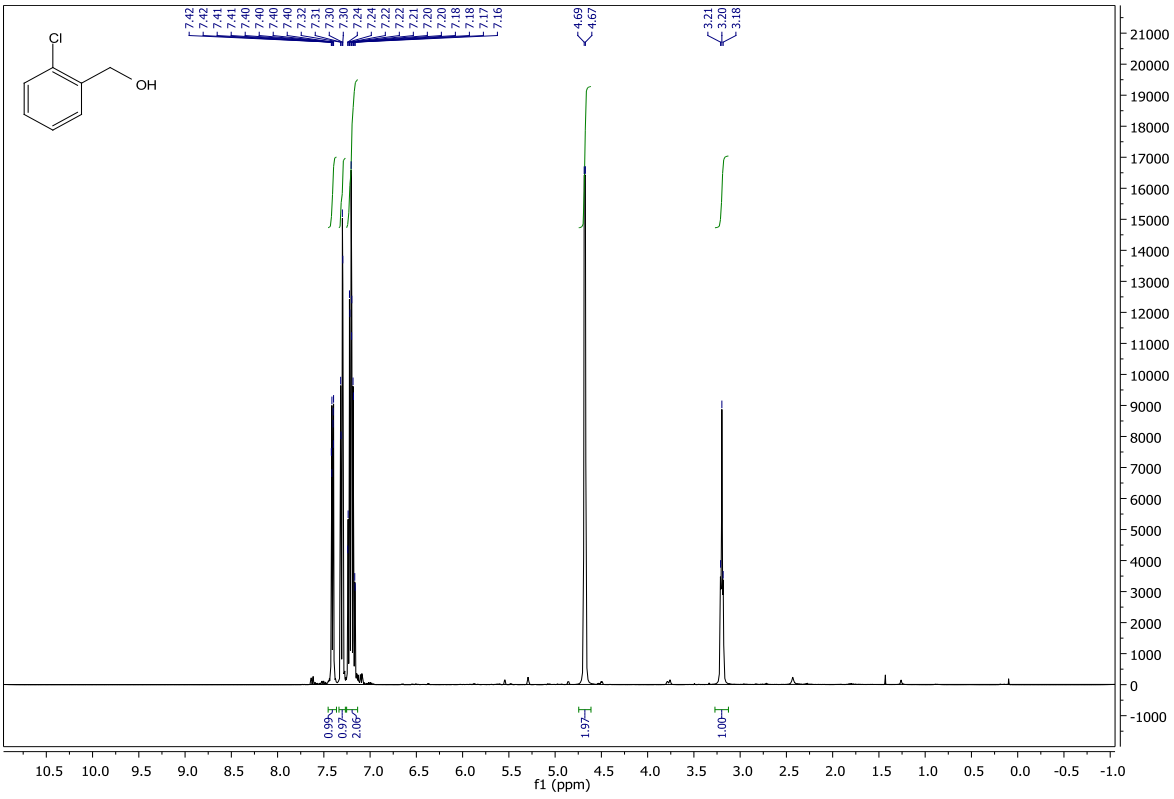

Figure 6.211. ^{1}H NMR for **2-g**

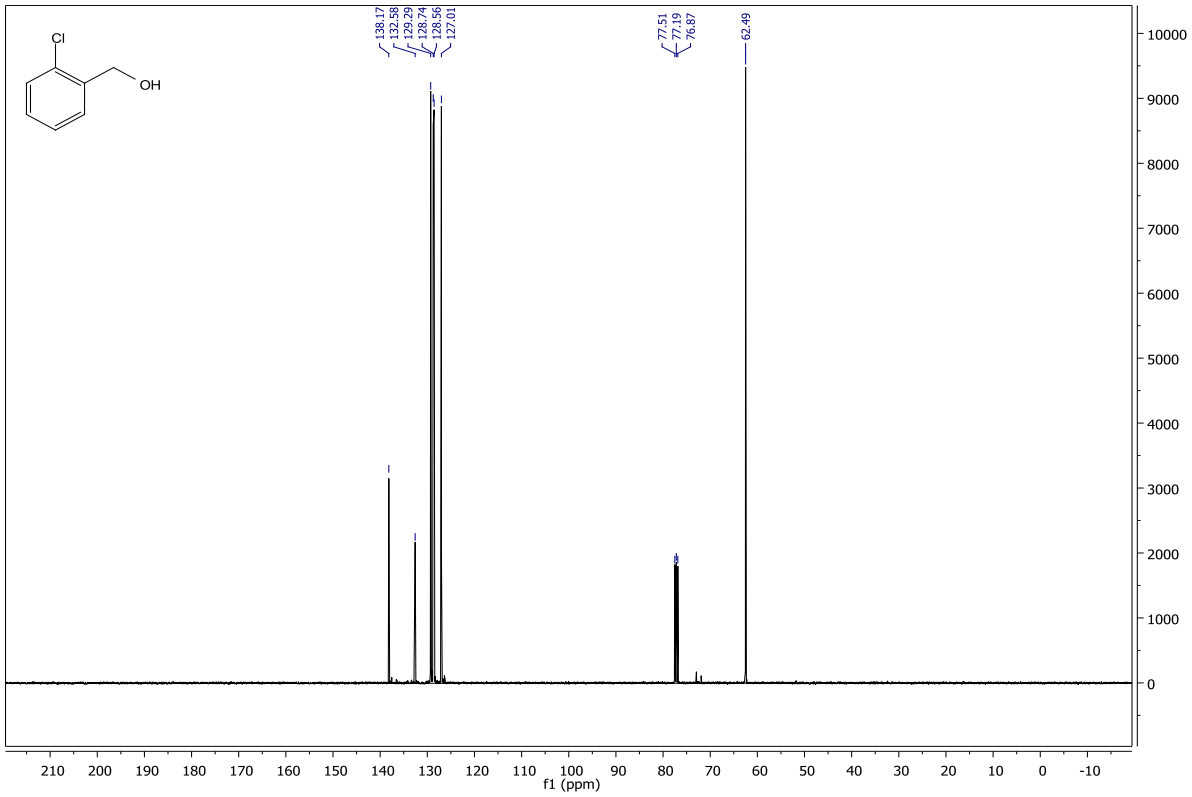

Figure 6.212. ^{13}C NMR for **2-g**

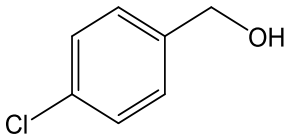

(4-chlorophenyl) methanol (2-h)

(4-chlorophenyl) methanol **(2-h)** was prepared from 4-chlorobenzaldehyde **(1-h)** by the procedure outlined in chapter 4. NMR analysis showed 100% conversion in 1 hour. 89% isolated yield of alcohol product was obtained after complete workup. ^{1}H NMR (400 MHz, $CDCl_3$) δ 7.21 (ddd, *J* = 8.7, 4.3, 1.2 Hz, 4H), 4.50 (s, 2H), 3.18 (s, 1H). ^{13}C NMR (101 MHz, $CDCl_3$) δ 139.20, 133.26, 128.63, 128.29, 77.49, 77.17, 76.85, 64.20.

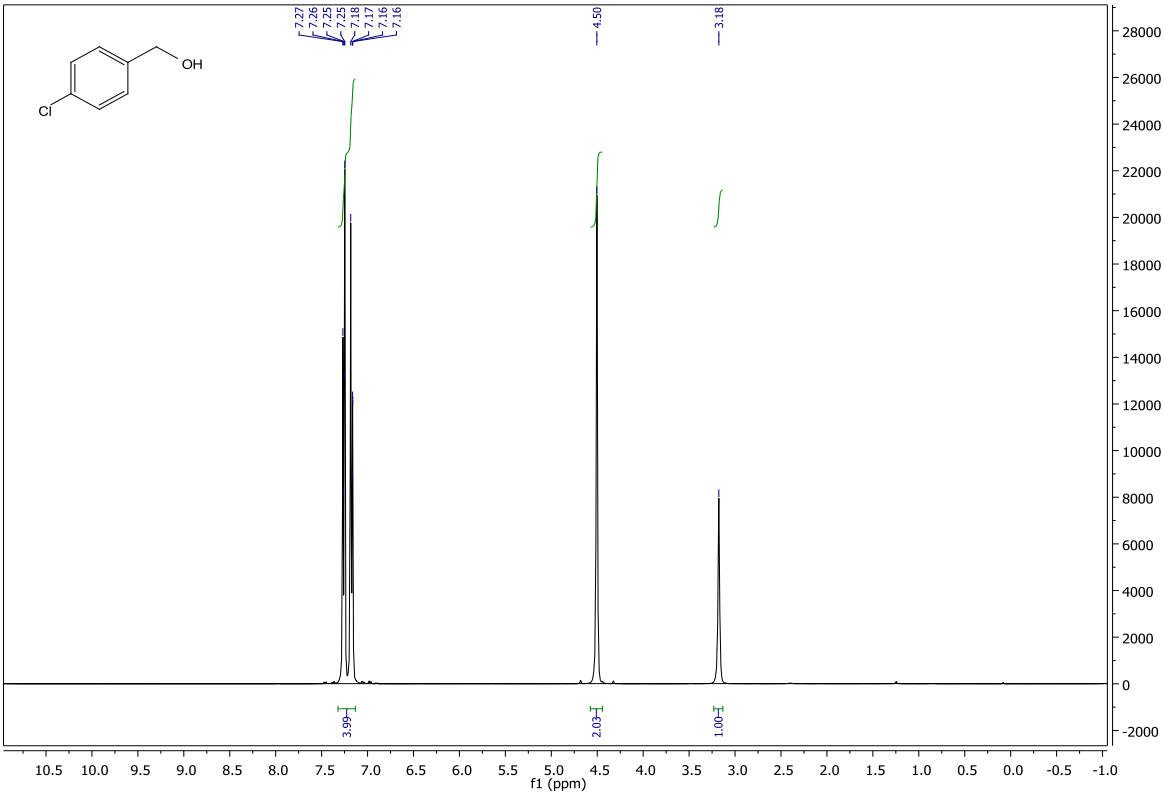

Figure 6.213. ^{1}H NMR for **2-h**

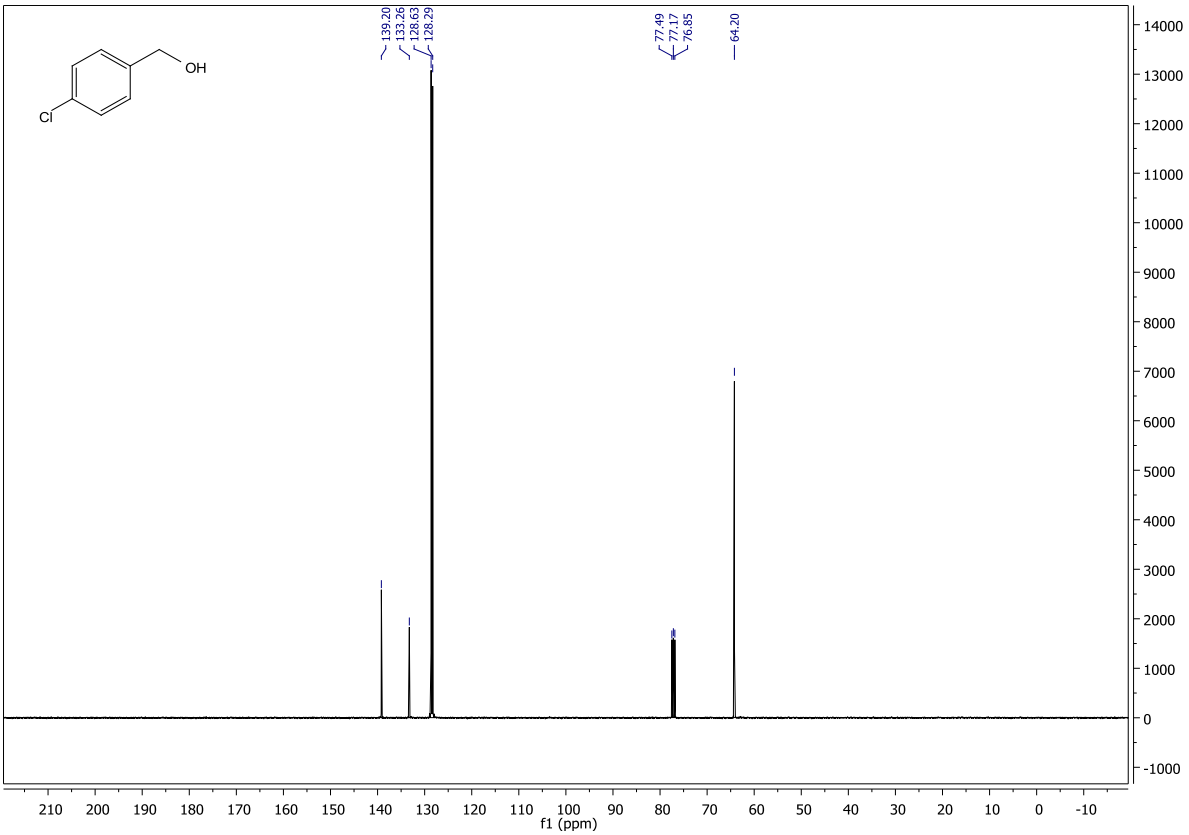

Figure 6.214. ^{13}C NMR for **2-h**

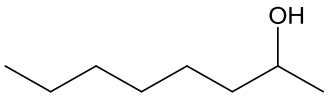

2-octanol (2-i)

2-octanol **(2-i)** was prepared from 2-octanone **(1-i)** by the procedure outlined in chapter 4. NMR analysis showed 100% conversion in 2 hours. 79% isolated yield of alcohol product was obtained after complete workup. ^{1}H NMR (500 MHz, $CDCl_3$) δ 3.79 – 3.71 (m, 1H), 2.00 (s, 1H), 1.48 – 1.34 (m, 3H), 1.26 (s, 7H), 1.15 (d, *J* = 6.2 Hz, 3H), 0.85 (t, *J* = 6.8 Hz, 3H). ^{13}C NMR (126 MHz, $CDCl_3$) δ 77.32, 77.06, 76.81, 68.02, 39.33, 31.83, 29.32, 25.73, 23.36, 22.59, 14.03.

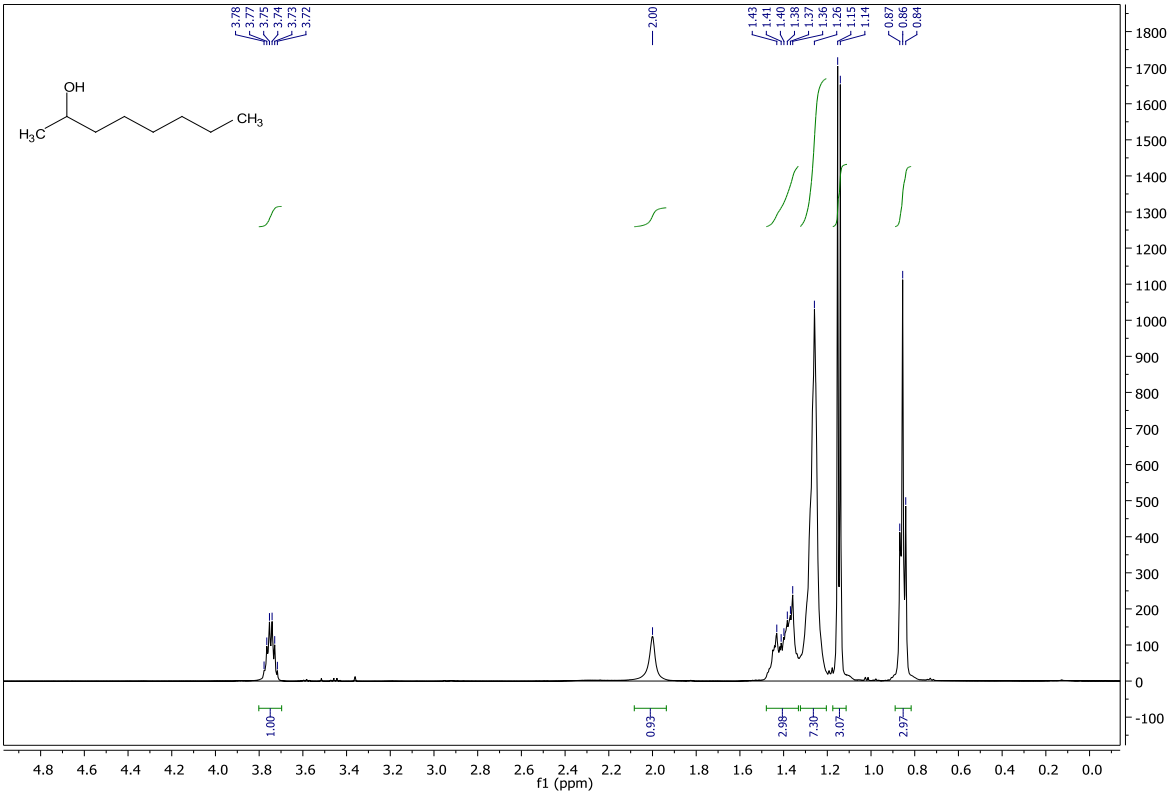

Figure 6.215. ^{1}H NMR for **2-i**

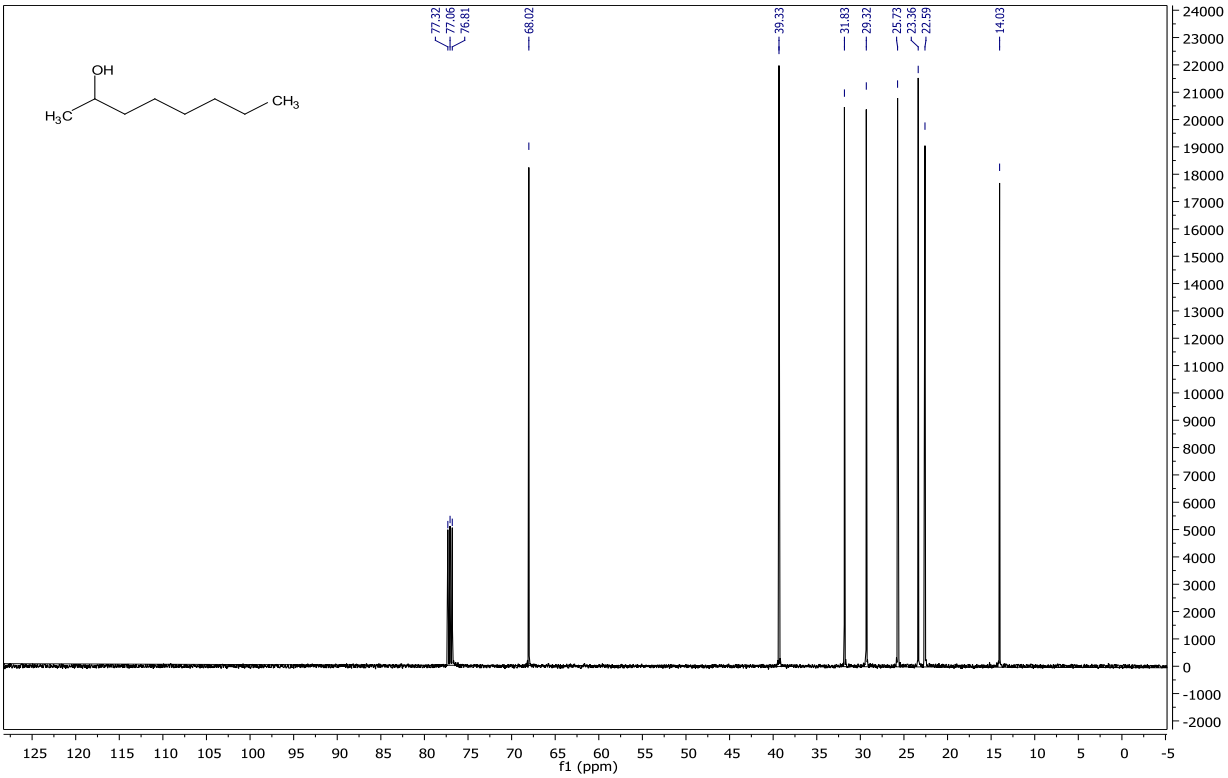

Figure 6.216. ^{13}C NMR for **2-i**

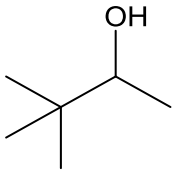

3,3-dimethylbutan-2-ol (2-j)

3,3-dimethylbutan-2-ol **(2-j)** was prepared from 3,3-dimethylbutan-2-one **(1-j)** by the procedure outlined in chapter 4. NMR analysis showed 100% conversion in 2 hours. 72% isolated yield of alcohol product was obtained after complete workup. ^{1}H NMR (400 MHz, $CDCl_3$) δ 3.43 (q, *J* = 6.4 Hz, 1H), 1.50 (s, 1H), 1.08 (d, *J* = 6.4 Hz, 3H), 0.85 (s, 9H). ^{13}C NMR (101 MHz, $CDCl_3$) δ 77.38, 77.06, 76.74, 75.64, 34.90, 25.42, 17.87.

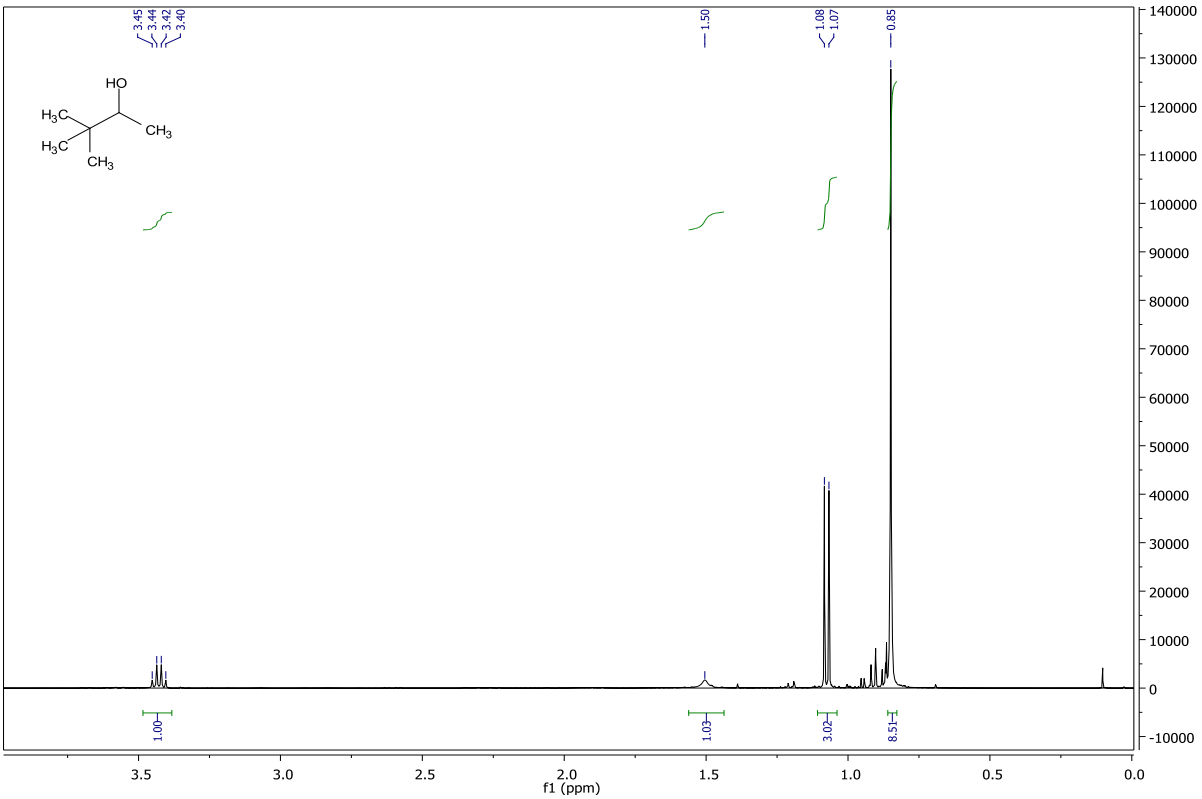

Figure 6.217. ^{1}H NMR for **2-j**

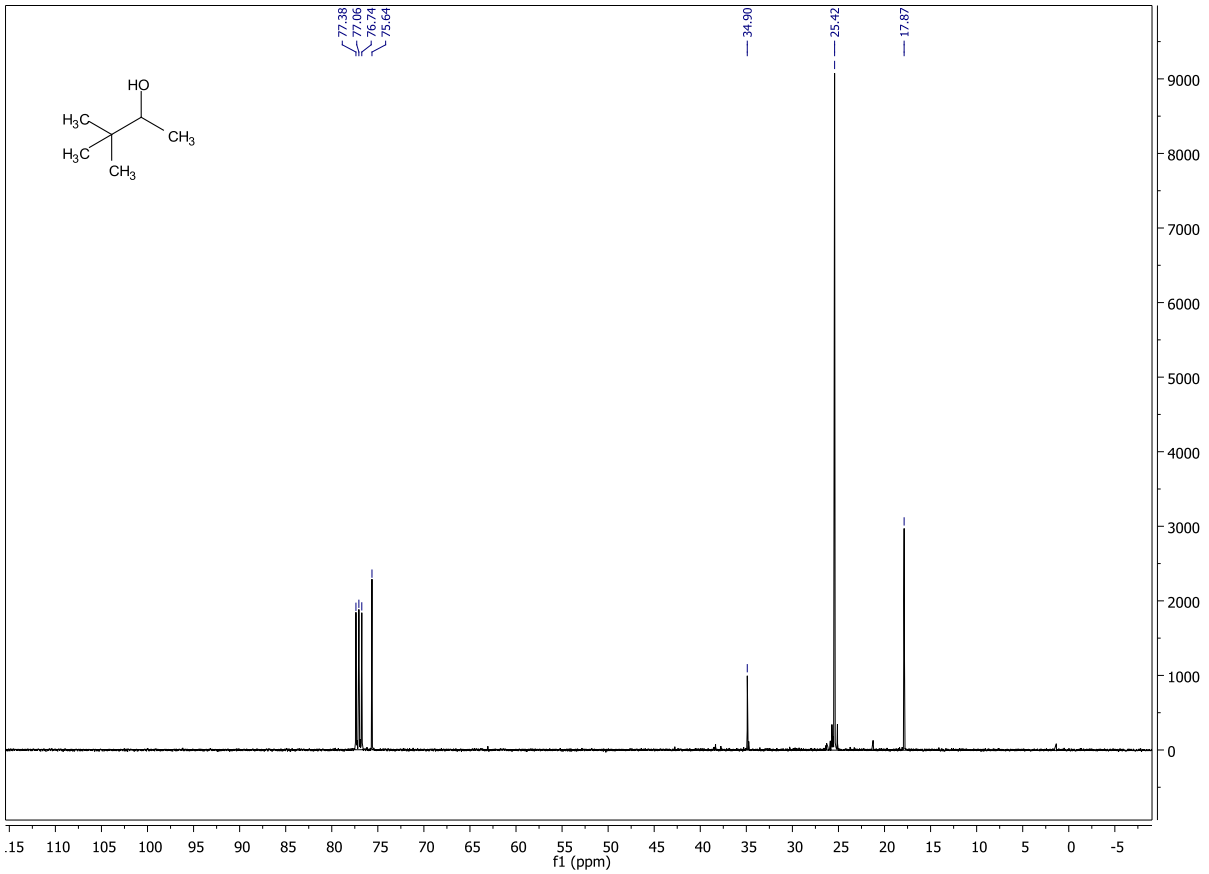

Figure 6.218. ^{13}C NMR for **2-j**

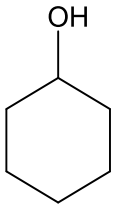

Cyclohexanol (2-k)

Cyclohexanol **(2-k)** was prepared from cyclohexanone **(1-k)** by the procedure outlined in chapter 4. NMR analysis showed 100% conversion in 2 hours. 43% isolated yield of alcohol product was obtained after complete workup. Note: Some of the product was lost during work up due to evaporation on the rotavap. ^{1}H NMR (500 MHz, $CDCl_3$) δ 3.59 (dt, *J* = 9.1, 4.3 Hz, 1H), 1.93 – 1.81 (m, 3H), 1.72 (dd, *J* = 8.7, 4.1 Hz, 2H), 1.54 (d, *J* = 11.7 Hz, 1H), 1.32 – 1.20 (m, 4H), 1.17 (dd, *J* = 16.3, 7.8 Hz, 1H). ^{13}C NMR (126 MHz, $CDCl_3$) δ 77.31, 77.06, 76.81, 70.29, 35.52, 25.45, 24.15.

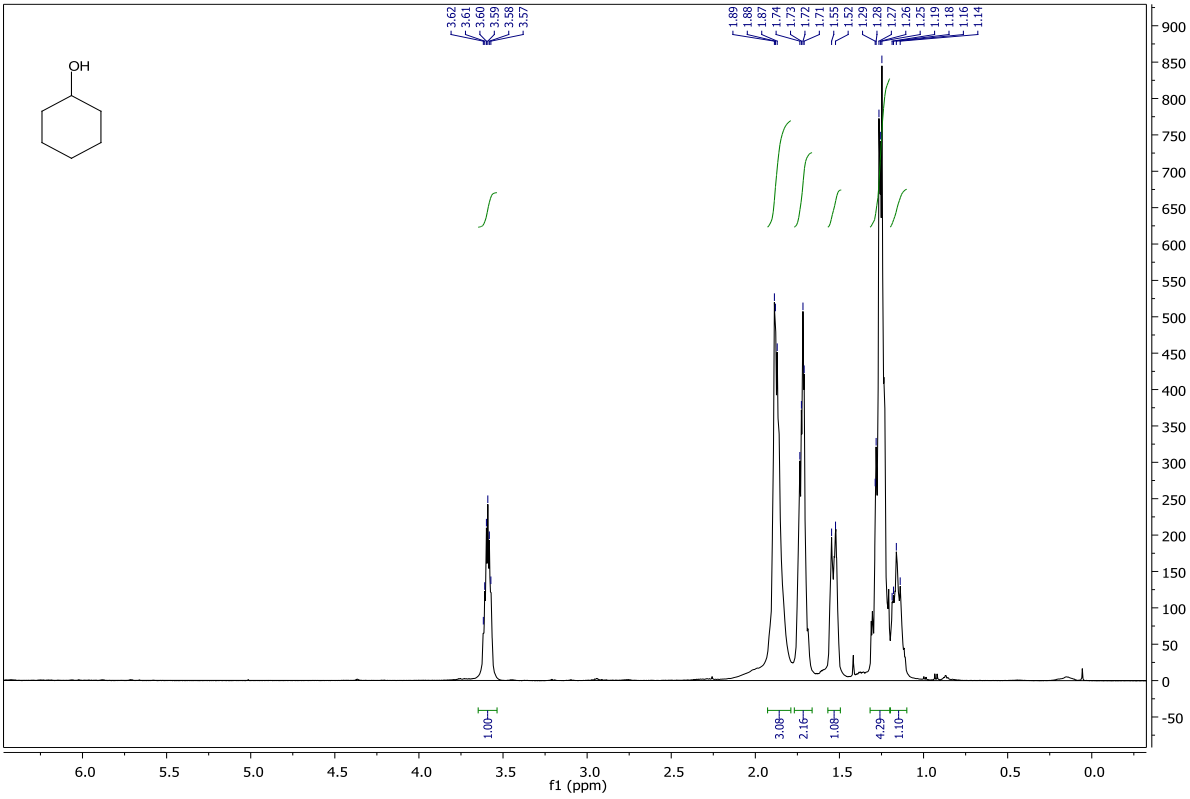

Figure 6.219. ^{1}H NMR for **2-k**

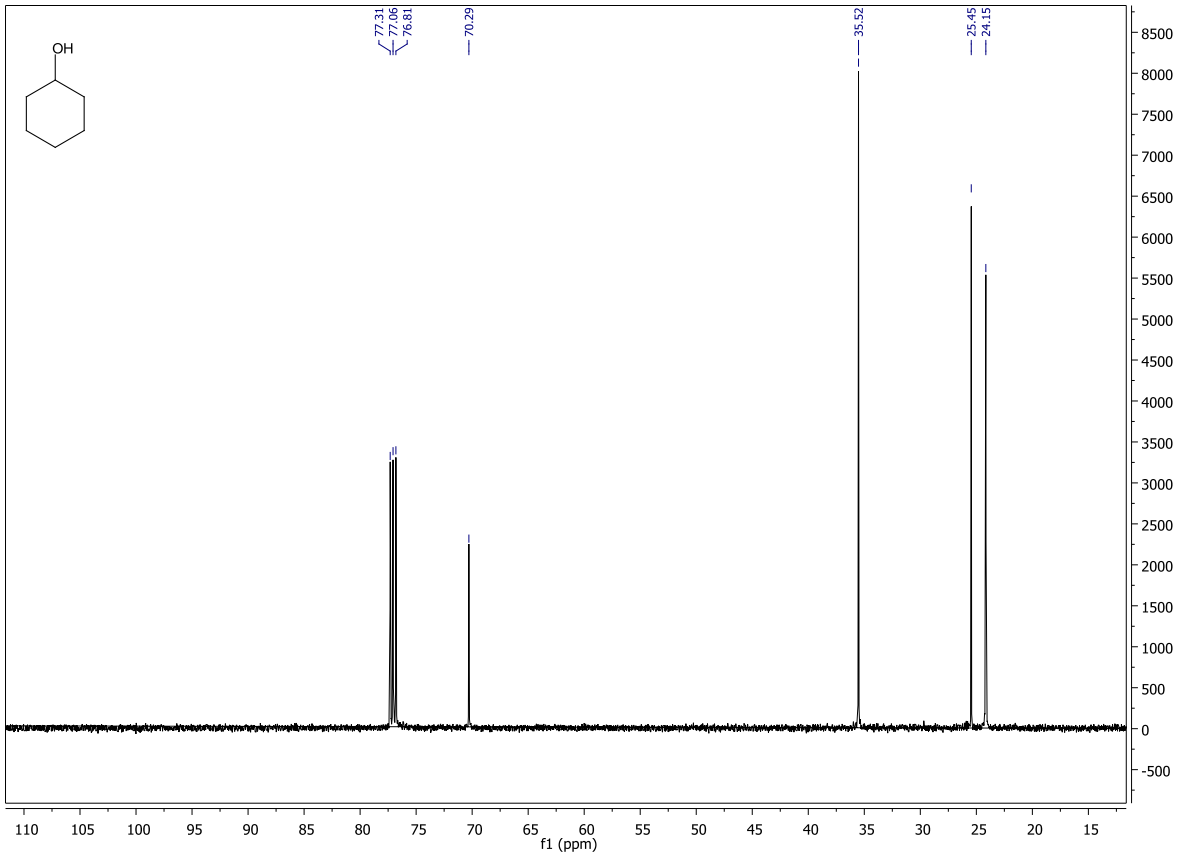

Figure 6.220. ^{13}C NMR for **2-k**

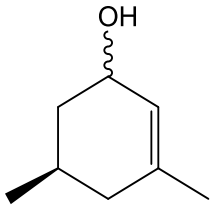

3,5-dimethylcyclohex-2-ene-1-ol (2-l)

3,5-dimethylcyclohex-2-ene-1-ol **(2-l)** was prepared from 3,5-dimethylcyclohex-2-en-1-one **(1-l)** by the procedure outlined in chapter 4. NMR analysis showed 100% conversion in 2 hours. 84% combined isolated yield of alcohol product was obtained after complete workup.

Determining ratio for *cis* isomer using H11 (See NMR spectra for 2-l)

(1.00/(1.00+0.22))*100% = 82%

Ratio for *trans* isomer

(0.22/(1.00+0.22)) *100% = 18%

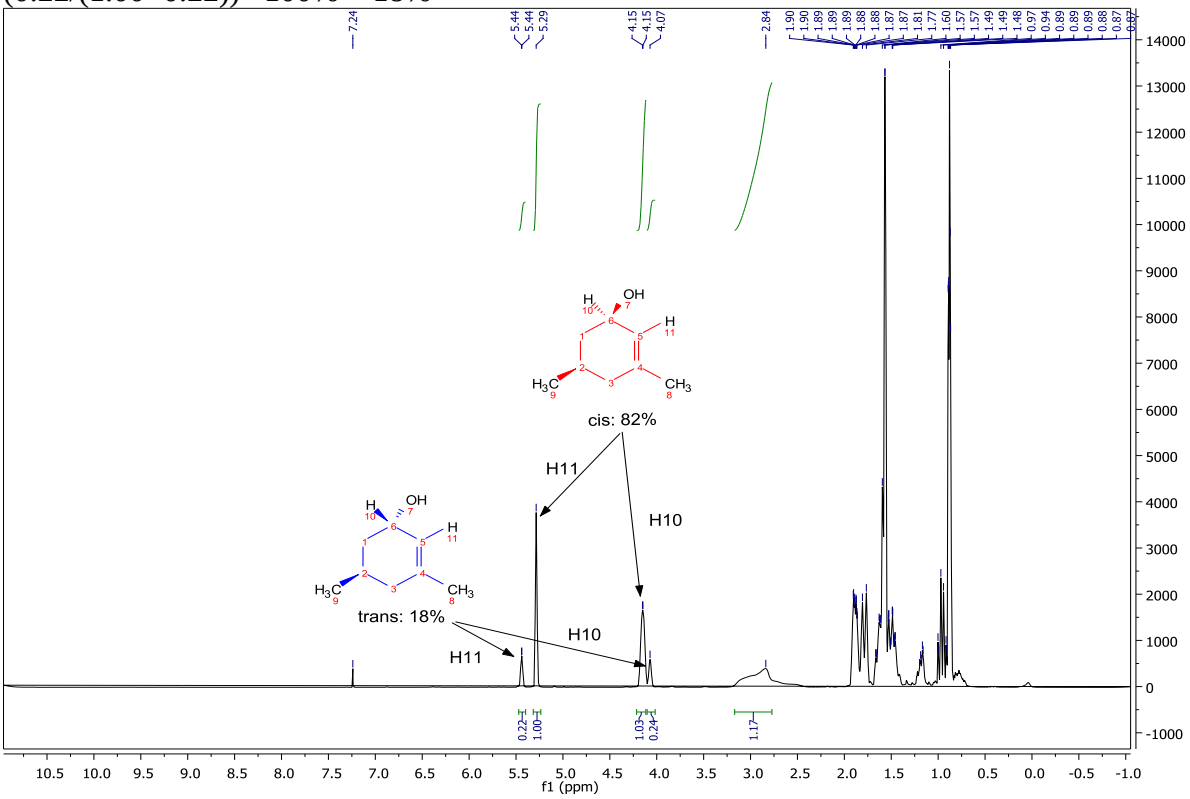

Figure 6.221. ^{1}H NMR for **2-l** and calculating ratio of cis vs. trans alcohol product

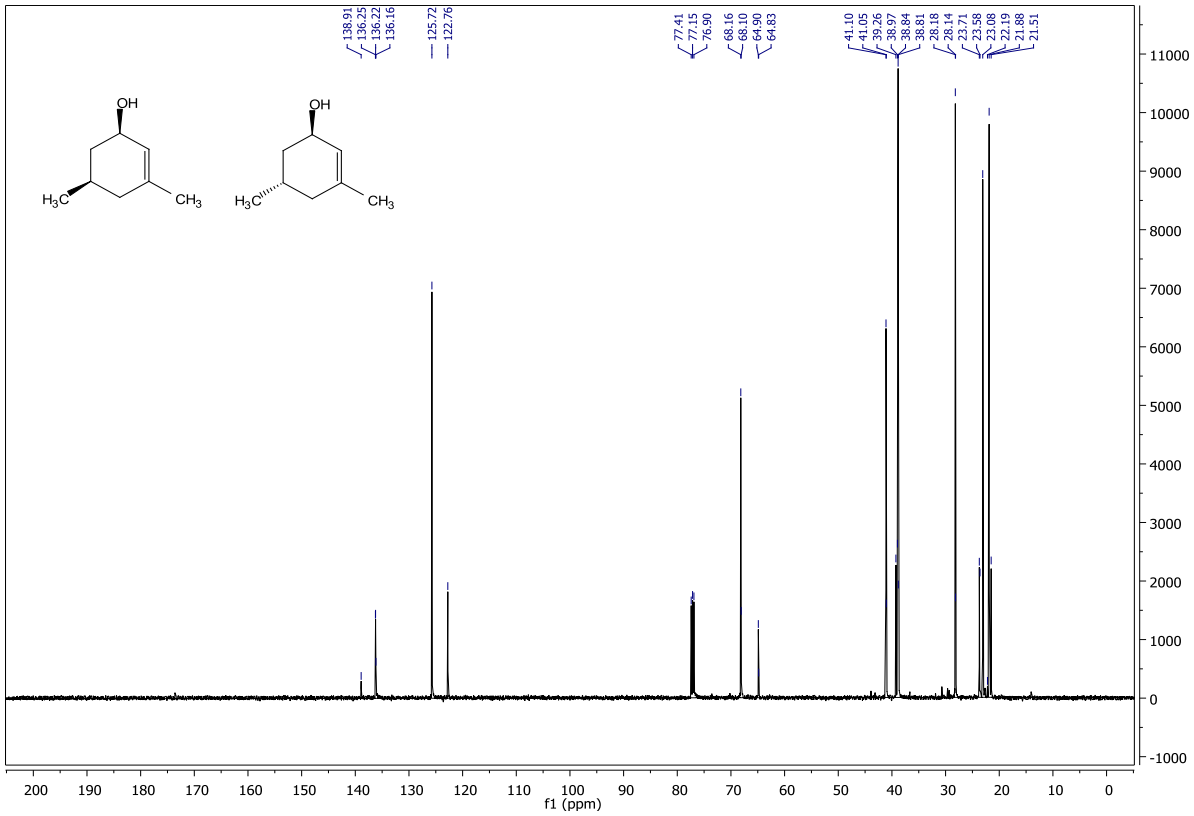

Figure 6.222. ^{13}C NMR for **2-l** (cis + trans alcohol products)

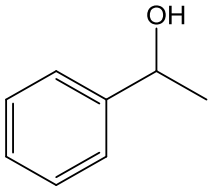

1-phenylethan-1-ol (2-m)

1-phenylethan-1-ol **(2-m)** was prepared from acetophenone **(1-m)** by the procedure outlined in chapter 4. NMR analysis showed 100% conversion in 2 hours. 73% isolated yield of alcohol product was obtained after complete workup. ^{1}H NMR (500 MHz, $CDCl_3$) δ 7.40 – 7.26 (m, 5H), 4.88 (q, *J* = 6.5 Hz, 1H), 2.42 (s, 1H), 1.50 (d, *J* = 6.5 Hz, 3H).^{13}C NMR (126 MHz, $CDCl_3$) δ 145.90, 128.51, 127.45, 125.45, 77.39, 77.14, 76.88, 70.35, 25.18.

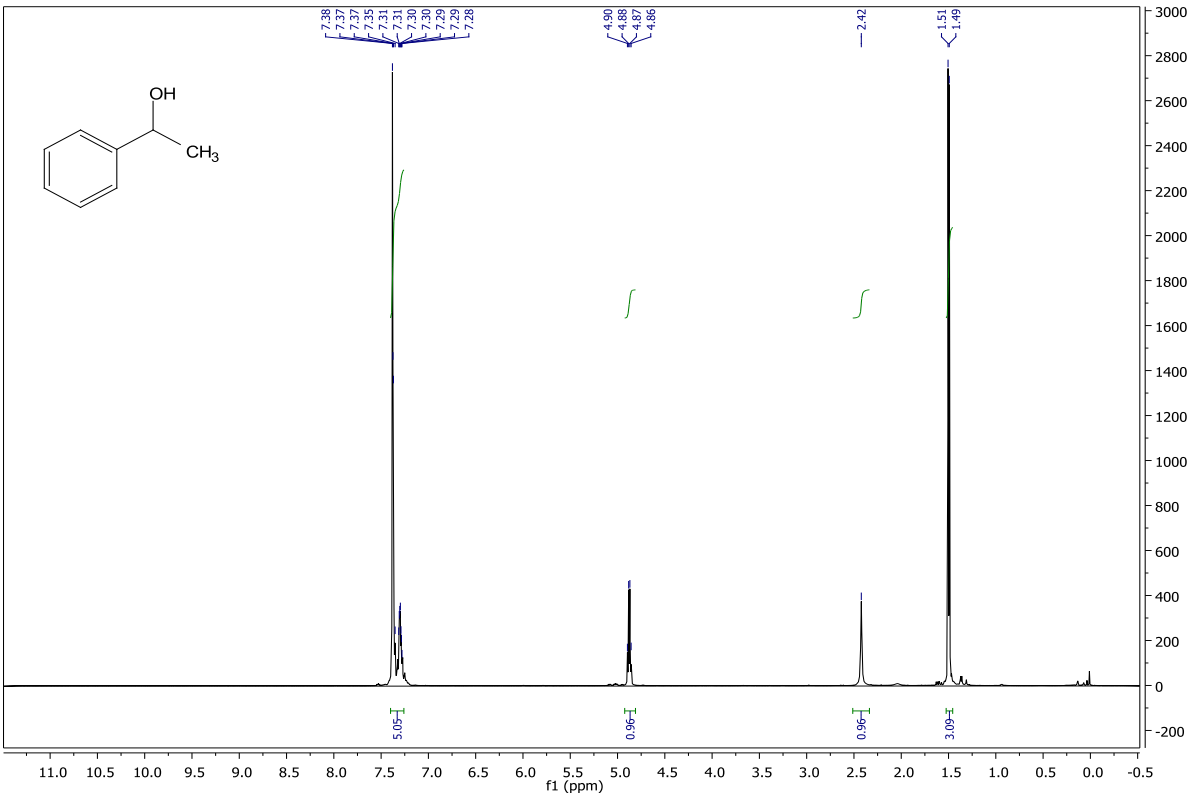

Figure 6.223. ^{1}H NMR for 2-m

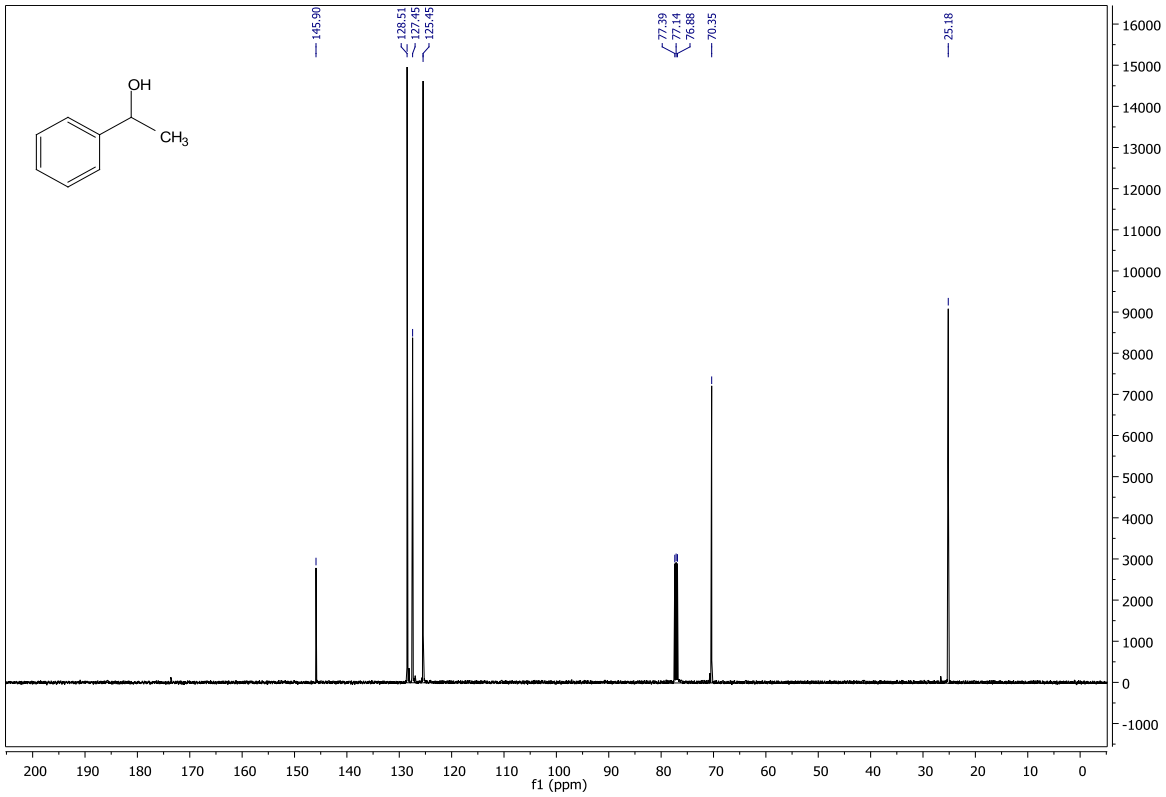

Figure 6.224. ^{13}C NMR for **2-m**

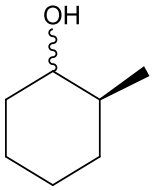

2-methylcyclohexanol (2-n)

2-methylcyclohexanol **(2-n)** was prepared from 2-methylcyclohexanone **(1-n)** by the procedure outlined in chapter 4. NMR analysis showed 100% conversion in 2 hours. 85% combined isolated yield of alcohol product was obtained after complete workup.

Determining ratio for *cis* isomer using H9 (See NMR spectra for 2-n)

(1.00/(1.00+0.49))*100% = 67%

Ratio for *trans* isomer

(0.49/(1.00+0.49)) *100% = 33%

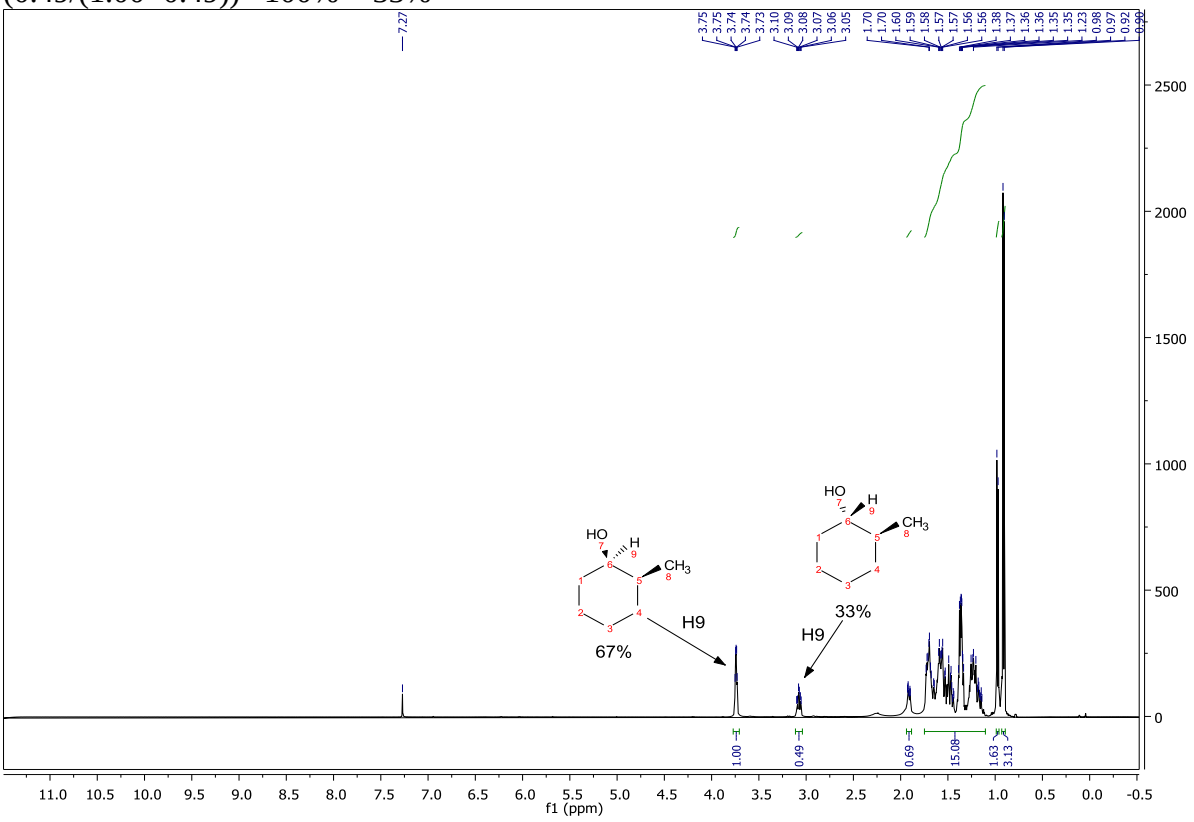

Figure 6.225. ^{1}H NMR for **2-n** and calculating ratio of cis vs. trans alcohol product

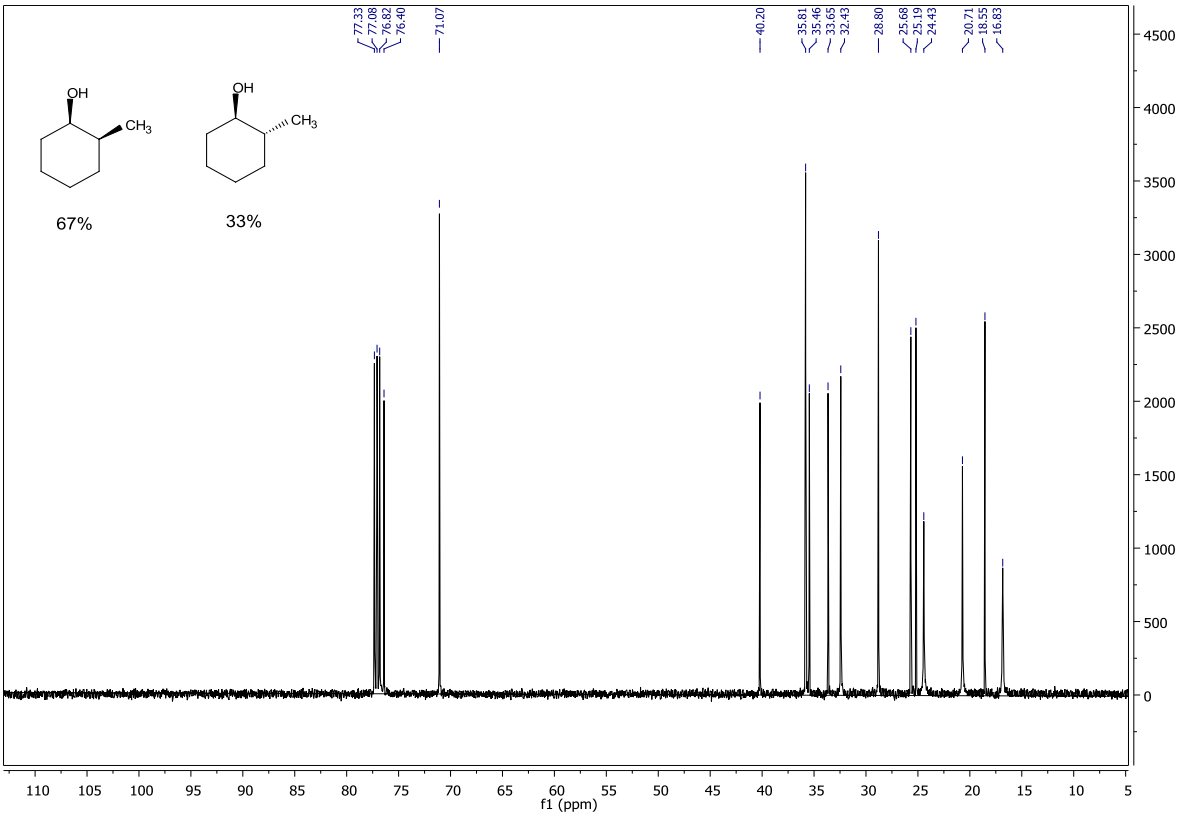

Figure 6.226. ^{13}C NMR for **2-n** (cis + trans alcohol products)

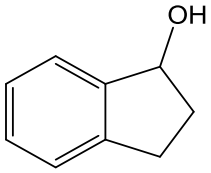

2,3-dihydro-1H-inden-1-ol (2-o)

2,3-dihydro-1H-inden-1-ol **(2-o)** was prepared from 2,3-dihydro-1H-inden-1-one **(1-o)** by the procedure outlined in chapter 4. NMR analysis showed 100% conversion in 2 hours. 89% isolated yield of alcohol product was obtained after complete workup. ^{1}H NMR (400 MHz, $CDCl_3$) δ 7.38 (d, *J* = 6.7 Hz, 1H), 7.30 – 7.19 (m, 3H), 5.16 (t, *J* = 6.1 Hz, 1H), 3.22 (s, 1H), 3.02 (ddd, *J* = 16.0, 8.6, 4.7 Hz, 1H), 2.83 – 2.73 (m, 1H), 2.46 – 2.36 (m, 1H), 1.89 (dddd, *J* = 13.2, 8.6, 6.8, 5.5 Hz, 1H). ^{13}C NMR (101 MHz, $CDCl_3$) δ 145.09, 143.34, 128.22, 126.68, 124.88, 124.39, 77.60, 77.28, 76.96, 76.16, 35.74, 29.86.

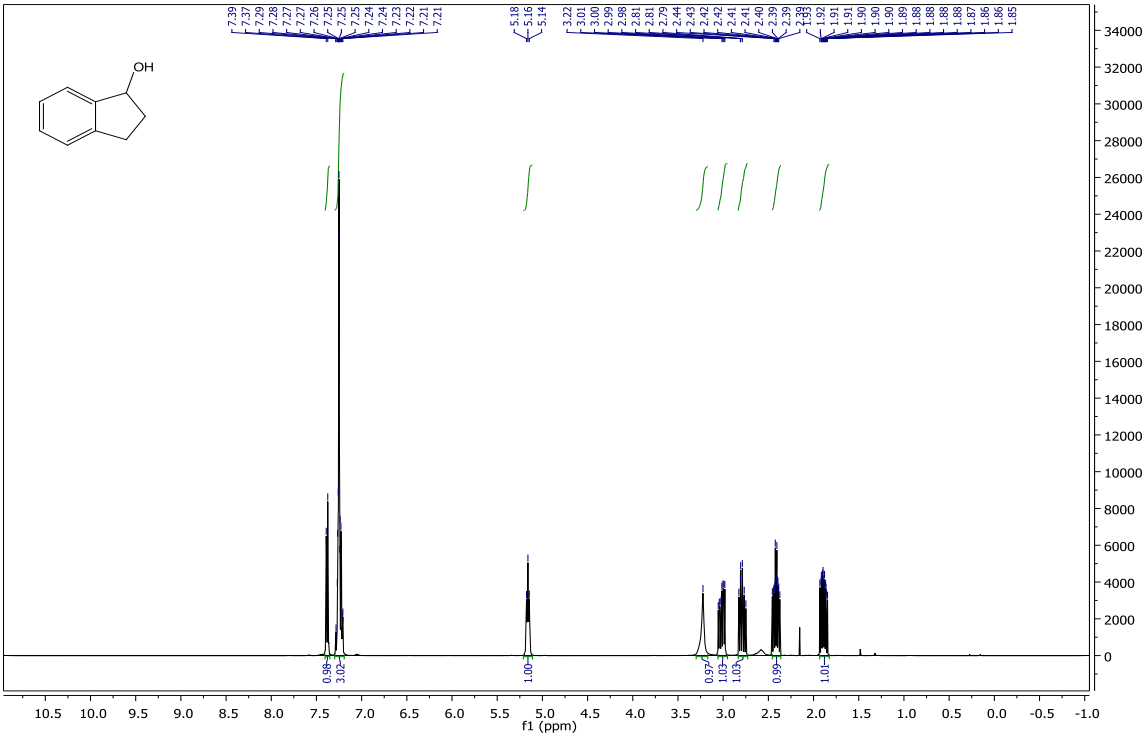

Figure 6.227. ^{1}H NMR for **2-o**

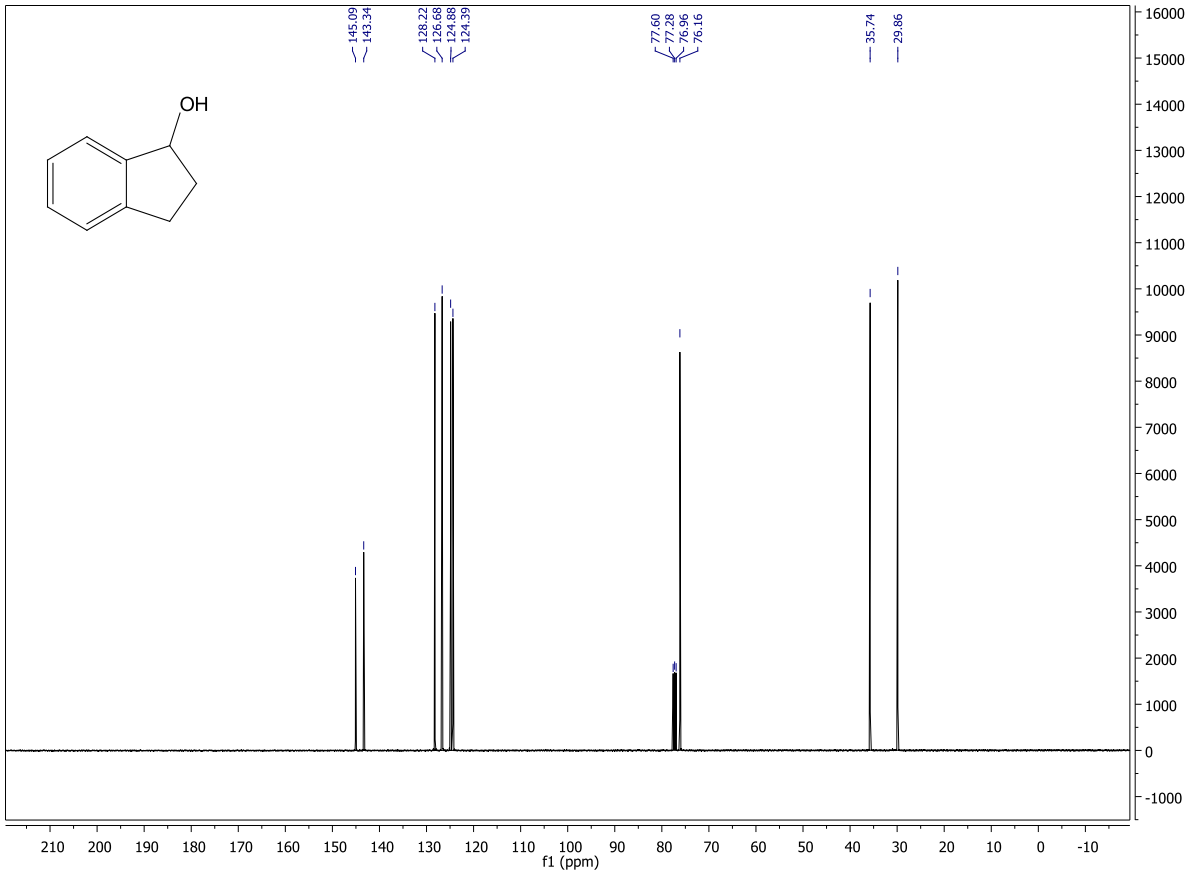

Figure 6.228. ^{13}C NMR for **2-o**

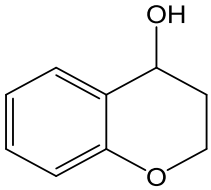

Chroman-4-ol (2-p)

Chroman-4-ol **(2-p)** was prepared from chroman-4-one **(1-p)** by the procedure outlined in chapter 4. NMR analysis showed 100% conversion in 2 hours. 82% isolated yield of alcohol product was obtained after complete workup. ^{1}H NMR (400 MHz, $CDCl_3$) δ 7.22 (dd, *J* = 7.6, 1.7 Hz, 1H), 7.19 – 7.13 (m, 1H), 6.87 (td, *J* = 7.4, 1.2 Hz, 1H), 6.80 (dd, *J* = 8.2, 1.2 Hz, 1H), 4.60 (d, *J* = 3.2 Hz, 1H), 4.20 – 4.07 (m, 2H), 3.35 (d, *J* = 3.2 Hz, 1H), 2.04 – 1.92 (m, 1H), 1.90 – 1.82 (m, 1H). ^{13}C NMR (101 MHz, $CDCl_3$) δ 154.52, 129.91, 129.62, 124.31, 120.56, 116.97, 77.58, 77.26, 76.94, 62.98, 62.01, 30.83.

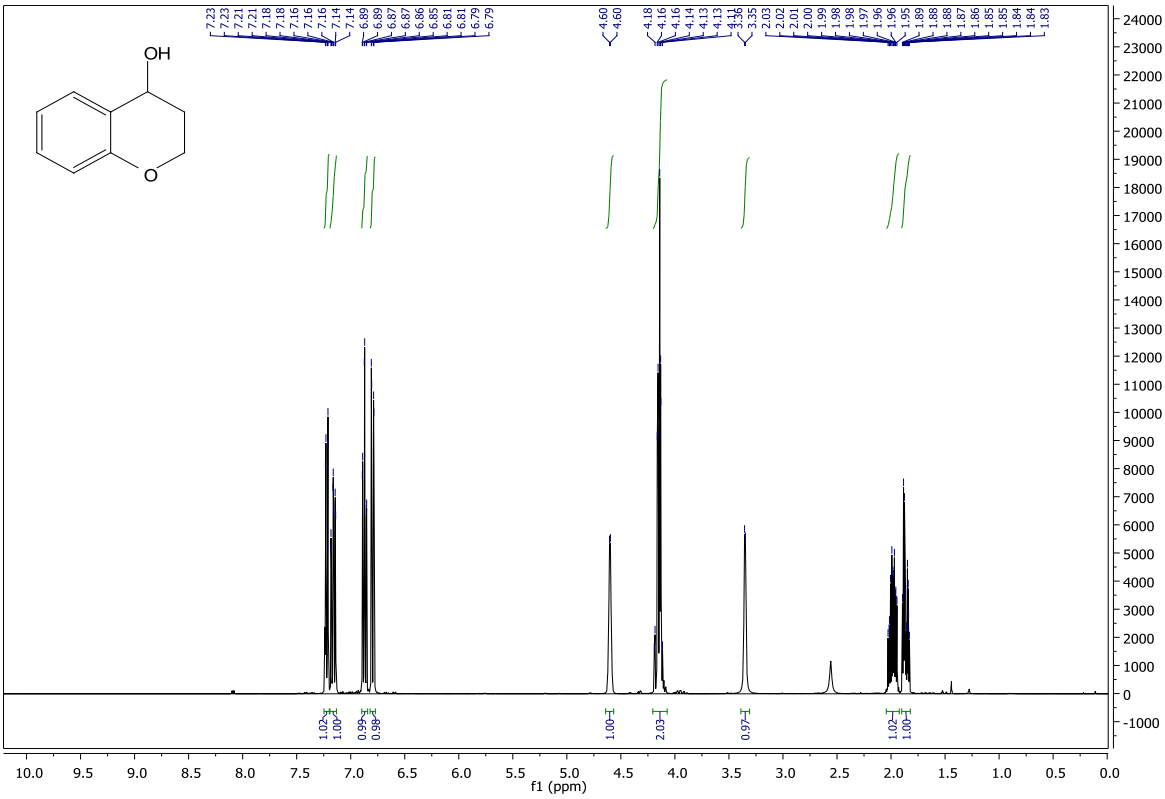

Figure 6.229. ^{1}H NMR for **2-p**

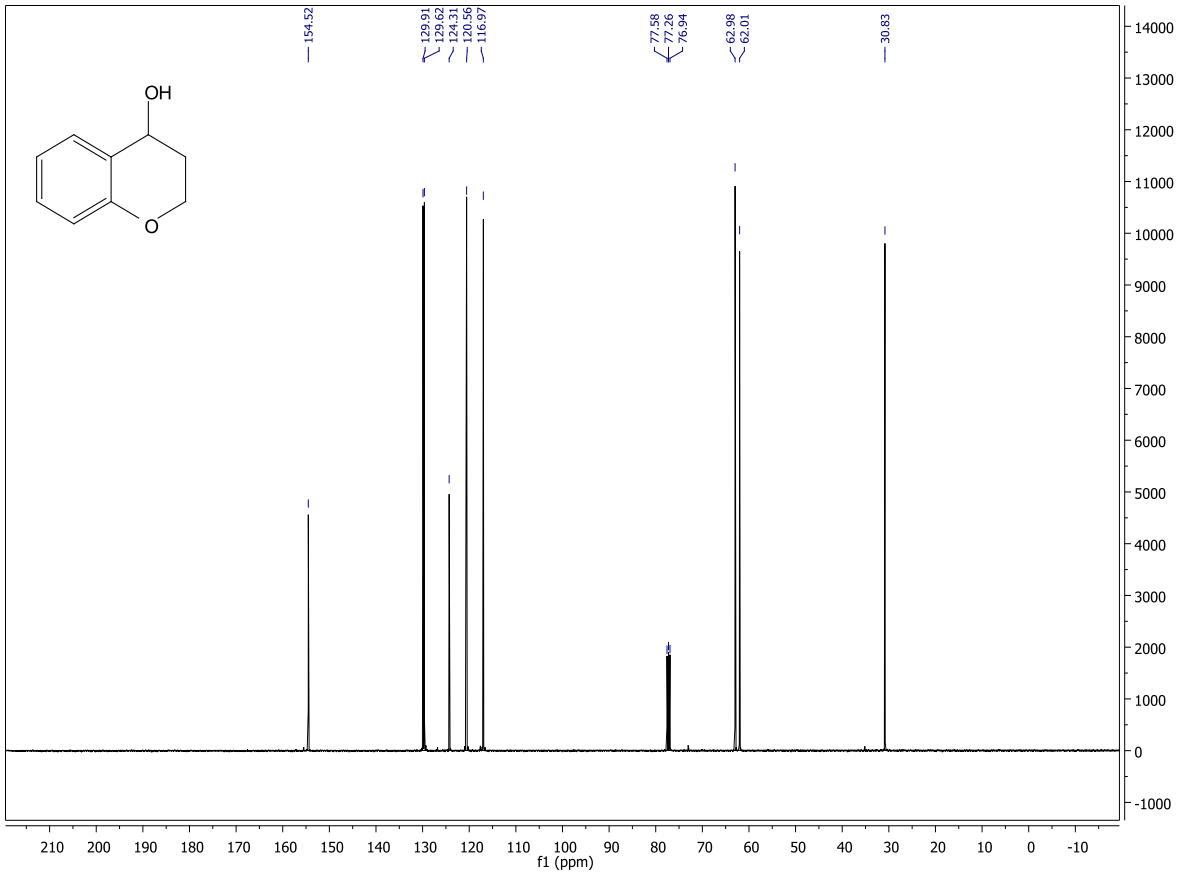

Figure 6.230. ^{13}C NMR for **2-p**

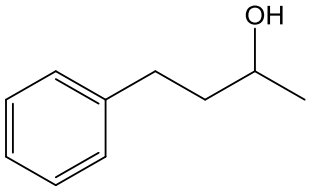

4-phenylbutan-2-ol (2-q)

4-phenylbutan-2-ol **(2-q)** was prepared from 4-phenylbutan-2-one **(1-q)** by the procedure outlined in chapter 4. NMR analysis showed 100% conversion in 2 hours. 97% isolated yield of alcohol product was obtained after complete workup. ^{1}H NMR (400 MHz, $CDCl_3$) δ 7.33 – 7.27 (m, 2H), 7.25 – 7.18 (m, 3H), 3.83 (d, *J* = 5.7 Hz, 1H), 2.73 (dddd, *J* = 37.5, 13.8, 9.4, 6.5 Hz, 2H), 2.31 (d, *J* = 2.5 Hz, 1H), 1.87 – 1.70 (m, 2H), 1.24 (d, *J* = 6.2 Hz, 3H). ^{13}C NMR (101 MHz, $CDCl_3$) δ 142.21, 128.49, 128.47, 125.87, 77.54, 77.23, 76.91, 67.44, 40.91, 32.22, 23.61.

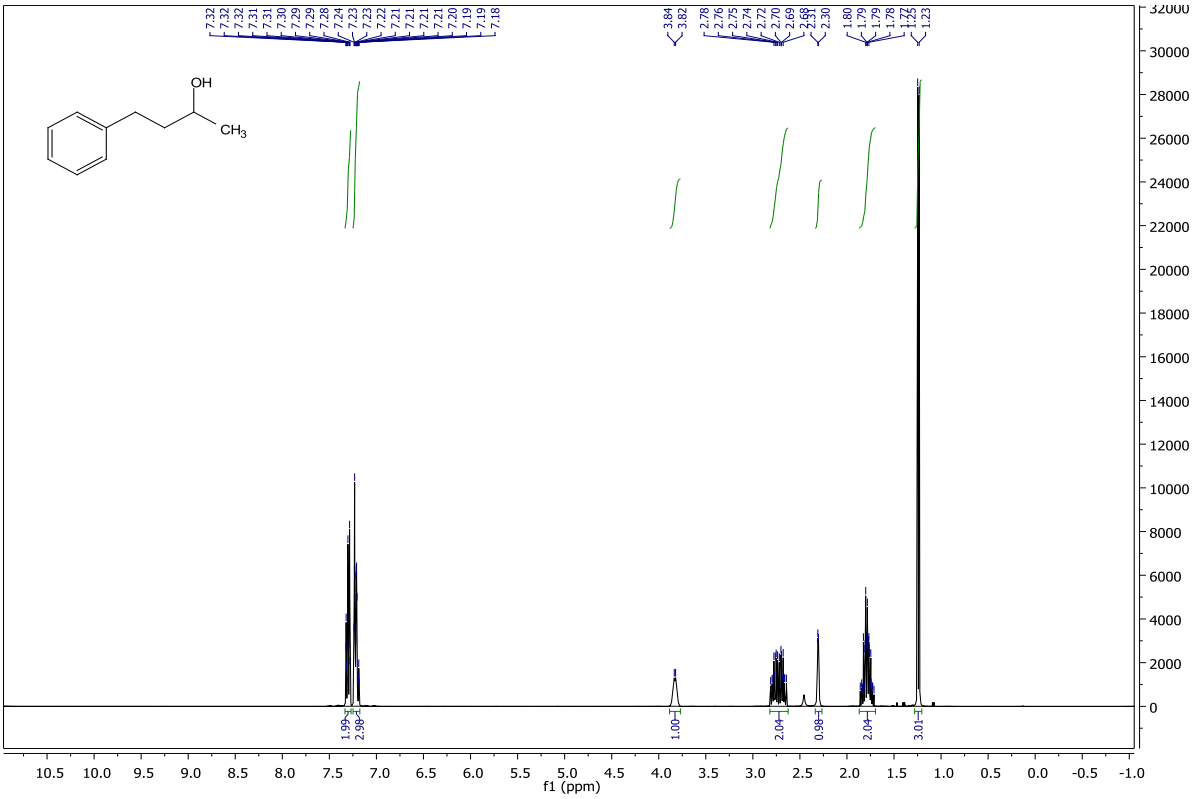

Figure 6.231. ^{1}H NMR for **2-q**

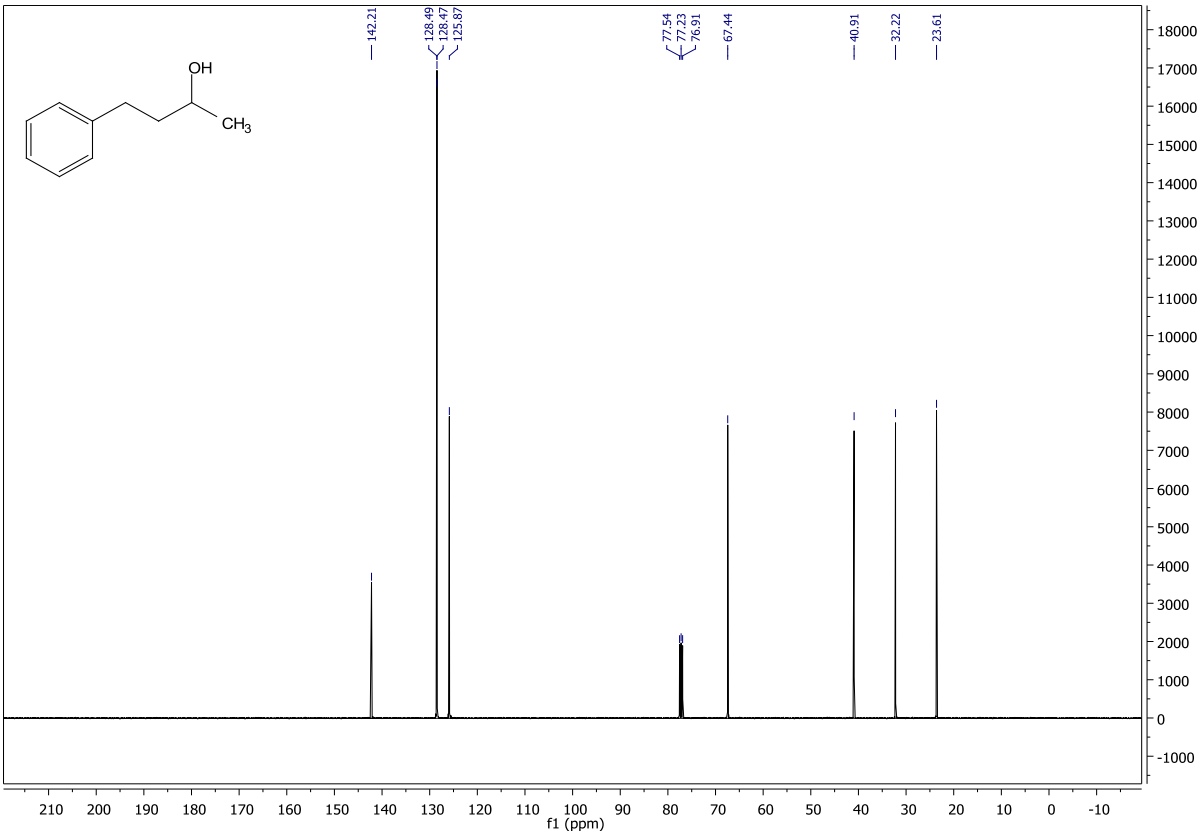

Figure 6.232. ^{13}C NMR for **2-q**

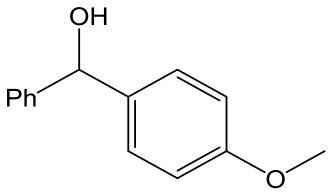

(4-methoxyphenyl) (phenyl) methanol (2-r)

(4-methoxyphenyl) (phenyl) methanol **(2-r)** was prepared from (4-methoxyphenyl) (phenyl) methanone **(1-r)** by the procedure outlined in chapter 4. NMR analysis showed 100% conversion in 2 hours. 88% isolated yield of alcohol product was obtained after complete workup. ^{1}H NMR (400 MHz, $CDCl_3$) δ 7.41 – 7.24 (m, 7H), 6.91 – 6.85 (m, 2H), 5.69 (d, *J* = 2.8 Hz, 1H), 3.77 (s, 3H), 3.37 (d, *J* = 3.3 Hz, 1H). ^{13}C NMR (101 MHz, $CDCl_3$) δ 158.95, 144.30, 136.45, 128.50, 128.10, 127.43, 126.60, 113.91, 77.70, 77.38, 77.06, 75.67, 55.33.

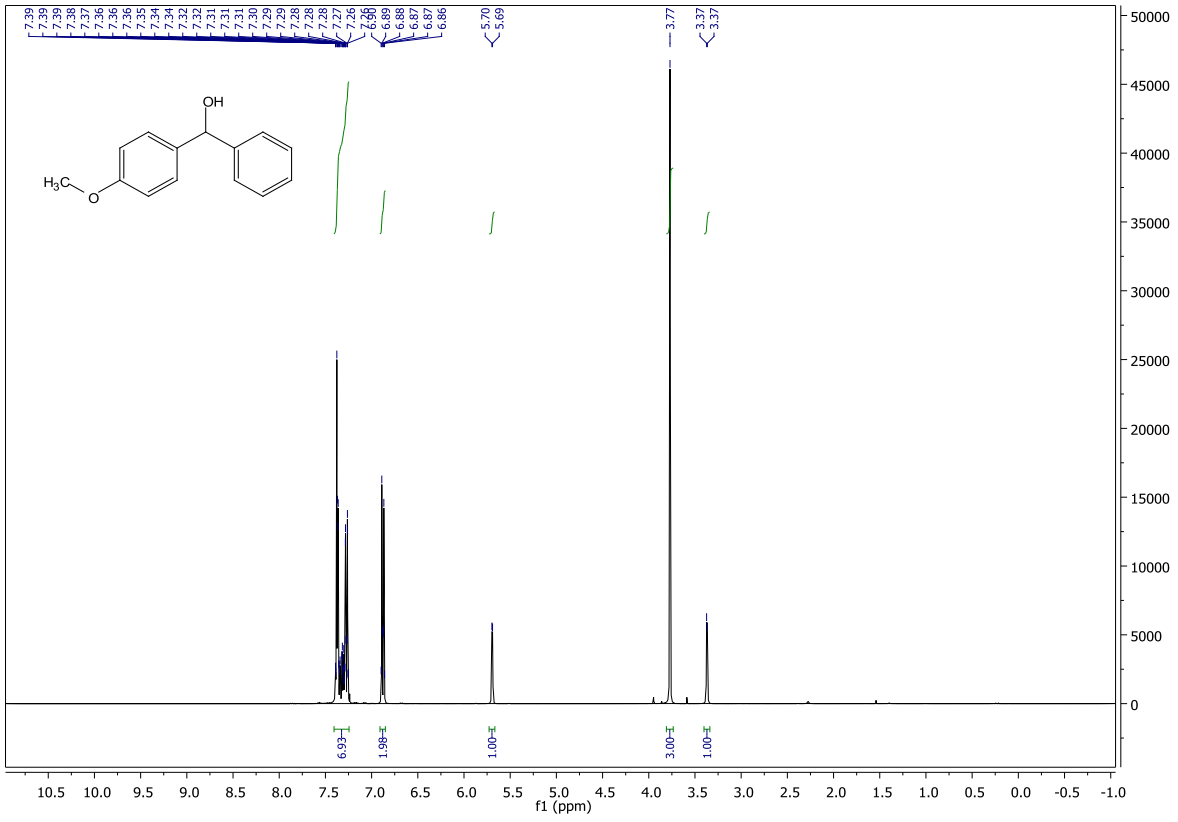

Figure 6.233. ^{1}H NMR for **2-r**

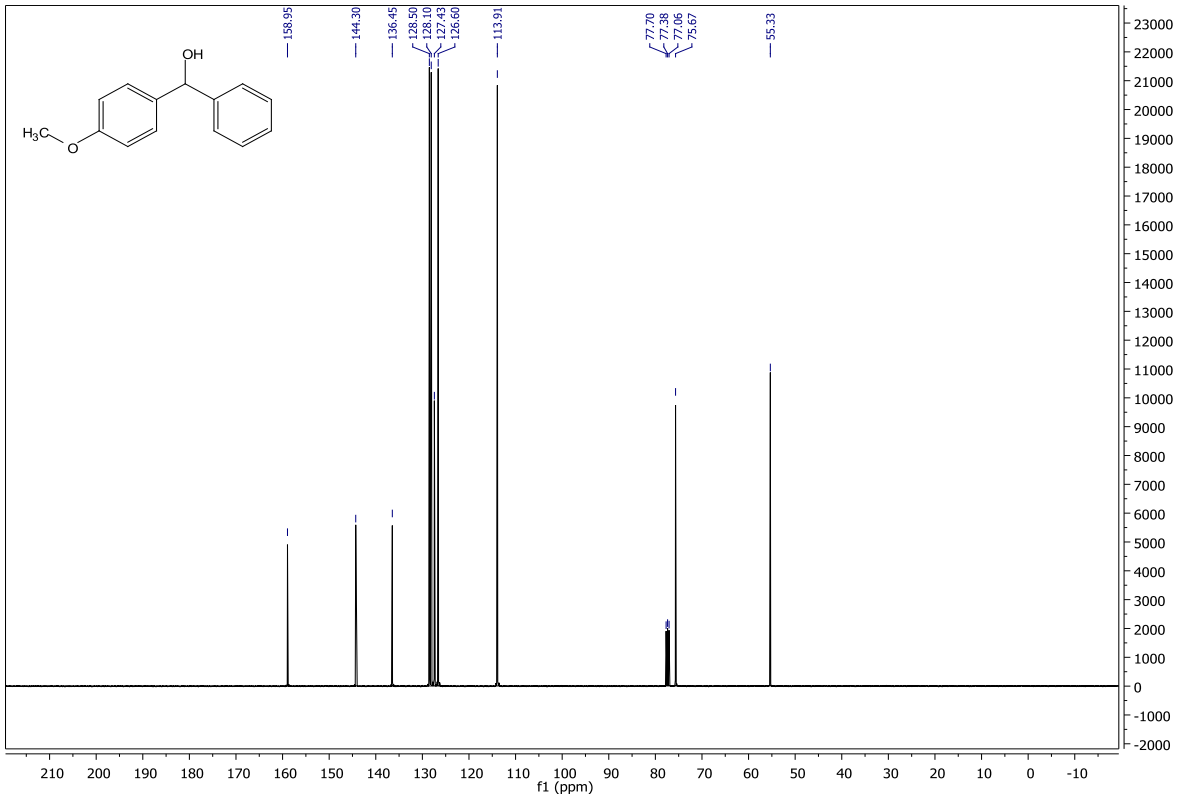

Figure 6.234. ^{13}C NMR for **2-r**

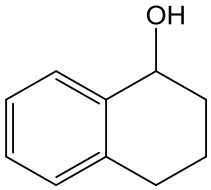

1,2,3,4-tetrahydronaphthalen-1-ol (2-s)

1,2,3,4-tetrahydronaphthalen-1-ol **(2-s)** was prepared from 3,4-dihydronaphthalen-1(2H)-one **(1-s)** by the procedure outlined in chapter 4. NMR analysis showed 100% conversion in 2 hours. 92% isolated yield of alcohol product was obtained after complete workup. ^{1}H NMR (400 MHz, CDCl3) δ 7.45 – 7.39 (m, 1H), 7.24 – 7.18 (m, 2H), 7.14 – 7.08 (m, 1H), 4.74 – 4.69 (m, 1H), 2.83 (ddd, *J* = 16.9, 8.2, 4.1 Hz, 1H), 2.73 (ddd, *J* = 16.5, 8.0, 5.8 Hz, 2H), 2.03 – 1.91 (m, 2H), 1.91 – 1.82 (m, 1H), 1.82 – 1.70 (m, 1H). ^{13}C NMR (101 MHz, CDCl3) δ 138.93, 137.16, 129.00, 128.82, 127.52, 126.16, 77.60, 77.29, 76.97, 68.02, 32.29, 29.34, 18.98.

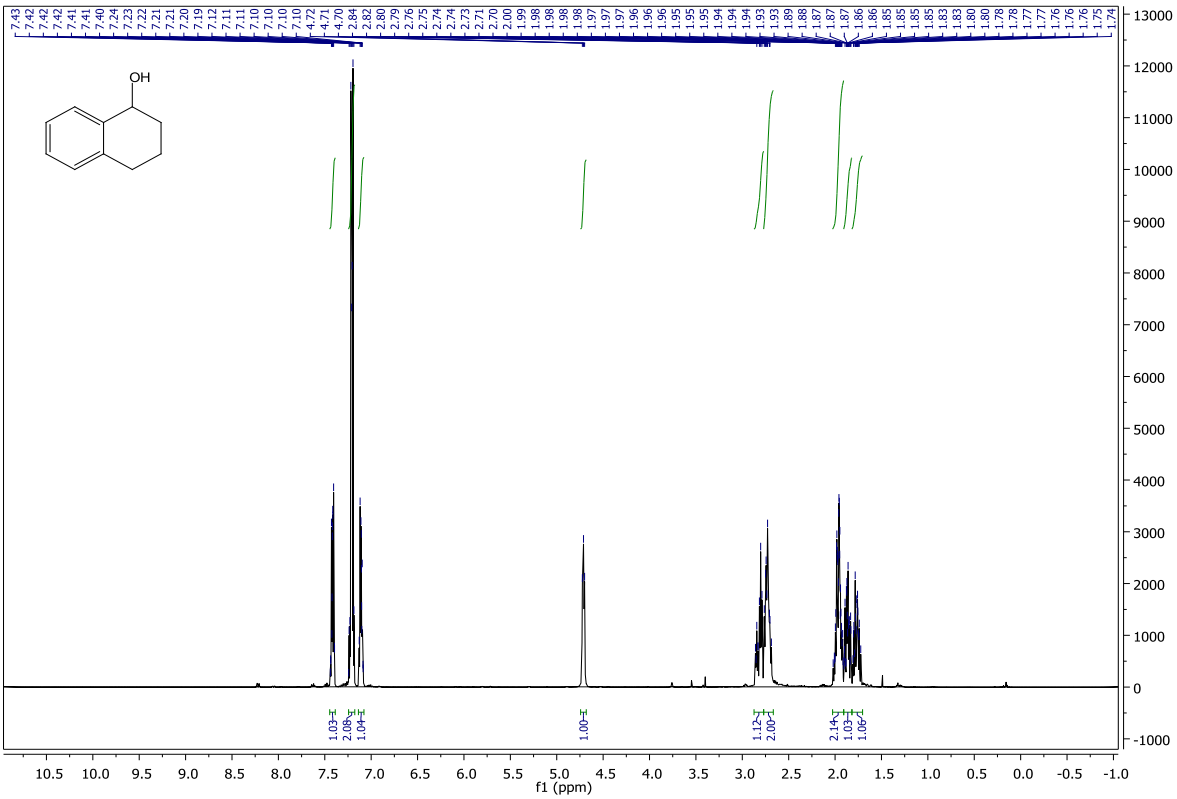

Figure 6.235. ^{1}H NMR for **2-s**

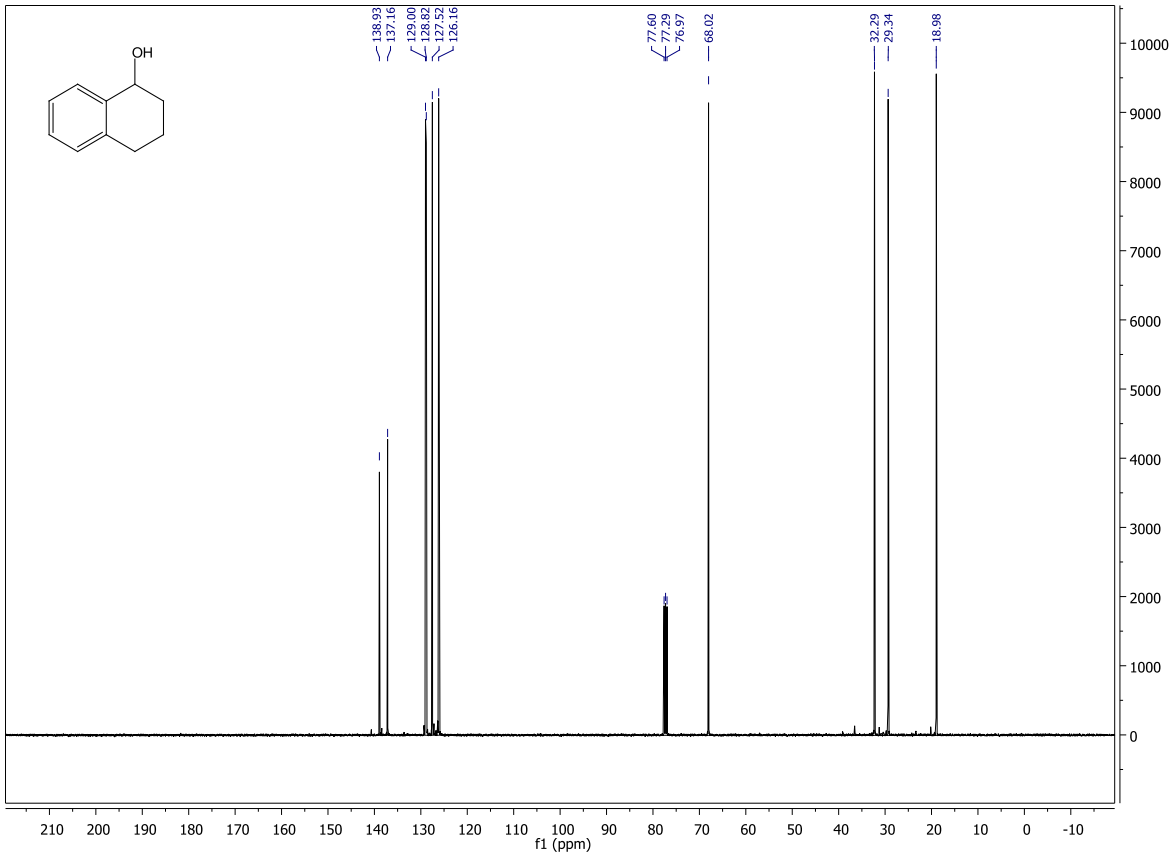

Figure 6.236. ^{13}C NMR for **2-s**

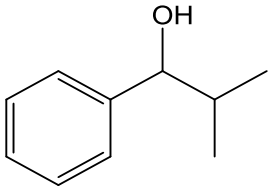

2-methyl-1-phenylpropan-1-ol (2-t)

2-methyl-1-phenylpropan-1-ol **(2-t)** was prepared from 2-methyl-1-phenylpropan-1-one **(1-t)** by the procedure outlined in chapter 4. NMR analysis showed 100% conversion in 2 hours. 99% isolated yield of alcohol product was obtained after complete workup. ^{1}H NMR (400 MHz, $CDCl_3$) δ 7.35 – 7.29 (m, 2H), 7.29 – 7.23 (m, 3H), 4.27 (d, *J* = 6.9 Hz, 1H), 2.80 (s, 1H), 1.98 – 1.84 (m, *J* = 6.8 Hz, 1H), 0.99 (d, *J* = 6.7 Hz, 3H), 0.78 (d, *J* = 6.8 Hz, 3H). ^{13}C NMR (101 MHz, $CDCl_3$) δ 143.75, 128.15, 127.35, 126.74, 79.93, 77.58, 77.27, 76.95, 35.24, 19.01, 18.48.

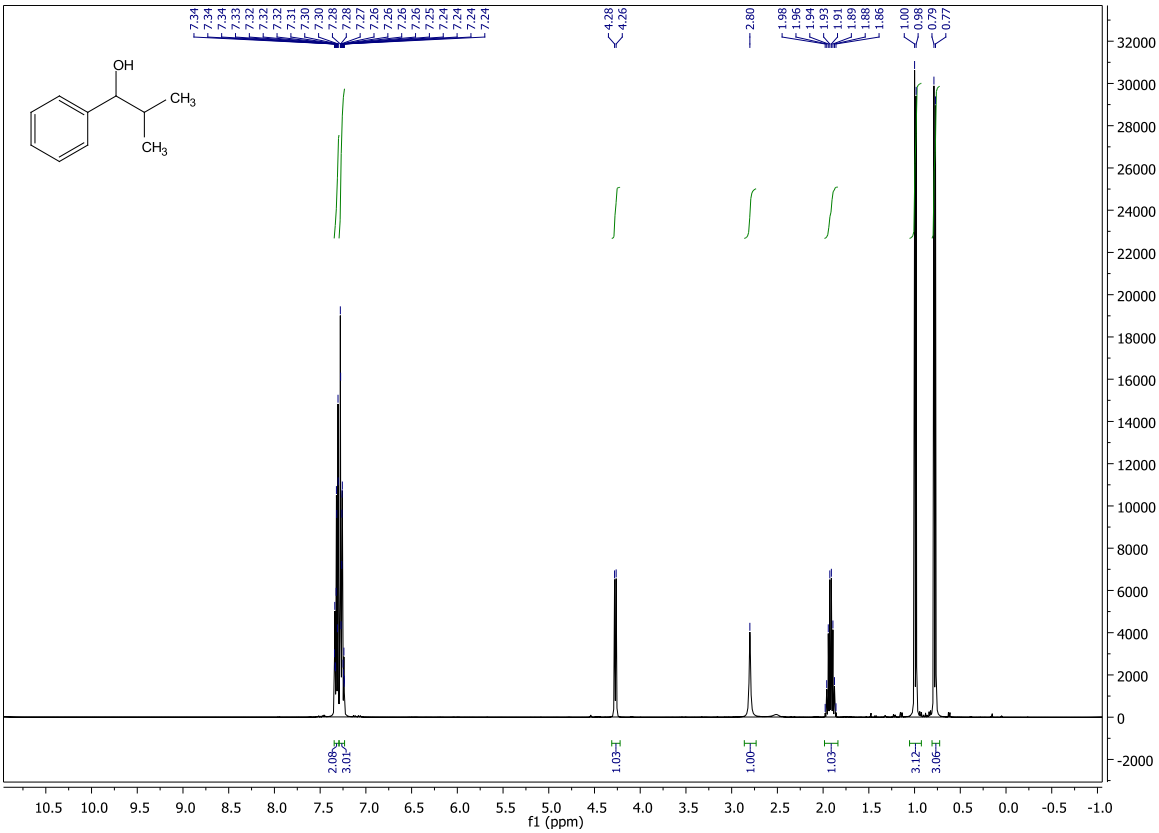

Figure 6.237. ^{1}H NMR for **2-t**

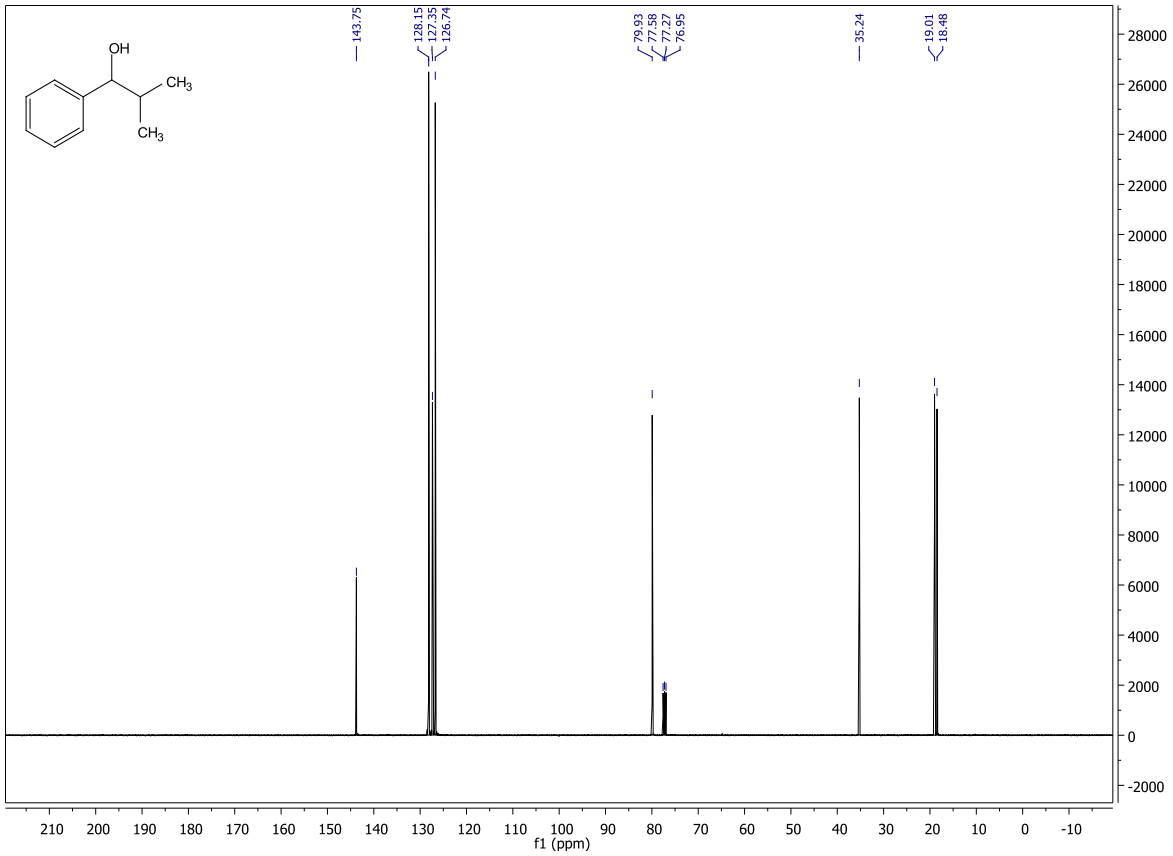

Figure 6.238. ^{13}C NMR for **2-t**

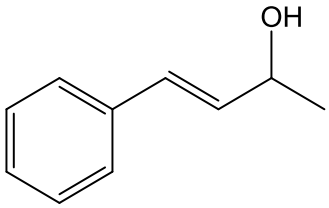

4-phenylbut-3-en-2-ol (2-u)

4-phenylbut-3-en-2-ol **(2-u)** was prepared from 4-phenylbut-3-en-2-one **(1-u)** by the procedure outlined in chapter 4. NMR analysis showed 66% conversion in 2 hours. Reaction did not proceed any further and 63% isolated yield of alcohol product was obtained after complete workup and flash chromatography (Hex: EtOAc = 70:30). ^{1}H NMR (400 MHz, $CDCl_3$) δ 7.36 (dt, *J* = 2.9, 1.9 Hz, 2H), 7.33 – 7.28 (m, 2H), 7.25 – 7.21 (m, 1H), 6.55 (d, *J* = 15.9 Hz, 1H), 6.25 (dd, *J* = 15.9, 6.4 Hz, 1H), 4.47 (pd, *J* = 6.4, 1.2 Hz, 1H), 2.17 (s, 1H), 1.36 (d, *J* = 6.4 Hz, 3H). ^{13}C NMR (101 MHz, $CDCl_3$) δ 136.74, 133.63, 129.35, 128.64, 127.67, 126.50, 77.47, 77.15, 76.84, 68.92, 23.45.

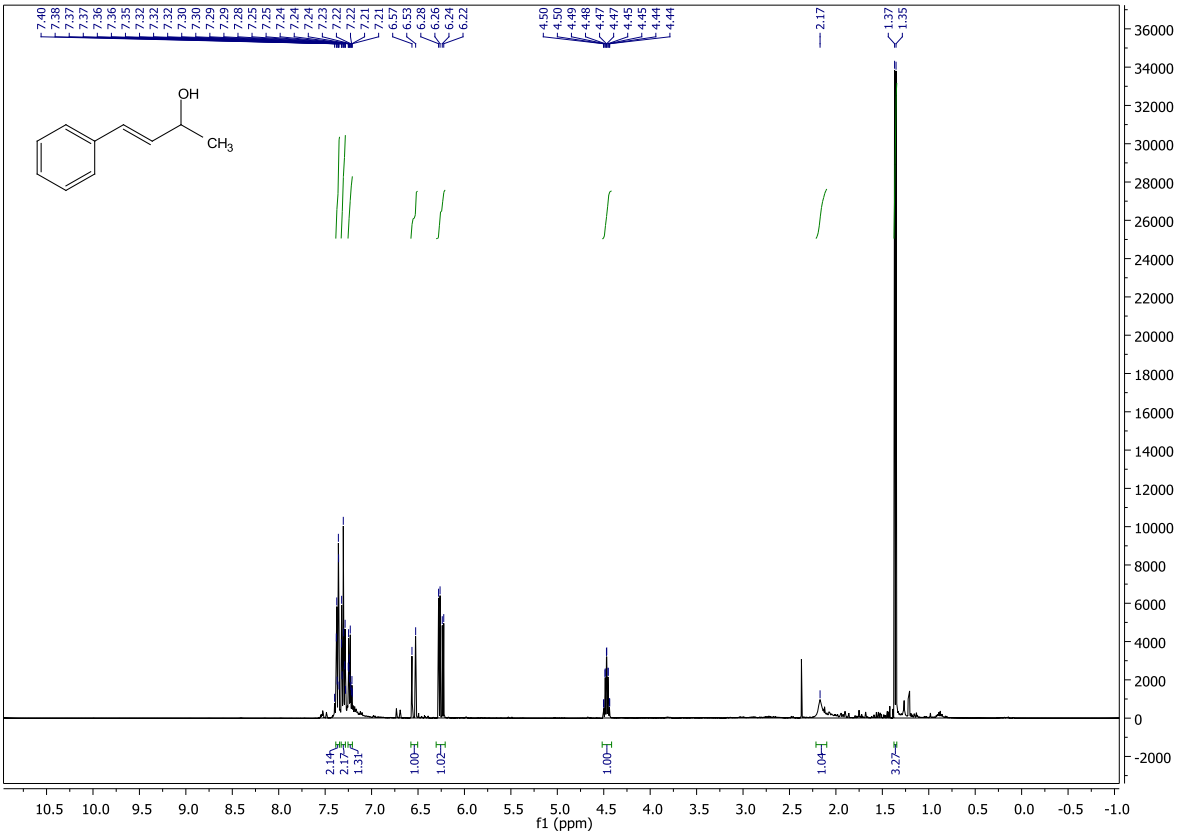

Figure 6.239. ^{1}H NMR for **2-u**

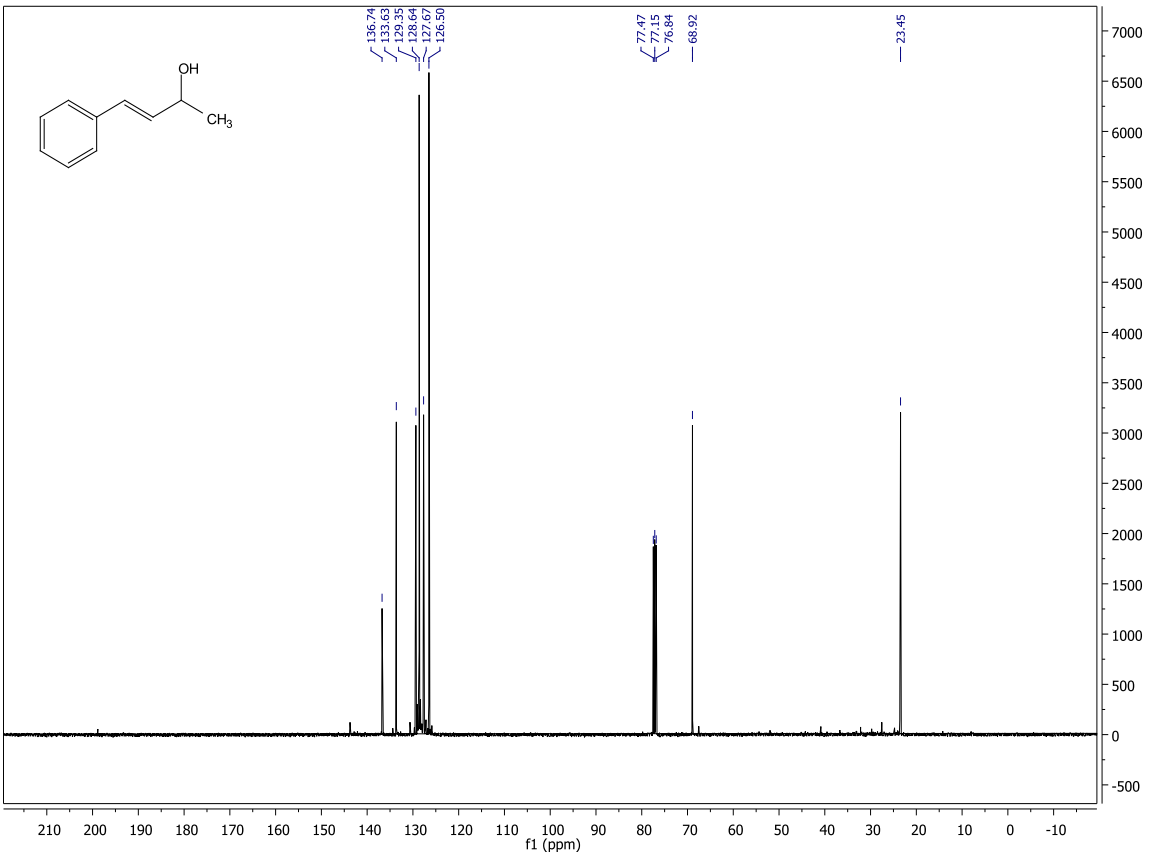

Figure 6.240. ^{13}C NMR for **2-u**

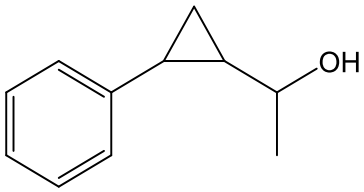

1-(2-phenylcyclopropyl) ethan-1-ol (2-v)

1-(2-phenylcyclopropyl) ethan-1-ol **(2-v)** was prepared from 1-(2-phenylcyclopropyl) ethan-1-one **(1-v)** by the procedure outlined in chapter 4. NMR analysis showed 100% conversion in 3 hours. 73% isolated yield of alcohol product was obtained after complete workup. ^{1}H NMR (400 MHz, $CDCl_3$) δ 7.32 – 7.25 (m, 2H), 7.21 – 7.15 (m, 1H), 7.12 – 7.06 (m, 2H), 3.40 – 3.31 (m, 1H), 2.67 (s, 1H), 1.95 – 1.75 (m, 1H), 1.52 – 1.46 (m, 1H), 1.34 (dd, *J* = 6.3, 2.3 Hz, 3H), 1.31 – 1.22 (m, 1H), 1.09 – 0.87 (m, 2H). ^{13}C NMR (101 MHz, $CDCl_3$) δ 142.96, 128.43, 128.42, 125.99, 125.89, 125.69, 125.62, 77.61, 77.29, 76.97, 71.64, 71.57, 30.86, 30.79, 22.84, 22.53, 21.45, 20.78, 14.05, 13.51.

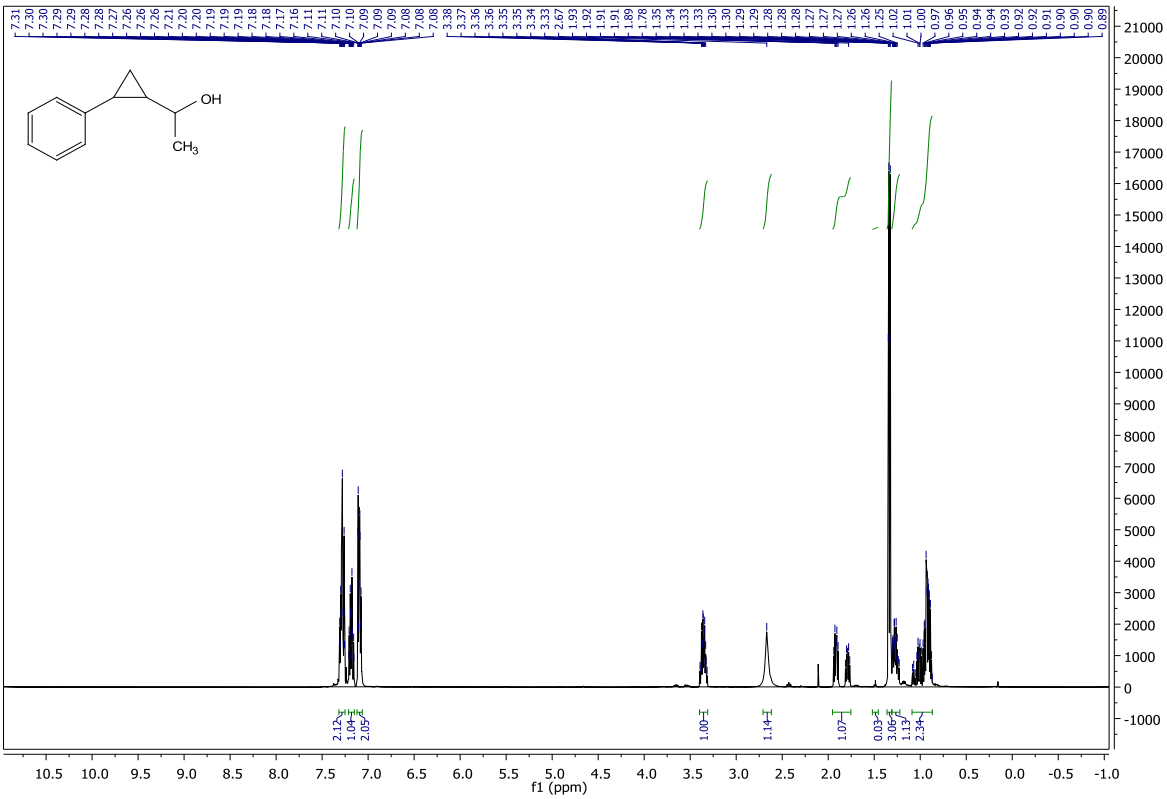

Figure 6.241. ^{1}H NMR for **2-v**

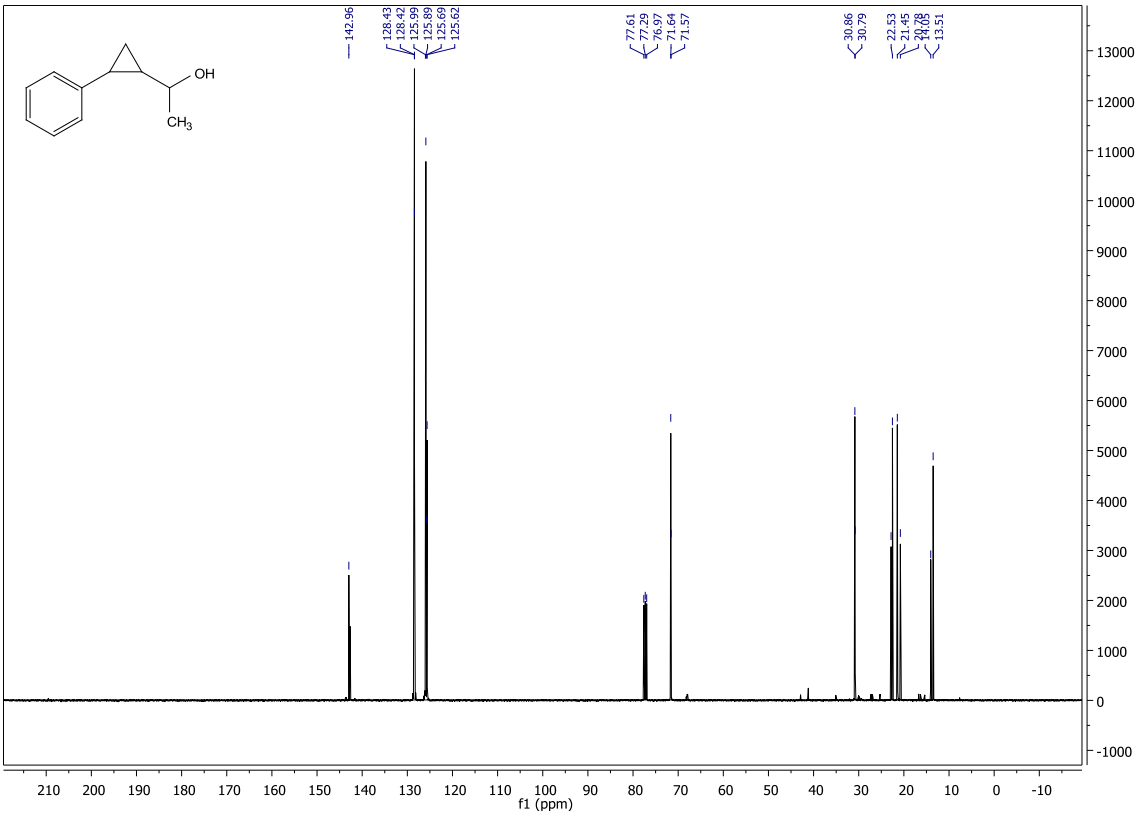

Figure 6.242. ^{13}C NMR for **2-v**

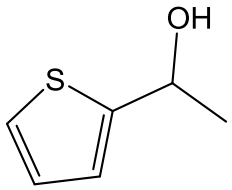

1-(thiophen-2-yl) ethan-1-ol (2-w)

1-(thiophen-2-yl) ethan-1-ol **(2-w)** was prepared from 1-(thiophen-2-yl) ethan-1-one **(1-w)** by the procedure outlined in chapter 4. NMR analysis showed 100% conversion in 3 hours. 89% isolated yield of alcohol product was obtained after complete workup. ^{1}H NMR (400 MHz, $CDCl_3$) δ 7.20 (dd, *J* = 5.1, 2.0 Hz, 1H), 6.96 – 6.88 (m, 2H), 5.05 (q, *J* = 6.3 Hz, 1H), 2.82 (s, 1H), 1.54 (d, *J* = 6.4 Hz, 3H). ^{13}C NMR (101 MHz, $CDCl_3$) δ 149.97, 126.68, 124.40, 123.23, 77.51, 77.20, 76.88, 66.14, 25.27.

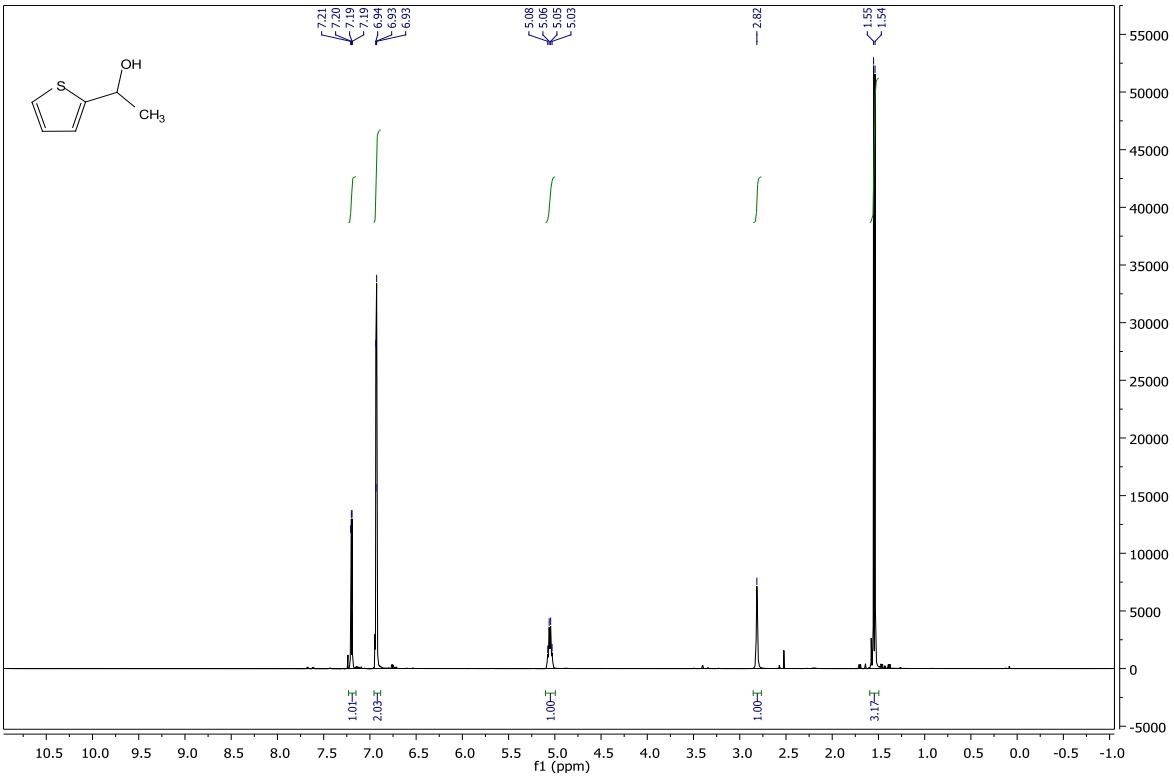

Figure 6.243. ^{1}H NMR for **2-w**

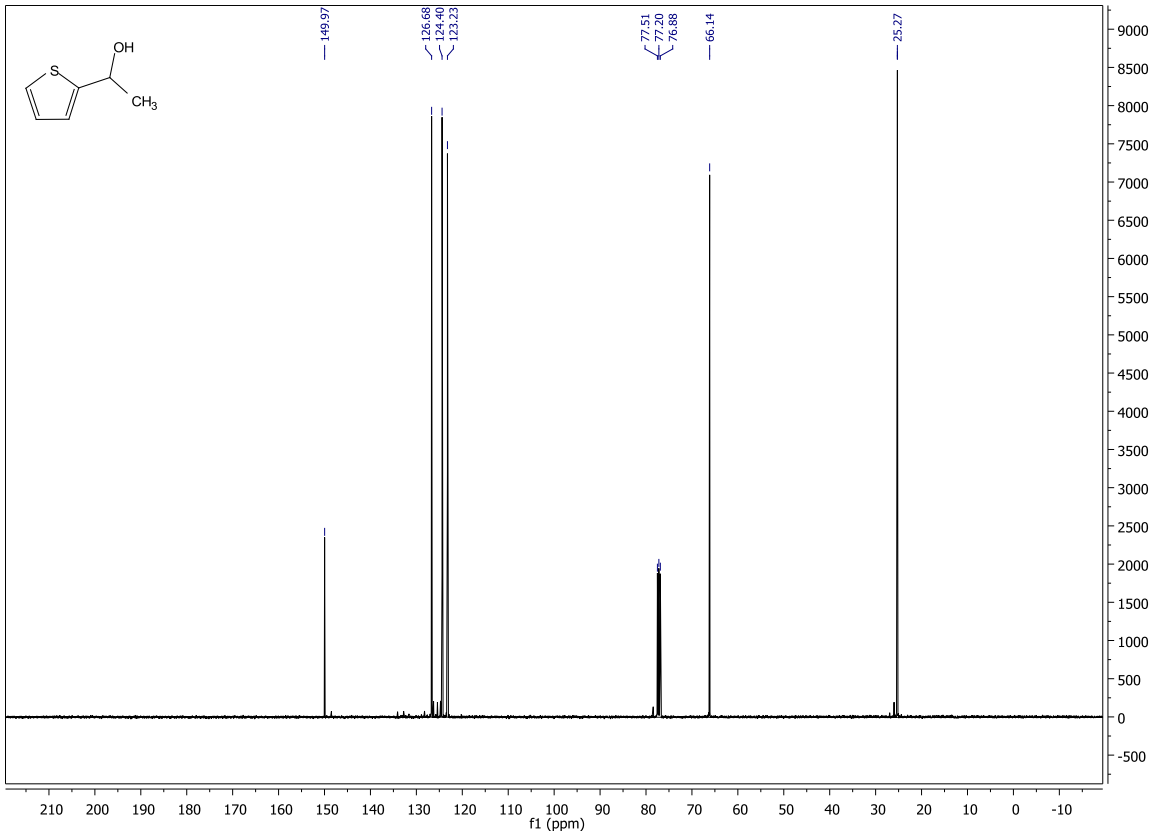

Figure 6.244. ^{13}C NMR for **2-w**

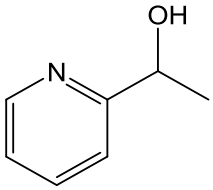

1-(pyridin-2-yl) ethan-1-ol (2-x)

1-(pyridin-2-yl) ethan-1-ol **(2-x)** was prepared from 1-(pyridin-2-yl) ethan-1-one **(1-x)** by the procedure outlined chapter 4. NMR analysis showed 92% conversion when left to stir overnight. Reaction did not proceed any further and 85% isolated yield of alcohol product was obtained after complete workup and flash chromatography (Hex: EtOAc = 70:30). ^{1}H NMR (400 MHz, $CDCl_3$) δ 8.42 (ddd, *J* = 4.9, 1.7, 1.0 Hz, 1H), 7.65 – 7.56 (m, 1H), 7.29 – 7.22 (m, 1H), 7.11 (ddd, *J* = 7.5, 4.9, 0.9 Hz, 1H), 4.83 (q, *J* = 6.6 Hz, 1H), 4.69 (s, 1H), 1.43 (d, *J* = 6.6 Hz, 3H). ^{13}C NMR (101 MHz, $CDCl_3$) δ 163.39, 148.09, 136.88, 122.21, 119.81, 77.46, 77.14, 76.82, 69.09, 24.20.

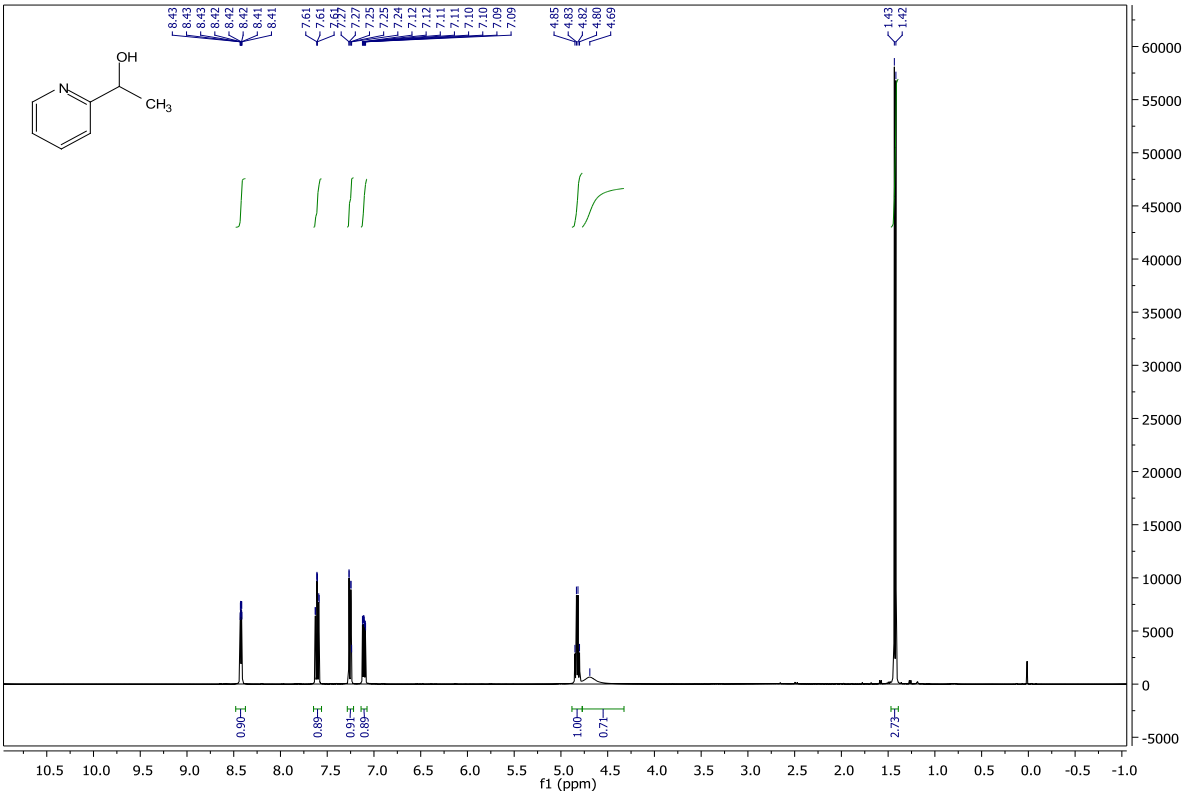

Figure 6.245. ^{1}H NMR for **2-x**

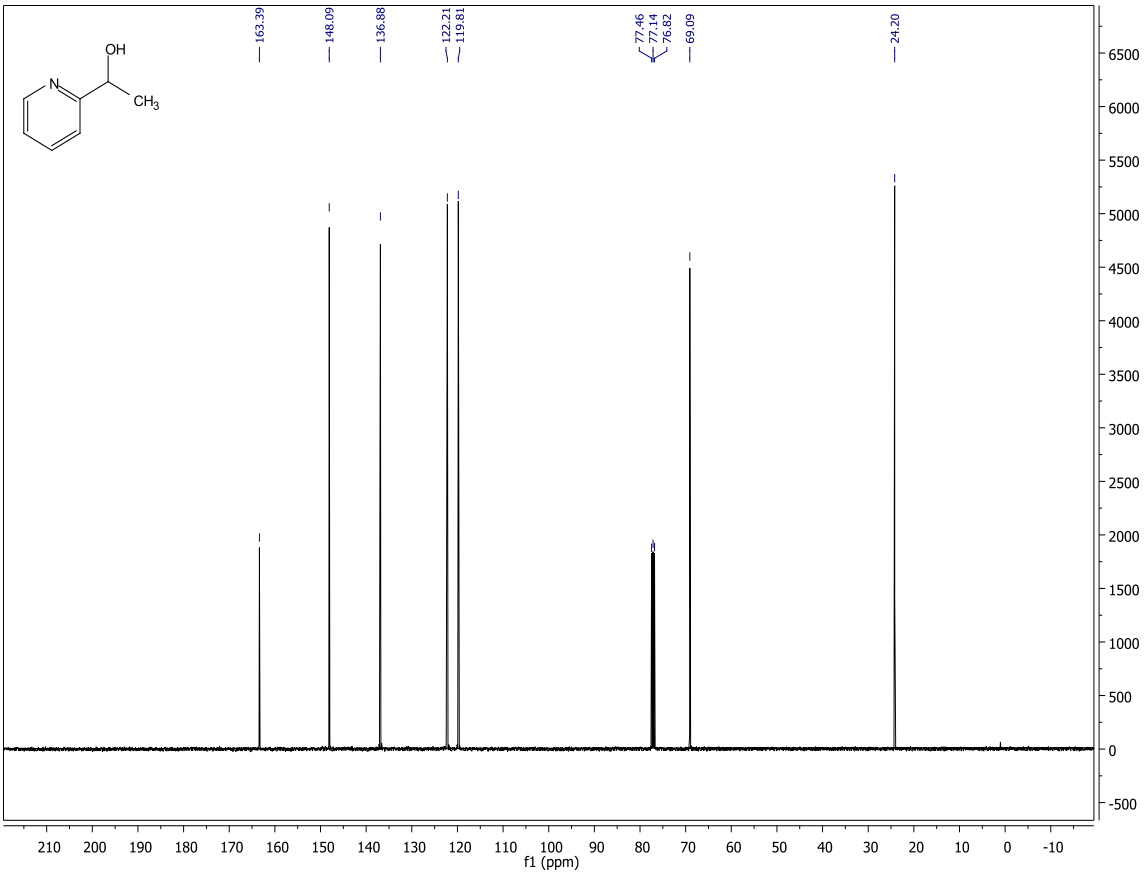

Figure 6.246. ^{13}C NMR for **2-x**

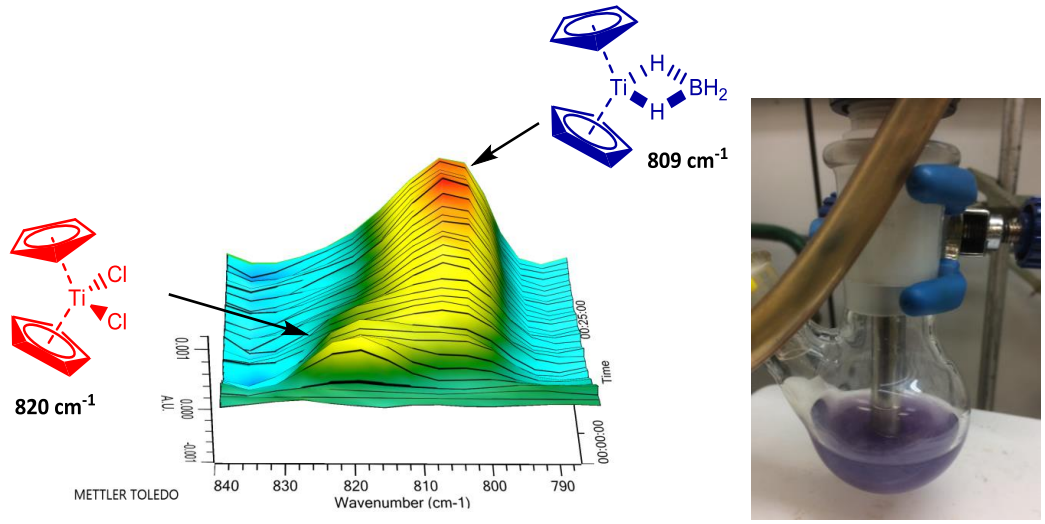

Figure 6.247. Formation of titanocene borohydride monitored by ReactIR.

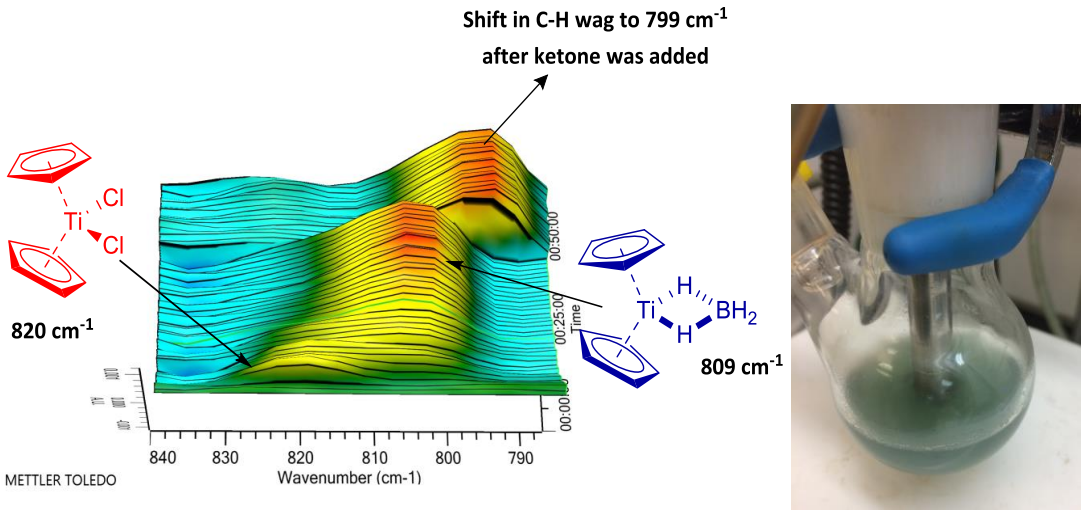

Figure 6.248. Shift in C-H wag upon ketone addition

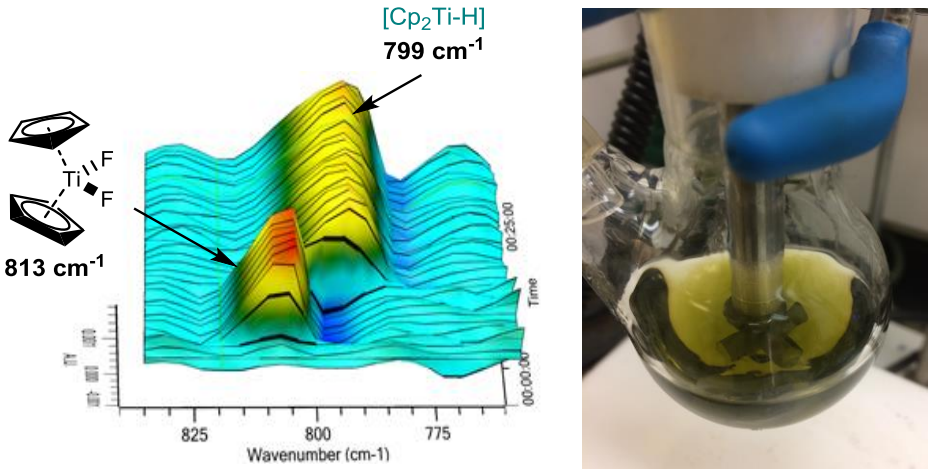

Figure 6.249. Formation of titanocene(III) hydride monitored by ReactIR.

a. 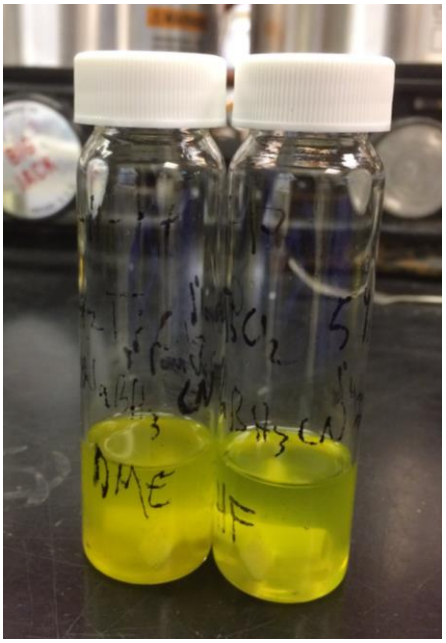

b. 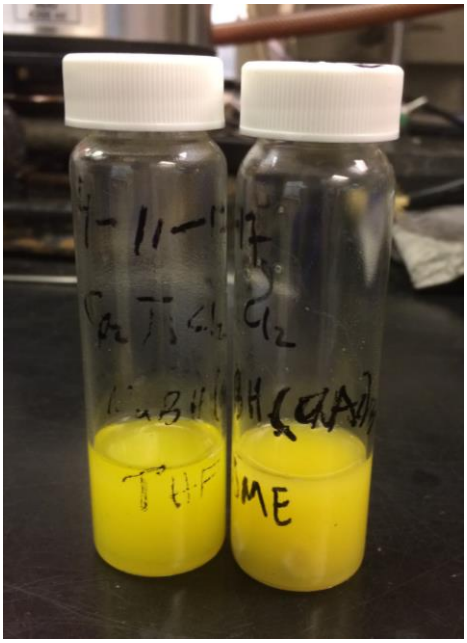

Figure 6.250. a. Solution of Cp_2TiCl_2, NaH_3CN, and **1** in THF and DME; **b.** Mixture of Cp_2TiCl_2, $NaH(OAc)_3$, and **1** in THF and DME.

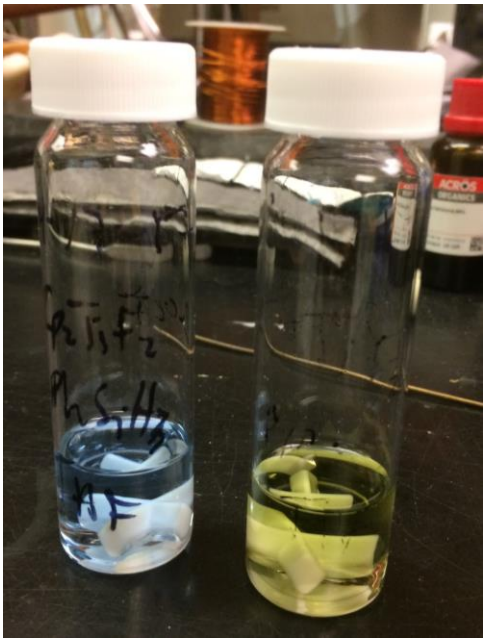

Figure 6.251. Solution of Cp_2TiF_2**,** $PhSiH_3$, and **1** in THF (Left); Solution of Cp_2TiF_2**,** PMHS, and **1** in THF

a. 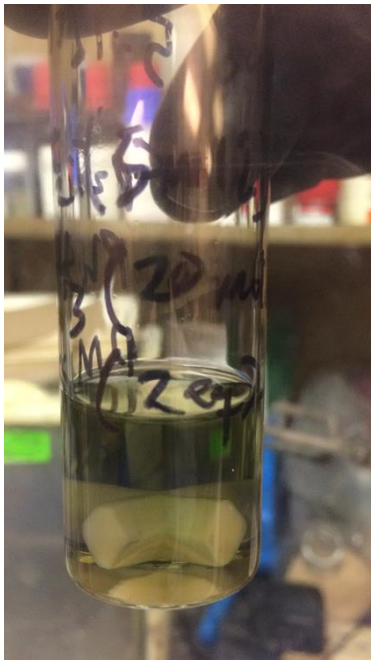 b. 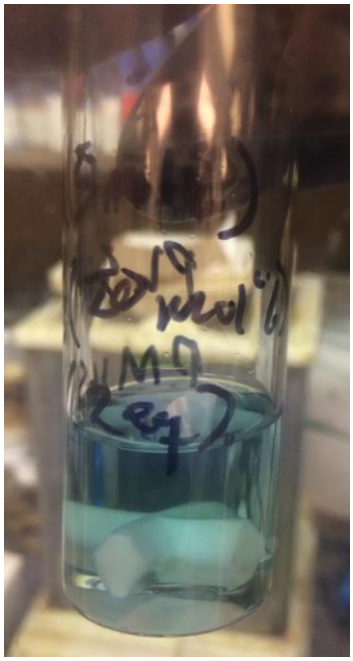

Figure 6.252. a. Solution of Cp_2TiF_2**,** 20 mol% $PhSiH_3$, 2 equiv PMHS in THF; **b.** Solution of Cp_2TiF_2**,** 20 mol% $PhSiH_3$, 2 equiv PMHS and **1** in THF

a.  b. 

Figure 6.253. a. Solution of Cp_2TiF_2**,** PMHS in THF at reflux; **b.** Solution of Cp_2TiF_2**,** PMHS, and **1** in THF at reflux (**Table 2S**, Entry 2) (**Table 2S**, Entry 4)

Sample NMR calculation for product distribution for 1-v Entry

1-v

3H = 1.64

Ratio= 1.64/3 = 0.55

% yield = [0.55/(0.55 + 1.00 + 0.27)]*100% = 30%

2-v

1H = 1.00

Ratio= 1.00/1 = 1.00

% yield = [1.00/(0.55 + 1.00 + 0.27)]*100% = 55%

3-v

2H = 0.53

Ratio= 0.53/2 = 0.27

% yield = [0.27/(0.55 + 1.00 + 0.27)]*100% = 15%

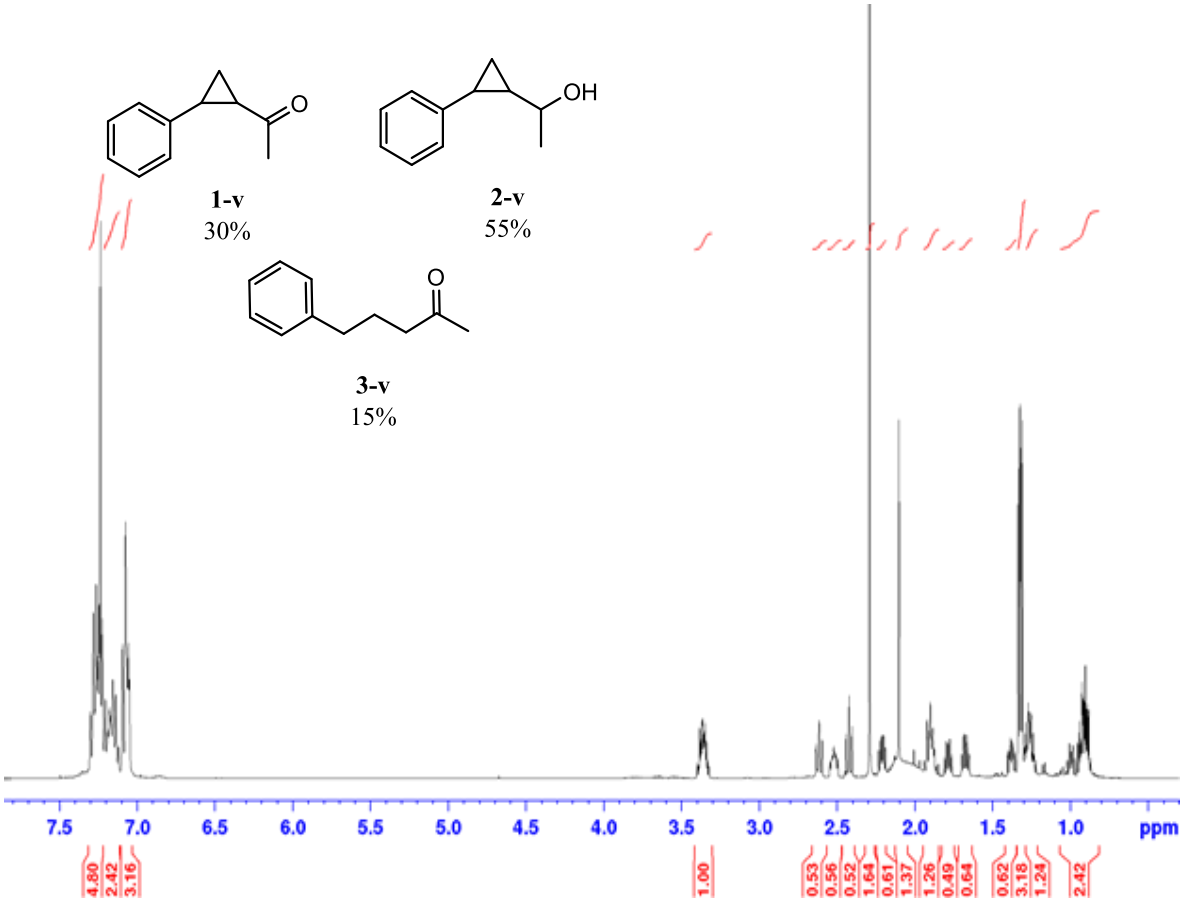

Figure 6.254. NMR spectra for crude product for reaction in table 4.4 entry 2

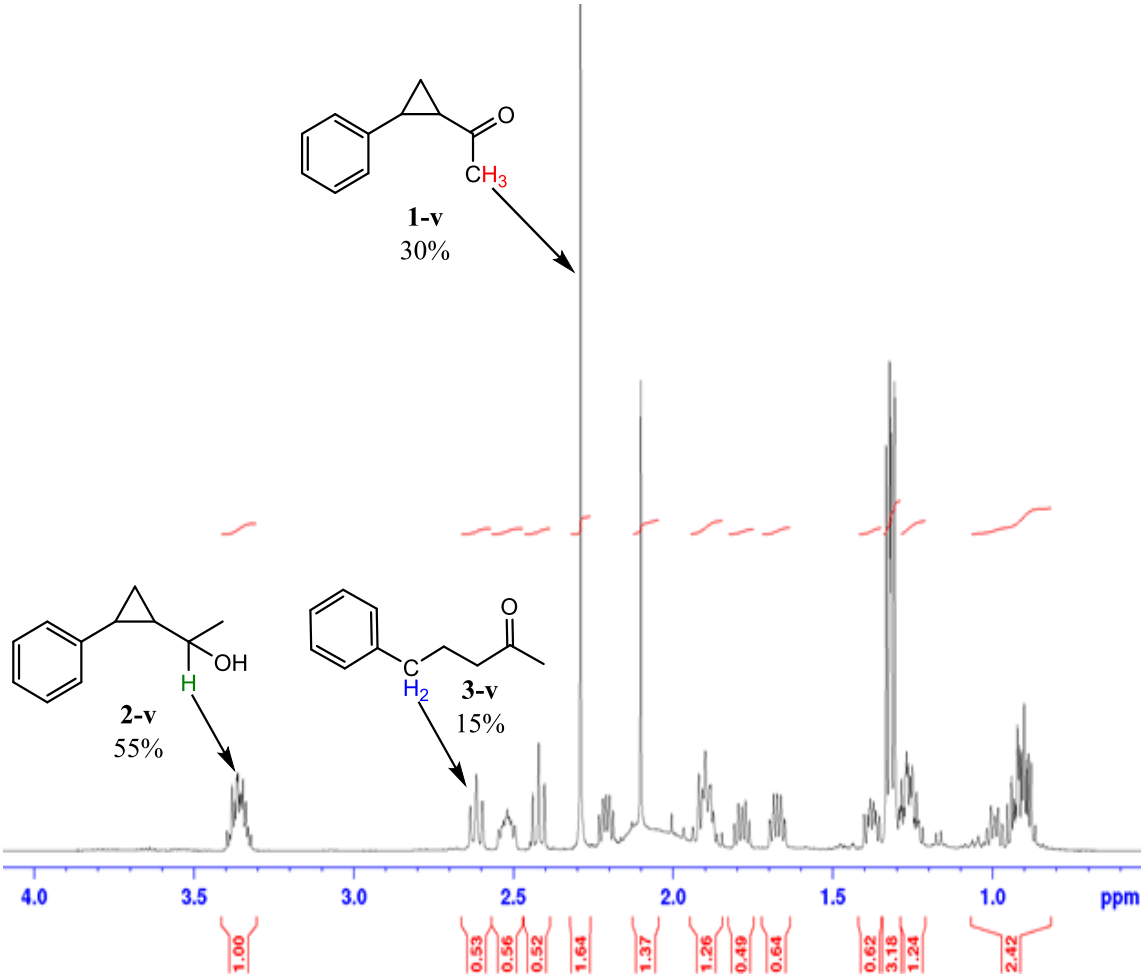

Figure 6.255. NMR calculation for crude product distribution for reaction in table 4.4 entry 2

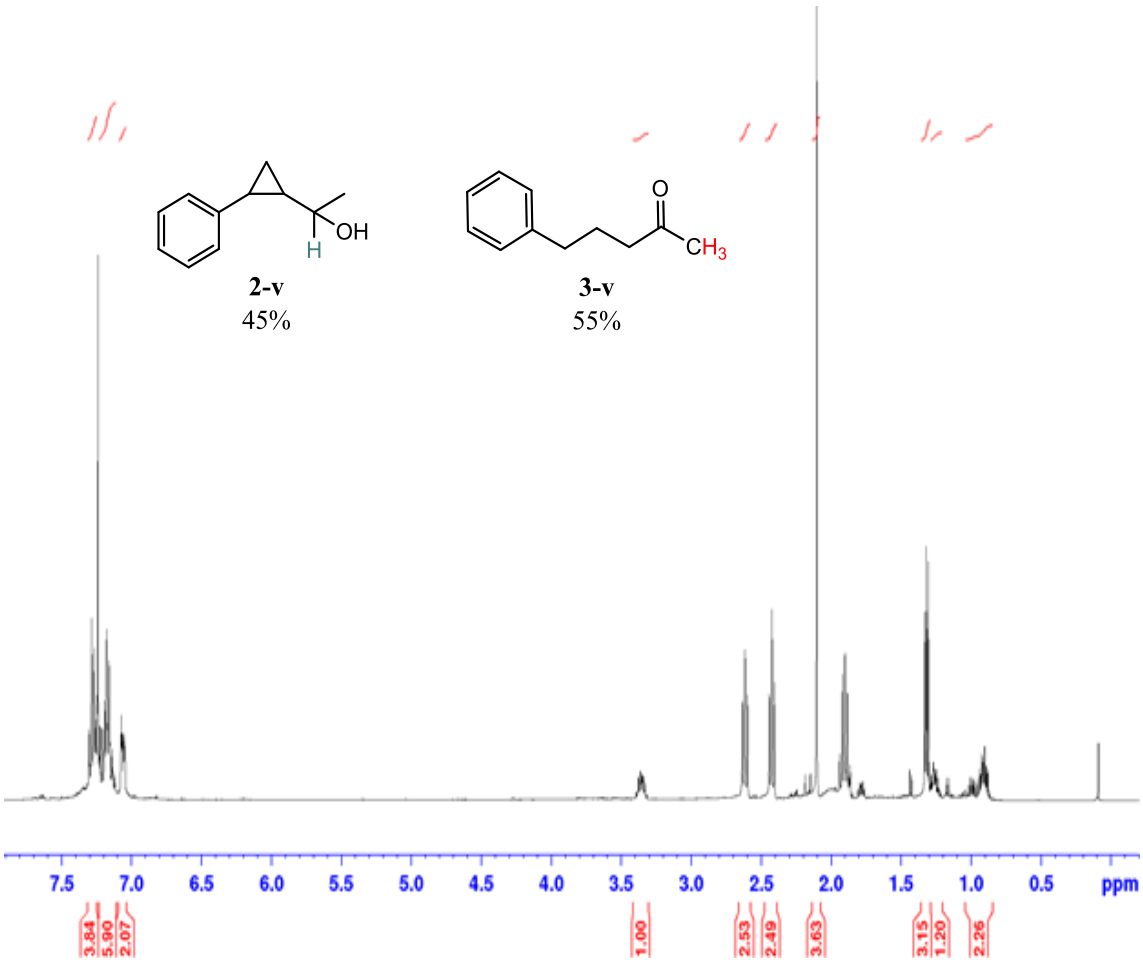

Figure 6.256. NMR spectra for crude product for reaction in table 4.4 entry 3

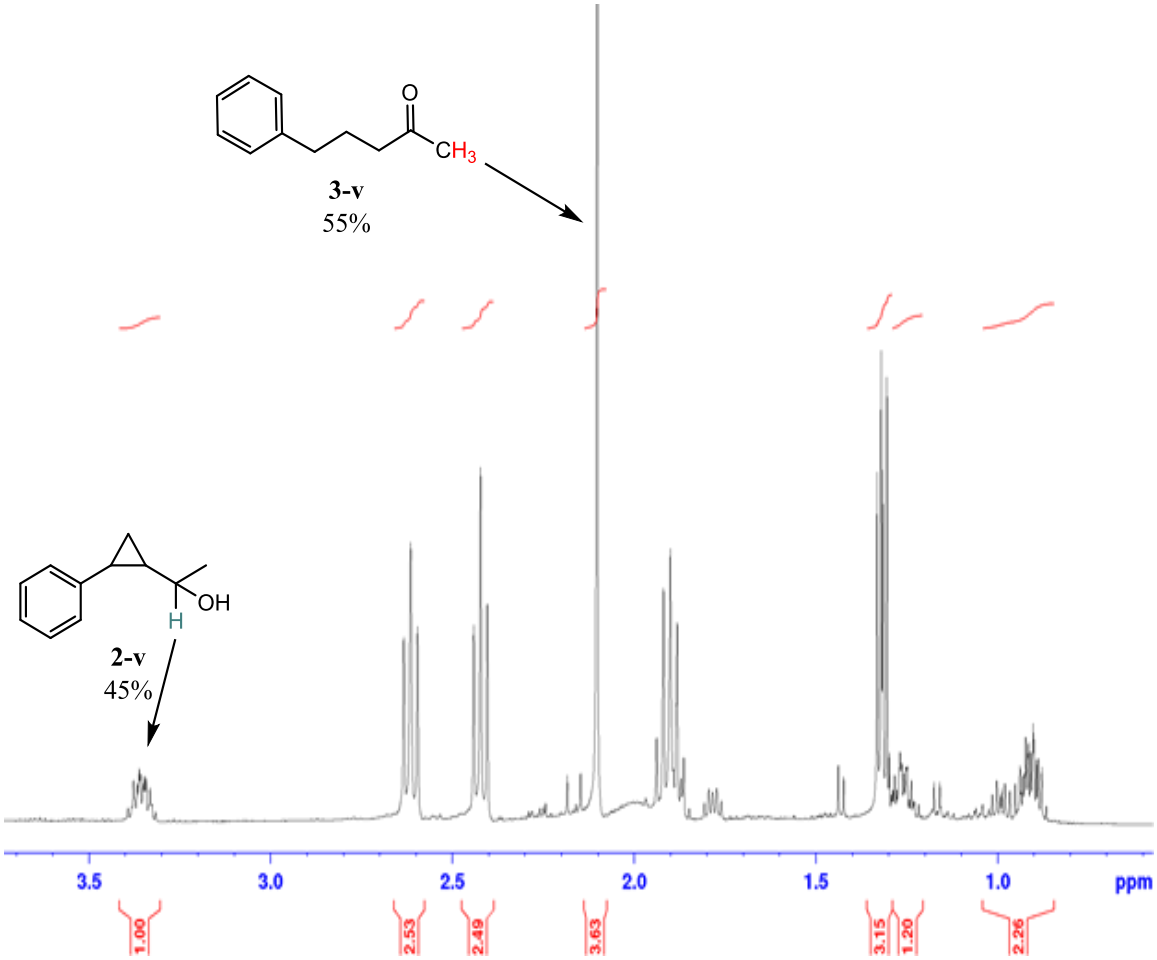

Figure 6.257. NMR calculation for crude product distribution for reaction in table 4.4 entry 3

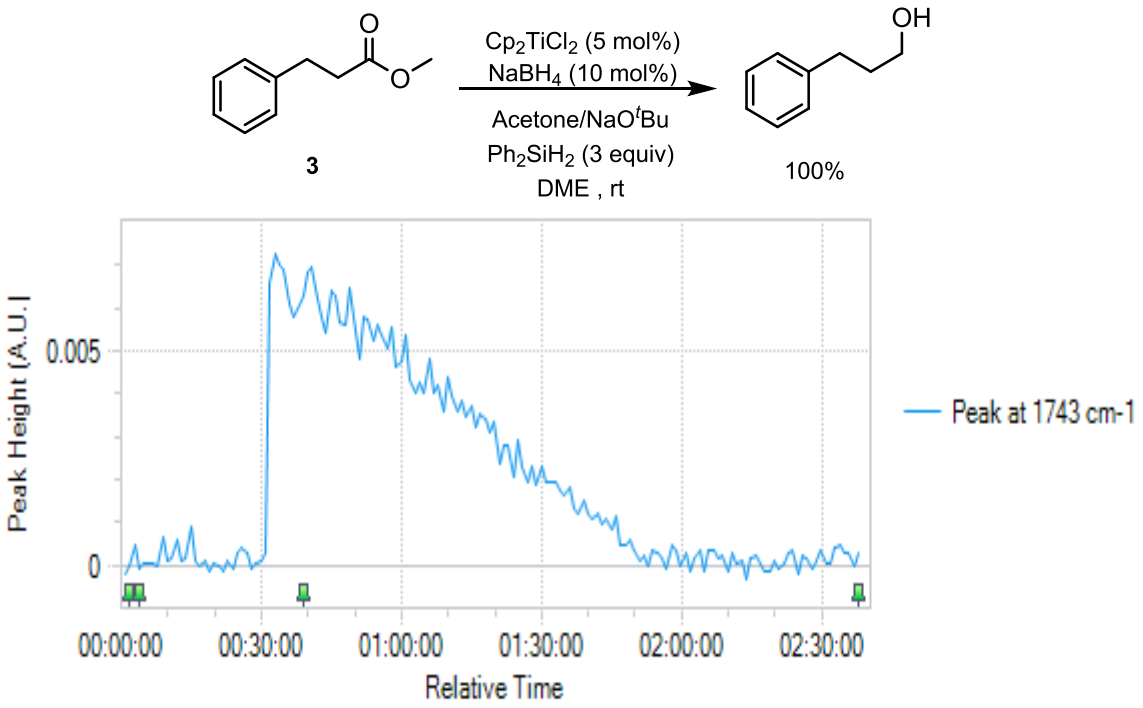

Figure 6.258. Reduction of **3** with acetone (40 mol%) as an additive. Reaction time was 80 min

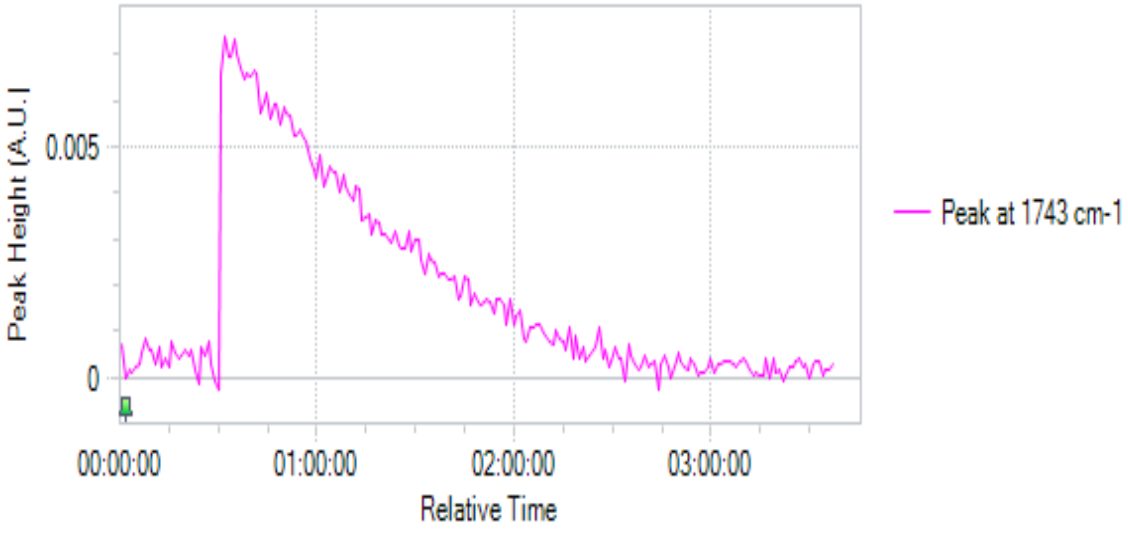

Figure 6.259. Reduction of **3** with NaO^{t}Bu (7 mol%) as an additive. Reaction time was 120 min

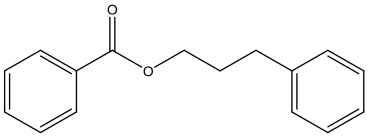

3-phenylpropyl benzoate

^{1}H NMR (400 MHz, $CDCl_3$) δ 8.11 – 7.99 (m, 2H), 7.59 – 7.53 (m, 1H), 7.48 – 7.41 (m, 2H), 7.31 (dd, *J* = 10.7, 4.1 Hz, 2H), 7.23 (dd, *J* = 8.2, 1.1 Hz, 3H), 4.35 (td, *J* = 6.4, 1.2 Hz, 2H), 2.80 (t, *J* = 7.6 Hz, 2H), 2.18 – 2.05 (m, 2H). ^{13}C NMR (101 MHz, $CDCl_3$) δ 166.64, 141.24, 132.95, 130.40, 129.61, 128.53, 128.50, 128.41, 126.09, 64.31, 32.36, 30.36.

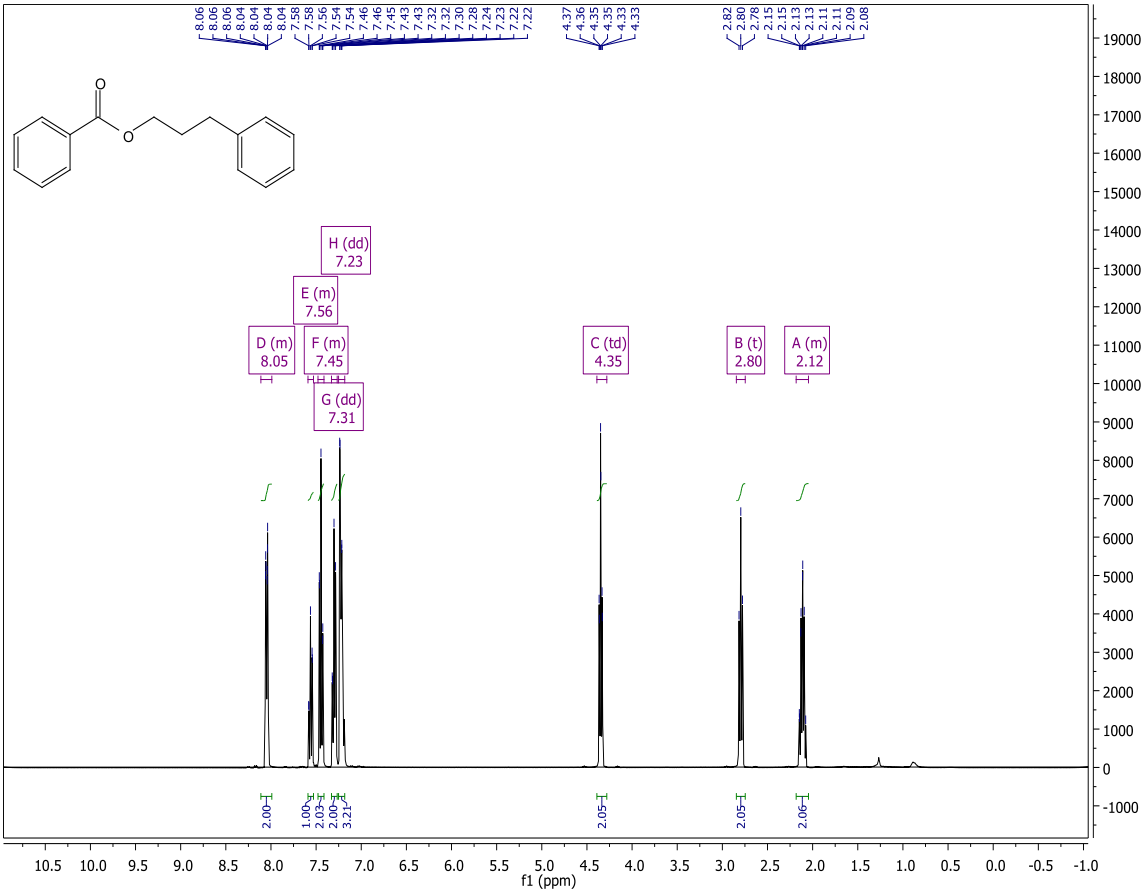

Figure 6.260. ^{1}H NMR for 3-phenylpropyl benzoate

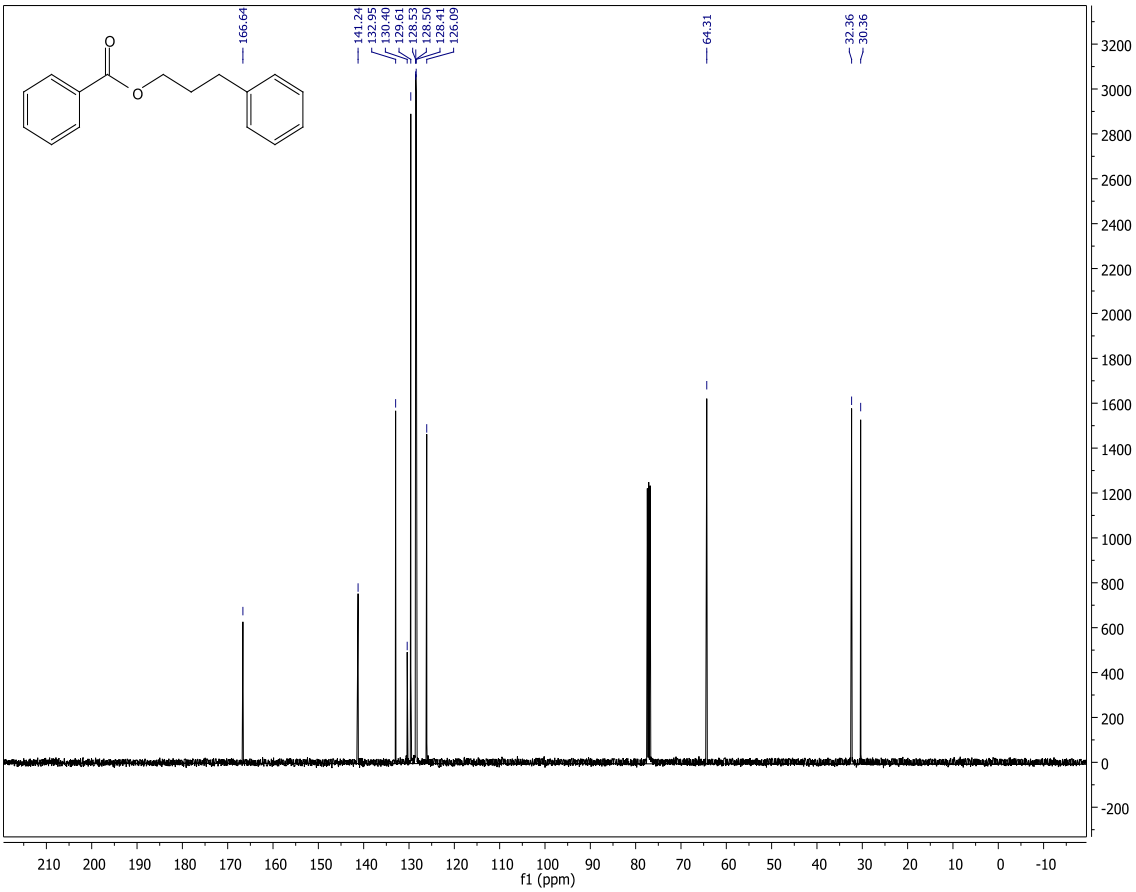

Figure 6.261. ^{13}C NMR for 3-phenylpropyl benzoate

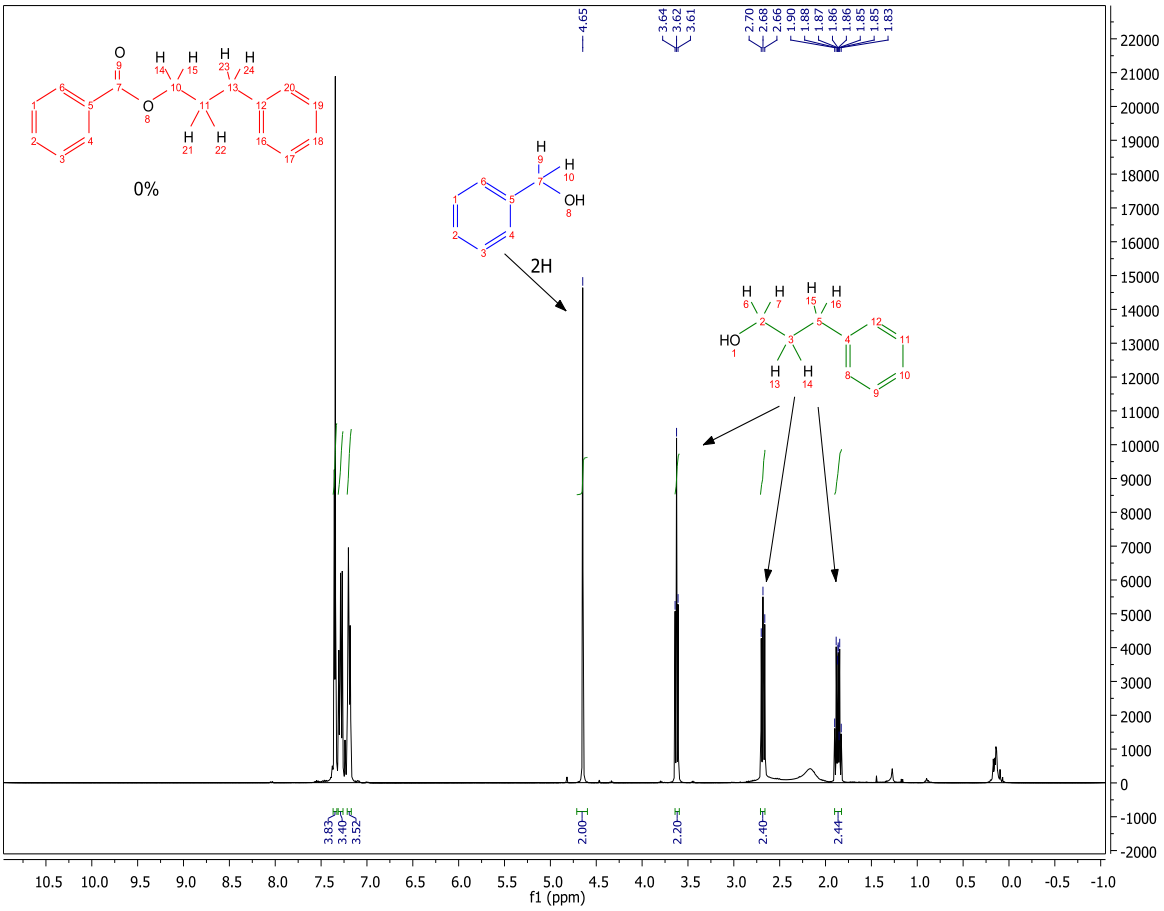

Figure 6.262. ^{1}H NMR for reduction of 3-phenylpropyl benzoate with Cp_2TiBH_4/NaO^{t}Bu/PMHS in DME

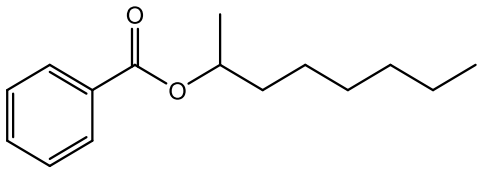

octan-2-yl benzoate

^{1}H NMR (400 MHz, $CDCl_3$) δ 8.06 – 7.99 (m, 2H), 7.57 – 7.48 (m, 1H), 7.45 – 7.37 (m, 2H), 5.20 – 5.09 (m, 1H), 1.82 – 1.66 (m, 1H), 1.66 – 1.51 (m, 1H), 1.42 – 1.21 (m, 11H), 0.86 (dd, *J* = 8.3, 5.6 Hz, 3H). ^{13}C NMR (101 MHz, $CDCl_3$) δ 166.24, 132.70, 130.94, 129.53, 128.29, 71.76, 36.09, 31.78, 29.20, 25.45, 22.63, 20.11, 14.10.

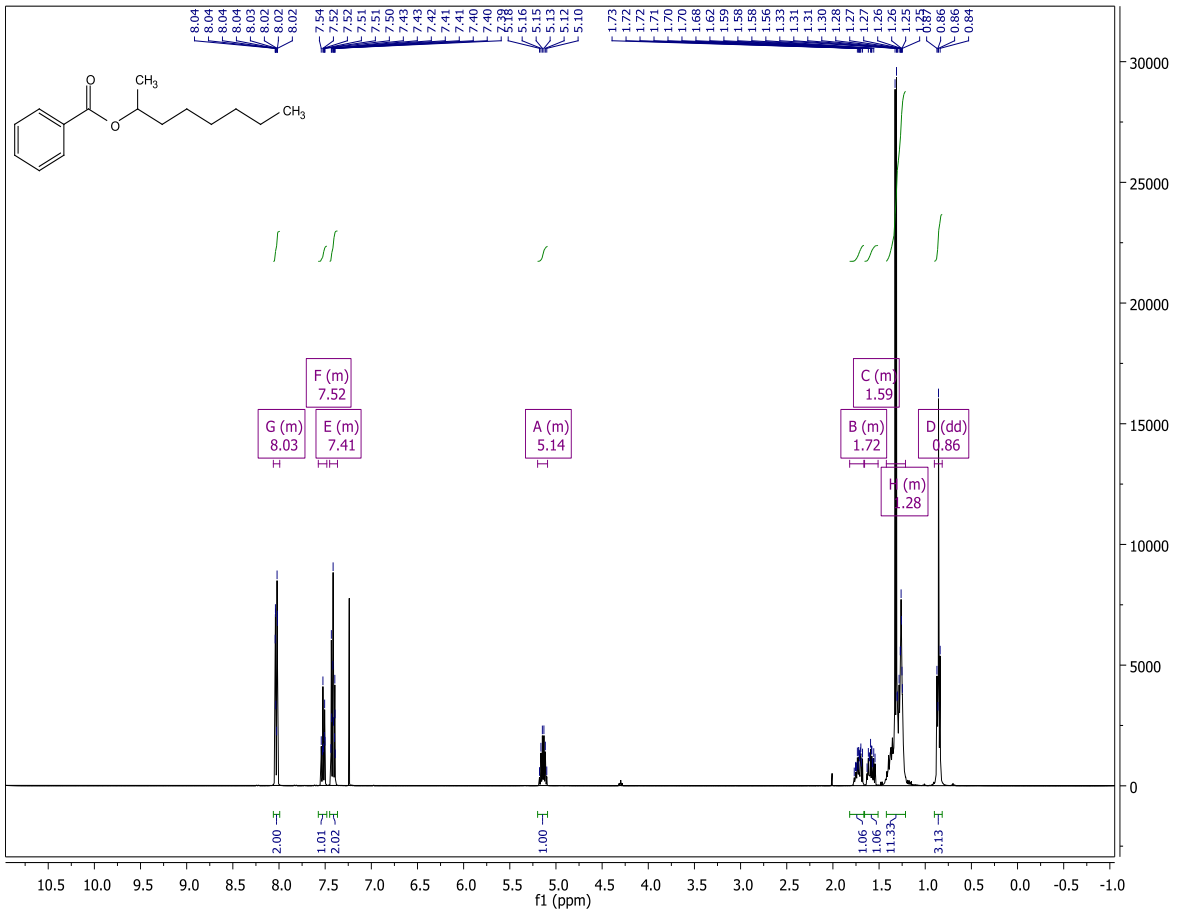

Figure 6.263. ^{1}H NMR for octan-2-yl benzoate

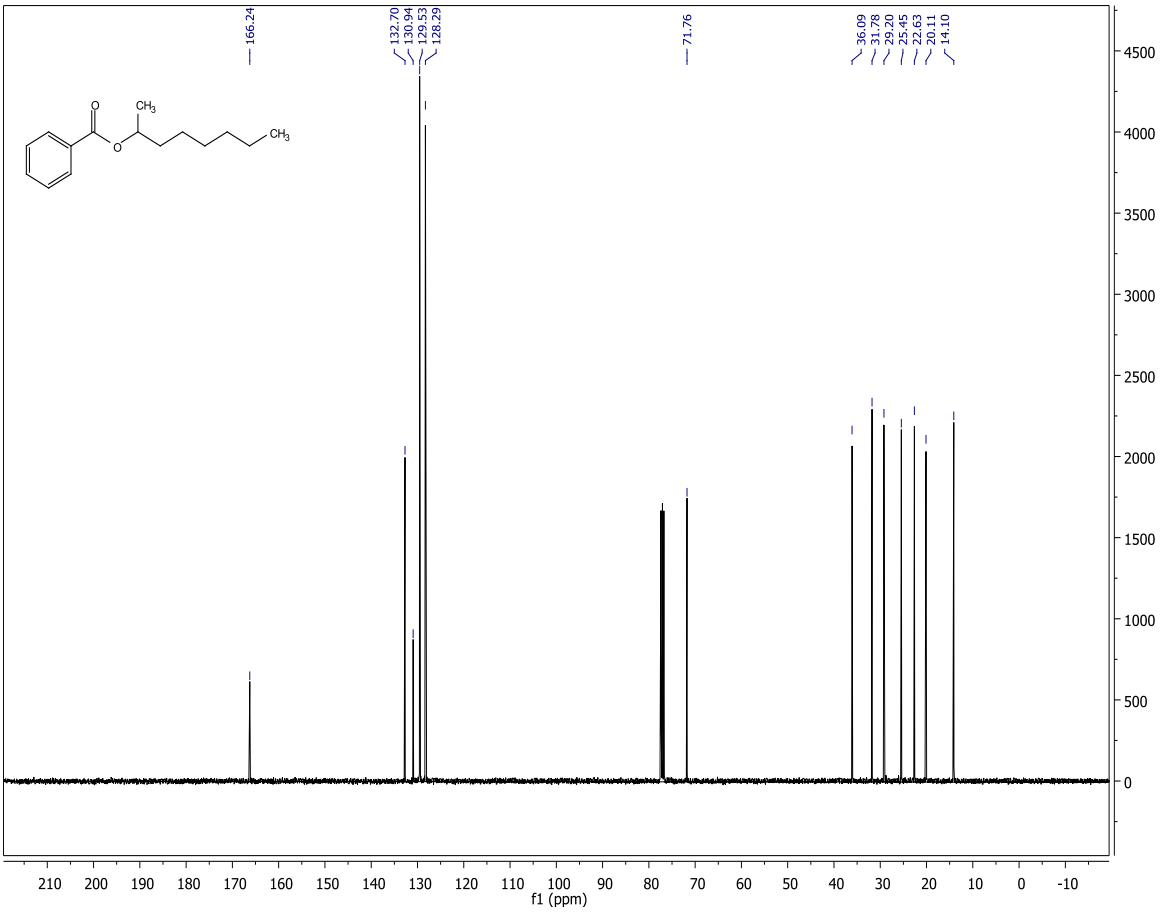

Figure 6.264. ^{13}C NMR for octan-2-yl benzoate

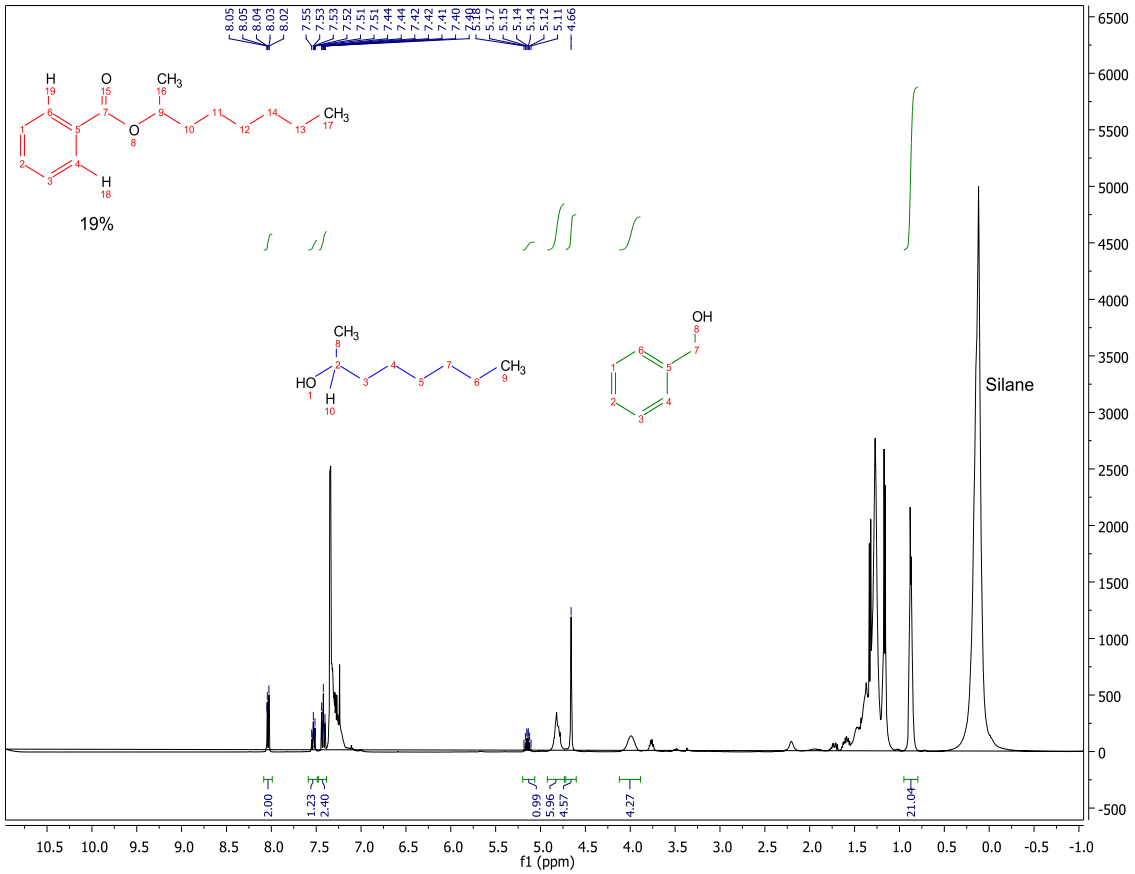

Figure 6.265. ^{1}H NMR for reduction of octan-2-yl benzoate with Cp_2TiBH_4/NaO^{t}Bu/PMHS in DME

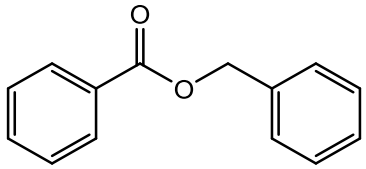

Benzyl benzoate

^{1}H NMR (400 MHz, $CDCl_3$) δ 8.08 (ddd, *J* = 4.1, 1.7, 0.7 Hz, 2H), 7.58 – 7.52 (m, 1H), 7.48 – 7.30 (m, 7H), 5.36 (s, 2H). ^{13}C NMR (101 MHz, $CDCl_3$) δ 166.48, 136.08, 133.09, 130.14, 129.75, 128.65, 128.42, 128.29, 128.22, 66.73.

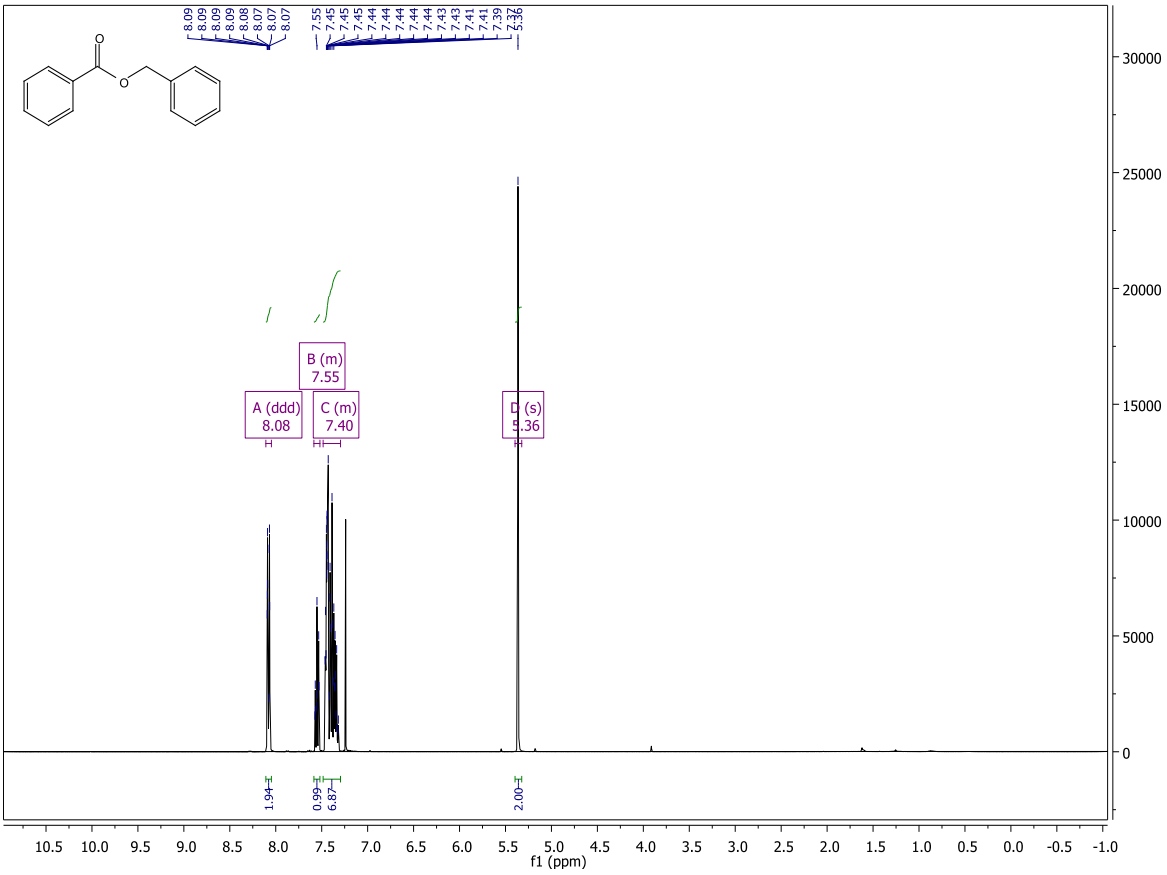

Figure 6.266. ^{1}H NMR for benzyl benzoate

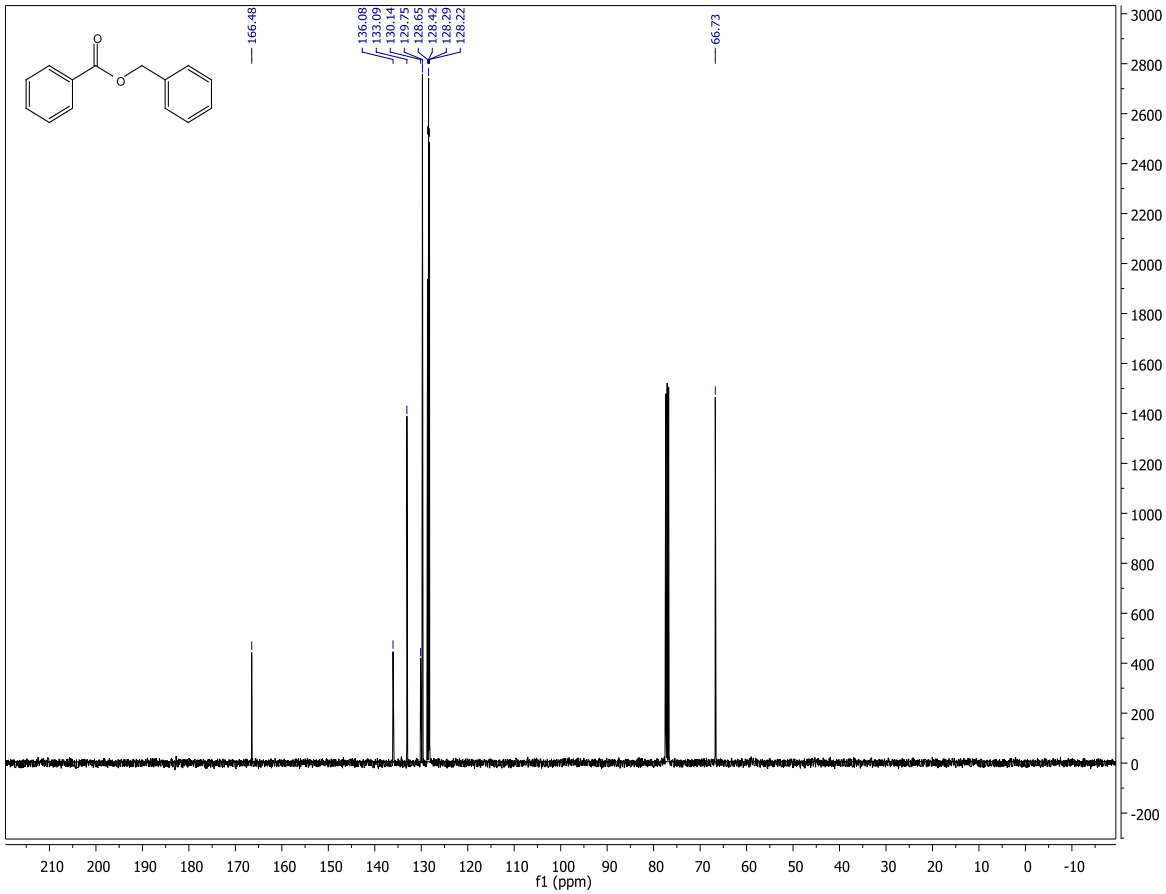

Figure 6.267. ^{13}C NMR for benzyl benzoate

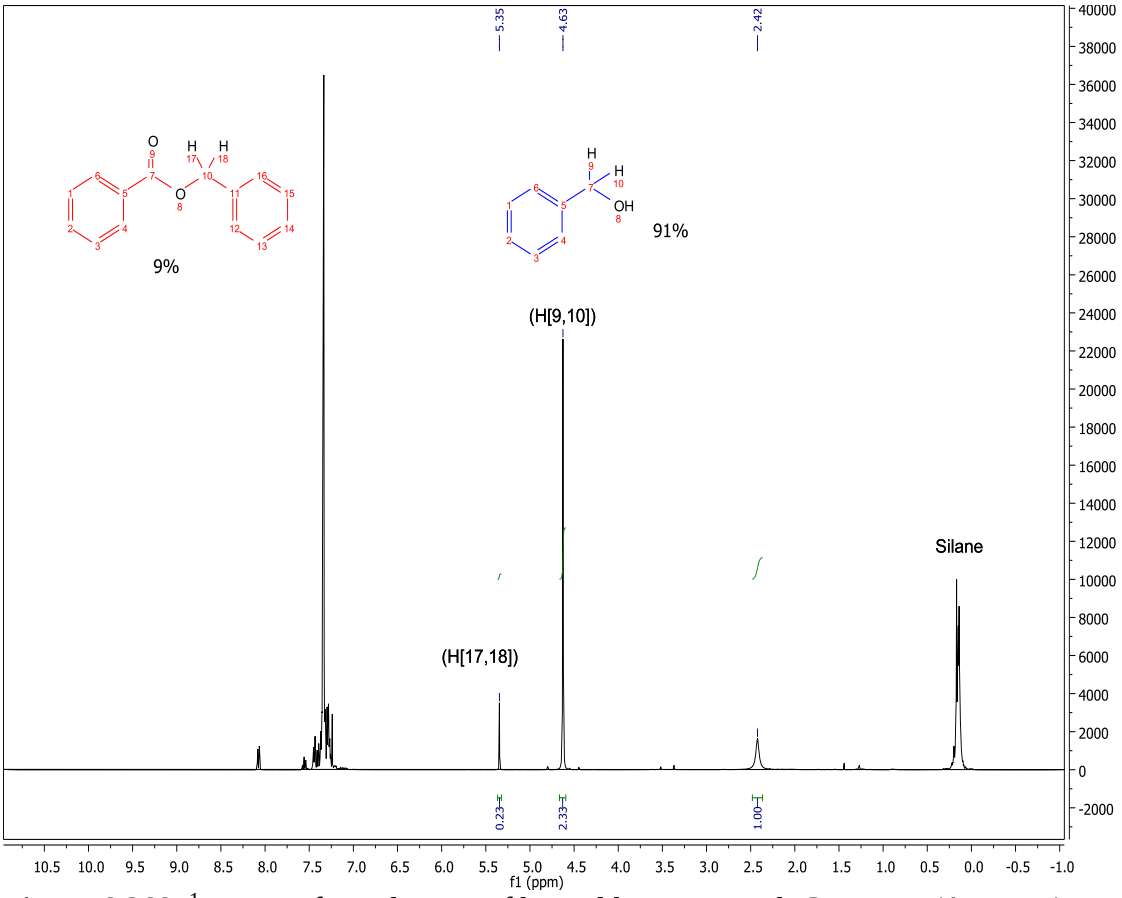

Figure 6.268. ^{1}H NMR for reduction of benzyl benzoate with Cp_2TiBH_4/Acetone/PMHS in DME

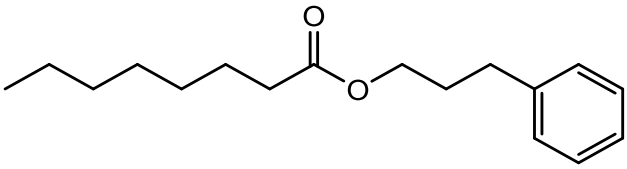

3-phenylpropyl octanoate

^{1}H NMR (400 MHz, $CDCl_3$) δ 7.30 – 7.25 (m, 2H), 7.18 (td, *J* = 6.8, 1.5 Hz, 3H), 4.07 (t, *J* = 6.5 Hz, 2H), 2.73 – 2.61 (m, 2H), 2.29 (t, *J* = 7.5 Hz, 2H), 1.94 (ddt, *J* = 13.1, 9.1, 6.5 Hz, 2H), 1.67 – 1.54 (m, 2H), 1.33 – 1.24 (m, 8H), 0.87 (t, *J* = 6.9 Hz, 3H). ^{13}C NMR (101 MHz, $CDCl_3$) δ 173.99, 141.27, 128.46, 128.43, 126.02, 63.58, 34.40, 32.22, 31.71, 30.29, 29.16, 28.98, 25.06, 22.65, 14.12.

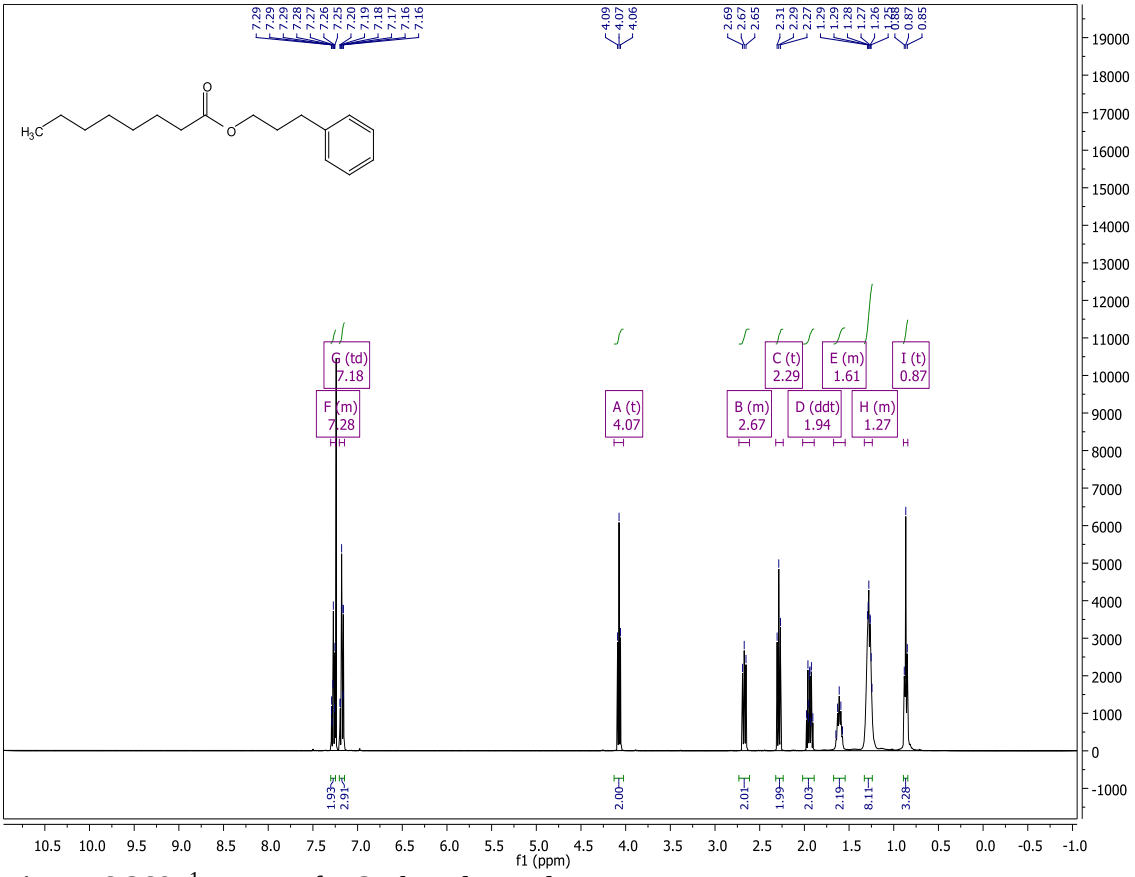

Figure 6.269. ^{1}H NMR for 3-phenylpropyl octanoate

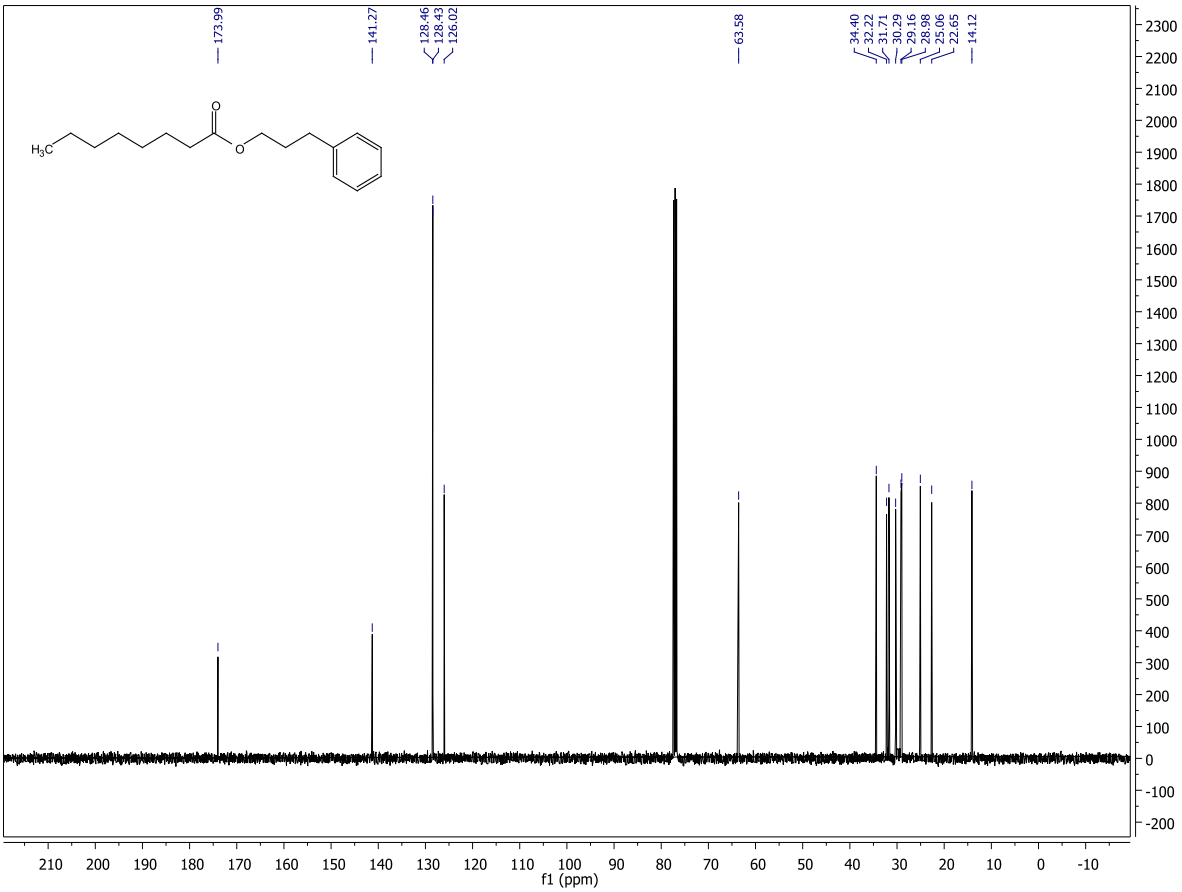

Figure 6.270. ^{13}C NMR for 3-phenylpropyl octanoate

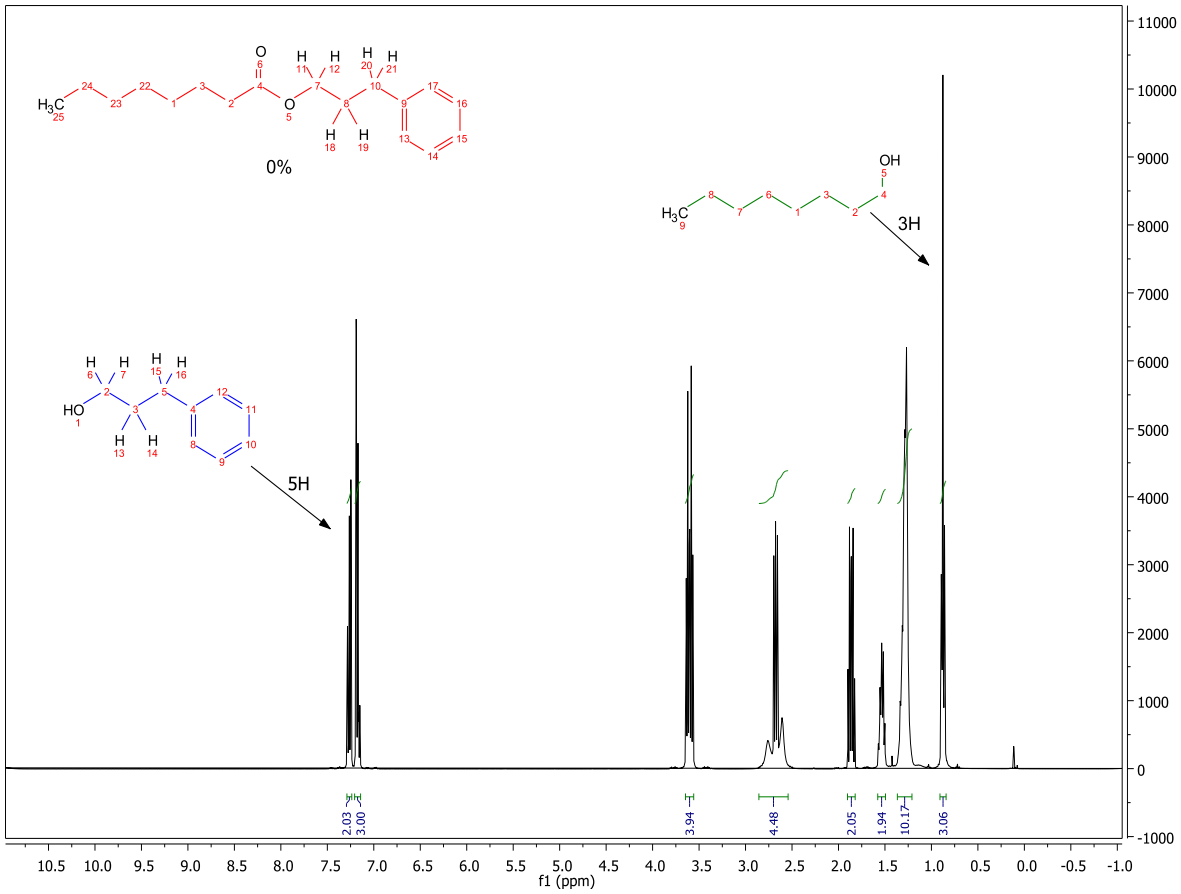

Figure 6.271. ^{1}H NMR for reduction of 3-phenylpropyl octanoate with Cp_2TiBH_4/NaO^{t}Bu/PMHS in DME

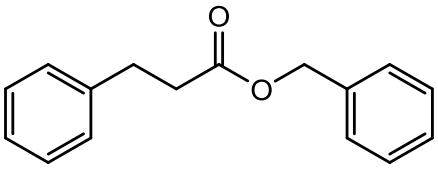

Benzyl 3-phenylpropanoate

^{1}H NMR (400 MHz, $CDCl_3$) δ 7.38 – 7.25 (m, 7H), 7.23 – 7.16 (m, 3H), 5.11 (s, 2H), 2.97 (t, *J* = 7.8 Hz, 2H), 2.68 (t, *J* = 7.8 Hz, 2H). ^{13}C NMR (101 MHz, $CDCl_3$) δ 172.78, 140.44, 135.92, 128.59, 128.55, 128.35, 128.27, 126.31, 66.33, 35.94, 30.97.

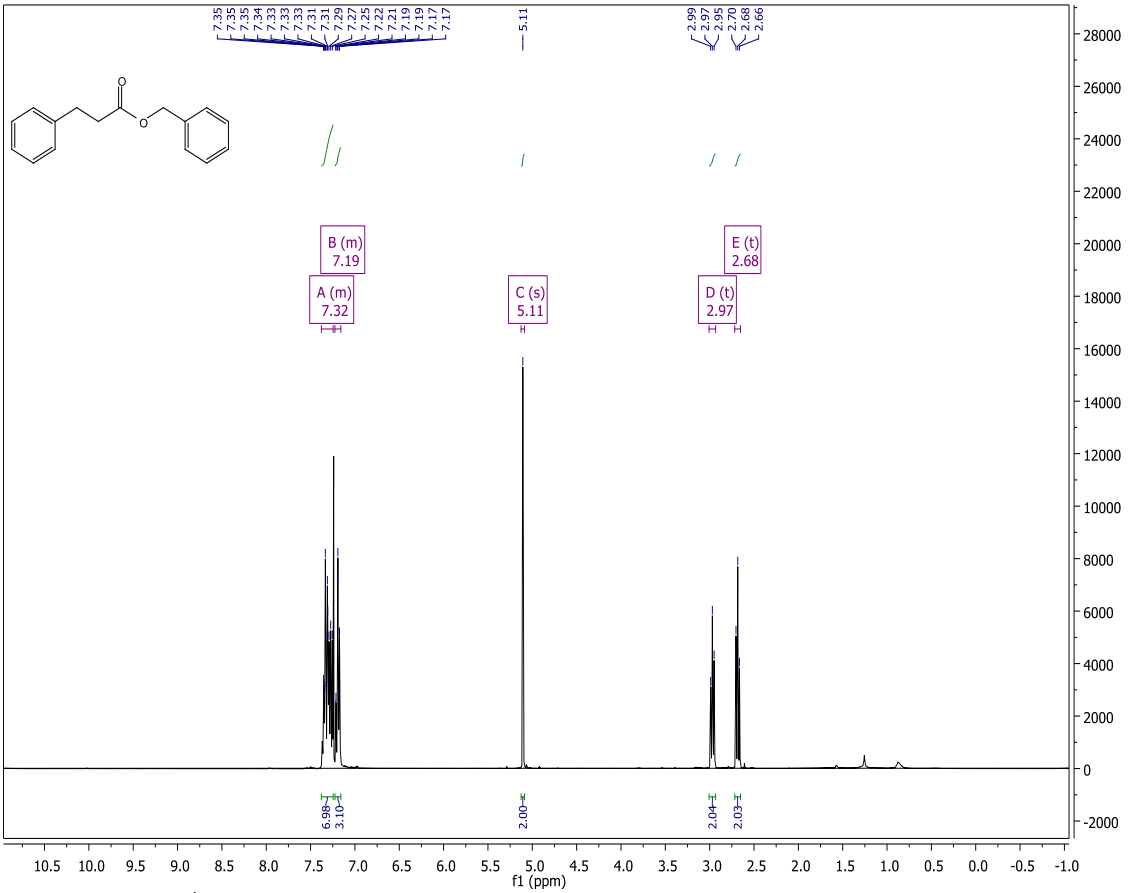

Figure 6.272. ^{1}H NMR for benzyl 3-phenylpropanoate

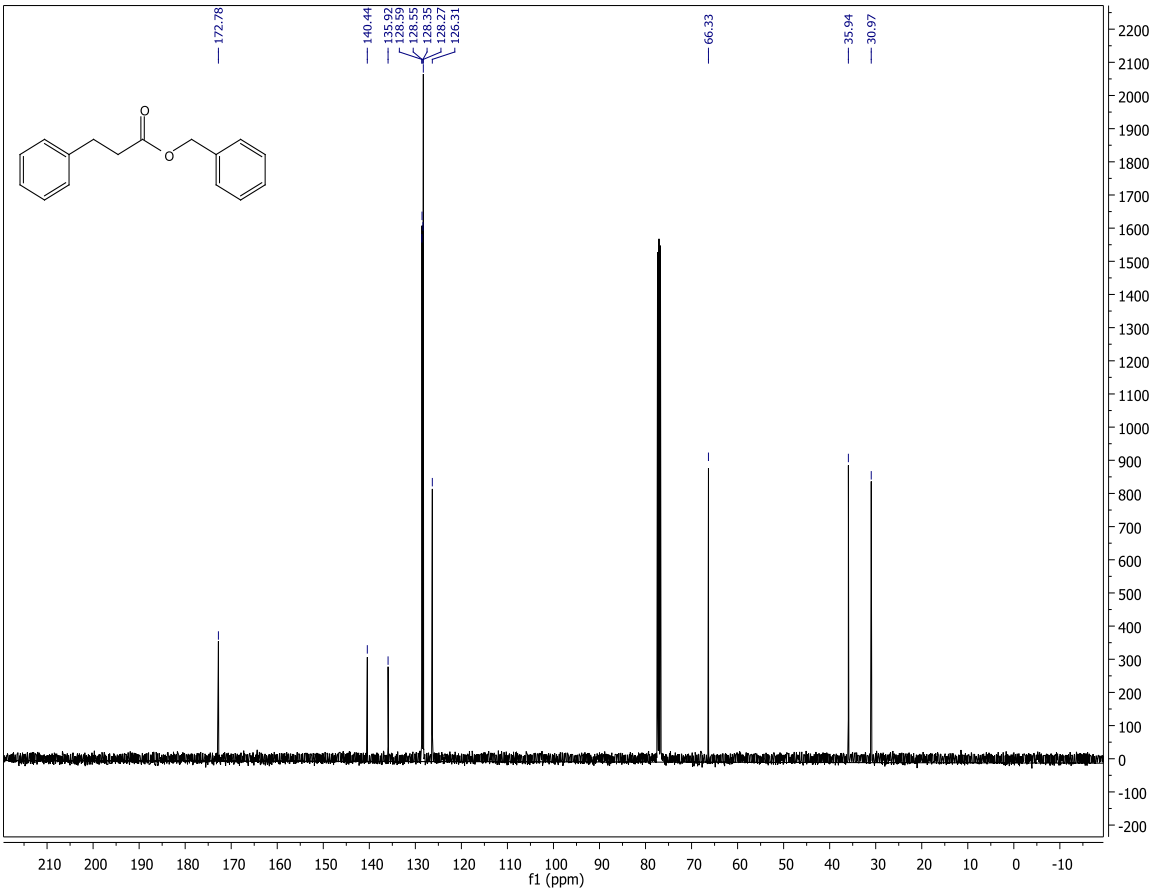

Figure 6.273. ^{13}C NMR for benzyl 3-phenylpropanoate

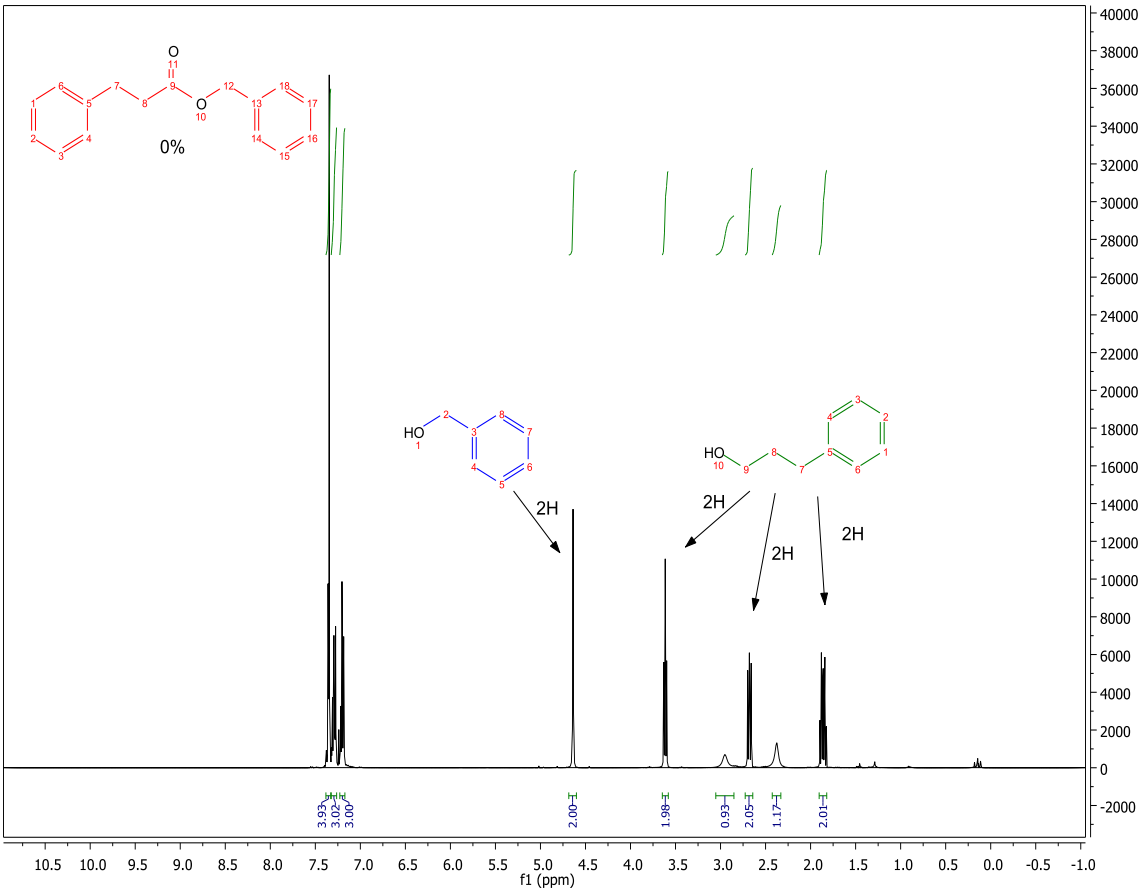

Figure 6.274. ^{1}H NMR for reduction of benzyl 3-phenylpropanoate with Cp_2TiBH_4/ NaO^{t}Bu/ PMHS in DME

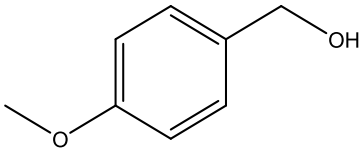

^{1}H NMR (400 MHz, $CDCl_3$) δ 7.25 (d, *J* = 6.8 Hz, 2H), 6.85 (d, *J* = 8.5 Hz, 2H), 4.55 (s, 2H), 3.77 (s, 3H).

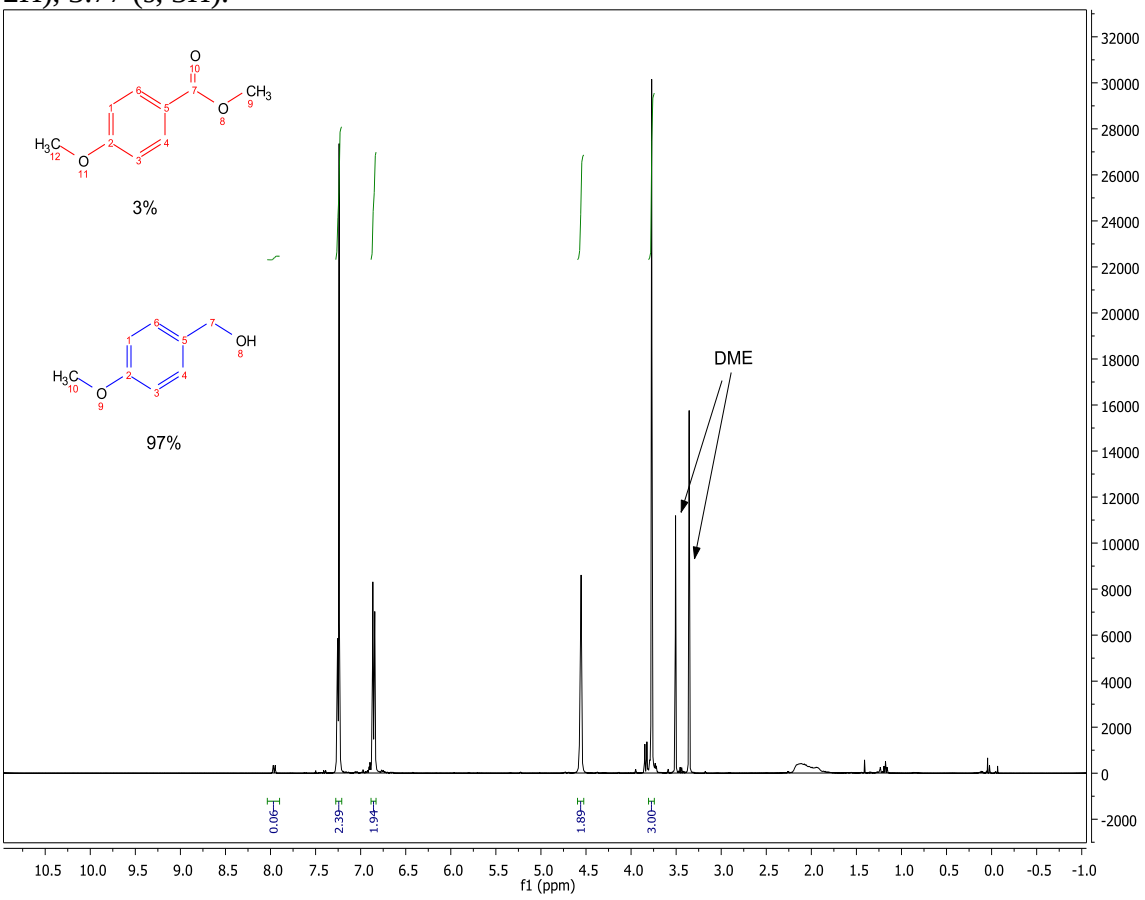

Figure 6.275. ^{1}H NMR for reduction of methyl 4-methoxybenzoate with Cp_2TiBH_4/ Acetone/ PMHS in DME

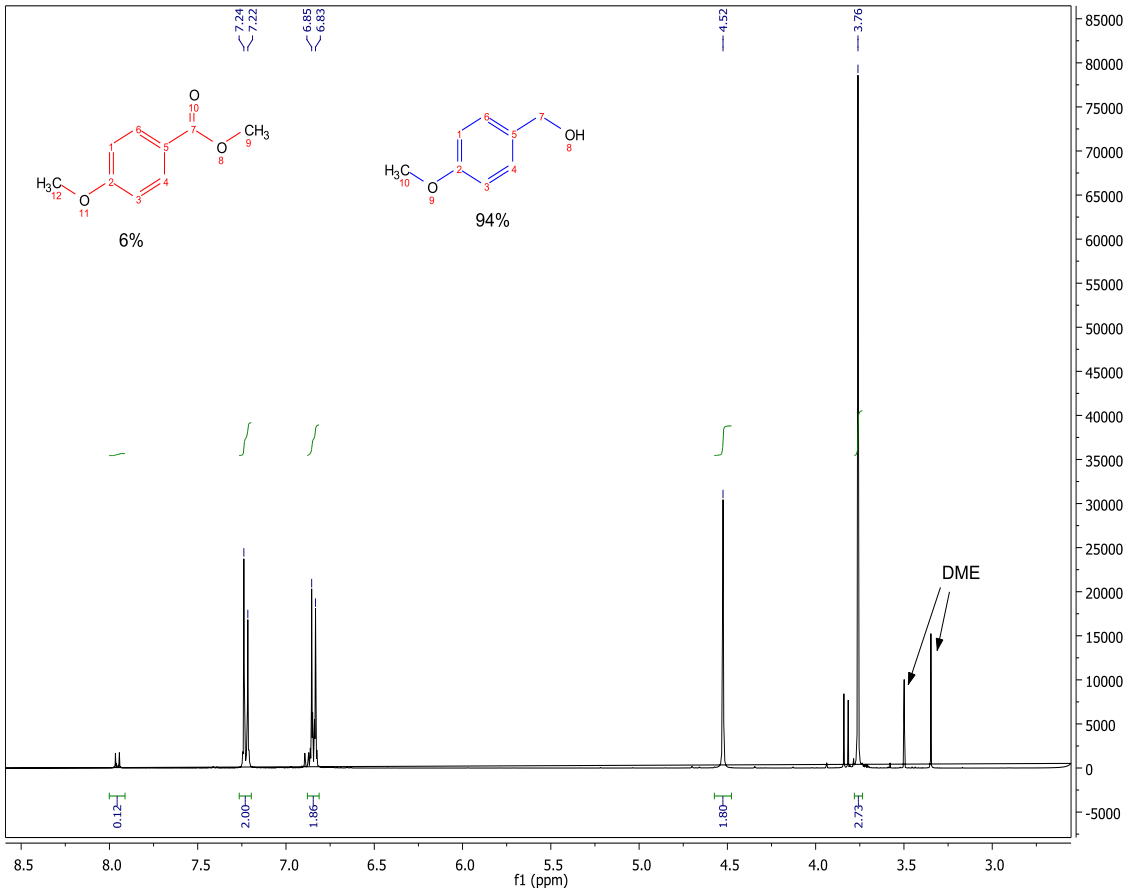

Figure 6.276. ^{1}H NMR for reduction of methyl 4-methoxybenzoate with Cp_2TiBH_4/ NaO^{t}Bu/ PMHS in DME

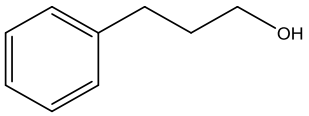

3-phenylpropan-1-ol

^{1}H NMR (500 MHz, $CDCl_3$) δ 7.31 (t, *J* = 7.5 Hz, 2H), 7.25 – 7.20 (m, 3H), 3.69 (t, *J* = 6.4 Hz, 2H), 2.78 – 2.68 (m, 2H), 1.92 (dq, *J* = 9.1, 6.5 Hz, 2H), 1.77 (s, 1H). ^{13}C NMR (126 MHz, $CDCl_3$) δ 141.88, 128.47, 128.44, 125.90, 62.25, 34.25, 32.11.

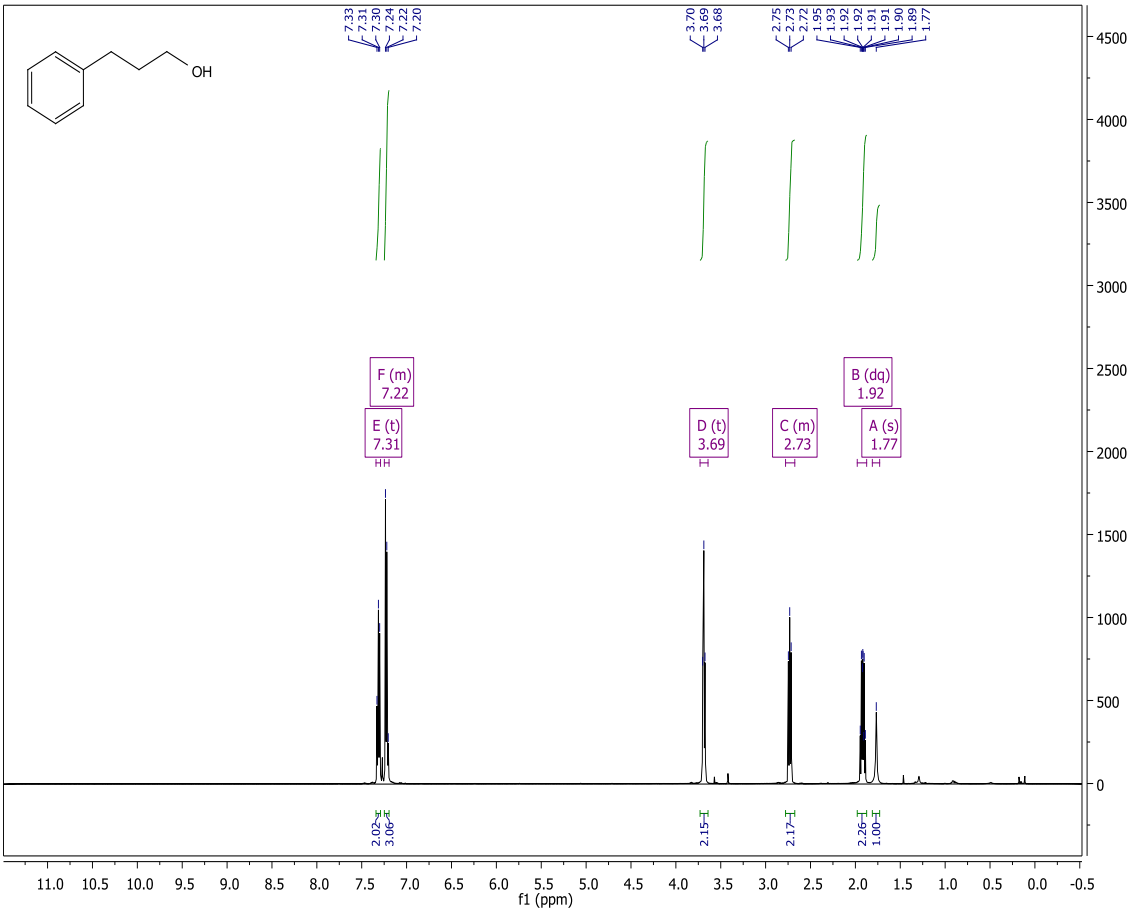

Figure 6.277. ^{1}H NMR for 3-phenylpropan-1-ol

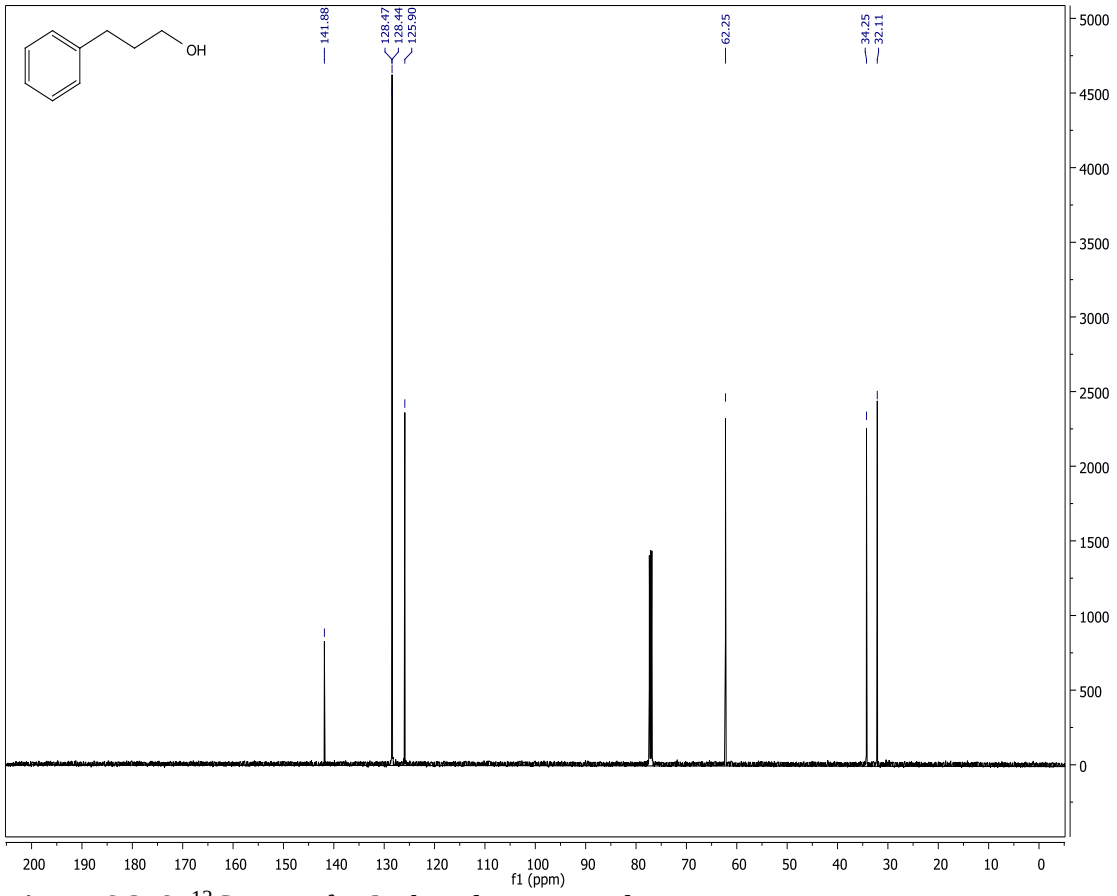

Figure 6.278. ^{13}C NMR for 3-phenylpropan-1-ol

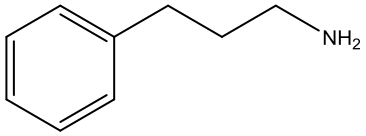

3-phenylpropan-1-amine

The amine was reduced with Yield after workup was 54 %

^{1}H NMR (400 MHz, $CDCl_3$) δ 7.30 – 7.24 (m, 2H), 7.21 – 7.13 (m, 3H), 2.77 – 2.67 (m, 2H), 2.67 – 2.60 (m, 2H), 1.89 – 1.71 (m, 4H). ^{13}C NMR (101 MHz, $CDCl_3$) δ 142.08, 128.40, 128.39, 125.82, 41.70, 35.26, 33.28.

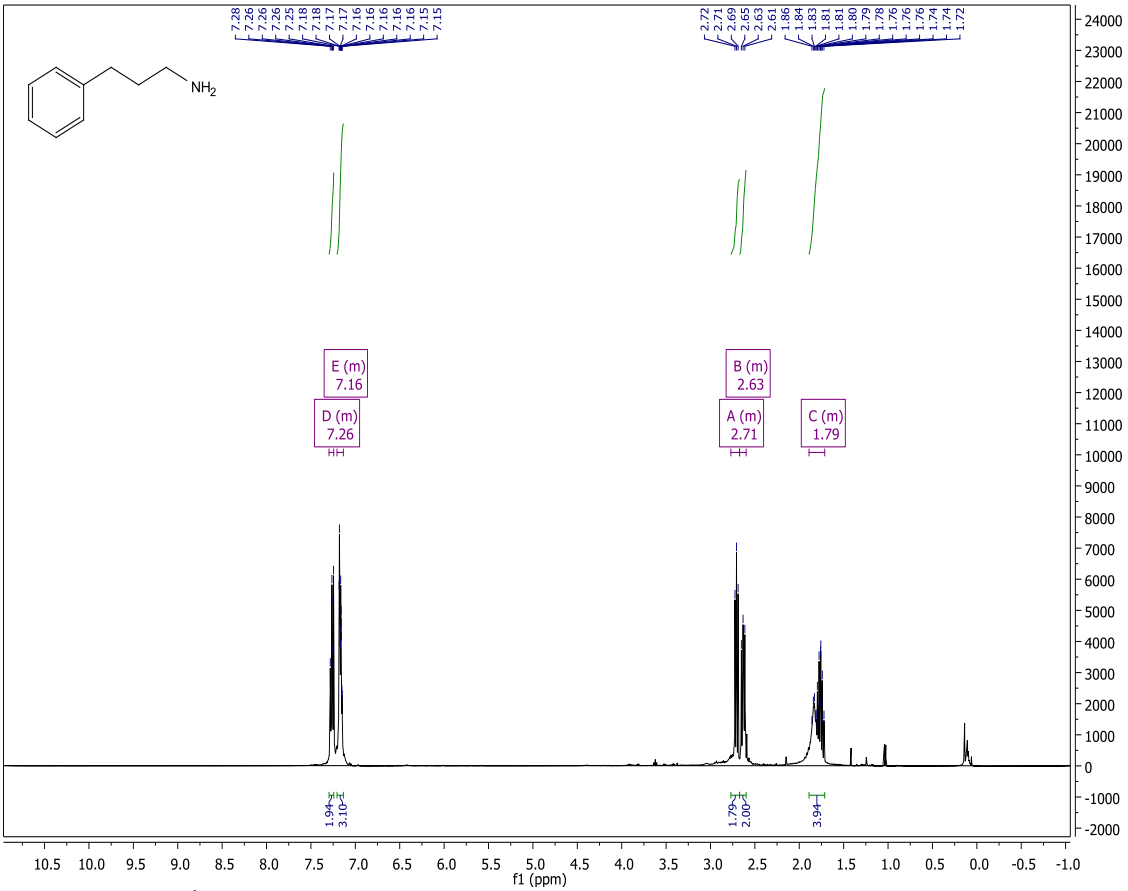

Figure 6.279. ^{1}H NMR for 3-phenylpropan-1-amine

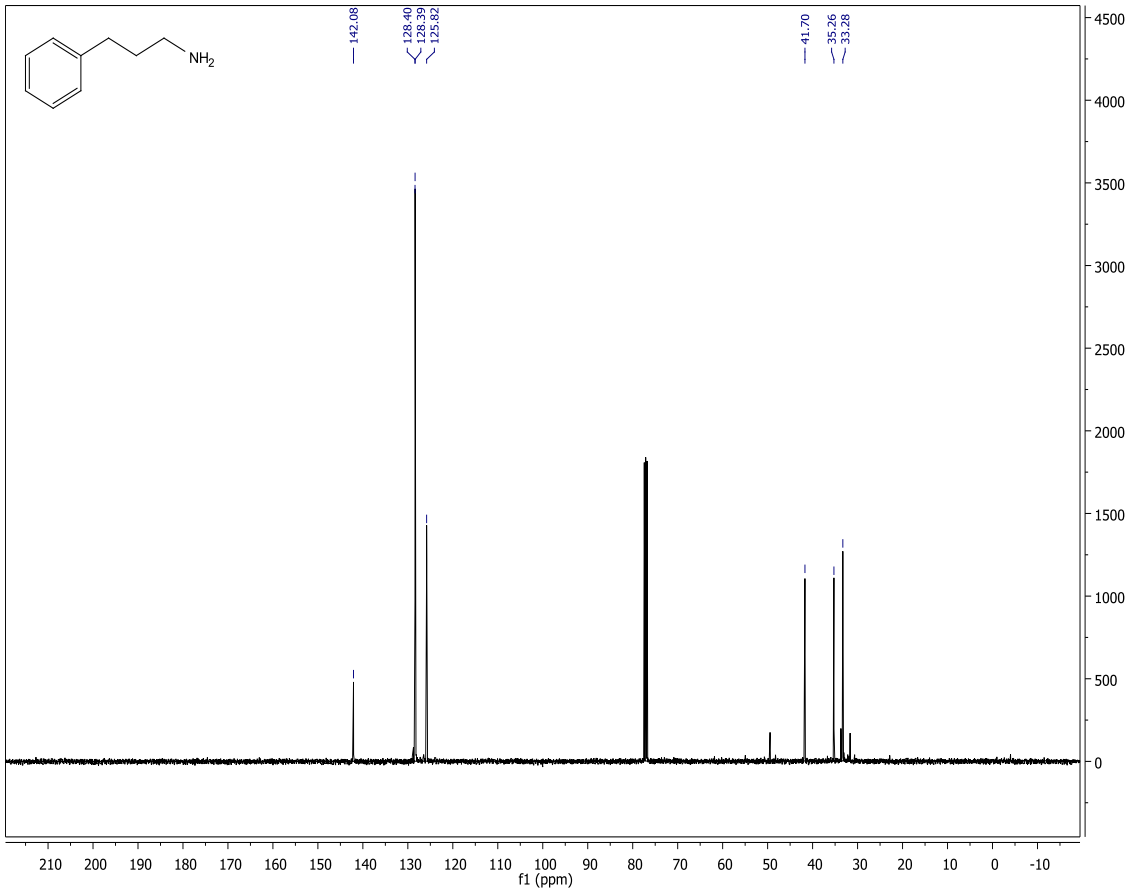

Figure 6.280. ^{13}C NMR for 3-phenylpropan-1-amine

Godfred Delali Fianu

Email: gdf212@lehigh.edu

EDUCATION

LEHIGH UNIVERSISTY, Bethlehem, PA August 2012- Summer 2017

- *Ph.D., Chemistry*

LEHIGH UNIVERSISTY, Bethlehem, PA
August 2012- 2014

- *M.S., Chemistry*

PRINCIPIA COLLEGE, Elsah, IL August 2007-*June 2011*

- *B.S. Chemistry*

RESEARCH EXPERIENCE

LEHIGH UNIVERSITY
Research Assistant
Adviser: Professor Robert A. Flowers II

- Mechanistic studies on atom-economical, titanocene-catalyzed homolytic aromatic substitution reactions.
- Mechanistic studies on titanocene borohydride catalyzed reductions.
- Experienced in methods of kinetic analysis of complex reactions.
- Applied understanding from kinetic studies to method development.
- Mentored undergraduate students.
- **Instrumentation:** ReactIR, GC, GC-MS, UV-Vis, SpectroVis, NMR (^{1}H, and ^{13}C), FTIR, Glovebox, Stopped-Flow Spectrophotometry.
- **Laboratory Skills:** Chemical kinetics measurements, flash column chromatography, crystallization, organic synthesis, purification techniques, spectral analysis, advanced wet chemistry.
- **Technical Skills:** MS Excel, Word, PowerPoint, OriginPro, SciFinder Scholar, ChemDraw, NMR Topspin, MestReNova, Mendeley, Gaussian09, Spartan.

PRINCIPIA COLLEGE
Undergraduate Researcher
Adviser: Professor Jeffrey Cornelius

- Studied methods for extracting an essential oil rich in eugenol from clove.

- Analyzed extracted oil with NMR and FTIR.

TEACHING EXPERIENCE

LEHIGH UNIVERSITY

Teaching Assistant

- **Intro to Chemical Principles (Fall 2016)**
- **Chemical Equilibrium in Aqueous Systems (Spring 2017)**
- Instructed, supervised, and assisted students with multiple step synthesis and analysis of compounds designed to teach laboratory, chemical, analytical, kinetic, and electrochemical principles.
- Tutored students on writing comprehensive lab reports.
- Graded laboratory reports.
- Proctored and graded exams.

PRINCIPIA COLLEGE

Laboratory Assistant **(2008-2011)**

- Supervised, and assisted students during laboratory experiments.
- Tutored students on homework assignments.
- Graded laboratory reports.

CONFERENCE PRESENTATIONS

ACS National Meeting & Exposition, Philadelphia, PA

- Mechanistic Studies of Titanocene(III) Reductions and Bond-Forming Reactions
- Oral Presentation
- August 2016

ACS National Meeting & Exposition, Denver, CO

- Radical Arylation of Epoxides by Low-Valent Titanocene Complexes: Mechanistic Studies and Method Development
- Oral Presentation
- March 2015

Catalysis Club of Philadelphia

- The Development and Mechanistic Studies of Additive Free Titanocene (III) Bond-Forming Reactions
- Poster Presentation
- November 2016

PUBLICATIONS

- Fianu, G. D.; Schipper, K. C.; Flowers, R. A., II. Catalytic carbonyl hydrosilylations *via* a titanocene borohydride–PMHS reagent system. *Catal. Sci. Technol.* **2017**, 7, 3469-3473.
- Gansäuer, A.; Hildebrandt, S.; von Laufenberg, D.; Kube, C.; Dahmen, T.; Michelmann, A.; Fianu, G. D.; Flowers, R. A., II. Cationic Titanocene(III) Complexes for Catalysis in Single-Electron Steps. *Angew. Chem., Int. Ed.* **2015**, *54*, 7003-7009.
- Gansäuer, A.; von Laufenberg, D.; Kube, C.; Dahmen, T.; Michelmann, A.; Behlendorf, M.; Sure, R.; Seddiqzai, M.; Grimme, S.; Fianu, G. D.; Sadasivam, D. V.; Flowers, R. A., II. Mechanistic Study of the Titanocene(III)-Catalyzed Radical Arylation of Epoxides. *Chem. Eur. J.* **2015**, *21*, 280-289.
- Gansäuer, A.; Kube, C.; Daasbjerg, K.; Sure, R.; Grimme, S.; Fianu, G. D.; Sadasivam, D. V.;
  Flowers, R. A., II. Substituent Effects and Supramolecular Interactions of Titanocene(III) Chloride: Implications for Catalysis in Single-Electron Steps. *J. Am. Chem. Soc.* **2014**, *136*, 1663-1671.

AWARDS AND AFFILIATIONS

- Member of the American Chemical Society
- University Graduate Fellowship *Fall 2012-2013*
- Academic Scholarship *Fall 2007-2011*
- Mark Crystal Achievement Award *2010-2011*
- Outstanding Junior Chemistry Award
- Best Chemistry Student Award *Fall 2007*